A SYSTEM RELIABILITY APPROACH TO THE LIFETIME OPTIMIZATION OF INSPECTION AND REPAIR OF HIGHWAY BRIDGES

by

Allen C. Estes

B.S., United States Military Academy, 1978

M.S., Stanford University, Const. Mgmt., 1987

M.S., Stanford University, Structures, 1987

M.B.A., Long Island University, 1989

M.M.A.S., U.S. Army Command and General Staff College, 1991

DISTRIBUTION STATEMENT A

Approved for public release;
Distribution Unlimited

A thesis submitted to the

Faculty of the Graduate School of the

University of Colorado in partial fulfillment

of the requirements for the degree of

Doctor of Philosophy

Department of Civil, Environmental and Architectural Engineering

1997

19971106 137

DTIC QUALITY INSPECTED 3

This thesis for the Doctor of Philosophy degree by

Allen C. Estes

has been approved for the

Department of

Civil, Environmental and Architectural Engineering

by

Dr. Dan M. Frangopol

Dr. George Hearn

Dr. Chung-Ha Suh

Dr. Benson Shing

Dr. John Dow

Date Apl 18/92

Allen C. Estes (Ph. D., Civil, Environmental and Architectural Engineering)

A SYSTEM RELIABILITY APPROACH TO THE LIFETIME OPTIMIZATION OF INSPECTION AND REPAIR OF HIGHWAY BRIDGES

Thesis directed by Professor Dan M. Frangopol

The United States has a national inventory of almost 600,000 highway bridges, many of which have deteriorated substantially and will require large expenditures to repair. Given that funds and resources are scarce, system reliability and optimization techniques have the potential to more efficiently maintain an adequate level of safety in these highway bridges while minimizing the total expected life-cycle cost. This study develops a reliability-based methodology for optimizing the inspection and repair of highway bridges.

An optimization method for inspection is proposed which relies on an event tree and the probability of making a repair to determine the optimal timing and number of inspections over the life of a structure. The method is developed and illustrated using a hypothetical structure, deterioration model, cost data, and inspection techniques. The method is later applied to an actual bridge deck using actual cost data, a chloride penetration model, and the half-cell potential method.

First-Order Reliability Method theory for component and system reliability is covered. A computer program RELSYS (RELiability of SYStems) is developed which computes the reliability index and probability of failure for any structural system which can be modeled as a series-parallel combination of components. The program is completely described through numerical examples and a comprehensive user's manual.

Using a system reliability approach, a hypothetical deterioration model is applied to statically determinate and indeterminate truss structures. Repairs are made whenever the system reliability index of the truss falls below a prescribed minimum level. A component reliability threshold is established to determine which components are repaired. The optimum component threshold reliability is based on minimizing total life-cycle cost from which a repair strategy is developed.

This system reliability approach is applied to the existing Colorado State Highway Bridge E-17-AH. All relevant bridge failure modes are identified and their component reliabilities are computed. The bridge is modeled as a series-parallel combination of these failure modes. Both the load rating and the system reliability of the index of the bridge are computed and compared. Using realistic live-load and deterioration models, the system reliability index of the bridge is evaluated over time. Considering several realistic repair options, the bridge is repaired every time its system reliability falls below a prescribed minimum value. The optimum lifetime repair strategy is based on all feasible combinations of repair options and cost data developed in consult with the Colorado Department of Transportation. Since the system reliability model is entirely strength-based, serviceability issues are addressed through serviceability flags.

A method for updating the bridge repair strategy over time is introduced based on the results of inspections. Updating the reliability of a bridge using data from the PONTIS Bridge Management System is investigated. The repair strategy is updated based on the hypothetical results of specifically selected non-destructive evaluation tests.

Dedication

To my wife

Peggy A. B. Estes and

my parents

Major General (Retired) Howard M. Estes Jr., Ph.D.

and Joan T. Estes

ACKNOWLEDGEMENTS

In an effort of this magnitude, there are a number of people who helped, guided, encouraged, and inspired me along the way. First and foremost, I want to thank my thesis advisor, Dr. Dan Frangopol, who directed this research and ensured that I finished on time. I am particularly grateful to Dr. Frangopol for the opportunity to present papers at several conferences and to jointly author over ten conference papers and journal articles. Dr. Frangopol introduced me to many of the international experts in structural reliability, and through him, I was able to meet many of the sources who appear in my bibliography. Every student should be so fortunate. I am deeply indebted to Dr. Frangopol for providing enough frequent and critical guidance to keep me on track and sufficient freedom to take this research where I wanted it to go.

I offer my sincere thanks to Professors George Hearn, Benson Shing, Chung-Ha Suh, John Dow, and James Diekmann who served on my thesis committee and evaluated my work. I am especially grateful to Dr. George Hearn who reviewed each chapter in detail as it was written and offered insightful comments for improvement.

I gratefully acknowledge the United States Army which funded my study and assigned me to the University of Colorado for three years to complete this program. In particular, I thank Colonels Kip Nygren, Terry Hand,

and Tom Lenox who were instrumental in my selection for this program and supported me returning to West Point to teach cadets.

The Colorado Department of Transportation (CDOT) assisted me greatly in this research. I am grateful to Walt Mystkowski, head of the Bridge Management Branch at CDOT, who offered his cooperation and resources to support this research. I especially thank Steve White who copied blueprints, found manuals, provided contacts, and took me through the data base to find a suitable bridge to analyze. Tom Moss' assistance was invaluable as he introduced me to the PONTIS bridge management system and allowed me to accompany him on bridge inspections on two different occasions. My thanks to Dana Christensen for arranging my inspection visits, Hap Ellsworth for describing the CDOT quality assurance inspection program, Mike Mohseni for answering questions on the BARS system, and Sharon Wilson for discussing bridge repair options and costs. In addition, I appreciate the assistance from Dick Hines from the Staff Material Branch with regard to the half-cell potential test and its associated capabilities and costs. My thanks to Ken Wood and Gerry Peterson from the Regional Materials Labs who also provided input on the half-cell potential test.

I offer special thanks to Dr. John Sørensen from the University of Aalborg, Denmark who explained some key system reliability concepts. He assisted me greatly with the Hohenbichler approximation and with equivalent alpha vectors. My thanks as well to Anne Lunke, a fellow student, who translated the comments from the Hohenbichler approximation computer code from Danish to English.

I am grateful to University of Colorado students who have gone before me and whose research greatly contributed to my own. The work done by Samer Hendawi and Yong-Hak Lee in developing RELTRAN helped immensely in the development of RELSYS. Kai-Yung Lin's research on optimum inspection strategies was very helpful toward developing my own. I especially appreciate Dave Renn's research on segment-based inspection, Steve Marshall's study on quantifying the capabilities of half-cell potential tests, and Tianna Szanyi's survey of condition rate deterioration models.

I appreciate the assistance, cooperation, and friendship provided by my office mates Adelino de Almeida, Emhaidy Gharaibeh, Yutaka Ide, Kai-Yung Lin, and Ichiro Iwaki during the past three years. A special thanks to Mike Enright who listened to my problems, found lots of my mistakes, and was a terrific friend throughout this whole process.

Finally and most importantly, I offer my sincere thanks and love to my wife Peggy and my parents Howard and Joan Estes, to whom this thesis is dedicated. I am grateful to Peggy who is my best friend and life companion, and to my parents who raised me and firmly instilled in me the value of an education.

CONTENTS

CHAPTER

I. INTRODUCTION 1

1.1 Overview 1

1.2 Objective 4

1.3 State of the Art 4

1.3.1 Reliability Theory 5

1.3.2 Random Variables 6

1.3.3 Bridge Inspection and Bridge Management 7

1.4 Benefits of the Study 9

1.5 Limitations of the Study 10

1.6 Organization of the Thesis 15

1.7 Units 19

II. INSPECTION OPTIMIZATION 21

2.1 Overview and Objectives 21

2.2 Description of the Problem: Single Component System . . 22

2.2.1 Deterioration Model 25

2.2.2 Inspection Methods 25

2.2.3 Probability of Repair 28

2.2.4 Cost of Repair 31

2.2.5 Single Component System: Two Lifetime Inspections 32

2.2.6 Single Component System – Four Lifetime Inspections 38

2.2.7 Program: OptimumInspect 47

2.3 Results of the Single Component System for Two, Three, and Four Inspections 48

2.4 Series System 62

2.5 Results of the Series System for Two Inspections 81

2.6 Two-Bar Parallel System 89

2.7 Conclusions 94

III. RELIABILITY OF SYSTEMS 101

3.1 Introduction 101

3.2 Reliability and Failure 102

3.3 Limit state functions 105

3.4 First Order Reliability Method (FORM) 106

3.4.1 Example of FORM 107

3.5 Correlation 111

3.5.1 FORM with Random Variable Correlation 116

3.5.2 Uncorrelated Non-Normal Variables 117

3.5.3 Correlated Non-Normal Variables 119

3.5.4 Sensitivity Measures 121

3.6 System Reliability 122

3.6.1 Series Structures – Probability of Failure 123

3.6.2 Series System Example 127

3.6.3 Parallel Structures – Probability of Failure 131

3.6.4 General Systems 140

3.7 Monte Carlo Simulation 149

3.8 RELSYS 151

3.9 Testing RELSYS 152

3.9.1 Parallel Systems 152

3.9.2 Series-Parallel System 156

3.9.3 Other RELSYS Tests 166

3.10 Strengths and Limitations of RELSYS 166

3.11 Potential Improvements for RELSYS 173

IV. OPTIMIZED REPAIR STRATEGY 174

4.1 Introduction 174

4.2 Establishing a Component Reliability Threshold 174

4.3 Series System: Seven Bar Truss 175

4.4 Parallel System 183

4.5 Series-Parallel System: Three Bar Indeterminate Truss . . 186

4.6 Summary 198

V. COLORADO BRIDGE E-17-AH: A CASE STUDY 199

5.1 Introduction 199

5.2 Bridge E-17-AH 202

5.3 Load Rating of Bridge E-17-AH 209

5.3.1 Load Rating: Slab 212

5.3.2 Load Rating: Shear on Critical Girder 215

5.3.3 Load Rating: Moment on Critical Girder 219

5.3.4 Load Rating: Serviceability on Critical Girder . . . 221

5.3.5 Final Load Rating of the Bridge 222

5.4 Component Reliability of Bridge E-17-AH 222

5.4.1 Random Variables 224

5.4.2 Limit State Equations 225

5.4.3 Reliability Results For An HS-20 Truck 230

5.4.4 A Reliability-Based Approach to Inventory and Operating Load Ratings 232

5.5 Live Load Models 233

5.5.1 Ghosn Live Load Model 234

5.5.2 Nowak Live Load Model 239

5.6 Other Failure Modes 247

5.6.1 Additional Failure Modes in the Superstructure . . 248

5.6.2 Failure Modes in the Substructure 253

5.7 Component Reliability Results 279

5.7.1 Sensitivity With Respect To Random Variables . . 279

5.8 Reliability of the Bridge as a System at a Fixed Point of Time 285

5.9 Time Dependent Deterioration of the Bridge 297

5.9.1 Deterioration of the Concrete Slab and Pier Cap . . 299

5.9.2 Deterioration of the Girders 310

5.10 System Reliability Over Time 325

5.11 Repair Criteria and Repair Options 330

5.12 Optimum Lifetime Repair Strategy 335

5.13 Serviceability Flags 354

5.13.1 Condition States 360

5.13.2 Condition State Deterioration Models 363

5.13.3 Markov Chain Models 366

5.13.4 Example Using Serviceability Flags 374

5.14 Summary 378

VI. STRATEGY UPDATES BASED ON INSPECTION RESULTS 381

6.1 Introduction 381

6.2 Current PONTIS Inspection 384

6.3 Updating Serviceability Flags Based on Routine Inspection Results 391

6.4 Updating System Reliability Based on Routine Inspection Results 396

6.4.1 Segment-Based Inspection 397

6.4.2 Reliability Update 405

6.4.3 General Approach 406

6.4.4 Bridge E-17-AH Girder Inspection Results 409

6.4.5 Using Inspection Results to Project Future Performance 428

6.4.6 Updating the Reliability of Other Components . . . 430

6.5 Reliability Updates Based on Non-Destructive Evaluation (NDE) Methods 433

6.5.1 Steel Girder Thickness 435

6.5.2 Active Corrosion in the Deck 443

6.5.3 Rate of Corrosion in the Deck 454

6.6 Updated Strategy for Bridge E-17-AH 463

VII. LIFETIME INSPECTION OPTIMIZATION OF CONCRETE DECKS USING THE HALF-CELL POTENTIAL TESTS 474

7.1 Introduction 474

7.2 Applying the Inspection Optimization Method 475

7.2.1 Failure Criterion 476

7.2.2 Deterioration Model and Repair Options 479

7.2.3 Inspection Methods, Capabilities, and Costs 482

7.2.4 Probability of Repair 499

7.2.5 The Optimization Problem 504

7.3 Optimum Inspection Strategy for the Deck 507

7.4 Updating the Optimum Inspection Strategy 512

7.4.1 Effect of Repair Probabilities on Updating 525

7.4.2 Updating the Deterioration Model 534

7.5 Effects of Other Variables 539

7.5.1 Service Life, Number of Inspections and Quality of Inspections 539

7.5.2 Replacement Policy and Probability of Replacement Approach 546

7.5.3 Effect of Discount Rate 554

7.5.4 Effect of $-350mV$ Threshold 554

7.6 Concluding Remarks 559

VIII. CONCLUSIONS AND RECOMMENDATIONS 564

8.1 Summary 564

8.2 Conclusions 573

8.3 Recommendations For Further Research 578

IX. REFERENCES 586

APPENDIX

A. RELSYS USER'S MANUAL 601

B. RELSYS FLOW CHARTS AND SUBROUTINES 670

C. NOTATIONS 704

TABLES

Table

2.1 **Parameters Associated With Four Inspection Techniques** 27

2.2 **Optimum Inspection Strategy and Total Costs for Two Lifetime Inspections** 49

2.3 **Optimum Inspection Strategy and Total Costs for Three Lifetime Inspections** 50

2.4 **Optimum Inspection Strategy and Total Costs for Four Lifetime Inspections** 51

2.5 **Optimal Inspection Strategy For Different Structures** . . 66

2.6 **Optimum Inspection Strategy and Costs for Two Bar Series System with Two Lifetime Inspections** 82

2.7 **Optimum Inspection Strategy and Costs for Two Bar Series System with Unequal Bar Resistances, Inspection Technique C** 85

2.8 **Optimum Inspection Strategy and Costs for Two Bar Parallel System with Two Lifetime Inspections** 91

2.9 **Optimum Inspection Strategy and Costs for Two-Bar Parallel System with Unequal Bar Resistances, Inspection Technique B** 93

3.1 **Iterative FORM Solution for** $g(\mathbf{X}) = 2X_1^2 - 2X_2 = 0$ **Where** X_1**=N[2.0, 0.2] and** X_2**=N[3.0,0.3]** 112

3.2 **Random Variables** X_1, X_2, **and** X_3 128

3.3 **Component Reliability Results for** $g(1)$, $g(2)$, **and** $g(3)$. . . 128

3.4 **Joint Probability Results for** $g(1)$, $g(2)$, **and** $g(3)$. 130

3.5 **Rank Ordering of $g(1)$, $g(2)$, and $g(3)$.** 131

3.6 **Bivariate Normal Distribution Approximations (β)** . . . 134

3.7 **Bivariate Normal Distribution Approximations ($P_f \cdot 10^{-3}$)** 135

3.8 **Trivariate Normal Distribution Approximations (β)** . . . 138

3.9 **Trivariate Normal Distribution Approximations ($P_f \cdot 10^{-3}$)** 139

3.10 **Adjusted System Reliabilities For Two Member Parallel System Based on the Sensitivities With Respect to the Random Variables X_1, X_2, and X_3** 146

3.11 **Adjusted System Reliabilities For Three Member Parallel System Based on the Sensitivities of the Random Variables X_1, X_2, and X_3** 148

3.12 **Results for Components 1, 4, and 5** 148

3.13 **Mean Resistance in Each Bar for Two, Three, Four, and Five-Bar Systems Which Are 0%, 25%, and 50% Unbalanced** 155

4.1 **Repair Costs for a Semi-Ductile Three Bar Indeterminate Truss for Different Resistance Correlation Values** 197

5.1 **Summary of Load Ratings for Colorado Highway Bridge E-17-AH** 223

5.2 **Random Variables in System Reliability Analysis of Colorado Highway Bridge Number E-17-AH** 226

5.3 **Variables in System Reliability Analysis of Colorado Highway Bridge Number E-17-AH** 227

5.4 **Comparison of Load Ratings to Reliability for Colorado Highway Bridge E-17-AH Using a Deterministic HS-20 Truck** 231

5.5 **Reliability Associated With the HS-20 Truck, the Inventory Rated Truck and the Operating Rated Truck** . 234

5.6 a and m Factors for Ghosn Live Load Model Based on Bridge Span [Ghosn and Moses 1986] 236

5.7 H Factors for Ghosn Live Load Model Based on Bridge Span and Traffic Volume [Ghosn and Moses 1986] 237

5.8 Average Daily Truck Traffic as a Function of Average Daily Traffic on Different Highways 237

5.9 Reliability Index (β) Associated With Load Ratings and Different Live Load Models 247

5.10 Critical Loading on the Pier Cap 258

5.11 Deterministic Analysis of the Pier Cap to Determine the Most Critical Section With Respect to Shear 263

5.12 Reliability and Sensitivity Analysis of Failure Modes for Colorado Highway Bridge Number E-17-AH 280

5.13 System Reliability Results for Bridge E-17-AH Using Different System Models and Different Correlation Between Girder Resistances 297

5.14 Random Variables (RV) Used To Compute the Deterioration of Reinforcing Steel in the Slab and Pier Cap Due To Chloride Penetration of the Concrete 304

5.15 Point Estimate Method Results for Finding the Mean and Standard Deviation for the Corrosion Initiation Time T_I for the Concrete Slab 306

5.16 Point Estimate Method Results for Finding the Mean and Standard Deviation for the Area of Steel After 30 Years $A(30)$ for the Concrete Slab 307

5.17 Statistical Parameters A and B for Predicting the Corrosion Propagation in the Bridge E-17-AH Girders [Albrecht and Naeemi 1984] 314

5.18 **Point Estimate Method Results for Finding the Mean and Standard Deviation for the Plastic Section Modulus After 30 Years, $Z(30)$, for the Interior-Exterior Girder** 319

5.19 **Repair Options and Associated Repair Costs for Bridge E-17-AH (Using 1996 U.S. Dollars)** 334

5.20 **Optimum Lifetime Repair Strategy for Bridge E-17-AH Using Simplified Series-Parallel Model Requiring Failure of Three Adjacent Girders** 340

5.21 **Optimum Lifetime Repair Strategy for Bridge E-17-AH Using Simplified Series-Parallel Model Requiring Failure of Three Adjacent Girders and the Corrosion Rate of the Pier Cap is Halved** 344

5.22 **Optimum Lifetime Repair Strategy for Bridge E-17-AH Using Simplified Series-Parallel Model Requiring Failure of Two Adjacent Girders** 346

5.23 **Cost of Available Repair Strategy for Bridge E-17-AH Using Simplified Series-Parallel Model Requiring Failure of Two Adjacent Girders for Discount Rates of 1% Through 6%** 351

5.24 **Optimum Lifetime Repair Strategy for Bridge E-17-AH Using Simplified Series-Parallel Model Requiring Failure of Two Adjacent Girders With the Discount Rate Raised to 6%** 353

5.25 **Optimum Lifetime Repair Strategy for Bridge E-17-AH Using Simplified Series Model Requiring Failure of a Single Girder** 356

5.26 **National Bridge Inventory Condition Ratings, Their Meaning, and Associated Repair Actions** 362

5.27 **PONTIS [1995] Condition State (CS) Ratings for An Unprotected Concrete Deck with Asphalt Concrete Overlay** 363

5.28 **Linear Condition State Deterioration Models for RC Decks, Railings, and RC Substructures [Hearn *et al.* 1995]** 365

5.29 Transition Probabilities for Concrete Bridge Substructures Using Markov Chains [Jiang and Sinha 1989] 367

5.30 Simulation Results for 10,000 Concrete Bridge Substructures Using Markov Chains (Year 0-35) 369

5.31 Simulation Results for 10,000 Concrete Bridge Substructures Using Markov Chains (Year 36-70) 370

5.32 New York State Condition Ratings and Their Definitions [Cesare *et al.* 1992] 372

5.33 Optimum Lifetime Repair Strategy for Bridge E-17-AH Using Simplified Series-Parallel Model Requiring Failure of Three Adjacent Girders (Serviceability Flags Included) 376

6.1 Inspection Results for PONTIS Bridge Elements for Bridge E-17-AH 386

6.2 PONTIS Condition State (CS) Ratings for Element 359: Soffit (Under Surface) of Concrete Decks and Slabs 387

6.3 CDOT Suggested Condition State (CS) Ratings for Element 359: Soffit (Under Surface) of Concrete Decks and Slabs 388

6.4 CDOT Suggested Condition State (CS) Ratings for Element 107: Painted Open Steel Girders 389

6.5 Comparison of Shear Area A_v and Plastic Section Modulus Z Over Time for an Interior-Exterior Girder Based on Same Corrosion Thickness Loss 390

6.6 PONTIS Condition State (CS) Ratings for Element 234: Concrete Pier Cap 391

6.7 PONTIS Condition State (CS) Ratings for Element 333: Miscellaneous Bridge Rating 395

6.8 Results of the Segment-Based Inspection on Bridge E-17-AH for the Interior Girders Where Moment Capacity is Critical 411

6.9 Results of the Segment-Based Inspection on Bridge E-17-AH for the Interior Girders Where Shear Capacity is Critical 413

6.10 Results of the Segment-Based Inspection on Bridge E-17-AH for the Interior-Exterior Girders 414

6.11 Results of the Segment-Based Inspection on Bridge E-17-AH for the Exterior Girders 415

6.12 Reliability-Based Condition State (CS) Ratings for Element 107: Painted Open Steel Girders 417

6.13 Inspection Program Categories Based on the Programs Implemented to Ensure Inspector Accuracy and Consistency 419

6.14 Probability Distributions: Condition State (CS) Ratings for Element 107 (Painted Open Steel Girders) for Inspection Categories A, B, and C 421

6.15 Updated Distribution Parameters for Area of Web (A_w) and Plastic Section Modulus (Z) for Girders 1-5 on Bridge E-17-AH Based on Inspection Results 425

6.16 Comparison of Area of Web (A_w) and Plastic Section Modulus (Z) Results for Girders 1-5 on Bridge E-17-AH Based on Inspection Results and Deterioration Model Prediction 427

6.17 Comparison of Component and System Reliability of Bridge E-17-AH Based on Inspection Results and Deterioration Model Prediction of the Bridge Girders 429

6.18 Projected % Section Loss in Girders V-1, M-4, and V-5 for 20 Years After Inspection Based on Linear Condition State Deterioration 431

6.19 Common Groups of Girder Thickness Readings Using Simplified Series-Parallel Model for Bridge E-17-AH 438

6.20 **Thickness Results for Exterior Girder Shear Failure Mode (V-1) for Inspections at 15, 30, and 55 Years of Service** 440

6.21 **Thickness Results for Exterior, Interior-Exterior and Interior Girders for Inspections at 15, 30, and 55 Years of Service** 440

6.22 **Results of Half-Cell Potential Inspections Based on 0.05 Volt Intervals on a Deck at 20, 40 and 60 Years of Service** 450

6.23 **Results of Half-Cell Inspection of Deck Based on Cumulative Percentage of Readings after 20, 40, and 60 Years** 452

6.24 **Results of Hypothetical Three Electrode Linear Polarization (3LP) Test on Deck of Bridge E-17-AH** . . . 462

6.25 **Updated Optimum Lifetime Repair Strategy for Bridge E-17-AH Using Simplified Series-Parallel Model Requiring Failure of Three Adjacent Girders** . . . 472

7.1 **Inspection Techniques A, B, and C Based on Spacing of Half-Cell Potential Readings** 495

7.2 **Expected Cost of Repair For Concrete Bridge Deck with 45 Year Service Life, Three Lifetime Inspections, *Proactive* Approach, Inspection Technique A, and 2% Discount Rate** 511

7.3 **Updated Optimization Results for Inspection of a Deck with a 45 Year Service Life Using a *Proactive* Approach, Inspection Technique A, and Discount Rate $r = 2\%$** 519

7.4 **Updated Optimization Results for Inspection of a Deck with a 45 Year Service Life Using an *Accelerated Linear* Approach** 534

7.5 **Updated Optimization Results for Inspection of a Deck with a 45 Year Service Life Using a *Proactive* Approach and Updated Deterioration Model** 536

7.6 **Optimum Inspection Strategy for a 40 Year Deck with a 60% Replacement Policy and Two Lifetime Inspections Considering Various Repair Approaches** 552

7.7 **Optimum Inspection Times and Expected Cost for Different Discount Rates on a 40 Year Deck with Four Lifetime Inspections and a *Proactive* Approach** 556

7.8 **Comparison of Inspection Optimization Using a Calibrated Threshold and a -350 mV Threshold for a 40 Year Deck with Three Lifetime Inspections** 561

A.1 **Distributions Available in RELSYS** 614

A.2 **Distributions Type Number in RELSYS** 615

A.3 **Random Variables: Example 1** 621

A.4 **Basic Variables Example 2** 625

A.5 **Random Variables: Example 3** 629

A.6 **Random Variables: Example 4** 632

A.7 **Random Variables: Example 5** 635

A.8 **Random Variables: Example 6** 639

A.9 **Random Variables: Example 7** 643

A.10 **Random Variables: Example 8** 648

A.11 **Random Variables: Example 9** 654

A.12 **Random Variables: Example 10** 663

FIGURES

Figure

1.1 **Total Cost, Failure Cost, and Initial Cost Versus Reliability** 11

2.1 **Single Component Structure Subjected to Centric Axial Load and Section Loss Due to Deterioration** 23

2.2 **Deterioration of Cross-Sectional Area Over Time** 26

2.3 **Density Distribution and Probability of Detection for Four Inspection Techniques** 29

2.4 **Repair Paths and Time Line for Two Lifetime Inspections on a Single Component Structure** 34

2.5 **Repair Paths for Four Lifetime Inspections on a Single Component Structure** 40

2.6 **Timeline for Four Lifetime Inspections on a Single Component Structure** 41

2.7 **Expected Total Costs for Techniques A, B, C, and D: Single Component Structure, Two Lifetime Inspections** 52

2.8 **Expected Total Costs for Techniques A, B, C, and D: Single Component Structure, Three Lifetime Inspections** 53

2.9 **Expected Total Costs for Techniques A, B, C, and D: Single Component Structure, Four Lifetime Inspections** 54

2.10 **Optimum Timing of Inspections Using Inspection Technique A for Two Lifetime Inspections,** $\delta_R = 0.10$ . . . 58

2.11 **Optimum Timing of Inspections Using Inspection Technique B for Three Lifetime Inspections,** $\delta_R = 0.10$ . . . 59

2.12 Optimum Timing of Inspections Using Inspection Technique C for Four Lifetime Inspections, $\delta_R = 0.10$ . . . 60

2.13 Optimum Timing of Inspections Using Inspection Technique A for Four Lifetime Inspections, $\delta_R = 0.10$ . . . 61

2.14 Effect of Various Inspection Techniques on a Structure With Mean Resistance $R = 14$ for Two Lifetime Inspections, $\delta_R = 0.10$ 63

2.15 Effect of Various Inspection Techniques on a Structure With Mean Resistance $R = 15$ for Four Lifetime Inspections, $\delta_R = 0.10$ 64

2.16 Expected Total Costs for a Single Component Structure with a Mean Resistance $R = 14$ for Two, Three, and Four Lifetime Inspections, $\delta_R = 0.10$ 65

2.17 Two Bar Series System 66

2.18 Repair Paths For Three Lifetime Inspections on a Two Bar System 68

2.19 Repair Paths For Three Lifetime Inspections on a Two Bar System: Top Quarter, Section A From Fig. 2.18 69

2.20 Repair Paths For Three Lifetime Inspections on a Two Bar System: Second Quarter, Section B From Fig. 2.18 70

2.21 Repair Paths For Three Lifetime Inspections on a Two Bar System: Third Quarter, Section C From Fig. 2.18 71

2.22 Repair Paths For Three Lifetime Inspections on a Two Bar System: Bottom Quarter, Section D From Fig. 2.18 72

2.23 The Probabilities of Failure for a Two Component System With Two Lifetime Inspections 75

2.24 The Additional Probabilities of Failure for a Two Component System With Three Lifetime Inspections . . . 76

2.25 Expected Total Costs for Techniques A, B, C, and D: Two Bar Series Structure, Two Lifetime Inspections . 83

2.26 **Two Component Series System Where Mean Resistance $R = 15$ and $\delta_R = 0.10$ For Both Bars, Varying Inspection Techniques** 86

2.27 **Two Component Series System with Two Inspections, Inspection Technique C, Varying Mean Resistances** 87

2.28 **Series System: Unequal Mean Bar Resistances, Two Inspections, Inspection Technique C** 88

2.29 **Two Bar Parallel System** 90

2.30 **Expected Total Costs for Techniques A, B, C, and D: Two-Bar Parallel Structure, Two Lifetime Inspections** 92

2.31 **Two Component Parallel System with Two Inspections, Inspection Technique B, Varying Mean Resistances, $\delta_R = 0.10$** 95

2.32 **Parallel System: Unequal Mean Bar Resistances, Two Lifetime Inspections, Inspection Technique B, $\delta_R = 0.10$** 96

2.33 **Comparison of Parallel, Single Component, and Series System: Two Lifetime Inspections, Inspection Technique B** 97

3.1 **Differential Reliability of a Structure Based on the Distributions of the Load and Resistance** 104

3.2 **Results of FORM Iterations in the Reduced Space** . . . 113

3.3 **Results of FORM Iterations in the Original Space** 114

3.4 **Correlation Between Two Failure Modes** 127

3.5 **Series Model of $g(1)$, $g(2)$, and $g(3)$** 128

3.6 **Reduction of a Series-Parallel System to an Equivalent Series System** 141

3.7 **Reduction of a Series-Parallel System to an Equivalent Single Component** 145

3.8 Parallel Systems With Two, Three, Four, and Five Bars 153

3.9 Comparison of Results for a Two-Bar Ductile Parallel System Between RELSYS, CALREL, and MCREL . 157

3.10 Comparison of Results for a Three-Bar Ductile Parallel System Between RELSYS, CALREL, and MCREL 158

3.11 Comparison of Results for a Four-Bar Ductile Parallel System Between RELSYS, CALREL, and MCREL . 159

3.12 Comparison of Results for a Five-Bar Ductile Parallel System Between RELSYS, CALREL, and MCREL . 160

3.13 Comparison of RELSYS Results to CALREL for Balanced Parallel Systems 161

3.14 Comparison of RELSYS Results to CALREL for 25% Unbalanced Parallel Systems 162

3.15 Two Bar Parallel System Modeled as a Series-Parallel System 163

3.16 Three Bar Parallel System Modeled as a Series-Parallel System 164

3.17 Four Bar Parallel System Modeled as a Series-Parallel System 165

3.18 Comparison of RELSYS Results to Hendawi and Frangopol [1994b] for Series-Parallel Systems, ($\rho(R_i, R_j) = 0.0$) 167

3.19 Comparison of RELSYS Results to Hendawi and Frangopol [1994b] for Series-Parallel Systems, ($\rho(R_i, R_j) = 0.5$) 168

3.20 Comparison of RELSYS Results to Hendawi and Frangopol [1994b] for Ductile, Perfectly Correlated, Series-Parallel Systems 169

3.21 Comparison of RELSYS Results to Hendawi and Frangopol [1994b] for Semi-ductile, Partially Correlated, Series-Parallel Systems 170

3.22 **Comparison of RELSYS Results to Hendawi and Frangopol [1994b] for Brittle, Uncorrelated, Series-Parallel Systems** 171

4.1 **Seven Bar Statically Determinate Truss Modeled as a Series System** 176

4.2 **Repair Plan for a Seven Bar Statically Determinate Truss, Initial Equal Importance of Bars;** $\beta_{threshold} = 7.0$; $Cost = 80$ 179

4.3 **Repair Plan for a Seven Bar Statically Determinate Truss, Initial Equal Importance of Bars;** $\beta_{threshold} = 4.0$; $Cost = 50$ 180

4.4 **Repair Plan for a Seven Bar Statically Determinate Truss, Initial Equal Importance of Bars;** $\beta_{threshold} = 2.6$; $Cost = 55$ 181

4.5 **Total Cost of Repair With Varying Values** $\beta_{threshold}$ **for a Seven Bar Statically Determinate Truss, Initial Equal Importance of Bars** 182

4.6 **Repair Plan for a Seven Bar Statically Determinate Truss, Initial Equal Bar Areas;** $\beta_{threshold} = 4.0$; $Cost = 180$ 184

4.7 **Total Cost of Repair With Varying Values** $\beta_{threshold}$ **for a Seven Bar Statically Determinate Truss, Initial Equal Bar Areas** 185

4.8 **Material Behavior Using a Ductility Factor** η 186

4.9 **Repair Plan for a Ductile Three Bar Parallel System with Equal Bar Areas** $A_1 = A_2 = A_3 = 2.0$, **Load: N[1.5,0.3], Resistance: N[0.5, 0.05], No Correlation.** 187

4.10 **Repair Plan for a Semi-Ductile Three Bar Parallel System with Equal Bar Areas** $A_1 = A_2 = A_3 = 2.0$, **Load: N[1.5,0.3], Resistance: N[0.5, 0.05], No Correlation.** 188

4.11 **Repair Plan for a Ductile Three Bar Parallel System with Unequal Bar Areas** $A_1 = 0.5$, $A_2 = 2.0$, $A_3 = 3.5$, **Load: N[1.5,0.3], Resistance: N[0.5, 0.05], No Correlation.** 189

4.12 **Three Bar Indeterminate Truss Modeled as a Series-Parallel System** 191

4.13 **Repair Plan for a Ductile Three Bar Indeterminate Truss With Equal Bar Areas;** $\beta_{threshold} = 7.0$; $Cost = 60$ 193

4.14 **Repair Plan for a Ductile Three Bar Indeterminate Truss With Equal Bar Areas;** $\beta_{threshold} = 4.0$; $Cost = 45$ 194

4.15 **Repair Plan for a Brittle Three Bar Indeterminate Truss With Equal Bar Areas;** $\beta_{threshold} = 7.0$; $Cost = 100$ . . 195

4.16 **Repair Plan for a Brittle Three Bar Indeterminate Truss With Equal Bar Areas;** $\beta_{threshold} = 4.0$; $Cost = 90$ . . . 196

5.1 **Profile of Colorado State Highway Bridge E-17-AH** . . . 203

5.2 **Profile Photograph of Colorado State Highway Bridge E-17-AH** 204

5.3 **Roadway Photograph of Colorado State Highway Bridge E-17-AH** 204

5.4 **Cross Section of Colorado State Highway Bridge E-17-AH** 205

5.5 **Standard Shape Dimensions for the WF 33x132 and WF 33x125 Beams** 206

5.6 **Abutment Photograph of Colorado State Highway Bridge E-17-AH** 207

5.7 **Column Pier Photograph of Colorado State Highway Bridge E-17-AH** 208

5.8 **HS-20 Truck Configuration** 211

5.9 **Cross Section of Concrete Slab Showing Placement of Reinforcement** 213

5.10 **(a) Actual and (b) Equivalent Approximation for Stress on Cross Section of Concrete Slab** 213

5.11 Critical Location for HS-20 Truck on Girder to Produce Maximum Shear 217

5.12 Critical Location for HS-20 Truck on Girder to Produce Maximum Moment 220

5.13 Series Model of Bridge E-17-AH Based on Three Failure Modes 232

5.14 Maximum Moment Over Time for Interior Girders in Bridge E-17-AH Based on the Nowak Live Load Model 244

5.15 Weight of Truck (top) and Maximum Shear in Interior Girders (bottom) Over Time in Bridge E-17-AH Based on Nowak Live Load Model 246

5.16 Identification of Exterior, Interior-Exterior, and Interior Girders on Bridge E-17-AH 249

5.17 Critical Loading Condition on Pier Cap Modeled as an Indeterminate Beam 254

5.18 Cross-section of Pier Cap 3 in the Positive Moment Area (Note there are 8-#9 bars on the top row in the negative moment region) 256

5.19 Cross-section of Pier Cap 2 in the Positive Moment Area (Note there are 8-#9 bars on the top row in the negative moment region) 257

5.20 Composite Shear Diagram for the Pier Cap on Bridge E-17-AH for the Most Critical Four Truck Case . 259

5.21 Composite Moment Diagram for the Pier Cap on Bridge E-17-AH for the Most Critical Four Truck Case . 260

5.22 Location and Spacing of Shear Steel in the Pier Cap Compared with the Locations of Maximum Shear . . 262

5.23 Dimensions and Placement of Steel in the Top and Bottom Columns 267

5.24 Dimensions and Location of Steel Reinforcement in the Column Footings 270

5.25 One-Way Shear on Column Footing: Beam Action at a Distance d Away From the Support Face 271

5.26 Two-Way Shear on Column Footing: Failure Plane of Column Punching Through Footing 273

5.27 Moment Failure on Column Footing: Critical Plane at the Support Face 275

5.28 Detail of the Expansion Bearing 278

5.29 RELSYS Sensitivity Values for Each Random Variable for Failure Due to Moment on an Interior Girder on Bridge E-17-AH With a Deterministic HS-20 Truck Live Load 283

5.30 Exact Sensitivity Values for Mean Values of Each Random Variable for Failure Due to Moment on an Interior Girder on Bridge E-17-AH With a Deterministic HS-20 Truck Live Load 284

5.31 Exact Sensitivity Values for Standard Deviation of Each Random Variable for Failure Due to Moment on an Interior Girder on Bridge E-17-AH With a Deterministic HS-20 Truck Live Load 286

5.32 Exact Sensitivity Values for Standard Deviation Plotted on the Same Scale as the Mean Values of Each Random Variable for Failure Due to Moment on an Interior Girder on Bridge E-17-AH With a Deterministic HS-20 Truck Live Load 287

5.33 Sensitivity Analysis on Random Variables: Failure Modes 1 (Concrete Slab) and 2 (Interior Girder due to Shear) 288

5.34 Sensitivity Analysis on Random Variables: Failure Modes 3 (interior Girder due to Moment) and 4 (Exterior Girder due to Moment) 289

5.35 Series-Parallel Model for Bridge E-17-AH: Superstructure 292

5.36 Series-Parallel Model for Bridge E-17-AH: Substructure and Slab 293

5.37 **Series-Parallel Model for Bridge E-17-AH: Deck, Superstructure, and Substructure** 294

5.38 **Simplified Series-Parallel Model for Bridge E-17-AH: Failure of Three Adjacent Girders Required for System Failure** 295

5.39 **Layout of Girders in Bridge E-17-AH** 296

5.40 **Simplified Series-Parallel Model for Bridge E-17-AH: Failure of Two Adjacent Girders Required for System Failure** 298

5.41 **Simplified Series-Parallel Model for Bridge E-17-AH: Failure of A Single Girder Required for System Failure** 298

5.42 **Area of Reinforcing Steel in the Top of a One-Foot (0.305 m) Section of the Slab Over Time With Deterioration Caused by Chloride Penetration of the Concrete** 309

5.43 **Coefficient of Variation of the Area of Steel Over Time Subject to Corrosion of the Reinforcing Steel** 311

5.44 **Corrosion Pattern on Steel Girders on Bridge E-17-AH** 315

5.45 **Dimensions for Computing the Plastic Section Modulus of a Steel Beam Corroding Over Time** 317

5.46 **Deterioration of the Plastic Section Modulus Z Due to Corrosion at the Midpoint of an Interior-Exterior Girder** 321

5.47 **Deterioration of the Plastic Section Modulus Z Due to Corrosion at the Midpoint of an Interior Girder** . 322

5.48 **Deterioration of the Web Area A_w Due to Corrosion at the Support of an Interior-Exterior Girder** 323

5.49 **Coefficient of Variation over Time for the Plastic Section Modulus Z and the Web Area A_w for Corroding Girders in Bridge E-17-AH** 324

5.50 System and Girder Moment Component Reliability Over Time for Bridge E-17-AH 327

5.51 System and Girder Shear Component Reliability Over Time for Bridge E-17-AH 328

5.52 Slab, Pier Cap, and Column Footing Component Reliability and System Reliability Over Time for Bridge E-17-AH 329

5.53 Results of Repair Option 1 on Bridge E-17-AH Using Simplified Series-Parallel Model Requiring the Failure of Three Adjacent Girders 336

5.54 Results of Repair Option 4 on Bridge E-17-AH Using Simplified Series-Parallel Model Requiring the Failure of Three Adjacent Girders 338

5.55 All Feasible Repair Options For Bridge E-17-AH Using Simplified Series-Parallel Model Requiring the Failure of Three Adjacent Girders 341

5.56 Results of Repair Option 1 on Bridge E-17-AH Using Simplified Series-Parallel Model Requiring the Failure of Three Adjacent Girders and the Corrosion Rate of the Pier Cap is Halved ($i_{corr} = 0.049$) . . 343

5.57 All Feasible Repair Options For Bridge E-17-AH Using Simplified Series-Parallel Model Requiring the Failure of Three Adjacent Girders and the Pier Cap Corrosion Rate is Halved 345

5.58 Results of Repair Option 1 (Replace Slab) on Bridge E-17-AH Using Simplified Series-Parallel Model Requiring the Failure of Two Adjacent Girders 347

5.59 Results of Repair Option 1 (Replace Slab) Followed By Repair Option 3 (Replace Slab and Exterior Girders) on Bridge E-17-AH Using Simplified Series-Parallel Model Requiring the Failure of Two Adjacent Girders 348

5.60 All Feasible Repair Options For Bridge E-17-AH Using Simplified Series-Parallel Model Requiring the Failure of Two Adjacent Girders Using A Discount Rate of 2% 349

5.61 All Feasible Repair Options For Bridge E-17-AH Using Simplified Series-Parallel Model Requiring the Failure of Two Adjacent Girders Using A Discount Rate of 6% 352

5.62 Results of Repair Option 3 (Replace Slab and Exterior Girders) on Bridge E-17-AH Using Simplified Series Model Requiring the Failure of a Single Girder 355

5.63 All Feasible Repair Options For Bridge E-17-AH Using Simplified Series Model Requiring the Failure of a Single Girder 357

5.64 Condition States (CS) for Concrete Bridge Substructures Over Time Using Markov Chains 371

5.65 Condition States (CS) for Cast-In-Place Bridge Deck Over Time Using Markov Chains and New York State Condition Ratings (1-7) 373

5.66 Results of Repair Option 1 (Replace Slab) on Bridge E-17-AH Using Simplified Series-Parallel Model Requiring the Failure of Three Adjacent Girder Including Serviceability Flags 375

5.67 All Feasible Repair Options For Bridge E-17-AH Using Simplified Series-Parallel Model Requiring the Failure of Three Adjacent Girders (Serviceability Flags Included) 377

6.1 Segment-Based Inspection Results for Bridge E-17-AH: Top of Concrete Deck 400

6.2 Segment-Based Inspection Results for Bridge E-17-AH: Bottom of Concrete Deck and Superstructure . . 401

6.3 Segment-Based Inspection Results for Bridge E-17-AH: Pier 2 402

6.4 Segment-Based Inspection Results for Bridge E-17-AH: Pier 3 403

6.5 Segment-Based Inspection Results for Bridge E-17-AH: Abutment 1 (Top) and Abutment 4 (Bottom) . . 404

6.6 Assumed Random Distribution of Deterioration for Element 107 in Condition State 4 When Inspectors are Correct 90% of the Time 408

6.7 Conservative Random Distribution of Deterioration for Element 107 in Condition State 4 When Inspectors are Correct 90% of the Time 410

6.8 Density Distributions Associated With Condition State (CS) Ratings CS1-CS5 for Element 107: Painted Open Steel Girders for Inspection Category A 423

6.9 Density Distributions Associated With Condition State (CS) Ratings CS1-CS5 for Element 107: Painted Open Steel Girders for Inspection Category C 424

6.10 Possible Pattern of Thickness Readings on a Bridge Girder 437

6.11 Results of Thickness Tests on Exterior Girder Shear Failure Mode (V-1) for Inspections at 15, 30, and 55 Years of Service 441

6.12 Revised Models for the Mean and Coefficient of Variation of the Corrosion Depth over Time For Exterior, Interior-Exterior, and Interior Girders Based on Inspection Results 444

6.13 Comparison of the Original Corrosion Model to the Revised Corrosion Model Based on Inspection Results for Exterior, Interior-Exterior, and Interior Girders 445

6.14 Testing Apparatus for Copper-Copper Sulfate Half-Cell Potential Test 447

6.15 Determination of the Percent Damage to a Deck Based on the Cumulative Distribution of Half-Cell Potential Readings From Inspections After 20, 40 and 60 Years of Service 453

6.16 Testing Apparatus for the Three Electrode Linear Polarization (3LP) Test 458

6.17 Updated System and Girder Moment Component Reliability Over Time for Bridge E-17-AH 464

6.18 **Updated System and Girder Shear Component Reliability Over Time for Bridge E-17-AH** 465

6.19 **Updated Slab, Pier Cap, and Column Footing Component Reliability and System Reliability Over Time for Bridge E-17-AH** 466

6.20 **Updated Results of Repair Option 1 on Bridge E-17-AH Using Simplified Series-Parallel Model Requiring the Failure of Three Adjacent Girders** 469

6.21 **Updated Results of Repair Option 4 on Bridge E-17-AH Using Simplified Series-Parallel Model Requiring the Failure of Three Adjacent Girders** 470

6.22 **Updated Feasible Repair Options and Costs (2% Discount Rate) For Bridge E-17-AH Using Simplified Series-Parallel Model Requiring the Failure of Three Adjacent Girders** 471

7.1 **Cumulative Distribution Function (CDF) and Probability Density Function (PDF) of the Corrosion Initiation Time T_I of the Deck** 481

7.2 **Half-Cell Potential Testing Equipment (Photo Courtesy of the Colorado Dept. of Transportation)** 483

7.3 **Probability Density Functions (PDF) of Half-Cell Potentials in Areas Where the Deck is Known to be Damaged and Undamaged [Marshall 1996]** 485

7.4 **Probability of Damage and No Damage for Individual Half-Cell Potential Readings** 487

7.5 **A Comparison of the Actual Damage in a Deck to the Interpreted Damage From a Half-Cell Potential Test Using Thresholds of $-350\ mV$, $-200\ mV$, and $-285.7\ mV$** 492

7.6 **A Comparison of the Inspection Techniques A, B, and C when the Deck is 20%, 50%, and 80% Damaged** . . 497

7.7 **Half-Cell Potential Test (Photo Courtesy of the Colorado Department of Transportation)** 499

7.8 **Four Approaches to the Probability of Replacing the Deck Based on Inspection Results: *Delayed*, *Linear*, *Proactive*, and *Idealized*** 501

7.9 **The Interpreted Damage to the Deck Provided by Inspection Technique B When the Deck is 50% Damaged Divided into Equal 1% Intervals** 503

7.10 **Optimum Inspection Strategy and Expected Damage for a Bridge Deck with 45 Year Service Life, Three Lifetime Inspections, *Proactive* Approach, Inspection Technique A, and 2% Discount Rate** 509

7.11 **Event Tree for the Optimum Inspection Strategy for a 45 Year Bridge Deck Using a *Proactive* Approach and Three Lifetime Inspections** 512

7.12 **Event Tree and Branches 1 Through 4 for the Optimum Inspection Strategy for a 45 Year Bridge Deck Using a *Proactive* Approach and Three Lifetime Inspections** 513

7.13 **Branches 5 Through 8 on the Event Tree for the Optimum Inspection Strategy for a 45 Year Bridge Deck Using a *Proactive* Approach and Three Lifetime Inspections** 514

7.14 **Two-Inspection Event Tree for the Updated Optimum Inspection Strategy for the 45 Year Bridge Deck After 10 Years of Service** 516

7.15 **Branches 1 Through 4 on the Two-Inspection Event Tree for the Updated Optimum Inspection Strategy for the 45 Year Bridge Deck After 10 Years of Service** 517

7.16 **Branches 1 and 2 on the Single-Inspection Event Tree for the Updated Optimum Inspection Strategy for the 45 Year Bridge Deck After 18 Years of Service** 520

7.17 **Updated Optimum Strategies for a 45 Year Bridge Deck Following the Most Probable Repair Path When Placed Into Service, After 10 Years, and After 18 Years** 521

7.18 **Updated Optimum Strategies for a 45 Year Bridge Deck Following the Most Probable Repair Path After 34 Years, 36 Years, and 43 Years** 522

7.19 **The One-Inspection Event Tree for the Updated Optimum Inspection Strategy for a 45 Year Bridge Deck After 34 Years of Service** 523

7.20 **The One-Inspection Event Tree for the Updated Optimum Inspection Strategy for a 45 Year Bridge Deck After 36 Years of Service** 524

7.21 **Event Tree for the Optimum Inspection Strategy for a 45 Year Bridge Deck Using a *Delayed* Approach and Three Lifetime Inspections** 527

7.22 **Branches 1 Through 4 for the Optimum Inspection Strategy for a 45 Year Bridge Deck Using a *Delayed* Approach and Three Lifetime Inspections** 528

7.23 **Branches 5 Through 8 for the Optimum Inspection Strategy for a 45 Year Bridge Deck Using a *Delayed* Approach and Three Lifetime Inspections** 529

7.24 **An *Accelerated Linear* Approach to Replacing the Deck Based on Percent Damage** 530

7.25 **Two Inspection Event Tree for the Initial Inspection Optimization of a Deck with 45 Year Service Life Using an *Accelerated Linear* Approach to the Probability of Repair** 531

7.26 **Updated Inspection Optimization for a New Deck with 27 Remaining Years Service Life Using an *Accelerated Linear* Approach to the Probability of Repair** 532

7.27 **Updated Inspection Optimization for a New Deck with 13 Remaining Years Service Life Using an *Accelerated Linear* Approach to the Probability of Repair** 533

7.28 **Single-Inspection Event Tree for the Updated Optimization for a 45 Year Deck with 35 Remaining Years Service Life Using a *Proactive* Approach and a Revised Deterioration Model** 537

7.29 **Single-Inspection Event Tree for the Updated Optimization for a 45 Year Deck with 25 Remaining Years Service Life Using a *Proactive* Approach and a Revised Deterioration Model** 538

7.30 **Expected Costs (in 1996 Dollars) Associated With Half-Cell Inspection Techniques A, B, and C for Concrete Decks with Service Lives of 20, 25, and 30 Years** 541

7.31 **Expected Costs (in 1996 Dollars) Associated With Half-Cell Inspection Techniques A, B, and C for Concrete Decks with Service Lives of 40, 50, and 60 Years** 542

7.32 **Comparison of Optimum Inspection Times t_1, t_2, and t_3 for Different Service Lives of a Concrete Deck Using Three Lifetime Inspections** 544

7.33 **Expected Costs (in 1996 Dollars) Associated With *Delayed*, *Linear*, and *Proactive* Approaches for Concrete Decks with Service Lives of 20, 40, and 60 Years** 548

7.34 **Comparison of Optimum Inspection Times t_1 and t_2, and Total Expected Cost (in 1996 Dollars) for Different Service Lives of a Concrete Deck Using *Delayed*, *Linear*, and *Proactive* Approaches** 550

7.35 **Comparison of Expected Lifetime Costs (in 1996 Dollars) for Different Service Lives for Replacement Policies of 50% and 60% for a Concrete Deck Using Two Lifetime Inspections** 551

7.36 **Comparison of Expected Damage and Optimum Strategies for Replacement Policies of 50% and 60% for a 40 Year Concrete Deck Using Two Lifetime Inspections** 553

7.37 **Comparison of Expected Damage and Optimum Strategies for Various Replacement Approaches on a 40 Year Concrete Deck Using Two Lifetime Inspections and a Replacement Policy of 60%** 555

7.38 **Optimum Inspection Times and Expected Cost (in 1996 Dollars) for Different Discount Rates on a 40 Year Deck with Four Lifetime Inspections and a *Proactive* Approach** 557

7.39 **Calibrating the *Linear* Probability Approach for Deck Replacement to Accommodate a -350 mV Half-Cell Threshold Value** 560

7.40 **Comparison of Optimum Inspection Strategies for a 40 Year Deck with Three Lifetime Inspections Using a Calibrated Threshold, 50% Policy, and a *Linear* Approach Versus Using a -350 mV Threshold, 28% Policy, and a *Calibrated Linear* Approach** 562

A.1 **Reduction of a Series-Parallel System to an Equivalent Series System** 607

A.2 **Four Bar Parallel Systems Example 7** 644

A.3 **Reduction of a Series-Parallel System to an Equivalent Single Component** 649

A.4 **Three Bar Parallel System Modeled as a Series-Parallel System** 654

A.5 **Three Bar Indeterminate Truss Modeled as a Series-Parallel System** 664

B.1 **Flow Chart for the Program RELSYS: Part 1 of 5** 672

B.2 **Flow Chart for the Program RELSYS: Part 2 of 5** 673

B.3 **Flow Chart for the Program RELSYS: Part 3 of 5** 674

B.4 **Flow Chart for the Program RELSYS: Part 4 of 5** 675

B.5 **Flow Chart for the Program RELSYS: Part 5 of 5** 676

B.6 **Subroutine Tree Structure for the Program RELSYS** . . 677

CHAPTER I

INTRODUCTION

1.1 Overview

After years of planning, construction, and coordination between many crafts and professions, the opening of a new bridge, dam, or airport is a significant triumph. To many, the ribbon cutting ceremony represents the final chapter in a long process that started with a concept and worked its way through design, funding, permits, contracts, construction, and acceptance of the final product. For most civil engineering structures with expected useful lives that can range from thirty to over one hundred years, deterioration over time is expected. After the design and construction are complete, an equally costly and important process of inspection and maintenance is needed to sustain this new structure at an adequate and safe level of performance over its useful life.

In the past, inspection and repair programs have largely been based on common sense, past experience, and local practice. Only recently have the techniques of reliability and structural optimization been used to develop maintenance programs which make the most efficient use of available resources. This study will focus on only one type of civil engineering structure, the highway bridge, and examine how system reliability techniques can be employed to

optimize its inspection and repair. In a recent survey of the field of reliability-based studies, Frangopol and Corotis [1996] concluded that there is a major gap between the progress of reliability optimization theory and its application to the practice of structural engineering. This thesis will hopefully help "bridge that gap".

With the maintenance of almost 600,000 U.S. highway bridges funded by the federal government alone [O'Connor and Hyman 1989], the annual cost of inspection and repair of bridges is significant. With ever increasing budgetary constraints and the continuing decay of the nation's infrastructure, it is more important than ever to use these funds efficiently. The cost of inspection and repair is high but the cost of no action is even higher in terms of loss of life, eroded confidence, and interrupted commerce. Comparing this cost of failure to the cost of inspection and repair provides insight to the optimal level of funding needed.

The risk of failure in a highway bridge or any other structure can never be totally eliminated. The risk can be reduced but eventually a point of diminished marginal returns is reached where minor reductions in risk require unjustified costs. Because the acceptance of risk requires that uncertainty be quantified, reliability techniques are useful and appropriate. A deterministic analysis of the problem provides output which is precise and appears exact, but which ignores the uncertainty of the input. Even a crude reliability approach provides an indication of the risk being assumed.

This study will attempt to optimize the inspection and repair of high-

way bridges using a system reliability approach. For example, the bridge deck may be deteriorating over time due to cracks and spalls in the concrete, the steel girders are experiencing section loss due to corrosion, and the expansion joints are eroding due to the combined effects of weather and traffic. While the individual reliabilities of these components may be above a minimum specified level, the combined effects of this deterioration may cause the bridge to be unsafe. Given the planned life of the structure, the optimal degree of repair must be assessed. It may be that repairing the deck or the girder alone will provide sufficient safety to the structure for its remaining life. A more complete repair may be required.

In order for a defect to be repaired, it must first be detected. All bridges in the U.S. undergo periodic visual inspections, usually every two years. Many defects such as concrete spalls, steel beam corrosion, and non-functioning roller bearings can be easily seen by an inspector. Other defects such as fatigue cracking or chloride ion penetration in concrete are much more difficult to detect and may require expensive non-destructive inspection techniques such as ultrasound, radar, or thermography. Reliability methods can be used to help optimize the timing and the technique for effective inspection.

The flow of this study is from the abstract and theoretical to the specific and practical. The early chapters develop inspection and repair models using fictitious cost data and simplified hypothetical structures and deterioration models to illustrate the theory behind the methodology and to observe critical trends. The later chapters will apply the models to a specific bridge us-

ing realistic deterioration models and Colorado Department of Transportation cost data. The ultimate goal is to integrate the reliability-based model into the existing bridge management system where data from inspections can be used to assess reliability and update the maintenance strategy for the bridge.

1.2 Objective

The objective of this study is to develop and demonstrate a methodology for evaluating the system reliability of a highway bridge over time and to develop an optimum inspection and repair strategy for that bridge that can be updated as new information becomes available.

1.3 State of the Art

Attempting to apply system reliability to current bridge applications crosses many areas of current research. The current state of reliability theory, uncertainty modeling, deterioration research, and bridge inspection progress provided both the means and the barriers to conducting this study. The progress in reliability theory and the availability of uncertainty data on many relevant random variables made this research possible. The lack of agreement in the literature in areas such as deterioration models, live load models, and non-destructive evaluation testing makes any choice of model controversial and subject to criticism. In many cases, tests and models from the literature were used recognizing that they were not perfect and future research may invalid them. Fortunately, the focus of this research is the methodology, so as new

models and data are developed, they can replace the current models and data as modules without affecting the validity of the methodology.

1.3.1 Reliability Theory

With improvements in the size and speed of digital computers, the development of reliability theory and applications has increased exponentially over the past two decades. Component reliability has developed to an advanced level where many computer programs and techniques exist to estimate the reliability of a single component of a structure. Reliability as it applies to the entire structural system is less developed. For example, if the steel reinforcement within a concrete beam is deteriorating, it is relatively straightforward to calculate the probability of failure of that beam with respect to moment capacity providing one knows the uncertainty and correlation associated with the input variables. It is more difficult to assess the probability of failure with respect to the bridge's overall ability to carry traffic because of the deterioration of the reinforcing steel in one beam.

Relatively few system reliability computer programs exist and many of them rely on Monte Carlo simulation. Monte Carlo simulation, while accurate, is too time consuming for this study. Since non-Monte Carlo system reliability software was not available, a crucial step in this study was to either procure or develop such a program.

As structural reliability theory has progressed, it has been widely accepted among researchers and increasingly acknowledged among practicing en-

gineers. Modern design codes (AASHTO LRFD Bridge Design Specifications, Ontario Bridge Design Code, LRFD Steel Design) are increasingly based on reliability techniques. Reliability-based research is progressing from hypothetical structures toward real-world applications where realistic data is needed to support the studies.

1.3.2 Random Variables

Many of the random variables needed for the reliability analysis of a highway bridge have been extensively studied. The literature provided many sources which offered the probabilistic parameters (i.e., mean, coefficient of variation) associated with such variables as the yield strength of steel, concrete cover, and the thickness of asphalt layers. Some studies even assess the model uncertainty associated with applying a theoretical equation to a real situation. The challenge was deciding which study to use. The sources used for all random variables are clearly indicated throughout this study.

A number of studies have been completed on modeling the uncertainty of the live loads on highway bridges, mostly as a result of weigh-in motion studies. By combining these truck traffic studies with extreme value statistics, it is possible to model the effects of increased maximum live load over time.

Much research has been conducted into the deterioration of bridge structures over time due to corrosion of steel members, fatigue, and penetration of chlorides in concrete. Some studies such as the deterioration of concrete

decks due to chloride penetration by Thoft-Christensen *et al.* [1997] attempt to understand the deterioration mechanism and assess the uncertainty in the random variables associated with the process. Other studies such as the Albrecht and Naeemi [1984] corrosion study make no attempt to understand the process, but rather observe performance over time and perform a regression analysis to develop the model. Deterioration functions which do not model the process are less desirable in system reliability studies. The only random variables are time and the regression parameters which will be difficult to correlate with other random variables in the system. Unfortunately, the deterioration process is often not well enough understood to accurately model it.

1.3.3 Bridge Inspection and Bridge Management

Numerous advances have been made in bridge management systems over the past two decades. The federal government has mandated that bridge inspections occur every two years and has developed a National Bridge Inventory data base from the results of reported inspections. Many studies have used this data base to develop models of how bridge systems and subsystems deteriorate over time.

The 1991 Intermodal Surface Transportation Efficiency Act (ISTEA) required state transportation departments to implement bridge management systems to more efficiently plan maintenance, monitor the condition of bridges and allocate resources. The PONTIS Bridge Management System has been adopted by several states and uses Markov chains to predict future condition

ratings of a bridge. The data for the PONTIS system comes from visual inspections. Under the current system, it is not possible to update the load rating of a bridge using PONTIS inspection data, although Renn [1995] suggests a way to do this. No studies were found which update the reliability of a bridge based on PONTIS inspection data.

If the reliability of a bridge is to be updated from a visual inspection, the condition states have to be very well defined, preferably with numerically quantifiable ratings such as percent section loss or size of cracks. The Colorado Department of Transportation has attempted this by supplementing the PONTIS inspection guides.

There are numerous non-destructive evaluation (NDE) tests available to detect specific defects. In some cases, there are multiple tests available for the same defect and their results are taken in combination to assess condition. Some tests are well established and new tests are being investigated all of the time. This study attempts to focus on NDE tests which will measure the section loss due to corrosion in steel girders, the initiation of corrosion in a concrete deck, and the rate of corrosion in the steel reinforcement once the corrosion starts.

Case studies and data from a specific structure or a laboratory study are common for most tests. Studies which provide a global probabilistic assessment of a particular technique are much less common. The case studies are often site-specific and are contradicted by other studies. The development of the probabilistic detection capability of the half-cell potential test by Marshall

[1996] was particularly helpful.

1.4 Benefits of the Study

1. A potentially useful reliability-based optimization method for the inspection and repair of highway bridges is introduced. As reliability theory gains greater prominence, there will be an even larger need for practical methods to apply it. Even if the methodology is not immediately adopted by a transportation department, it will hopefully contribute ideas and logic to a method that is eventually adopted and used.

2. A non-Monte Carlo system reliability program is added to the computer software library at the University of Colorado.

3. The National Science Foundation sponsored a workshop in Boulder, Colorado, on *Structural Reliability in Bridge Engineering* in October 1996. This was one of the first events where researchers and practicing engineers together discussed the advances and research needs in structural reliability. In the final workshop report to the National Science Foundation [1997], high priority research needs included reliability-based optimization, modeling of uncertainties, limit state definitions, systems reliability, target reliability levels, expected life-cycle costs, bridge resistance and load models, human issues, time dependency, deterioration models, bridge networks, maintaining reliability, non-destructive testing, performance forecasting, and support for new codes. This study addresses many of those listed areas.

4. In a study of this breadth, a number of decisions and compromises

had to be made. To develop and update an optimum inspection and repair strategy, choices must be made regarding uncertainties in random variables, live load and deterioration models, costs, repair options, inspection methods, reliability method, and system modeling of the bridge. All of the decisions regarding these important topics are potentially controversial. The reasoning behind all of these decisions will contribute to the debate.

1.5 Limitations of the Study

1. Inspection and repair of highway bridges requires analysis of existing structures. Revising the design of new bridges to optimize their inspection and repair is much more complex and beyond the scope of this study. This limits the availability of replacement options as bridge components are replaced with what was originally designed. In reality, bridge managers often use repair situations as an opportunity to upgrade or improve a design.

2. Throughout this thesis, a minimum system reliability is prescribed, usually $\beta_{min} = 2.0$, and the deteriorating structure is not allowed to fall below that value. The minimum system reliability is a measure of acceptable risk. Frangopol and Moses [1994] illustrated how an optimum degree of risk can be found by minimizing the total cost of a structure as shown in Fig. 1.1.

The total cost was defined as the initial cost of the structure which decreases as the acceptable risk increases plus the failure cost which increases as the acceptable risk increases. The failure cost is equal to the cumulative

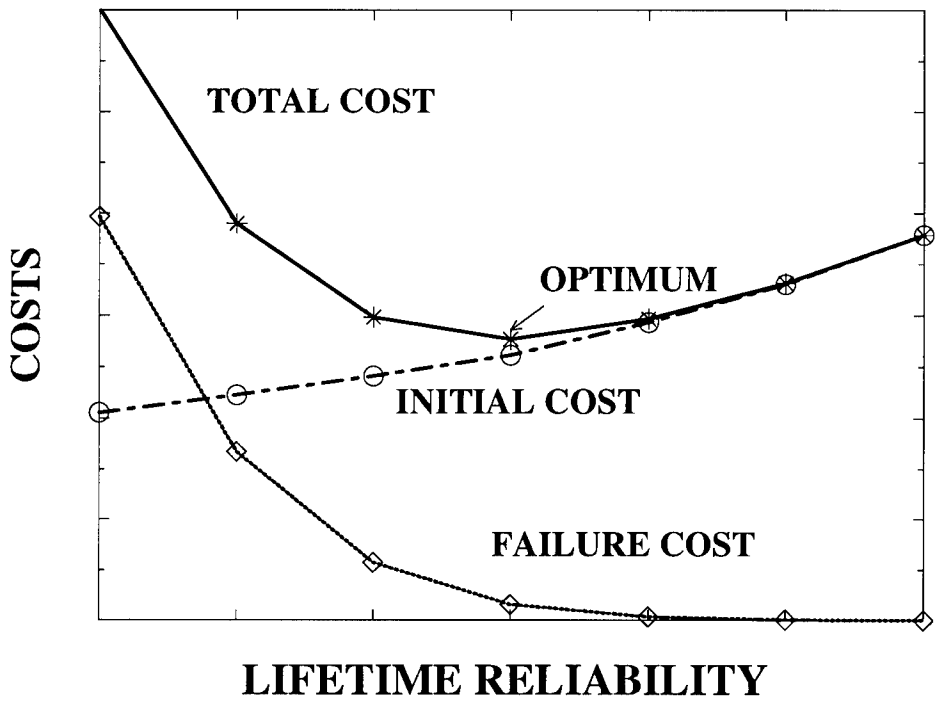

Figure 1.1: **Total Cost, Failure Cost, and Initial Cost Versus Reliability**

cost of failure in terms of loss of life, reconstruction, traffic delay and rerouting, lawsuits, increased government regulation, and loss of good will multiplied by the probability of occurrence. The minimum total expected cost would define the optimal acceptable risk (i.e., optimal lifetime reliability level).

This study does not attempt to quantify the failure cost of the bridge which would depend on a number of factors such as the predicted loss of life associated with a particular failure mechanism, the importance of the bridge in the overall traffic network, the detour length, the traffic volume, etc. While research in the area of failure costs exists, the attempt to quantify

the failure costs associated with a particular bridge could comprise an entire thesis in itself. This study chooses an arbitrary minimum system reliability index assuming that it adequately reflects acceptable risk. The Report to the National Science Foundation [1997] listed target reliability levels and failure costs as areas which require further research.

The question of costs is not trivial as the availability of scarce funds which must be allocated efficiently to the entire system of bridges may affect the ability to maintain a specified safety level in a particular bridge. The situation becomes more complex as the opportunity cost of using available funds on bridge repair must be weighed against the benefits of spending the money on national defense, foreign aid, education or medical research. Include political considerations and the problem becomes even more intractable. This thesis focuses only on minimizing the cost of maintaining a prescribed level of safety in a bridge. It does not address whether these funds are available or whether they could be better spent on some other activity.

3. This study is restricted to repairs based on deterioration of the bridge. It is estimated that over 35% of all highway bridges are either structurally deficient or functionally obsolete and that over $78 billion is needed to correct the defects [FHWA 1993]. Many of these defects, however, involve safety concerns such as deck width, sight distance, excessive curvature, or vertical clearance. While very important, such issues are not associated with deterioration and will not be considered. Likewise, those rehabilitations which address vulnerability issues such as seismic retrofit, collision, and fracture crit-

ical situations are neglected.

4. The deterioration models used in this study are not specific to the State of Colorado. The Albrecht and Naeemi [1984] corrosion model used for the bridge girders was developed from bridges throughout Europe and the United States. Furthermore, the corrosion model does not account for the protection provided by the paint on the steel girders. The Thoft-Christensen *et al.* [1997] model for chloride penetration and corrosion of steel reinforcement in the slab was based on concrete decks in Denmark and the United Kingdom. Since the purpose of this study is to illustrate a methodology, the lack of a deterioration model specific to Colorado bridges is not a serious limitation. In addition, the updating process illustrates how a general deterioration model can be revised to accommodate specific site inspection results.

5. In developing limit state equations for failure modes on a selected bridge, this study uses the same equations as those used by the Colorado Department of Transportation when computing a load rating for the same bridge. The intent is to compare the system reliability index with the bridge load rating and to use equations that are already generally accepted by the agency charged with managing the Colorado bridges. The load rating software, Bridge Analysis and Rating System (BARS), is based on the AASHTO [1992] design specifications. Although an LRFD-based AASHTO [1994a] specification is available, it has not yet been incorporated into the load rating of Colorado bridges. Some of the limit state equations used in this thesis are therefore based on the AASHTO [1992] specifications. Similarly, no 3-D finite

element analysis was performed on the highway bridge, just as no such analysis is usually performed on a typical highway bridge.

6. This study ignores the interaction between failure modes. For example, if a girder fails, the slab must span a greater distance between girders. If a roller bearing collects debris and will not rotate, these girders are subjected to additional stresses. These effects are not considered.

7. Under existing bridge management systems, it is not possible to update the reliability of a bridge using the results of a visual inspection. This study demonstrates how it could be done based on using a segment-based inspection, rewriting the condition state definition, defining the distribution of the condition state, and quantifying the subjective uncertainty associated with the inspector's assessments. There is a lack of available research in some of these areas. This study illustrates how the reliability could be updated if the research was available. As a result, the numerical quantities used to redefine the condition states, define the condition state distributions, and quantify the inspector uncertainty were hypothetical.

8. There is limited inspection data available on Bridge E-17-AH, the highway bridge used in this study. Several PONTIS inspection reports were readily available, but some of the NDE tests recommended in this study were not conducted on this bridge. There is no record of a weigh-in-motion study, half-cell potential test, 3-electrode linear polarization, or a test of girder flange thickness being conducted on this bridge. The first priority in this study is to use actual data from Bridge E-17-AH whenever it is available. The next

alternative was to use actual data from a similar bridge and apply it to the bridge in question. Only as a last resort was a hypothetical inspection result developed based on general findings or trends found in the literature.

Specifically, in this study, the three-electrode linear polarization (3LP) test data was taken directly from a deck structure in the northeastern United States [Clear 1992]. The 3LP method is relatively new, but is the only available method for measuring the rate of corrosion in reinforcing steel embedded in concrete. Using the 3LP method in the field requires a number of assumptions, some of which are debatable. The hypothetical half-cell potential test results on the deck were based on results from corrosion studies on bridge decks in Kansas [Crumpton and Bukovatz 1974]. Finally, the girder thickness results were purely hypothetical based generally on trends observed from the visual inspection and the Albrecht and Naeemi [1984] corrosion model. Although the inspections were not conducted on the bridge under investigation, inspection results over time were needed to fully and completely illustrate the updating process.

9. This study neglects uncertainty associated with human error in design, construction, or testing. It suggests a method of incorporating inspector error into the assessment of visual inspection data, but otherwise neglects human error.

1.6 Organization of the Thesis

Chapter 1 serves as an introduction to the research conducted in

this thesis.

Chapter 2 develops a model to optimize the inspection of very simple single component, series, and parallel structures which deteriorate over time. Four sample inspection techniques are offered. The optimization program ADS is linked with the reliability program RELTRAN to optimize the timing, number, and method of inspection based on minimum cost and expected life.

Chapter 3 presents a system reliability program, RELSYS, developed in this study which calculates the system reliability of any structure which can be expressed as a series and parallel combination of components. The algorithm and accompanying theory for the first-order, second-moment component and system reliability are described and illustrated with numerical examples. The results of the program are compared with two Monte Carlo simulation programs. The resulting strengths and limitations of the program are discussed. The User's Manual for RELSYS is in Appendix A. A detailed description of RELSYS to include flow chart, listing of variables, and subroutine descriptions is presented in Appendix B.

Chapter 4 develops a minimum cost repair strategy for systems of components. A minimum allowable system reliability is established based on the maximum assumable risk allowed over the life of the structure. Inspections occur every two years as the structure deteriorates over time. The structure must be repaired whenever the system reliability index falls below the prescribed minimum. Individual components are repaired based on whether they

are above or below a component threshold reliability level at the time of inspection. This threshold reliability level is varied until an optimum lifetime repair strategy is developed. The model is applied to a statically determinate five-bar truss (series system) and a three-bar statically indeterminate truss (series-parallel system) using a hypothetical deterioration model and cost data.

Chapter 5 applies the methodology described in Chapters 3 and 4 to Colorado State Highway Bridge E-17-AH. Using 24 separate random variables and 16 different failure modes, the reliability of each bridge component is computed. The bridge is modeled as a series-parallel combination of the individual failure modes and the system reliability is computed. The system reliability is compared to the bridge load rating and a sensitivity analysis with respect to all random variables is performed.

The reliability of the structure decreases over time as the maximum live load increases and the bridge deteriorates. The bridge girders are subject to corrosion and the concrete bridge deck and pier cap are subject to chloride penetration and subsequent corrosion of the steel reinforcement. The bridge is repaired any time the system reliability index falls below the prescribed minimum value. Five distinct repair options and their associated costs are considered. All feasible combinations of these options are investigated until an optimum repair strategy is developed. Since the system reliability model is strength-based, the concept of serviceability flags is introduced to handle relevant failure modes not based on strength.

Chapter 6 uses biennial visual inspections and selected NDE tests to

update the optimum repair strategy for Bridge E-17-AH. The original lifetime repair strategy is developed based on theoretical models when the bridge is placed in service. The updated repair strategy is based on actual structural performance as determined by inspection results. Future performance is then extrapolated from the inspection trends.

The actual PONTIS bridge inspections are used to update the serviceability flags and future performance of the bridge is predicted based on assumed linear condition-state deterioration. A segment-based inspection technique is introduced to allow PONTIS inspection results to update bridge reliability. With several key assumptions regarding condition state deterioration and the quality of the inspection program, the reliability of some components of Bridge E-17-AH is updated.

Finally, three NDE tests are proposed which allow the reliability of the bridge to be updated – although these tests were never actually conducted on the bridge. Measuring the flange thickness on the girders allows the actual corrosion of the girders to be assessed. The half-cell potential test provides data on the chloride initiation time and the three-electrode linear polarization test provides a reinforcement corrosion rate. It is demonstrated how the results of a particular inspection can be used to update the reliability and the results at several points in time can establish a trend and predict future performance. Based on these hypothetical test results, an updated optimum repair strategy for Bridge E-17-AH is developed.

Once the relevant NDE tests have been identified, **Chapter 7** applies

the inspection optimization methodology introduced in Chapter 2 to the concrete bridge deck from Bridge E-17-AH using the half-cell potential method. The uncertainty of the half-cell method is addressed relative to the quality of the equipment, the correlation between potential readings and the existence of active corrosion, and the ability to assess the condition of the entire deck based on a series of half-cell readings. Failure of the deck is defined as active corrosion occurring in at least 50% of the deck area. Three different inspection techniques based on different spacings of readings and their costs are introduced. Four approaches to repair (delayed, linear, proactive, idealized) are considered.

Using the same event tree methodology introduced in Chapter 2, the optimum number and timing of lifetime inspections is developed based on the expected life of the concrete deck. As repair decisions are made, the optimum inspection plan is updated. This is illustrated with an example which consistently follows the most likely path on the event tree. The effects on the optimum strategy of varying the discount rate, repair approach, repair policy, expected life, and the deterioration model are all examined.

Chapter 8 presents conclusions and recommendations for future research.

1.7 Units

While the original intent of this thesis was to use S.I. (metric) units, it became unfeasible to do so. Virtually all sources used for the practical

applications were in English units. The design equations, the blueprints for the bridge, the BARS load rating output, and the PONTIS inspection data were all in English units. As a result, the constants in the component limit state equations are based on English units. It would be misleading and difficult for any future researcher looking to follow or verify this study if S.I. units were used. The convention used in this thesis is to present all material in English units with S.I units in parenthesis wherever practicable.

CHAPTER II

INSPECTION OPTIMIZATION

2.1 Overview and Objectives

Any structure which is deteriorating over time may need to be repaired at some point during its lifetime. The needed repair will only be made if the relevant defect is detected. This requires that the structure be inspected and evaluated. There are different types of inspections that may be performed.

The Federal Highway Administration requires that highway bridges be inspected every two years [Tonias 1995] by a certified bridge inspector, not necessarily a licensed professional engineer. In many cases, the biannual inspection is visual and reports the general condition of the bridge in terms of degree of spalling on the deck, exposed reinforcing bars, condition of bearings, etc. This type of inspection is practical and worthwhile because it is inexpensive, does not require much time, and the inspector does not need design expertise or an engineering degree. Examining every bridge for obvious hazardous situations and maintaining a record over time for each bridge is good public policy especially toward maintaining public confidence in the performance of these structures.

Some states supplement these two year inspections with a five year inspection by a professional engineer competent to address design performance

and strengthening measures [Tonias 1995]. While most inspection information on bridges comes from these inspections, specialized tests may be required to detect defects that cannot be seen visually.

Often there are a variety of inspection methods from which to choose for a particular defect. Testing for adequate concrete cover, for example, can be done with a pachometer which locates reinforcing steel from a magnetic field or other methods such as ultrasound are available. For other defects, inspection methods could include acoustic, ultrasonic, electrical, infrared, thermographic, radar, and nuclear methods [AASHTO,1994a]. All methods have associated costs and detection capabilities. The decision concerning which inspection method to use and when in the life of the structure it should be employed is worthy of study.

This chapter is based on an optimization approach suggested by Thoft-Christensen and Sørensen [1987], Thoft-Christensen [1987], and Sørensen and Faber [1991]. The approach is significantly modified in this study to optimize the timing and method of inspection over the life of a structure. The method is illustrated on each of the simplest possible single component, series, and parallel structures and the results are analyzed.

2.2 Description of the Problem: Single Component System

The structure to be analyzed is a single bar with a constant cross-section subjected to a centric axial load as shown in Figure 2.1. The resistance

(R) and load (P) are normally distributed random variables while the cross-sectional area (A) is deterministic. The initial values for these variables are:

Resistance (R): $\mu_R = 14.0$; $\sigma_R = 1.4$

Load (P): $\mu_P = 8.0$; $\sigma_P = 0.8$

Area (A): $A_{init} = 1.0$

where μ_X and σ_X are the mean and standard deviation of X, respectively, and A_{init} is the initial (undamaged) cross-sectional area.

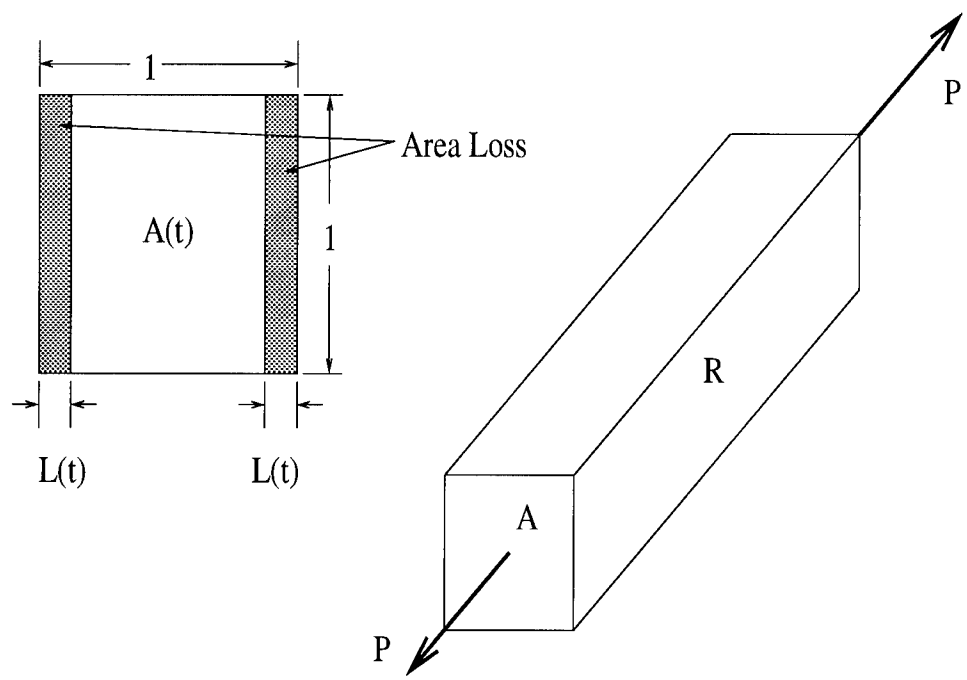

Figure 2.1: **Single Component Structure Subjected to Centric Axial Load and Section Loss Due to Deterioration**

The structure will fail if:

$$R - P/A \leq 0 \tag{2.1}$$

To understand and analyze the model, it is necessary to modify these variables to create different structures. In developing new structures, the mean (μ_R) and the standard deviation (σ_R) of the resistance were changed to simplify understanding. The coefficient of variation $\delta_R = 0.10$ remained the same throughout. In charts and graphs, where the resistance (R) of a structure is listed, it is in fact referring to μ_R because the resistance is a random variable.

The probability of failure of the structure is expressed through the reliability index (β) which is discussed more fully in the next chapter. In relation to the probability of failure of the structure, $P_f = \Phi(-\beta)$ where Φ is the distribution function of the standard normal variate. A higher value of β represents a lower probability of failure of the structure. This reliability index was calculated using the program RELTRAN (RELiability TRANsformation) [Lee *et al.* 1993].

Given the structure described in Fig. 2.1, the goal is to develop an inspection strategy that will minimize total cost of the inspection and repair and prevent the structure from deteriorating to an unacceptable level of reliability at any point during the usable life of the structure. The expected useful life of this structure is 10 years and the reliability index will not be permitted to fall below $\beta = 2.0$. There will be two, three, or four inspections allocated over the life of the structure. The design variables are the times and qualities of the inspections.

It is difficult to directly optimize the number of inspections (n) because the number of design variables depends on the number of lifetime inspections. The number of inspections is an integer quantity. Mixing real and integer design variables complicates the optimization problem considerably. The most practical option is to work the problem for discrete values of n and compare the results.

2.2.1 Deterioration Model

The structure is deteriorating over time resulting in loss of cross-sectional area as shown in Fig. 2.1. The expected thickness loss is expressed as:

$$L(t) = Dt^B \tag{2.2}$$

where: $L(t)$ = average thickness loss over time; t = time (years); and D, B = deterioration parameters. The area of the structure at any time, t, is:

$$A(t) = A_{init} - 2.0L(t) = A_{init} - 2.0(0.051t^{0.57}) \tag{2.3}$$

The deterioration of the structure over time assuming that no repairs are made is shown in Figure 2.2. There is a rapid exponential decrease in area where only half the original area remains after approximately 17 years.

2.2.2 Inspection Methods

If a fault in a structure exists, there is no guarantee that a given inspection will find it. A higher quality inspection is more likely to discover an existing defect but it will also result in a greater cost. In reality, the availability

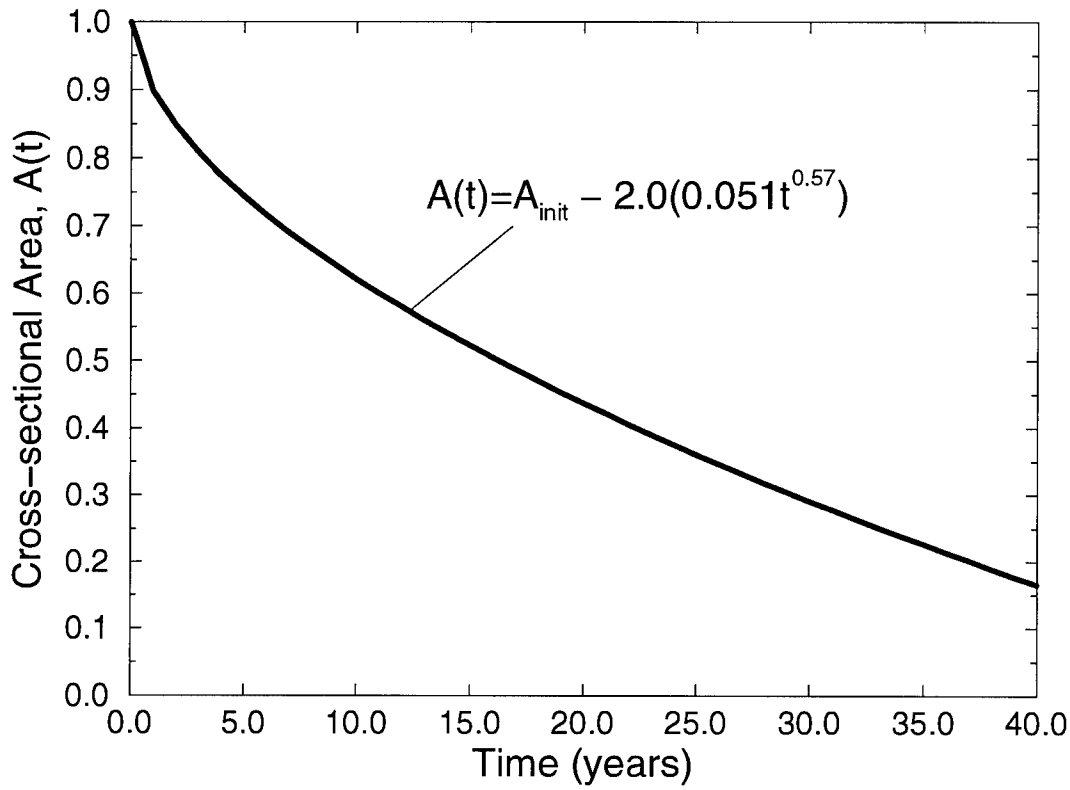

Figure 2.2: **Deterioration of Cross-Sectional Area Over Time**

of inspection techniques or qualities is not a continuous function but rather a series of discrete techniques which are available to detect a specific defect. The techniques vary in cost and detection ability. This example considers four such hypothetical techniques.

The qualities of all four techniques are random variables which have some uncertainty associated with their detection abilities. The quality of each inspection is assumed to be normally distributed although it could realistically take any distribution. The ability of these methods to detect damage is based on the intensity of the structural damage. Mori and Ellingwood [1994]

described the degree of damage using a damage intensity factor η_{str} defined as:

$$\eta_{str} = (A_{init} - A(t))/A_{init} \tag{2.4}$$

where $A(t)$ is the deteriorated cross-sectional area at any time t. The value ranges from $\eta = 0$, which indicates no damage, to a value of $\eta = 1$, which indicates that the element no longer exists.

The parameters which describe the four techniques used here are shown in Table 2.1 where:

$\eta_{0.5}$ = damage intensity at which there is a 50-50 chance of detection;

σ_{insp} = standard deviation of the detection ability of the inspection;

η_{min} = damage intensity below which detection is impossible; and

η_{max} = damage intensity above which detection is absolutely certain.

Table 2.1: **Parameters Associated With Four Inspection Techniques**

Technique	$\eta_{0.5}$	σ_{insp}	η_{min}	η_{max}	Inspection Cost
A	0.05	.005	.035	.065	1.5
B	0.1	0.01	0.07	0.13	1.0
C	0.2	0.04	0.08	0.32	.75
D	0.3	0.03	0.21	0.39	.50

As suggested by Lin [1995], the minimum and maximum intensity

values are calculated as three standard deviations above and below the mean:

$$\eta_{min} = \eta_{0.5} - 3.0\sigma_{insp} \tag{2.5}$$

$$\eta_{max} = \eta_{0.5} + 3.0\sigma_{insp} \tag{2.6}$$

The probability of a defect being detected (P_{det}) at any time t is dependent on the damage intensity of the structure η_{str} at the time of the inspection and the inspection technique being employed:

$$P_{det} = \Phi((\eta_{str} - \eta_{0.5})/\sigma_{insp}) \tag{2.7}$$

The probability density function of each technique and the shape of it cumulative distribution function are shown in Figure 2.3. This approach is applicable to real world problems if the data on the relevant inspection technique can be gathered and its distribution approximated.

2.2.3 Probability of Repair

To optimize the timing of a limited number of available inspections, the inspection should be made when (1) there is a high probability that a repair will be needed but (2) before the defect has been allowed to progress to where the safety constraints of the structure are violated. It is necessary, therefore, to calculate the probability of making a repair, assuming the defect is detected.

Repairs on structures are often determined by a repair policy developed by the engineer charged with maintaining the structure. A reliability-based repair policy might be that the structure is repaired when $\beta = 3.0$ or

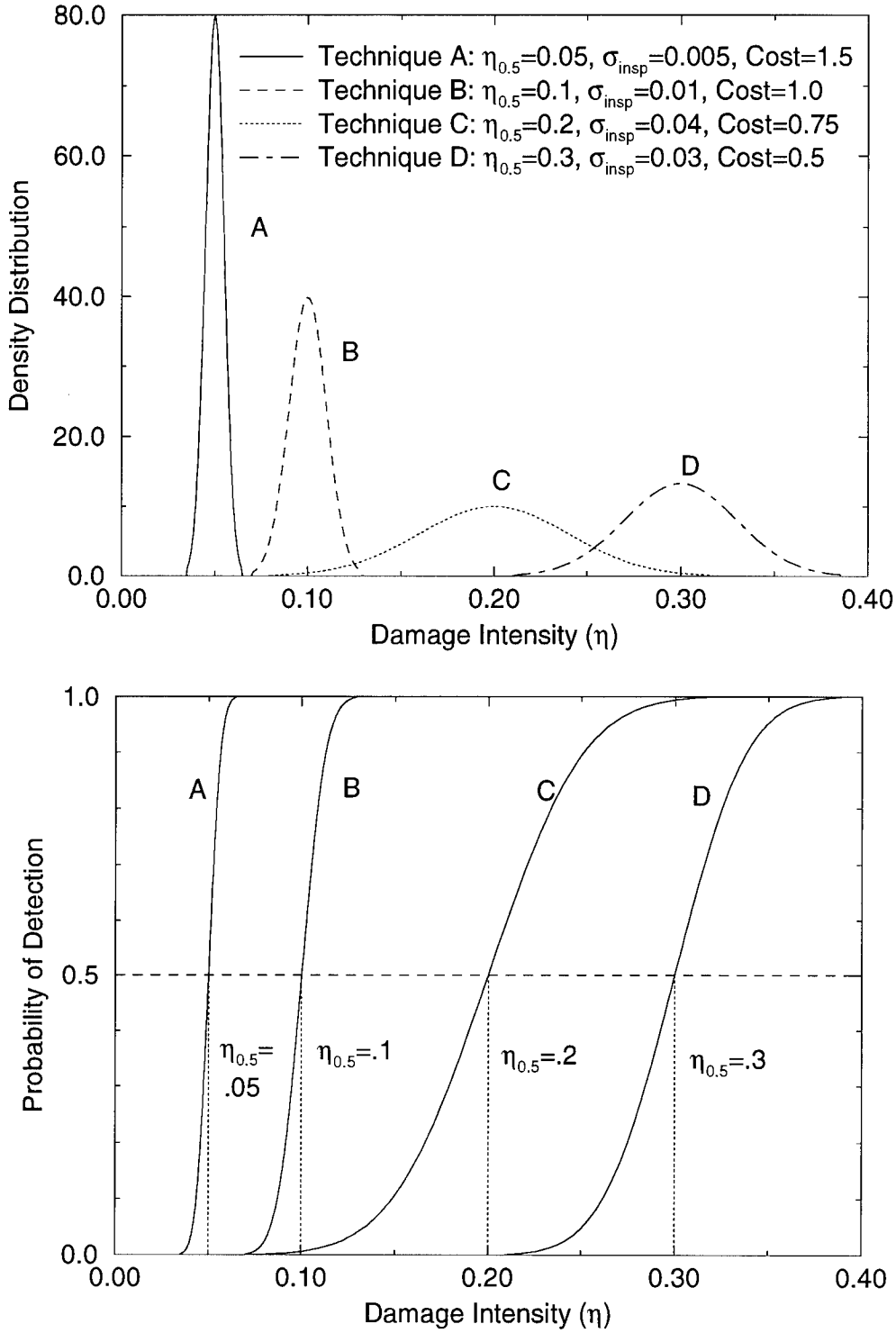

Figure 2.3: **Density Distribution and Probability of Detection for Four Inspection Techniques**

$\beta = 2.5$. The probability of repair can be based on the adherence to the repair policy. A proactive manager may repair the structure early. More likely, a competition for scarce maintenance funds may force the repairs to be made later, after the policy has been violated. Clearly, as the deterioration of a structure increases and its reliability decreases, the likelihood that it will be repaired increases.

The probability of making a repair in this example is based on the difference between the original reliability and the constrained minimum allowable reliability of the structure. If a defect has been detected, the probability of making the repair (P_{rep}) is calculated as:

$$P_{rep} = \begin{cases} 0.0 & \text{for} \quad \beta_{str}(t) > \beta_{init} \\ (\beta_{init} - \beta_{str}(t))/(\beta_{init} - \beta_{min}) & \text{for} \quad \beta_{min} \leq \beta_{str}(t) \leq \beta_{init} \\ 1.0 & \text{for} \quad \beta_{str}(t) < \beta_{min} \end{cases} \tag{2.8}$$

where:

β_{init} = reliability index of structure when placed in service;

$\beta_{str}(t)$ = reliability index of structure at time t; and

β_{min} = minimum acceptable reliability index of structure.

The range of probabilities will range from $P_{rep} = 0$ when the structure is in its original state or when a complete repair has been made to $P_{rep} = 1.0$ when the minimum reliability index of the structure is reached. The inherent assumption is that a repair will return a structure to its original reliability

state. This assumption could easily be modified to return a structure to some specified percentage of its original reliability after a repair. That specified percentage could even decrease over time indicating the difficulty of returning an old bridge to its original state.

After an inspection, a decision regarding whether or not to repair the structure based on the degree of damage that was detected in the inspection must be made. As the number of inspections increases, the number of decision paths increases by 2^n where n is the number of inspections [Lin 1995]. The probability of taking any path or branch (P_b) is equal to:

$$P_b = \prod_{i=1}^{n} P_{sub_i} \tag{2.9}$$

where P_{sub_i} is the probability of taking any sub-branch along the path. The probability of taking a sub-branch which involves making a repair (R^+) is equal to

$$P_{sub_{R+}} = P_{det} P_{rep} \tag{2.10}$$

which using conditional probability accounts for both the damage intensity and the ability of the chosen inspection technique to detect the damage, where P_{det} and P_{rep} are given by Eqs. 2.7 and 2.8, respectively. Similarly, the probability of taking any sub-branch where a repair is not made (R^-) is equal to

$$P_{sub_{R-}} = 1 - P_{sub_{R+}} \tag{2.11}$$

2.2.4 Cost of Repair

Realistically, a repair which is made after a greater period of time when more deterioration has occurred should be more expensive than a repair made when the deterioration is minor. Even the most minor repair has a fixed cost associated which might include the salary of the workers, the transportation to the site, and destruction/repair associated with getting to the damaged area, such as chipping away concrete to get to the corroded rebar.

In this example, the cost of repair is assumed to be equal to the sum of a fixed cost C_{fix} which occurs every time a repair is made (i.e., planning, getting to the site, exposing the element) and a variable cost C_{var} which depends on the degree of damage (i.e, the amount of material that needs to be replaced).

$$C_{rep} = C_{fix} + C_{var} \tag{2.12}$$

where $C_{fix} = 5.0$ and $C_{var} = 5.0\ \eta_{rep}$.

2.2.5 Single Component System: Two Lifetime Inspections

The total cost associated with the inspection program (C_{tot}) is equal to:

$$C_{tot} = \sum_{i=1}^{n} C_{insp} + \sum_{j=1}^{m} C_{rep} \tag{2.13}$$

where n = number of lifetime inspections, and $m \leq n$ is the number of lifetime repairs. It is this total cost that will be minimized to optimize the timing and method of inspection. For the case of the single component structure in Fig. 2.1, the optimization problem can be formulated as:

Minimize: C_{tot}

such that:

$$\beta_{t_1} \geq \beta_{min} = 2.0 \tag{2.14}$$

$$\beta_{t_2} \geq \beta_{min} = 2.0 \tag{2.15}$$

$$\beta_{10\ years} \geq \beta_{min} = 2.0 \tag{2.16}$$

$$0.5 \leq t_1 \leq 7.0 \tag{2.17}$$

$$0.5 \leq t_2 - t_1 \leq 7.0 \tag{2.18}$$

$$t_2 \leq 10.0 \tag{2.19}$$

where t_1 and t_2 are the times (in years) that the two inspections will be conducted. Eqns. 2.14 through 2.16 ensure that the reliability of the structure never falls below the minimum allowable reliability level ($\beta_{min} = 2.0$). This is accomplished by checking the reliability at the two inspection times and at the end of the useful life of the structure. Eqns. 2.17 and 2.18 ensure the inspections are at least six months apart but not more than seven years apart.

At time t_1, a decision must be made whether or not to repair the structure based on the damage reported by the inspection as indicated by Eqn. 2.10. Let R_1^+ indicate that a repair was made at time, t_1, and R_1^- indicate that a repair was not made. Similarly, at time t_2, a decision must again be made whether or not to repair the structure where R_2^+ indicates repair and R_2^- indicates no repair. The decision at time, t_2, must account for whether repairs were or were not made at time t_1. Fig. 2.4 illustrates these possibilities.

At time, t_1, there are two options:

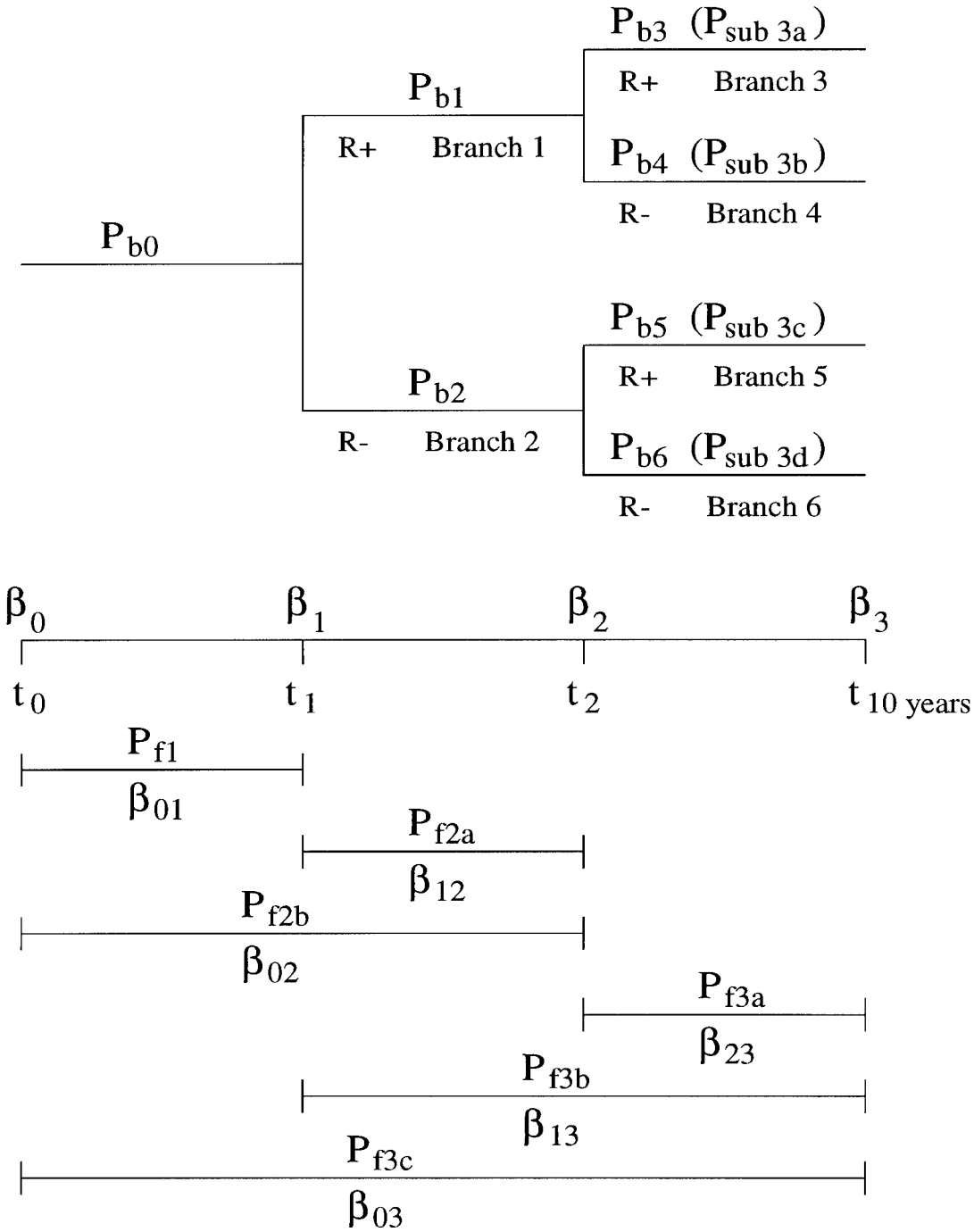

Figure 2.4: **Repair Paths and Time Line for Two Lifetime Inspections on a Single Component Structure**

a) Repair at time, t_1 (branch 1: R_1^+)

$$P_{b_1} = P(R_1^+) = P_{det_1} P_{rep_1} \tag{2.20}$$

b) No repair at time, t_1 (branch 2: R_1^-)

$$P_{b_2} = P(R_1^-) = 1 - P_{b_1} \tag{2.21}$$

where:

P_{b_1} = the probability of taking branch 1;

$P_{det_1} = \Phi((\eta_1 - \eta_{0.5})/\sigma_{insp})$ = the probability of detection of the damage at time, t_1;

$P_{rep_1} = (\beta_{init} - \beta_{0x1})/(\beta_{init} - \beta_{min})$ = the probability that a repair will be made if the defect is detected at time, t_1;

$\beta_{01} = \beta_{t_1}$ = the reliability index of the structure at time, t_1; and

η_1 = the damage intensity of the structure at time, t_1.

At time, t_2, the four considerations are:

a) Repair at time t_2, if a repair was made at t_1 (branch 3: $R_1^+ \bigcap R_2^+$)

$$P_{b_3} = P(R_1^+ \bigcap R_2^+) = P_{b_1} P_{sub_{3a}} \tag{2.22}$$

where:

$P_{sub_{3a}} = P_{det_{2a}} P_{rep_{2a}}$ = probability of making the repair R_2^+, given that a repair was made at time t_1. Referring to Fig. 2.4, note that $2a$ identifies actions at time t_2 given that the previous repair was made at time t_1. Similarly, $2b$ identifies the actions at time t_2, given that the previous repair was at t_0. In

addition

$P_{det_{2a}} = \Phi((\eta_{2a} - \eta_{0.5})/\sigma_{insp})$;

$P_{rep_{2a}} = (\beta_{init} - \beta_{12})/(\beta_{init} - \beta_{min})$; and

$\beta_{12} = \beta_{t_{2a}}$ = the reliability index of the structure at time, t_2 where last repair was made at t_1.

b) No repair at t_2, if a repair was made at t_1 (branch 4: $R_1^+ \bigcap R_2^-$)

$$P_{b_4} = P(R_1^+ \bigcap R_2^-) = P_{b_1} P_{sub_{3b}} \tag{2.23}$$

where: $P_{sub_{3b}} = 1 - P_{sub_{3a}}$

c) Repair at t_2, if no repair was made at t_1 (branch 5: $R_1^- \bigcap R_2^+$)

$$P_{b_5} = P(R_1^- \bigcap R_2^+) = P_{b_2} P_{sub_{3c}} \tag{2.24}$$

where: $P_{sub_{3c}} = P_{insp_{2b}} P_{rep_{2b}}$

d) No repair at t_2, if no repair was made at t_1 (branch 6: $R_1^- \bigcap R_2^-$)

$$P_{b_6} = P(R_1^- \bigcap R_2^-) = P_{b_2} P_{sub_{3d}} \tag{2.25}$$

where: $P_{sub_{3d}} = 1 - P_{sub_{3c}}$.

The reliability of the structure must be evaluated at times t_1, t_2, and $t_{10\ years}$ to ensure that the minimum reliability constraint is not violated. To calculate the probability of failure of the structure after these inspections,

the weighted effect of each of the repair paths must be considered. For each branch b_i, the probability of failure of the structure at a point in time given that b_i was taken (i.e., $P_f(t)|b_i$) is multiplied by the probability of that branch being taken, P_{b_i}. The total probability of failure is equal to the sum over all branches. The reliability index, β, at any time t can be expressed as:

$$\beta(t) = -\Phi^{-1}[\sum_{i=1}^{2^n} P_f(t)|b_i(P_{b_i})] \tag{2.26}$$

where n = number of lifetime inspections.

At time t_1, the reliability index β_1 is calculated directly from the reduction in section area since no decisions concerning repair have been made yet and there are no branches to consider. At t_2, either branch 1 (R_1^+) or branch 2 (R_1^-) has already been chosen. The reliability index β_2 is therefore:

$$\begin{aligned} \beta_2 &= -\Phi^{-1}(\Phi(-\beta(t_2 - t_1))P(R_1^+) + \Phi(-\beta(t_2))P(R_1^-)) \\ &= -\Phi^{-1}(\Phi(-\beta_{12})P_{b_1} + \Phi(-\beta_{02})P_{b_2}) \end{aligned} \tag{2.27}$$

Likewise, at time $t_{10\ years}$, the useful life of the structure, either branch 3 ($R_1^+ \bigcap R_2^+$), branch 4 ($R_1^+ \bigcap R_2^-$), branch 5 ($R_1^- \bigcap R_2^+$), or branch 6 ($R_1^- \bigcap R_2^-$) has been chosen. The reliability index $\beta_{10\ years}$ is:

$$\begin{aligned} \beta_{10\ years} &= -\Phi^{-1}(\Phi(-\beta(t_{10\ years} - t_2))P(R_1^+ \bigcap R_2^+) \\ &\quad +\Phi(-\beta(t_{10\ years} - t_1))P(R_1^+ \bigcap R_2^-) \\ &\quad +\Phi(-\beta(t_{10\ years} - t_2))P(R_1^- \bigcap R_2^+) \\ &\quad +\Phi(-\beta(t_{10\ years})) * P(R_1^- \bigcap R_2^-)) \\ &= -\Phi^{-1}[\Phi(-\beta_{23})P_{b_3} + \Phi(-\beta_{13})P_{b_4} \end{aligned}$$

$$+\Phi(-\beta_{23})P_{b_5} + \Phi(-\beta_{03})P_{b_6}] \tag{2.28}$$

The cost of repair associated with each branch C_r is different since branch 3 requires two repairs, branches 4 and 5 require one repair, and branch 6 involves no repairs. The cost of repair calculation becomes:

$$C_{rep} = \sum_{i=1}^{2^n} C_r(r_i)P_{b_i} \tag{2.29}$$

where:

C_r = the cost of a repair on a branch which is a function of the fixed and variable cost as described in Eqn. 2.12; and r_i = number of repairs required in branch i.

The cost of repair for this two-inspection, single-component example is:

$$\begin{aligned}
C_{b_3} &= P_{b_3}(2(C_{fix}) + C_{var}(\eta_1 + \eta_{2a})) \\
C_{b_4} &= P_{b_4}(1(C_{fix}) + C_{var}\eta_1) \\
C_{b_5} &= P_{b_5}(1(C_{fix}) + C_{var}\eta_{2b}) \\
C_{b_6} &= 0 \\
C_{rep} &= C_{b_3} + C_{b_4} + C_{b_5} + C_{b_6} \\
C_{tot} &= 2(C_{insp}) + C_{rep}
\end{aligned}$$

2.2.6 Single Component System – Four Lifetime Inspections

The formulation of the problem for the single component system which has four inspections over its lifetime is listed below. By examining the solution to the four inspection problem, the three inspection problem will become apparent.

Minimize: C_{tot}

such that:

$$\beta_{t_1} \geq \beta_{min} = 2.0 \tag{2.30}$$

$$\beta_{t_2} \geq \beta_{min} = 2.0 \tag{2.31}$$

$$\beta_{t_3} \geq \beta_{min} = 2.0 \tag{2.32}$$

$$\beta_{t_4} \geq \beta_{min} = 2.0 \tag{2.33}$$

$$\beta_{10\ years} \geq \beta_{min} = 2.0 \tag{2.34}$$

$$0.5 \leq t_1 \leq 7.0 \tag{2.35}$$

$$0.5 \leq t_2 - t_1 \leq 7.0 \tag{2.36}$$

$$0.5 \leq t_3 - t_2 \leq 7.0 \tag{2.37}$$

$$0.5 \leq t_4 - t_3 \leq 7.0 \tag{2.38}$$

$$t_4 \leq 10.0 \tag{2.39}$$

As the number of inspections increase, the number of possibilities increase as shown in Fig. 2.5. At time t_4, there are 16 possible branches of repair to consider.

The notation can easily become complex and is consistent with the two inspection case. Every possible time interval between inspections is iden-

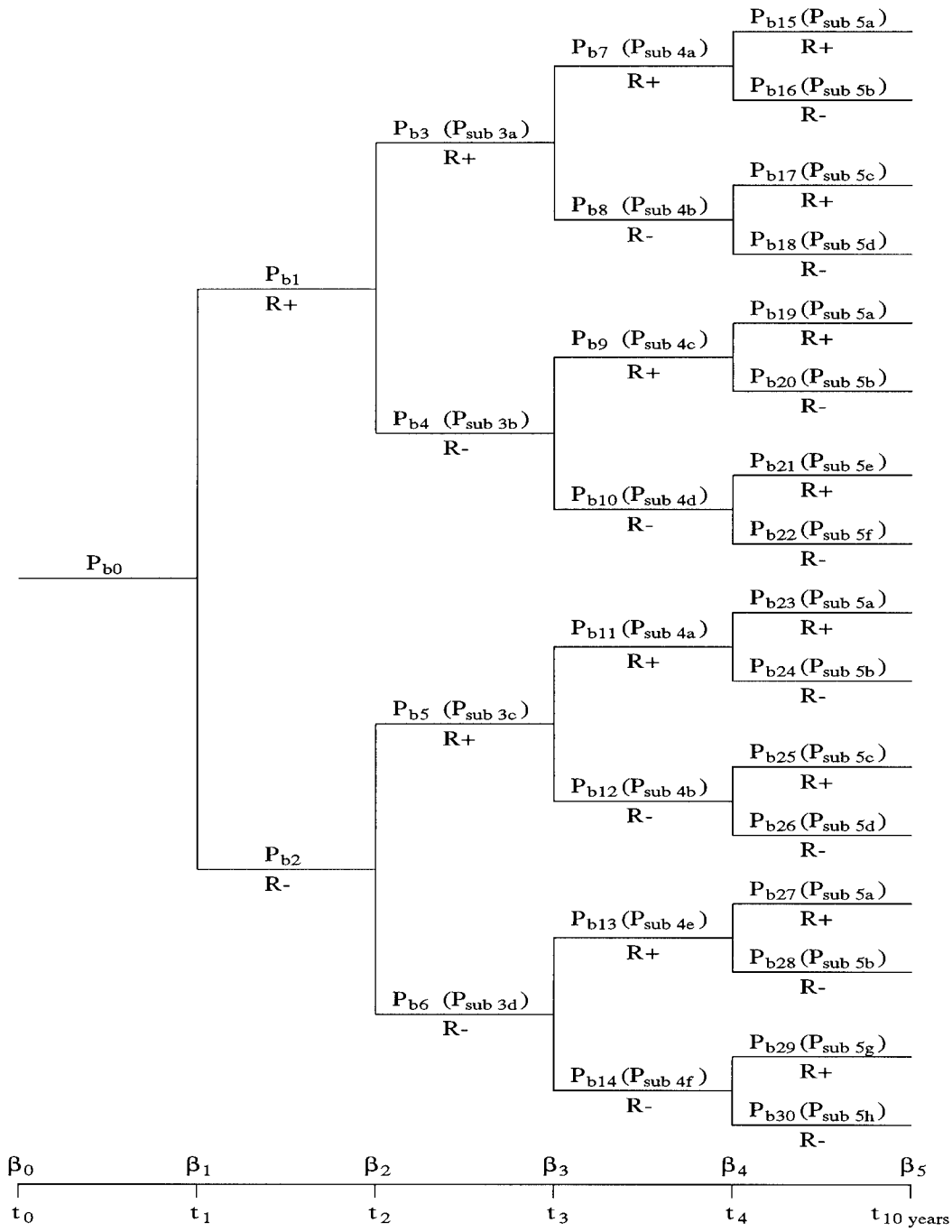

Figure 2.5: **Repair Paths for Four Lifetime Inspections on a Single Component Structure**

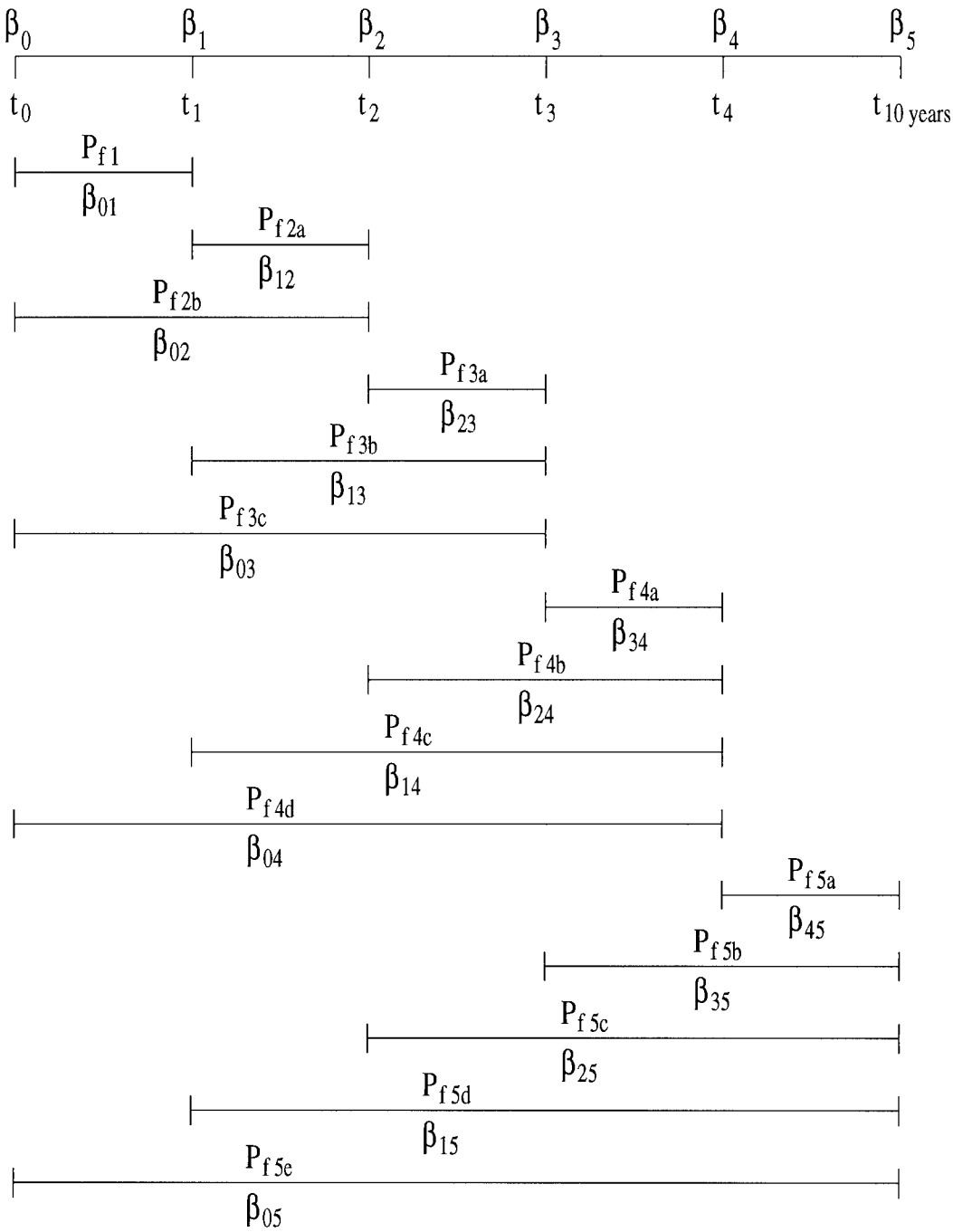

Figure 2.6: **Timeline for Four Lifetime Inspections on a Single Component Structure**

tified and notation which describes the probability of failure and the reliability index over these intervals is developed. Also, the damage intensity η must be tracked over every time interval.

Let:

$$
\begin{aligned}
P_{f_1} &= \Phi(-\beta(t_1)) = \Phi(-\beta_{01}) \qquad \eta = \eta_1 \\
P_{f_{2a}} &= \Phi(-\beta(t_2 - t_1)) = \Phi(-\beta_{12}) \qquad \eta = \eta_{2a} \\
P_{f_{2b}} &= \Phi(-\beta(t_2)) = \Phi(-\beta_{02}) \qquad \eta = \eta_{2b} \\
P_{f_{3a}} &= \Phi(-\beta(t_3 - t_2)) = \Phi(-\beta_{23}) \qquad \eta = \eta_{3a} \\
P_{f_{3b}} &= \Phi(-\beta(t_3 - t_1)) = \Phi(-\beta_{13}) \qquad \eta = \eta_{3b} \\
P_{f_{3c}} &= \Phi(-\beta(t_3)) = \Phi(-\beta_{03}) \qquad \eta = \eta_{3c} \\
P_{f_{4a}} &= \Phi(-\beta(t_4 - t_3)) = \Phi(-\beta_{34}) \qquad \eta = \eta_{4a} \\
P_{f_{4b}} &= \Phi(-\beta(t_4 - t_2)) = \Phi(-\beta_{24}) \qquad \eta = \eta_{4b} \\
P_{f_{4c}} &= \Phi(-\beta(t_4 - t_1)) = \Phi(-\beta_{14}) \qquad \eta = \eta_{4c} \\
P_{f_{4d}} &= \Phi(-\beta(t_4)) = \Phi(-\beta_{04}) \qquad \eta = \eta_{4d} \\
P_{f_{5a}} &= \Phi(-\beta(t_5 - t_4)) = \Phi(-\beta_{45}) \qquad \eta = \eta_{5a} \\
P_{f_{5b}} &= \Phi(-\beta(t_5 - t_3)) = \Phi(-\beta_{35}) \qquad \eta = \eta_{5b} \\
P_{f_{5c}} &= \Phi(-\beta(t_5 - t_2)) = \Phi(-\beta_{25}) \qquad \eta = \eta_{5c} \\
P_{f_{5d}} &= \Phi(-\beta(t_5 - t_1)) = \Phi(-\beta_{15}) \qquad \eta = \eta_{5d} \\
P_{f_{5e}} &= \Phi(-\beta(t_5)) = \Phi(-\beta_{05}) \qquad \eta = \eta_{5e}
\end{aligned}
$$

Fig. 2.6 shows a time line which provides a pictorial description of

these values. Over each of these time periods, the damage intensity η is calculated. From the damage and the quality of the inspection technique used, the probability of detection P_{det_i} is calculated where i indicates variable subscripts which uniquely identify that particular inspection. Similarly, the probability of repair P_{rep_i} is calculated over every possible time period with the subscripts uniquely defining that specific repair. With these values, the probability of each branch and sub-branch as numbered in Fig. 2.5 can be calculated.

For time t_1:

$$\begin{aligned} P_{b_1} &= P(R_1^+) = P_{det_1} P_{rep_1} \\ P_{b_2} &= P(R_1^-) = 1 - P_{b_1} \end{aligned}$$

For time t_2:

$$\begin{aligned} P_{sub_{3a}} &= P_{det_{2a}}(P_{rep_{2a}}) \\ P_{sub_{3b}} &= 1 - P_{sub_{3a}} \\ P_{sub_{3c}} &= P_{det_{2b}}(P_{rep_{2b}}) \\ P_{sub_{3d}} &= 1 - P_{sub_{3c}} \\ P_{b_3} &= P(R_1^+ \bigcap R_2^+) = P_{b_1} P_{sub_{3a}} \\ P_{b_4} &= P(R_1^+ \bigcap R_2^-) = P_{b_1} P_{sub_{3b}} \\ P_{b_5} &= P(R_1^- \bigcap R_2^+) = P_{b_2} P_{sub_{3c}} \\ P_{b_6} &= P(R_1^- \bigcap R_2^-) = P_{b_2} P_{sub_{3d}} \end{aligned}$$

For time t_3:

$$
\begin{aligned}
P_{sub_{4a}} &= P_{det_{3a}} P_{rep_{3a}} \\
P_{sub_{4b}} &= 1 - P_{sub_{4a}} \\
&\ldots\ldots \\
P_{sub_{4e}} &= P_{insp_{3e}} P_{rep_{3e}} \\
P_{sub_{4f}} &= 1 - P_{sub_{4e}} \\
P_{b_7} &= P(R_1^+ \bigcap R_2^+ \bigcap R_3^+) = P_{b_3} P_{sub_{4a}} \\
P_{b_8} &= P(R_1^+ \bigcap R_2^+ \bigcap R_3^-) = P_{b_3} P_{sub_{4b}} \\
P_{b_9} &= P(R_1^+ \bigcap R_2^- \bigcap R_3^+) = P_{b_4} P_{sub_{4c}} \\
P_{b_{10}} &= P(R_1^+ \bigcap R_2^- \bigcap R_3^-) = P_{b_4} P_{sub_{4d}} \\
P_{b_{11}} &= P(R_1^- \bigcap R_2^+ \bigcap R_3^+) = P_{b_5} P_{sub_{4a}} \\
P_{b_{12}} &= P(R_1^- \bigcap R_2^+ \bigcap R_3^-) = P_{b_5} P_{sub_{4b}} \\
P_{b_{13}} &= P(R_1^- \bigcap R_2^- \bigcap R_3^+) = P_{b_6} P_{sub_{4e}} \\
P_{b_{14}} &= P(R_1^- \bigcap R_2^- \bigcap R_3^-) = P_{b_6} P_{sub_{4f}}
\end{aligned}
$$

For time t_4:

$$
\begin{aligned}
P_{sub_{5a}} &= P_{det_{4a}} P_{rep_{4a}} \\
P_{sub_{5b}} &= 1 - P_{sub_{5a}} \\
&\ldots\ldots \\
P_{sub_{5g}} &= P_{det_{4d}} P_{rep_{4d}} \\
P_{sub_{5h}} &= 1 - P_{sub_{5g}}
\end{aligned}
$$

$$
\begin{aligned}
P_{b_{15}} &= P(R_1^+ \bigcap R_2^+ \bigcap R_3^+ \bigcap R_4^+) = P_{b_7} P_{sub_{5a}} \\
P_{b_{16}} &= P(R_1^+ \bigcap R_2^+ \bigcap R_3^+ \bigcap R_4^-) = P_{b_7} P_{sub_{5b}} \\
P_{b_{17}} &= P(R_1^+ \bigcap R_2^+ \bigcap R_3^- \bigcap R_4^+) = P_{b_8} P_{sub_{5c}} \\
P_{b_{18}} &= P(R_1^+ \bigcap R_2^+ \bigcap R_3^- \bigcap R_4^-) = P_{b_8} P_{sub_{5d}} \\
P_{b_{19}} &= P(R_1^+ \bigcap R_2^- \bigcap R_3^+ \bigcap R_4^+) = P_{b_9} P_{sub_{5a}} \\
P_{b_{20}} &= P(R_1^+ \bigcap R_2^- \bigcap R_3^+ \bigcap R_4^-) = P_{b_9} P_{sub_{5b}} \\
P_{b_{21}} &= P(R_1^+ \bigcap R_2^- \bigcap R_3^- \bigcap R_4^+) = P_{b_{10}} P_{sub_{5e}} \\
P_{b_{22}} &= P(R_1^+ \bigcap R_2^- \bigcap R_3^- \bigcap R_4^-) = P_{b_{10}} P_{sub_{5f}} \\
P_{b_{23}} &= P(R_1^- \bigcap R_2^+ \bigcap R_3^+ \bigcap R_4^+) = P_{b_{11}} P_{sub_{5a}} \\
P_{b_{24}} &= P(R_1^- \bigcap R_2^+ \bigcap R_3^+ \bigcap R_4^-) = P_{b_{11}} P_{sub_{5b}} \\
P_{b_{25}} &= P(R_1^- \bigcap R_2^+ \bigcap R_3^- \bigcap R_4^+) = P_{b_{12}} P_{sub_{5c}} \\
P_{b_{26}} &= P(R_1^- \bigcap R_2^+ \bigcap R_3^- \bigcap R_4^-) = P_{b_{12}} P_{sub_{5d}} \\
P_{b_{27}} &= P(R_1^- \bigcap R_2^- \bigcap R_3^+ \bigcap R_4^+) = P_{b_{13}} P_{sub_{5a}} \\
P_{b_{28}} &= P(R_1^- \bigcap R_2^- \bigcap R_3^+ \bigcap R_4^-) = P_{b_{13}} P_{sub_{5b}} \\
P_{b_{29}} &= P(R_1^- \bigcap R_2^- \bigcap R_3^- \bigcap R_4^+) = P_{b_{14}} P_{sub_{5g}} \\
P_{b_{30}} &= P(R_1^- \bigcap R_2^- \bigcap R_3^- \bigcap R_4^-) = P_{b_{14}} P_{sub_{5h}}
\end{aligned}
$$

Recalling Eqn. 2.26 for the reliability index at time t, the reliability index β_4 at time t_4 can be calculated using the notation above as:

$$
\begin{aligned}
\beta_4 &= -\Phi^{-1}[P_{f_{4a}}(P_{b_7} + P_{b_9} + P_{b_{11}} + P_{b_{13}}) + P_{f_{4b}}(P_{b_8} + P_{b_{12}}) \\
&\quad + P_{f_{4c}} P_{b_{10}} + P_{f_{4d}} P_{b_{14}}]
\end{aligned}
$$

and the reliability index $\beta_{10\ years}$ at time $t_{10\ years}$ can be calculated as:

$$\begin{aligned}\beta_{10\ years} &= -\Phi^{-1}[P_{f_{5a}}(P_{b_{15}} + P_{b_{17}} + P_{b_{19}} + P_{b_{21}} + P_{b_{23}} + P_{b_{25}} + P_{b_{27}} + P_{b_{29}}) \\ &\quad + P_{f_{5b}}(P_{b_{16}} + P_{b_{20}} + P_{b_{24}} + P_{b_{28}}) + P_{f_{5c}}(P_{b_{18}} + P_{b_{26}}) \\ &\quad + P_{f_{5d}}P_{b_{22}} + P_{f_{5e}}P_{b_{30}}]\end{aligned}$$

The cost of repair calculation includes fixed and variable costs which account for the damage intensity at every repair. The number of repairs varies because one branch offers 4 repairs, four branches offer 3 repairs, six branches offer 2 repairs, four branches offer 1 repair, and one branch has no repairs. Using Eqn. 2.29, the cost of repair calculation becomes:

$$\begin{aligned}C_{b_{15}} &= P_{b_{15}}(4(C_{fix}) + C_{var}(\eta_1 + \eta_{2a} + \eta_{3a} + \eta_{4a})) \\ C_{b_{16}} &= P_{b_{16}}(3(C_{fix}) + C_{var}(\eta_1 + \eta_{2a} + \eta_{3a})) \\ C_{b_{17}} &= P_{b_{17}}(3(C_{fix}) + C_{var}(\eta_1 + \eta_{2a} + \eta_{4b})) \\ C_{b_{18}} &= P_{b_{18}}(2(C_{fix}) + C_{var}(\eta_1 + \eta_{2a})) \\ C_{b_{19}} &= P_{b_{19}}(3(C_{fix}) + C_{var}(\eta_1 + \eta_{3b} + \eta_{4a})) \\ C_{b_{20}} &= P_{b_{20}}(2(C_{fix}) + C_{var}(\eta_1 + \eta_{3b})) \\ C_{b_{21}} &= P_{b_{21}}(2(C_{fix}) + C_{var}(\eta_1 + \eta_{4c})) \\ C_{b_{22}} &= P_{b_{22}}(1(C_{fix}) + C_{var}(\eta_1)) \\ C_{b_{23}} &= P_{b_{23}}(3(C_{fix}) + C_{var}(\eta_{2b} + \eta_{3a} + \eta_{4a})) \\ C_{b_{24}} &= P_{b_{24}}(2(C_{fix}) + C_{var}(\eta_{2b} + \eta_{3a})) \\ C_{b_{25}} &= P_{b_{25}}(2(C_{fix}) + C_{var}(\eta_{2b} + \eta_{4b})) \\ C_{b_{26}} &= P_{b_{26}}(1(C_{fix}) + C_{var}(\eta_{2b}))\end{aligned}$$

$$
\begin{aligned}
C_{b_{27}} &= P_{b_{27}}(2(C_{fix}) + C_{var}(\eta_{3c} + \eta_{4a})) \\
C_{b_{28}} &= P_{b_{28}}(1(C_{fix}) + C_{var}(\eta_{3c})) \\
C_{b_{29}} &= P_{b_{29}}(1(C_{fix}) + C_{var}(\eta_{4d})) \\
C_{b_{30}} &= 0
\end{aligned}
$$

$$
C_{rep} = \sum_{i=15}^{30} C_{b_i}
$$

$$
C_{tot} = 4(C_{insp}) + C_{rep}
$$

2.2.7 Program: OptimumInspect

The FORTRAN code which optimizes the timing of the inspections for a specified inspection technique is OptimumInspect written by the author. The program is written in Fortran 77 and links the structural reliability program RELTRAN (RELiability TRANsformation) [Lee *et al.* 1993] with the optimization program ADS (Automated Design Synthesis) [Vanderplaats 1986]. A different version of the program was written to accommodate two, three, and four lifetime inspections, respectively.

The user is required to complete subroutines which define the limit state equations and the accompanying gradients. The limit state equations describe the behavior of the structure being investigated. The user also inputs data which describe the random variables, correlation, and limit state equation parameters. This information is needed by RELTRAN which has the capability to calculate the reliability of single components and series systems.

The user also inputs data for the initial section properties, minimum allowable reliability index, life of structure, and cost data. While ADS provides many optimization options, numerous sample trials revealed that ISTRAT=0, IOPT=4, and IONED=5 provide the best answer with the fewest iterations and no violated constraints. This translates to skipping a specific strategy and going directly to the optimizer (ISTRAT=0), using the method of feasible directions as the optimizer technique (IOPT=4), and using the golden section method for a constrained function (IONED=5) as detailed in Vanderplaats [1984].

Given the deterioration model, the inspection technique capabilities, and all of the equations described earlier which reflect the possible repair paths, the program computes the optimum inspection times based on minimizing the total cost. The results are sent to a graphing subroutine which produces the data needed to create a graph of β versus time.

2.3 Results of the Single Component System for Two, Three, and Four Inspections

The model described above was tested for structures whose mean resistance (R) was 12.5, 13, 14, 15, 16, and 17 for inspection techniques A, B, C, and D, and $\delta_R = 0.10$. Figure 2.7 compares the associated inspection and repair costs for each case when only two inspections were allowed over the life of the structure. Figures 2.8 and 2.9 list the same for the cases of three and four inspections respectively. Tables 2.2, 2.3, and 2.4 show the optimum timing of the inspections and the associated total costs for various bar resistances and

inspection techniques considering two, three, and four lifetime inspections, respectively.

Table 2.2: **Optimum Inspection Strategy and Total Costs for Two Lifetime Inspections**

Lifetime Inspections	Inspection Technique	Mean Bar Resistance	Inspection Times		Total Cost
			t_1	t_2	
2	A	13.0	3.42	6.76	14.6
2	A	14.0	4.40	4.90	10.1
2	A	15.0	3.33	3.83	8.6
2	A	16.0	0.51	1.21	5.1
2	A	17.0	0.51	1.01	4.7
2	B	13.0	3.42	6.76	13.8
2	B	14.0	4.45	4.96	8.1
2	B	15.0	3.36	3.88	7.1
2	B	16.0	0.50	1.00	3.5
2	B	17.0	0.50	1.01	2.6
2	C	14.0	4.67	5.17	7.6
2	C	15.0	4.05	4.66	6.4
2	C	16.0	2.12	2.90	2.7
2	C	17.0	0.50	1.00	1.5
2	D	15.0	4.20	7.55	6.1
2	D	16.0	4.00	5.92	2.2
2	D	17.0	2.91	3.50	1.0

Note: $\delta_R = 0.10$ for all cases.

The less expensive inspection techniques will not work for the structures with smaller resistances where early detection of the damage is essential to maintaining the structure above the minimum reliability index. For example, when the mean resistance, R, is equal to 13, inspection technique D is

Table 2.3: **Optimum Inspection Strategy and Total Costs for Three Lifetime Inspections**

Lifetime Inspections	Inspection Technique	Mean Bar Resistance	Inspection Times			Total Cost
			t_1	t_2	t_3	
3	A	12.5	2.56	5.08	7.56	21.7
3	A	13.0	3.18	6.23	6.74	17.5
3	A	14.0	3.95	4.47	4.97	13.1
3	A	15.0	2.43	2.94	3.45	11.1
3	A	16.0	0.50	1.01	1.52	7.9
3	A	17.0	0.51	1.02	1.53	7.5
3	B	13.0	3.24	6.35	6.85	14.6
3	B	14.0	4.11	4.62	5.14	10.1
3	B	15.0	2.53	3.02	3.52	8.7
3	B	16.0	0.50	1.00	1.50	5.1
3	B	17.0	0.50	1.00	1.50	4.9
3	C	14.0	4.25	4.77	5.27	8.4
3	C	15.0	3.17	3.92	4.43	7.3
3	C	16.0	1.41	2.11	2.88	3.5
3	C	17.0	0.50	1.01	1.53	2.3
3	D	15.0	4.01	6.03	7.32	6.5
3	D	16.0	3.98	5.11	5.70	2.7
3	D	17.0	1.67	2.44	3.17	1.50

Note: $\delta_R = 0.10$ for all cases.

Table 2.4: **Optimum Inspection Strategy and Total Costs for Four Lifetime Inspections**

Lifetime Inspections	Inspection Technique	Mean Bar Resistance	Inspection Times				Total Cost
			t_1	t_2	t_3	t_4	
4	A	12.18	2.00	4.00	6.00	8.00	29.0
4	A	12.2	2.00	4.00	6.00	8.00	28.7
4	A	12.5	1.85	3.91	5.70	7.8	25.7
4	A	13.0	0.51	3.25	6.25	6.75	20.4
4	A	14.0	0.51	3.97	4.48	4.99	15.7
4	A	15.0	0.50	2.45	2.95	3.45	13.4
4	A	16.0	0.51	1.02	1.52	2.03	10.9
4	A	17.0	0.51	1.01	1.53	2.03	10.4
4	B	12.2	2.00	4.00	6.00	8.00	26.7
4	B	12.5	1.85	3.91	5.70	7.80	23.7
4	B	13.0	2.80	3.32	6.39	6.90	15.9
4	B	14.0	0.50	4.12	4.62	5.13	11.0
4	B	15.0	0.50	2.50	3.01	3.52	9.7
4	B	16.0	0.51	1.03	1.53	2.03	7.5
4	B	17.0	0.51	1.02	1.52	2.05	7.2
4	C	13.0	3.60	4.84	7.13	8.12	13.8
4	C	14.0	0.54	4.26	4.75	5.28	9.2
4	C	15.0	0.58	3.34	3.87	4.37	8.0
4	C	16.0	0.67	1.18	1.71	3.04	4.2
4	C	17.0	0.51	1.02	1.53	2.03	3.3
4	D	14.0	2.00	5.48	5.98	7.99	8.0
4	D	15.0	2.00	4.01	6.03	7.32	7.0
4	D	16.0	2.00	3.97	5.10	5.70	3.2
4	D	17.0	2.00	2.51	3.13	3.63	2.0

Note: $\delta_R = 0.10$ for all cases.

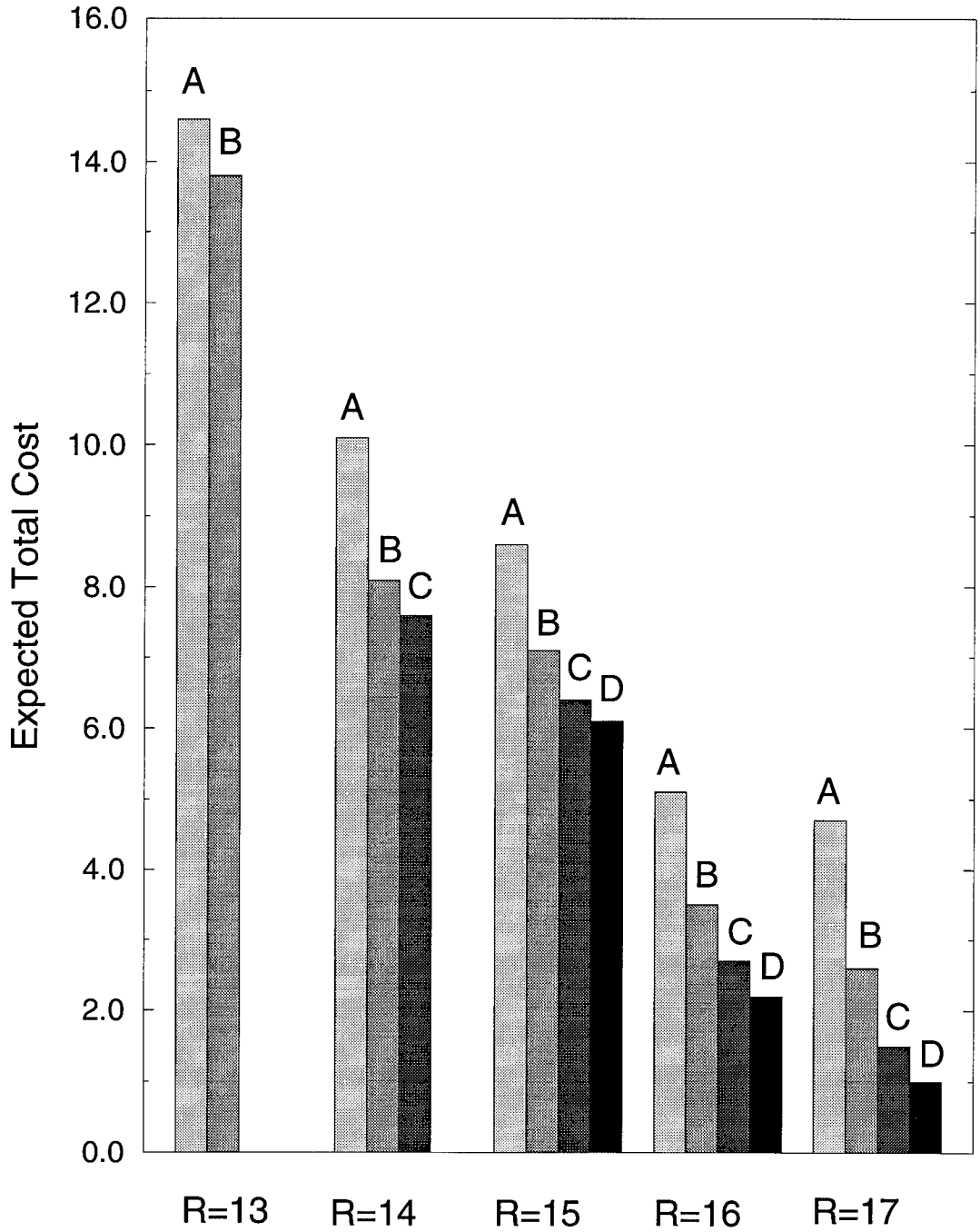

Figure 2.7: **Expected Total Costs for Techniques A, B, C, and D: Single Component Structure, Two Lifetime Inspections**

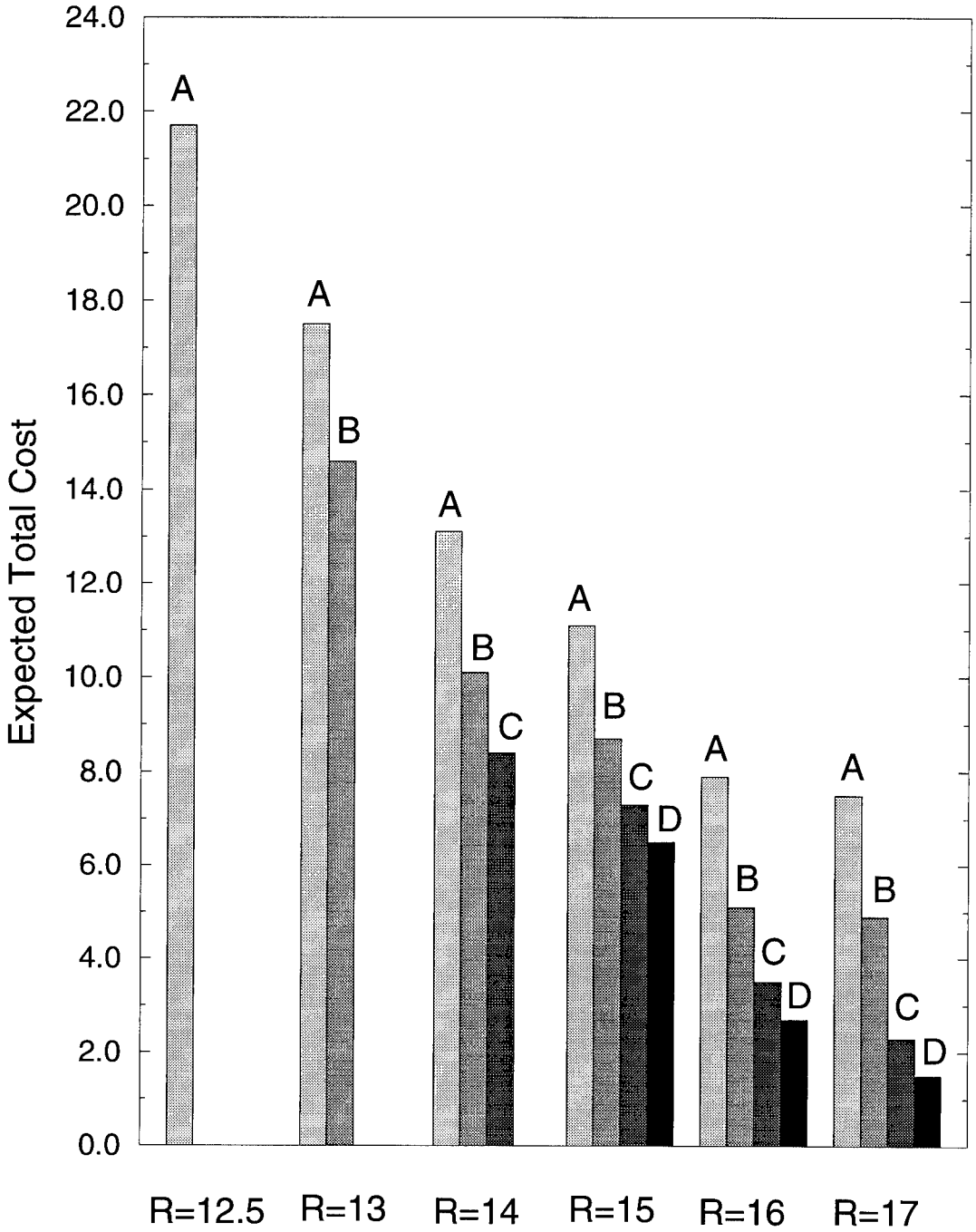

Figure 2.8: **Expected Total Costs for Techniques A, B, C, and D: Single Component Structure, Three Lifetime Inspections**

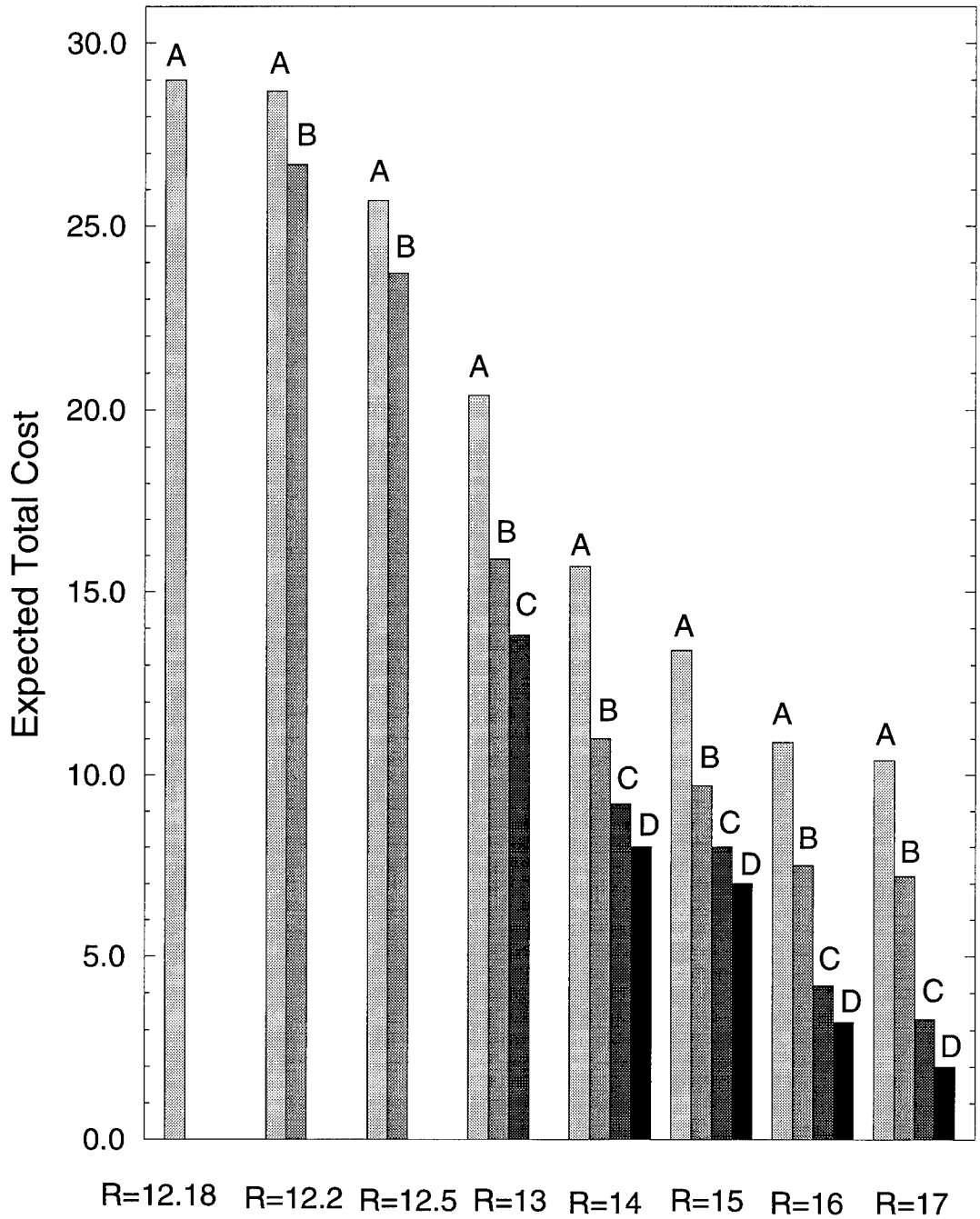

Figure 2.9: **Expected Total Costs for Techniques A, B, C, and D: Single Component Structure, Four Lifetime Inspections**

unsatisfactory for two, three, or four inspections. Inspection technique C will work for R=13 but only if four inspections are allowed. Inspection techniques A and B will work for all cases when R=13.

At one extreme where R=12.18, only inspection technique A with four inspections will solve the problem without violating any constraints. At the other extreme where R=17, any technique will work but inspection technique D with two inspections provides the lowest cost solution where the probability of repair is so small that the cost of inspection is the only cost that appears.

The lowest quality inspection technique that provides an answer also provides the lowest cost. The selection of the proper technique for the problem at hand is important. Looking, for example, at the four inspection case (Fig. 2.9), if one chose inspection technique A for the structure having the mean resistance R=17, one would be paying over five times as much as if inspection technique D was chosen. On the other hand, if R=13, using inspection technique A would cost about 1.5 times as much as the optimum but inspection technique D lacks the detection ability to keep the structure from falling below the minimum reliability index. The consequences of a poor selection of an inspection technique are either additional cost or potential violation of the imposed reliability constraints.

The cost effect of the choice of technique is greatest when the expected number of repairs is small. In the cases of two, three, or four inspections, the percent difference in costs for the different techniques is greatest

when R=17. The number of expected repairs is small and the total cost is dominated by the inspection cost. As the expected number of repairs increases such as for R=13, the cost of repair dominates the total cost and the percent cost differential between the techniques drops.

For these examples, the general conclusion is that if the number of repairs is expected to be small, the cheapest technique that will do the job should be chosen. The cost savings will be significant and there is little chance of violating the constraints. If the number of repairs is expected to be large, the best technique available should be selected because the extra cost is small relative to the total cost of inspection/repair and the penalty of a bad choice is a high likelihood of violated reliability constraints. In these examples, the cost of inspection is relatively close to the cost of repair. For examples where the cost of repair is much larger than the cost of inspection, that conclusion is probably invalid.

The timing of inspection and likelihood of repair for different structures are investigated next where the number of inspections and the inspection technique are fixed. Fig. 2.10 shows the case of two inspections using inspection technique A. Figs. 2.11 and 2.12 show the cases of three inspections using inspection technique B and four inspections using technique C, respectively. The results are similar in all three figures. At the higher resistances, the probability of repair is low and the effect of the repair barely appears on the graphs. As the resistances become lower , the probability of repair becomes greater and the effect of the repair is much more visible.

When the inspections are not needed, they tend to be as early in the life of the structure as the constraints allow. Fig. 2.10 shows this for the structures where R=16 and R=17. As the mean resistance decreases, the mean timing of the inspections comes later in the life of the structure and the interval between inspections becomes larger. Figs. 2.11 and 2.12 demonstrate as well that the additional inspections are scheduled as early in the life of the structure as possible where their effect is minimal if they are not needed. As the mean resistance decreases, the effects of the third and fourth inspection are more pronounced. The most extreme case is shown in Fig. 2.13 for the four inspection case with inspection technique A where R=12.18. The timing of the inspections is stretched out to 2, 4, 6, and 8 years with maximum probability of repair at each inspection. If the mean resistance was reduced even slightly, there would be violated constraints.

The effect of the different inspection techniques where the structure and the number of inspections are held constant is investigated next. Fig. 2.14 shows the case of two inspections when the mean resistance is $R = 14$ and $\delta_R = 0.10$. Fig. 2.15 shows the four inspection case when the mean resistance is $R = 15$ and $\delta_R = 0.10$. The timing of the inspections for the higher quality techniques occurs earliest in the life of the structure and grows progressively later as the quality of the inspection technique drops. The probability of making the repairs is higher for the higher quality inspection techniques because the probability of detection is higher.

In Fig. 2.15, the expected probability of making a repair is so small

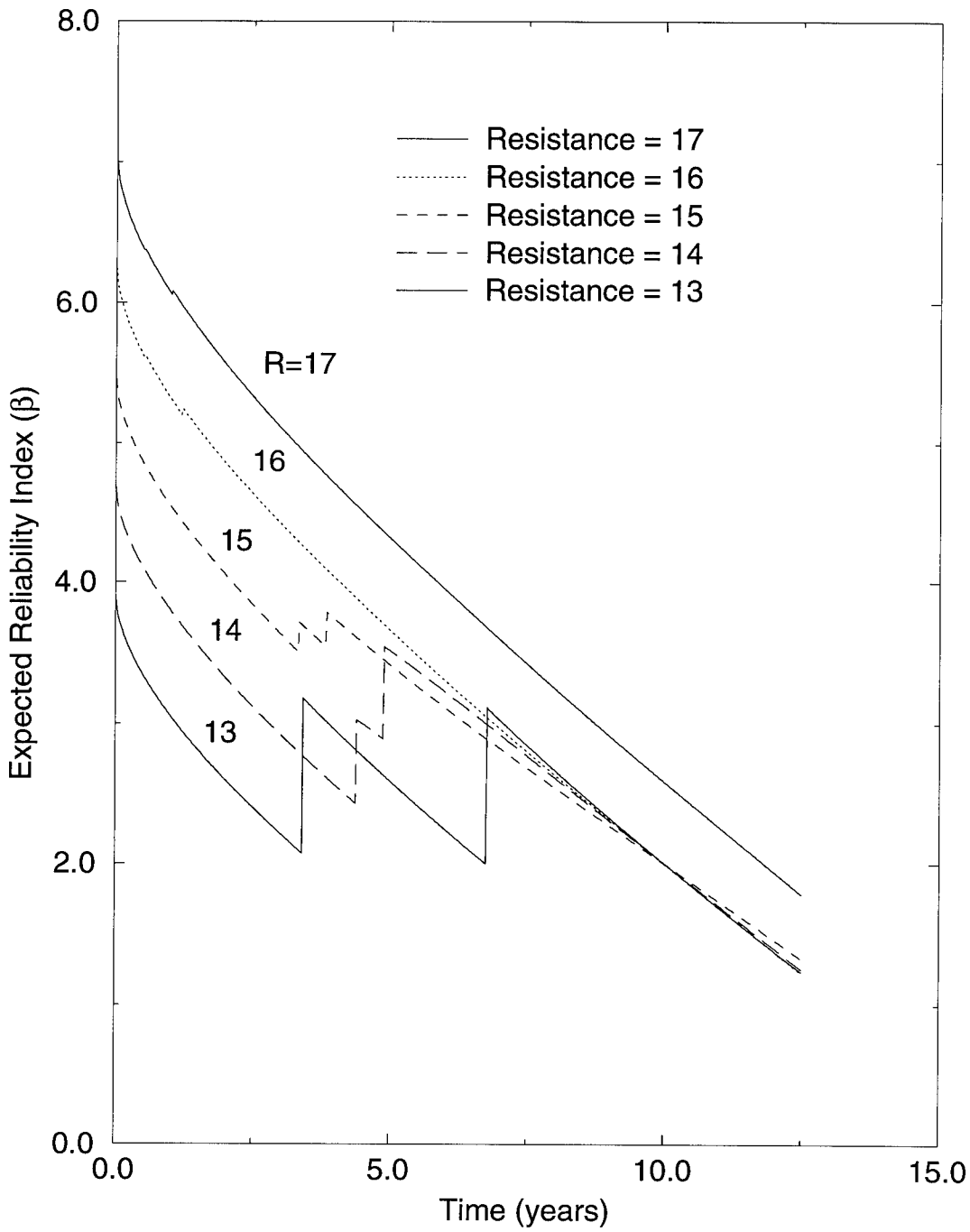

Figure 2.10: **Optimum Timing of Inspections Using Inspection Technique A for Two Lifetime Inspections,** $\delta_R = 0.10$

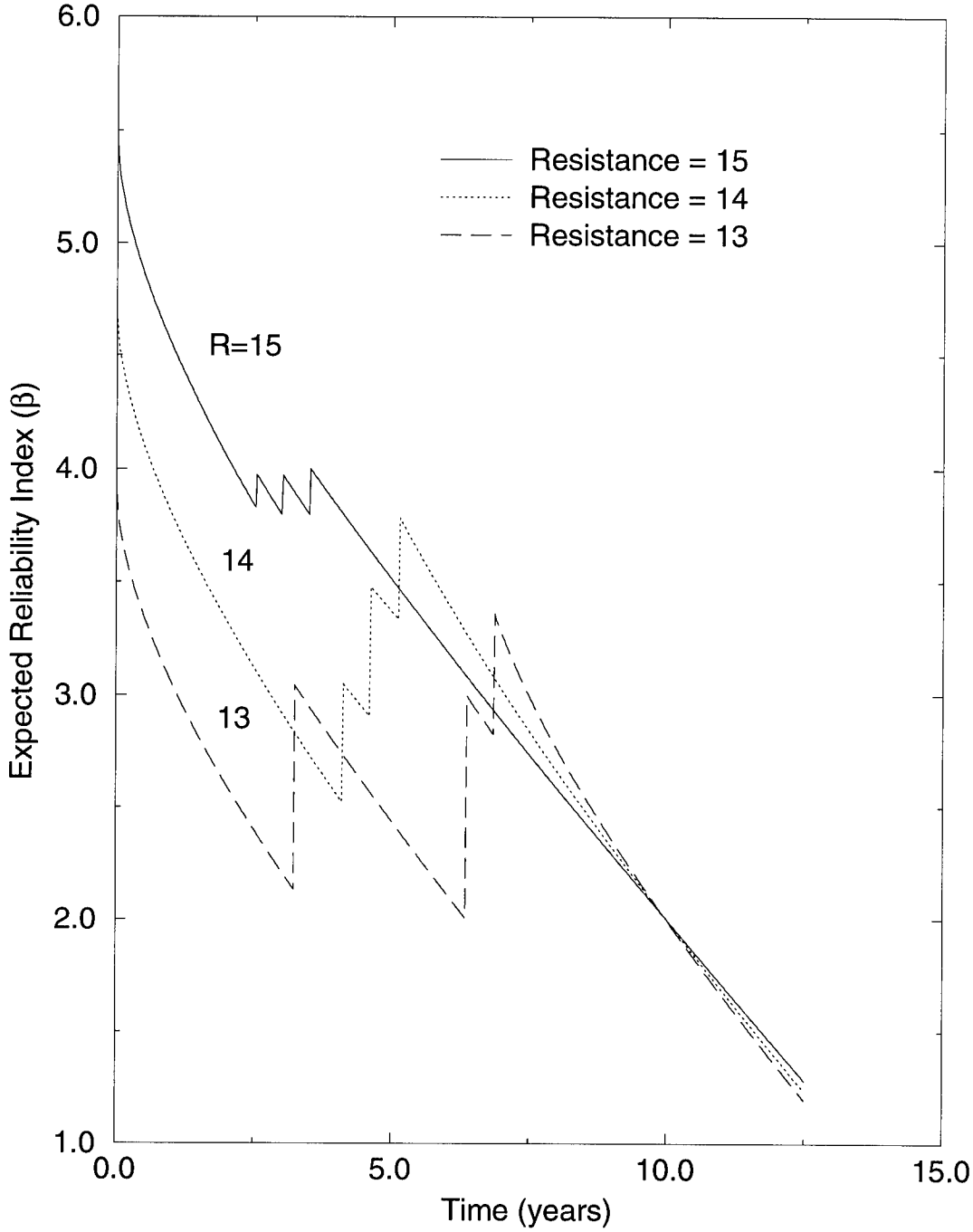

Figure 2.11: **Optimum Timing of Inspections Using Inspection Technique B for Three Lifetime Inspections,** $\delta_R =$ 0.10

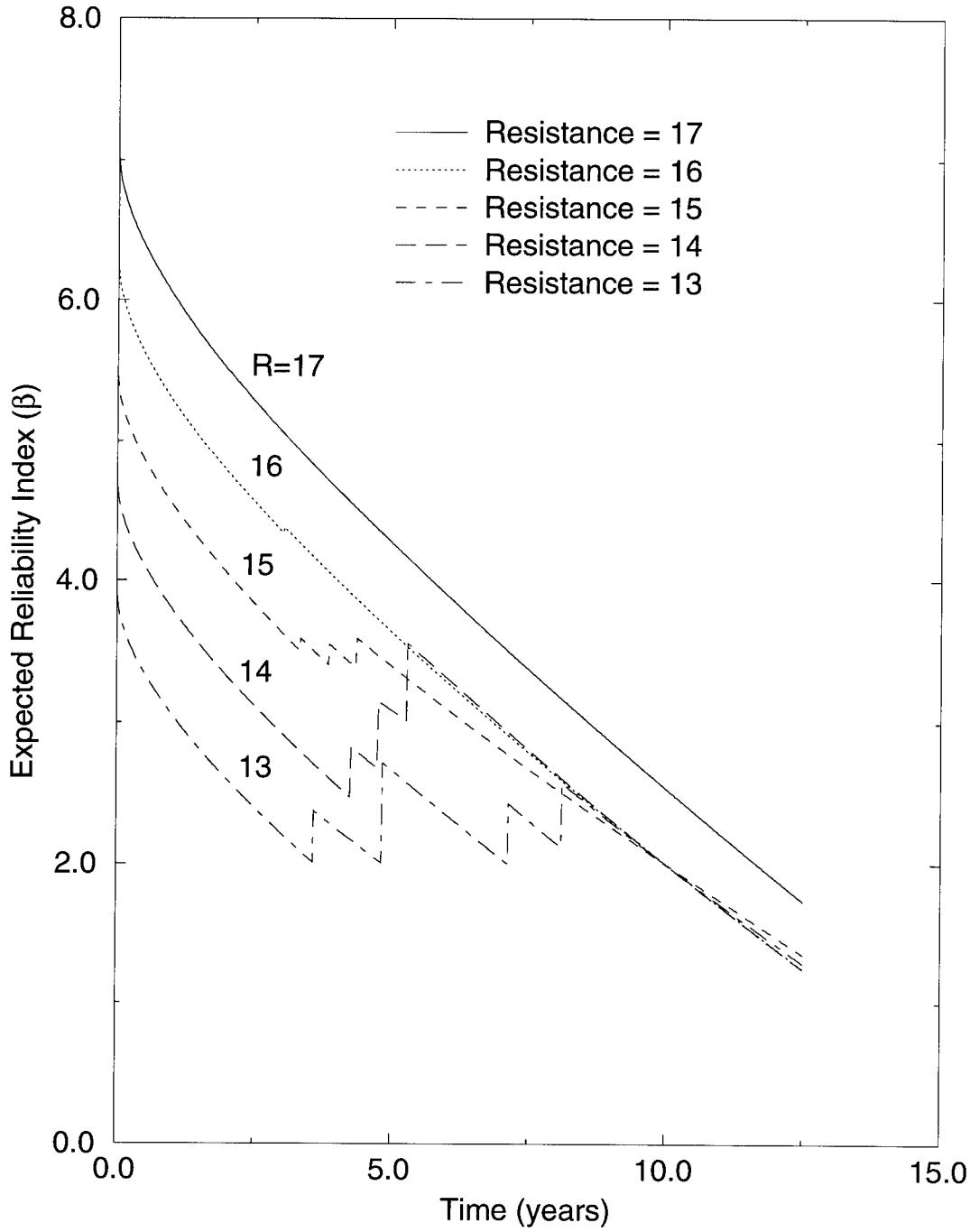

Figure 2.12: **Optimum Timing of Inspections Using Inspection Technique C for Four Lifetime Inspections,** $\delta_R = 0.10$

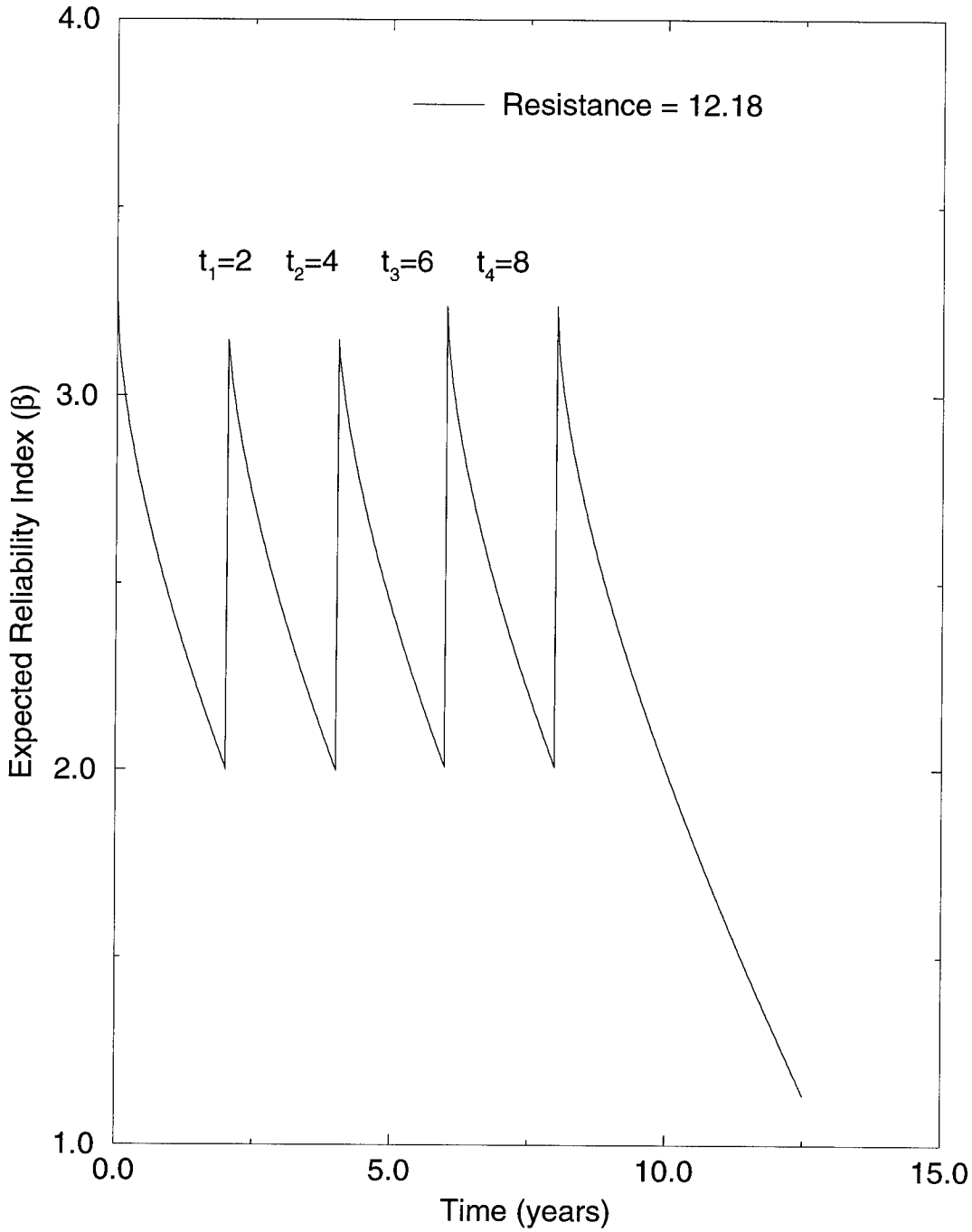

Figure 2.13: **Optimum Timing of Inspections Using Inspection Technique A for Four Lifetime Inspections,** $\delta_R = 0.10$

that the effect of the repair is not visible on the graph. This indicates that the fourth inspection was not needed for this structure. In fact, the graph for three lifetime inspections is almost identical to the four inspection graph in Fig. 2.15. As shown in Figs. 2.8 and 2.9, the only difference in the costs between the three and four inspection case is the cost of the fourth inspection. For techniques C and D, however, it appears that even the third inspection was not necessary, and only two repairs appear on the graph. For techniques C and D in the four inspection case, there were two unnecessary inspections early in the life of the structure.

Finally, the optimum inspection strategy for a given structure can be selected. Figure 2.16 shows the costs for all possibilities for a structure when the mean resistance $R = 14$ and $\delta_R = 0.10$. The best solution for this structure is to conduct two lifetime inspections using technique C where the cost is 7.6. Other acceptable solutions where the cost is within ten percent of the optimum would be four inspections with technique D, three inspections with technique C or two inspections with technique B. Technique A would be a waste of money in this case.

Similarly, the optimum solution for other structures based on minimum cost are shown in Table 2.5

2.4 Series System

A similar analysis is now performed on a two bar series system as shown in Fig. 2.17. In a series system, the failure of any member causes the

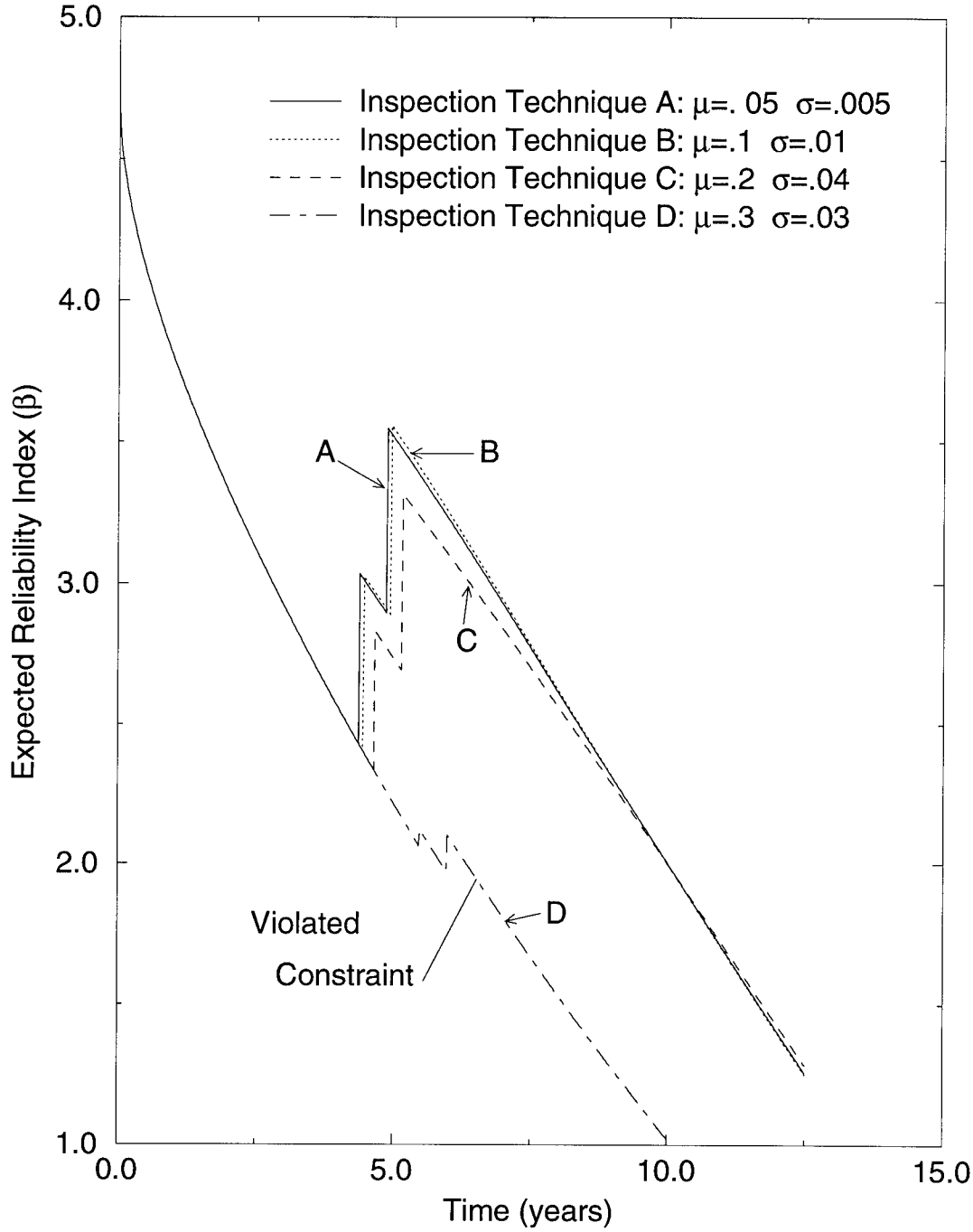

Figure 2.14: **Effect of Various Inspection Techniques on a Structure With Mean Resistance $R = 14$ for Two Lifetime Inspections, $\delta_R = 0.10$**

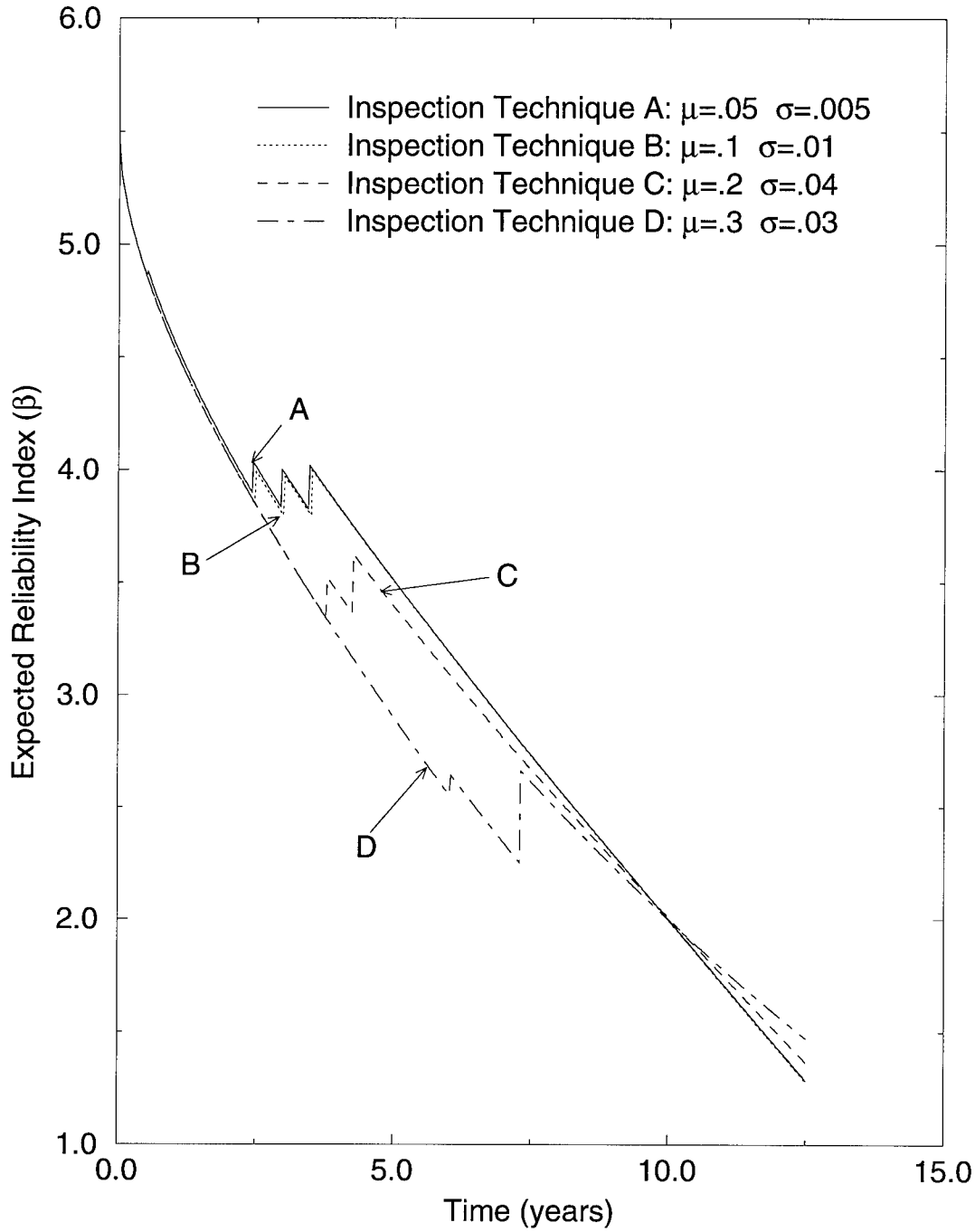

Figure 2.15: **Effect of Various Inspection Techniques on a Structure With Mean Resistance $R = 15$ for Four Lifetime Inspections, $\delta_R = 0.10$**

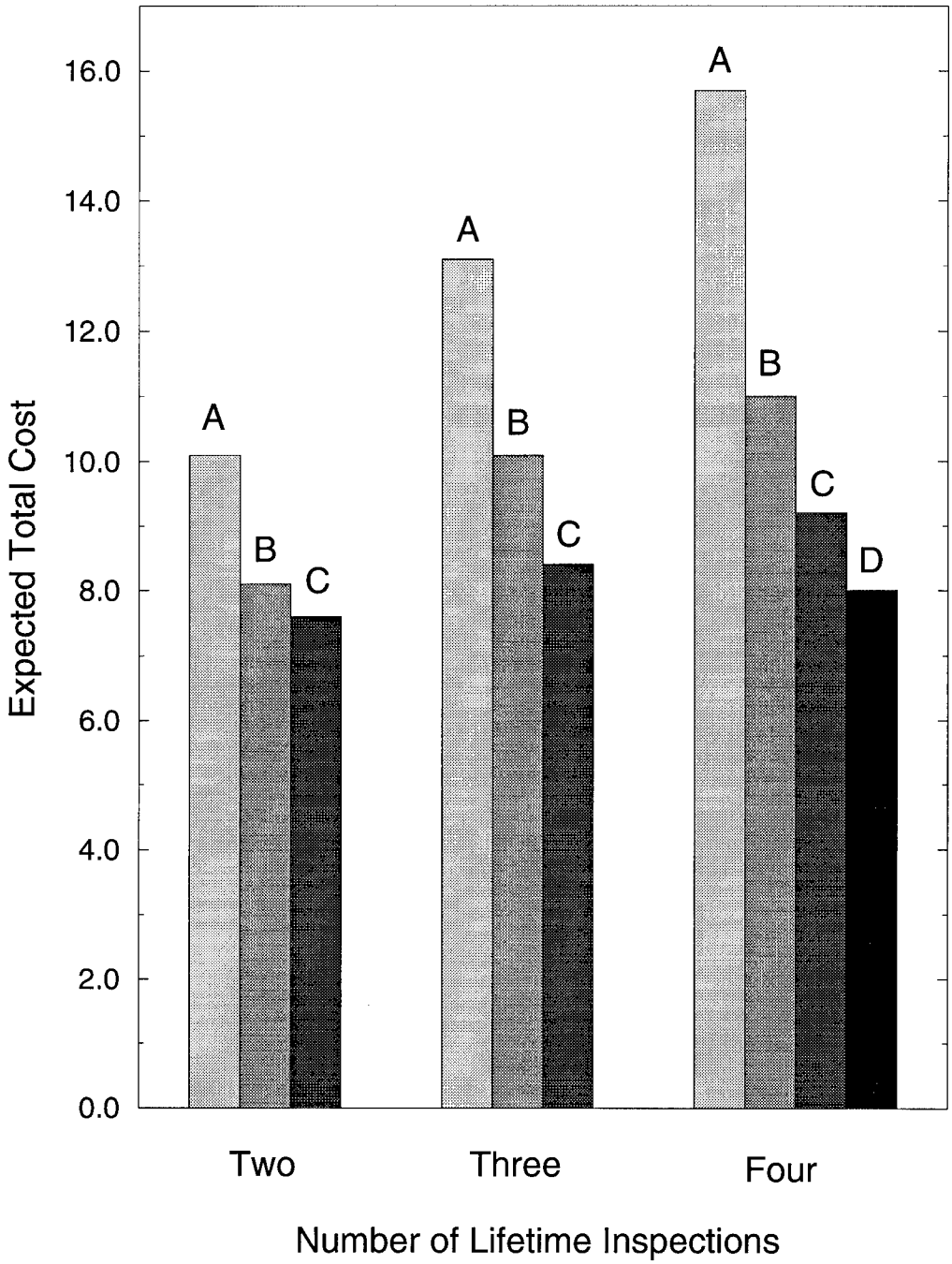

Figure 2.16: **Expected Total Costs for a Single Component Structure with a Mean Resistance $R = 14$ for Two, Three, and Four Lifetime Inspections, $\delta_R = 0.10$**

Table 2.5: **Optimal Inspection Strategy For Different Structures**

Mean Resistance	Number of Inspections	Optimal Technique
12.18	4	A
12.5	3	A
13	2	B
14	2	C
15	2	C
16	2	D
17	2	D
Note: $\delta_R = 0.10$ for all cases.		

entire system to fail. The system is still subjected to a centric axial load and the resistance, load, and area of the bars have not changed. The resistances of the bars are assumed to be uncorrelated. The same deterioration model (Eq. 2.3) is used.

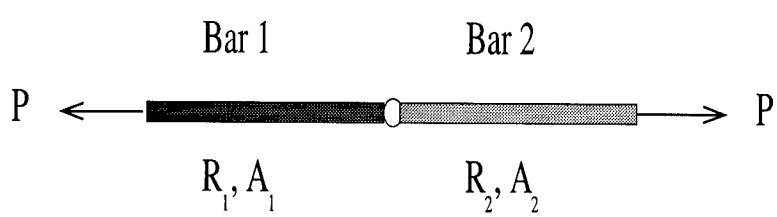

Figure 2.17: **Two Bar Series System**

The major difference in the problem is that there are four options after every inspection: (a) repair both bars, (b) repair bar 1 but not bar

2, (c) repair bar 2 but not bar 1, or (d) repair neither bar. For a series system with k bars, the number of branches expands to $(2^k)^n$ where n is the number of lifetime inspections. The current two bar structure ($k = 2$) with two inspections ($n = 2$) will have 16 possible paths and with three inspections ($n = 3$), there will be 64 paths.

The two bar series structure was analyzed for two and three lifetime inspections. Figs. 2.18, 2.19, 2.20, 2.21, and 2.22 show the 64 paths, the numbering system for the three inspection problem and the probabilities associated with each path. Fig. 2.18 shows the 64 branches and Figs. 2.19 through 2.22 breaks the event tree into quarters and shows the notation in more detail. The problem statement for the three inspection case is identical to that for the single component structure as indicated below.

Minimize: C_{tot}

such that:

$$\beta_{t_1} \geq \beta_{min} = 2.0 \tag{2.40}$$

$$\beta_{t_2} \geq \beta_{min} = 2.0 \tag{2.41}$$

$$\beta_{t_3} \geq \beta_{min} = 2.0 \tag{2.42}$$

$$\beta_{10\ years} \geq \beta_{min} = 2.0 \tag{2.43}$$

$$0.5 \leq t_1 \leq 7.0 \tag{2.44}$$

$$0.5 \leq t_2 - t_1 \leq 7.0 \tag{2.45}$$

$$0.5 \leq t_3 - t_2 \leq 7.0 \tag{2.46}$$

$$t_3 \leq 10.0 \tag{2.47}$$

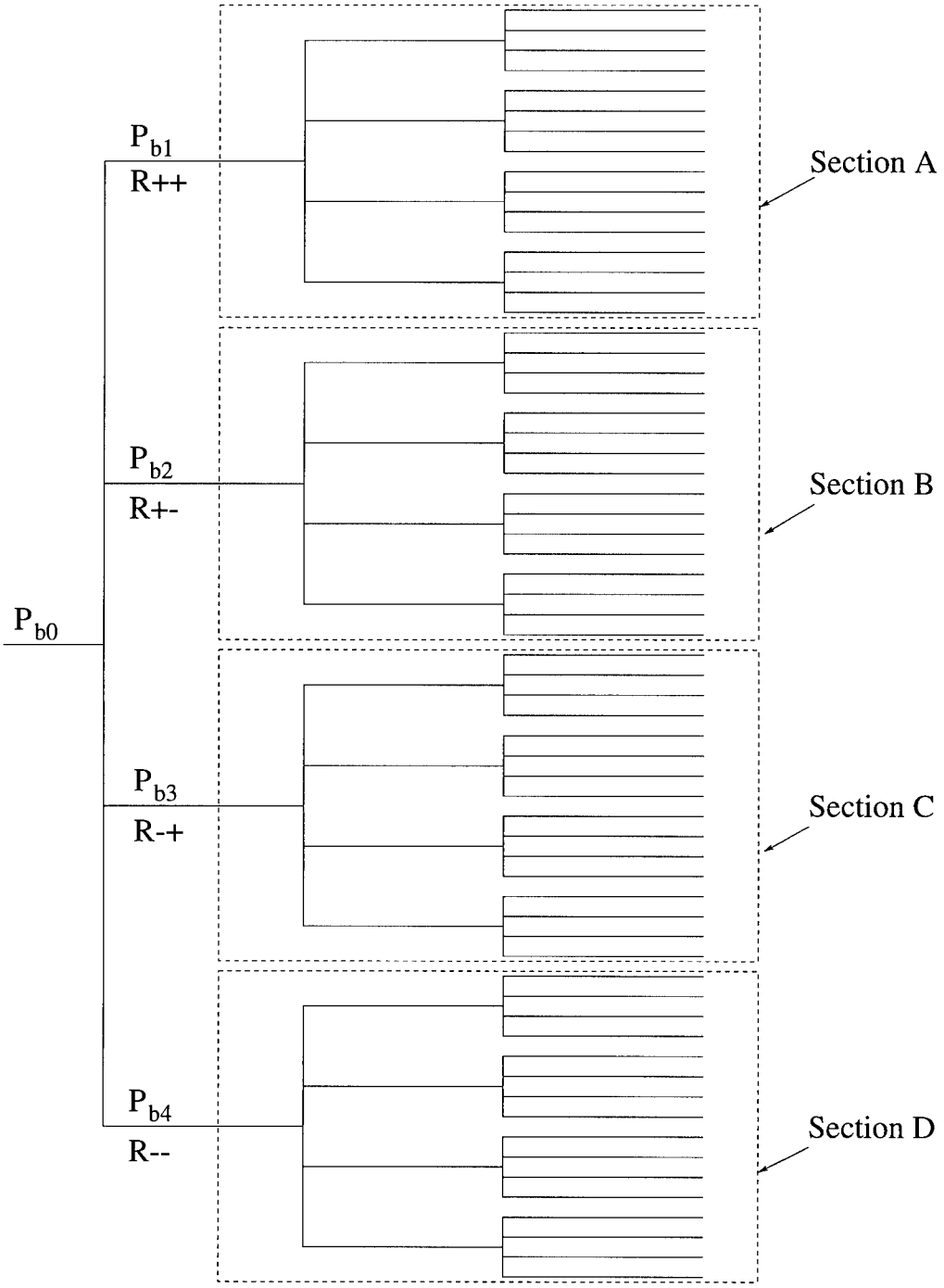

Figure 2.18: **Repair Paths For Three Lifetime Inspections on a Two Bar System**

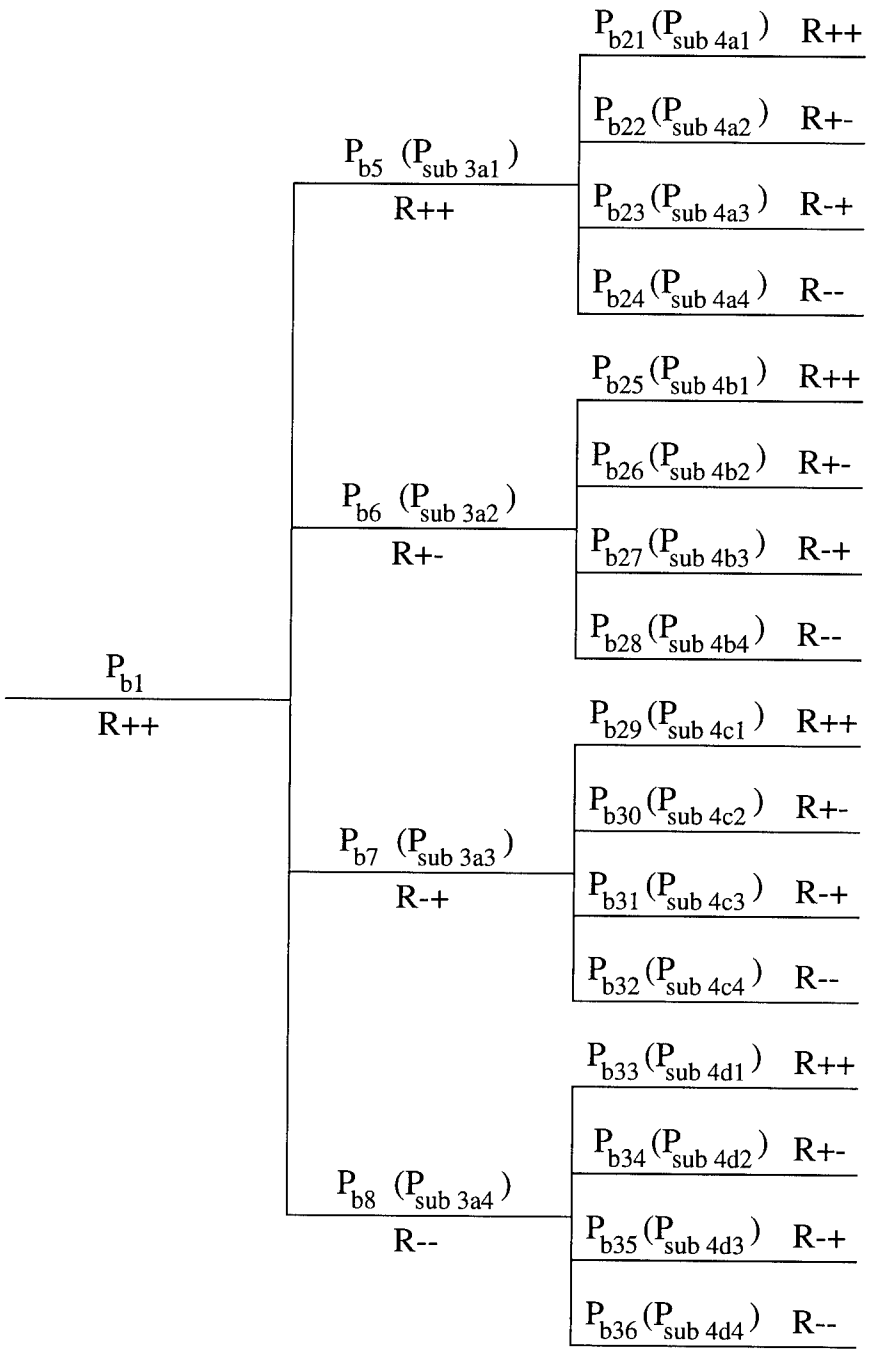

Figure 2.19: **Repair Paths For Three Lifetime Inspections on a Two Bar System: Top Quarter, Section A From Fig. 2.18**

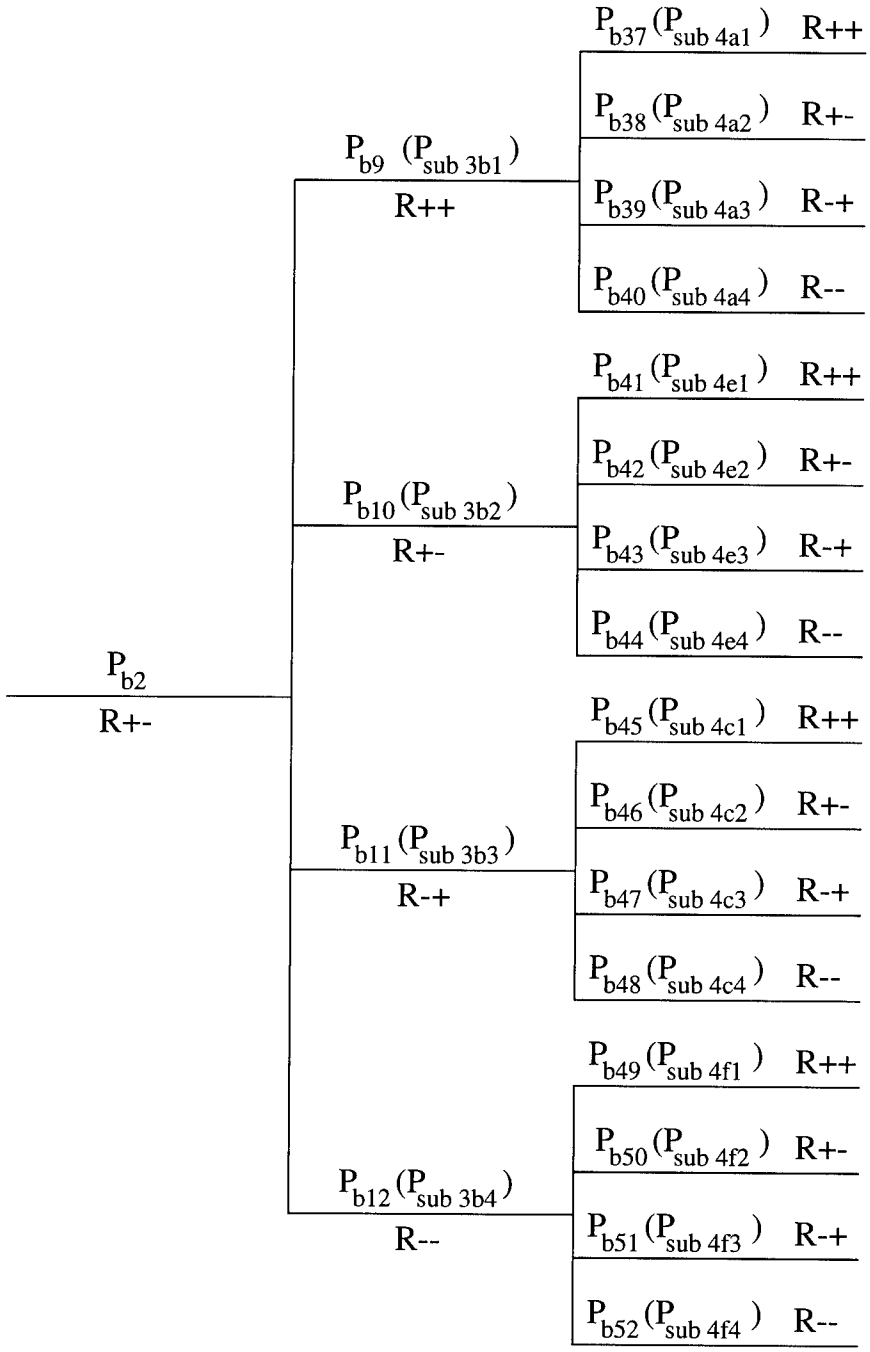

Figure 2.20: **Repair Paths For Three Lifetime Inspections on a Two Bar System: Second Quarter, Section B From Fig. 2.18**

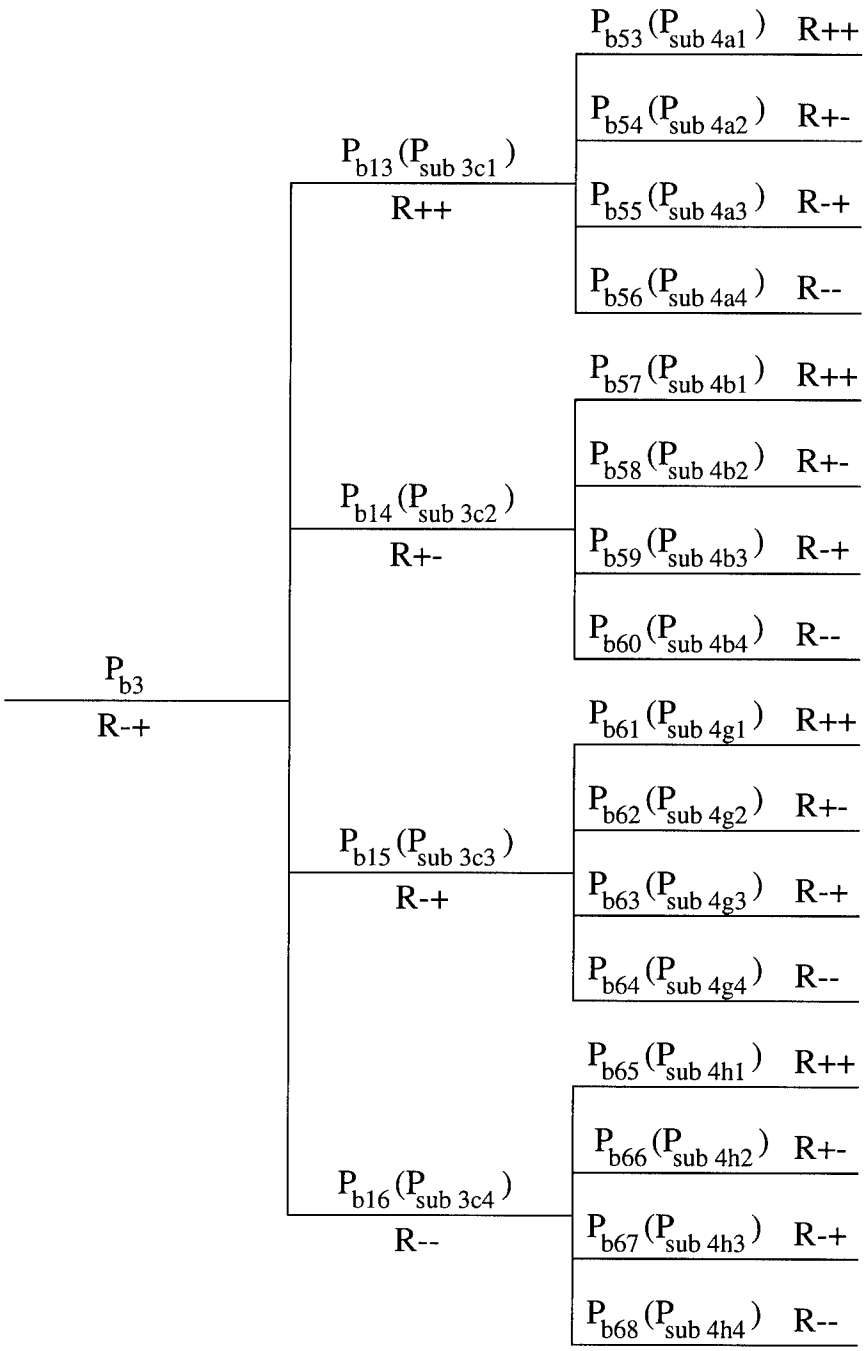

Figure 2.21: **Repair Paths For Three Lifetime Inspections on a Two Bar System: Third Quarter, Section C From Fig. 2.18**

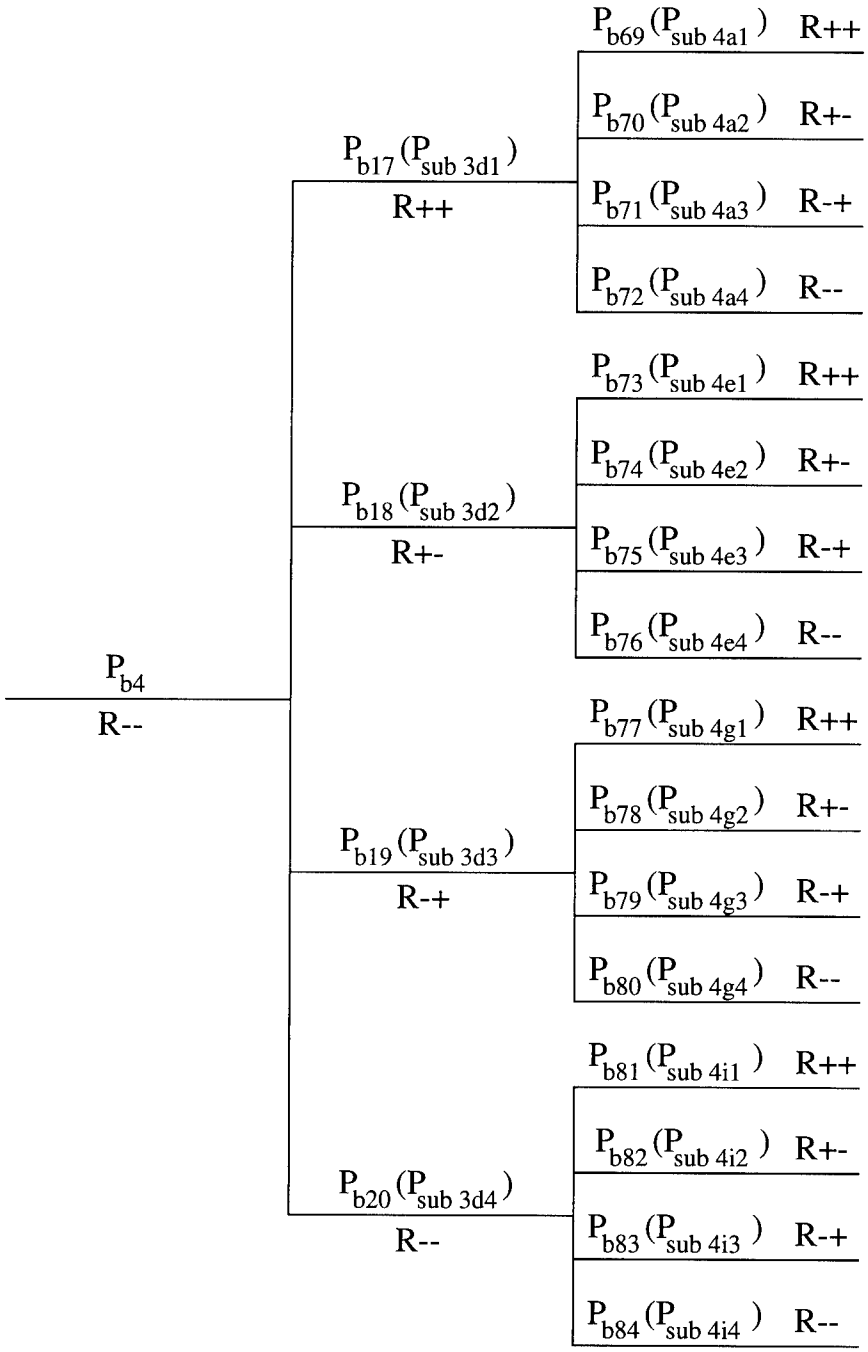

Figure 2.22: **Repair Paths For Three Lifetime Inspections on a Two Bar System: Bottom Quarter, Section D From Fig. 2.18**

With so many branches, consistent notation is critical to following the problem and trouble-shooting for errors. Again, every possible time interval between inspections is identified and notation which describes the probability of failure and the reliability index over these intervals is developed. Also, the damage intensity, η, must be tracked over every time interval.

Let:

$$
\begin{aligned}
P_{f_1} &= \Phi(-\beta_1) \quad \eta_{bar1} = \eta_{1_{b1}} \quad \eta_{bar2} = \eta_{1_{b2}} \\
P_{f_{2a}} &= \Phi(-\beta_{1212}) \quad \eta_{bar1} = \eta_{2a_{b1}} \quad \eta_{bar2} = \eta_{2a_{b2}} \\
P_{f_{2b}} &= \Phi(-\beta_{1202}) \quad \eta_{bar1} = \eta_{2a_{b1}} \quad \eta_{bar2} = \eta_{2b_{b2}} \\
P_{f_{2c}} &= \Phi(-\beta_{0212}) \quad \eta_{bar1} = \eta_{2b_{b1}} \quad \eta_{bar2} = \eta_{2a_{b2}} \\
P_{f_{2d}} &= \Phi(-\beta_{0202}) \quad \eta_{bar1} = \eta_{2b_{b1}} \quad \eta_{bar2} = \eta_{2b_{b2}} \\
P_{f_{3a}} &= \Phi(-\beta_{2323}) \quad \eta_{bar1} = \eta_{3a_{b1}} \quad \eta_{bar2} = \eta_{3a_{b2}} \\
P_{f_{3b}} &= \Phi(-\beta_{2313}) \quad \eta_{bar1} = \eta_{3a_{b1}} \quad \eta_{bar2} = \eta_{3b_{b2}} \\
&\ldots\ldots \\
P_{f_{3h}} &= \Phi(-\beta_{0313}) \quad \eta_{bar1} = \eta_{3c_{b1}} \quad \eta_{bar2} = \eta_{3b_{b2}} \\
P_{f_{3i}} &= \Phi(-\beta_{0303}) \quad \eta_{bar1} = \eta_{3c_{b1}} \quad \eta_{bar2} = \eta_{3c_{b2}} \\
P_{f_{4a}} &= \Phi(-\beta_{3434}) \quad \eta_{bar1} = \eta_{4a_{b1}} \quad \eta_{bar2} = \eta_{4a_{b2}} \\
P_{f_{4b}} &= \Phi(-\beta_{3424}) \quad \eta_{bar1} = \eta_{4a_{b1}} \quad \eta_{bar2} = \eta_{4b_{b2}} \\
&\ldots\ldots \\
P_{f_{4o}} &= \Phi(-\beta_{0414}) \quad \eta_{bar1} = \eta_{4d_{b1}} \quad \eta_{bar2} = \eta_{4c_{b2}} \\
P_{f_{4p}} &= \Phi(-\beta_{0404}) \quad \eta_{bar1} = \eta_{4d_{b1}} \quad \eta_{bar2} = \eta_{4d_{b2}}
\end{aligned}
$$

The probabilities and reliability indices listed above are based on the entire system. The system reliability is calculated based on the state of repair of each bar. For example, β_{ikjk} is the reliability index at time t_k when the first bar was last repaired at time t_i and the second bar was last repaired at time t_j. As such, β_{0313} is the reliability index at time t_3 when the first bar was last repaired at time t_0 which means it has never been repaired and the second bar was last repaired at time t_1. Figure 2.23 shows a time line which provides a pictorial description of these values for the two inspection case. Over each of these time periods, the damage intensity, η, is calculated. Figure 2.24 shows the additional values needed for the three inspection case.

From the damage and the quality of the inspection technique used, the probability of detection (P_{det_i}) is again calculated for each bar separately where i indicates variable subscripts which uniquely identify that particular inspection. Similarly, the probability of repair (P_{rep_i}) is calculated over every possible time period with the subscripts uniquely defining that specific repair. The probability of repair is based on the system reliability index rather than the reliability of any individual member. With these values, the probability of each branch and sub-branch as numbered in Figs. 2.19 through 2.22 can be calculated. Note that R_3^{+-} indicates that at time t_3, Bar 1 is repaired (+) and Bar 2 is not repaired (-).

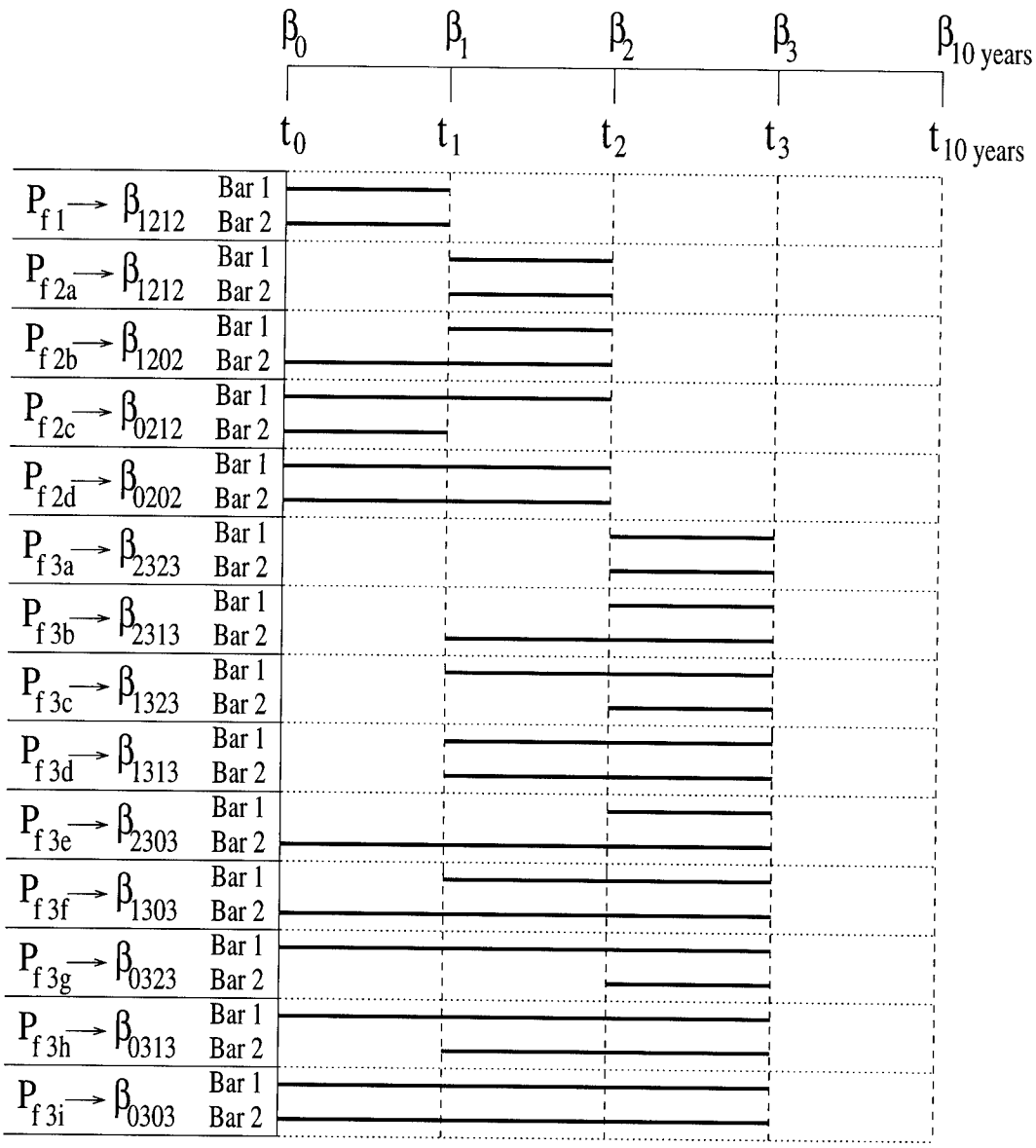

Figure 2.23: **The Probabilities of Failure for a Two Component System With Two Lifetime Inspections**

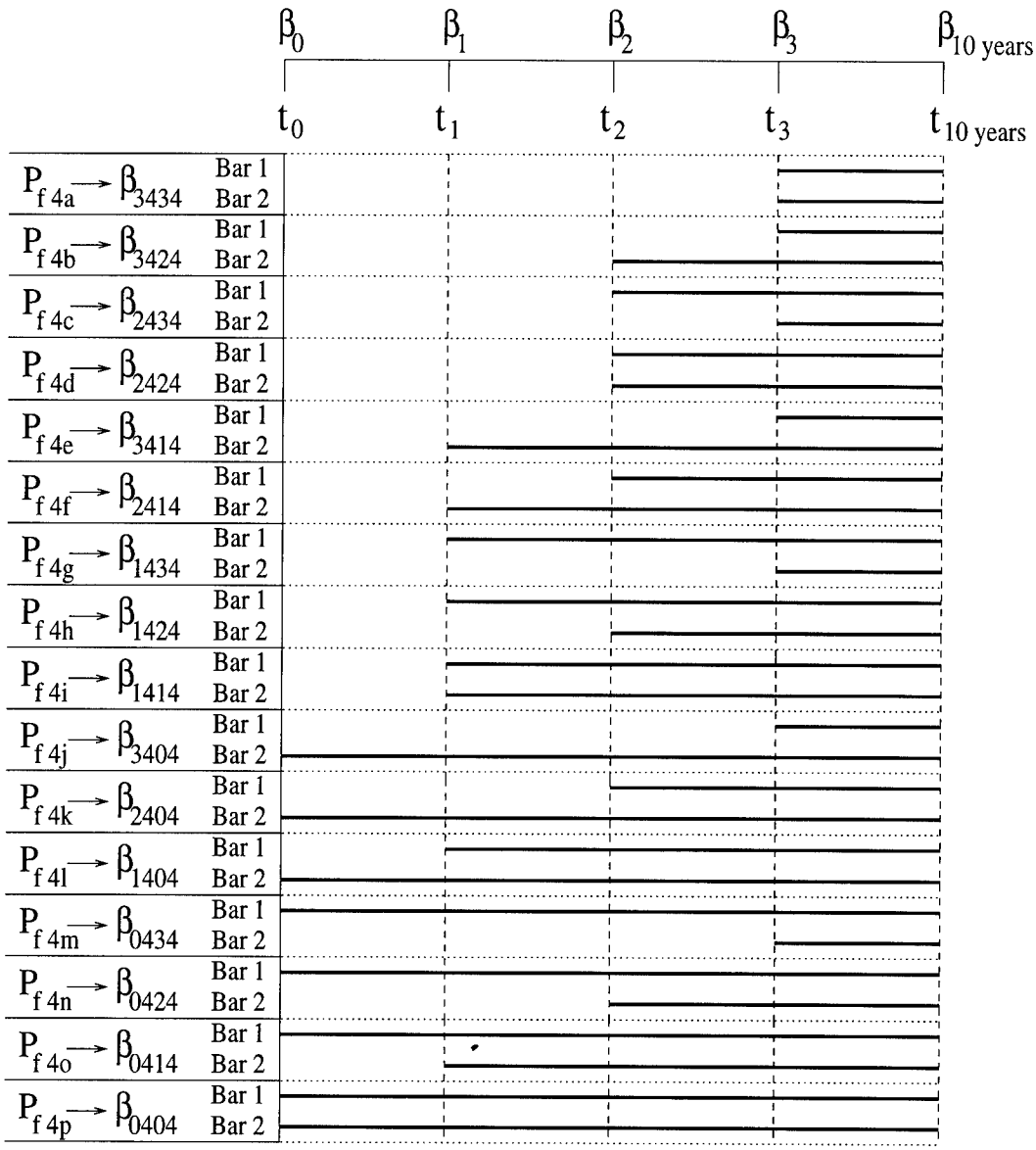

Figure 2.24: **The Additional Probabilities of Failure for a Two Component System With Three Lifetime Inspections**

For time t_1:

$$
\begin{aligned}
P_{b_1} &= P(R_1^{++}) = P_{det_{1_{b1}}} P_{det_{1_{b2}}} P_{rep_1} \\
P_{b_2} &= P(R_1^{+-}) = P_{det_{1_{b1}}} (1.0 - P_{det_{1_{b2}}}) P_{rep_1} \\
P_{b_3} &= P(R_1^{-+}) = (1.0 - P_{det_{1_{b1}}}) P_{det_{1_{b2}}} P_{rep_1} \\
P_{b_4} &= P(R_1^{--}) = 1.0 - (P_{b_1} + P_{b_2} + P_{b_3})
\end{aligned}
$$

For time t_2:

$$
\begin{aligned}
P_{sub_{3a_1}} &= P_{det_{2a_{b1}}} P_{det_{2a_{b2}}} P_{rep_{2a}} \\
P_{sub_{3a_2}} &= P_{det_{2a_{b1}}} (1.0 - P_{det_{2a_{b2}}}) P_{rep_{2a}} \\
P_{sub_{3a_3}} &= (1.0 - P_{det_{2a_{b1}}}) P_{det_{2a_{b2}}} P_{rep_{2a}} \\
P_{sub_{3a_4}} &= 1.0 - (P_{sub_{3a_1}} + P_{sub_{3a_2}} + P_{sub_{3a_3}}) \\
P_{b_5} &= P(R_1^{++} \bigcap R_2^{++}) = P_{b_1} P_{sub3_{a1}} \\
P_{b_6} &= P(R_1^{++} \bigcap R_2^{+-}) = P_{b_1} P_{sub3_{a2}} \\
P_{b_7} &= P(R_1^{++} \bigcap R_2^{-+}) = P_{b_1} P_{sub3_{a3}} \\
P_{b_8} &= P(R_1^{++} \bigcap R_2^{--}) = P_{b_1} P_{sub3_{a4}} \\
&\ldots\ldots \\
P_{sub_{3d_1}} &= P_{det_{2b_{b1}}} P_{det_{2b_{b2}}} P_{rep_{2d}} \\
P_{sub_{3d_2}} &= P_{det_{2b_{b1}}} (1.0 - P_{det_{2b_{b2}}}) P_{rep_{2d}} \\
P_{sub_{3d_3}} &= (1.0 - P_{det_{2b_{b1}}}) P_{insp_{2b_{b2}}} P_{rep_{2d}} \\
P_{sub_{3d_4}} &= 1.0 - (P_{sub_{3d_1}} + P_{sub_{3d_2}} + P_{sub_{3d_3}}) \\
P_{b_{17}} &= P(R_1^{--} \bigcap R_2^{++}) = P_{b_4} P_{sub3_{d1}}
\end{aligned}
$$

$$P_{b_{18}} = P(R_1^{--} \bigcap R_2^{+-}) = P_{b_4} P_{sub3_{d2}}$$

$$P_{b_{19}} = P(R_1^{--} \bigcap R_2^{-+}) = P_{b_4} P_{sub3_{d3}}$$

$$P_{b_{20}} = P(R_1^{--} \bigcap R_2^{--}) = P_{b_4} P_{sub3_{d4}}$$

For time t_3:

$$P_{sub4_{a_1}} = P_{det_{3a_{b1}}} P_{det_{3a_{b2}}} P_{rep_{2a}}$$

$$P_{sub4_{a_2}} = P_{det_{3a_{b1}}} (1.0 - P_{det_{3a_{b2}}}) P_{rep_{2a}}$$

$$P_{sub4_{a_3}} = (1.0 - P_{det_{3a_{b1}}}) P_{det_{3a_{b2}}} P_{rep_{2a}}$$

$$P_{sub4_{a_4}} = 1.0 - (P_{sub4_{a_1}} + P_{sub4_{a_2}} + P_{sub4_{a_3}})$$

$$P_{b_{21}} = P(R_1^{++} \bigcap R_2^{++} \bigcap R_3^{++}) = P_{b_5} P_{sub4_{a1}}$$

$$P_{b_{22}} = P(R_1^{++} \bigcap R_2^{++} \bigcap R_3^{+-}) = P_{b_5} P_{sub4_{a2}}$$

$$P_{b_{23}} = P(R_1^{++} \bigcap R_2^{++} \bigcap R_3^{-+}) = P_{b_5} P_{sub4_{a3}}$$

$$P_{b_{24}} = P(R_1^{++} \bigcap R_2^{++} \bigcap R_3^{--}) = P_{b_5} P_{sub4_{a4}}$$

.....

$$P_{sub4_{i_1}} = P_{det_{2b_{b1}}} P_{det_{2b_{b2}}} P_{rep_{2d}}$$

$$P_{sub4_{i_2}} = P_{det_{2b_{b1}}} (1.0 - P_{det_{2b_{b2}}}) P_{rep_{2d}}$$

$$P_{sub4_{i_3}} = (1.0 - P_{det_{2b_{b1}}}) P_{det_{2b_{b2}}} P_{rep_{2d}}$$

$$P_{sub4_{i_4}} = 1.0 - (P_{sub_{3d_1}} + P_{sub_{3d_2}} + P_{sub_{3d_3}})$$

$$P_{b_{81}} = P(R_1^{--} \bigcap R_2^{--} \bigcap R_3^{++}) = P_{b_{20}} P_{sub4_{i1}}$$

$$P_{b_{82}} = P(R_1^{--} \bigcap R_2^{--} \bigcap R_3^{+-}) = P_{b_{20}} P_{sub4_{i2}}$$

$$P_{b_{83}} = P(R_1^{--} \bigcap R_2^{--} \bigcap R_3^{-+}) = P_{b_{20}} P_{sub4_{i3}}$$

$$P_{b_{84}} = P(R_1^{--} \bigcap R_2^{--} \bigcap R_3^{--}) = P_{b_{20}} P_{sub4_{i4}}$$

Recalling Eqn. 2.26, for the reliability index at time t, the reliability index β_3 at t_3 can be calculated using the notation above as:

$$\begin{aligned}\beta_4 &= -\Phi^{-1}[P_{f_{3a}}(P_{b_5} + P_{b_9} + P_{b_{13}} + P_{b_{17}}) \\ &\quad + P_{f_{3b}}(P_{b_6} + P_{b_{14}}) + P_{f_{4c}}(P_{b_7} + P_{b_{11}}) \\ &\quad + P_{f_{3d}}(P_{b_8}) + P_{f_{3e}}(Pb_{10} + P_{b_{18}}) + P_{f_{3f}}(P_{b_{12}}) \\ &\quad + P_{f_{3g}}(P_{b_{15}} + P_{b_{19}}) + P_{f_{3h}}(P_{b_{16}}) + P_{f_{4i}}(P_{b_{20}})]\end{aligned}$$

and the reliability index $\beta_{10\ years}$ can be calculated as:

$$\begin{aligned}\beta_{10\ years} &= -\Phi^{-1}[P_{f_{4a}}(P_{b_{21}} + P_{b_{25}} + P_{b_{29}} + P_{b_{33}} + P_{b_{37}} + P_{b_{41}} + P_{b_{45}} + \\ &\quad P_{b_{49}} + P_{b_{53}} + P_{b_{57}} + P_{b_{61}} + P_{b_{65}} + P_{b_{69}} + P_{b_{73}} + P_{b_{77}} + P_{b_{81}}) + \\ &\quad P_{f_{4b}}(P_{b_{22}} + P_{b_{30}} + P_{b_{38}} + P_{b_{46}} + P_{b_{54}} + P_{b_{62}} + P_{b_{70}} + P_{b_{78}}) + \\ &\quad P_{f_{4c}}(P_{b_{23}} + P_{b_{27}} + P_{b_{39}} + P_{b_{43}} + P_{b_{55}} + P_{b_{59}} + P_{b_{71}} + P_{b_{75}}) + \\ &\quad P_{f_{4d}}(P_{b_{24}} + P_{b_{40}} + P_{b_{56}} + P_{b_{72}}) + \\ &\quad P_{f_{4e}}(P_{b_{26}} + P_{b_{34}} + P_{b_{58}} + P_{b_{66}}) + \\ &\quad P_{f_{4f}}(P_{b_{28}} + P_{b_{60}}) + \\ &\quad P_{f_{4g}}(P_{b_{31}} + P_{b_{35}} + P_{b_{47}} + P_{b_{51}}) + \\ &\quad P_{f_{4h}}(P_{b_{32}} + P_{b_{48}}) + \\ &\quad P_{f_{4i}}(P_{b_{36}}) + \\ &\quad P_{f_{4j}}(P_{b_{42}} + P_{b_{50}} + P_{b_{74}} + P_{b_{82}}) + \\ &\quad P_{f_{4k}}(P_{b_{44}} + P_{b_{76}}) +\end{aligned}$$

$$P_{f_{4l}}(P_{b_{52}}) +$$

$$P_{f_{4m}}(P_{b_{63}} + P_{b_{67}} + P_{b_{79}} + P_{b_{83}}) +$$

$$P_{f_{4n}}(P_{b_{64}} + P_{b_{80}}) +$$

$$P_{f_{4o}}(P_{b_{68}}) +$$

$$P_{f_{4p}}(P_{b_{84}})]$$

The computation of the cost of repair is complicated by including fixed and variable costs which requires tracking the damage intensity at every repair for both bars. The number of repairs varies because each branch offers a different number of repairs. Branch 21 (Fig. 2.18), for example, repairs both bars three times. Branch 46 (Fig. 2.20) repairs bar 1 two times and bar 2 only once. Branch 84 (Fig. 2.22) has no repairs of either bar. The cost of inspection and the fixed cost of repair calculation is the same as the single component structure. The fixed cost is applied if either bar is repaired. The additional cost appears in the variable cost because there is a second bar to repair. Using Eqn. 2.29, the cost of repair is calculated as follows:

$$\begin{aligned}
C_{b_{21}} &= P_{b_{21}}(3(C_{fix}) + C_{var}(\eta_{1_{b1}} + \eta_{1_{b2}} + \eta_{2a_{b1}} + \eta_{2a_{b2}} + \eta_{3a_{b1}} + \eta_{3a_{b2}})) \\
C_{b_{22}} &= P_{b_{22}}(3(C_{fix}) + C_{var}(\eta_{1_{b1}} + \eta_{1_{b2}} + \eta_{2a_{b1}} + \eta_{2a_{b2}} + \eta_{3a_{b1}})) \\
C_{b_{23}} &= P_{b_{23}}(3(C_{fix}) + C_{var}(\eta_{1_{b1}} + \eta_{1_{b2}} + \eta_{2a_{b1}} + \eta_{2a_{b2}} + \eta_{3a_{b2}})) \\
&\ldots\ldots \\
C_{b_{82}} &= P_{b_{82}}(1(C_{fix}) + C_{var}(\eta_{3d_{b1}}))
\end{aligned}$$

$$C_{b_{83}} = P_{b_{83}}(1(C_{fix}) + C_{var}(\eta_{3d_{b2}}))$$

$$C_{b_{84}} = 0$$

$$C_{rep} = \sum_{i=21}^{84} C_{branches}$$

$$C_{tot} = 3(C_{insp}) + C_{rep}$$

The system reliability index for the two-bar series system was computed using the upper Ditlevsen bound provided by RELTRAN. The load P and the resistances of both bars, R_{bar1} and R_{bar2}, were all normally distributed. The optimum inspection strategy was obtained by linking RELTRAN with ADS as described in Section 2.2.7.

2.5 Results of the Series System for Two Inspections

Figure 2.25 shows the respective total costs for the two bar series structure with two inspections. Both bars had equal resistances in each case. The trend was similar to the single bar system in that the percent difference in total costs was largest for the highest resistance where the effect of the inspection cost is prominent. The optimum timing of the inspections and total costs associated with the various inspection techniques and bar resistances are shown in Table 2.6.

The costs were higher overall than in the case of the single bar structure for two reasons. The variable cost of repair was greater because of the

Table 2.6: **Optimum Inspection Strategy and Costs for Two Bar Series System with Two Lifetime Inspections**

Bar 1		Bar 2		Insp.	Time	Time	Total Cost
μ_R	σ_R	μ_R	σ_R	Tech.	t_1	t_2	C_{tot}
13.5	1.35	13.5	1.35	A	3.83	6.18	15.0
14.0	1.40	14.0	1.40	A	4.70	5.19	11.8
15.0	1.50	15.0	1.50	A	3.90	4.39	10.3
16.0	1.60	16.0	1.60	A	2.18	2.69	7.7
17.0	1.70	17.0	1.70	A	0.50	1.01	4.9
14.0	1.40	14.0	1.40	B	4.59	5.17	9.4
15.0	1.50	15.0	1.50	B	3.85	4.43	8.6
16.0	1.60	16.0	1.60	B	2.09	2.72	6.3
17.0	1.70	17.0	1.70	B	0.51	1.01	3.0
14.0	1.40	14.0	1.40	C	4.83	5.42	9.9
15.0	1.50	15.0	1.50	C	4.55	5.05	9.1
16.0	1.60	16.0	1.60	C	3.55	4.05	7.0
17.0	1.70	17.0	1.70	C	0.50	1.00	1.5
15.0	1.50	15.0	1.50	D	6.86	7.40	10.4
16.0	1.60	16.0	1.60	D	3.93	7.22	6.7
17.0	1.70	17.0	1.70	D	2.77	3.38	1.0

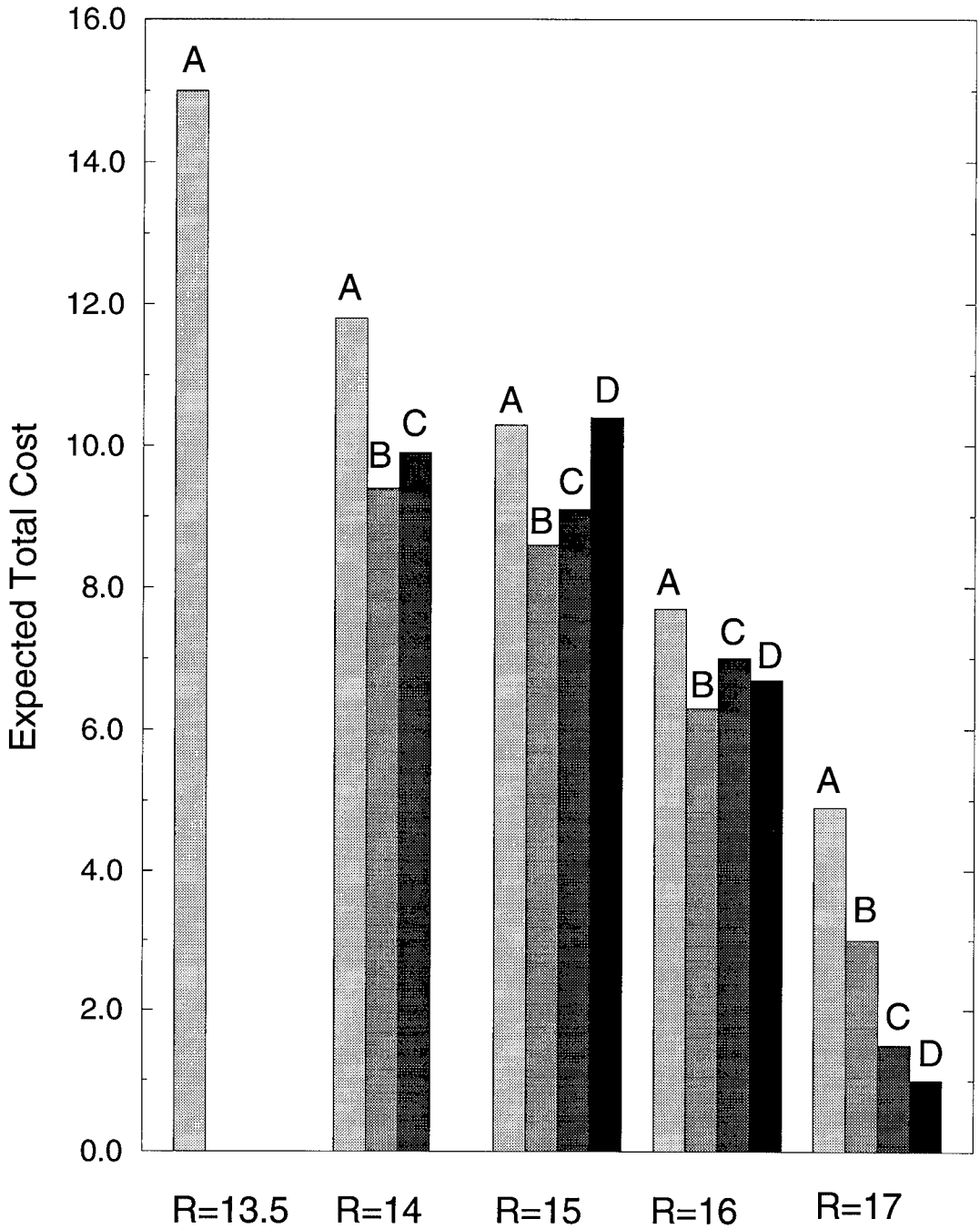

Figure 2.25: **Expected Total Costs for Techniques A, B, C, and D: Two Bar Series Structure, Two Lifetime Inspections**

additional bar and the series structure with uncorrelated resistances is inherently less reliable than a single component structure of the same size. The series system is only as strong as its weakest member and the chances of getting one member weaker than the others are increased if the resistances are independent. This is reflected by inspection technique B being unable to provide an answer which meets the constraints when the mean resistance of both bars is R=13, while an acceptable solution was provided for the single component system. The costs were almost identical however at the higher resistances where only the inspection costs were involved.

The biggest surprise was associated with the structures where the mean resistances of both bars were R=15 and R=16. The lower quality inspection techniques did not provide the lowest cost contrary to the trend established for the single component structure. Figure 2.26 shows the results for the R=15 structure for the different inspection techniques. Inspection techniques A and B were close together with similar times of inspection and similar probabilities of repair. As a result, the cost for inspection technique B was lower since the cost of inspection was less. Inspection technique D had inspection times much later in the life of the structure and the probability of repair was much higher. The increase in cost due to the higher probability of repair offset the lesser inspection cost. This does not appear to happen often but seems to be a result of the poorer detection capability causing higher repairs later in the life of the structure.

Fig. 2.27 shows the results for varying resistances with the number of

inspections and the inspection technique fixed. Using inspection technique C, the trends are the same as for a single component structure. As the resistance decreases, the effects of the repairs are larger. The mean time of inspection occurs later in the structure's life and the time interval between inspections becomes larger.

Finally, Fig. 2.28 and Table 2.7 show the results for structures where the resistances of the two bars are not equal. With a series system which is only as strong as its weakest member, it is expected that the structure with equal resistances would be more reliable. In Fig. 2.28, the combined resistance of the two bars was the same but the distribution became increasingly unequal. As expected, the structure where R_{bar1}=16 and R_{bar2}=16 required less repair and produced the lowest total cost. Similarly, the structure with the most unequal resistances, R_{bar1}=18 and R_{bar2}=14, produced the highest cost and had the highest probability of needing repair.

Table 2.7: **Optimum Inspection Strategy and Costs for Two Bar Series System with Unequal Bar Resistances, Inspection Technique C**

Bar 1		Bar 2		Insp.	Time	Time	Total Cost
μ_R	σ_R	μ_R	σ_R	Tech.	t_1	t_2	C_{tot}
16.0	1.60	16.0	1.6	C	3.55	4.05	7.02
17.0	1.70	15.0	1.50	C	4.10	4.65	8.27
18.0	1.80	14.0	1.40	C	4.53	5.03	9.26

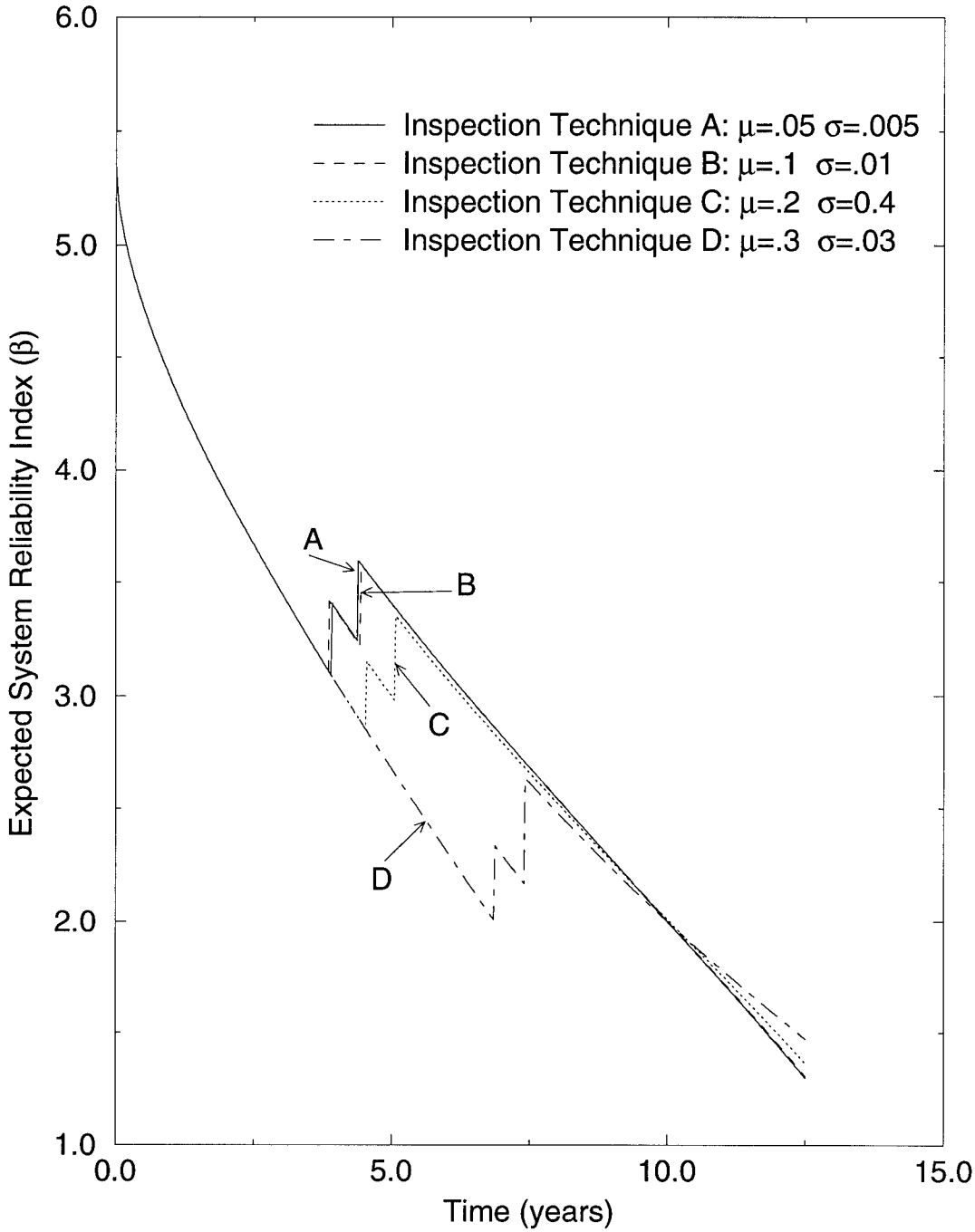

Figure 2.26: **Two Component Series System Where Mean Resistance $R = 15$ and $\delta_R = 0.10$ For Both Bars, Varying Inspection Techniques**

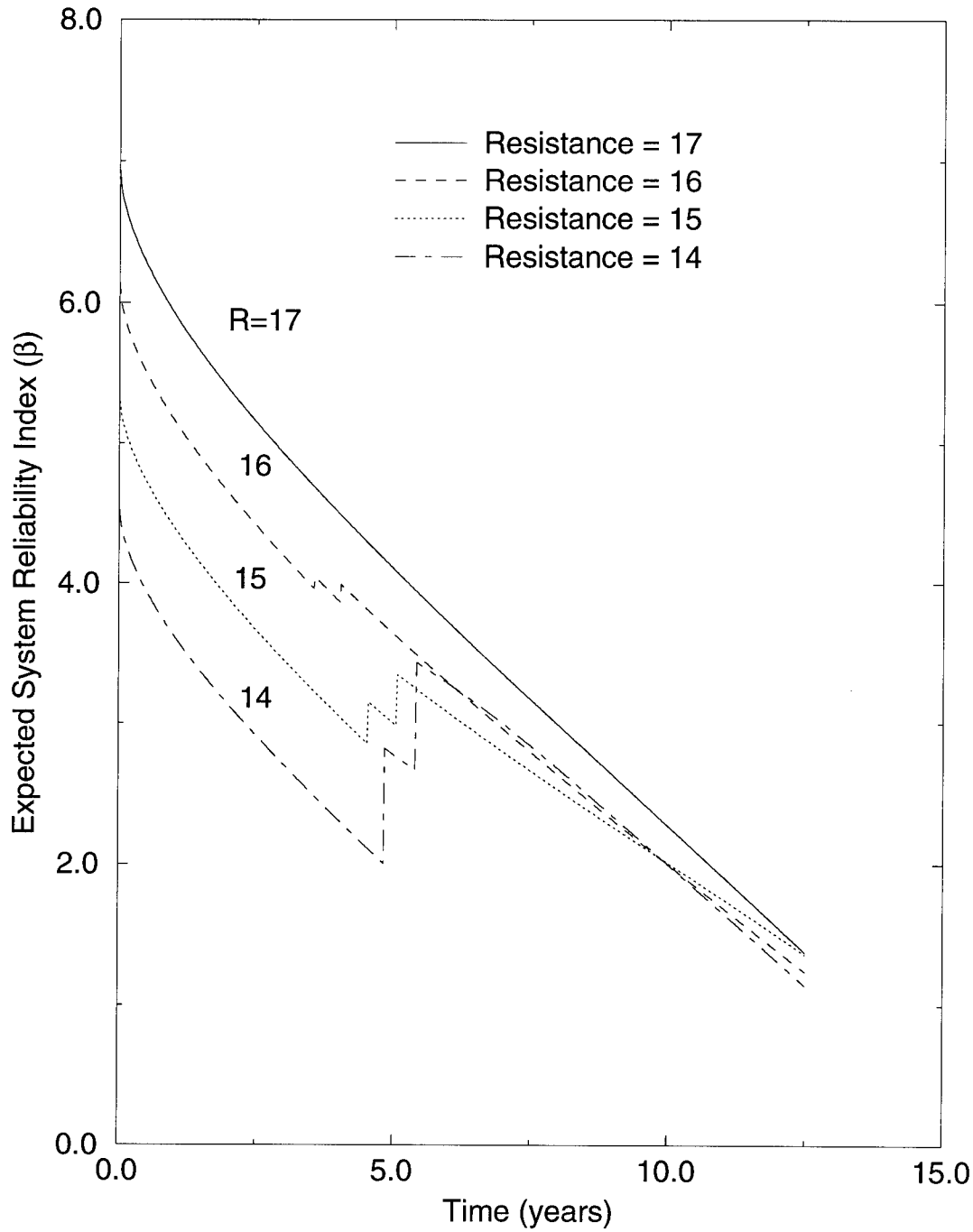

Figure 2.27: **Two Component Series System with Two Inspections, Inspection Technique C, Varying Mean Resistances**

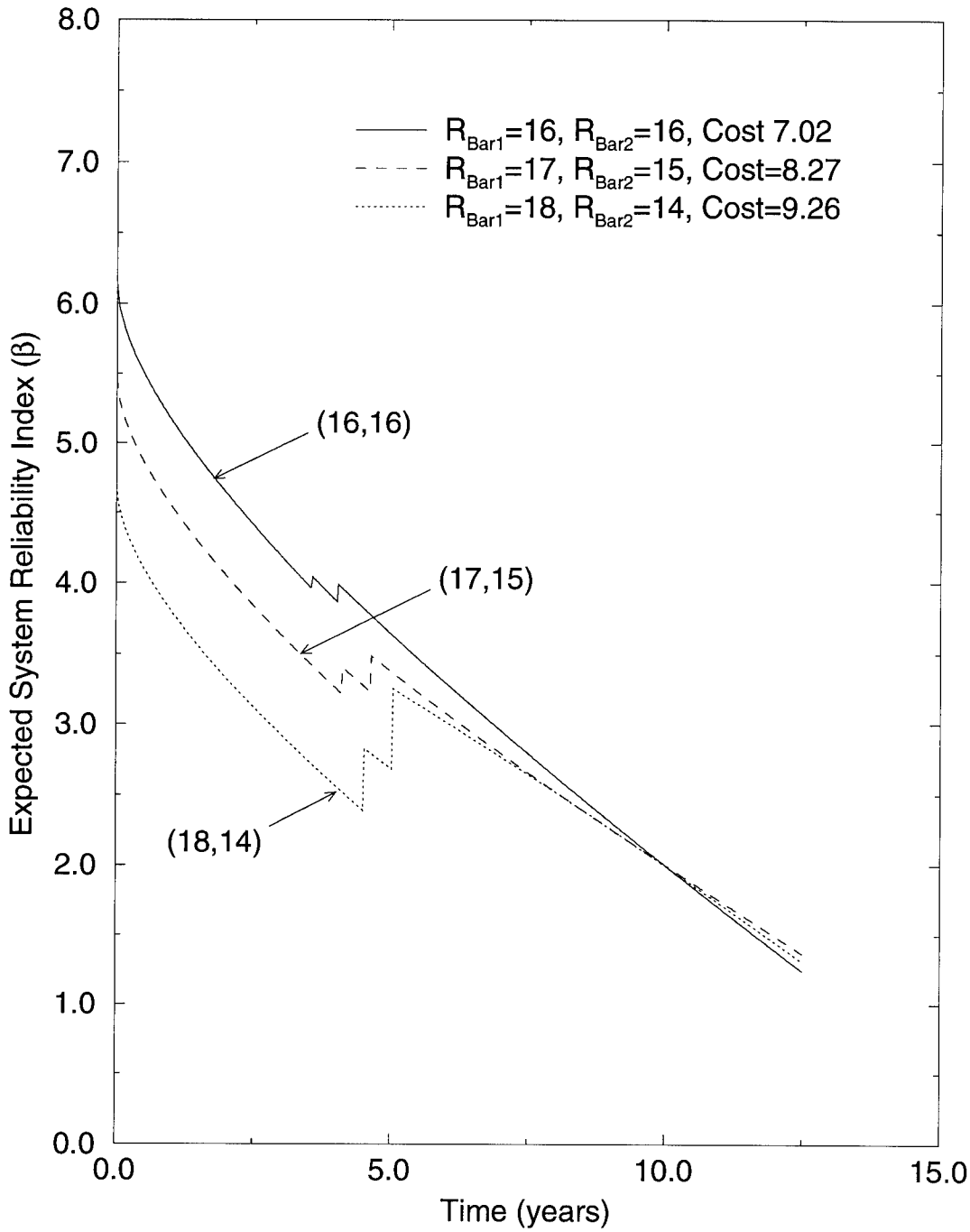

Figure 2.28: **Series System: Unequal Mean Bar Resistances, Two Inspections, Inspection Technique C**

2.6 Two-Bar Parallel System

The next structure to be analyzed is the two-bar parallel system. Whereas a series system is only as strong as its weakest member, a parallel system is at least as strong as its strongest member. A parallel structure does not fail until all of its members have failed. Figure 2.29 shows the two bar structure again subjected to a centric axial load. The load and area remain the same as in the previous examples (i.e., the load P is normally distributed ($\mu_P = 8.0$ and $\sigma_P = 0.8$) and the initial areas of the bars are $A_1 = A_2 = 1.0$). The mean value of the resistances were halved (i.e., $\mu_R = 7.0$ and $\sigma_R = 0.7$ for both bars) in order to make a fair comparison with the series and single component structures considered earlier. The coefficient of variation $\delta = 0.1$ was unchanged.

Fortunately, the nature of the problem is identical to that of the series system where the number of paths and methods for determining probability of repair and detection likelihood are exactly the same. The only difference is that the system reliability index is calculated for a parallel system. The force (P) is distributed to the two bars in relation to their stiffnesses which in this case is in proportion to their cross-sectional areas. The system is assumed to be ductile and again the resistances are assumed to be uncorrelated.

The system reliability index was determined using the system reliability program RELSYS which is described in the next chapter. RELSYS

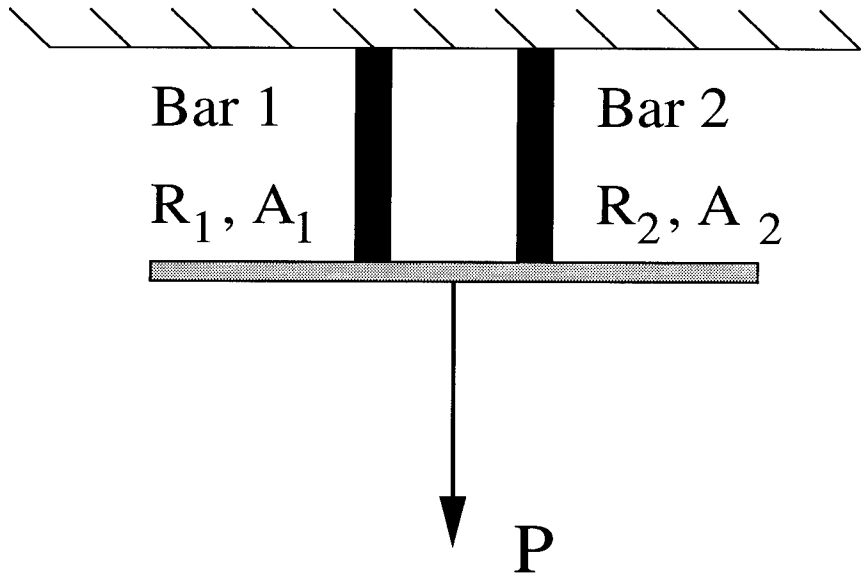

Figure 2.29: **Two Bar Parallel System**

was linked with the optimization program ADS to determine the optimum inspection strategy as described in Section 2.2.7.

Fig. 2.30 shows the costs for the two-inspection, two-bar parallel system for varying resistances and inspection techniques. Table 2.8 shows the optimum times and costs for different resistances using all four inspection techniques. The general trend is the same as that for the series and single component systems. The costs are similar and the same effects regarding cost differential and inspection quality still hold. Even though the resistances of the bars in the parallel system were halved relative to the series and single component structures, the parallel structure was still more reliable. Inspection techniques A and B provided answers with no violated constraints for mean resistances as low as R=6.0. Neither the single component or series structure

came close.

Table 2.8: **Optimum Inspection Strategy and Costs for Two Bar Parallel System with Two Lifetime Inspections**

Bar 1		Bar 2		Insp.	Time	Time	Total Cost
μ_R	σ_R	μ_R	σ_R	Tech.	t_1	t_2	C_{tot}
6.0	0.60	6.0	0.6	A	3.28	6.73	17.07
6.25	0.625	6.25	0.625	A	4.0	6.0	14.43
6.5	0.65	6.5	0.65	A	4.52	5.03	11.29
6.75	0.675	6.75	0.675	A	4.04	4.55	9.67
7.0	0.70	7.0	0.70	A	3.61	4.13	8.49
7.5	0.75	7.5	0.75	A	1.95	2.45	5.96
6.0	0.60	6.0	0.6	B	1.93	2.45	4.63
6.25	0.625	6.25	0.625	B	4.0	6.0	13.44
6.5	0.65	6.5	0.65	B	4.38	5.02	8.89
6.75	0.675	6.75	0.675	B	3.94	4.57	7.69
7.0	0.70	7.0	0.70	B	3.57	4.18	6.79
7.5	0.75	7.5	0.75	B	1.93	2.45	4.63
6.5	0.65	6.5	0.65	C	4.27	5.63	6.62
6.75	0.675	6.75	0.675	C	4.23	5.09	6.00
7.0	0.70	7.0	0.70	C	4.17	4.67	5.39
7.5	0.75	7.5	0.75	C	3.12	3.63	4.06
7.0	0.70	7.0	0.70	D	6.22	6.73	4.97
7.5	0.75	7.5	0.75	D	5.62	6.13	3.50

Fig. 2.31 looks at varying resistances for two inspections when the inspection technique is fixed – in this case, inspection technique B. The resistances are the same in both bars. The trend is the same as already observed for series and single component structures. As the resistance decreases, the mean time of inspection is later, the interval between inspections increases,

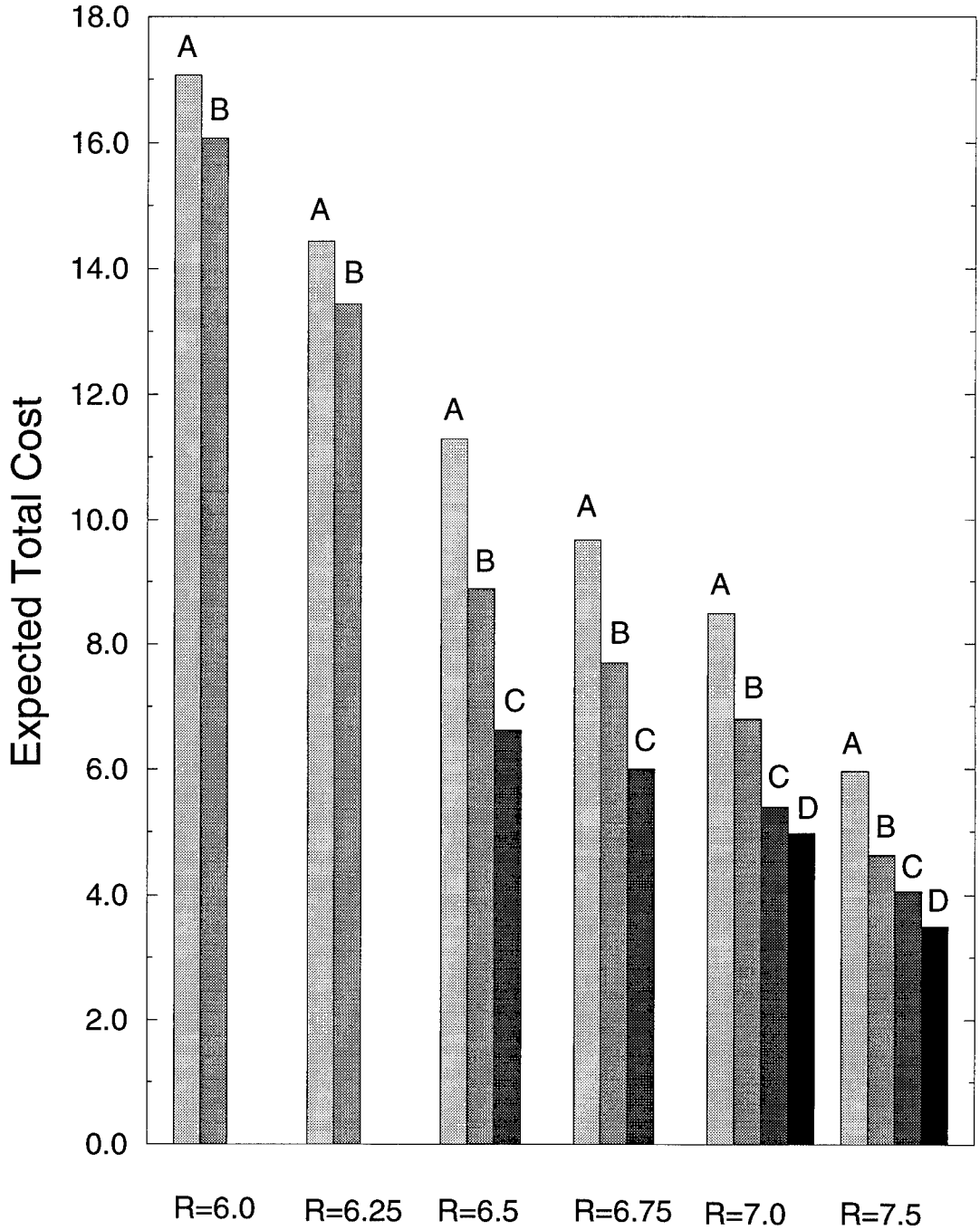

Figure 2.30: **Expected Total Costs for Techniques A, B, C, and D: Two-Bar Parallel Structure, Two Lifetime Inspections**

and the probability of making the repairs increases significantly.

Fig. 2.32 investigates the effect of unequal bar resistances. With a parallel system, it is expected that if the sum of the mean resistances of the bars are equal, the most unequal distribution will produce the most reliable structure. This is verified in Fig. 2.32 and Table 2.9 where the structure which has the highest probability of repair and the most costly inspection program occurs when R_{bar1}=6.0 and R_{bar2}=6.0. Totally opposite to the effect observed in the series structure, as the resistances become more unequal, the reliability of the structure increases and the cost of repair and maintenance drops considerably.

Table 2.9: **Optimum Inspection Strategy and Costs for Two-Bar Parallel System with Unequal Bar Resistances, Inspection Technique B**

Bar 1		Bar 2		Insp.	Time	Time	Total Cost
μ_R	σ_R	μ_R	σ_R	Tech.	t_1	t_2	C_{tot}
6.0	0.60	6.0	0.6	B	1.93	2.45	4.63
7.0	0.70	5.0	0.50	B	2.02	5.49	11.03
8.0	0.80	4.0	0.40	B	2.83	3.42	5.57
9.0	0.90	3.0	0.30	B	0.50	1.01	2.86

As a final comparison, Fig. 2.33 shows the results for an equivalent series, single component, and parallel system using two inspections and inspection technique B. As expected, the parallel system behaves much better than the single component system with only a small probability of repair early

in the life of the structure. The series system behaves worse than the single component system with a later mean inspection time and a higher probability of repair. If the bar failures were correlated, this effect would be diminished. If the member resistances were perfectly correlated, the three structures would be expected to produce results identical to those of the single component structure [Hendawi 1994].

While the model optimizes the timing of the inspections to minimize the total cost, it does not provide assistance in determining whether it is better to repair one member or both. And if only one member is to be repaired, which should it be? Understanding the system behavior of series and parallel structures would help in this decision. In a parallel system, it would be most beneficial to repair the strongest member. Conversely, in a series system, the reliability would be most improved by repairing the weakest member.

2.7 Conclusions

After minimizing the total cost of inspection and repair of simple series, parallel, and single component structures for several different inspection techniques, the following conclusions can be reached:

1. The method described herein has application primarily for those inspections which would be used in special cases and are sufficiently expensive to justify this kind of analysis. This method could also be justified for a choice between inexpensive inspection techniques which would be applied to a large number of bridges where a large total cost could be affected by the

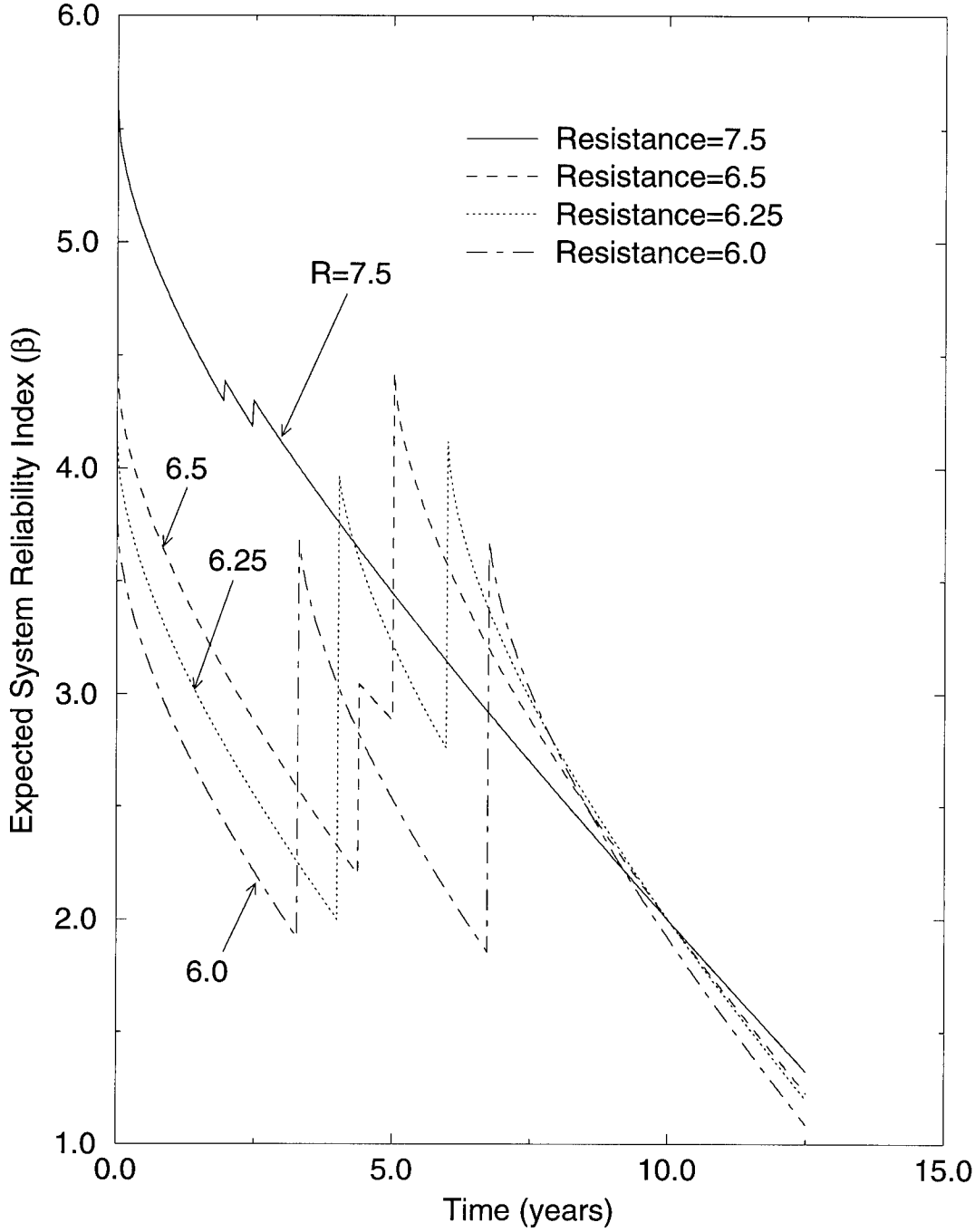

Figure 2.31: **Two Component Parallel System with Two Inspections, Inspection Technique B, Varying Mean Resistances,** $\delta_R = 0.10$

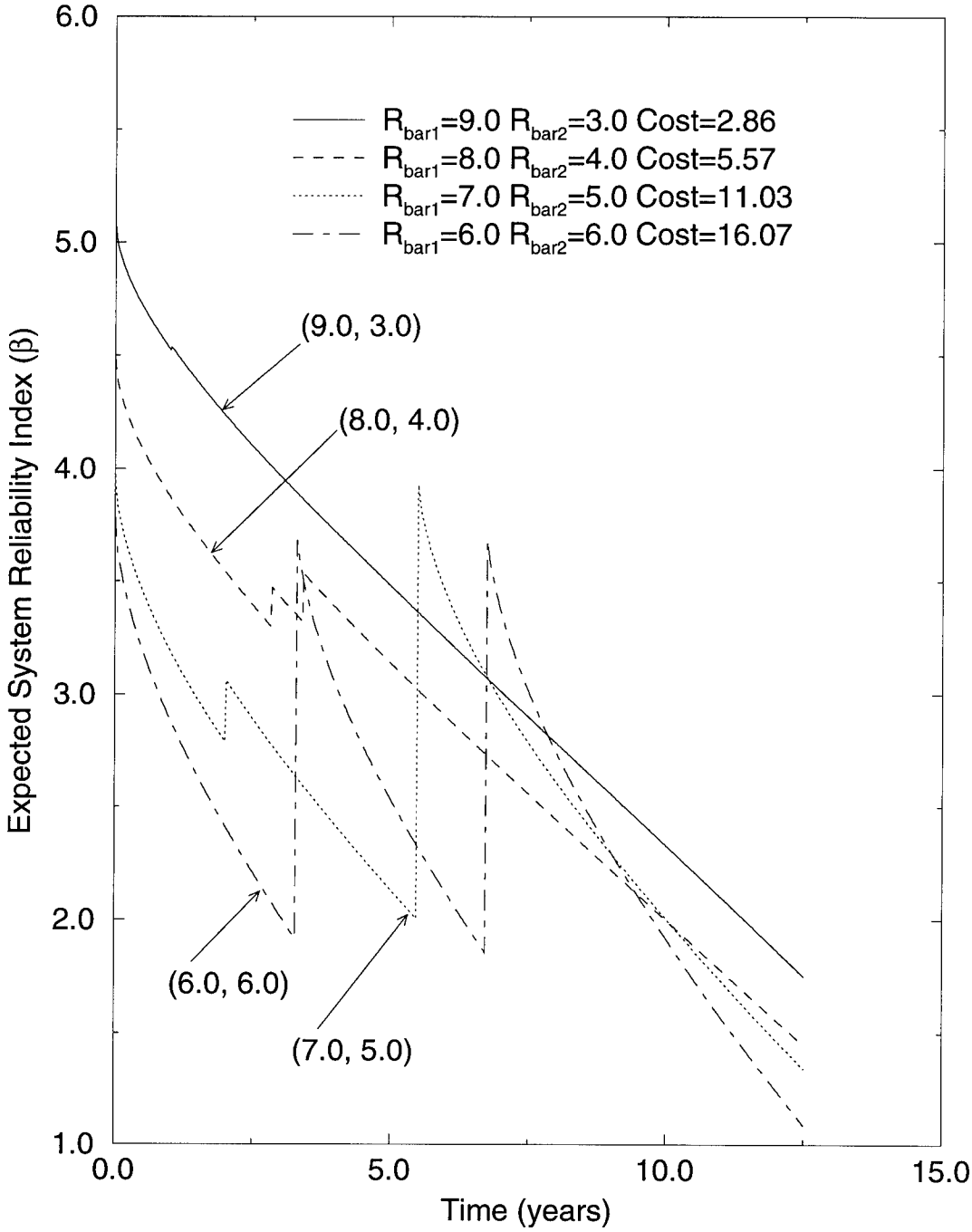

Figure 2.32: **Parallel System: Unequal Mean Bar Resistances, Two Lifetime Inspections, Inspection Technique B,** $\delta_R = 0.10$

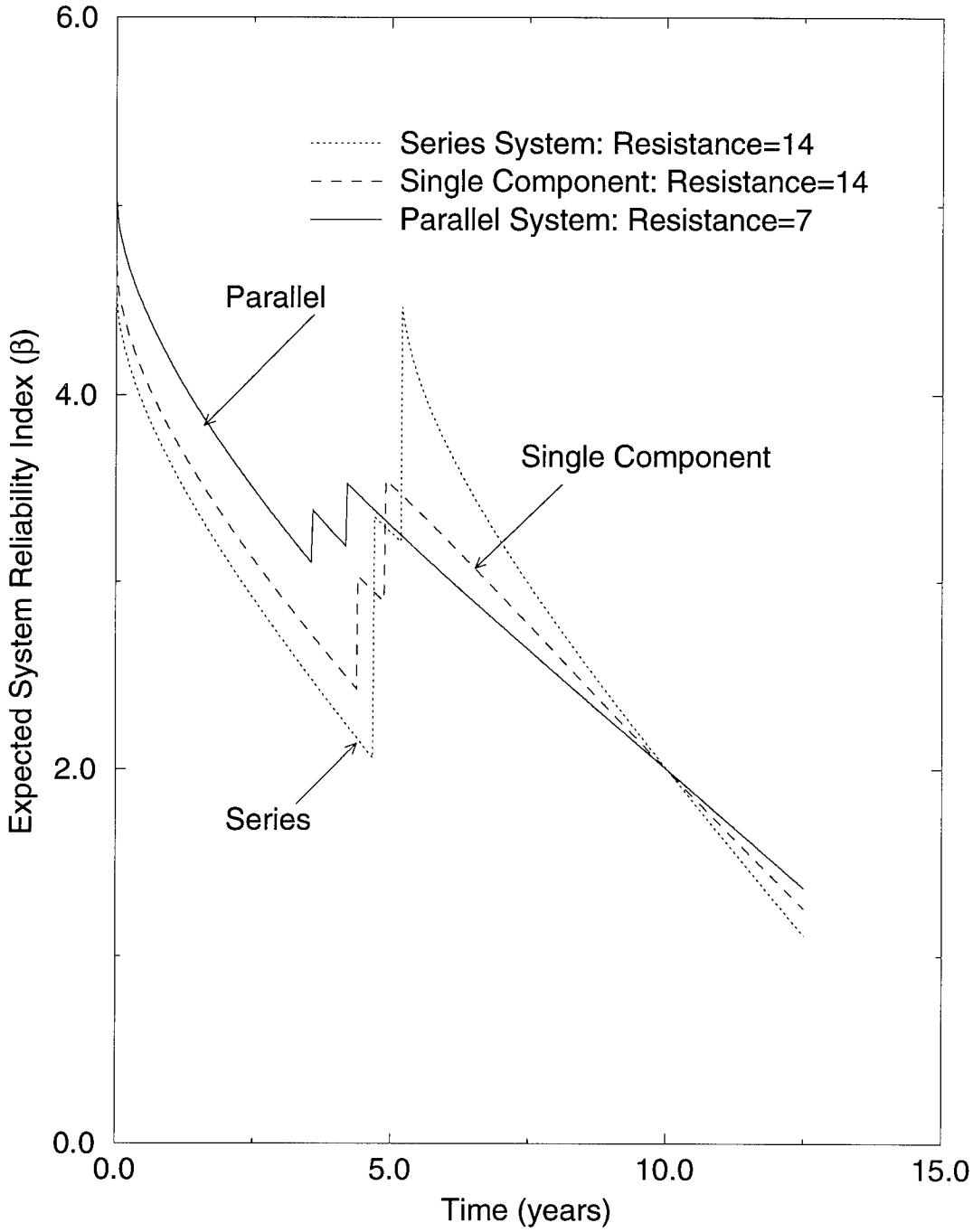

Figure 2.33: **Comparison of Parallel, Single Component, and Series System: Two Lifetime Inspections, Inspection Technique B**

result. The options at inspection points should be complete repair or no repair. Attempting to repair one member without repairing another complicated the problem considerably without contributing much to the solution. The analysis could be based on either the component or system reliability index. If the inspection is focusing on a specific defect, a component reliability analysis may be more appropriate.

2. By limiting the analysis to complete repair or no repair decisions, the number of possible branches is limited to 2^n where n is the number of lifetime inspections. Still a structure with 10 inspections, for example, would involve 1024 possibilities which becomes impractical. One suggested technique to reduce the number of branches is to eliminate any branch whose probability of occurrence is less than one percent of the probability of the largest branch [Thoft-Christensen and Sørensen 1987]. It is a good idea but programming the constraint would be a challenge. A different solution would be to shorten the time period over which the inspection program is being designed using fewer inspection periods and extrapolate to the larger desired time period.

3. The selection of an inspection technique is important. For the examples used in this chapter where the cost of inspection is relatively close to the cost of repair, one should choose the least expensive technique that will provide a solution but it is difficult to determine this in advance. For a structure where there exists a large probability of repair, a high quality technique should be chosen. The percent cost differential between techniques relative to the total inspection/repair cost is small and a bad selection will result in vio-

lated reliability constraints. If the probability of repair is small, a low quality technique should be chosen. The percent cost differential is significant between techniques and the chance of violating the reliability constraints by a poor selection is much less. This conclusion is not necessarily valid for cases where the cost of repair is several orders of magnitude larger than the cost of inspection.

4. For series, single component, and parallel systems, the total cost of inspection/repair rose as the mean resistance of the structure became less. As the resistance became less for the same inspection technique, the mean time of inspection was later in the life of the structure, the time interval between inspections became greater, and the probability of making repairs increased.

5. In general, for series, single component, and parallel systems, the total cost of inspection/repair dropped as the quality of the inspection diminished. There were some clear exceptions to this however. The mean times of inspection tended to be later in the life of the structure for the lower quality inspection techniques and the probability of needing repair sometimes was greater and sometimes was lower depending on the structure. For some structures, the poorer detectability was an advantage resulting in fewer repairs, while in others, the inability to detect defects caused greater repair costs later on. In some cases, the additional costs of repairs more than offset the savings in inspection cost.

6. The series structures were less reliable than the equivalent single component structure and required more repairs and a higher expected total

cost. The parallel structures were more reliable than the equivalent single component structure and demonstrated a lower probability of repair. The expected total cost associated with the parallel system was still higher than the single component system because there were more components in the structure. These differences in both the series and parallel structures would have been less if the resistances of the members had been correlated.

CHAPTER III

RELIABILITY OF SYSTEMS

3.1 Introduction

While it is desirable to consider the reliability of an entire structural system, this reliability can be quite difficult to calculate – which is the primary reason it has been neglected in the past. Numerous methods and approximate techniques exist which can accurately calculate the reliability of a single component with respect to a single failure mode. These include: first-order approximation (FORM) [Ang and Tang 1984], second-order approximation [Melchers 1987], directional simulation [Bjerager 1988], radial-space division method [Katsuki and Frangopol 1994], and discrete value methods [USACE 1992 and 1993]. Computer programs such as Radial Space Division [Katsuki 1995], CALREL [Liu *et al* 1989] and RELTRAN [Lee *et al* 1993] have employed these techniques. The same availability of methods and software does not exist for the system reliability problem. Other than Monte Carlo simulation programs such as CALREL and MCREL [Lin 1995], system reliability software is scarce. Monte Carlo simulation can be too time consuming for many applications. Without such a tool, calculating the system reliability of a highway bridge at various stages of its useful life would not be feasible. Commercially developed system reliability programs include PRADDS [Sϕrensen 1987a], PROBAN [Bjerager 1996], and STRUREL [Rackwitz 1996].

The purpose of this chapter is to introduce RELSYS (Reliability of Systems), a computer program which quickly calculates the reliability index for any structure which can be modeled as a combination of components in series and parallel. This chapter will cover the challenges involved in calculating system reliability, summarize the methods used by RELSYS for both component and system reliability, compare the results from RELSYS with those obtained by Monte Carlo simulation, discuss the strengths and limitations of the program, and suggest potential improvements. The User's Manual for RELSYS is in Appendix A and a complete program description including variable listings, subroutine descriptions, and a flowchart is in Appendix B.

3.2 Reliability and Failure

Engineers design structures to withstand the loads that will be placed on them. The designer's objective is to provide, with a very high degree of certainty, a structure that will perform as intended. This section addresses how that degree of certainty can be calculated.

An individual structural member is considered safe or reliable when the strength, resistance, or capacity of the member exceeds the demand or the load acting on it. There will most likely be a degree of uncertainty associated with the strength or resistance (R) of the member and the load (L). If the designer has some knowledge about the random nature of R and L, the uncertainty can be quantified and evaluated. If the probability density functions are known or can be accurately estimated, then the reliability or probability

of safe performance (P_s) can be expressed as:

$$P_s = P(R > L) = P(R - L > 0) = \int\int_{R>L} f_{R,L}(r,l)drdl \tag{3.1}$$

where $f_R(r)$ and $f_L(l)$ are the probability density functions of R and L and $f_{R,L}(r,l)$ is their joint probability density function.

If R and L are independent, then Fig. 3.1 illustrates the probability of failure for the individual component member. If an incremental load value dl is considered, the probability of the load value falling into the interval dl and the strength value simultaneously exceeding the load value at that point gives the reliability of that segment dP_s which can be expressed as [Rao, 1992]:

$$dP_s = f_L(l)dl \int_l^{\infty} f_R(r)dr = f_L(l)dl[1 - F_R(l)] \tag{3.2}$$

where: F_R represents the cumulative distribution function of R and $F_R(l)$ is indicated as area A_r in Fig. 3.1. The term, $f_L(l)dl$, is represented by area A_l.

Since the reliability of the member involves the probability of the strength exceeding the load, the total reliability (P_s) of the member is expressed as:

$$P_s = \int dP_s = \int_{-\infty}^{\infty} f_L(l)[\int_l^{\infty} f_R(r)dr]dl = \int_{-\infty}^{\infty} f_L(l)[1 - F_R(l)]dl \tag{3.3}$$

Failure is defined as the probability that the member will not survive. This means that the probability of failure (P_f) can be expressed as:

$$P_f = 1 - P_s = 1 - P(R \geq L) = \int_{-\infty}^{\infty} f_L(l)F_R(l)dl \tag{3.4}$$

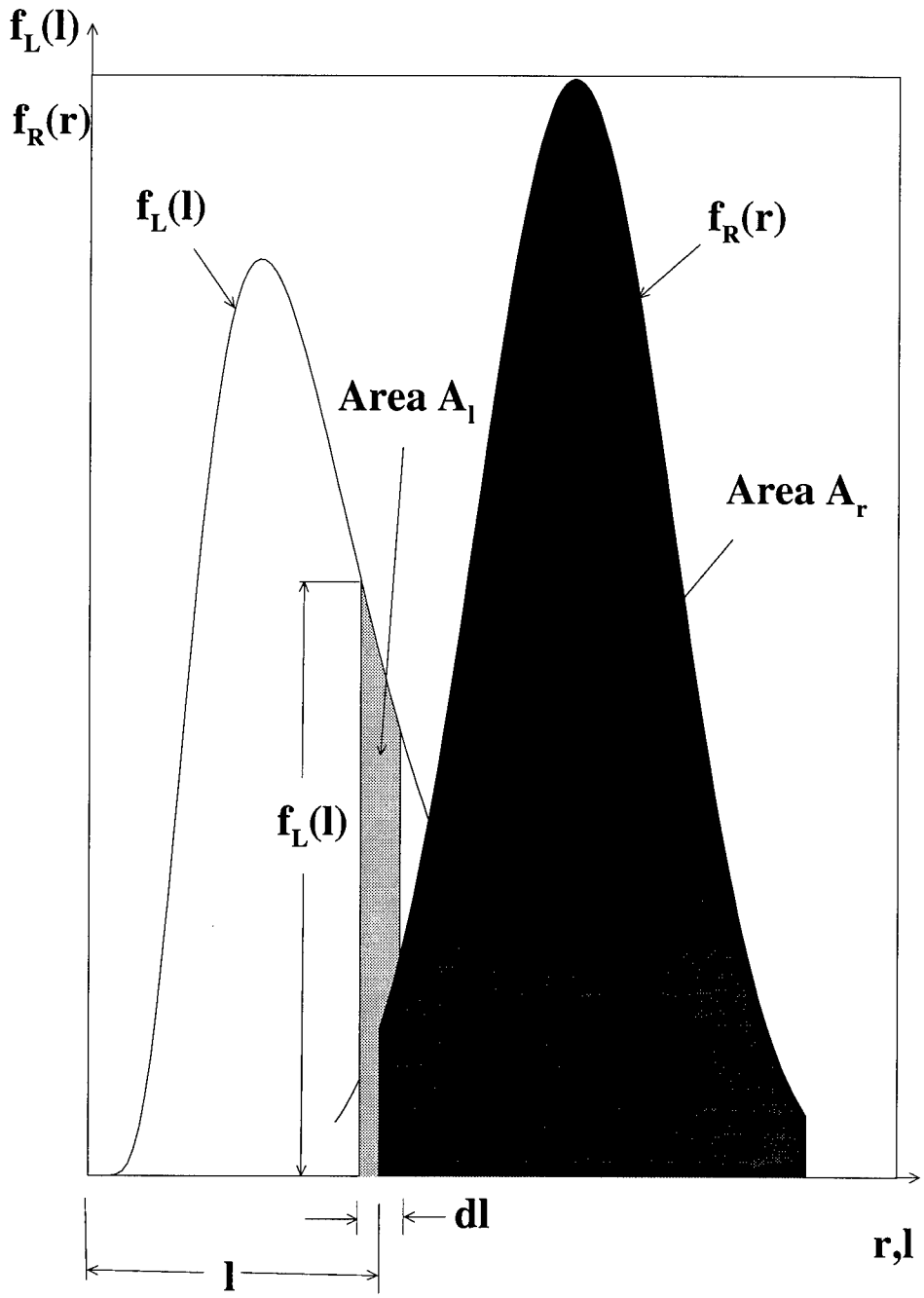

Figure 3.1: **Differential Reliability of a Structure Based on the Distributions of the Load and Resistance**

The failure probability is often computed from the reliability index β.

$$P_f = \Phi(-\beta) \tag{3.5}$$

where Φ is the distribution function of the standard normal variate. If R and L are uncorrelated, the reliability index β of the member can be determined by:

$$\beta = \frac{\mu_g}{\sigma_g} = \frac{\mu_{R-L}}{\sigma_{R-L}} = \frac{\mu_R - \mu_L}{\sqrt{\sigma_R^2 + \sigma_L^2}} \tag{3.6}$$

The reliability index graphically depicts the shortest distance from the origin to a failure surface in standard normal space defined by $f(r, l) = r - l = 0$. A first-order approximate solution is based on this definition of β.

3.3 Limit state functions

A reliability problem may be a function of many random variables other than just resistance R and load L. The generalized structural reliability problem is formulated in terms of a vector of basic random variables of the structural system, $\mathbf{X} = \{X_1, X_2, ..., X_n\}^T$, where $X_1, X_2, ..., X_n$ are basic random variables that may describe loads, structural component dimensions, material characteristics, and section properties. A limit state function, $g(\mathbf{X})$=0, describes the performance of the structural system in terms of the basic random variables, $\mathbf{X}$; and defines the failure surface which separates the survival region from the failure region. It follows that

$$g(\mathbf{X}) > \mathbf{0} \text{ defines the "survival or safe region"} \tag{3.7}$$

$$g(\mathbf{X}) \leq \mathbf{0} \text{ defines the "failure region"} \tag{3.8}$$

If the joint probability distribution function of the design variables $X_1, X_2, ..., X_n$ is $f_{X_1,X_2,...,X_n}(X_1, X_2, ..., X_n)$, the probability of the safe state is

$$P_s = \int \cdots \int_{g(\mathbf{X})>\mathbf{0}} f_{X_1,X_2,...,X_n}(X_1, X_2, ..., X_n) dx_1 \ldots dx_n \tag{3.9}$$

which may be written as

$$P_s = \int_{g(\mathbf{X})>\mathbf{0}} f_{\mathbf{X}}(\mathbf{x}) \mathbf{dx} \tag{3.10}$$

where Eq. 3.10 represents the volume integral of $f_{\mathbf{X}}(\mathbf{x})$ over the safe region $g(\mathbf{X}) > \mathbf{0}$. Conversely, the failure probability would be the corresponding volume integral over the failure region

$$P_f = \int_{g(\mathbf{X})<\mathbf{0}} f_{\mathbf{X}}(\mathbf{x}) \mathbf{dx} \tag{3.11}$$

The integral describing the joint distribution $g(\mathbf{X})$ can easily become too complex to solve directly. Approximate techniques are developed to approximate this convolution integral and solve for structural reliability. This study uses a first-order reliability method (FORM) to search for and approximate the shortest distance between the origin and the limit state surface $g(\mathbf{X}) = \mathbf{0}$ in the reduced space of standard normal variates.

3.4 First Order Reliability Method (FORM)

In the First Order Reliability Method (FORM), the limit state function at any point is approximated by a first-order Taylor series expansion about that point. This creates a straight line which is tangent to the limit state function at the point of interest. The minimum distance β from the origin to this

line is:

$$\beta = \frac{\mu_g}{\sigma_g} = \frac{\sum_{i=1}^{n} U_i^* (\frac{\partial g}{\partial U_i^*})}{\sqrt{\sum_{i=1}^{n} (\frac{\partial g}{\partial U_i^*})^2}} \tag{3.12}$$

where $(U_1^*, U_2^*, \ldots, U_n^*)$ is the most probable failure point and the derivatives $(\partial g / \partial U_i^*)$ are evaluated at this same point.

Based on the user's guess for the most probable point of failure, the method involves an iterative search which relies on the gradients of the limit state function at the point of failure and the direction cosines to find this minimum distance. The detailed theory behind the FORM approach is presented in Ang and Tang [1984]. This iterative process is best illustrated by an example.

3.4.1 Example of FORM

Given the limit state equation, $g(\mathbf{X}) = g(X_1, X_2) = 2X_1^2 - 2X_2 = 0$, the reliability index can be calculated by finding the minimum distance from the origin in standard normal space to the failure surface described by $g(\mathbf{X})$. The limit state equation $g(\mathbf{X})$ is in the original space which will be denoted as the x-space. The minimum distance in question is found in the standard normal or reduced space, hereafter referred to as the u-space. Let us assume that the variable X_1 is normally distributed with a mean value $\mu_{X_1} = 2.0$ and a standard deviation $\sigma_{X_1} = 0.2$ which can be expressed as $X_1 = N[2.0, 0.2]$. The parameters for X_2 are $N[3.0, 0.3]$. With these uncorrelated, normally distributed variables, the transformation equation from the original space x to

the reduced space u is:

$$U_i = \frac{X_i - \mu_{X_i}}{\sigma_{X_i}} \qquad i = 1, 2, \ldots, n \tag{3.13}$$

In terms of the reduced variates, U_i, the limit state would be

$$g(\mathbf{X}) = g(\sigma_{X_1} U_1 + \mu_{X_1}, \ldots, \sigma_{X_n} U_n + \mu_{X_n}) = 0 \tag{3.14}$$

or in matrix form

$$\mathbf{X} = [\sigma_X]\mathbf{U} + \mu_X \tag{3.15}$$

where $\mathbf{U} = \{U_1, U_2, ..., U_n\}^T$, $\mu_X = \{\mu_{X_1}, \mu_{X_2}, ..., \mu_{X_n}\}^T$, and

$$[\sigma_X] = \begin{pmatrix} \sigma_{X_1} & 0 & \cdots & 0 \\ 0 & \sigma_{X_2} & \cdots & 0 \\ \vdots & \vdots & \ddots & \vdots \\ 0 & 0 & \cdots & \sigma_{X_n} \end{pmatrix} \tag{3.16}$$

The limit state equation $g(\mathbf{X}) = 0$ could be transformed directly to the u-space using Eq. 3.13 to obtain $g(\mathbf{U}) = 0$

$$g(\mathbf{X}) = 0.133U_1^2 + 2.67U_1 - U_2 + 3.33 = 0 \tag{3.17}$$

The algorithm is structured, however, so that the transformation from the x-space to the u-space is never explicitly made. This allows for computer code where the problem and the solution are provided in the original x-space and the user is not aware of the existence of the u-space. The algorithm uses the Direct Derivation approach developed by Lee [1994] which was originally incorporated into the program RELTRAN [Lee *et al.* 1993]. The method simultaneously

iterates to find the optimal search direction and ensures that the failure point is on the failure surface. The method also allows the user to express the limit state equation in its original x-space form.

Using the stated example problem, this iterative FORM approach proceeds as follows:

1) For each random variable, make an initial guess of the most probable point of failure in the original space (X_i^*). Usually the mean value is a reasonable starting guess. For purposes of illustrating the convergence process, this example will make an intentionally bad initial guess. Therefore, let $X_1^* = 6.0$ and $X_2^* = 0.5$.

2) Calculate the gradient with respect to each random variable $\partial g/\partial X_i^*$ based on the initial guess value. The gradient will establish the search direction for this iteration.

$$\begin{aligned}
\partial g/\partial X_1 &= 4X_1 \\
\partial g/\partial X_1^* &= 4X_1^* = 4(6) = 24 \\
\partial g/\partial X_2 &= -2 \\
\partial g/\partial X_2^* &= -2
\end{aligned}$$

3) Calculate the gradients in the reduced space.

$$\begin{aligned}
\partial g/\partial U &= \partial g/\partial X(\partial X/\partial U) \quad where: \; X = \sigma_x U + \mu_x \;\; and \; \partial X/\partial U = \sigma_x \\
\partial g/\partial U &= \partial g/\partial X(\sigma_x) \\
\partial g/\partial U^* &= \partial g/\partial X^*(\sigma_x)
\end{aligned}$$

$$\partial g/\partial U_1^* = \partial g/\partial X_1^*(\sigma_{x_1}) = 24(0.2) = 4.8$$

$$\partial g/\partial U_2^* = \partial g/\partial X_2^*(\sigma_{x_2}) = -2.0(0.3) = -0.6$$

4) Compute $\Delta\beta$ based on Taylor series expansion about U^*.

$$\Delta\beta = \frac{g_x(X^*)}{\sqrt{\sum(\frac{\partial g}{\partial U^*})^2}}$$

$$g_x(X^*) = 2X_1^{*^2} - 2X_2^* = 2.0(6.0)^2 - 2.0(0.5) = 71$$

$$\sqrt{\sum(\frac{\partial g}{\partial U^*})^2} = \sqrt{(\frac{\partial g}{\partial U_1^*})^2 + (\frac{\partial g}{\partial U_2^*})^2} = \sqrt{4.8^2 + (-0.6)^2} = 4.837$$

$$\Delta\beta = 71/4.837 = 14.68$$

5) Compute the updated reliability index β_{new}.

$$\beta_{new} = \beta_{old} + \Delta\beta = 0.0 + 14.68 = 14.68$$

6) Compute the direction cosines, α_{g_1,u_1}.

$$\alpha_{g_1,u_1} = \frac{\partial g/\partial U_i}{\sqrt{\sum_{i=1}^{n}(\frac{\partial g}{\partial U_i^*})^2}}$$

$$\alpha_{1,1} = \frac{\partial g/\partial U_1^*}{\sqrt{(\frac{\partial g}{\partial U_1^*})^2 + (\frac{\partial g}{\partial U_2^*})^2}} = 4.8/4.837 = .9923$$

$$\alpha_{1,2} = -0.6/4.837 = -.1240$$

7) Compute the new failure point in the reduced space, U_i^*.

$$U_i^* = -\alpha_{g1,i}\beta$$

$$U_1^* = -\alpha_{1,1}\beta = -.9923(14.86) = -14.68$$

$$U_2^* = -\alpha_{1,2}\beta = -(-.1240)(14.86) = 1.82$$

8) Compute the new failure point in the original space, X_i^*.

$$X_1^* = \mu_{X_1} + u_1^* \sigma_{x_1} = 2 + (-14.68)(0.2) = -.9128$$

$$X_2^* = \mu_{X_2} + u_2^* \sigma_{x_2} = 3 + 1.82(0.3) = 3.546$$

9) Let $\epsilon = .00001$. Substitute the new failure points X_1^* and X_2^* into the limit state equation $g(\mathbf{X})$. If $\mid g(\mathbf{X}^*) \mid < \epsilon$, then the iteration is complete and the solution has converged. If not, perform another iteration using the new values of X_1^* and X_2^*.

In this case, the solution did not converge and ten more iterations were necessary. On the eleventh iteration, the value for $\mid g(\mathbf{X}^*) \mid$ was less than 0.00001 and the solution was sufficiently precise. Table 3.1 shows the values for these iterations. Figs. 3.2 and 3.3 show the iterations graphically in the reduced and original spaces, respectively. After the eighth iteration, the changes were too small to be shown on the graphs. The final reliability index was $\beta = 1.2317$. The program RELSYS uses this method to compute reliability indices. This problem is Example 1 in the RELSYS User's Manual in Appendix A.

3.5 Correlation

The random variables in the limit state equation may be correlated meaning that a linear relationship exists which relates the behavior of one random variable to another. This relationship can affect the overall behavior of the failure component. One measure of this relationship between two random variables X_1 and X_2 is the covariance $cov(X_1, X_2)$ which is denoted by

Table 3.1: **Iterative FORM Solution for $g(\mathbf{X}) = 2X_1^2 - 2X_2 = 0$ Where X_1=N[2.0, 0.2] and X_2=N[3.0,0.3]**

Iter.	Step (2)		Step (3)		Step (4)		Step (5)
Num.	$\partial g/\partial X_1^*$	$\partial g/\partial X_2^*$	$\partial g/\partial U_1^*$	$\partial g/\partial U_2^*$	$g(X^*)$	$\Delta\beta$	β_{new}
1	24.0	-2.0	4.80	-0.60	71.0	14.68	14.68
2	-3.65	-2.0	-0.73	-0.60	-5.426	-5.74	8.94
3	13.52	-2.0	2.70	-0.60	13.458	4.85	13.79
4	-2.77	-2.0	-0.55	-0.60	-6.831	-8.36	5.43
5	10.95	-2.0	2.19	-0.60	6.597	2.91	8.34
6	1.57	-2.0	0.31	-0.60	-7.016	-10.37	-2.03
7	8.75	-2.0	1.75	-0.60	4.649	2.51	0.49
8	7.63	-2.0	1.53	-0.60	1.186	0.72	1.21
9	7.10	-2.0	1.42	-0.60	0.035	0.02	1.23
10	7.09	-2.0	1.42	-0.60	-6E-04	0.00	1.23
11	7.09	-2.0	1.42	-0.60	-1E-07	0.00	1.23

Iter.	Step (6)		Step (7)		Step (8)	
Num.	$\alpha_{1,1}$	$\alpha_{1,2}$	U_1^*	U_2^*	X_1^*	X_2^*
1	0.9923	-0.1240	-14.56	1.82	-0.91	3.55
2	-0.7727	-0.6348	6.90	5.67	3.38	4.70
3	0.9763	-0.2166	-13.47	2.99	-0.69	3.90
4	-0.6788	-0.7342	3.69	3.99	2.74	4.20
5	0.9644	-0.2643	-8.04	2.20	0.39	3.66
6	0.4626	-0.8866	0.94	-1.80	2.19	2.46
7	0.9459	-0.3243	-0.46	0.16	1.91	3.05
8	0.9307	-0.3658	-1.12	0.44	1.77	3.13
9	0.9211	-0.3892	-1.13	0.48	1.77	3.17
10	0.9210	-0.3896	-1.13	0.48	1.77	3.17
11	0.9210	-0.3896	-1.13	0.48	1.77	3.17

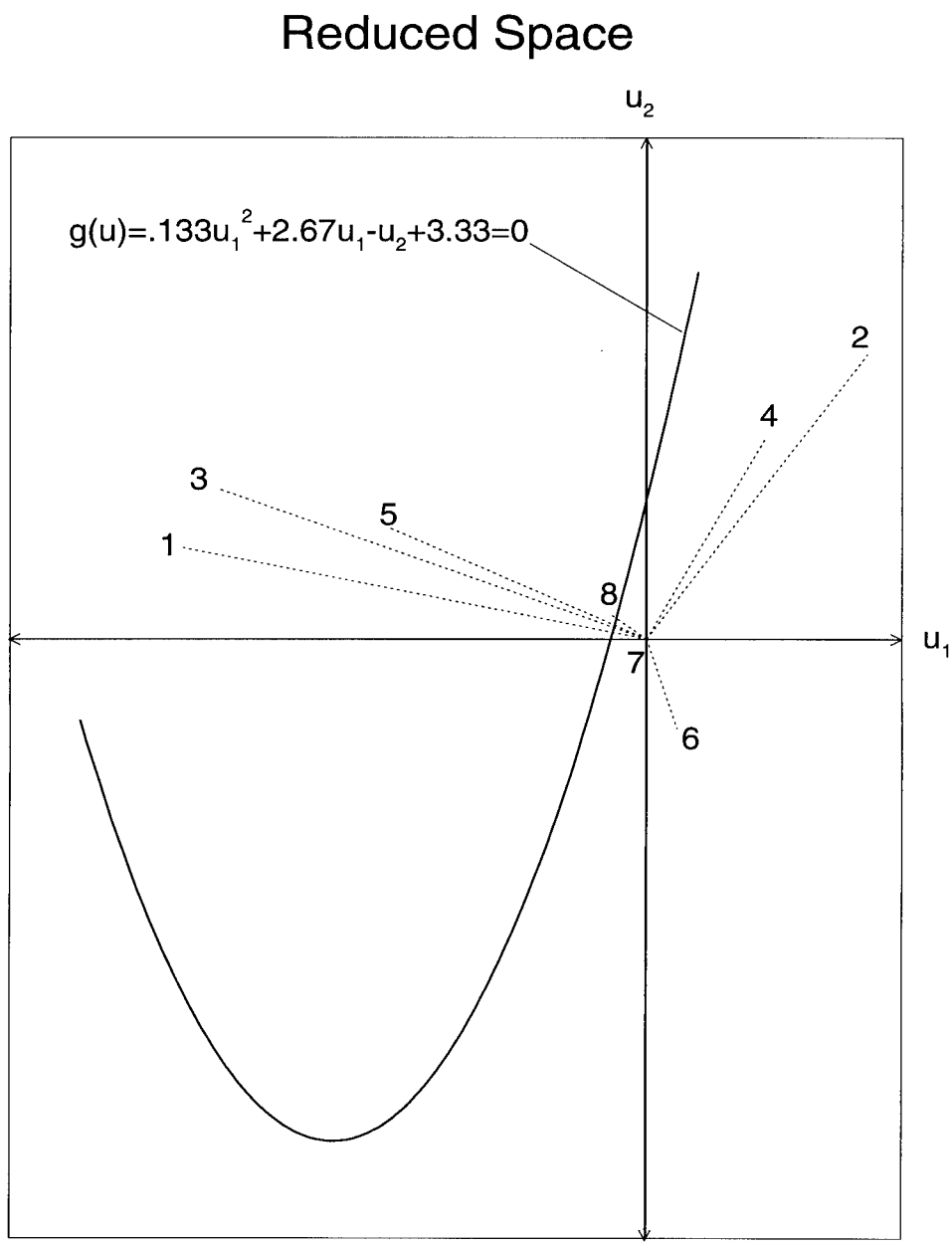

Figure 3.2: **Results of FORM Iterations in the Reduced Space**

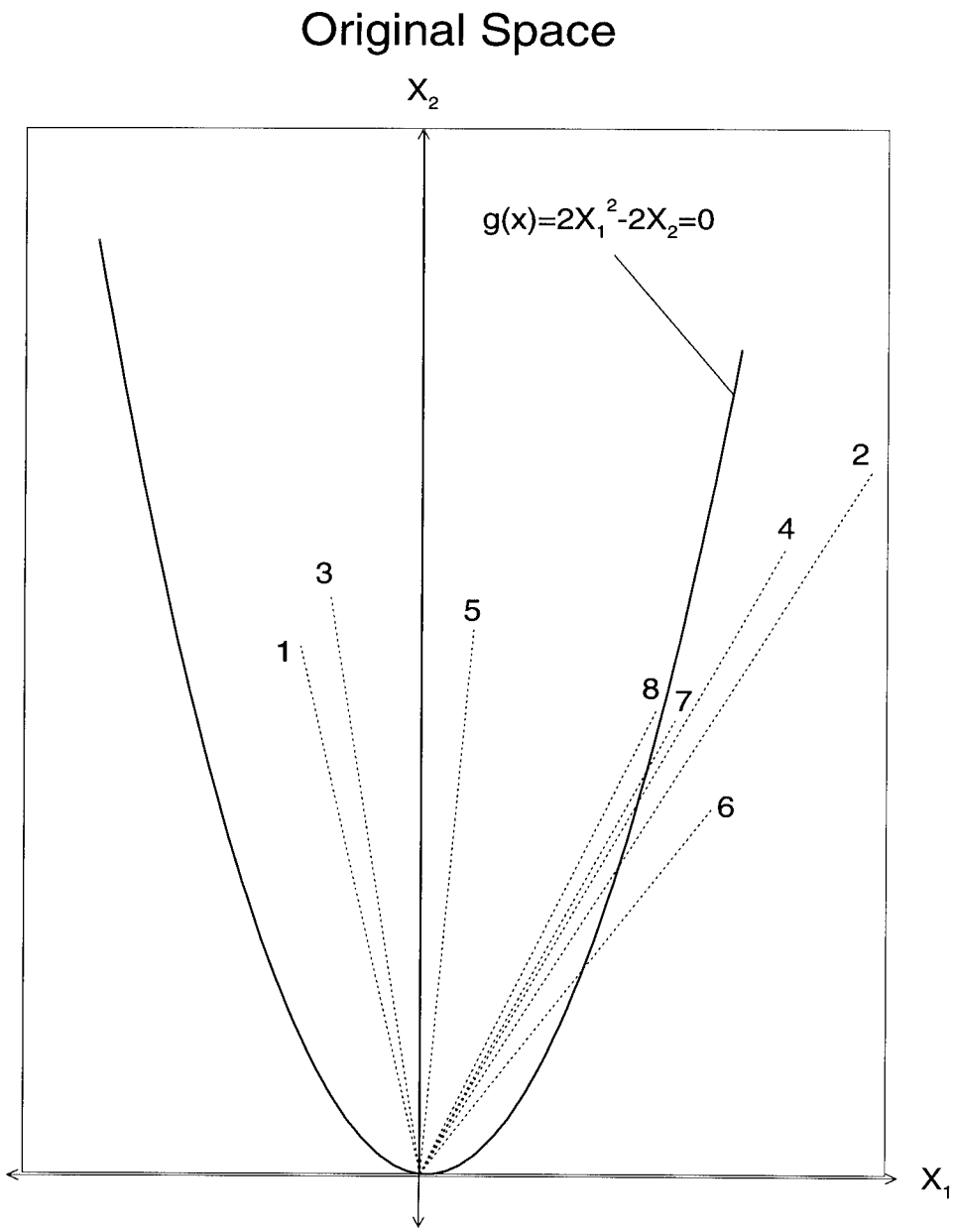

Figure 3.3: **Results of FORM Iterations in the Original Space**

[Benjamin and Cornell 1970]:

$$cov(X_1, X_2) = \int_{-\infty}^{\infty} \int_{-\infty}^{\infty} (x_1 - \mu_{X_1})(x_2 - \mu_{X_2}) f(x_1, x_2) dx_1 dx_2 \tag{3.18}$$

where $f(x_1, x_2)$ is the joint probability distribution of X_1 and X_2. It is often preferable to use the normalized form of the covariance which is called the correlation coefficient ($\rho_{X_1 X_2}$) where:

$$\rho_{X_1 X_2} = \frac{cov(X_1, X_2)}{\sigma_{X_1} \sigma_{X_2}} \tag{3.19}$$

The values for ρ range from $-1 \leq \rho \leq +1$. A value of $+1$ would indicate a perfect linear relationship between the variables X_1 and X_2. If X_1 were to increase by a specific amount, we could predict exactly how much X_2 would rise. If $\rho_{X_1,X_2} = 0$, the variables X_1 and X_2 are statistically independent and the behavior of one variable offers no basis for predicting the behavior of the other. Perfect negative correlation is indicated by $\rho_{X_1,X_2} = -1$. If X_1 were to increase by a certain amount, one could predict exactly how much X_2 would decrease. Values of ρ between these extremes indicate that the degree of linear relationship between the variables is somewhere between these extremes.

All correlation values ρ_{ij} between all random variables can be collected in a symmetric correlation matrix ρ

$$\rho = \begin{pmatrix} \rho_{11} & \rho_{12} & \cdots & \rho_{1n} \\ \rho_{21} & \rho_{22} & \cdots & \rho_{2n} \\ \vdots & \vdots & \ddots & \vdots \\ \rho_{n1} & \rho_{n2} & \cdots & \rho_{nn} \end{pmatrix} \tag{3.20}$$

where $\rho_{ij} = \rho_{ji}$ and $\rho_{ii} = 1.0$.

3.5.1 FORM with Random Variable Correlation

The FORM algorithm described in Section 3.4.1 can be modified to accommodate random variable correlation by introducing an addition transformed space, the y-space. The x-space is the original space in which the problem is formed, the u-space is the correlated reduced standard normal space, and the y-space is the uncorrelated reduced standard normal space. The reliability index β is the shortest distance from the origin to the failure surface $g(\mathbf{Y}) = 0$ in the uncorrelated, reduced standard normal y-space where $\mathbf{Y} = \{Y_1, Y_2, ..., Y_n\}^T$. The solution procedure is the same except that an additional transformation is required from the u-space to the y-space.

The transformation from the u-space to the y-space is made through a transformation matrix $\mathbf{T}$ such that

$$\mathbf{Y} = \mathbf{T}^T\mathbf{U} \quad and \quad \mathbf{U} = \mathbf{TY} \tag{3.21}$$

where $\mathbf{T}$ is an orthogonal matrix composed of the eigenvectors corresponding to the correlation matrix ρ. Using this transformation, Eq. 3.15 becomes

$$\mathbf{X} = [\sigma_X]\mathbf{TY} + \mu_X \tag{3.22}$$

Consider, for example, a limit state equation with three random variables X_1, X_2, and X_3. The correlation between these random variables would be included in a 3x3 correlation matrix $[\rho]$. From this correlation matrix, three eigenvalues λ_1, λ_2, and λ_3 are computed. From λ_1, the corresponding

normalized eigenvector $\mathbf{\Phi}_1 = \{\phi_{11}, \phi_{12}, \phi_{13}\}^T$ is computed. Similarly, λ_2 and λ_3 produce $\mathbf{\Phi}_2 = \{\phi_{21}, \phi_{22}, \phi_{23}\}^T$ and $\mathbf{\Phi}_3 = \{\phi_{31}, \phi_{32}, \phi_{33}\}^T$, respectively. The transformation matrix $\mathbf{T}$ would be

$$\mathbf{T} = \begin{pmatrix} \phi_{11} & \phi_{21} & \phi_{31} \\ \phi_{12} & \phi_{22} & \phi_{32} \\ \phi_{13} & \phi_{23} & \phi_{33} \end{pmatrix} \tag{3.23}$$

Using Eq. 3.22, the failure points in the original x-space (X_1^*, X_2^*, X_3^*) are computed from the failure points in the y-space (Y_1^*, Y_2^*, Y_3^*) as

$$\begin{aligned} X_1^* &= Y_1^*\sigma_1\phi_{11} + Y_2^*\sigma_1\phi_{21} + Y_3^*\sigma_1\phi_{31} \\ X_2^* &= Y_1^*\sigma_2\phi_{12} + Y_2^*\sigma_2\phi_{22} + Y_3^*\sigma_2\phi_{32} \\ X_3^* &= Y_1^*\sigma_3\phi_{13} + Y_2^*\sigma_3\phi_{23} + Y_3^*\sigma_3\phi_{33} \end{aligned} \tag{3.24}$$

Step 3 in the algorithm in Section 3.4.1 requires computing the gradients in the reduced space. These gradients in the y-space $\partial g/\partial Y_i$ are

$$\partial g/\partial Y_i = \sum_{j=1}^{n} \partial g/\partial U_j(\partial U_j/\partial Y_i) = \sum_{j=1}^{n} \sigma_{X_j}(\partial g/\partial X_j)\partial U_j/\partial Y_i \tag{3.25}$$

Using the same limit state equation with three random variables and Eqs. 3.21 and 3.25, the first gradient in y-space $\partial g/\partial Y_1$ is

$$\begin{aligned} \partial g/\partial Y_1 &= \sigma_1(\partial g/\partial X_1)\partial U_1/\partial Y_1 + \sigma_2(\partial g/\partial X_2)\partial U_2/\partial Y_1 + \sigma_3(\partial g/\partial X_3)\partial U_3/\partial Y_1 \\ \partial g/\partial Y_1^* &= \sigma_1(\partial g/\partial X_1^*)\phi_{11} + \sigma_2(\partial g/\partial X_2^*)\phi_{12} + \sigma_3(\partial g/\partial X_3^*)\phi_{13} \end{aligned} \tag{3.26}$$

All other steps shown in Section 3.4.1 remain the same.

3.5.2 Uncorrelated Non-Normal Variables

The transformation from the x-space to the u-space for a normally distributed variable was shown in Eq. 3.13. Most variables are not normally distributed but an equivalent normal distribution can be created for a corresponding non-normal distribution for a specific point on the failure surface X_i^*. The equivalent normal distribution is valid only for that specific failure point. In an iterative process where a new failure point is being chosen for each trial, a new equivalent normal distribution must be created for each trial. Once the equivalent mean $\mu_{X_i}^N$ and equivalent standard deviation $\sigma_{X_i}^N$ have been computed, the solution process is the same as shown in Section 3.4.1. The transformation from the x-space to the u-space becomes

$$U_i = \frac{X_i - \mu_{X_i}^N}{\sigma_{X_i}^N} \qquad i = 1, 2, \ldots, n \tag{3.27}$$

The equivalent normal standard deviation $\sigma_{X_i}^N$ is computed [Ang and Tang 1984] as

$$\sigma_{X_i}^N = \frac{\phi\{\Phi^{-1}[F_{X_i}(x_i^*)]\}}{f_{X_i}(x_i^*)} \tag{3.28}$$

where $F_{X_i}(x_i^*)$ and $f_{X_i}(x_i^*)$ are the cumulative distribution function (CDF) and probability density function (PDF), respectively of the non-normal distribution evaluated at the current point of failure X_i^*. The symbols $\Phi(-)$ and $\phi(-)$ represent the CDF and PDF of the standard normal distribution, respectively. The equivalent normal mean value $\mu_{X_i}^N$ is

$$\mu_{X_i}^N = X_i^* - \sigma_{X_i}^N\{\Phi^{-1}[F_{X_i}(x_i^*)]\} \tag{3.29}$$

Consider, for example, a problem where the non-normal distribution is the shifted-exponential distribution. Assume the mean time to failure is

15 years so the number of occurrences per year is $\lambda = 1/15$. Assume the offset time is $a = 2$ years. If the assumed failure point is $X^* = 4$ years, the parameters of the equivalent normal distribution would be computed as follows.

$$\begin{aligned}
F_X(x^*) &= 1 - e^{-\lambda(x^*-a)} = 1 - e^{-1/15(4-2)} = 0.125 \\
\Phi^{-1}(F_X(x^*)) &= \Phi^{-1}(0.125) = -1.15 \\
\phi\{\Phi^{-1}(F_X(x^*))\} &= \frac{1}{\sqrt{2\pi}} e^{-1/2(-1.15)^2} = 0.2059 \\
f_x(x^*) &= \lambda e^{-\lambda(x^*-a)} = 1/15 e^{-1/15(4-2)} = 0.05834 \\
\sigma_{X^*}^N &= \frac{\phi\{\Phi^{-1}(F_X(x^*))\}}{f_x(x^*)} = \frac{0.2059}{0.05834} = 3.529 \\
\mu_{X^*}^n &= X^* - \sigma^N \Phi_{-1}(F_X(x^*)) = 4 - 3.529(-1.15) = 8.058
\end{aligned} \tag{3.30}$$

Once a new failure point is chosen, a new equivalent normal distribution must be computed.

3.5.3 Correlated Non-Normal Variables

If the random variables have non-normal distributions and are correlated, the dependence between the variables could be expressed using conditional probabilities through the Rosenblatt transformation [Ang and Tang 1984], but this is cumbersome. The Rosenblatt transformation can be avoided and the problem can be solved in the same manner as for correlated normal distributions if equivalent correlation coefficients ρ_{ij}^N can be found. Der Kiureghian and Liu [1986] developed approximate expressions for ρ_{ij}^N for the

uniform, shifted exponential, shifted Rayleigh, Type-I largest value, Type-I smallest value, lognormal, gamma, Type-II largest value and Type-III smallest value distributions. Therefore, these are the distributions that are included in RELSYS.

Der Kiureghian and Liu [1986] define the uniform, shifted exponential, shifted Rayleigh, Type-I largest and Type-I smallest distributions as Group 1 distributions. Similarly the lognormal, gamma, Type-II largest and Type-III smallest are Group 2 distributions. The equivalent correlation coefficient ρ_{ij}^N is equal to the actual correlation between the two random variables X_i and X_j multiplied by a factor φ.

$$\rho_{ij}^N = \rho_{ij}(\varphi) \tag{3.31}$$

The factor φ is dependent on whether X_i and X_j are normal, Group 1, or Group 2 distributions.

If X_i is normally distributed and X_j is a Group 1 distribution or vice versa, the factor φ is a constant. For example, if X_i is normal and X_j is uniform, then φ=1.023. If X_i is normally distributed and X_j is a Group 2 distribution or vice versa, φ is a function of the coefficient of variation δ of the Group 2 distribution. For example, if X_i is normal and X_j is a gamma distribution, then

$$\varphi = 1.001 - 0.007\delta_j + 0.118\delta_j^2 \tag{3.32}$$

When X_i and X_j are both Group 1 distributions, φ is a function of the correlation ρ_{ij} between them. For example, if X_i is uniform and X_j is

Type-I largest, then

$$\varphi = 1.064 - 0.069\rho_{ij} + 0.005\rho_{ij}^2 \tag{3.33}$$

Similarly, if X_i is a Group 1 distribution and X_j is Group 2, then φ is a function of ρ_{ij} and δ_j. If both variables are Group 2 distributions, φ is a function of ρ_{ij}, δ_i and δ_j. If X_i is shifted-exponential and X_j is lognormal, then

$$\varphi = 1.098 + 0.003\rho_{ij} + 0.019\delta_j + 0.025\rho_{ij}^2 + 0.3038\delta_j^2 - 0.437\rho_{ij}\delta_j \tag{3.34}$$

If X_i is lognormal and X_j is Type-II largest, then

$$\begin{aligned} \varphi &= 1.026 + 0.082\rho_{ij} - 0.019\delta_i + 0.222\delta_j + 0.018\rho_{ij}^2 + 0.288\delta_i^2 \\ &\quad +0.379\delta_j^2 - 0.441\rho_{ij}\delta_i + 0.126\delta_i\delta_j - 0.277\rho_{ij}\delta_j \end{aligned} \tag{3.35}$$

The expressions for φ for all possible combinations of these distributions for X_i and X_j are listed in Der Kiureghian and Liu [1986], along with the maximum error associated with each. The program RELSYS uses these equations to compute the equivalent correlation coefficients ρ_{ij}^N.

3.5.4 Sensitivity Measures

After the reliability of a structural component has been computed, it is useful to examine the sensitivity of the reliability with respect to the random variables which contribute to the uncertainty in the problem [Frangopol 1985, Karamchandani and Cornell 1992]. A sensitivity analysis will reveal which random variables are most worthy of continued study – where the reduced uncertainty will most improve the component reliability. A complete sensitivity analysis with respect to all random variables can be a tedious process.

Hohenbichler and Rackwitz [1986] showed that the direction cosines were good approximate measures of the stochastic importance of a random variable. The sensitivity $sens_{\mu_j}$ with respect to the mean value of random variable X_j in component a is

$$sens_{\mu_j} = \alpha_{aj} \tag{3.36}$$

where α_{aj} is the direction cosine with respect to the failure point of random variable X_j in the uncorrelated reduced space. These direction cosines were computed in Step 6 of the iterative solution process shown in Section 3.4.1. The sensitivity $sens_{\sigma_j}$ with respect to the standard deviation of random variable X_j is

$$sens_{\sigma_j} = -\beta\alpha_{aj}^2 \tag{3.37}$$

These sensitivity values are used in RELSYS. The validity of the sensitivity measures will be evaluated on an actual bridge example in Chapter 5.

3.6 System Reliability

The first-order approximation method describe herein is used to compute the reliability of a single component. A structural system can have multiple components. Failure of a single component (series system) may cause failure of the entire system or the system may have redundancies where multiple components must fail (parallel system) for the system to fail. The interrelationship of the failure components is important in evaluating the reliability of an entire system. When describing system reliability, it is often difficult to determine whether a subscript in an equation is referring to a component

or a random variable – particularly regarding correlation coefficients and direction cosines. The convention used in this study is to reserve subscripts $(i, j, k, \ldots, n)$ for random variables. The remaining subscripts $(a, b, c, \ldots, h)$ and $(o, \ldots, z)$ are used for components.

3.6.1 Series Structures – Probability of Failure

While a structure can consist of just one member, it is usually comprised of a system of members. If the failure of a single member will lead to the failure of the entire structure, the system is considered a series structure. If a structural system is treated as a series system of z elements, the probability of failure P_f can be written as the probability of a union of events

$$P_f = P\left(\bigcup_{a=1}^{z} \{g_a(X) \leq 0\}\right) \tag{3.38}$$

To calculate the exact reliability of a structure with many members can be cumbersome process involving multiple integrals and necessary approximations. A more practical approach is to compute the lower and upper bounds on the reliability of the series system. The uni-modal or Cornell bounds are formed by considering the cases where the correlation between the failure modes (as described by the limit state equations) is either zero or one. Assuming the probability of failure for each individual element is known, the upper bound is calculated by assuming that all of the members are statistically independent ($\rho_{sys_{ab}} = 0$). The survival of the structure, which is the intersection of all members surviving, is equal to the product of the probabilities of

each member surviving. Therefore, the upper bound failure for the overall structure is equal to:

$$P_{f_{upper}} = 1 - \prod_{a=1}^{z}(1 - P_f(a)) \tag{3.39}$$

A lower bound can be calculated by assuming perfect correlation between the members ($\rho_{sys_{ab}} = 1$). In this case, if one member survives, then all members will survive, so the member with the least chance of survival (largest probability of failure) is identified. The lower bound indicates that, at best, the series structure is only as strong as its weakest member. Therefore:

$$P_{f_{lower}} = max[P_f(a)] \tag{3.40}$$

A set of bounds on the probability of failure for a series structure can be expressed as:

$$P_f(a)_{max} \leq P_f \leq 1 - \prod_{a=1}^{z}(1 - P_f(a)) \tag{3.41}$$

In many cases, the interval between these bounds can be very large. Ditlevsen [1979] developed tighter bounds which account for the actual correlation between the members of the series system. The lower bound can be written as:

$$P_{f_{lower}} = P(F_1) + \sum_{a=2}^{z} max[P(F_a) - \sum_{b=1}^{a-1}(P(F_a \bigcap F_b); 0] \tag{3.42}$$

The lower bound is based on considering only the individual component probabilities, $P(F_a)$, and all possible combinations of joint probabilities involving two members, $P(F_a \bigcap F_b)$. By neglecting joint probabilities involving three or more members (i.e., $P(F_a \bigcap F_b \bigcap F_c)$), which are more difficult to calculate, a

lower bound is assured. The upper bound for the probability of the system failure can be written as

$$P_{f_{upper}} = \sum_{a=1}^{z} P(F_a) - \sum_{a=2,b<a}^{z} max[P(F_b \bigcap F_a)] \tag{3.43}$$

The upper bound also considers only the individual probabilities and the joint probabilities involving two members. The upper bound is computed by selectively excluding certain two-member joint probabilities. The best bounds are obtained by rank ordering the failure events, $(F_1, ..., F_z)$ from the highest probability of failure to lowest [Melchers, 1987]. The actual probability of failure of the structure falls within these bounds and as the correlation between the members increases, the reliability of the system increases.

The individual component reliabilities in the Ditlevsen bounds $P(F_a)$ are computed using the algorithm described in Section 3.4.1. The two-member joint probability $P(F_a \bigcap F_b)$ is computed by numerically integrating the bivariate normal distribution function:

$$P(F_1 \bigcap F_2) = \int_{\beta_1}^{\infty}\int_{\beta_2}^{\infty} \frac{1}{2\pi\sqrt{1-\rho_{sys_{ab}}^2}} e^{-1/2(1-\rho_{sys_{ab}}^2)(\beta_a^2+\beta_b^2-2\rho_{sys_{ab}}\beta_a\beta_b)} d\beta_a d\beta_b \tag{3.44}$$

where β_a and β_b are the reliability indices associated with $P(F_a)$ and $P(F_b)$, respectively, and $\rho_{sys_{ab}}$ is the correlation between component failure events F_a and F_b.

The correlation between the random variables within each limit state function is known and was used to calculate the reliabilities of the individual components. The correlation between the components which comprise the

system has to be developed. This is done using the direction cosines (α^*_{aj}) associated with each random variable of each component. While β provides the shortest distance from the origin to the failure surface which is the magnitude of the reliability vector, the direction cosines (α^*_{aj}) provide the contribution to the direction of the reliability vector from each random variable. Using this notation, α^* is the direction cosine at the most probable point of failure, j is the random variable whose contribution is being evaluated, and a is the component under consideration.

As shown in Fig. 3.4, the correlation coefficient between any two components ($\rho_{sys_{ab}}$) is equal to the cosine of the angle between the two reliability vectors associated with a and b. This can be calculated using the direction cosines (α^*_{aj}):

$$\rho_{sys_{a,b}} = \frac{Cov(a,b)}{\sigma_a \sigma_b} = \sum_{k=1}^{n} \alpha^*_{ak} \alpha^*_{bk} \tag{3.45}$$

A system correlation matrix ρ_{sys} can now be assembled:

$$\rho_{sys} = \begin{pmatrix} \rho_{sys_{11}} & \rho_{sys_{12}} & \cdots & \rho_{sys_{1z}} \\ \rho_{sys_{21}} & \rho_{sys_{22}} & \cdots & \rho_{sys_{2z}} \\ \vdots & \vdots & \ddots & \vdots \\ \rho_{sys_{z1}} & \rho_{sys_{z2}} & \cdots & \rho_{sys_{zz}} \end{pmatrix} \tag{3.46}$$

With the system correlation matrix ρ_{sys} and the component reliabilities $\beta_a, \beta_b, ...\beta_z$, the Ditlevsen bounds for a series system can be calculated using Eqns. 3.42 and 3.43. The reliability of the series system is the average

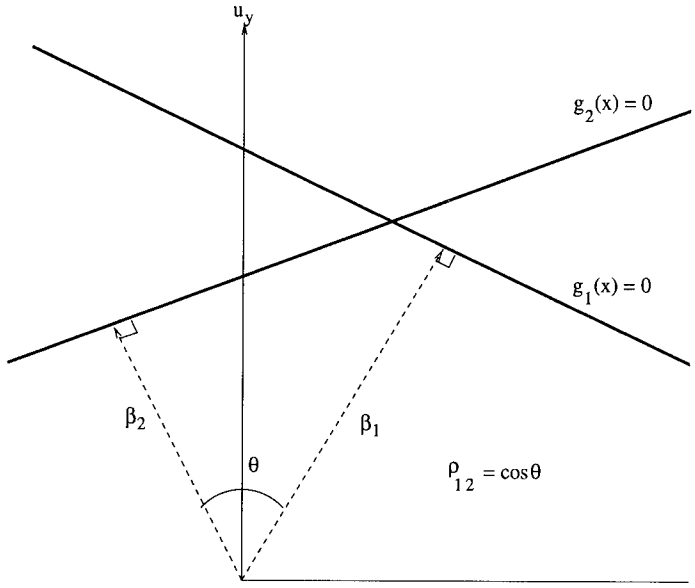

Figure 3.4: **Correlation Between Two Failure Modes**

of the Ditlevsen bounds for that system.

$$\beta_{sys} = \frac{\beta_{lower} + \beta_{upper}}{2} \tag{3.47}$$

3.6.2 Series System Example

Consider the following series system comprised of three failure components as described by limit state equations $g(1)$, $g(2)$, and $g(3)$.

$$g(1) = 2X_1^2 - 2X_2$$

$$g(2) = X_1 - X_3$$

$$g(3) = 1.5X_1 + 0.5X_3^2 - X_2$$

The system fails if any of the three components fail as modeled in Fig. 3.5. The random variables X_1, X_2, and X_3 are uncorrelated and normally distributed. The parameters for these variables are shown in Table 3.2.

Table 3.2: **Random Variables X_1, X_2, and X_3**

Variable	Mean Value	Standard Deviation	Distribution
X_1	2.0	0.2	Normal
X_2	3.0	0.3	Normal
X_3	1.0	0.1	Normal

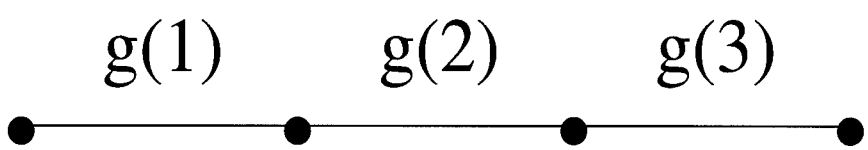

Figure 3.5: **Series Model of $g(1)$, $g(2)$, and $g(3)$**

Note that $g(1)$ is the same component analyzed in Section 3.4.1. Table 3.3 shows the component reliability results and direction cosines at the point of failure for components $g(1)$, $g(2)$, and $g(3)$.

Table 3.3: **Component Reliability Results for $g(1)$, $g(2)$, and $g(3)$.**

Component	β	P_f	P_s	α^*_{a1}	α^*_{a2}	α^*_{a3}
g(1)	1.2317	0.1090	0.8910	0.9210	-0.3896	0.0
g(2)	4.4721	0.3875E-5	1.0	0.8944	0.0	-0.4472
g(3)	1.1479	0.1255	0.8750	0.6892	-0.6892	0.2238

The upper and lower unimodal bounds which are based on no correlation and perfect correlation between failure modes, respectively can be

computed directly.

$$
\begin{aligned}
P_{f_{upper}} &= 1 - \prod_{a=1}^{z}(1 - P_f(a)) = 1 - (0.8910)(1.0)(0.8750) = 0.2286 \\
P_{f_{lower}} &= max[P_f(a)] = max[0.1090, 0.3875E-5, 0.1255] = 0.1255
\end{aligned}
\tag{3.48}
$$

The upper and lower bi-modal bounds require the correlation between failure modes to be computed.

$$
\begin{aligned}
\rho_{sys_{a,b}} &= \sum_{k=1}^{n} \alpha^*_{ak}\alpha^*_{bk} \\
\rho_{sys_{12}} &= \alpha^*_{11}\alpha^*_{21} + \alpha^*_{12}\alpha^*_{22} + \alpha^*_{13}\alpha^*_{23} \\
&= 0.9210(0.8944) + (-0.3896)(0.0) + 0.0(-0.4472) = 0.8238 \\
\rho_{sys_{13}} &= \alpha^*_{11}\alpha^*_{31} + \alpha^*_{12}\alpha^*_{32} + \alpha^*_{13}\alpha^*_{33} \\
&= 0.9210(0.6892) + (-0.3896)(-0.6892) + 0(0.2238) = 0.9033 \\
\rho_{sys_{23}} &= \alpha^*_{21}\alpha^*_{31} + \alpha^*_{22}\alpha^*_{32} + \alpha^*_{23}\alpha^*_{33} \\
&= 0.8944(0.6892) + 0(-0.6892) + (-0.4472)(0.2238) = 0.5163
\end{aligned}
\tag{3.49}
$$

Using these failure mode correlation coefficients and Eq. 3.44, the joint probabilities $P[g(1) \bigcap g(2)]$, $P[g(1) \bigcap g(3)]$, and $P[g(2) \bigcap g(3)]$ are computed. The results are shown in Table 3.4.

To obtain the narrowest bounds, the three events $g(1)$, $g(2)$, and $g(3)$ are rank ordered from the highest probability of failure to the lowest as shown in Table 3.5. By applying these rank ordered results to Eqs. 3.42 and 3.43, the upper and lower bimodal bounds $P_{f_{upper}}$ and $P_{f_{lower}}$ can be computed.

Table 3.4: **Joint Probability Results for $g(1)$, $g(2)$, and $g(3)$.**

Joint Distribution	β_a	β_b	$\rho_{sys_{ab}}$	$P_{f_{sys}}$	β_{sys}
$g(1) \bigcap g(2)$	1.2317	4.4721	0.8238	3.873E-06	4.4719
$g(1) \bigcap g(3)$	1.2317	1.1479	0.9033	0.08226	1.4690
$g(2) \bigcap g(3)$	4.4721	1.1479	0.5163	3.599E-06	4.4877

$$
\begin{aligned}
P_{f_{lower}} &= P(F_1) + P(F_2) - P(F_2 \bigcap F_1) + P(F_3) - P(F_3 \bigcap F_2) - P(F_3 \bigcap F_1) \\
&= 0.1255 + 0.1090 - 0.08226 + 3.875(10^{-6}) - 3.599(10^{-6}) - 3.873(10^{-6}) \\
&= 0.1522 \\
P_{f_{upper}} &= P(F_1) + P(F_2) + P(F_3) - max[P(F_2 \bigcap F_1)] \\
&\quad -max[P(F_3 \bigcap F_2), P(F_3 \bigcap F_1)] \\
&= 0.1255 + 0.1090 + 3.875(10^{-6}) - max[0.08226] \\
&\quad -max[3.599(10^{-6}), 3.873(10^{-6})] = 0.1522
\end{aligned} \tag{3.50}
$$

RELSYS computes the probability of failure of this series system as the average of these upper and lower bimodal bounds. In this case, the upper and lower bounds are the same to four decimal places and $P_{f_{sys}} = 0.1522$. The Ditlevsen bounds are furthest apart when the series system contains a large number of members with relatively equal probabilities of failure. This series

Table 3.5: **Rank Ordering of $g(1)$, $g(2)$, and $g(3)$.**

Ordered Event	Original Event	P_f
F_1	$g(3)$	0.1255
F_2	$g(1)$	0.1090
F_3	$g(2)$	3.875E-06
$F_1 \bigcap F_2$	$g(3) \bigcap g(1)$	0.08226
$F_1 \bigcap F_3$	$g(3) \bigcap g(2)$	3.599E-06
$F_2 \bigcap F_3$	$g(1) \bigcap g(2)$	3.873E-06

system is Example 5 in the RELSYS User's Manual (Appendix A).

3.6.3 Parallel Structures – Probability of Failure

If the remaining members of a structure will continue to carry the required loads when a single member fails, the system is considered a parallel structure. The upper and lower unimodal bounds for the probability of failure for a ductile parallel structure are easily established. Brittle systems, which cannot redistribute loads between members like a ductile system, are usually modeled as series systems.

If the structural system is modeled as a parallel system, the probability of failure of this system P_f can be written as a probability of intersection of events:

$$P_f = P\left(\bigcap_{a=1}^{z} \{g_a(X) \leq 0\}\right) \tag{3.51}$$

where z is the number of elements which have to fail in order to cause system failure.

A lower bound failure probability is found by assuming statistical independence ($\rho_{sys_{ab}} = 0$) between the structural members. The probability of the structure failing is equal to the product of the individual failure probabilities of members. Therefore,

$$P_{f_{lower}} = \prod_{a=1}^{z} (1 - P_f(a)) \tag{3.52}$$

The upper bound is calculated when there is perfect correlation between the members ($\rho_{sys_{ab}} = 1.0$). The structure will be at least as strong as its strongest member. The member with the lowest P_f value provides the upper bound for the probability of failure for the structure.

$$P_{f_{upper}} = min[P_f(a)] \tag{3.53}$$

A set of bounds on the probability of failure of a parallel structure can be expressed as:

$$\prod_{a=1}^{z} (1 - P_f(a)) \leq P_f \leq min[P_f(a)] \tag{3.54}$$

In contrast to the series system, the reliability of a parallel system decreases with increased member correlation. For parallel systems, there is no equivalent to the Ditlevsen bounds and the bounds listed above are often too wide to be useful.

Since this first-order approach to solving the component reliability problem reduces all random variables to equivalent normal distributions, a solution to the parallel system can be found by solving the n-dimensional joint standardized distribution integral [Thoft-Christensen and Murotsu 1986].

$$P(F_1 \bigcap F_2 \bigcap \cdots \bigcap F_z) = \int_{\beta_1}^{\infty}\int_{\beta_2}^{\infty}\cdots\int_{\beta_z}^{\infty} \frac{1}{(2\pi)^{z/2}\sqrt{det[\rho_{sys}]}} e^{-1/2\{\beta\}[\rho_{sys}]^{-1}\{\beta\}^T} d\{\beta\} \tag{3.55}$$

where $\{\beta\} = \{\beta_a, \beta_b, \cdots, \beta_z\}$, ρ_{sys} is the system correlation matrix, and z is the number of members in the parallel system.

3.6.3.1 Bivariate Normal Distribution

For a two-member parallel system, Eq. 3.55 reduces to the bivariate normal distribution shown in Eq. 3.44. Several numerical approximations of the bivariate normal distribution were attempted using Composite Simpson's rule [Burden and Faires 1993], the Hohenbichler approximation [Hohenbichler and Rackwitz 1983], and Gaussian quadrature with 5, 11, 25, and 51 Gauss points [Stroud and Secrest 1966]. The Hohenbichler approximation uses conditional probability to successively reduce the dimension of a multi-normal integral by one dimension for every iteration until it is reduced to a single integral. A recursive algorithm is then used to reverse the process and solve the multi-dimensional integral [Thoft-Christensen and Murotsu 1986]. Tables 3.6 and 3.7 show the results for the system reliability index β_{sys} and the system probability of failure $P_{f_{sys}}$ using all of these methods for various two-member parallel systems. All of the methods, with the exception of Gaussian quadrature using only five Gauss points, yield approximately the same results. RELSYS uses the Composite Simpson's rule to solve this integral.

Table 3.6: **Bivariate Normal Distribution Approximations (β)**

β_1	β_2	$\rho_{1,2}$	Simpson's	Hohenb.	Gauss 5	Gauss 11	Gauss 25	Gauss 51
2.5	2.5	0.2	3.6136	3.6137	3.6077	3.6136	3.6136	3.6136
2.5	4.5	0.4	4.7855	4.7880	4.7920	4.7856	4.7856	4.7856
2.5	3.6	0.6	3.8282	3.8286	3.8314	3.8282	3.8282	3.8282
4.0	2.5	0.6	4.1535	4.1539	4.1638	4.1535	4.1535	4.1535
3.0	3.0	0.7	3.5032	3.5031	3.4881	3.5032	3.5032	3.5032
2.5	4.5	0.8	4.5042	4.5046	4.4942	4.5041	4.5042	4.5042
4.0	4.0	0.8	4.4142	4.4135	4.4008	4.4142	4.4142	4.4142
2.5	3.0	0.9	3.0597	3.0596	3.0716	3.0597	3.0596	3.0596
4.5	2.5	0.9	4.4998	4.4998	4.4100	4.4973	4.4999	4.4999

Table 3.7: **Bivariate Normal Distribution Approximations** ($P_f \cdot 10^{-3}$)

β_1	β_2	$\rho_{1,2}$	Simpson's	Hohenb.	Gauss 5	Gauss 11	Gauss 25	Gauss 51
2.5	2.5	0.2	.1511	.1510	.1545	.1511	.1511	.1511
2.5	4.5	0.4	.0008520	.0008431	.0008249	.0008519	.0008519	.0008519
2.5	3.6	0.6	.06456	.06446	.06372	.06456	.06456	.06456
4.0	2.5	0.6	.01637	.01635	.01565	.01637	.01637	.01637
3.0	3.0	0.7	.2300	.2300	.2434	.2300	.2300	.2300
2.5	4.5	0.8	.003330	.003328	.003490	.003330	.003329	.003329
4.0	4.0	0.8	.005068	.005090	.005391	.005068	.005068	.005068
2.5	3.0	0.9	1.109	1.108	1.066	1.109	1.109	1.109
4.5	2.5	0.9	.003398	.003404	.005166	.003440	.003397	.003397

3.6.3.2 Trivariate Normal Distribution

The trivariate normal distribution is used to compute the reliability of a three-member parallel system. The trivariate normal distribution can be expressed as:

$$P(F_1 \bigcap F_2 \bigcap F_3) = \int_{\beta_1}^{\infty}\int_{\beta_2}^{\infty}\int_{\beta_3}^{\infty} f_3(\beta_1, \beta_2, \beta_3; [\rho_{sys}]) d\beta_c d\beta_b d\beta_a \tag{3.56}$$

where:

$$f_3(\beta_1, \beta_2, \beta_3; [\rho_{sys}]) = \frac{1}{(2\pi)^{3/2}\sqrt{det[\rho_{sys}]}} e^{[-1/2\{\beta_1,\beta_2,\beta_3\}[\rho_{sys}]^{-1}\{\beta_1,\beta_2,\beta_3\}^T]} \tag{3.57}$$

in which $[\rho_{sys}]$ is the correlation coefficient matrix of $\{\beta_1, \beta_2, \beta_3\}$ given by:

$$[\rho_{sys}] = \begin{pmatrix} \rho_{11} & \rho_{12} & \rho_{13} \\ \rho_{21} & \rho_{22} & \rho_{23} \\ \rho_{31} & \rho_{32} & \rho_{33} \end{pmatrix} = \begin{pmatrix} 1 & \rho_{12} & \rho_{13} \\ \rho_{12} & 1 & \rho_{23} \\ \rho_{13} & \rho_{23} & 1 \end{pmatrix}$$

and the inverse of the correlation matrix is:

$$[\rho_{sys}]^{-1} = \frac{1}{\det[\rho_{sys}]} \begin{pmatrix} 1.0 - \rho_{23}^2 & -\rho_{12} + \rho_{13}\rho_{23} & -\rho_{13} + \rho_{12}\rho_{23} \\ -\rho_{12} + \rho_{13}\rho_{23} & 1.0 - \rho_{13}^2 & -\rho_{23} + \rho_{12}\rho_{13} \\ -\rho_{13} + \rho_{12}\rho_{23} & -\rho_{23} + \rho_{12}\rho_{13} & 1.0 - \rho_{12}^2 \end{pmatrix}$$

and where:

$$\det[\rho_{sys}] = 1.0 + \rho_{12}\rho_{23}\rho_{13}(2.0) - \rho_{12}^2 - \rho_{13}^2 - \rho_{23}^2 \tag{3.58}$$

The approximate solution of the trivariate normal distribution was investigated using Gaussian quadrature with 5, 11, 25, and 51 Gauss points; the Hohenbichler approximation; and a lower bound solution proposed by Ramachandran [1986]. This lower bound solution of $P(F_i \bigcap F_j \bigcap F_k)$ is developed using only the intersection of two events:

$$P(F_i \bigcap F_j \bigcap F_k) \geq \frac{P(F_i \bigcap F_j)P(F_i \bigcap F_k)}{P(F_i)} \tag{3.59}$$

Tables 3.8 and 3.9 show the system reliability indices and probabilities of failure for several three-member parallel structures using all listed approximate methods. If $\rho_{sys_{ab}} < 0.9$ for all of the correlation coefficients, then the Gaussian quadrature using 11 Gauss points provides results that are close to the exact solution. If any member correlation is greater than 0.9, better results are achieved with 25 Gauss points. Raising the number of Gauss points to 51 requires greater computational effort but does not appear to significantly improve the results. For the reliability of a three-member parallel system, RELSYS numerically integrates the trivariate normal distribution using Gaussian quadrature with 11 Gauss points if $\rho_{sys_{ab}} < 0.9$ and 25 Gauss points if $\rho_{sys_{ab}} \geq 0.9$.

For parallel systems with four members of more, the number of computations to numerically integrate the multinormal distribution becomes too large and the Hohenbichler approximation is used. The Hohenbichler approximation is solved using a FORTRAN 77 subroutine provided to the author by Sørensen [1987]. The Hohenbichler approximation works best for failure events that are perfectly correlated or independent. The accuracy is less for

Table 3.8: **Trivariate Normal Distribution Approximations (β)**

β_1	β_2	β_3	$\rho_{1,2}$	$\rho_{1,3}$	$\rho_{2,3}$	Ramach.	Hohenb	Exact
2.78	3.28	3.81	0.61	0.87	0.67	4.19	4.20	4.18
1.77	2.16	3.47	0.39	0.93	0.08	4.32	4.51	4.32
2.26	2.64	3.68	0.46	0.78	0.12	4.67	4.80	4.64
1.92	2.10	1.63	0.99	0.35	0.27	2.78	2.78	2.77
1.67	1.72	1.39	0.75	0.32	0.80	2.62	2.33	2.33
0.38	0.40	0.93	0.54	0.26	0.82	1.42	1.37	1.37
2.99	2.61	2.38	0.64	0.56	0.98	3.57	3.41	3.41
0.62	0.03	1.38	0.12	0.22	0.30	1.97	1.96	1.95
3.59	4.03	1.53	0.25	0.39	0.59	5.17	5.12	5.12

β_1	β_2	β_3	$\rho_{1,2}$	$\rho_{1,3}$	$\rho_{2,3}$	Gauss 5	Gauss 11	Gauss 25	Gauss 51
2.78	3.28	3.81	0.61	0.87	0.67	4.22	4.18	4.18	4.18
1.77	2.16	3.47	0.39	0.93	0.08	4.92	4.39	4.31	4.31
2.26	2.64	3.68	0.46	0.78	0.12	4.57	4.65	4.65	4.65
1.92	2.10	1.63	0.99	0.35	0.27	3.20	2.89	2.76	2.77
1.67	1.72	1.39	0.75	0.32	0.80	2.24	2.33	2.33	2.33
0.38	0.40	0.93	0.54	0.26	0.82	1.52	1.37	1.37	1.37
2.99	2.61	2.38	0.64	0.56	0.98	3.16	3.36	3.41	3.41
0.62	0.03	1.38	0.12	0.22	0.30	1.98	1.96	1.96	1.96
3.59	4.03	1.53	0.25	0.39	0.59	5.13	5.16	5.16	5.16

Table 3.9: **Trivariate Normal Distribution Approximations** ($P_f \cdot 10^{-3}$)

β_1	β_2	β_3	$\rho_{1,2}$	$\rho_{1,3}$	$\rho_{2,3}$	Ramach.	Hohenb	Exact
2.78	3.28	3.81	0.61	0.87	0.67	.0141	.0136	.0144
1.77	2.16	3.47	0.39	0.93	0.08	.0077	.0033	.0078
2.26	2.64	3.68	0.46	0.78	0.12	.0015	.00080	.0017
1.92	2.10	1.63	0.99	0.35	0.27	2.750	2.777	2.790
1.67	1.72	1.39	0.75	0.32	0.80	4.350	9.951	10.000
0.38	0.40	0.93	0.54	0.26	0.82	78.47	85.72	86.03
2.99	2.61	2.38	0.64	0.56	0.98	0.180	0.319	0.320
0.62	0.03	1.38	0.12	0.22	0.30	24.22	25.14	25.67
3.59	4.03	1.53	0.25	0.39	0.59	.00012	.00015	.00015

β_1	β_2	β_3	$\rho_{1,2}$	$\rho_{1,3}$	$\rho_{2,3}$	Gauss 5	Gauss 11	Gauss 25	Gauss 51
2.78	3.28	3.81	0.61	0.87	0.67	.0123	.0148	.0148	.0148
1.77	2.16	3.47	0.39	0.93	0.08	.00044	.00057	.00081	.00080
2.26	2.64	3.68	0.46	0.78	0.12	.0024	.0017	.0017	.0017
1.92	2.10	1.63	0.99	0.35	0.27	.676	1.932	2.852	2.841
1.67	1.72	1.39	0.75	0.32	0.80	12.593	9.994	9.980	9.980
0.38	0.40	0.93	0.54	0.26	0.82	64.59	85.74	85.68	85.68
2.99	2.61	2.38	0.64	0.56	0.98	0.790	0.388	0.320	0.319
0.62	0.03	1.38	0.12	0.22	0.30	24.03	25.18	25.18	25.18
3.59	4.03	1.53	0.25	0.39	0.59	.00014	.00013	.00013	.00013

events with medium dependencies. The approximation has the largest error if the probabilities of failure are the same and the correlation between events is also the same. As expected, the error also increases as the number of members in the parallel system increases [Hohenbichler and Rackwitz 1983]. The accuracy is best when the individual component β values are rank-ordered from smallest to largest [Ditlevsen and Madsen 1996].

3.6.4 General Systems

A general system can be modeled as any combination of series and parallel systems. Consider a series system consisting of y parallel systems. Each parallel system a has z_a components. Then, the probability of failure is given as:

$$P_f = P\left(\bigcup_{a=1}^{y} \bigcap_{b=1}^{z_a} \{g_{ab}(X) \leq 0\}\right) \tag{3.60}$$

The reliability of a series system and a parallel system can be solved separately using the reliabilities and the direction cosines at the point of failure of the individual components. The approach for a complex system will be to sequentially break the system down into simpler equivalent subsystems. The example series-parallel system in Fig. 3.6 illustrates how the equivalent components are created and the system is simplified until a single system reliability index can be calculated. The original problem consists of six limit state equations $g(1) = 0$ through $g(6) = 0$ and the reliability of each can be calculated using the FORM described earlier. Using the direction cosines

associated with the most probable points of failure for each limit state, the system correlation matrix is calculated.

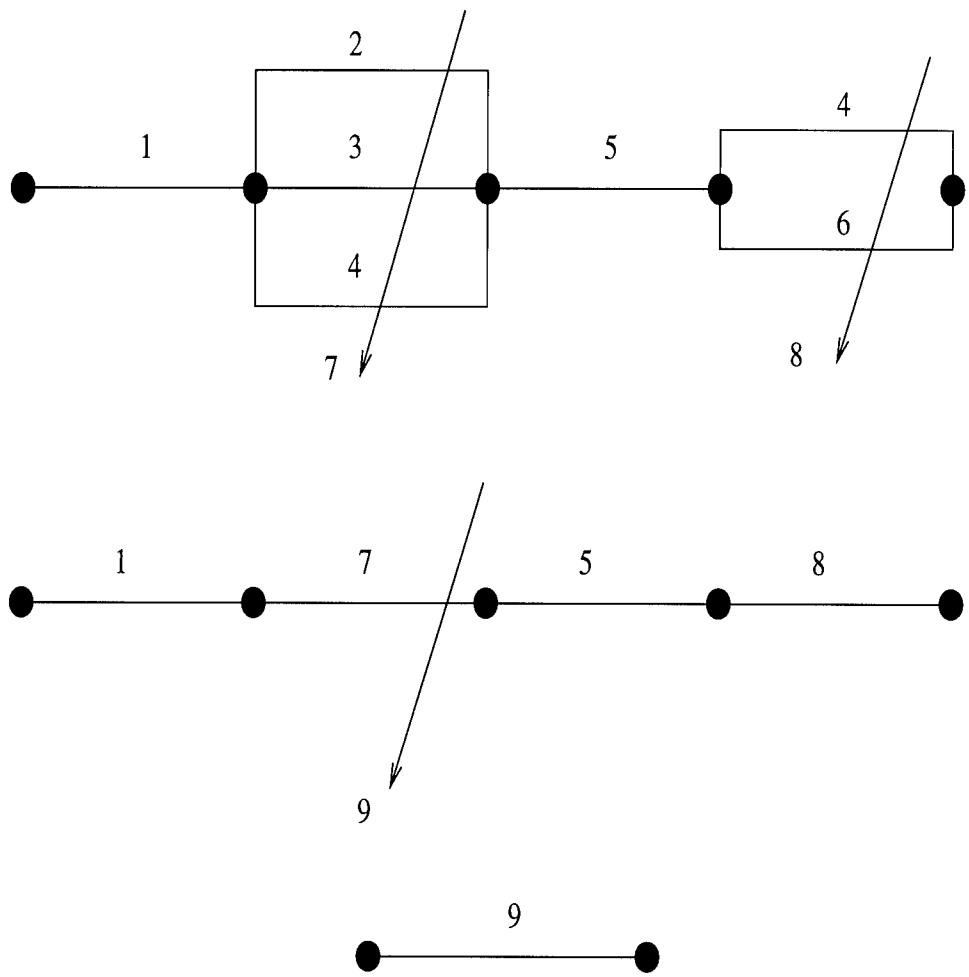

Figure 3.6: **Reduction of a Series-Parallel System to an Equivalent Series System**

Using the trivariate normal distribution (Eq. 3.57), the reliability of the parallel system comprised of $g(2)$, $g(3)$, and $g(4)$ is found and an equivalent component $g(7)$ is created. Similarly, the bivariate normal distribution

(Eq. 3.44) is used to find the reliability of the two-member parallel system of $g(4)$ and $g(6)$, and create the equivalent component $g(8)$. The intermediate result is a series system of components $g(1)$, $g(7)$, $g(5)$, and $g(8)$. The equivalent single component $g(9)$ is the average of the bimodal bounds for this series system. Since the reliability of a system is dependent on the correlation of the individual members of the system, the equivalent correlation of the equivalent components must be included.

3.6.4.1 Equivalent Alpha Vectors

The equivalent correlation coefficients $\rho_{sys-equiv_{ab}}$ that are associated with the equivalent components created in the system analysis are a function of equivalent alpha vectors of equivalent direction cosines associated with each random variable in the sub-system analysis,

$$\rho_{sys-equiv_{ab}} = \sum_{k=1}^{n} \alpha_{equiv_{ak}} \alpha_{equiv_{bk}} \tag{3.61}$$

where $\alpha_{equiv_{ak}}$ is the equivalent direction cosine for equivalent component a with respect to random variable k. Just as with Eq. 3.18, the equivalent direction cosines are a function of the gradients. The gradient under consideration however is the change in the system reliability with respect to each random variable in the system $\frac{\partial(\beta_{sys})}{\partial(X_k)}$.

$$\alpha_{equiv_{ak}} = \frac{\partial(\beta_{sys})/\partial(X_k)}{\sqrt{\sum_{i=1}^{n} (\frac{\partial(\beta_{sys})}{\partial(X_i)})^2}} \tag{3.62}$$

The gradients $\frac{\partial(\beta_{sys})}{\partial(X_k)}$ are computed by using the direction cosines associated with each component α^*_{ak} in a system to individually assess the

effect of each random variable on the reliability of the system. The effect or sensitivity of the system reliability with respect to each random variable becomes the equivalent direction cosine for that random variable. Consider random variable X_k for a series or parallel system with z components. The reliability index associated with an individual component β_a are varied by a small amount β_{ak} which is an arbitrary small constant ψ multiplied the direction cosine α^*_{ak}.

$$\begin{aligned} \beta_{ak} &= \beta_a + \psi(\alpha^*_{ak}) \\ \beta_{bk} &= \beta_b + \psi(\alpha^*_{bk}) \\ \vdots &= \vdots \\ \beta_{zk} &= \beta_z + \psi(\alpha^*_{zk}) \end{aligned} \tag{3.63}$$

Using these altered reliability indices and the original system correlation matrix ρ_{sys}, the revised system reliability index for the series or parallel system $\beta_{sys_{new(k)}}$ with respect to the random variable X_k is computed. The system gradient with respect to X_k is computed as

$$\frac{\partial(\beta_{sys})}{\partial(X_k)} = \frac{\beta_{sys} - \beta_{sys_{new(k)}}}{\psi} \tag{3.64}$$

This process is completed with respect to the rest of the random variables in the system from which the remainder of the system gradients are computed. Eq. 3.62 uses these gradients to create the equivalent alpha vectors and Eq. 3.61 computes the equivalent correlation coefficients.

3.6.4.2 General System Example

Consider the following general series-parallel system shown in Fig. 3.7 containing the same three failure components 1, 2, and 3 represented by the limit state equations $g(1)$, $g(2)$, and $g(3)$ used in earlier examples.

$$\begin{aligned} g(1) &= 2X_1^2 - 2X_2 \\ g(2) &= X_1 - X_3 \\ g(3) &= 1.5X_1 + 0.5X_3^2 - X_2 \end{aligned} \tag{3.65}$$

The general system is a parallel system of components 1 and 3 in series with component 1, in series with a parallel combination of components 1, 2, and 3. The parameters of random variables X_1, X_2, and X_3 are listed in Table 3.2 and the direction cosines and reliability associated with each component is shown in Table 3.3.

Considering the parallel system of components 1 and 3, Eq. 3.49 uses the direction cosines α_{ak}^* to compute the system correlation coefficient $\rho_{sys_{13}} = 0.9033$. The bivariate normal distribution (Eq. 3.44) is used to compute the reliability of the parallel system $\beta_{sys} = 1.3902$ for $\beta_1 = 1.2317$, $\beta_3 = 1.1479$, and $\rho_{sys_{13}} = 0.9033$.

The effect of random variable X_1 on the system reliability is considered first. Setting $\psi = 0.001$, the adjusted component reliabilities based on the sensitivity of X_1 are:

$$\begin{aligned} \beta_{11} &= \beta_1 - \psi(\alpha_{11}^*) = 1.2317 + 0.001(0.9210) = 1.2326 \\ \beta_{21} &= \beta_2 - \psi(\alpha_{21}^*) = 1.1479 + 0.001(0.6892) = 1.1485 \end{aligned} \tag{3.66}$$

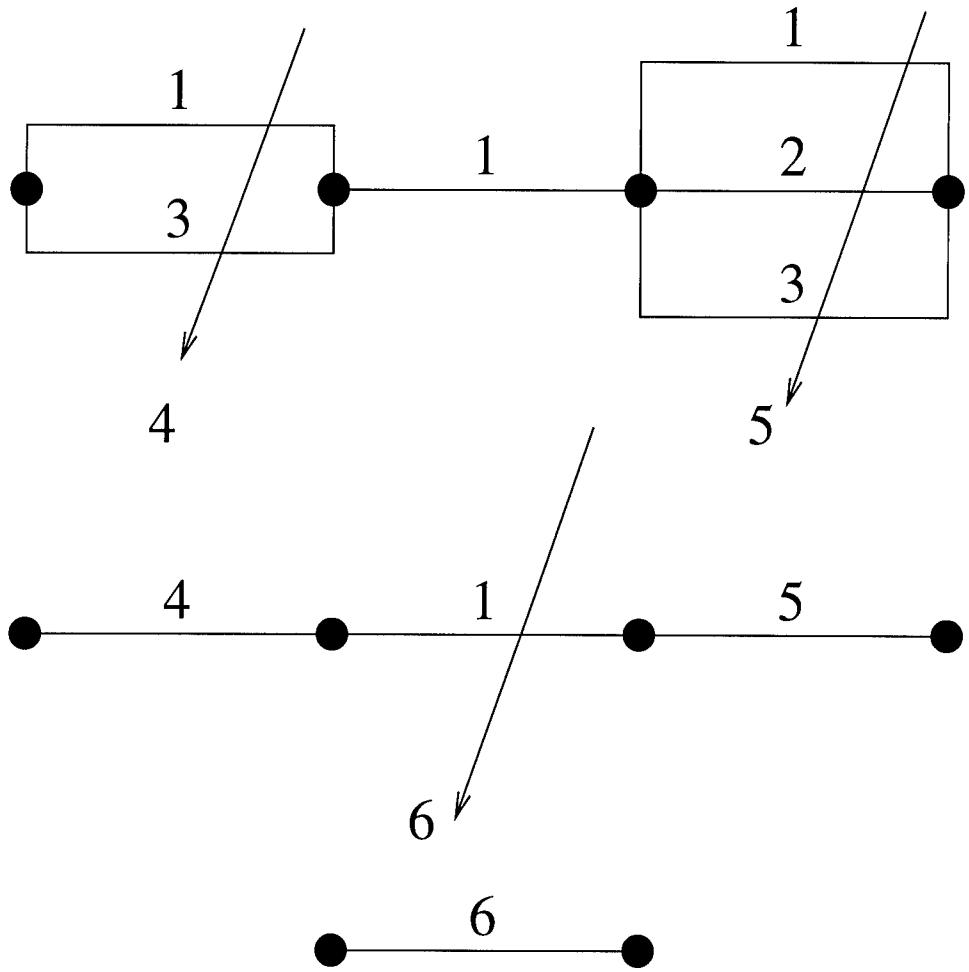

Figure 3.7: **Reduction of a Series-Parallel System to an Equivalent Single Component**

Solving the bivariate normal distribution where $\beta_{11} = 1.2326$, $\beta_{21} = 1.1479$ and $\rho_{sys_{11,21}} = 0.9033$ yields $\beta_{sys_{new(1)}} = 1.3911$. Table 3.10 shows the results for β_{1i}, β_{2i}, and $\beta_{sys_{new(i)}}$ for random variables X_2 and X_3.

Table 3.10: **Adjusted System Reliabilities For Two Member Parallel System Based on the Sensitivities With Respect to the Random Variables X_1, X_2, and X_3**

Random	Component 1		Component 2		System
Variable	α^*_{1i}	β_{1i}	α^*_{2i}	β_{2i}	$\beta_{sys_{new(i)}}$
X_1	0.9210	1.2326	0.6892	1.1485	1.3911
X_2	-0.3896	1.2313	-0.6892	1.1472	1.3897
X_3	0.0	1.2317	0.2238	1.1481	1.3903

The gradients of the system reliability with respect to each random variable are:

$$\begin{aligned}
\frac{\partial(\beta_{sys})}{\partial(X_1)} &= \frac{\beta_{sys} - \beta_{sys_{new(1)}}}{\psi} = \frac{1.3902 - 1.3911}{0.001} = 0.8344 \\
\frac{\partial(\beta_{sys})}{\partial(X_2)} &= \frac{1.3902 - 1.3897}{0.001} = -0.5286 \\
\frac{\partial(\beta_{sys})}{\partial(X_3)} &= \frac{1.3902 - 1.3903}{0.001} = 0.0989
\end{aligned} \tag{3.67}$$

Using Eq. 3.62, the equivalent direction cosines $\alpha_{equiv_{ak}}$ which make up the equivalent alpha vector for equivalent component 4 are

$$\begin{aligned}
\alpha_{equiv_{41}} &= \frac{0.8344}{\sqrt{(0.8344)^2 + (-0.5286)^2 + (0.0996)^2}} = \frac{0.8344}{0.9855} = 0.8405 \\
\alpha_{equiv_{42}} &= \frac{-0.5286}{0.9855} = -0.5325
\end{aligned}$$

$$\alpha_{equiv_{43}} = \frac{0.0989}{0.9855} = 0.0996 \tag{3.68}$$

This equivalent alpha vector can be used to compute the equivalent correlation coefficients between component 4 and any of the other components in the system. The reliabilities of the two components 1 ($\beta_1 = 1.2317$) and 3 ($\beta_3 = 1.1479$) are relatively equal and each have relatively equal contributions to the reliability of the system. The equivalent direction cosines for each random variable in this case are close to the average of the individual direction cosines for each component.

The parallel system consisting of components 1, 2, and 3 is reduced to equivalent component 5 in a similar manner. Eq. 3.49 provides the system correlation coefficients $\rho_{sys_{12}} = 0.8238$, $\rho_{sys_{13}} = 0.9033$, $\rho_{sys_{23}} = 0.5163$ from which the system correlation matrix ρ_{sys} is created. The reliability of the parallel system $\beta_{sys} = 4.488$ is computed from the trivariate normal distribution (Eq. 3.57) using ρ_{sys} and $\beta = \{\beta_1, \beta_2, \beta_3\} = \{1.2317, 4.4721, 1.1479\}$. Table 3.11 shows the adjusted reliabilities of the components based on the sensitivities of the random variables and the resulting equivalent alpha vector for the three-member parallel system.

In this three-member system, component 2 has a much higher reliability than the other two members and has the dominant effect on the reliability of the system. The equivalent direction cosines are likewise dominated by the component 2.

The system has been reduced to an equivalent three-member series system of components 1, 4, and 5. The reliabilities and direction cosines for

Table 3.11: **Adjusted System Reliabilities For Three Member Parallel System Based on the Sensitivities of the Random Variables X_1, X_2, and X_3**

Ran.	Comp. 1	Comp. 2	Comp. 3	System			
Var.	β_{1i}	β_{2i}	β_{3i}	$\beta_{sys_{new(i)}}$	β_{sys}	$\frac{\partial(\beta_{sys})}{\partial(X_i)}$	$\alpha_{equiv_{5i}}$
X_1	1.2326	4.4730	1.1485	4.4891	4.4882	0.8885	0.9020
X_2	1.2313	4.4721	1.1472	4.4882	4.4882	-0.0174	-0.0177
X_3	1.2317	4.4717	1.1480	4.4878	4.4882	-0.4248	-0.4313

these three components are shown in Table 3.12 which is very similar to Table 3.3. The series system is solved in the same manner as shown in Section 3.6.2. The direction cosines are used to compute the system correlation coefficients. The component reliabilities and correlation coefficients are substituted into the bivariate normal distribution integral (Eq. 3.44) to compute all two-event joint probabilities. The upper and lower bimodal bounds are computed. For the series system of components 1, 4, and 5, the Ditlevsen bounds were $P_{f_{upper}} =$ 0.11281 and $P_{f_{lower}} = 0.11281$.

Table 3.12: **Results for Components 1, 4, and 5**

Component	β	P_f	P_s	α^*_{a1}	α^*_{a2}	α^*_{a3}
1	1.2317	0.1090	0.8910	0.9210	-0.3896	0.0
4	1.3902	0.0827	0.9173	0.8405	-0.5325	-0.0996
5	4.4882	0.3598E-05	1.0	0.9020	-0.0177	-0.4313

Using the average of the bi-modal bounds, the reliability index of equivalent component 6 and thus the reliability of the system is $\beta_{sys} = 1.2119$. The equivalent alpha vector could be computed in the same manner based on the contribution of the random variables to the system reliability, but there is no need since the solution is complete. RELSYS uses this method to break any system which can be modeled as a series-parallel combination of the individual components into successively smaller equivalent systems, until only a single equivalent component is remaining. This general system is Example 8 in the RELSYS User's Manual (Appendix A).

The approximate FORM approach described herein is very effective in many cases and provides good results with minimum computational effort. Until this method was developed, the most popular estimation methods for such analysis was Monte Carlo simulation [De and Cornell, 1990] which has some serious limitations, particularly for problems that will be executed many times.

3.7 Monte Carlo Simulation

Because of the difficulty in calculating the integral in Eq. 3.11, the previous inadequacy of the bounds for the parallel system, and the difficulty in calculating the effect of correlation in higher order systems, the technique of last resort has been Monte Carlo simulation. Rather than facing the mathematical complexities of the problem, Monte Carlo simulation generates the random variables that appear in the problem, transforms them to the assumed probability distribution, and evaluates the functions which constitute

the model a sufficient number of times to generate a credible answer. For a given limit state equation, $g(x) = 0$, the probability of failure (P_f) is calculated as:

$$P_f = n_f/n \tag{3.69}$$

where n is the number of times the simulation is run and n_f is the number of times that $g(x) \geq 0$ was not true.

Monte Carlo simulation experiences some degree of sampling problems unless the sample size is infinitely large. As the number of simulations becomes greater, the standard deviation of the probability of failure becomes less. Monte Carlo simulation can require large amounts of computer time particularly if the event is rare. The larger the probability of failure, the larger the number of simulations required to obtain a reasonable solution. The number of iterations required is based on the acceptable percent error. One relationship [Ang and Tang, 1984] is:

$$\%\ error = 200\sqrt{\frac{(1 - P_f)}{n(P_f)}} \tag{3.70}$$

Another general rule of thumb [Harbitz, 1986] is that the number of iterations required to obtain a reasonable error (i.e. roughly 30%) is:

$$n = 10/P_f \tag{3.71}$$

Structures are designed so that failure is necessarily a rare event. With most structures having reliability indices around $\beta = 3$ or $\beta = 4$ and some individual components of a structure having reliability indices of $\beta = 7$ or $\beta = 8$, it is common that millions and sometimes billions of simulations are required for

each calculation. When the system reliability calculation will be made many times to account for the entire life of the structure, the Monte Carlo method, while accurate, requires too much time to be useful.

3.8 RELSYS

RELSYS (Reliability of Systems) is a FORTRAN 77 program written by the author which calculates the reliability of any structure which can be modeled as a combination of series and parallel structures. The program uses the average of the Ditlevsen bounds for series systems, numerical integration of the multi-normal distribution for two and three-member systems, the Hohenbichler approximation for larger parallel systems, and correlation coefficients based on equivalent alpha vectors to calculate the system reliability index. The algorithm reduces the various series and parallel systems to equivalent single components, gradually reducing the entire system to a single simplified component. The program is divided into four parts:

relsys.f: The program shell which reads the input file and calls the subroutines which will calculate the system reliability. The purpose of this shell is to create an environment which allows the user to repeatedly calculate the reliability of the structure and to define the problem to be solved. Specifically for a highway bridge, the shell defines the cost data, the deterioration functions, the number of lifetime inspections, and the minimum acceptable reliability. It contains the aspects of the problem that do not involve the reliability calculations;

subrel.f: Main program for reliability calculation. It acts as the switchboard

which calls the necessary subroutines to calculate reliability;

subrel1.f: Contains all subroutines for calculating the reliability of individual components; and

subrel2.f: Contains all subroutines for calculating the system reliability.

3.9 Testing RELSYS

The results of RELSYS were compared with those obtained by the Monte Carlo simulation programs MCREL and CALREL for the same problems.

3.9.1 Parallel Systems

The first comparison was made on two-bar, three-bar, four-bar, and five-bar parallel systems as shown in Figure 3.8. In each case, the sum of the mean resistances of the members was 1.5 times as great as the mean load. Therefore, the System Safety Factor (SSF) of 1.5 was fixed. The Resistance Sharing Factor (RSF) which describes the relative stiffness of the bars for each system is $RSF = 1/n$ where n is the number of bars in the system. The bars have equal stiffnesses and therefore initially take an equal share of the load P. The coefficient of variation for all random variables (i.e., load and bar resistances) was $\delta = .10$ and the correlation of the bar resistances was varied between $\rho_{R_iR_j} = 0.0$ (statistically independent) and $\rho_{R_iR_j} = 1.0$ (perfectly correlated). The comparison was made on structures which were balanced, 25% unbalanced, and 50% unbalanced. In this context, a balanced system is one where the mean resistances of all bars are equal. The degree of unbalance

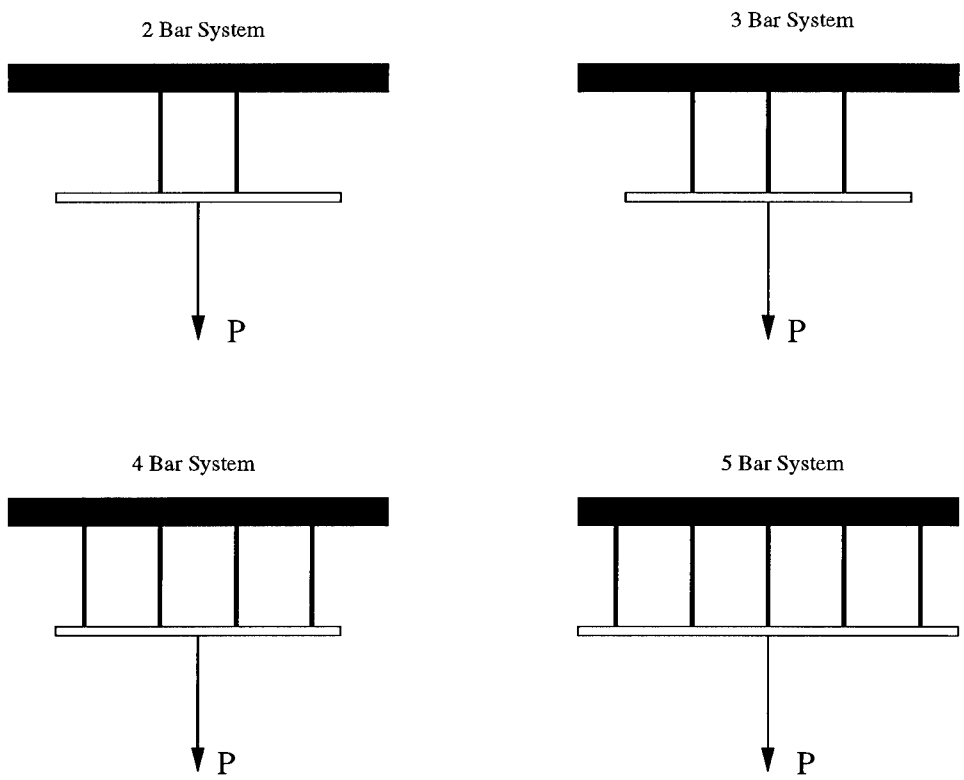

Figure 3.8: **Parallel Systems With Two, Three, Four, and Five Bars**

is computed based on the relative difference between the strongest and weakest member of the parallel system. The degree of unbalanced is calculated as [De and Cornell, 1990]:

$$\% \, Unbalance \; = 1 - \frac{\mu_{R_{Weakest}}}{\mu_{R_{Strongest}}} \tag{3.72}$$

The elastic modulus, area, and length of all bars were the same which provided an equal distribution of the load to all members. Table 3.13 shows the mean resistances in each bar for the two, three, four, and five-bar systems which are 0%, 25%, and 50% unbalanced. In each case, the mean value of the load is $\mu_P = 1.0$. Since $SSF = 1.5$, the sum of the mean bar resistances must equal 1.5. The coefficient of all random variables is $\delta = 0.10$.

The results for the two-bar system are shown in Fig. 3.9. The results obtained by RELSYS and CALREL were almost identical which was to be expected since RELSYS provides an exact answer for a 2 bar system. There was a large difference between CALREL and MCREL for the balanced system using intermediate correlation values.

The results for the three-bar, four-bar, and five-bar systems are shown in Figs. 3.10, 3.11, and 3.12, respectively. For the three-bar system, the trivariate normal distribution is integrated numerically and the RELSYS and CALREL results are almost identical. For the four and five-bar systems, the Hohenbichler approximation is used which provides excellent results for the four-bar system. The RELSYS results for the five-bar balanced system are slightly lower than those produced by CALREL. It is expected that the

Table 3.13: **Mean Resistance in Each Bar for Two, Three, Four, and Five-Bar Systems Which Are 0%, 25%, and 50% Unbalanced**

Percent Unbalanced	Two-Bar System: Mean Resistance				
	R_{bar1}	R_{bar2}	-	-	-
0	0.7500	0.7500	-	-	-
25	0.6428	0.8571	-	-	-
50	0.5000	1.0000	-	-	-
Percent Unbalanced	Three-Bar System: Mean Resistance				
	R_{bar1}	R_{bar2}	R_{bar3}	-	-
0	0.5000	0.5000	0.5000	-	-
25	0.4286	0.5000	0.8571	-	-
50	0.3333	0.5000	0.6667	-	-
Percent Unbalanced	Four-Bar System: Mean Resistance				
	R_{bar1}	R_{bar2}	R_{bar3}	R_{bar4}	-
0	0.3750	0.3750	0.3750	0.3750	-
25	0.3214	0.3482	0.4018	0.4286	-
50	0.2500	0.3125	0.4375	0.5000	-
Percent Unbalanced	Five-Bar System: Mean Resistance				
	R_{bar1}	R_{bar2}	R_{bar3}	R_{bar4}	R_{bar5}
0	0.3000	0.3000	0.3000	0.3000	0.3000
25	0.2572	0.2786	0.3000	0.3214	0.3428
50	0.2000	0.2500	0.3000	0.3500	0.4000

amount of error on the balanced system will increase as the number of bars increases. The effect was minimal in the unbalanced system where the weaker bars contribute relatively little to the overall safety of the system. The difference between RELSYS and CALREL was greatest for uncorrelated resistances and became less with increased correlation of the bar resistances. The difference between CALREL and MCREL became less with the larger number of bars.

Fig. 3.13 shows a comparison between RELSYS and CALREL for a perfectly balanced system where the CALREL results are normalized to 1.0. The RELSYS results were usually conservative. In the worst case, which is a five-bar system with no correlation between the bar resistances, the RELSYS value is low by only 5% and all other results improve from there. Fig. 3.14 makes the same comparison for a 25% unbalanced system where the results for all cases are within 2% of the CALREL results. The four-bar balanced parallel system is Example 7 in the RELSYS User's Manual (Appendix A).

3.9.2 Series-Parallel System

Hendawi [1994] made an extensive study on parallel systems using Monte Carlo simulation to calculate the system reliability of these parallel structures for different system safety factors, material behavior, and correlations. These parallel systems were modeled as series-parallel systems where every combination of failure paths was considered. In this section, the same problems were solved using RELSYS and the results are compared. Figures 3.15, 3.16, and 3.17 show two-bar, three-bar, and four-bar parallel systems along

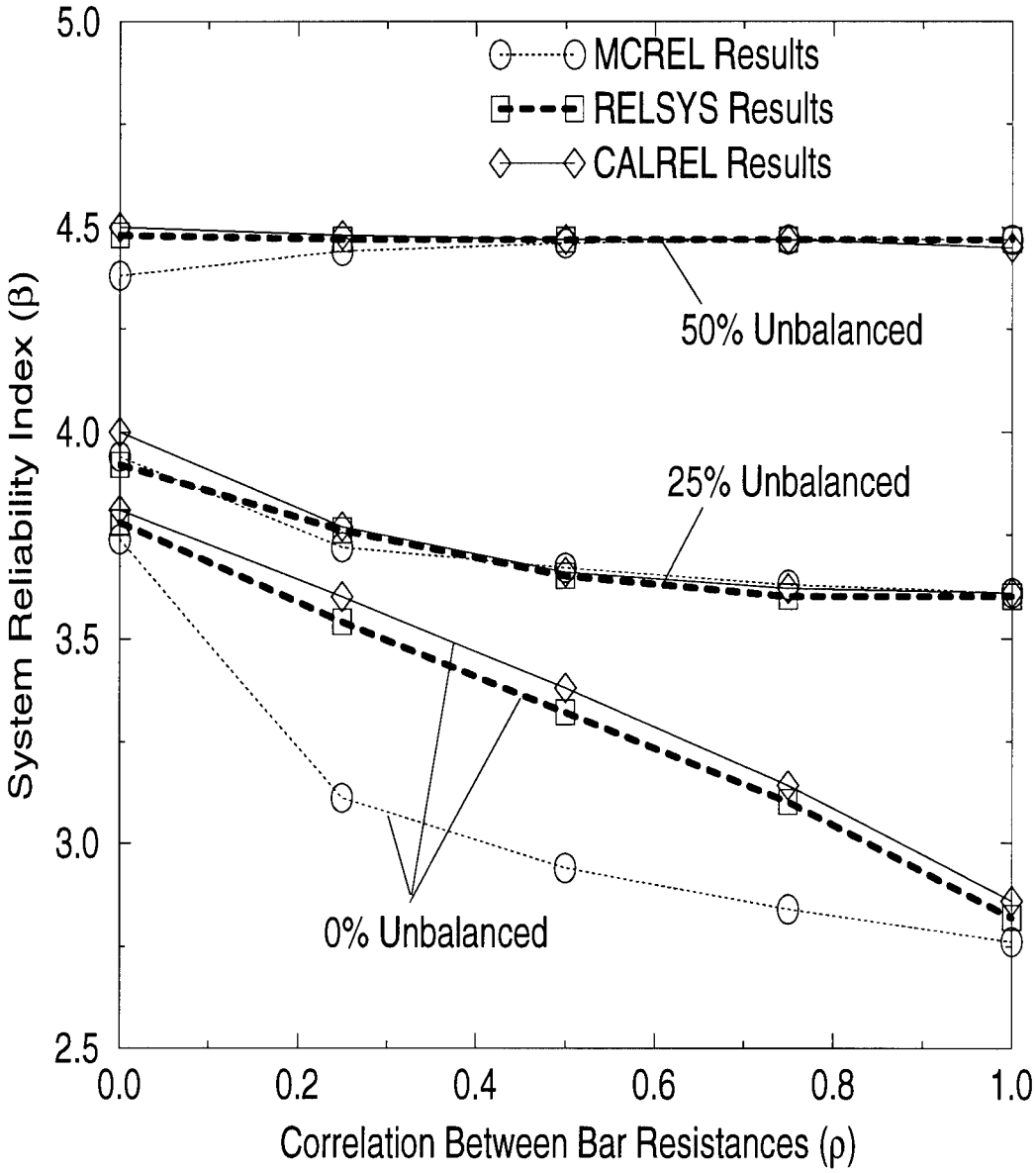

Figure 3.9: **Comparison of Results for a Two-Bar Ductile Parallel System Between RELSYS, CALREL, and MCREL**

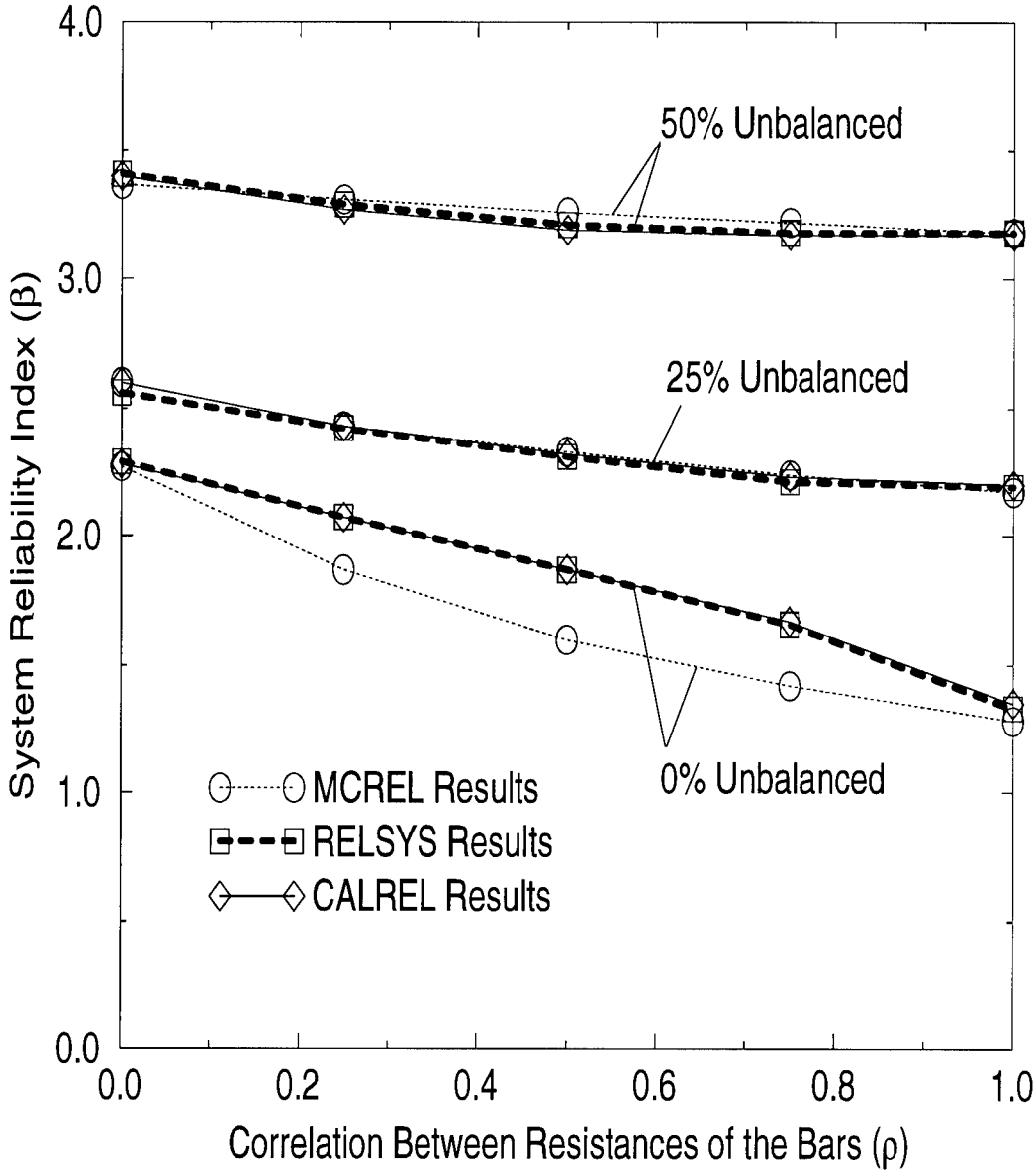

Figure 3.10: **Comparison of Results for a Three-Bar Ductile Parallel System Between RELSYS, CALREL, and MCREL**

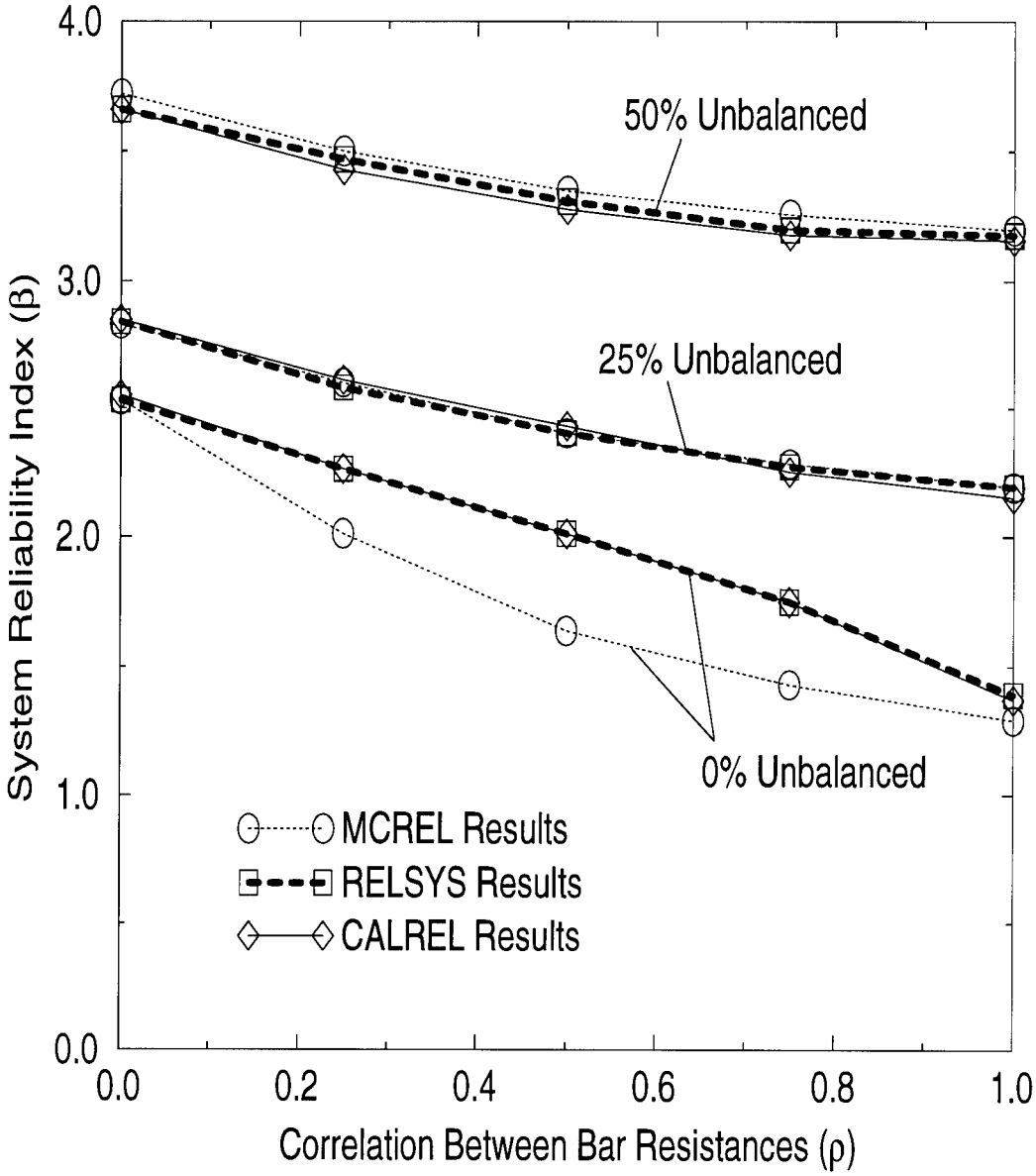

Figure 3.11: **Comparison of Results for a Four-Bar Ductile Parallel System Between RELSYS, CALREL, and MCREL**

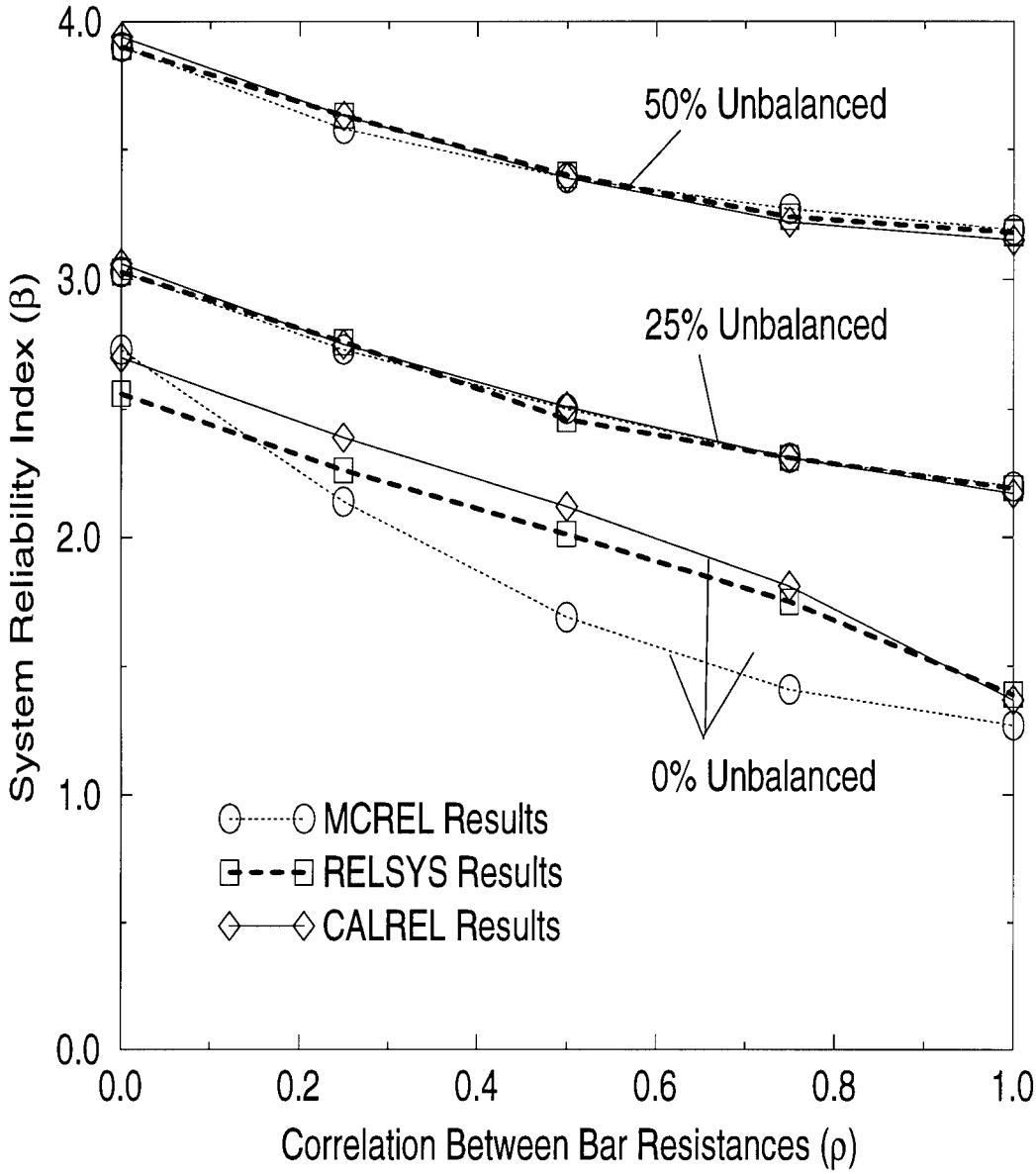

Figure 3.12: **Comparison of Results for a Five-Bar Ductile Parallel System Between RELSYS, CALREL, and MCREL**

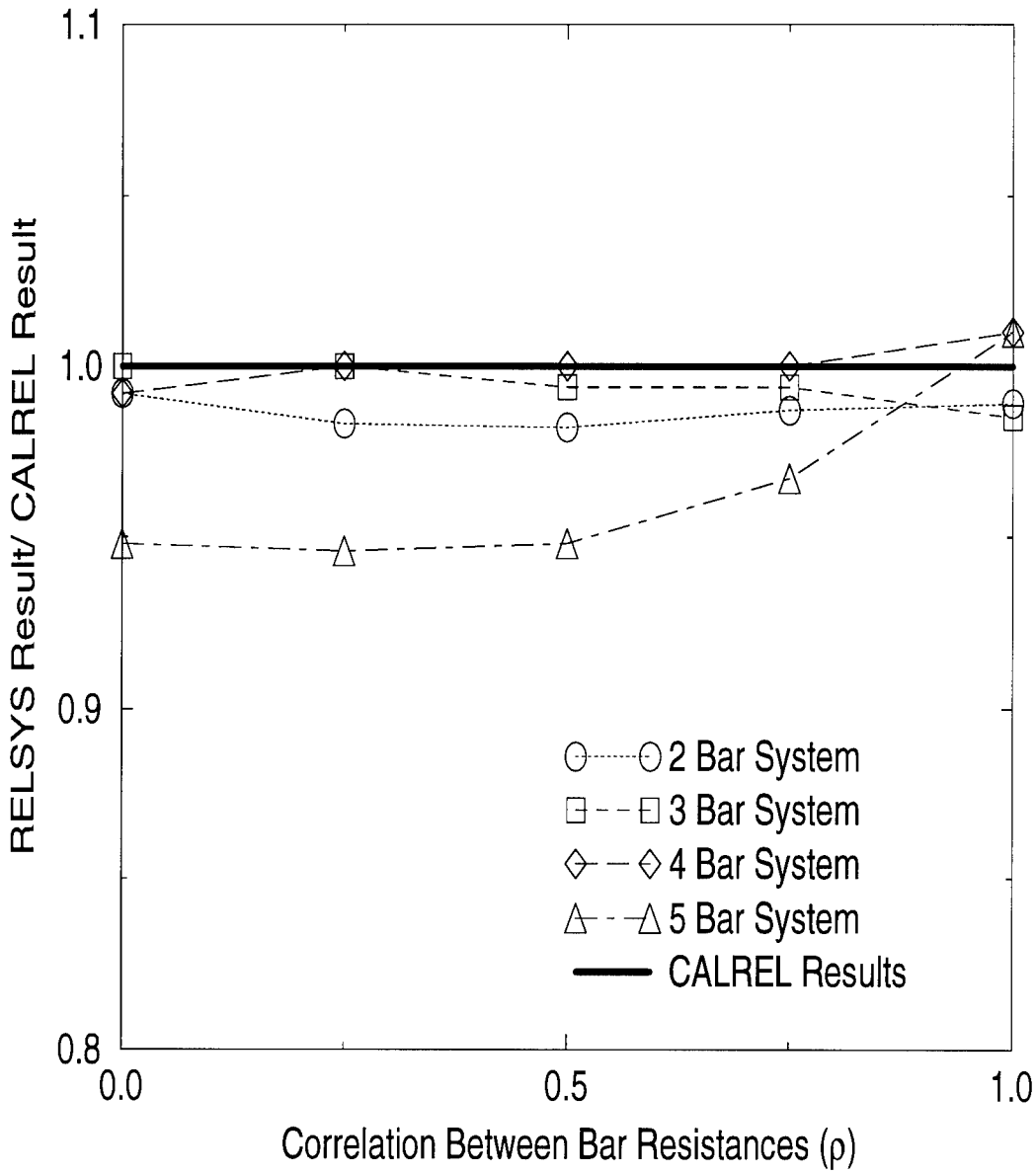

Figure 3.13: **Comparison of RELSYS Results to CALREL for Balanced Parallel Systems**

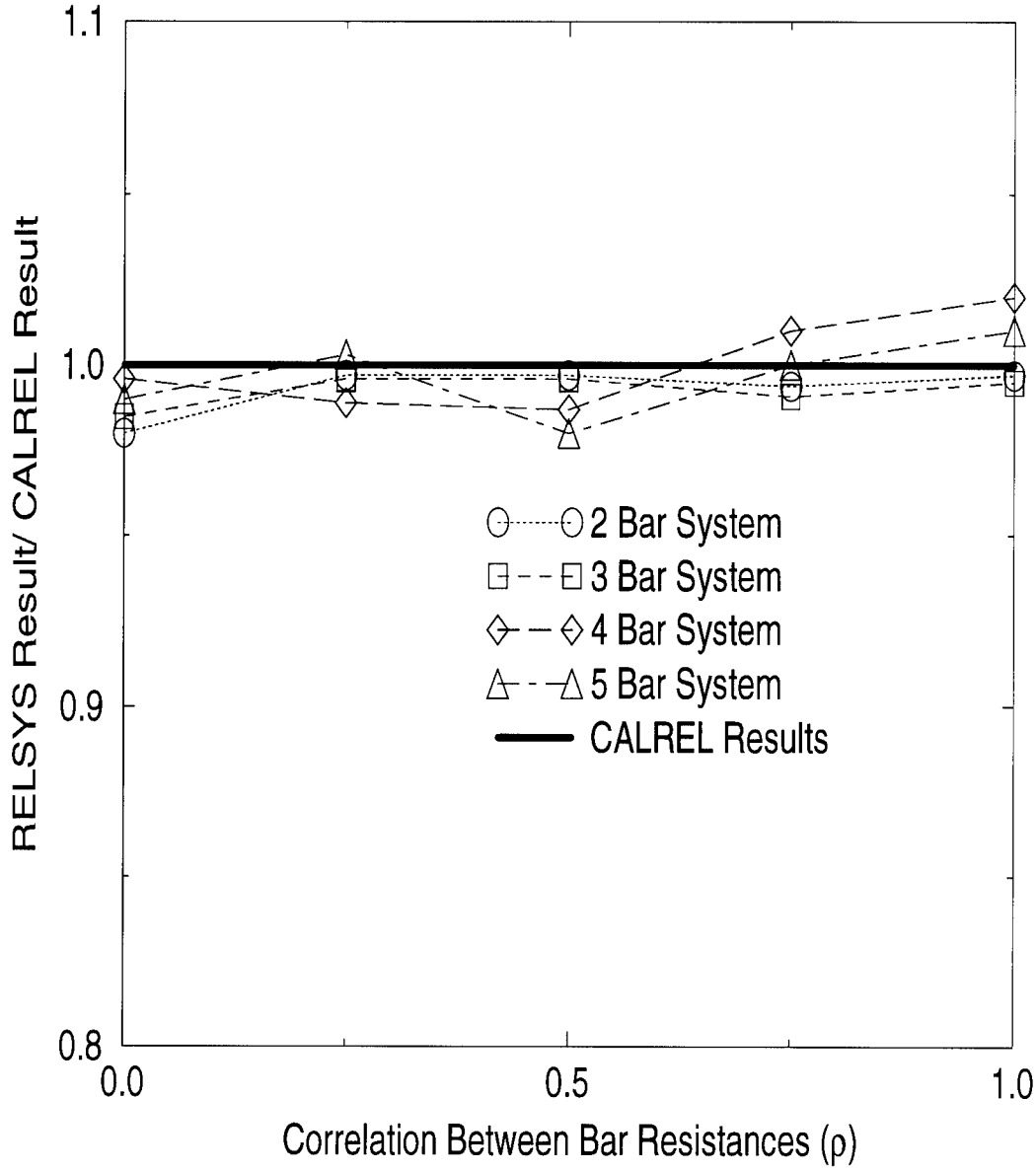

Figure 3.14: **Comparison of RELSYS Results to CALREL for 25% Unbalanced Parallel Systems**

with how they were modeled as series-parallel systems by Hendawi [1994]. Each parallel system represents a possible failure path and the structure is a series system of all possible failure paths. The two bar system, for example, is a series system with two possible failure paths. Either bar 1 fails followed by bar 2 (bar 2|1) or bar 2 fails followed by bar 1 (bar 1|2). The 3 and 4 bar structures are an expansion of the same theme.

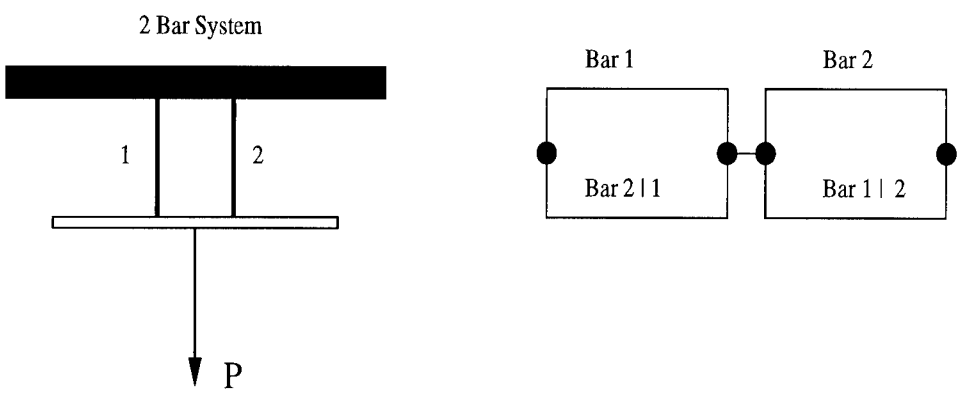

Figure 3.15: **Two Bar Parallel System Modeled as a Series-Parallel System**

Figure 3.18 compares the results obtained by Hendawi and Frangopol [1994b] to those of RELSYS where the correlation between bar resistances is 0.0 and the coefficient of variation of both the loads and resistances is 10%. The results are shown for three material behaviors indicated by the ductility factor (η). A perfectly ductile ($\eta = 1.0$), a semi-ductile ($\eta = 0.5$), and a brittle ($\eta = 0.0$) structure are considered.

The RELSYS results agree exactly for the two bar system and are

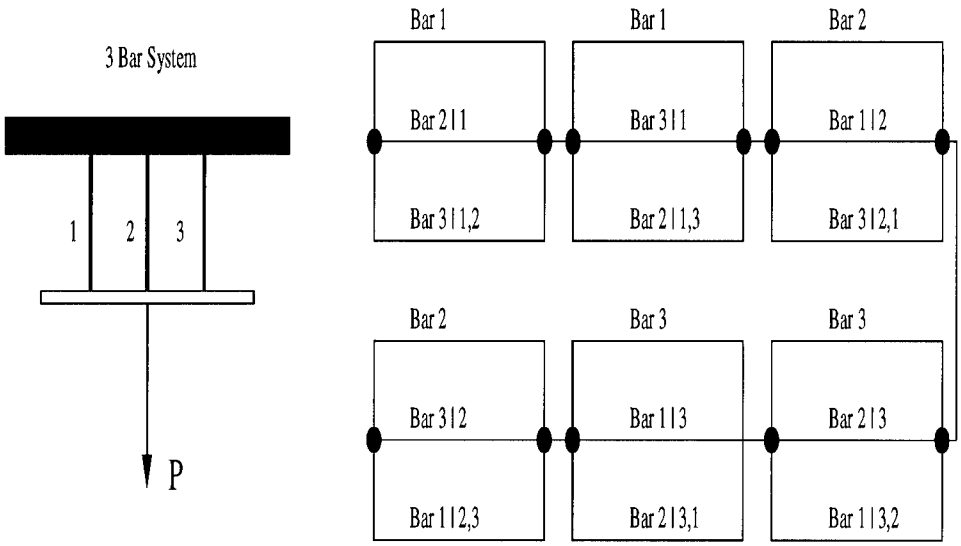

Figure 3.16: **Three Bar Parallel System Modeled as a Series-Parallel System**

progressively lower as the number of bars increases. For the worst case in the four bar structure, the RELSYS values are low by about 6%. The results are similar in Fig. 3.19 where the resistance correlation is increased to 0.5 and the worst case difference in results was 10%. With the parallel system, the RELSYS results improved with increased member resistance correlation. In the series-parallel system, this is not necessarily the case.

Figs. 3.20, 3.21, and 3.22 show three comparisons between the RELSYS and Hendawi and Frangopol [1994b] results for a ductile, perfectly correlated structure; semi-ductile, partially-correlated structure; and a brittle, uncorrelated structure, respectively. In each figure, the upper and lower Ditvelsen bounds are shown. As the number of bars increases, the gap between the

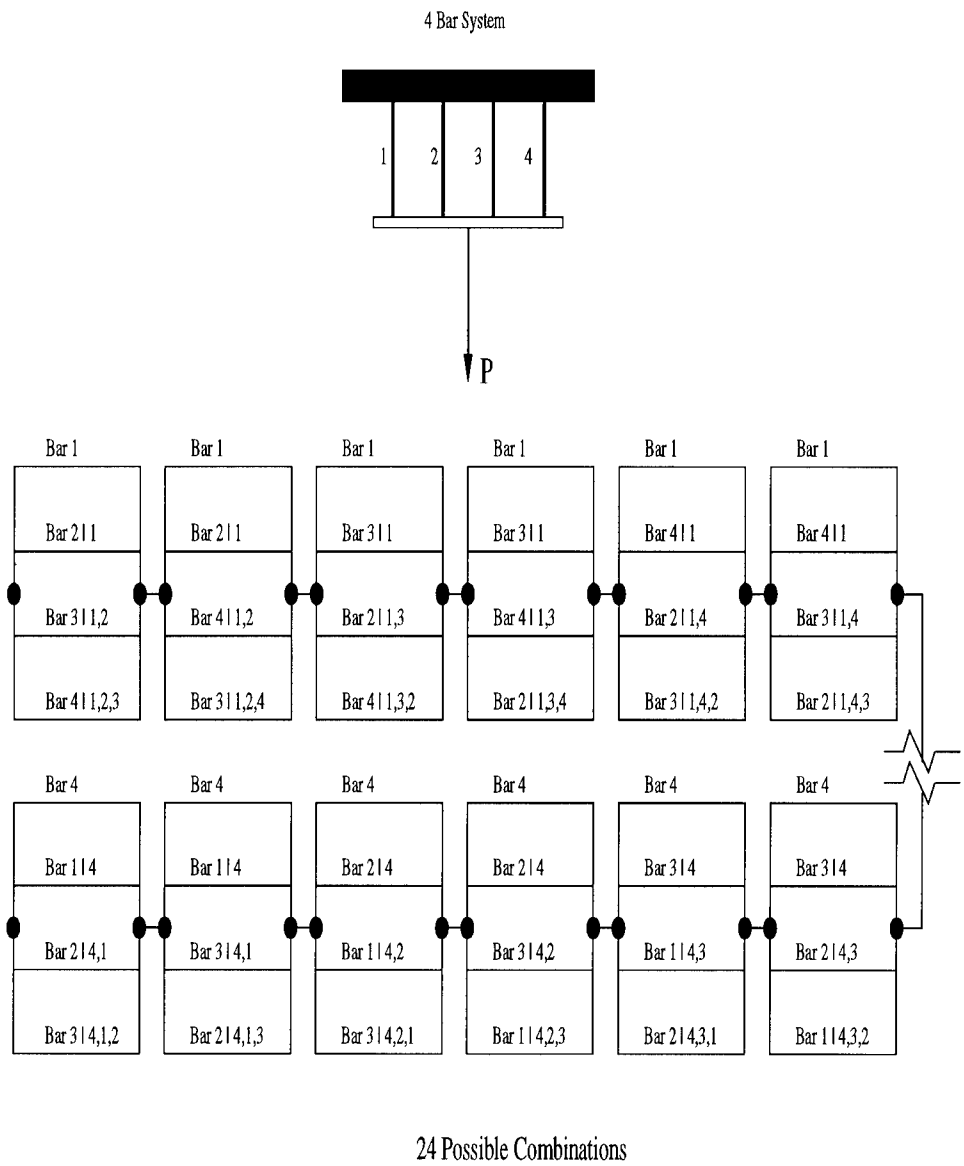

Figure 3.17: **Four Bar Parallel System Modeled as a Series-Parallel System**

Ditlevsen bounds diverges. Since the reliability of the equivalent series system is the average of these bounds, this divergence is also responsible for the difference between the RELSYS and Hendawi and Frangopol [1994b] results. This is a worst-case scenario since the Ditlevsen bounds are widest when the reliability of individual components are equal. The three bar parallel system modeled as a series-parallel system is Example 9 in the RELSYS User's Manual (Appendix A).

3.9.3 Other RELSYS Tests

RELSYS was also tested for a statically indeterminate truss modeled as a series-parallel system in Chapter 4. The RELSYS results are almost identical to those obtained from Monte Carlo simulation. The three-bar indeterminate truss is Example 10 in the RELSYS User's Manual (Appendix A).

3.10 Strengths and Limitations of RELSYS

RELSYS has the ability to compute the system reliability of any structure which can be modeled as a combination of series and parallel systems, regardless of the complexity. It is much faster than Monte Carlo simulation and gives reasonable and conservative results for most situations that are expected to be encountered in the investigation of highway bridges. RELSYS produces highly accurate results for all parallel systems with five or fewer members. The divergence of the Ditlevsen bounds produced the largest errors when the reliabilities of components in a series system were all equal, but even the worst

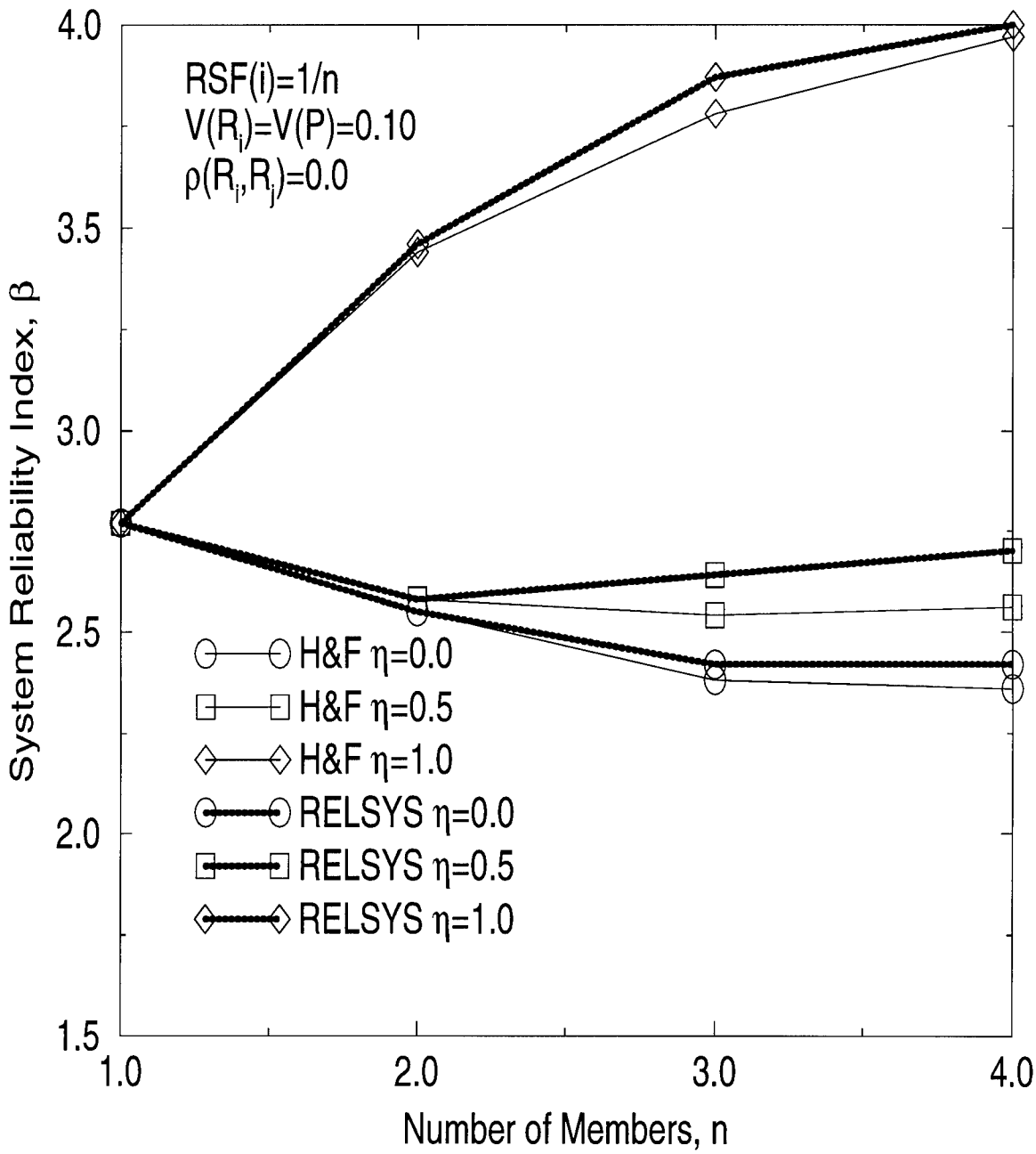

Figure 3.18: **Comparison of RELSYS Results to Hendawi and Frangopol [1994b] for Series-Parallel Systems,** $(\rho(R_i, R_j) = 0.0)$

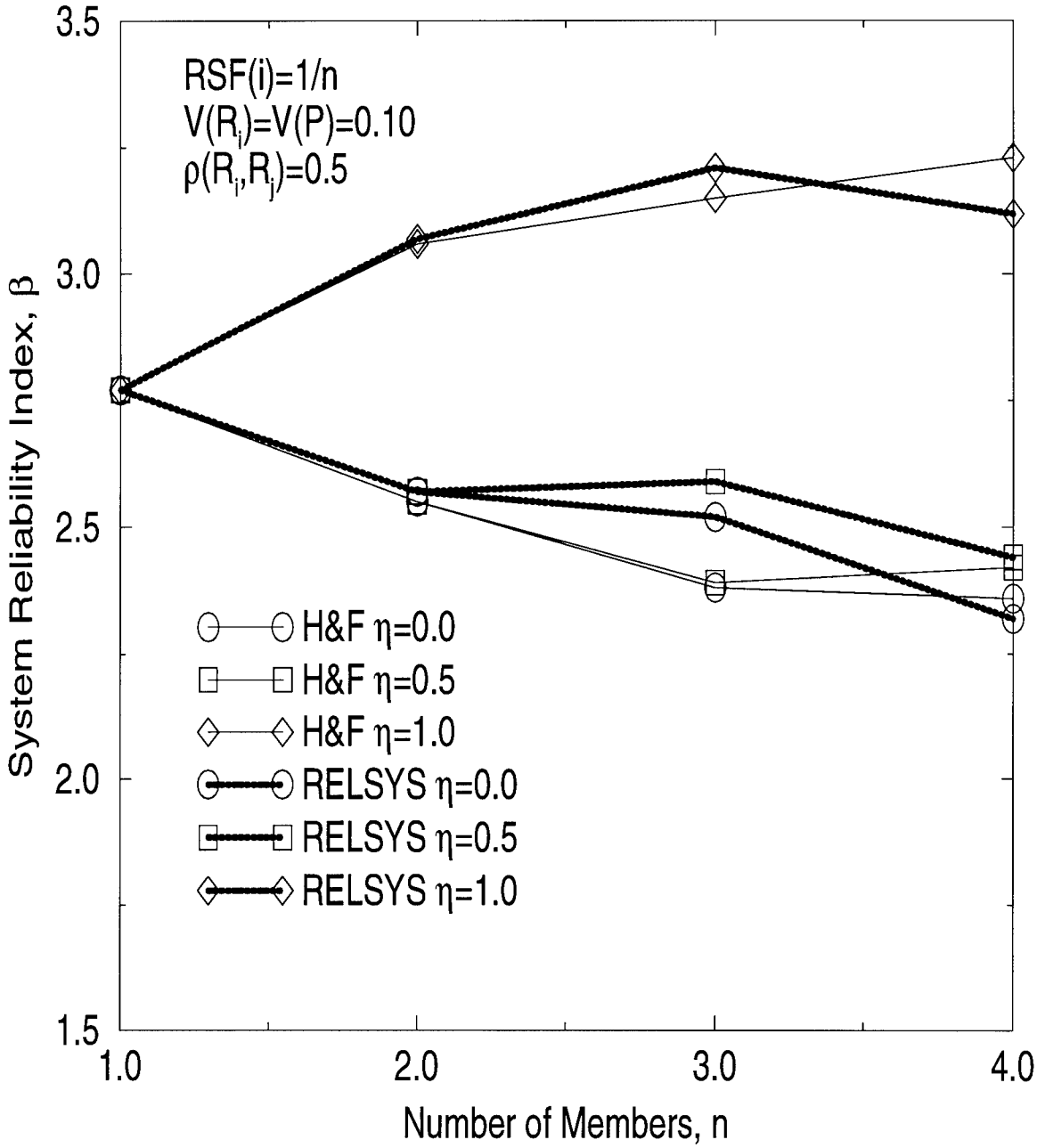

Figure 3.19: **Comparison of RELSYS Results to Hendawi and Frangopol [1994b] for Series-Parallel Systems,** $(\rho(R_i, R_j) = 0.5)$

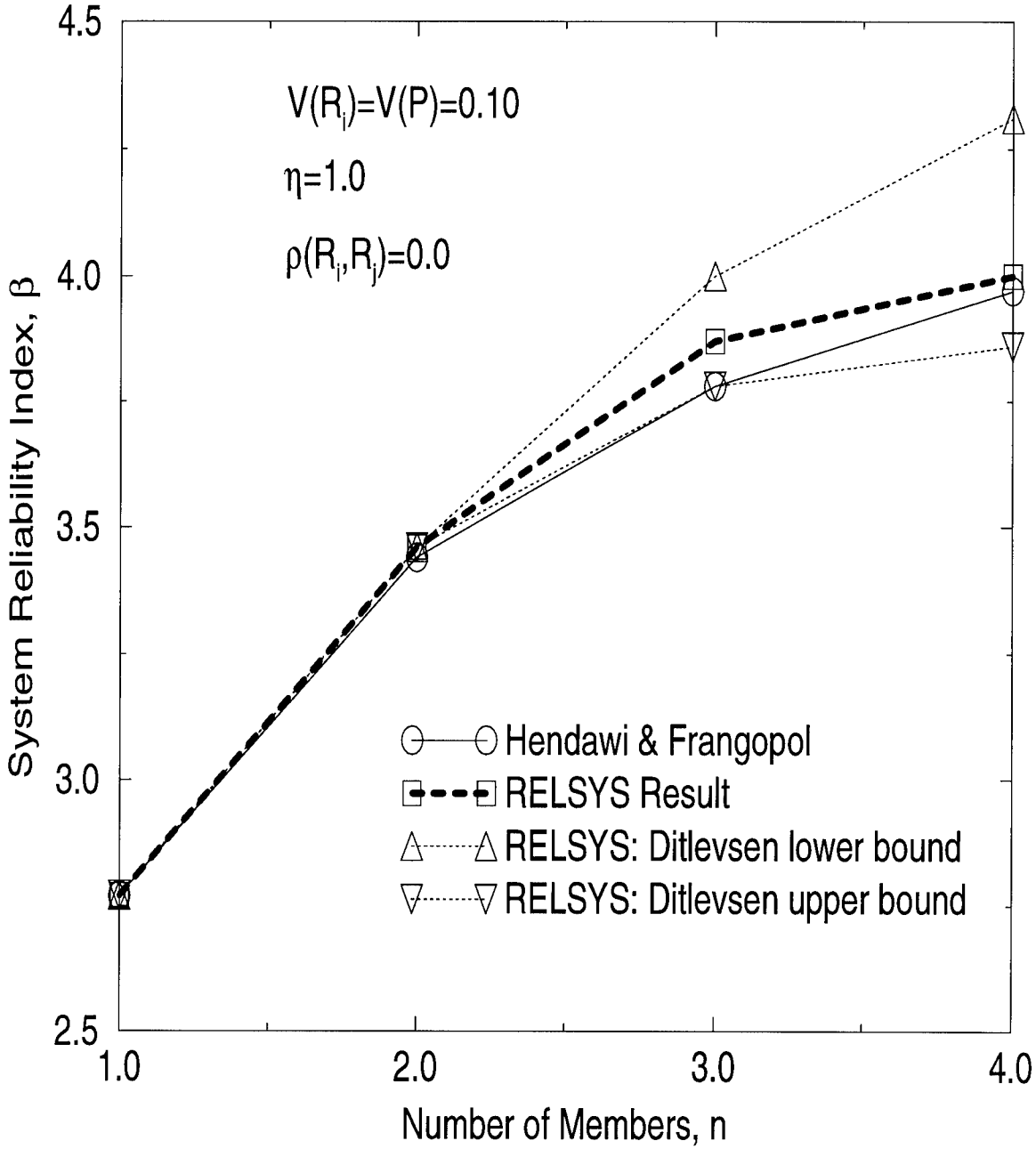

Figure 3.20: **Comparison of RELSYS Results to Hendawi and Frangopol [1994b] for Ductile, Perfectly Correlated, Series-Parallel Systems**

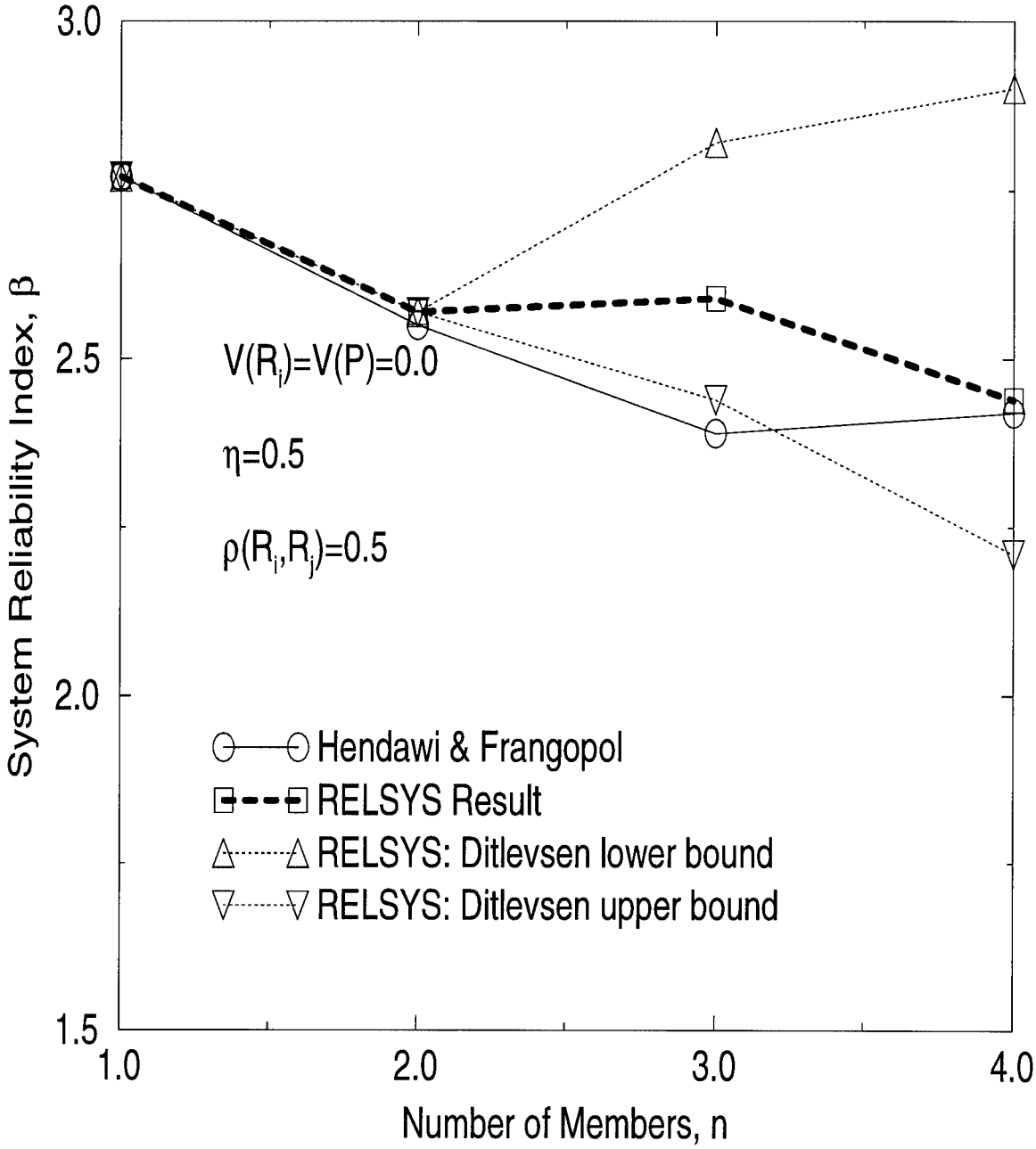

Figure 3.21: **Comparison of RELSYS Results to Hendawi and Frangopol [1994b] for Semi-ductile, Partially Correlated, Series-Parallel Systems**

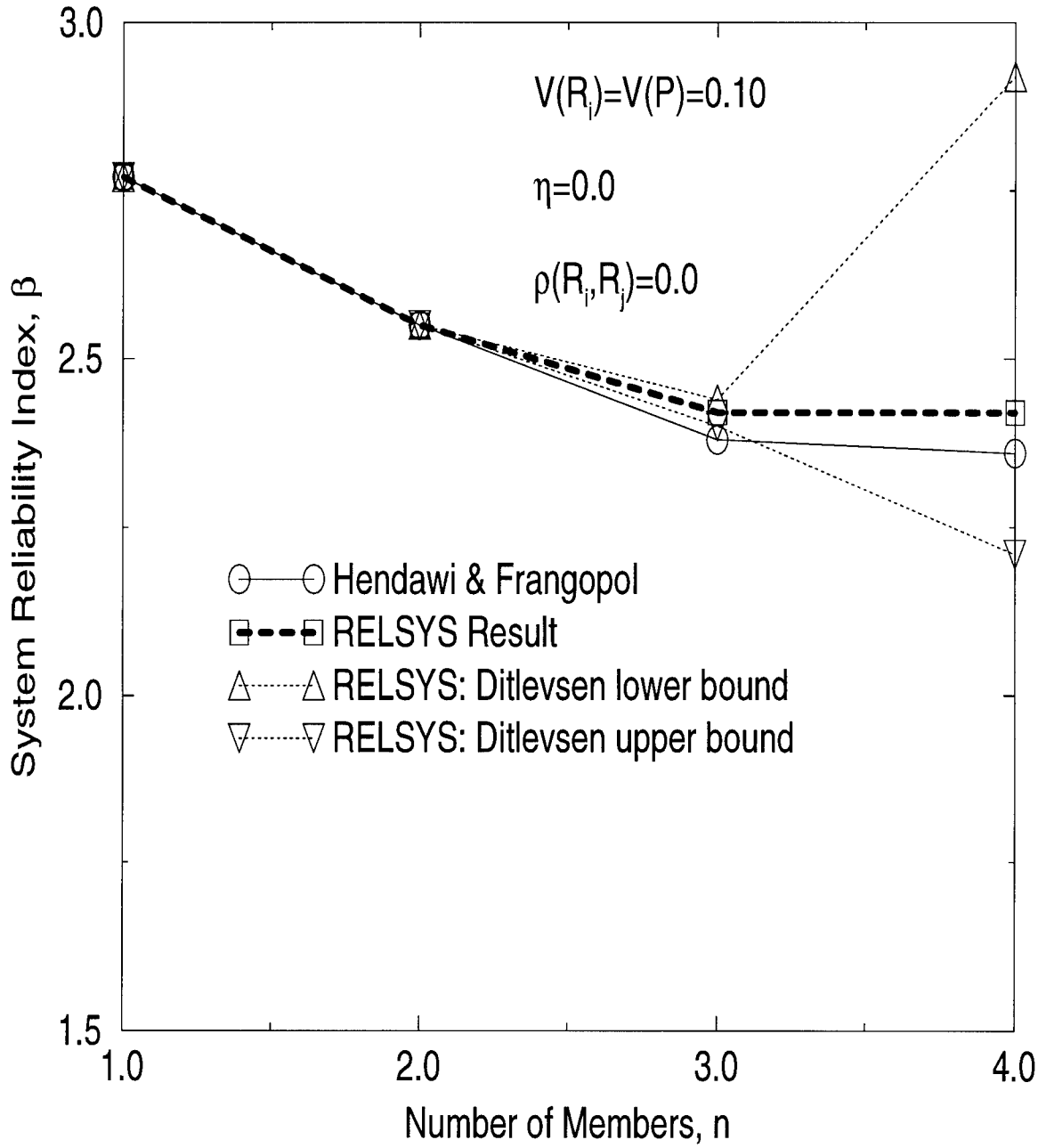

Figure 3.22: **Comparison of RELSYS Results to Hendawi and Frangopol [1994b] for Brittle, Uncorrelated, Series-Parallel Systems**

case produced answers that were within 10% of the Monte Carlo simulation solution. In general, RELSYS provides an excellent approximation for most problems with relatively little computational effort.

There are certain limitations to this approach. The FORM methods are approximations and have errors associated with them, especially with problems that are highly non-linear. Sometimes a local minimum is identified in the minimum distance optimization process and the global minimum distance to the failure surface is missed which causes the reliability to be over-estimated. This FORM approach is a level 2 reliability method, which indicates that only the mean and standard deviation are considered. Other distribution parameters such as skewness are ignored. Creating an equivalent normal distribution from a non-normal distribution can create errors, especially when that assumption is carried through the entire system analysis.

There is error associated with the bimodal bounds and the numerical integration of the multi-normal integral, especially when there is very high correlation between the components. In fact, any correlation higher than 0.99 is reduced to $\rho_{sys_{ab}} = 0.99$ which creates an additional minor error – especially for those failure modes which are perfectly correlated. It has been argued that a joint β-point is a more accurate measure of the reliability of a parallel system than the multi-normal integral solution [Enevoldsen 1991, Enevoldsen and Sϕrensen 1990, 1990a].

There is a potential problem with failure surfaces that are symmetrical or otherwise have multiple points that have the same minimum distance

from the origin to the failure surface. The β value would be the same for any of these points but the direction cosines could be very different which would have a profound effect on the system reliability.

3.11 Potential Improvements for RELSYS

Two potential areas for improvement in the RELSYS program would include:

a. Use the direct integration approach and the Hohenbichler approximation for series systems as well as parallel systems. This would reduce the inaccuracy associated with the divergence of the Ditlevsen bounds when all of the members of a series system have equal reliabilities. Since RELSYS has a routine for integrating the trivariate normal distribution, the Ditlevsen bounds could also be tightened by incorporating all three-member joint distributions in the bounds.

b. Only one search technique (gradient-based) is attempted for finding the shortest distance from the origin to the failure surface. In some cases the search does not converge. The program could be linked to ADS or some other general optimization programs to use other search strategies to improve convergence.

CHAPTER IV

OPTIMIZED REPAIR STRATEGY

4.1 Introduction

With the ability to calculate the structural reliability of an entire structural system, a minimum acceptable safety level can be specified. If the structure falls below that level, some type of remedial action needs to occur to return the structure to a safe level. With many parts of the structure deteriorating simultaneously, a choice needs to be made concerning which repairs to make. The decision involves costs of repairs, the effect of the repair on the overall reliability of the system, and the desired useful life of the structure. This chapter presents an optimization method which minimizes total lifetime cost yet avoids the complex probability tree developed in Chapter 2.

4.2 Establishing a Component Reliability Threshold

A minimum system reliability index for a structure needs to be specified. This index is a measure of acceptable risk. It defines the safety level above which the structure must remain throughout its useful life. Ideally, this system reliability is based on an analysis of the total cost of the structure. The costs of construction and maintenance are weighed against the costs of failure as described in Chapter 1. One would expect that the minimum system reliability index for a nuclear power plant or a hospital would be significantly

higher than for a grain silo or a pump house where the costs of failure are much less.

Through deterioration and/or load increase, the reliability of the system may fall below its specified minimum. Aside from demolishing the existing structure and building a new one, the only option is to repair some or all of the components which contribute to the system reliability. The approach offered here involves choosing a threshold component reliability index, $\beta_{threshold}$. When it is determined that a repair is needed because the system safety is too low, all components whose individual reliabilities fall below $\beta_{threshold}$ will be repaired. The value of $\beta_{threshold}$ is varied until an optimum repair strategy is formed based on minimum cost. In this model, the bridge is evaluated every two years and the system reliability is computed based on the results.

4.3 Series System: Seven Bar Truss

An optimum repair strategy for the seven bar, statically determinate truss shown in Fig. 4.1 will be developed. It is modeled as a series system as shown in Fig. 4.1. The areas are defined for the bottom chords (A_1), the diagonals (A_2), and the top chord (A_3). The limit state equations based on equilibrium are:

$$
\begin{aligned}
g(1) &= g(2) = R - .5(Q/A) \\
g(3) &= g(4) = g(5) = g(6) = R - .7071(Q/A) \\
g(7) &= R - Q/A
\end{aligned}
$$

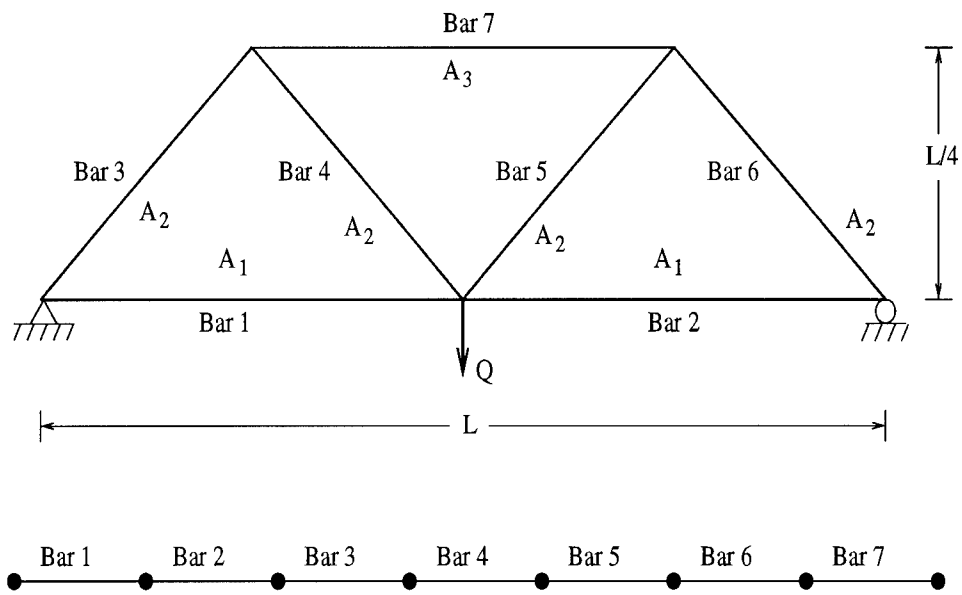

Figure 4.1: **Seven Bar Statically Determinate Truss Modeled as a Series System**

where R is the resistance of the bars; Q is the load on the truss; and A is the area of the bars which is changing over time using the same deterioration model described by Eqn. 2.3. The inherent assumptions are that the bar resistances are perfectly correlated and the resistance of each bar is the same in tension and compression.

The desired useful life of the truss is 70 years and the minimum allowable system reliability index is $\beta_{min} = 2.0$. The load (Q) and bar resistances (R) are normally distributed random variables with values equal to: $R = N[2, .2]$ and $Q = N[1, .1]$. The cost of a repair is equal to the sum of a variable cost ($C_{var} = 5.0$) which is charged for each bar repaired and a fixed cost ($C_{fix} = 5.0$) which is charged each time a repair is made. The cost model was deliberately kept simple to observe the trends in the problem. The model could easily be modified to include damage intensity and time value of money.

The first truss to be optimized is one where the areas of the bars have been designed ($A_1 = 1.0$; $A_2 = 1.4142$; $A_3 = 2.0$) so that each component has the same reliability when the truss is placed in service. Using the deterioration model in Eq. 2.3 and Fig. 2.2, the truss is inspected every two years. Because the bars have different sizes, the reliability of the bars will differ over time as the equal depth of deterioration has a different effect on these bars. Fig. 4.2 shows the results when $\beta_{threshold} = 7.4$ which causes every bar to be repaired whenever the system reliability falls below β_{min} and results in a total lifetime cost of 80. Repairs were required after 28 and 56 years of service.

Lowering $\beta_{threshold}$ to 4.0 as shown in Fig. 4.3 results in repairs after

28 and 50 years of service. Only bars 1 and 2 are fixed during the first repair. Bars 1 through 6 are repaired the second time and bar 7 is never repaired. The resulting cost is 50 which turns out to be the optimum solution.

Fig. 4.4 indicates that $\beta_{threshold}$ can be lowered further to 2.6 but the resulting lifetime cost is 55. Repairs are made at 28, 50 and 56 years. Bars 1 and 2 were not repaired at year 50 as they were in Fig. 4.3. As a result, a special repair was required at year 56 for bars 1 and 2 which resulted in additional cost.

All possibilities can be considered starting with a high enough $\beta_{threshold}$ value to ensure that all components must be repaired and then incrementally lowering the $\beta_{threshold}$ value until the structure cannot maintain the desired safety over its useful life. Fig. 4.5 shows the resulting costs associated with the varying $\beta_{threshold}$ values. The optimum solution occurs when $3.4 \leq \beta_{threshold} \leq 4.6$. The range for the optimum $\beta_{threshold}$ solution is wide because there are so few repair options in this problem. This technique is most efficient for cases where the number of discrete repair options is large.

The truss was analyzed again where all of the bars started with equal areas ($A_1 = A_2 = A_3 = 1.0$). In this case, the deterioration affects each bar equally but the component reliabilities are different because some bars take a larger proportion of the load. Fig. 4.6 shows the optimum solution using a value of $\beta_{threshold} = 4.0$. Repairs are required every eight years with bar 7 being repaired every time. Bars 3, 4, 5, and 6 get repaired every other time and bars 1 and 2 are repaired every third time. The total lifetime cost is 180. The cost

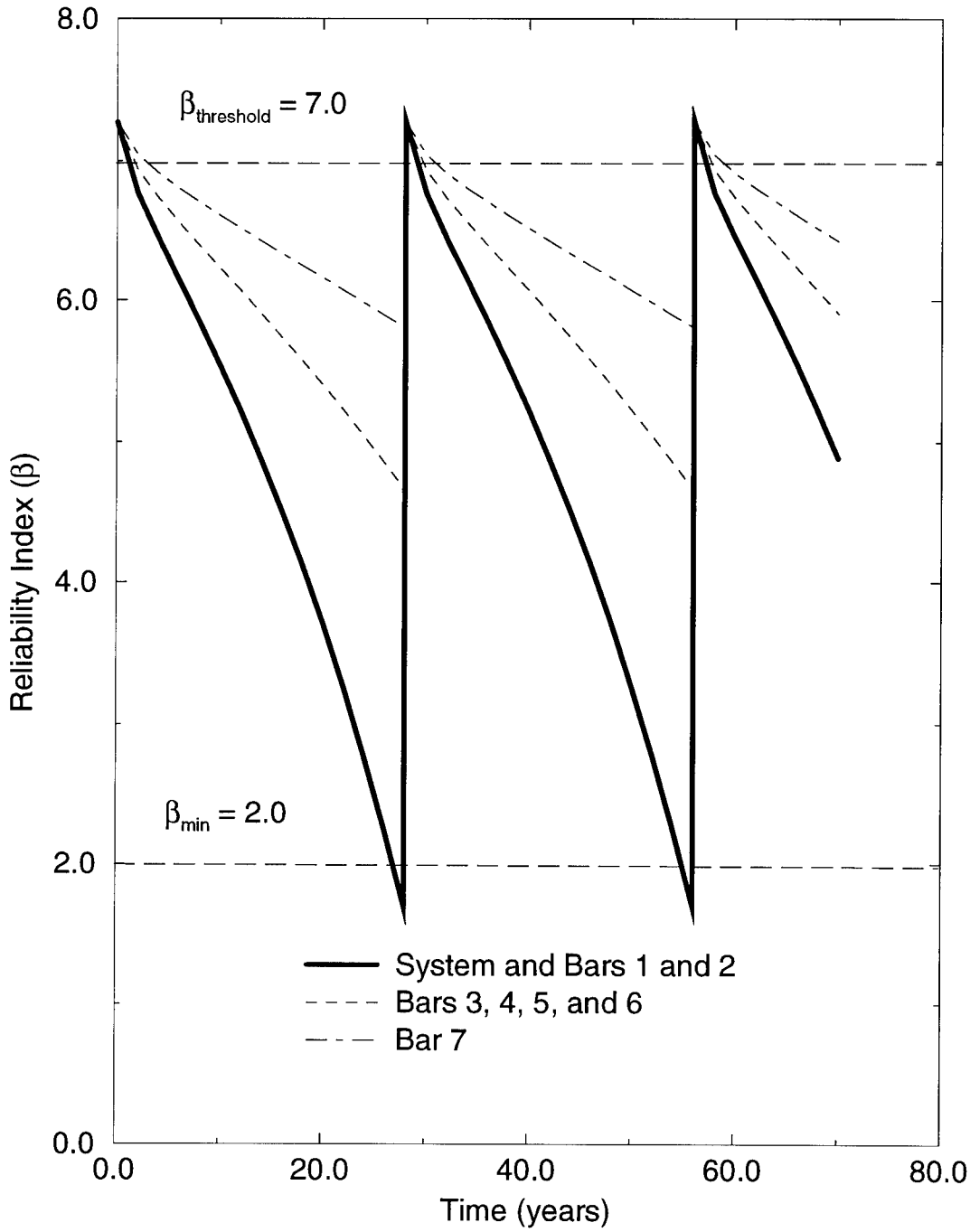

Figure 4.2: **Repair Plan for a Seven Bar Statically Determinate Truss, Initial Equal Importance of Bars;** $\beta_{threshold} = 7.0$; $Cost = 80$

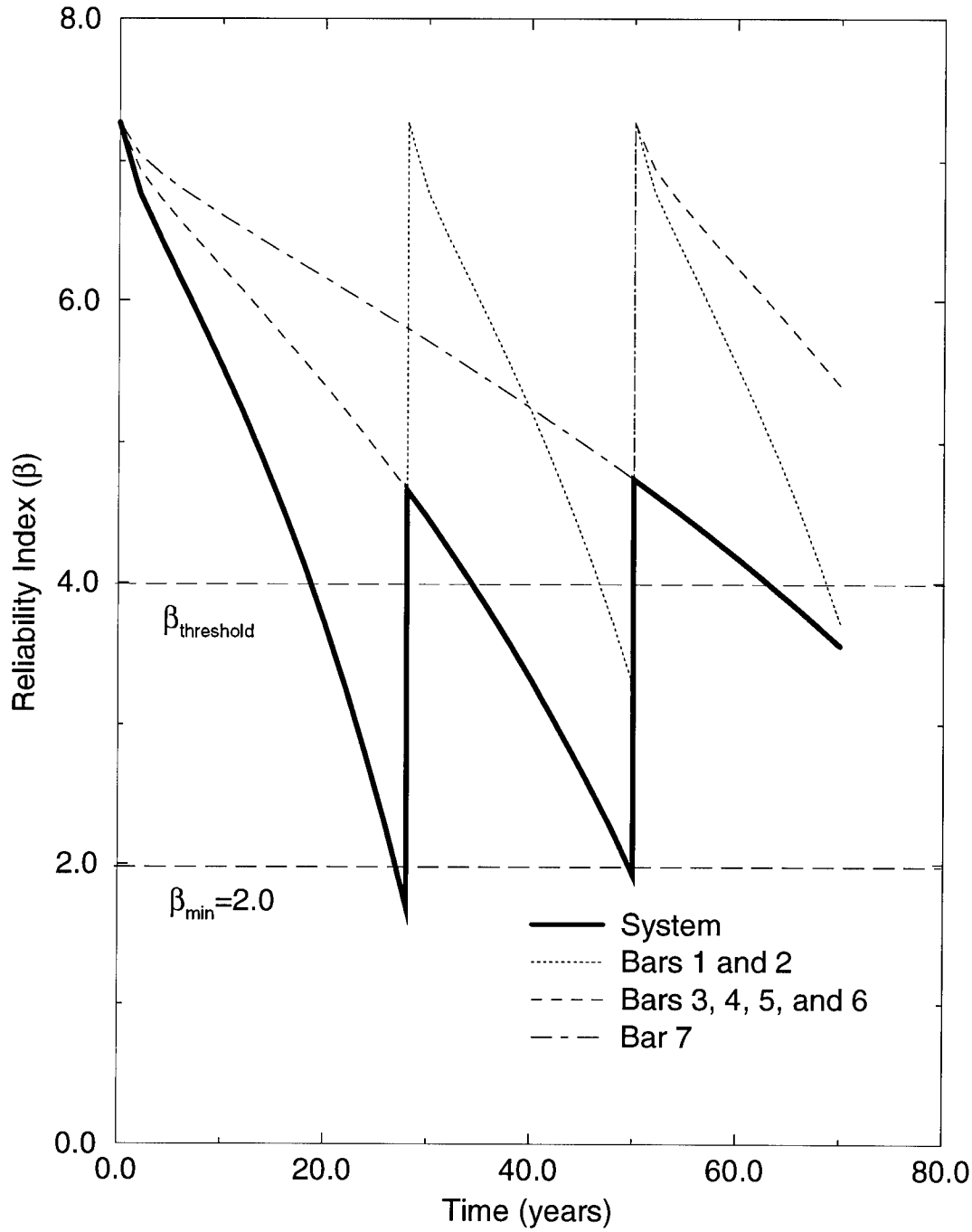

Figure 4.3: **Repair Plan for a Seven Bar Statically Determinate Truss, Initial Equal Importance of Bars;** $\beta_{threshold} = 4.0$; $Cost = 50$

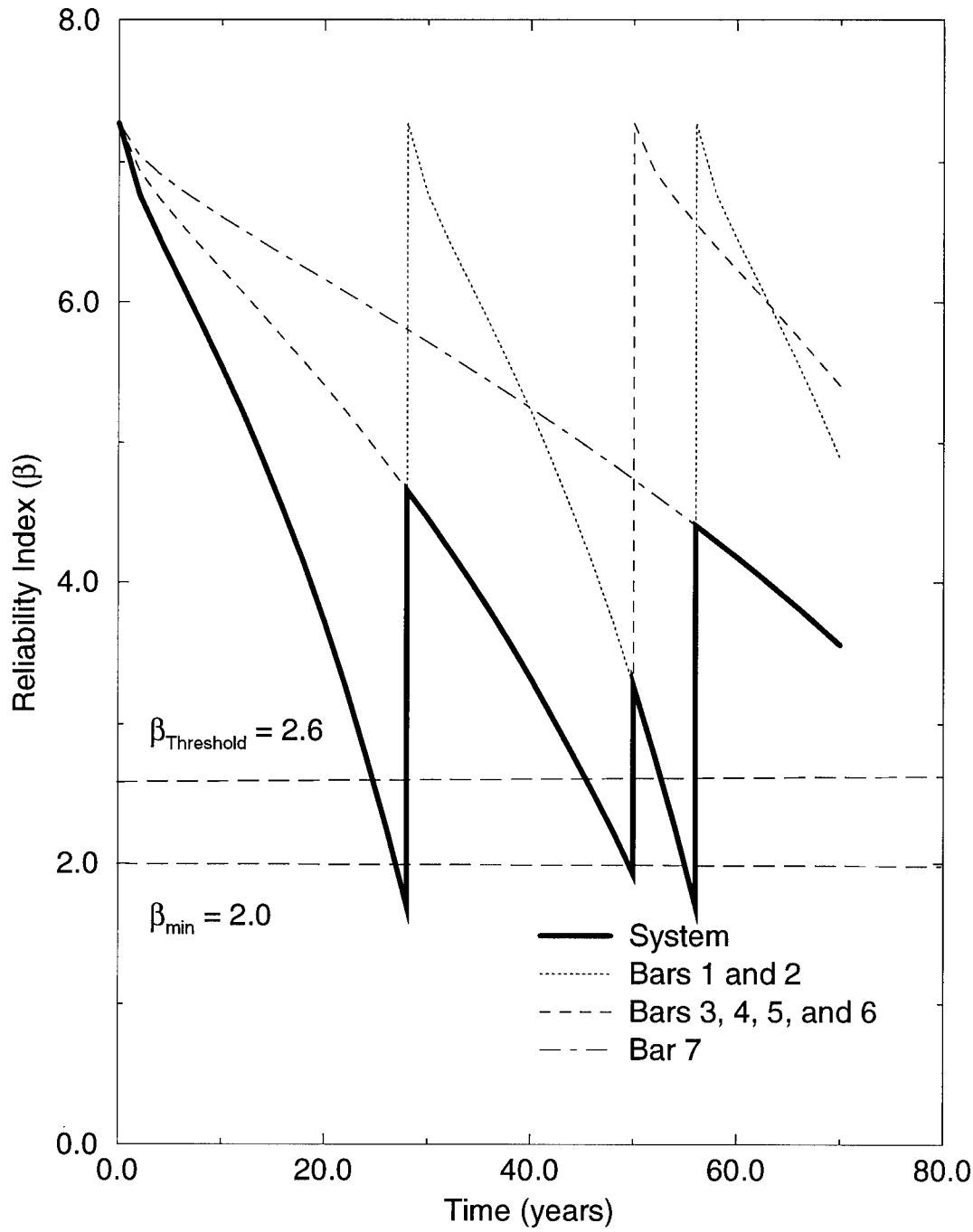

Figure 4.4: **Repair Plan for a Seven Bar Statically Determinate Truss, Initial Equal Importance of Bars;** $\beta_{threshold} = 2.6$; $Cost = 55$

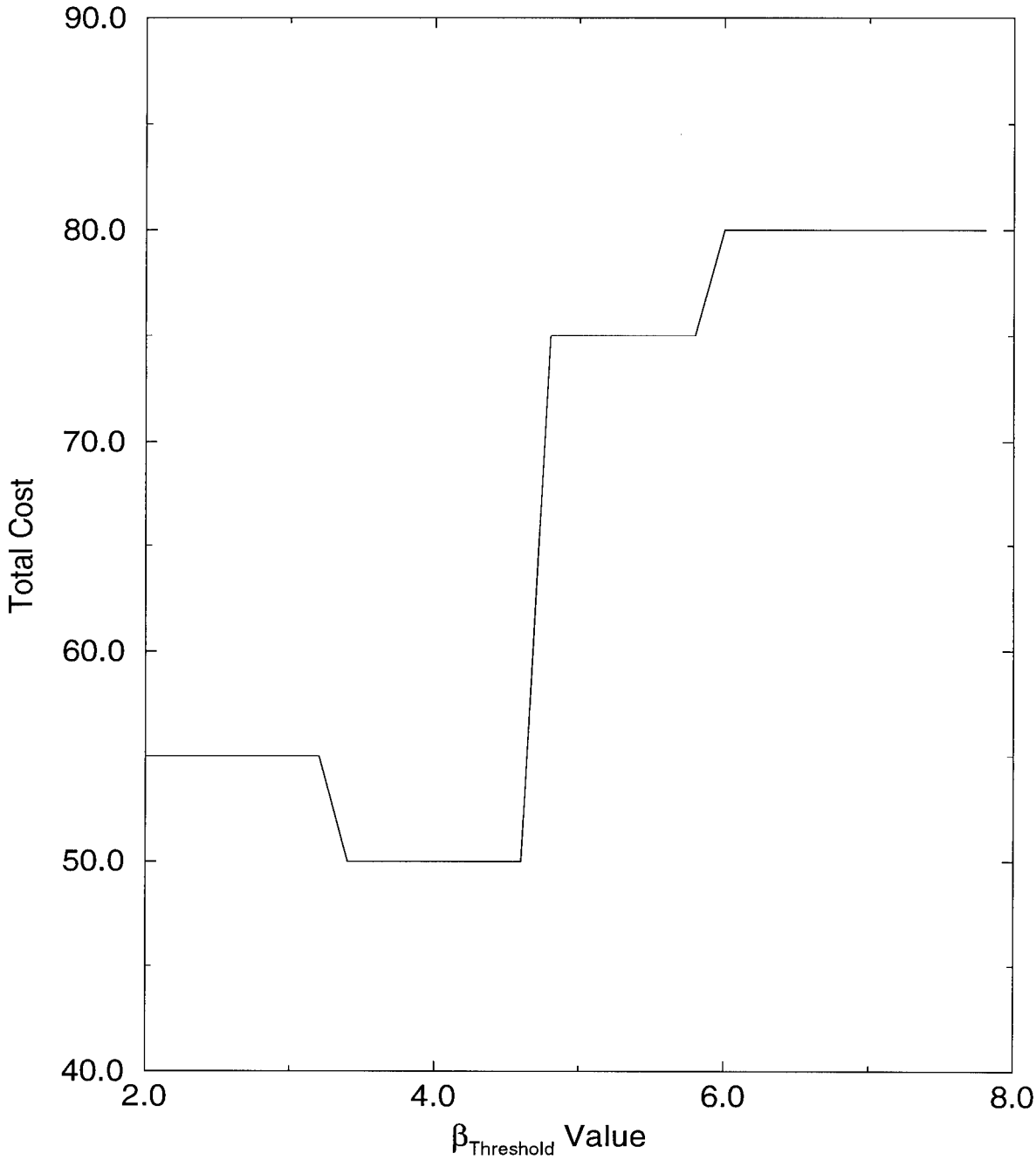

Figure 4.5: **Total Cost of Repair With Varying Values $\beta_{threshold}$ for a Seven Bar Statically Determinate Truss, Initial Equal Importance of Bars**

associated with all feasible $\beta_{threshold}$ values is shown in Fig. 4.7. Note there is a slight jump in cost from 180 to 185 when $\beta_{threshold} = 2.6$. This particular value represents a special case where some bars just missed the threshold for repair which caused an additional special repair later on.

4.4 Parallel System

The repair of the three bar parallel structure shown and modeled in Fig. 3.16 is optimized using the same useful life of 70 years and a minimum acceptable reliability of $\beta_{min} = 2.0$. The load (P) and bar resistances (R) are normally distributed with values equal to: $P = N[1.5, 0.3]$ and $R = N[.5, .05]$. All variables are uncorrelated.

For a balanced system (i.e., one where the bar resistances are the same), the component reliabilities are the same for all three bars at all times. The load is distributed to the members according to relative stiffness. As one member deteriorates, the other members take more load. The reliability of each member drops but the component reliabilities all remain equal. Fig. 4.9 shows this effect for the ductile three-bar structure in Fig. 3.16. The bar areas are equal ($A_1 = A_2 = A_3 = 2.0$) and the deterioration model is shown in Eq. 2.3 and Fig. 2.2. The individual reliabilities are allowed to fall below $\beta_{min} = 2.0$, yet the system reliability remains above the specified minimum. The optimal solution is trivial and requires repairing all bars at once.

The effect of material behavior can be observed using a ductility factor η which reflects the post-elastic capacity of the material as shown in

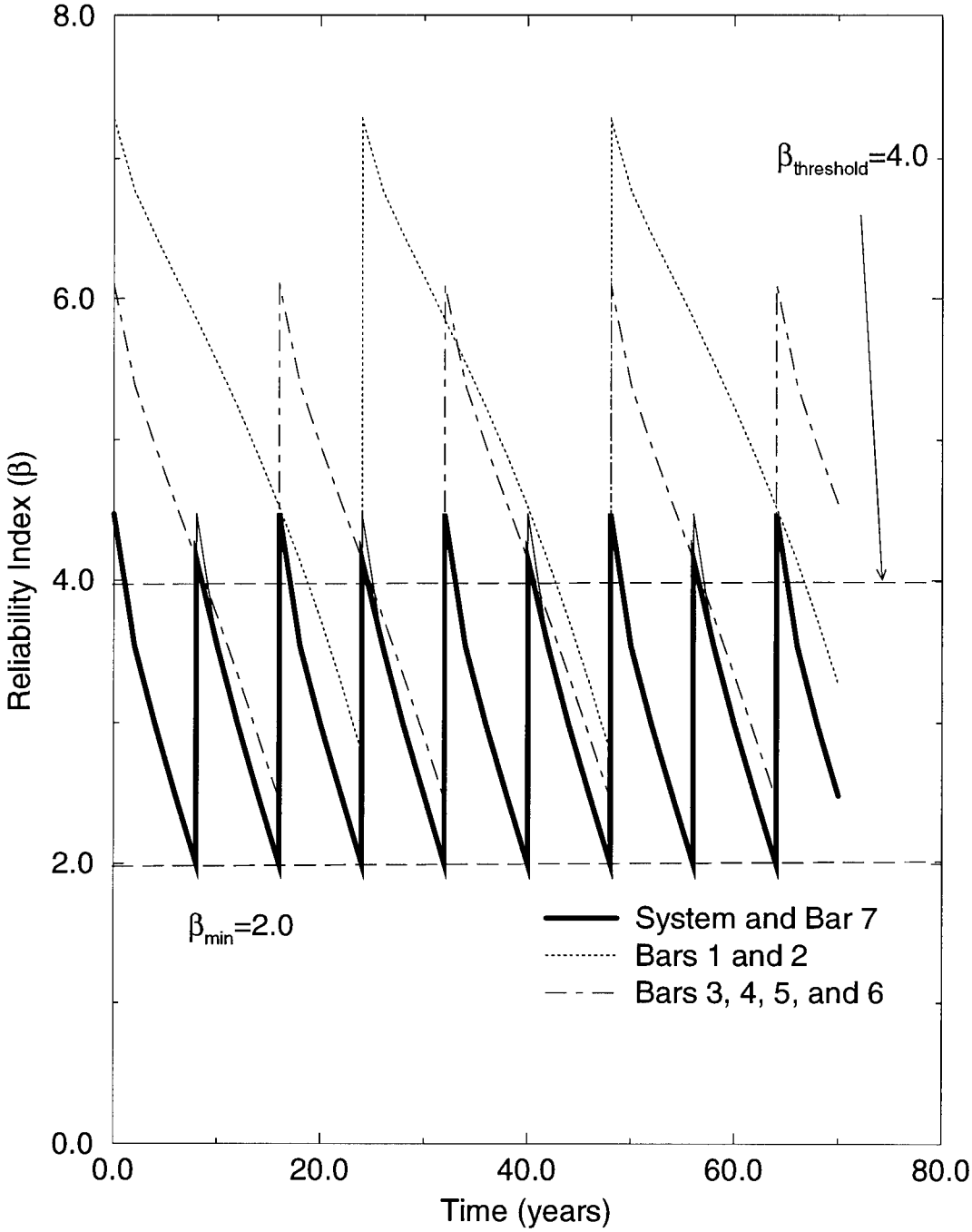

Figure 4.6: **Repair Plan for a Seven Bar Statically Determinate Truss, Initial Equal Bar Areas;** $\beta_{threshold} = 4.0$; $Cost =$ 180

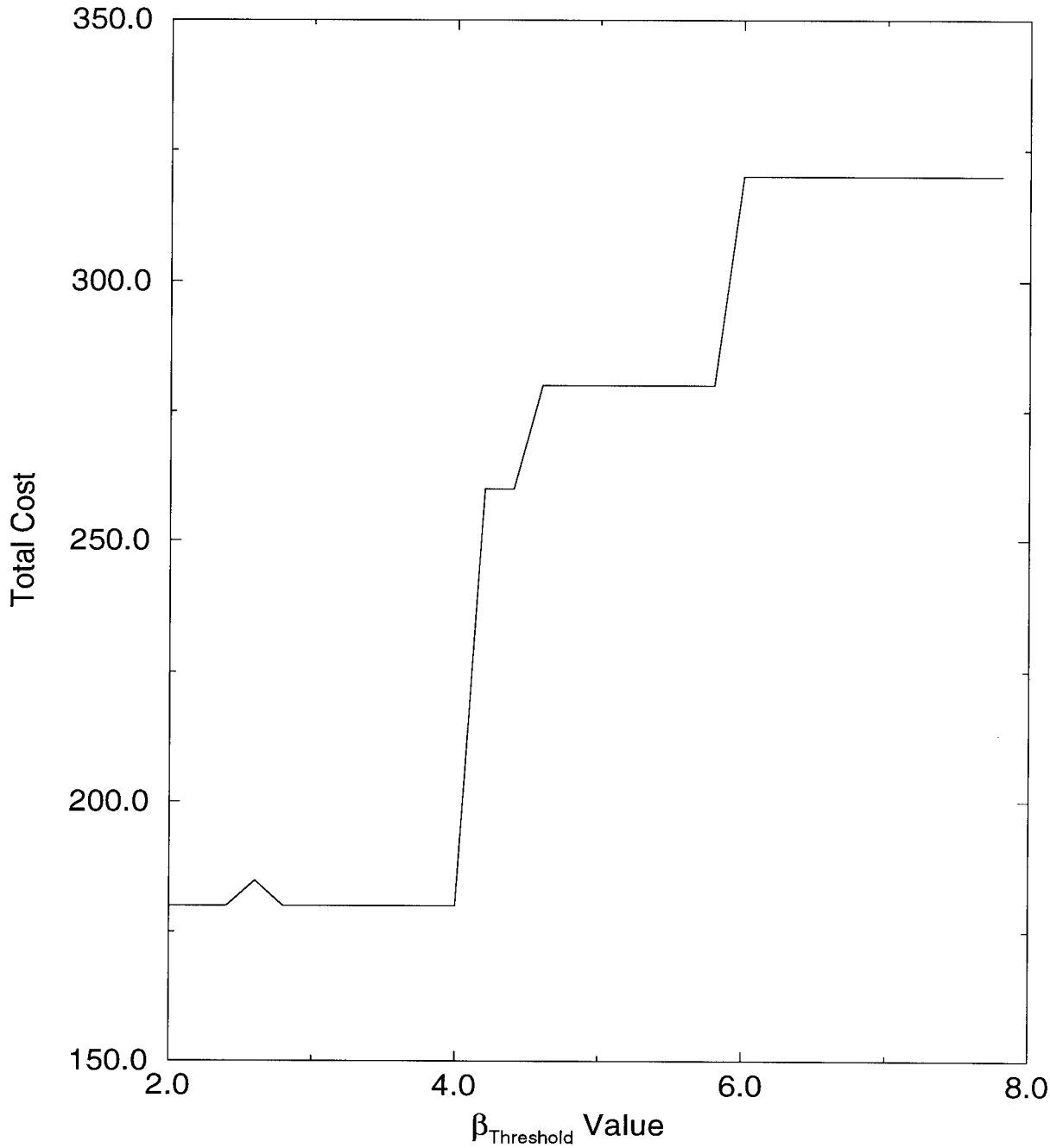

Figure 4.7: **Total Cost of Repair With Varying Values $\beta_{threshold}$ for a Seven Bar Statically Determinate Truss, Initial Equal Bar Areas**

Fig. 4.8. The values of η range from $\eta = 1.0$ for a ductile structure which retains full yield capacity after reaching its elastic limit to $\eta = 0.0$ for a brittle structure which has no post-yield capacity. The semi-ductile case ($\eta = 0.5$) for the three bar parallel structure is shown in Fig 4.10 where the individual component reliabilities must remain above the reliability of the system.

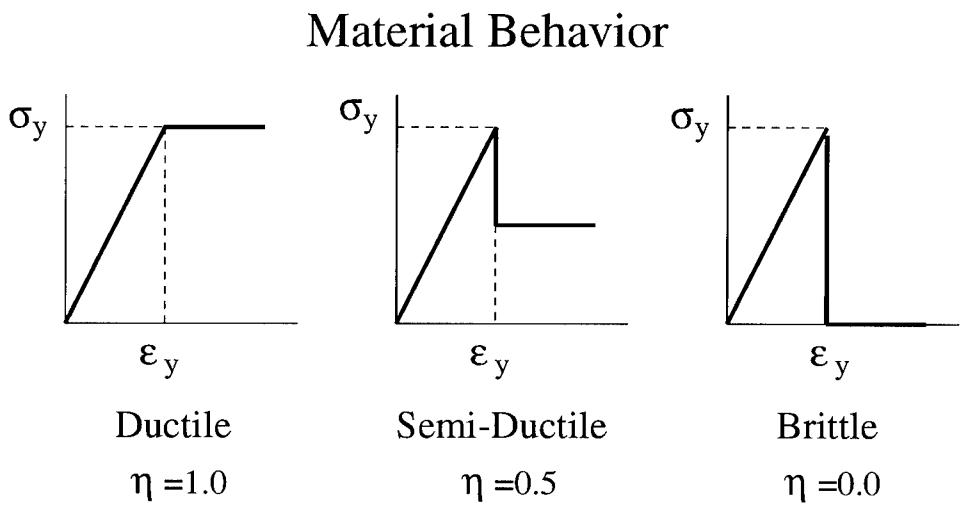

Figure 4.8: **Material Behavior Using a Ductility Factor** η

The respective reliabilities of the bars remain equal even if the bar areas are different ($A_1 = 0.5,\ A_2 = 2.0,\ A_3 = 3.5$). Fig. 4.11 shows that the smallest bar, Bar 1, eventually deteriorates to the point it no longer exists. The remaining two bars provide adequate system safety until their eventual deterioration forces a repair. Comparing Fig. 4.9 and 4.11, the reliability of the parallel system with bars of equal areas was higher and was repaired later in its structural life.

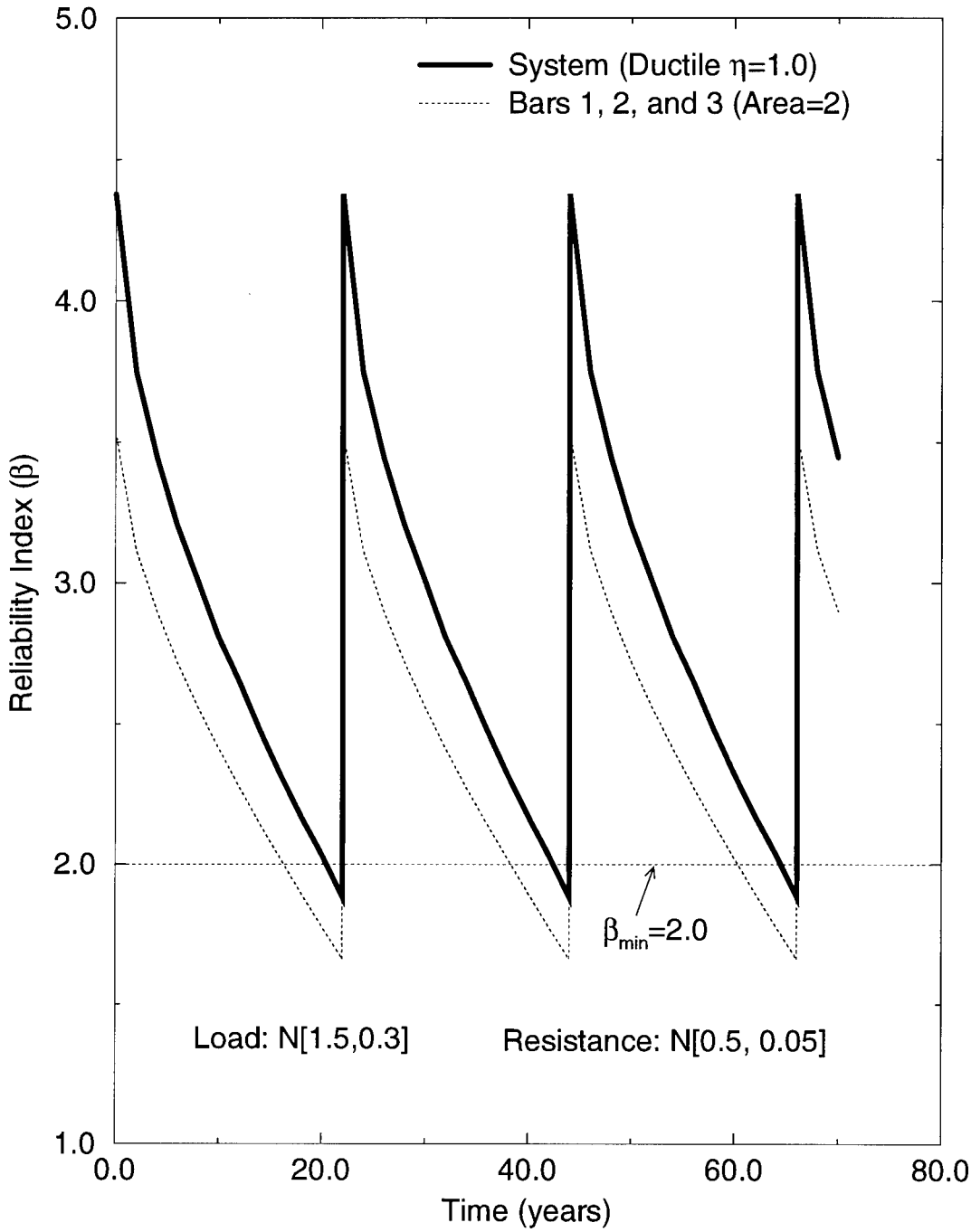

Figure 4.9: **Repair Plan for a Ductile Three Bar Parallel System with Equal Bar Areas $A_1 = A_2 = A_3 = 2.0$, Load: N[1.5,0.3], Resistance: N[0.5, 0.05], No Correlation.**

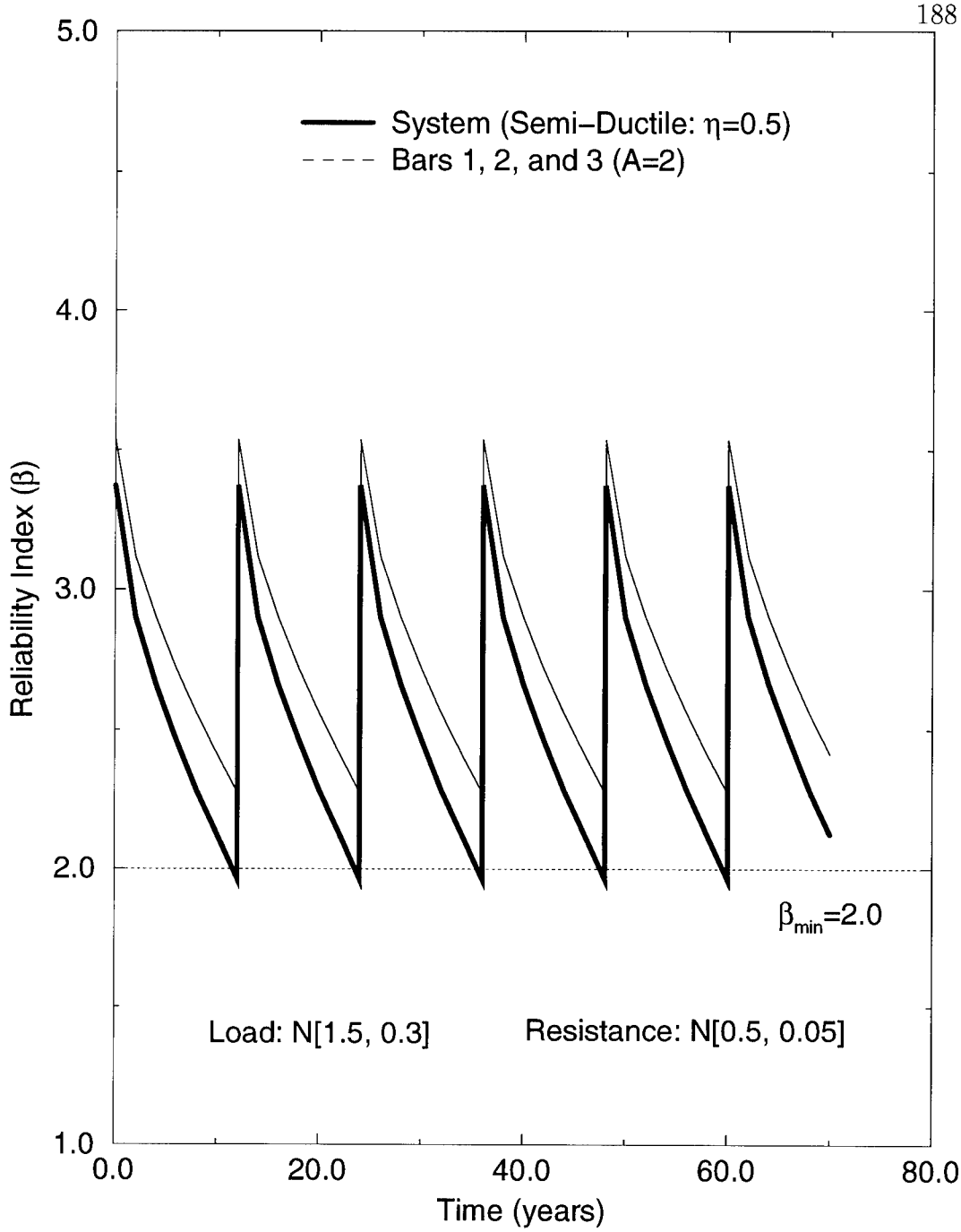

Figure 4.10: **Repair Plan for a Semi-Ductile Three Bar Parallel System with Equal Bar Areas $A_1 = A_2 = A_3 =$ 2.0, Load: N[1.5,0.3], Resistance: N[0.5, 0.05], No Correlation.**

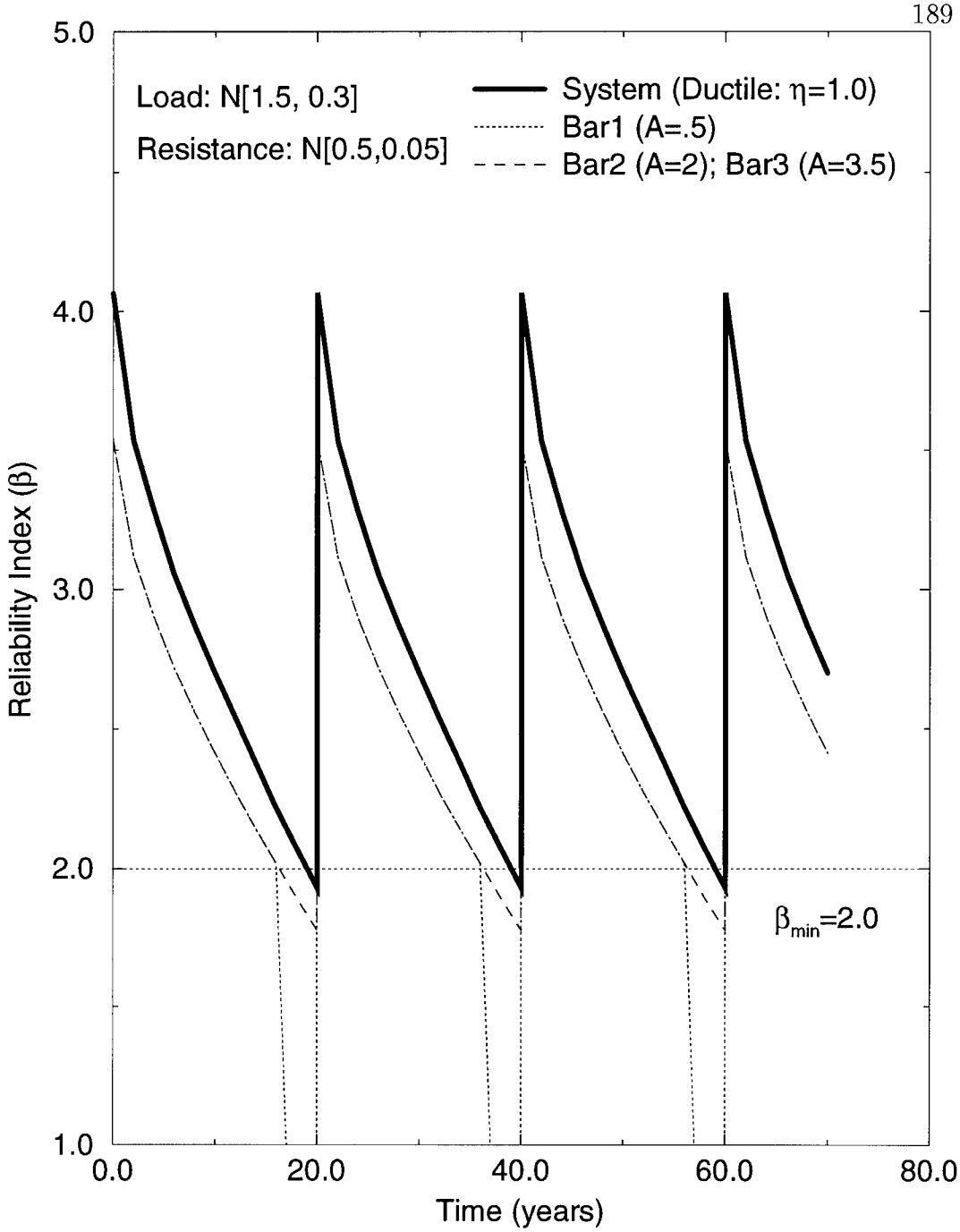

Figure 4.11: **Repair Plan for a Ductile Three Bar Parallel System with Unequal Bar Areas** $A_1 = 0.5$, $A_2 = 2.0$, $A_3 = 3.5$, **Load: N[1.5,0.3], Resistance: N[0.5, 0.05], No Correlation.**

4.5 Series-Parallel System: Three Bar Indeterminate Truss

The three bar indeterminate truss shown if Fig. 4.12 is modeled as a series-parallel system where the failure of any two bars will cause failure of the system. The useful life is 70 years and the allowable reliability level for the system is $\beta_{min} = 2.0$. The resistances of the three bars are: $R_{bar1} = N[15, 1.5]$, $R_{bar2} = N[15, 1.5]$, and $R_{bar3} = N[10, 1.0]$. The load on the truss is $P = N[20, 4.0]$. The deterioration model (Eq. 2.3) and the costs ($C_{fix} = 5.0$, $C_{var} = 5.0$) are unchanged. The limit state equations which describe the components in the series-parallel model (Fig. 4.12) are:

Prior to any bars failing (Bar 1, Bar 2, Bar 3)

$$
\begin{aligned}
g(1) &= R_1(2.0A_1A_3 + \sqrt{2}(A_1A_2 + A_3A_2)) - \sqrt{2}PA_1(cos\theta + sin\theta) - 2.0PA_2cos\theta \\
g(2) &= R_2(2.0A_1A_2 + \sqrt{2}(A_1A_2 + A_3A_2)) - \sqrt{2}P((A_1 - A_3)cos\theta + (A_1 + A_3)sin\theta) \\
g(3) &= R_3(\sqrt{2}A_1A_3 + A_1A_2 + A_3A_2) + P(A_3sin\theta - A_3cos\theta - \sqrt{2}A_2cos\theta)
\end{aligned}
$$

If Bar 1 fails (Bar 2|1, Bar 3|1):

$$
\begin{aligned}
g(4) &= R_2A_2 - P(sin\theta + cos\theta) + \sqrt{2}\eta R_1A_1 \\
g(5) &= R_3A_3 - P\sqrt{2}cos\theta + \eta R_1A_1
\end{aligned}
$$

If Bar 2 fails (Bar 1|2, Bar 3|2):

$$
\begin{aligned}
g(6) &= R_1A_1 - \sqrt{2}/2(P(sin\theta + cos\theta) + \eta R_2A_2 \\
g(7) &= R_3A_3 - \sqrt{2}/2(P(cos\theta - sin\theta) + \eta R_2A_2)
\end{aligned}
$$

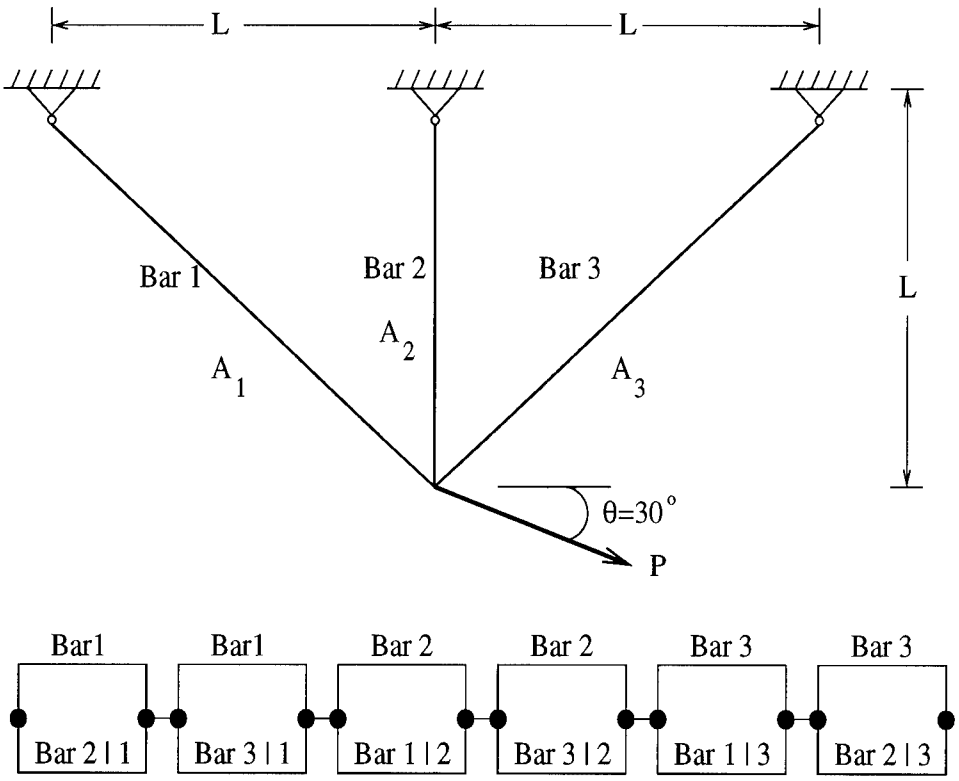

Figure 4.12: **Three Bar Indeterminate Truss Modeled as a Series-Parallel System**

If Bar 3 fails (Bar 1|3, Bar 2|3):

$$g(8) = R_1A_1 - \sqrt{2}Pcos\theta + \eta R_3A_3$$

$$g(9) = R_2A_2 - P(sin\theta - cos\theta) - \sqrt{2}\eta R_3A_3$$

Investigating a ductile truss and starting the optimization with a large value of $\beta_{threshold} = 7.0$, Fig. 4.13 shows that all three bars get repaired resulting in a lifetime cost value of 60. Lowering the component reliability threshold to $\beta_{threshold} = 4.0$ caused only bars 1 and 3 to be repaired as shown in Fig. 4.14. The resulting total cost was lowered to 45 which indicates that bar 2 did not need to ever be repaired. Attempting to lower $\beta_{threshold}$ to the point where bar 3 does not get repaired resulted in a repair plan where the minimum system safety could not be maintained for the life of the structure.

The same analysis was completed for a brittle truss using the same assumptions. Fig. 4.15 shows the brittle truss where $\beta_{threshold} = 7.0$. All three bars were repaired and the total lifetime cost was 100. Lowering the $\beta_{threshold}$ value to 4.0 resulted in bar 2 not being repaired and the total cost was 90. There were more lifetime repairs required using a lower $\beta_{threshold}$ value but the total cost was still less. It is interesting to note in Fig. 4.16 that the reliability of bar 3 improves as bar 2 deteriorates.

In both cases, the optimal solution was to repair only bars 1 and 3. As expected, the safety of the brittle structure was much more expensive to maintain. There are a number of items which could be investigated at this

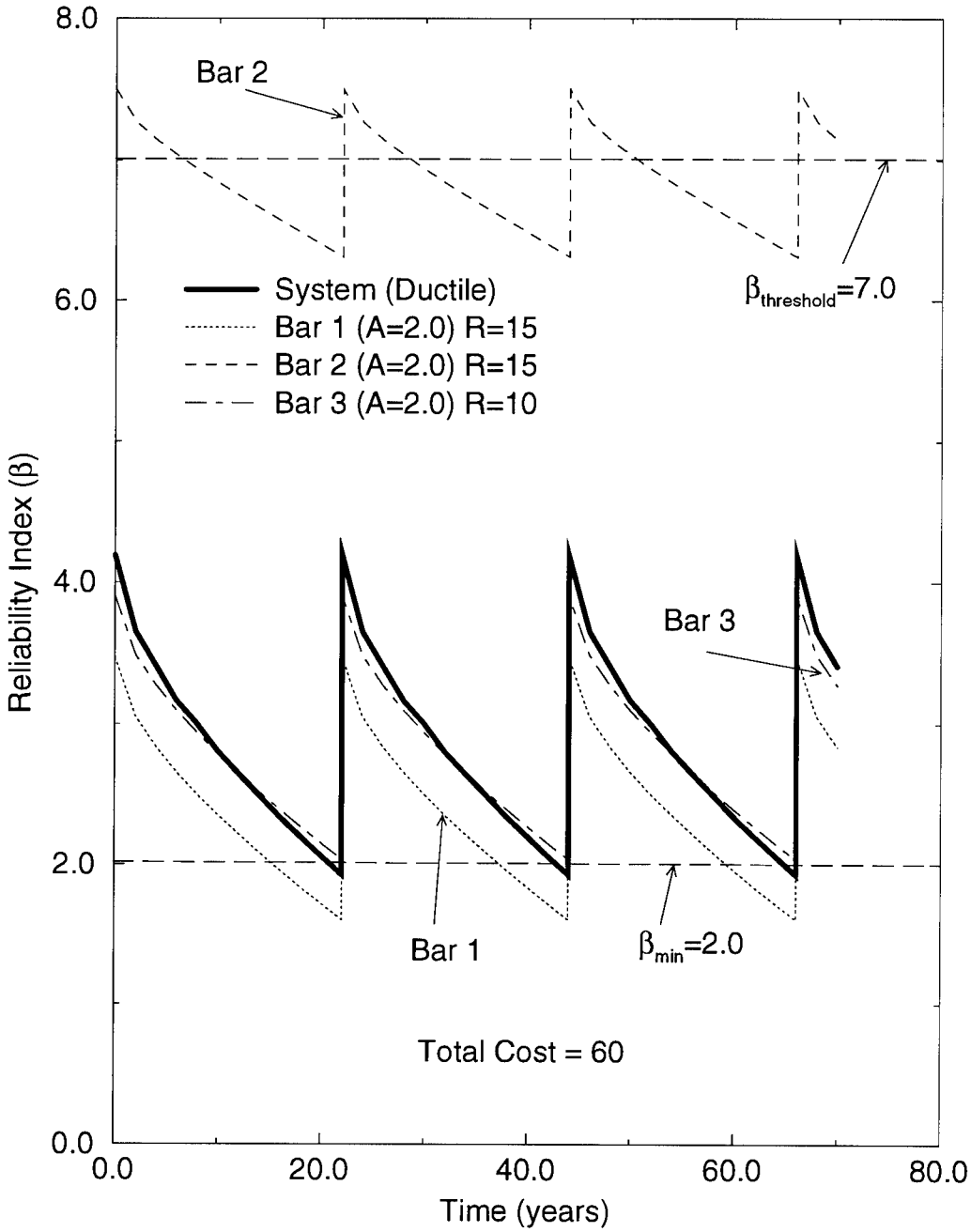

Figure 4.13: **Repair Plan for a Ductile Three Bar Indeterminate Truss With Equal Bar Areas;** $\beta_{threshold} = 7.0$; $Cost = 60$

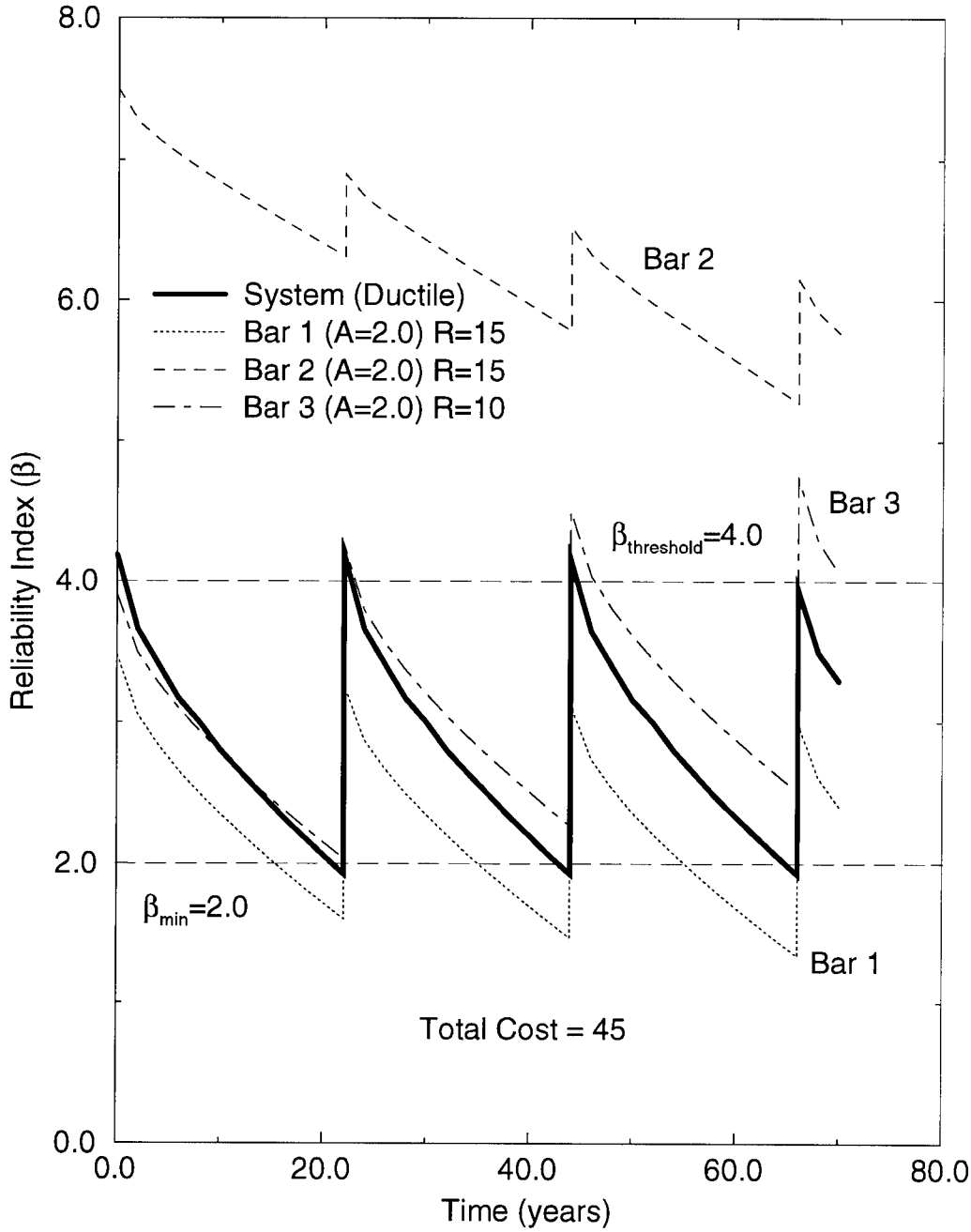

Figure 4.14: **Repair Plan for a Ductile Three Bar Indeterminate Truss With Equal Bar Areas;** $\beta_{threshold} = 4.0$; $Cost = 45$

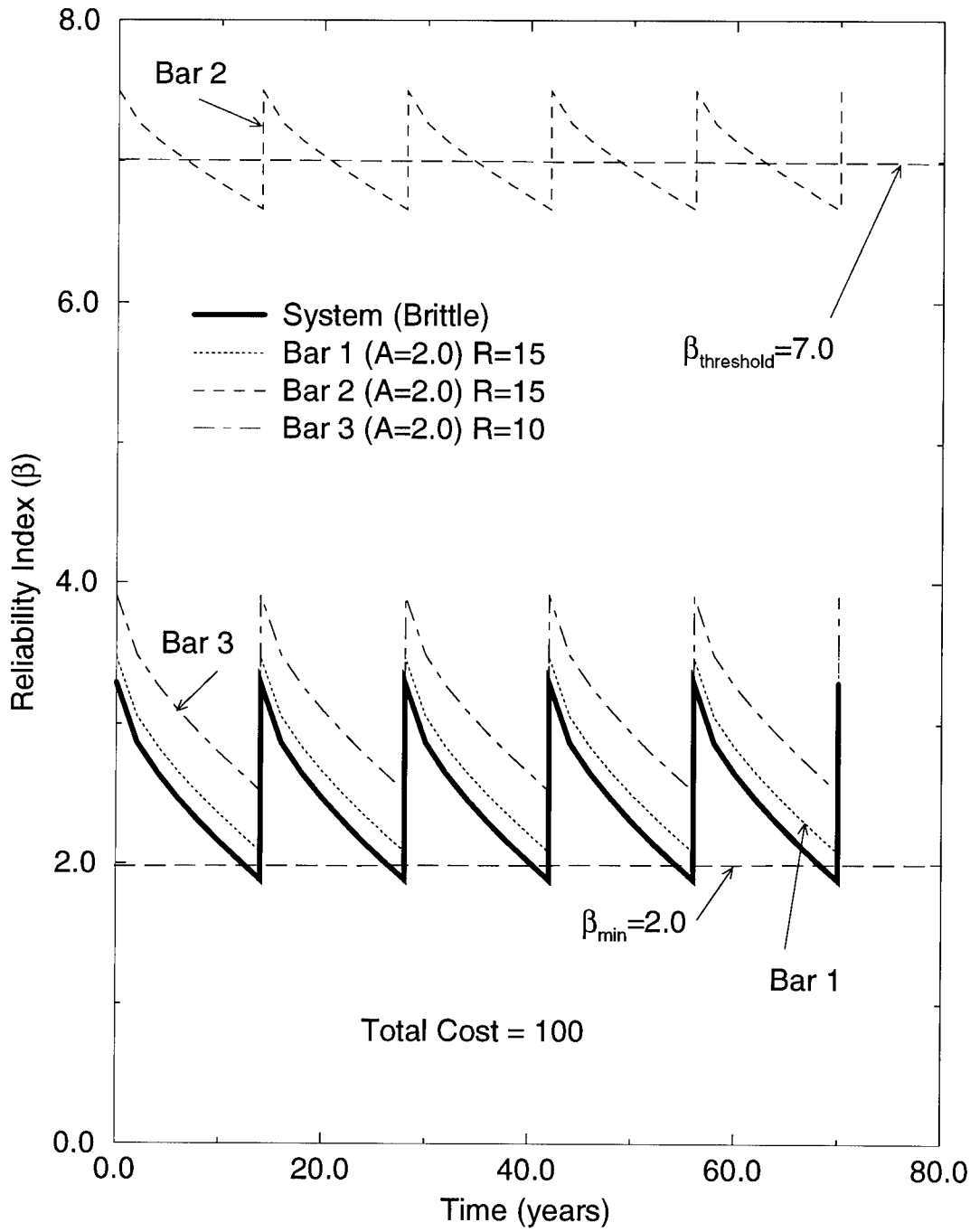

Figure 4.15: **Repair Plan for a Brittle Three Bar Indeterminate Truss With Equal Bar Areas;** $\beta_{threshold} = 7.0$; $Cost = 100$

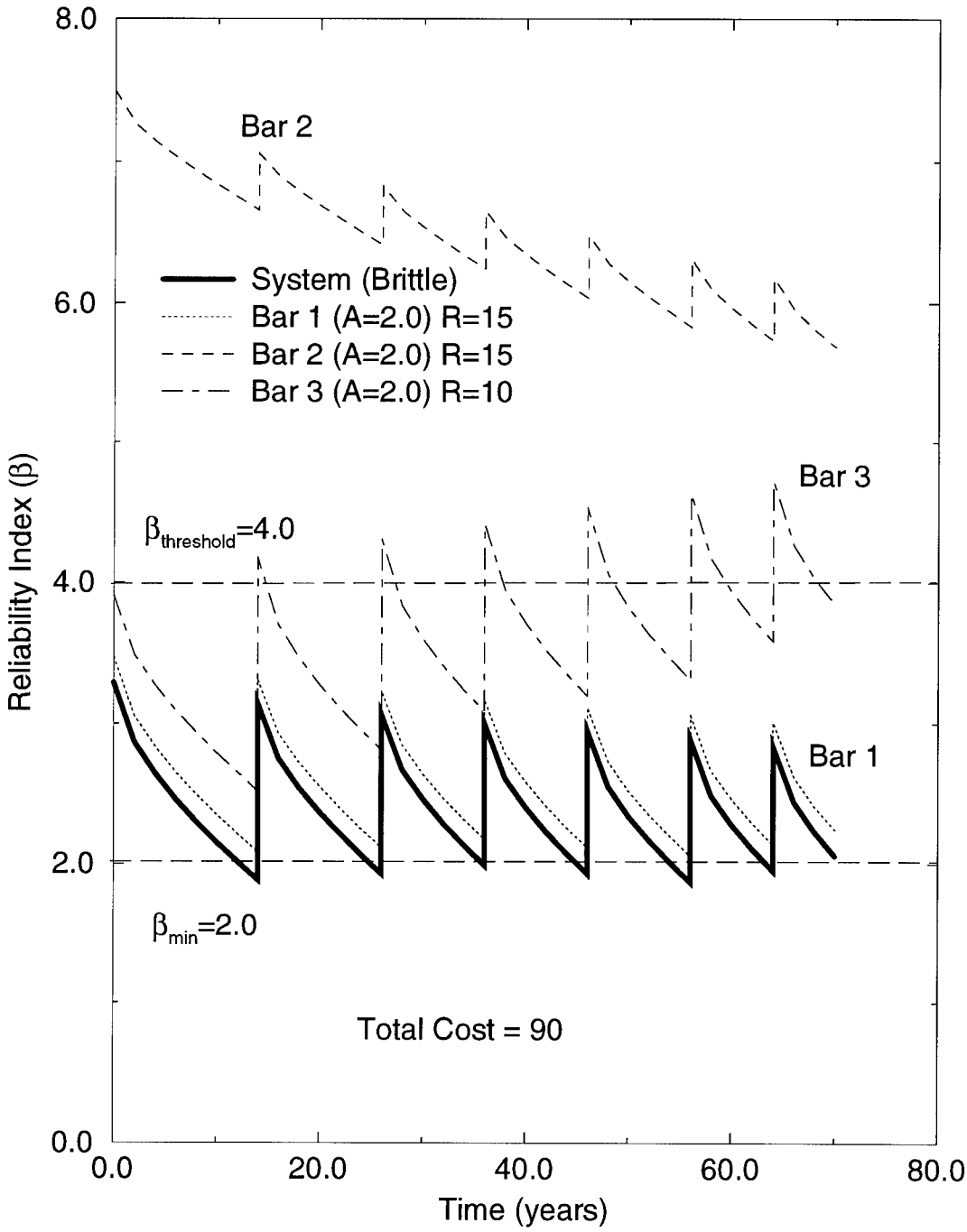

Figure 4.16: **Repair Plan for a Brittle Three Bar Indeterminate Truss With Equal Bar Areas;** $\beta_{threshold} = 4.0$; $Cost = 90$

point such as changing the direction of the load, changing the resistance or initial area of one or more bars, varying the material ductility properties, and/or varying the correlation among resistances. Correlation between the resistances is interesting in a series-parallel structure because increased resistance correlation improves the reliability of a series system but decreases the reliability of a parallel system. Looking at a partially ductile truss ($\eta = .5$), for example, for $\beta_{threshold}$ values of 7.0 and 4.0, the results are shown in Table 4.1.

Table 4.1: **Repair Costs for a Semi-Ductile Three Bar Indeterminate Truss for Different Resistance Correlation Values**

$\beta_{threshold}$	ρ_{R_1,R_2}	$cost$
7.0	0.0	100
7.0	0.5	80
7.0	1.0	100
4.0	0.0	90
4.0	0.5	90
4.0	1.0	90

For this case, the best solution occurred when all three bars were repaired and the resistances were partially correlated. In both cases, the repairs were made later for the partially correlated case. For the $\beta_{threshold}$ value of 7.0, the later repairs resulted in one less lifetime repair which was not true for

the case when $\beta_{threshold}$ was equal to 4.0.

4.6 Summary

For some simple structures, the optimal choice of a $\beta_{threshold}$ value appears to offer a repair strategy for a structure which minimizes cost and maintains a desired level of system safety for the life of the structure. While the choice of repairing one bar or another may appear simplistic, the method can be applied to the more realistic choice of repairing a deck, replacing a beam, rehabilitating an abutment, or some combination of these. A real application of this method will become more complex as the structure will be more sophisticated and a particular repair may have several competing options.

CHAPTER V

COLORADO BRIDGE E-17-AH: A CASE STUDY

5.1 Introduction

The previous chapter presented a method for optimizing the repair of a structure based on system reliability. Components of a system were chosen for repair based on minimizing the total cost while maintaining the reliability of the structural system above a prescribed minimum value for the lifetime of the structure. The method was illustrated for some simplified truss structures using hypothetical values for deterioration, cost, and load.

This chapter will apply this technique to an existing highway bridge in the State of Colorado. It will examine what complexities arise and what simplifications are needed to solve a real world problem and will assess how system reliability methods can be used to optimize the repair of a structure. Again the emphasis is on assessment rather than design since the structure already exists and the challenge is to maintain its reliability throughout the useful life of the structure. The organization of this chapter is as follows:

- Choose a sample bridge.
- Calculate the load rating capacity of the bridge for a standard AASHTO HS-20 truck

- Using the same equations as those used for the load rating, determine the reliability of the bridge components and the bridge system. The random variables must be defined. Initially the live load will be considered to be a deterministic HS-20 truck so that the load rating and the reliability index can be compared.

- Using available live load models for highway bridges, allow the bridge live load to become a random variable and observe the effect.

- Assess and develop limit state equations for the other potentially relevant failure modes in the bridge that are not included in a bridge load rating. The reliabilities of these failure modes will be computed and the sensitivity of the random variables will be examined.

- Considering all relevant failure modes, develop a series-parallel model of the bridge system and compute the system reliability. When examining all failure modes and possible correlations between random variables, the system model can quickly become quite complex. Based on the relative reliabilities of the components and some reasonable assumptions, the model can often be simplified without significant loss in accuracy.

- Examine how the bridge is deteriorating over time. Selected deterioration models from the literature such as corrosion of the structural steel and the corrosion of steel reinforcement in concrete due to the penetration of chlorides will be used. The effect of the deterioration on the component and system reliability over time will be shown.

- Using realistic repair options and their associated costs, the repair of the bridge will be optimized over time for several different scenarios. The cost data will be based on actual repairs made in the State of Colorado and on projected discount rates for money. The sensitivity key variables such as corrosion factors, the discount rate, and the nature of the bridge model with respect to system reliability and the optimum repair strategy will be examined.

- This analysis involves strength-based limit state equations. Some repairs are made based on serviceability constraints. The structure may still be sufficiently strong to carry the required load but spalling concrete or excessive potholes may necessitate a repair. The inclusion of serviceability flags as a means to accommodate serviceability concerns will be introduced and illustrated.

- From the examples shown, some conclusions can be drawn concerning the methodology and the potential usefulness of system reliability in solving real world problems.

This study is restricted to repairs based on deterioration of the bridge. While a substantial amount of bridge renovation has been done to address safety concerns such as deck width, sight distance, and excessive curvature, this study will only consider those repairs attributable to deterioration. Likewise, those rehabilitations which addressed vulnerability issues such

as seismic retrofit, collision and fracture critical situations will be neglected.

5.2 Bridge E-17-AH

Since a system reliability approach to highway bridges is still a new concept, the structure for this case study was chosen based on its simplicity and commonality. The focus is on the reliability technique. Complex structures under unusual conditions such as scour from waterways, complex trusses, non-prismatic plate girders, and suspension systems were deliberately avoided in this first attempt. Although reliability methods can be used on all of these structures, the complexity of the calculations obscures the point of the exercise. By choosing a common type of bridge, a demonstration that these reliability methods are useful provides applications to a large number of structures and offers the greatest possible benefit.

The structure chosen for this study is the Colorado State Highway Bridge E-17-AH located on 40th Avenue (State Highway 33) between Madison and Garfield Streets in Denver, Colorado. The bridge has three simple spans of equal length and has a total length of 137 feet (41.76 m) as shown in Figs. 5.1 and 5.2. The deck consists of nine inches of reinforced concrete and a three inch surface layer of asphalt. The east-west bridge has two lanes of traffic in each direction as shown in Fig. 5.3 with an average daily traffic (ADT) of 8500. The roadway width is 40 feet with five foot pedestrian sidewalks and handrailing on each side. The bridge offers a clearance of 22.17 feet (6.76 m) for the CB&Q railroad spur which runs underneath. There is no skew or curvature.

The slab is supported by nine standard-rolled, compact, non-composite steel girders as shown in Fig. 5.4. The two exterior girders, which support the pedestrian traffic are 33" (83.8 cm) WF (wide flange) beams which weigh 125 lb/ft (1824 N/m). The seven interior girders are all 33" (83.8 cm) WF beams at 132 lb/ft (1926 N/m). While these standard shapes are no longer produced today, their dimensions [AISC 1943] are shown in Fig. 5.5. The girders are stiffened by end diaphragms and intermediate diaphragms at the third points (all diaphragms are 15" (38.1 cm) channel sections at 33.9 lb/ft (494.7 N/m)). Each girder is supported at one end by a fixed bearing and an expansion bearing at the other.

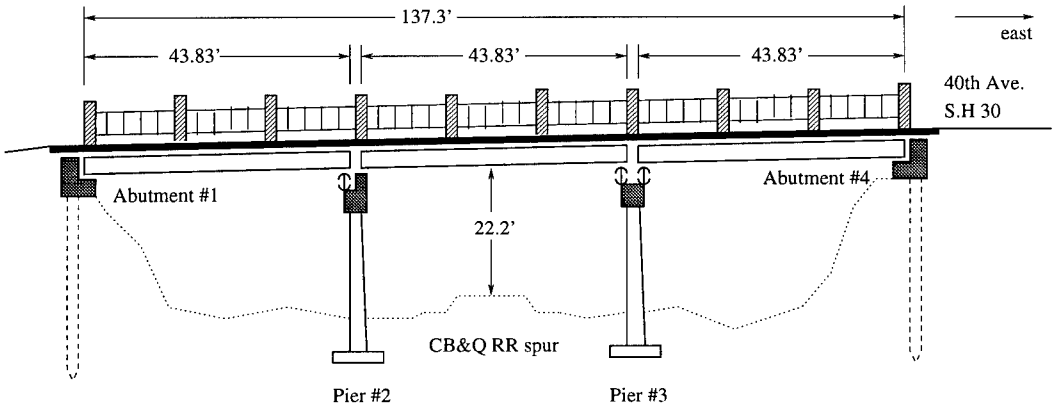

Figure 5.1: **Profile of Colorado State Highway Bridge E-17-AH**

The bridge is supported by abutments at the end and by two piers in the middle. The abutments are reinforced concrete beams supported by eleven reinforced concrete piles with exterior steel casings as shown in Fig. 5.6. The piers consist of reinforced concrete beams on which the girder bearings rest, supported by tapered reinforced square columns. Each column has a footing

Figure 5.2: **Profile Photograph of Colorado State Highway Bridge E-17-AH**

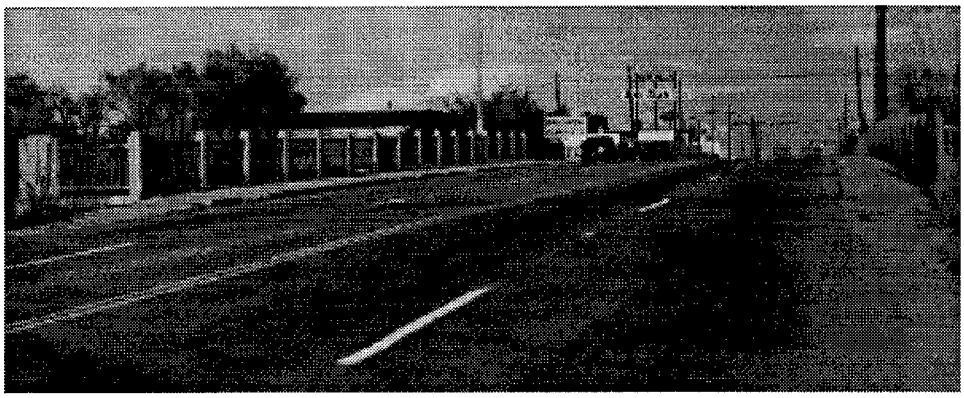

Figure 5.3: **Roadway Photograph of Colorado State Highway Bridge E-17-AH**

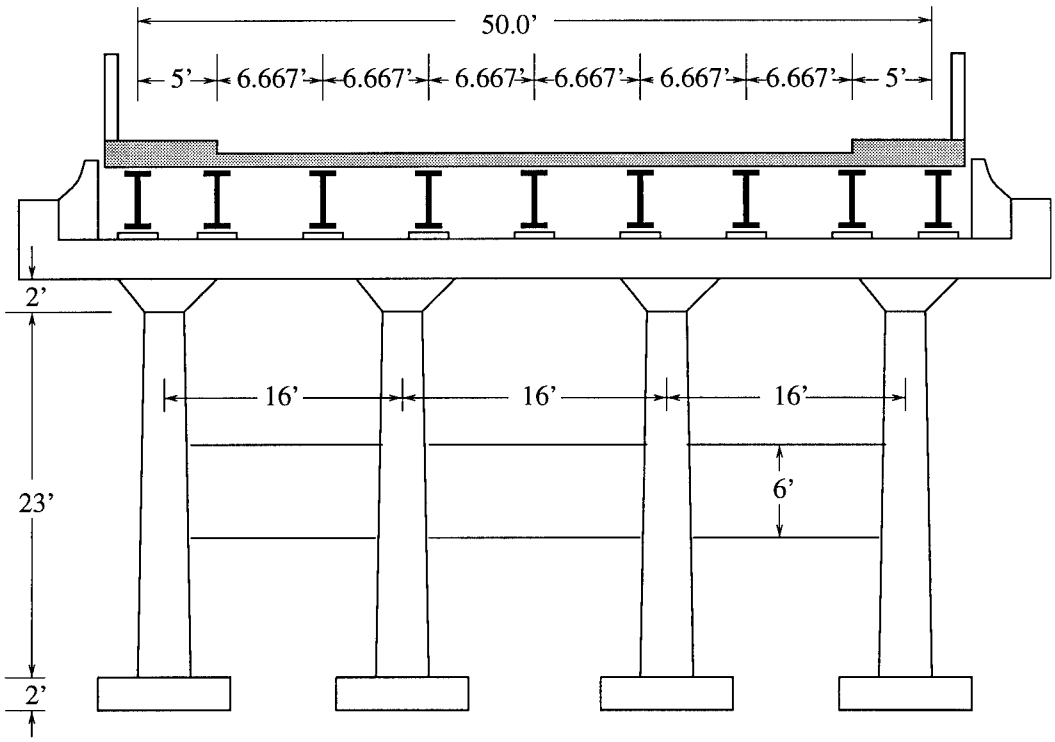

Figure 5.4: **Cross Section of Colorado State Highway Bridge E-17-AH**

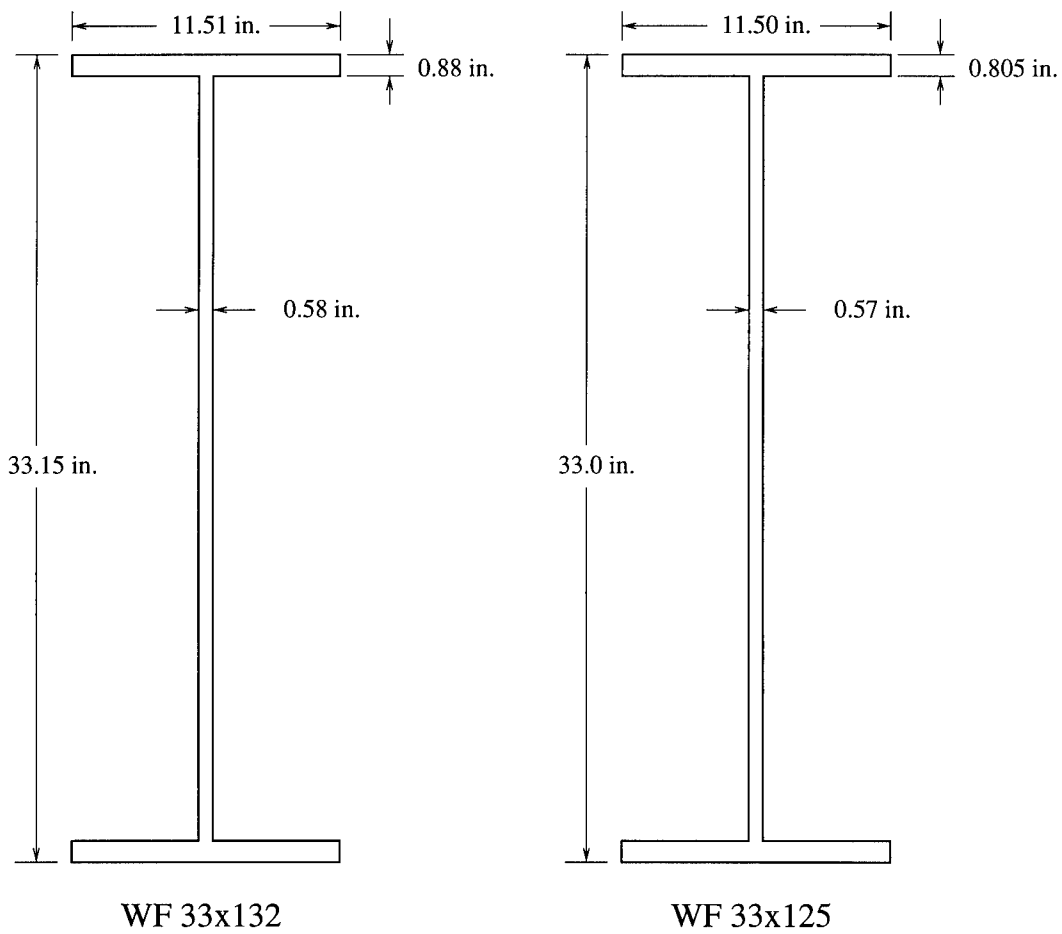

Figure 5.5: **Standard Shape Dimensions for the WF 33x132 and WF 33x125 Beams**

which distributes the load to the sand and gravel soil underneath. As shown in Figs. 5.4 and 5.7, there is a six foot (1.83 m) supporting wall which connects the four columns. Piers 2 and 3 are very similar. The only differences are the positioning of the supporting wall and the dimensions on the top beam. Pier 2 is designed to support a fixed bearing and an expansion bearing while Pier 3 supports two expansion bearings as shown in Figs. 5.19 and 5.18, respectively.

Figure 5.6: **Abutment Photograph of Colorado State Highway Bridge E-17-AH**

The bridge which includes 204,400 lbs (909 kN) of structural steel, 64,900 pounds (288 kN) of reinforcing steel, and 464 cubic yards (354.5 m^3) of concrete was constructed in 1942 at a cost of $393,000. The only major repair made on the bridge has been a $68,000 repair to the approach of the bridge in 1992 [CDOT 1995b]. The bridge has no toll, no postings, and no detour length is listed indicating the bridge can be bypassed. Bridge E-17-AH is currently considered functionally obsolete because of the 40 foot (12.2

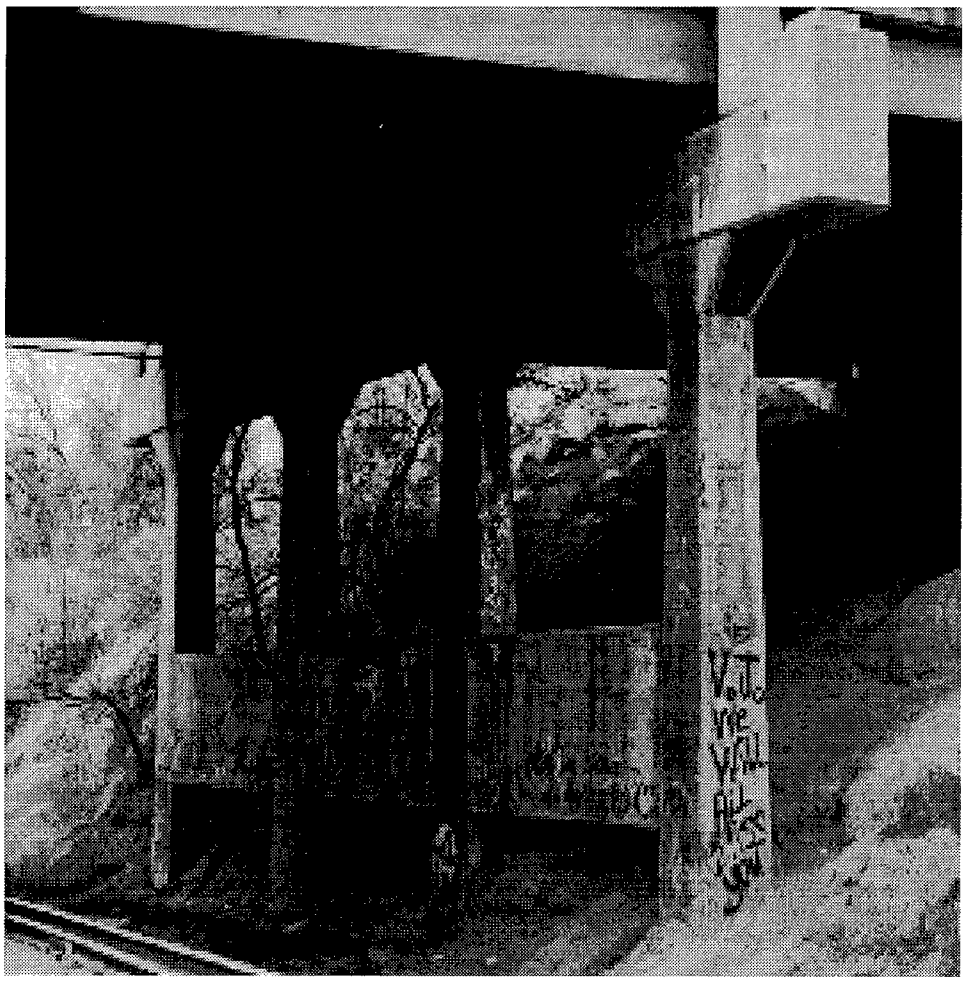

Figure 5.7: **Column Pier Photograph of Colorado State Highway Bridge E-17-AH**

m) road way width and has a sufficiency rating of 60.8. The sufficiency rating ranges from a high of 100 indicating an entirely sufficient bridge to 0 indicating an entirely insufficient bridge. The sufficiency rating is a function of structural adequacy and safety (55%), serviceability and functional obsolescence (30%), and essentiality for public use (15%) [FHWA 1988a].

5.3 Load Rating of Bridge E-17-AH

Agencies charged with operating and maintaining a bridge are responsible for its safety. They need to have an understanding of how much load a bridge can safely carry to ensure the safety of those who use the bridge. The most common method is to assign a load rating to a bridge which specifies its live load carrying capacity. Ratings are often in tons, metric tons, or HS capacity. A number of rating methods and live load standard vehicles are available which use both allowable stress and load factor approaches. The efforts of AASHTO and the National Cooperative Highway Research Program (NCHRP) have helped provide a standard approach [White *et al.* 1992]. AASHTO [1989] and AASHTO [1994] both provide widely used rating methods but there are numerous differences between them. This study will incorporate the most recent load rating calculations and equations used by the Colorado Department of Transportation for Bridge E-17-AH [CDOT 1995c]. It uses the Bridge Analysis and Rating System (BARS) program [BARS 1988] to compute the load rating and relies on a load factor approach which includes inventory and operating ratings.

The inventory rating is the lower of the two ratings and represents

the load level at which the structure is safe for an infinite period of time [White *et al.* 1992] (assuming no deterioration of the structure). The equation for the inventory rating factor (RF_{inv}) based on moment is

$$RF_{inv} = \frac{M_u - \gamma M_{dl}}{\beta \gamma M_{ll}} \tag{5.1}$$

The operating rating is the absolute maximum load that should be allowed on the bridge under any circumstances and the equation for the operating rating factor (RF_{opr}) based on moment is

$$RF_{opr} = \frac{M_u - \gamma M_{dl}}{\gamma M_{ll}} \tag{5.2}$$

where M_u is the ultimate moment capacity, M_{dl} is the dead load moment demand, M_{ll} is the live load moment demand and $\gamma = 1.3$ and $\beta = 1.67$ from paragraph 3.23 of AASHTO [1992].

The live load associated with the load rating is the AASHTO HS-20 truck [AASHTO 1992] which consists of a tractor truck and a semi-trailer as shown in Fig. 5.8. To obtain the gross weight of the vehicle in tons, the HS designation is multiplied by 1.8. An HS-20 truck for example weighs 36 tons (32.6 metric tons). The spacing between the truck wheels and the front wheels on the trailer is 14 feet (4.27 m) while the spacing between the trailer wheels can range from 14 feet (4.27 m) to 30 feet (9.14 m). The variable spacing allows the HS-20 truck to more accurately model the trucks actually traveling on the highways and allows the spacing to be varied to create the most critical cases for negative moment on continuous spans.

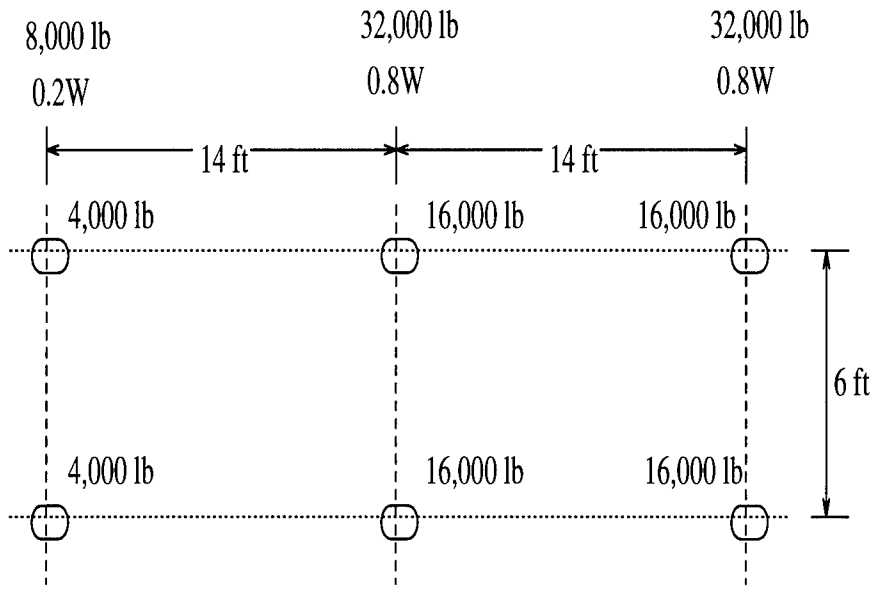

Figure 5.8: **HS-20 Truck Configuration**

The load rating is normally based on the superstructure only since the substructure does not usually dominate the design. The load rating for Bridge E-17-AH is based on the slab and the most critical girder. The slab is rated for moment capacity while the girder is evaluated based on moment, shear, and serviceability. The lowest rating for all of the failure modes is the load rating for the bridge. The load rating is a single value which describes the strength of the bridge. It is the deterministic equivalent of the system reliability index that this study is attempting to compute. It is therefore useful to compute the load rating of this bridge in detail and use the same equations to compute the system reliability index. This will provide a basis

for comparison.

5.3.1 Load Rating: Slab

The rating on the concrete slab is based on its ultimate moment capacity and the dead load and live load demand placed upon it. Fig. 5.9 shows the cross section of the slab and the placement of the steel reinforcement. The ultimate moment capacity of the slab is found by multiplying the yield force in the tensile reinforcement T_t by the distance between the tensile reinforcement and the centroid of the equivalent compression block $d_{eff} - a_t/2$ as shown in Fig. 5.10. The load rating is based on the resisting moment over the support, so in this case, the tension steel is in the top of the slab and d_{eff} is the distance from the bottom of the slab to the centerline of the top reinforcement. The analysis is based on a one-foot section of slab. The dimensions, steel placement, and yield strengths are taken from the bridge plans [CSHD 1941] and the BARS output [CDOT 1995c]. The ultimate moment M_u is

$$\begin{aligned} M_u &= T_t(d_{eff} - a_t/2)\phi \\ &= \frac{31,000lb(6.75in - 1.013/2in)(ft/12in)(.9)}{1000lb/kip} \\ &= 14.516ft - kip\ (19.681kN - m) \end{aligned} \tag{5.3}$$

where $\phi = 0.9$ is a reduction factor [AASHTO 92 (8.16.3.2.1)] and:

$$T_t = A_t f_y = .62in^2(50,000psi) = 31,000\ lb\ (137.9\ kN) \tag{5.4}$$

$$a_t = \frac{T_t}{.85f'_c} = \frac{31,000lb}{.85(3000psi)(12in/ft)(1ft)} = 1.013\ in\ (2.57\ cm) \tag{5.5}$$

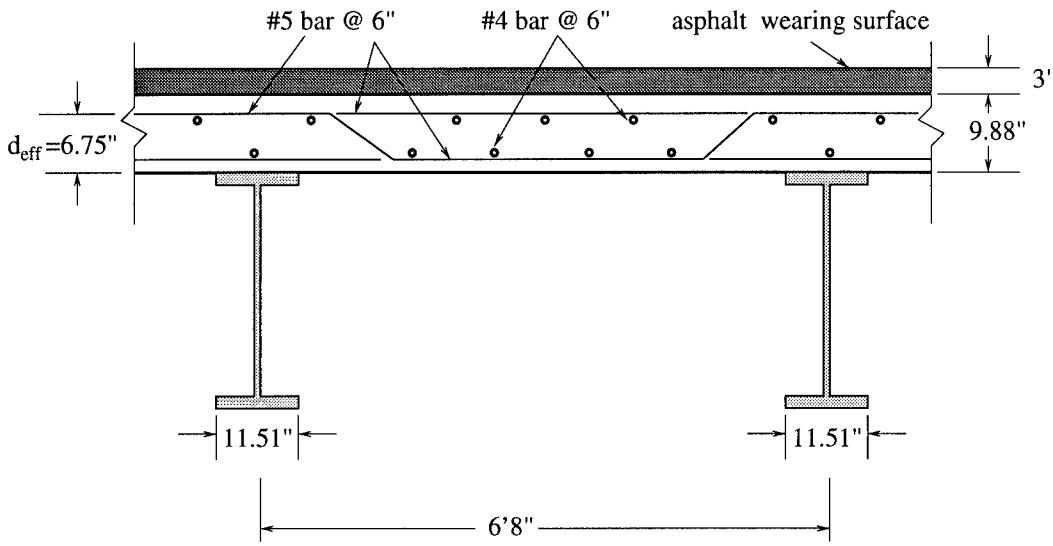

Figure 5.9: **Cross Section of Concrete Slab Showing Placement of Reinforcement**

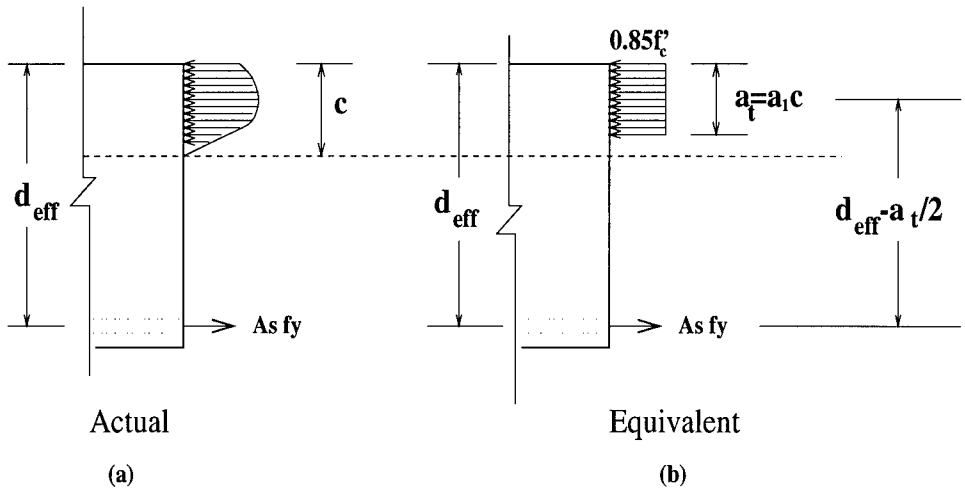

Figure 5.10: **(a) Actual and (b) Equivalent Approximation for Stress on Cross Section of Concrete Slab**

The dead load demand on the slab includes the weight of the concrete w_{conc} and the weight of the asphalt w_{asph} which are uniformly distributed over the 6.187 feet (1.886 m) which separate any two interior girders. The unit weights of the concrete γ_{conc} and asphalt γ_{asph} are 150 lb/ft^3 (2403 kg/m^3) and 144 lb/ft^3 (2307 kg/m^3), respectively. The dead load moment M_{dl} is

$$\begin{aligned} M_{dl} &= \frac{ws^2C_f}{8} \\ &= \frac{159.44lb/ft(6.187ft)(0.8)}{8}\frac{kip}{1000lb} = .61\ ft-kip \\ &= (0.827\ N-m) \end{aligned} \tag{5.6}$$

where the continuity factor $C_f = .8$ is used because the slab spans more than three girders [AASHTO 92 (3.24.3.1)] and:

$$\begin{aligned} w &= w_{asph} + w_{conc} = 123.44lb/ft + 36lb/ft = 159.44\ lb/ft\ (2327\ N/m) \\ w_{conc} &= t_{slab}\gamma_{conc} = \frac{9.875in}{12in/ft}(150lb/ft^3)(1ft) = 123.44\ lb/ft\ (1801\ N/m) \\ w_{asph} &= HMA\gamma_{asph} = \frac{3in}{12in/ft}(144lb/ft^3)(1ft) = 36.0\ lb/ft\ (525.3\ N/m) \end{aligned} \tag{5.7}$$

The live load moment M_{ll} on the slab is based on a single wheel L_{trk} from the HS-20 truck placed in the center of the slab which produces a 16 kip point load between two girders. The live load moment M_{ll} [AASHTO 92 (3.24.3.1)] includes both a continuity factor C_f and an impact factor I_f.

$$\begin{aligned} M_{ll} &= \frac{L_{trk}(s+2)}{32}C_fI_f = \frac{16kip(6.187ft+2ft)}{32}(.8)(1.3) \\ &= 4.26\ ft-kip\ (5.78\ kN-m) \end{aligned} \tag{5.8}$$

where $I_f = 1.3$ [AASHTO 92 (3.8.2)] and $C_f = .8$ [AASHTO 92 (3.24.3.1)]

With the moment demand and capacities, the inventory rating factor RF_{inv} can be calculated as:

$$RF_{inv} = \frac{M_u - \gamma M_{dl}}{\beta\gamma M_{ll}} = \frac{14.516 - 1.3(.61)}{1.67(1.3)(4.26)} = 1.487 \tag{5.9}$$

Using the rating factor, the load rating for the slab can be computed in tons, metric tons, or HS equivalents, as follows:

Inventory Rating: $36tons(RF_{inv}) = 36ton(1.487) = 53.56\ tons$

Metric: $53.56tons(\frac{2000lb/U.S.ton}{2204.6lb/met.ton}) = 48.59\ metric\ tons$

HS Rating: $HS20(RF_{inv}) = 20(1.487) = HS29.8$

The operating rating is calculated the same way.

$$RF_{opr} = \frac{M_u - \gamma M_{dl}}{\gamma M_{ll}} = \frac{14.516 - 1.3(.61)}{(1.3)(4.26)} = 2.479 \tag{5.10}$$

Inventory Rating: $36ton(RF_{opr}) = 36ton(2.479) = 89.26\ tons$

Metric: $89.26tons(\frac{2000lb/U.S.ton}{2204.6lb/met.ton}) = 80.98\ metric\ tons$

HS Rating: $HS20(RF_{opr}) = 20(1.487) = HS49.6$

5.3.2 Load Rating: Shear on Critical Girder

As with the slab, the load rating of the girder is a function of the shear capacity and shear load demand on the girder. The bridge girders are all compact sections. Assuming that the entire shear capacity of the girder comes from the web, the ultimate shear capacity V_u is a function of the strength of the steel F_y, and the depth d_w and thickness t_w of the web.

$$\begin{aligned} V_u &= .58F_y d_w t_w = .58(33,000psi)(31.35in)(.58in.)(lb/1000kips) \\ &= 348.02\ kips\ (1548\ kN) \end{aligned} \tag{5.11}$$

where it can be seen from Fig. 5.5 that for the WF 33x132 beam, the depth of the web $d_w = d - 2t_f = 33.15 - 2(.88) = 31.35\ in\ (79.63\ cm)$.

The dead load shear is computed by considering the concrete and asphalt as a uniformly distributed load based on the tributary area of the slab and the self-weight of the steel girder. The dead load of the concrete w_{conc} is

$$w_{conc} = 150lb/ft^3(\frac{9.875in}{12in/ft})(6.667ft) = 823\ lb/ft\ (12,010\ kN/m) \quad (5.12)$$

The dead load of the asphalt w_{asph} is

$$w_{asph} = 144lb/ft^3(\frac{3in}{12in/ft})(6.667ft) = 240\ lb/ft\ (3502\ N/m) \quad (5.13)$$

and the weight of the steel w_{stl} is 132 lb/ft (1926 N/m). The total dead load w_{tot} is the sum of the individual loads,

$$w_{tot} = w_{conc}+w_{asph}+w_{stl} = 823+240+132 = 1195\ lb/ft\ (17,439\ N/m) \quad (5.14)$$

The maximum dead load shear V_{dl} for a simply supported beam occurs at the supports and is equal to

$$V_{dl} = \frac{w_{tot}L}{2} = 1195lb/ft\frac{(43.833ft)}{2}(kip/1000lb) = 27.6\ kip\ (122.8\ kN) \quad (5.15)$$

The most critical live load shear occurs when the HS-20 truck has its rear wheel over the support as shown in Fig. 5.11 where the load represents one wheel line of the truck. It can be shown that the value of the maximum shear V_{max} which occurs at the left reaction for any length L can be calculated as:

$$V_{max} = 16(1 + \frac{L-14}{L} + \frac{L-28}{4L}) \quad (5.16)$$

Using the span length $L = 43.833\ ft$ (13.36 m), the critical shear is $V_{max} =$ 28.33 *kips* (126.0 kN). The amount of the truck load that is transferred to each girder is determined by the AASHTO distribution factors DF which are a function of the girder spacing S. For an interior steel beam with a reinforced concrete deck where the girder spacing is less than 14 feet (4.27 m), the distribution factor DF is [AASHTO 92 (3.23.3)]

$$DF = \frac{S}{5.5} = \frac{6.667ft}{5.5} = 1.212 \tag{5.17}$$

These distribution factors are best used for bridges with a constant deck width, four or more girders which are parallel and have similar stiffness, and bridge curvatures of four degrees or less. Bridge E-17-AH qualifies in all cases.

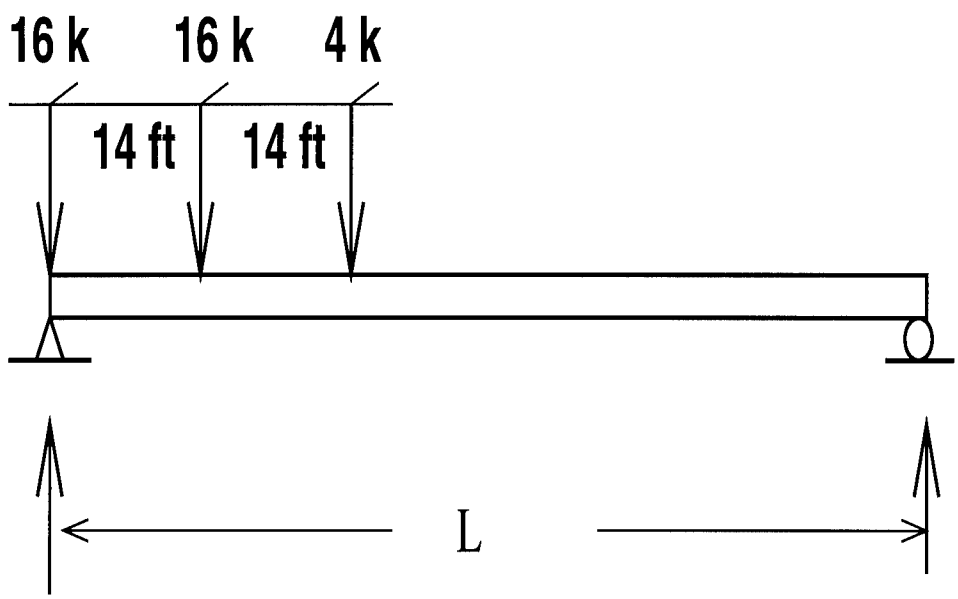

Figure 5.11: **Critical Location for HS-20 Truck on Girder to Produce Maximum Shear**

The dynamic amplification of the shear force that results from impact of the moving vehicle is included in an impact factor I which is a function of the length of the girder. Because the length of the girder L is 43.833 ft (13.36 m), the impact factor is [AASHTO 92]

$$I = \frac{50}{L + 125} = \frac{50}{43.833 + 125} = 0.296 \tag{5.18}$$

The maximum live load shear V_{ll} experienced by a single girder is a function of the maximum shear caused by the HS-20 truck V_{max}, the girder distribution factor DF, and the impact factor I as follows:

$$V_{ll} = V_{max} DF(1.0 + I) = 28.33 kips(1.212)(1.296) = 44.5\ kips\ (197.9\ kN) \tag{5.19}$$

The bridge rating considering failure of an interior girder due to shear is computed similarly to the slab rating. The inventory rating factor RF_{inv} can be calculated as:

$$RF_{inv} = \frac{V_u - \gamma V_{dl}}{\beta \gamma V_{ll}} = \frac{348.47 - 1.3(27.74)}{1.67(1.3)(44.5)} = 3.23 \tag{5.20}$$

The operating rating factor can be computed as $RF_{opr} = 1.67 RF_{inv} = 1.67(3.23) = 5.40$.

Using the rating factor, the load rating can be computed in tons, metric tons, or HS equivalents, as follows:

Inventory Rating: $36 tons(RF_{inv}) = 36 ton(3.23) = 116.3\ tons$

Metric: $116.3 tons(\frac{2000 lb/U.S.ton}{2204.6 lb/met.ton}) = 48.59\ metric\ tons$

HS Rating: $HS20(RF_{inv}) = 20(3.23) = HS64.6$

Similarly, the operating ratings are 194.4 *tons*, 176.4 *metric tons*, and $HS108.0$

5.3.3 Load Rating: Moment on Critical Girder

The critical girder is also evaluated for its moment strength. The ultimate moment capacity M_u is evaluated based on the plastic section modulus Z and the yield strength of the steel $F_y = 33,000\ psi$ (227.5 MPa). The plastic section modulus Z is a function of the dimensions of the WF 33x132 girder [AISC 1943] as shown in Fig. 5.5.

$$\begin{aligned} Z &= [\frac{33.15-2(0.88)}{2}(0.58)\frac{33.15-2(0.88)}{4}+(\frac{33.15}{2}-\frac{0.88}{2})(0.88)(11.51)]2 \\ &= 469.73\ in^3\ (7697\ cm^3) \end{aligned} \tag{5.21}$$

Since the girder is a compact section, the ultimate moment capacity M_u is therefore

$$\begin{aligned} M_u = ZF_y &= 469.73in^3(33,000psi)(\frac{kip}{1000lb})(\frac{ft}{12in}) \\ &= 1291.76\ ft-kips\ (1725\ kN-m) \end{aligned} \tag{5.22}$$

The dead load moment M_{dl} is computed using the same uniformly distributed load $w_{tot} = 1195\ lb/ft$ (Eq. 5.14) that was used to compute the shear for a simply-supported beam.

$$M_{dl} = \frac{w_{tot}L^2}{8} = \frac{1195lb/ft(43.833ft)^2}{8}(\frac{kip}{1000lb}) = 303.8\ ft{-}kips\ (411.8\ kN{-}m) \tag{5.23}$$

The most critical live load moment occurs when the wheels of the HS-20 truck are offset slightly from the center of the girder as shown in Fig. 5.12

where the load represents one wheel line of the truck. It can be shown that the value of the maximum moment M_{max} which occurs at the center of the girder for any length L can be calculated as:

$$M_{max} = [\frac{36}{L}(\frac{L}{2} - 2.33)^2 - 56] \tag{5.24}$$

Using the span length $L = 43.833\ ft$, the critical moment is $M_{max} = 259.0\ ft-kips$ $(351.1\ kN - m)$.

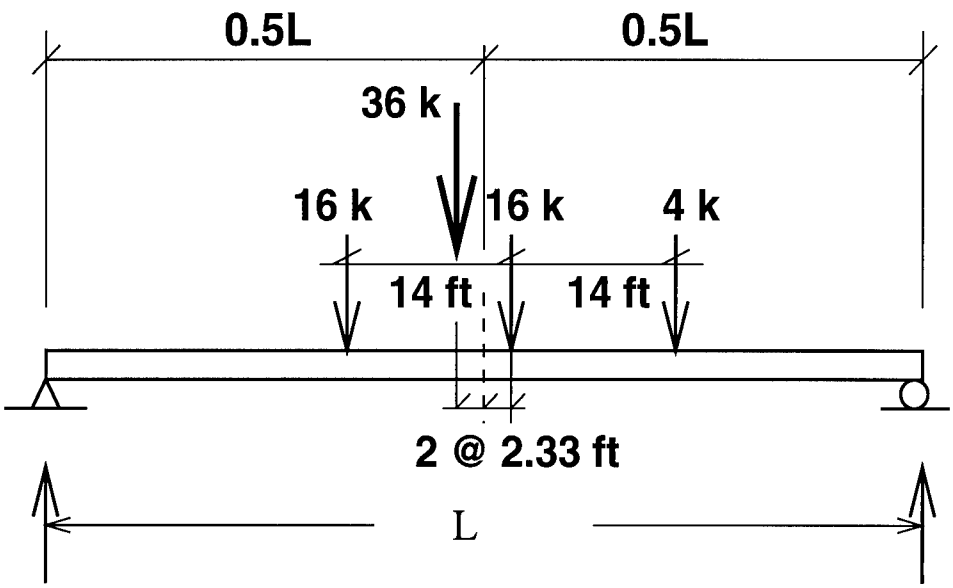

Figure 5.12: **Critical Location for HS-20 Truck on Girder to Produce Maximum Moment**

Using the same girder distribution factor DF and impact factor I as for the shear calculation (Eqs. 5.17 and 5.18), the maximum live load moment M_{ll} experienced by a single girder is

$$M_{ll} = M_{max}DF(1.0 + I) = 259.0ft - kips(1.212)(1.296)$$

$$= \ 399.7\ ft - kips\ (541.9\ kN - m) \tag{5.25}$$

The inventory rating factor RF_{inv} considering failure of an interior girder due to moment is:

$$RF_{inv} = \frac{M_u - \gamma M_{dl}}{\beta\gamma M_{ll}} = \frac{1291.76 - 1.3(303.8)}{1.67(1.3)(399.8)} = 1.035 \tag{5.26}$$

Similarly the operating rating factor can be computed as $RF_{opr} = 1.67RF_{inv} = 1.67(1.035) = 1.725$. Using the rating factor, the inventory load ratings for serviceability are computed as 37.26 US tons, 33.8 metric tons, and HS 20.7. Likewise, the operating ratings are 62.1 US tons, 56.34 metric tons, and HS 34.5.

5.3.4 Load Rating: Serviceability on Critical Girder

The final rating considered in this bridge is a so-called serviceability rating which is based on the moment strength of the most critical girder. The largest difference from the previous girder moment computation is that the elastic section modulus S_x is used rather than the plastic section modulus Z. The inventory rating factor RF_{inv} for serviceability is [CDOT 1995d]

$$RF_{inv} = \frac{\phi F_y S_x - M_{dl}}{\beta M_{ll}} = \frac{\frac{(0.8)(33{,}000psi)(408.5in^3)}{(12in/ft)(1000lb/kip)} - 303.8ft - kip}{1.67(399.8ft - kip)} = 0.8923 \tag{5.27}$$

The operating rating factor is $RF_{opr} = 1.67RF_{inv} = 1.67(0.8923) = 1.487$. Using the rating factor, the inventory load ratings are computed as 32.12 US tons, 29.14 metric tons, and HS 17.8. Likewise, the operating ratings are 53.5

US tons, 48.6 metric tons, and HS 29.7.

5.3.5 Final Load Rating of the Bridge

A summary of the separate load ratings is shown in Table 5.1. The lowest of the four ratings becomes the rating for the bridge. For Bridge E-17-AH, the overall load rating is determined by the serviceability rating. The bridge is therefore given an inventory rating of HS 17.8 and an operating rating of HS 29.7. The numerical results presented here differ slightly from the BARS output from the last CDOT load rating [CDOT 1995c]. The reasons for the differences are some discrepancies in the input data by CDOT, specifically the placement of the HS-20 truck, the unit weight of steel, and exact dimensions on the WF33x132 girder. The BARS program places the HS-20 truck in the exact center of the girder as opposed to the more critical offset position as shown in Fig. 5.12. Otherwise, the equations and input data used in this study and by CDOT are identical.

5.4 Component Reliability of Bridge E-17-AH

Using the same equations as those used for the load rating, the reliability of those same components or failure modes will be computed (i.e., moment failure in the slab, shear and moment failure in the critical girder). The serviceability criterion will not be used here, although serviceability will be discussed at the end of the chapter. This will provide a basis for comparison

Table 5.1: **Summary of Load Ratings for Colorado Highway Bridge E-17-AH**

Inventory Rating				
Failure Mode	Rating Factor	HS Rating	U.S. Tons Capacity	Metric Ton Capacity
slab	1.487	29.8	53.56	48.59
int. girder: flexure	1.035	20.7	37.26	33.80
int. girder: shear	3.23	64.6	116.3	105.5
serviceability	.8293	17.8	32.12	29.14
Operating Rating				
Failure Mode	Rating Factor	HS Rating	U.S. Tons Capacity	Metric Ton Capacity
slab	2.479	49.6	89.26	80.98
int. girder: flexure	1.725	34.5	62.1	56.34
int. girder: shear	5.4	108.0	194.4	176.4
serviceability	1.487	29.7	53.53	48.56

between the load rating and the reliability index.

5.4.1 Random Variables

The first step in this process is to define the random variables and the nature of their distributions. In this study, dimensions that can be physically measured will be considered deterministic such as the spacing and length of girders and the dimensions of the steel girder cross sections. Dimensions which cannot be easily measured such as the spacing of reinforcement in concrete and dimensions which may vary throughout the structure such as concrete cover and asphalt thickness will be random.

Wherever possible, the random variables and their uncertainties will be taken from the literature. There have been an increasing number of reliability studies which quantify most of the random variables needed for these computations. While they may not apply perfectly to bridge E-17-AH, they are the most realistic values currently available without conducting a site specific investigation.

Table 5.2 shows the random variables that will be used, their distribution, and the source from which they were taken. In many cases, these variables were described by a bias factor and coefficient of variation δ. The bias factor is a ratio between the mean value of the random distribution and the deterministic value of the variable. The mean value of the distribution which is needed for RELSYS is obtained by multiplying the bias factor by the deterministic quantity, usually taken from the bridge drawings [CSHD 1941].

Similarly, the standard deviation of the distribution is obtained by multiplying the mean value of the distribution by the coefficient of variation.

There are different types of uncertainties to consider such as material strength, dimensions that cannot be easily measured, live loads, and unit weight of materials. In some cases where no information was available on the uncertainty of a variable, such as the continuity factor C_f or the impact factor I_f for very short spans, the quantity was considered deterministic. The symbols used for these variables either apply to that variable directly (i.e., F_y or M_{trk-i}) or use the symbol λ (i.e., $\lambda_{d_{eff}}$ or λ_{conc}) which indicates an uncertainty factor.

Model uncertainty is included whenever possible. The equations for impact, distribution factors, moment and shear capacity are simplified models which attempt to describe the real world effect. As such there is some uncertainty associated with that model. The model uncertainty is considered by using the variables directly (i.e., DF_i or I_{beam}) or by using an uncertainty factor γ (i.e., γ_{msg}). The description of these variables and their assigned numbers (used in the RELSYS program) are listed in Table 5.3. Some of these random variables will not be introduced until later in the chapter. These random variables are those needed to analyze the bridge prior to any deterioration. As the deterioration of the bridge is analyzed over time, additional random variables will be introduced.

5.4.2 Limit State Equations

Table 5.2: **Random Variables in System Reliability Analysis of Colorado Highway Bridge Number E-17-AH**

Var.	Determin.	Random	Source	Bias	δ
λ_{rebar}	1.0	N[1.0, .015]	Nowak et.al. [1994]	1.0	.015
f_y	50 ksi	N[56.0, 6.16]	Nowak [1995]	1.12	0.11
$\lambda_{d_{eff}}$	1.0	N[1.0, .02]	Lu et.al. [1994]	1.0	.02
t_{slab}	9.875 in	N[9.875, 0.4]	Nowak [1995]	1.0	.0405
HMA	3 in	N[3.0, 0.75]	Nowak [1993]	1.0	0.25
γ_{mfc}	1.0	N[1.02, .061]	Nowak-Yamani [1995]	1.02	.06
λ^*_{trk}	1.0	N[1.27, .036]	Nowak [1993]	1.0	.028
V^*_{trk-i}	1.0	N[1.27, .036]	Nowak [1993]	1.0	.028
F_y	33 ksi	N[36.63, 4.21]	Nowak [1995]	1.11	.12
DF_i	1.212	N[1.309, .163]	Zokaie et.al. [1991]	.926	.124
DF_{i-e}	1.06	N[1.14, .142]	Zokaie et.al. [1991]	.926	.124
DF_e	0.090	N[0.982, .122]	Zokaie et.al. [1991]	.926	.124
I_{beam}	1.296	N[1.14, .114]	Nowak et. al. [1991]	.880	0.1
ω_{steel}	132 plf	N[135.96, 10.9]	Hendawi [1994]	1.03	0.08
M^*_{trk-i}	259.0 ft-kip	N[435.6, 14.76]	Nowak [1993]	1.68	0.033
f'_c	3 ksi	N[2.76, .497]	Nowak et.al. [1994]	.92	0.18
λ_{asph}	1.0	N[1.0, 0.25]	Nowak [1993]	1.0	0.25
λ_{conc}	1.0	N[1.05, 0.105]	Nowak [1993]	1.05	0.10
λ_{steel}	1.0	N[1.03, 0.082]	Nowak [1993]	1.03	0.08
γ_{msg}	1.0	N[1.14; .137]	Nowak [1995]	1.14	.12
γ_{mfg}	1.0	N[1.11; .128]	Nowak [1995]	1.11	.115
V^*_{trk-e}	1.0	N[0.905, 0.064]	Nowak [1993]	1.0	.071
M^*_{trk-e}	259.0 ft-kip	N[306.0, 22.76]	Nowak [1993]	1.35	0.12
γ_{msc}	1.0	N[1.075, .108]	Nowak-Yamani [1995]	1.075	.10
A_v/s	.178 in	N[.178, .00711]	Lu et.al. [1994]	1.0	.04
γ_{mcc}	.85	N[.85, .085]	Nawy [1990]	1.0	.10
E_s	29,000 ksi	N[29.0, 1.74](10^3)	Tabsh-Nowak [1991]	1.0	.06

* Variable is based on the 50 year load

Table 5.3: **Variables in System Reliability Analysis of Colorado Highway Bridge Number E-17-AH**

Variable	Random	Meaning
γ_{mfc}	vm(1)	Model uncertainty factor: concrete flexure, deck
λ_{rebar}	vm(2)	Uncertainty factor: reinforcing steel area in concrete
f_y	vm(3)	Yield stress of steel reinforcing in concrete deck
$\lambda_{d_{eff}}$	vm(4)	Effective depth of reinforcing steel in deck
f'_c	vm(5)	28 day yield strength of concrete
λ_{asph}	vm(6)	Uncertainty factor: weight of asphalt on deck
λ_{conc}	vm(7)	Uncertainty factor: weight of concrete on deck
λ_{trk}	vm(8)	Uncertainty factor: HS-20 truck in analysis of deck
F_y	vm(9)	Yield strength of steel in girders
γ_{msg}	vm(10)	Model uncertainty factor: shear in girders
λ_{steel}	vm(11)	Uncertainty factor: weight of steel girders
V_{trk-i}	vm(12)	Uncertainty factor: live load shear on interior girders
DF_i	vm(13)	Uncertainty: live load girder distribution, interior girders
I_{beam}	vm(14)	Uncertainty factor: impact on girders
γ_{mfg}	vm(15)	Model uncertainty: flexure in girders
M_{trk-i}	vm(16)	Uncertainty factor: live load moment on interior girders
DF_e	vm(17)	Uncertainty: live load girder distribution, exterior girders
DF_{i-e}	vm(18)	Uncertainty: live-load distribution, int-ext. girders
V_{trk-e}	vm(19)	Uncertainty: live-load shear, exterior girders
M_{trk-e}	vm(20)	Uncertainty: live-load moment, exterior girders
E_s	vm(21)	Modulus of Elasticity, steel
–	vm(22)	not used
γ_{msc}	vm(23)	Model uncertainty: shear in concrete
A_v/s	vm(24)	Area of shear reinforcement/ bar spacing
γ_{mcc}	vm(25)	Model uncertainty: eccentricity in short columns

The limit state equations for each failure mode (slab, moment in interior girder and shear in interior girder) need to be developed. This involves combining the random variables with the load rating equations already used. Recalling that a limit-state equation is always in the form of *Capacity* − *Demand*, a positive result indicates survival and a negative result represents failure of the component. A result equal to zero indicates a point on the failure surface.

For the slab which was only analyzed for moment capacity, the general form of the limit state equation would be

$$g(1) = M_{Capacity} - M_{Demand} = M_u - M_{dl} - M_{ll} = 0 \tag{5.28}$$

Recalling Eqs. 5.4, 5.4, and 5.5, the equation for ultimate moment capacity M_u can be expressed by substitution as

$$M_u = \frac{A_t f_y d_{eff}}{12} - \frac{a_t^2 f_y^2}{244.8 f_c'} \tag{5.29}$$

The random variables which account for the area of tension steel in a one-foot section of slab A_t and the effective depth of the slab d_{eff} are expressed as

$$\begin{aligned} A_t &= (.62in^2)\lambda_{rebar} \\ d_{eff} &= (6.75in)\lambda_{d_{eff}} \end{aligned}$$

By substitution into Eq. 5.29,

$$\begin{aligned} M_u &= \gamma_{mfc}[\frac{.62\lambda_{rebar} f_y (6.75\lambda_{d_{eff}})}{12} - \frac{(.62)^2\lambda_{rebar}^2 f_y^2}{244.8 f'c}] \\ &= \gamma_{mfc}[.349\lambda_{rebar} f_y \lambda_{d_{eff}} - \frac{.3844\lambda_{rebar}^2 f_y^2}{244.8 f_c'}] \end{aligned} \tag{5.30}$$

Using Eq. 5.6 and substituting for the random variables, the equation for the dead load moment M_{dl} becomes

$$\begin{aligned} M_{dl} &= \frac{ws^2C_f}{8(1000)} = \frac{w(6.187ft)^2(.8)}{8000} = .003817w \\ &= .003817(w_{conc} + w_{asph}) = .003817(36\lambda_{asph} + 123.44\lambda_{conc}) \\ &= .137\lambda_{asph} + .471\lambda_{conc} \end{aligned} \tag{5.31}$$

Similarly, using Eq. 5.8 and substituting random variables, the resulting equation for the live load moment on the slab is

$$\begin{aligned} M_{ll} &= \frac{L_{trk}(s+2)}{32}C_fI_f = \frac{16\lambda_{trk}(6.187+2)}{32}(.8)(1.3) \\ &= 4.27\lambda_{trk} \end{aligned} \tag{5.32}$$

By substituting the results from Eqs. 5.30, 5.31, and 5.32 into Eq. 5.28, the final limit state equation for failure of the slab due to moment that will be used for a reliability analysis is:

$$g(1) = \gamma_{mfc}[.349\lambda_{rebar}f_y\lambda_{D_{eff}} - \frac{.3844\lambda_{rebar}^2 f_y^2}{244.8f_c'}] - .137\lambda_{asph} - .471\lambda_{conc} - 4.26\lambda_{trk} \tag{5.33}$$

The exact same process is used to generate the limit state equations for failure due to shear and moment in the interior girders. The limit state equation for shear $g(2)$ is obtained by substituting random variables into Eqs. 5.11, 5.15, and 5.19 for V_u, V_{dl}, and V_{ll} respectively.

$$\begin{aligned} g(2) &= V_{Capacity} - V_{Demand} = V_u - V_{dl} - V_{ll} = 0 \\ &= 10.55F_y\gamma_{msg} - 18.04\lambda_{conc} - 5.26\lambda_{asph} - 2.89\lambda_{steel} - 28.33V_{trk-i}DF_iI_{beam} \end{aligned} \tag{5.34}$$

The limit state equation for moment in the interior girder is obtained by substituting random variables into Eqs. 5.22, 5.23, and 5.25 for M_u, M_{dl}, and M_{ll} respectively.

$$\begin{aligned} g(3) &= M_{Capacity} - M_{Demand} = M_u - M_{dl} - M_{ll} = 0 \\ &= 39.8F_y\gamma_{mfg} - 197.65\lambda_{conc} - 57.64\lambda_{asph} - 31.7\lambda_{steel} - M_{trk-i}DF_iI_{beam} \end{aligned} \tag{5.35}$$

5.4.3 Reliability Results For An HS-20 Truck

Using the limit state equations for the slab and girder shown in Eqs. 5.33, 5.34, and 5.35 and the values for the random variables shown in Table 5.2, the reliability with respect to each failure mode is computed. The only exception is the live load which is initially assumed to be a deterministic AASHTO HS-20 truck. Since the load rating was computed based on the HS-20 truck, this will allow a valid comparison. Using RELSYS, the reliability indices for the slab, girder (shear), and girder (moment) were $\beta = 6.72$, 6.81, and 4.00 respectively. A comparison with the load rating results is shown in Table 5.4.

The major difference between the reliability and load rating results is the relative disparity in importance of the slab and girder-shear failure modes. The load rating indicates that the slab can safely carry less than half the load that the girder can sustain with respect to shear failure (i.e., HS 29.8 vs. HS 64.6). However, the two failure modes have almost equal reliabilities.

Table 5.4: **Comparison of Load Ratings to Reliability for Colorado Highway Bridge E-17-AH Using a Deterministic HS-20 Truck**

Failure Mode	Inventory Rating (HS)	Operating Rating (HS)	Reliability Index (β)
slab	29.8	49.6	6.72
int. girder: shear	64.6	108.0	6.81
int. girder: flexure	20.7	34.5	4.00
serviceability	17.8	29.7	-
system	17.8	29.7	4.00

Having used identical equations, it demonstrates the effect that the relative uncertainty of the individual variables has on the results.

Taking the lowest component load rating as the load rating of the bridge is not a conservative assumption. The bridge at this point would undoubtedly be modeled as a series system as shown in Fig. 5.13 where failure of any of the components would constitute failure of the bridge. Taking the reliability of the weakest member as the reliability of the bridge assumes perfect correlation between the failure modes. Any partial correlation between failure modes would result in a lower system reliability. In this particular example, however, the point is not illustrated because the reliability of the girder with respect to flexure is so much lower than the reliability of the other two fail-

ure modes, that the system reliability index is 4.0. If the reliabilities of the components were closer together, the system reliability index would be lower than any of the individual component reliabilities. The load rating approach remains conservative in this case by including the serviceability criterion which dominates.

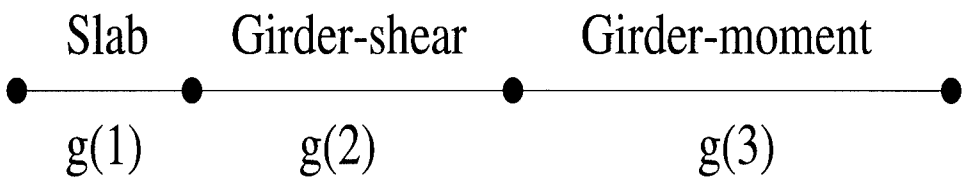

Figure 5.13: **Series Model of Bridge E-17-AH Based on Three Failure Modes**

5.4.4 A Reliability-Based Approach to Inventory and Operating Load Ratings

A load rating analysis informs the bridge manager which trucks can safely cross a particular bridge. In the case of Bridge E-17-AH, for example, it was found that the maximum load (i.e., operating rating) that one should take across the slab is an HS 49.6 equivalent truck while the girder with respect to shear could handle an HS 108.0 equivalent truck. It seems logical then that a reliability analysis with an HS 49.6 truck crossing the slab and an HS 108.0 truck crossing the girder would produce similar levels of safety with respect to these failure modes. This is not the case.

Table 5.5 shows the reliability results with respect to the three failure components from Fig. 5.13 for a deterministic HS-20 truck and for determin-

istic truck equivalents to its respective inventory and operating load ratings. For example, the slab was subjected to an HS 29.8 truck (inventory rating) and an HS 49.6 truck (operating rating). Table 5.5 shows that the levels of safety are not the same for the respective failure modes when subjected to their inventory and operating loads. In fact, the level of disparity is not the same looking at the inventory and operating results. For example, when the girder is subjected to its respective inventory load with respect to shear and moment, the girder is safer with respect to shear ($\beta_{shear} = 4.21, \beta_{moment} = 3.89$). When subjected to their operating loads, the girder is safer with respect to moment ($\beta_{shear} = 2.40, \beta_{moment} = 2.46$).

The different failure components should produce similar levels of safety when subjected to their inventory or operating loads. A reliability-based approach to load rating would provide this. For example, the inventory rating could be defined as the HS truck that would provide a reliability index $\beta = 4.0$ and the operating rating as the HS truck that produces $\beta = 2.5$. This approach would clearly produce different HS ratings than currently exist, would account for the relative uncertainty of random variables, and would produce similar levels of safety by definition.

5.5 Live Load Models

The reliability analysis so far has used a deterministic HS-20 truck as the live load on the bridge. In reality, the live load traffic on the bridge is one of the most uncertain random variables in the analysis. A number of studies and live load models have been proposed (i.e., Ellingwood *et al.* [1982],

Table 5.5: **Reliability Associated With the HS-20 Truck, the Inventory Rated Truck and the Operating Rated Truck**

Failure Mode	HS-20 Load	Inventory Load	Operating Load
slab	6.72	5.64	3.41
int. girder: shear	6.81	4.21	2.40
int. girder: flexure	4.00	3.89	2.46

Goble *et al.* [1992], Tan [1990], Bailey [1996]), usually as the result of field observations or weigh-in-motion studies. Quantifying the live load is difficult because the live load effect is a combination of individual truck weights, the spacing of individual truck axles, and the relative position of trucks on the bridge. This study will consider two of these models: Ghosn & Moses [1986] and Nowak [1993].

5.5.1 Ghosn Live Load Model

The Ghosn live load model was based on a weigh-in-motion study in conjunction with the FHWA and Ohio DOT [Ghosn 1981]. A weigh-in-motion study obtains truck weights in an undetectable manner using traffic sensors to obtain vehicle speed and axle spacing. Strain gages measure the effect of traffic on the bridge. The strain records are compared to the influence line of the bridge to obtain truck axle weights. The weigh-in-motion data ultimately

is used to develop traffic patterns which describe the position and weight of the vehicles going over the bridge.

The purpose of the live load model is to calculate the maximum live load expected at different times over the service life of the structure. Based on the results from a large number of sites, Ghosn and Moses [1984] developed a numerical integration approach to calibrate a load prediction formula applied to a range of span lengths. The result was a load model formula, best summarized in Ghosn and Moses [1986] which computes the mean value of the maximum bending moment M in 50 years as follows:

$$M = amW^{*}HgiG_{r} \tag{5.36}$$

where the listed variables include truck configuration, girder distribution, span, impact and growth. Looking at the variables individually and applying them to bridge E-17-AH, a is the only deterministic variable and is dependent on the truck configuration and the span. This model used two types of trucks: single and semi-trailer. For shorter spans (less than 60 ft (18.3 m), the single truck configuration was dominant. The variable m is a random coefficient based on span length and describes the variation of load effect for a given type truck. The values for a, m, and V_m (the coefficient of variation of m) are interpolated from Table 5.6 reprinted in part from Ghosn & Moses [1986].

Using a bridge span $L = 43.833\ ft$ (13.36 m) for Bridge E-17-AH and interpolating between spans of 40 ft (12.19 m) and 60 ft (18.29 m) on Table 5.6, the computed variables are $a = 9.52\ kip - ft/kip$ (2.90 $kN - m/kN$),

Table 5.6: a **and** m **Factors for Ghosn Live Load Model Based on Bridge Span [Ghosn and Moses 1986]**

Span (ft)	a $(kip - ft/kip)$	m	V_m	Type of Truck
30	6.07	0.92	0.15	Single
40	8.57	0.93	0.12	Single
60	13.57	0.94	0.06	Single

$m = .932$, and $V_m = 0.109$. The variable W^* is the 95th percentile weight for the dominant type truck for the bridge span. For the short span in this case, the single truck dominated which produced a 95th percentile weight $W^* = 47$ *kips* and $V_{W^*} = 0.15$. A headway factor H includes the likelihood of overloading by having closely spaced vehicles at the extreme tail of the weight distribution on the bridge. Since H is dependent on span and traffic volume, its value is based on the interpolation from Table 5.7 also reprinted in part from Ghosn and Moses [1986].

Average traffic volume is defined as 2000 trucks/day and low volume is considered 200 trucks/day. The average daily traffic (ADT) over Bridge E-17-AH is 8500 vehicles/day [CDOT 1995b]. State Highway 33 is classified as an Urban road (not interstate) which according to Table 5.8 [AASHTO 94 (C3.6.1.4.2)] would provide an estimated average daily truck traffic (ADTT) percentage as 10% or 850 trucks/day. The traffic over the bridge is somewhere between low and average. For average traffic volume, interpolation from Table

Table 5.7: **H Factors for Ghosn Live Load Model Based on Bridge Span and Traffic Volume [Ghosn and Moses 1986]**

Span (ft)	Heavy Volume	Average Volume	Low Volume
40	2.79	2.69	2.41
100	2.93	2.80	2.51

5.7 results in $H = 2.70$ and for low traffic volume, $H = 2.41$. In both cases, $V_H = 0.10$.

Table 5.8: **Average Daily Truck Traffic as a Function of Average Daily Traffic on Different Highways**

Class of Highway	Fraction of Trucks in Traffic
Rural, interstate	0.20
Urban, interstate	0.15
Other rural	0.15
Other urban	0.10

The distribution of the load to the girders is accounted for by g (Eq. 5.36) which makes the AASHTO distribution factor a random variable by applying a bias factor and coefficient of variation [Moses and Verma 1987].

The AASHTO distribution factor DF for the distribution of four wheel lines and a girder spacing $S = 6.667\ ft\ (2.032\ m)$ is

$$DF = \frac{S/5.5}{\#\ wheel\ lines} = \frac{6.667ft/5.5}{4} = .3030 \tag{5.37}$$

The bias factor for steel girders is $b_g = 0.9$ with a coefficient of variation of 0.13. This results in values of $g = b_g(DF) = 0.9(.3030) = .2727$ and $V_g = 0.13$. The dynamic amplification or impact factor i of the vehicles is found by transforming the deterministic AASHTO impact factor into a random variable where $i = 1.11$ and $V_i = 0.11$. Finally a variable for future growth G_r is included to account for the increased gross weight of heavy trucks on the highways over time. The values used by Ghosn [1986] were $G_r = 1.15$ and $V_{G_r} = 0.10$. Applying the values for these variables to the Ghosn live load model, the fifty year maximum moment M for average traffic volume is computed as

$$\begin{aligned} M &= amW^*HgiG_r \\ &= (9.52ft - kip/kip)(.932)(47kip)(2.70)(.2727)(1.11)(1.15) \\ &= 413.3\ ft - kips\ (560.4\ kN - m) \end{aligned} \tag{5.38}$$

For low traffic the mean maximum moment would be $M = 368.7\ ft - kips$ $(499.9\ kN - m)$. The coefficient of variation of the maximum moment V_M can be computed for both average and low traffic volume as

$$\begin{aligned} V_M &= \sqrt{V_a^2 + V_m^2 + V_{W^*}^2 + V_H^2 + V_b^2 + V_i^2 + V_{G_r}^2} \\ &= \sqrt{(0)^2 + (.109)^2 + (.15)^2 + (.10)^2 + (.13)^2 + (.11)^2 + (.10)^2} \\ &= .259 \end{aligned} \tag{5.39}$$

The reliability analysis on the interior girder due to moment failure can now be revised using the more realistic Ghosn live load model rather than the deterministic HS-20 truck. The live load moment on the bridge for average traffic is a random variable with a mean value $M = 413.3\ ft{-}kips$ ($560.3\ kN{-}m$) and a standard deviation $\sigma_M = (.259)(413.3) = 107.0\ ft{-}kips$ ($145.1\ kN{-}m$). Recall that for the deterministic HS-20 truck the live load moment was $M_{ll} = 259.0\ ft - kips$ ($351.2\ kN - m$).

As expected the reliability of the girder with respect to moment decreased using the Ghosn live load model. Recalling that $\beta = 4.00$ for the girder using the HS-20 truck, the reliability index drops to $\beta = 3.86$ for low volume traffic and to $\beta = 3.56$ for the average volume traffic. The use of a live load model provides a more realistic assessment of bridge safety but different live load models do not necessarily produce similar results.

5.5.2 Nowak Live Load Model

A live load model which predicts the maximum truck moments and shears for different length spans was developed by Nowak [1993]. The study covered 9,250 selected trucks from the Ontario Ministry of Transportation data base. The data base included number of axles, axle spacing, axle loads, and gross weight of the vehicles. The bending moments and shears were calculated for each truck in the survey for a wide range of spans. The cumulative distribution functions (CDF) of the span moments and shears were plotted on normal probability paper for spans ranging from 10 feet (3.05 m) to 200 feet

(60.96 m). The maximum moments and shears for different time periods were extrapolated from these distributions.

These CDFs were transformed to a standard normal distribution and the coefficients of variation for the maximum shears and moments were determined from the slope of the transformation. The end result was a series of graphs which provide a ratio of the mean shear and moment for the live load model to the shear and moment resulting from the standard HS-20 truck. This quantity is the bias factor needed for the random variable. The coefficients of variation for the maximum moment and shear are provided on other graphs. To read the graphs, one must know only the bridge span and the desired life of the bridge.

The Nowak graphs were based on a measured two week traffic flow which equates to approximately 1,000 trucks per day. It is estimated that 1.5 million trucks will pass over the bridge in five years, 15 million trucks in 50 years, and 20 million trucks in 75 years. The Nowak graphs are based on the statistics of extreme values where the probability of encountering a large truck at the extreme tail of the distribution increases as the number of trucks passing over the bridge increases. As a result, the mean values of the maximum moment and shear increase over time and the coefficients of variation decrease.

The Nowak graphs can be applied to a specific bridge where the daily traffic is known by reading the data for a single truck from the Nowak study and applying extreme value statistics to the actual traffic of the bridge under consideration. For Bridge E-17-AH which has a span of 43.833 ft (13.36 m),

the Nowak graphs [Nowak 1993] show that the ratio of the shear caused by one truck in the live load study to the shear caused by an HS-20 truck is 0.52 and the coefficient of variation is 0.29. Similarly, the ratio of the positive moment on a simple span for a single truck caused by the live load model to the moment caused by the HS-20 truck is 0.65 and the coefficient of variation is 0.32. As expected, the HS-20 truck provides a conservative estimate of the single truck crossing the bridge. The AASHTO HS-20 truck does not account, however, for the increased probability that an extreme value truck will cross the bridge as the number of occurrences increases.

Let the initial distribution of trucks crossing the bridge have a cumulative distribution function (CDF), $F_X(x)$, and probability density function (PDF), $f_X(x)$. The exact distribution of the maximum truck crossing the bridge CDF, F_{M_n}, and PDF, f_{M_n}, is a function of the number of occurrences n [Ang & Tang 1984]

$$\begin{aligned} F_{M_n}(m) &= [F_X(m)]^n \\ f_{M_n}(m) &= n[F_X(m)]^{n-1} f_X(m) \end{aligned} \tag{5.40}$$

Because the exact distribution is a function of another distribution and can contain many random variables, the computations can be very cumbersome. Fortunately, as the number of occurrences becomes larger, the extreme distribution approaches an asymtotic form which is not dependent on the original distribution. The normal and lognormal distributions approach a type I extreme value distribution with negligible differences as n is greater than 25. The type I extreme value distribution is only a function of the number of

occurrences n, the mean value of the initial distribution μ, and the standard deviation of the original distribution σ [Ang & Tang 1984].

$$\begin{aligned} F_{M_n}(m) &= e^{-e^{[\frac{-\alpha_n}{\sigma}(m-\mu-\sigma u_n)]}} \\ f_{M_n}(m) &= (\frac{\alpha_n}{\sigma})e^{[(\frac{\alpha_n}{\sigma})(m-\mu-\sigma u_n]}e^{-e^{[(\frac{-\alpha_n}{\sigma}(m-\mu-\sigma u_n]}} \end{aligned} \tag{5.41}$$

where

$$\begin{aligned} \alpha_n &= \sqrt{2ln(n)} \\ u_n &= \alpha_n - \frac{ln[ln(n)] + ln(4\pi)}{2\alpha_n} \end{aligned} \tag{5.42}$$

To apply the live load model to the reliability analysis of the bridge, only the mean and standard deviation of the extreme distribution are needed. Using the central and dispersion characteristics of the type I extreme distribution, the mean μ_{M_n} and standard deviation σ_{M_n} can be computed as [Ayyub and White 1995]

$$\begin{aligned} \mu_{M_n} &= \sigma u_n + \mu + (\gamma\sigma/\alpha_n) \\ \sigma_{M_n} &= (\pi/\sqrt{6})(\sigma/\alpha_n) \end{aligned} \tag{5.43}$$

where $\gamma = 0.577216$ (the Euler number).

Eq. 5.43 can be used to compute the mean and standard deviation of the live load effects over any time period using the values from the Nowak graphs and the number of occurrences. In order to compare the reliability results with those from the Ghosn model, a time period of 50 years is chosen. Considering the ADTT of 850 trucks per day, the number of occurrences n is

$$n = 850 trucks/day(365.25 days/year)(50 years) = 15,523,125\ trucks \tag{5.44}$$

Considering the 50 year maximum moment provided by this live load moment, recall that the Nowak graphs provide a ratio between the live load moment and the HS-20 moment of 0.65 and a coefficient of variation of 0.32. The HS-20 truck produced a live load moment of 259.0 $ft - kips$ (351.2 $kN - m$) (Eq. 5.24) which results in the mean μ and standard deviation σ for the moment caused by a single live load model truck as

$$\begin{aligned} \mu &= .65(259.0ft - kips) = 168.35\ ft - kips\ (228.25\ kN - m) \\ \sigma &= (168.35ft - kips)(0.32) = 53.87\ ft - kips\ (73.03\ kN - m) \end{aligned} \tag{5.45}$$

By substituting these values for n, μ, and σ into Eqns. 5.42 and 5.43, the mean value for the 50 year maximum moment M_{trk-i} is 435.6 $ft - kips$ (590.6 $kN - m$) and the standard deviation $\sigma_{M_{trk-i}}$ is 14.76 $ft - kips$ (20.01 $kN - m$). These values are used in the reliability analysis of $g(3)$, the most critical girder with respect to moment (see Eq. 5.35). The values for M_{trk-i} and $\sigma_{M_{trk-i}}$ for any time period can be seen in Fig. 5.14.

Through a similar analysis using the shear values from the Nowak graphs, the mean value for the 50 year maximum shear is 35.94 $kips$ (159.9 kN) and the standard deviation is 1.02 $kips$ (4.54 kN). Recalling from Eq. 5.16 that the live load shear caused by an HS-20 truck is 28.33 $kips$ (126.0 kN), the shear factor V_{trk-i} in Eq. 5.34 and its standard deviation $\sigma_{V_{trk-i}}$ are computed as

$$\begin{aligned} V_{trk-i} &= 35.94kips/28.33kips = 1.27 \\ \sigma_{V_{trk-i}} &= 1.02kips/35.94kip(1.27) = .036 \end{aligned} \tag{5.46}$$

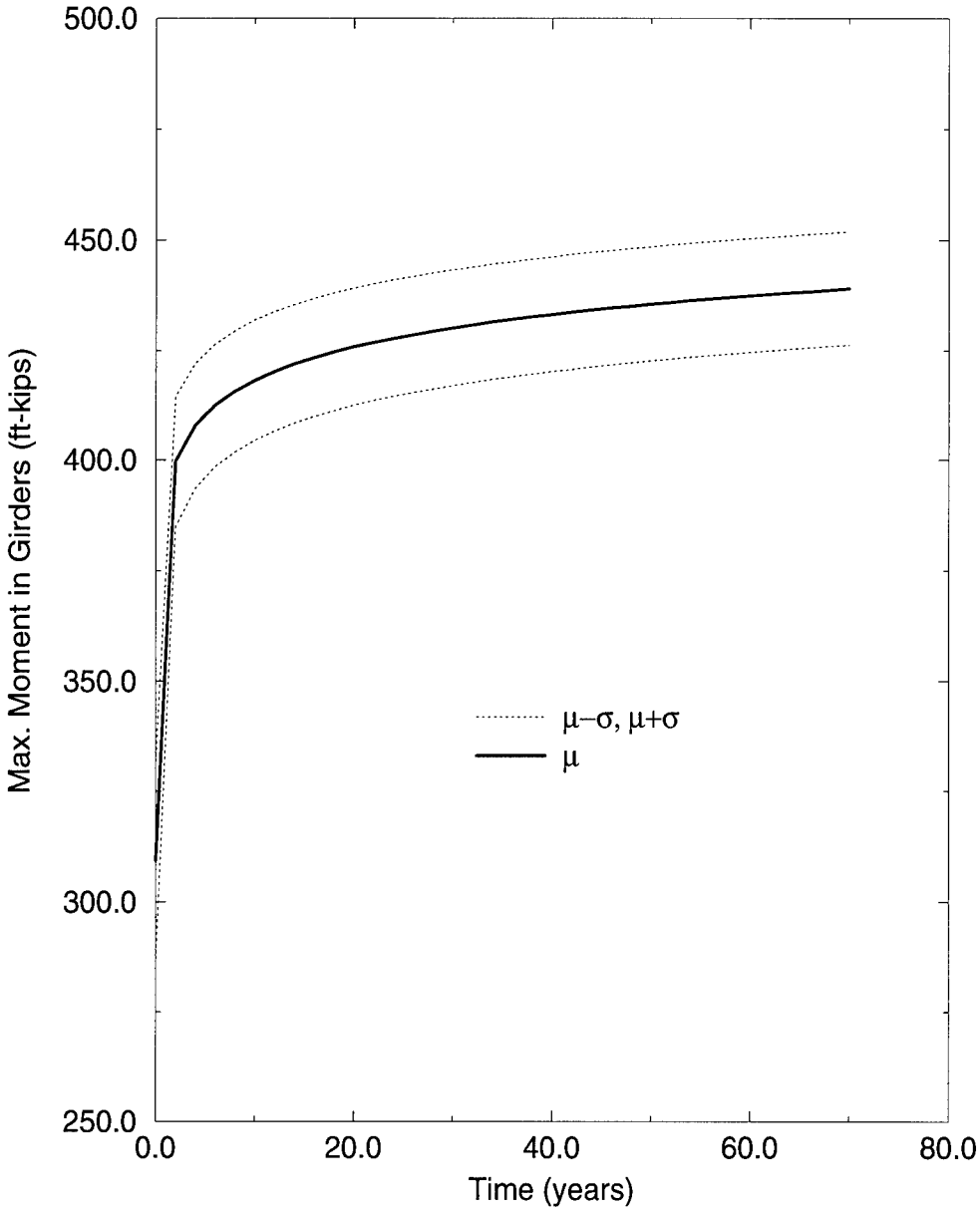

Figure 5.14: **Maximum Moment Over Time for Interior Girders in Bridge E-17-AH Based on the Nowak Live Load Model**

The shear data from the Nowak graphs can also be used to compute the equivalent truck 50 year live load to be used in the reliability analysis for the slab. Using the shear data for a single truck from the Nowak graphs, back calculating the weight of the truck and substituting into Eqs. 5.43 and 5.42, the mean value of a wheel line for the 50 year truck is 45.65 *kips* (203.1 kN) with a standard deviation of 1.31 *kips* (5.83 kN). Since the weight of a wheel line on an HS-20 truck is 36 *kips* (160 kN), the uncertainty factor associated with the live load truck λ_{trk} used in Eq. 5.33 becomes

$$\begin{aligned} \lambda_{trk} &= 45.65 kips/36.0 kips = 1.27 \\ \sigma_{\lambda_{trk}} &= 1.31 kips/45.65 kip(1.27) = .036 \end{aligned} \tag{5.47}$$

The mean values and the dispersion for the weight of the truck and the shear caused by the truck in the interior girders can be seen in Fig. 5.15.

The reliability analysis of the bridge was completed using the Nowak live load model with respect to each of the three limit state equations, $g(1)$, $g(2)$, and $g(3)$ (Eqs. 5.33, 5.34, and 5.35) and to the system as modeled in Fig. 5.13. The reliability index with respect to the slab was $\beta = 3.21$ and to the interior girder with respect to shear and moment was $\beta = 6.22$ and $\beta = 2.44$, respectively. The system reliability was dominated by the interior girder moment $g(3)$ where $\beta_{sys} = 2.43$. The Nowak live load model reliability results are similar to the reliability of the operating load rating (Table 5.5). Table 5.9 shows a comparison of the reliability results between the deterministic HS-20 truck, the Ghosn 50 year live load, and the Nowak 50 year live load.

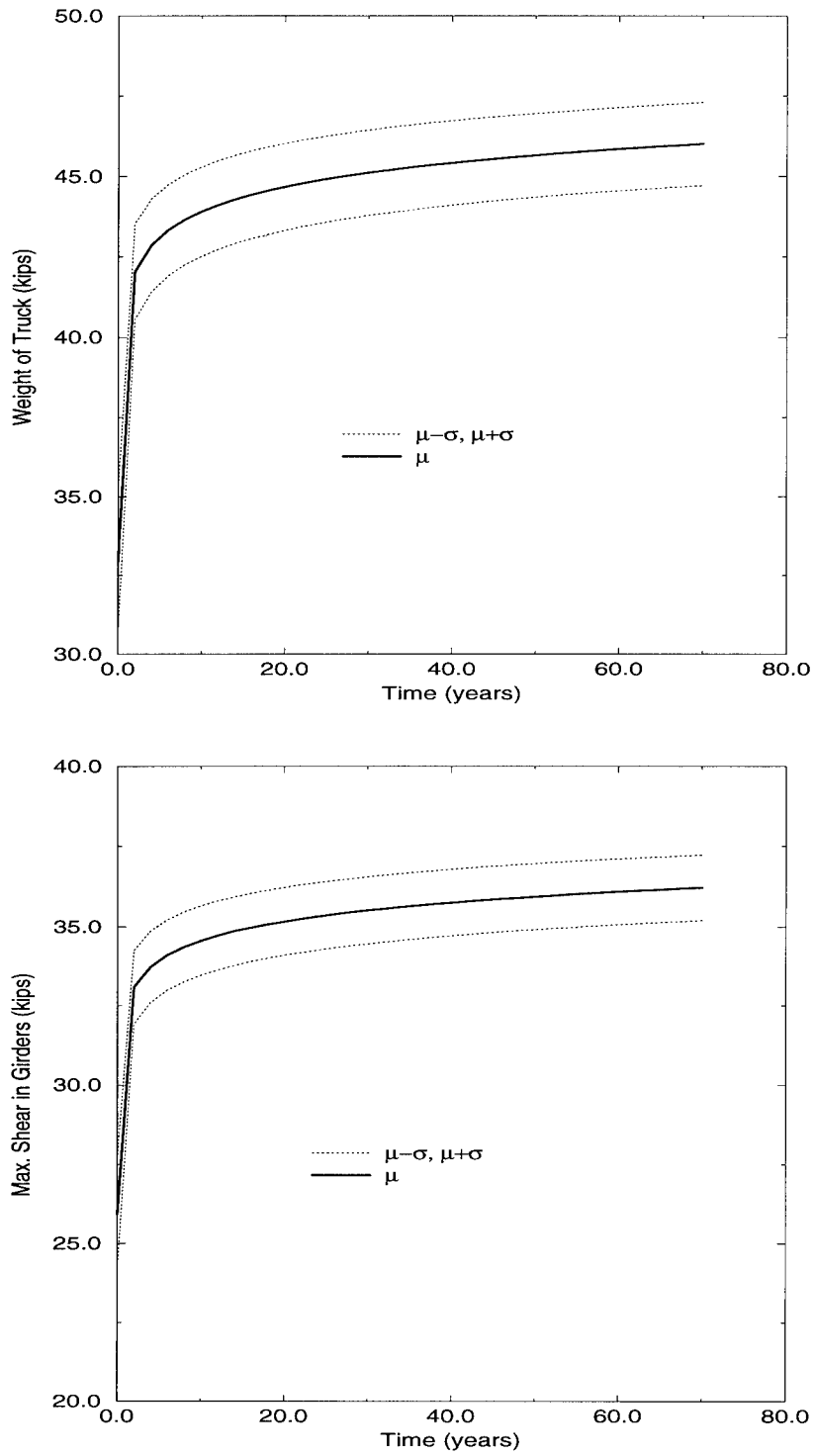

Figure 5.15: **Weight of Truck (top) and Maximum Shear in Interior Girders (bottom) Over Time in Bridge E-17-AH Based on Nowak Live Load Model**

Table 5.9: **Reliability Index (β) Associated With Load Ratings and Different Live Load Models**

Failure Mode	HS-20 Load	Ghosn 50 Year (low)	Ghosn 50 Year (avg)	Nowak 50 Year
slab	6.72			3.21
girder: shear	6.81			6.22
girder: flexure	4.00	3.86	3.56	2.44
system	4.00			2.43

The increased live load has a much larger effect on some failure modes than others. The reliability of the slab decreased significantly under the Nowak live load model while the reliability of the girder with respect to shear changed much less. While the HS-20 truck is conservative with regard to the single truck in the live load model, the HS-20 truck becomes unconservative when the large number of truck occurrences increases the likelihood of encountering an overweight truck at the tail of the distribution. The live load models account for this important fact. Unfortunately, the two live load models considered here did not produce similar results which indicates that further study and data collection in this area are needed. The Nowak live load model will be used for the remainder of this study because it is the more recent study and appears to be the more conservative model.

5.6 Other Failure Modes

The load rating classification includes only the failure of the slab and the failure of the most critical girder due to shear and moment. The substructure is not included in the load rating analysis. Therefore a number of possible failure modes are not considered. The load rating analysis does not include any effects of redundancy in a structure nor does it consider the correlation between failure modes. Using the reliability approach, this section will address these problems by incorporating additional failure modes and will model the structure so that correlation and redundancy are included in the analysis. Limit state equations will be developed for the additional failure modes and the individual component reliabilities will be computed. The system reliability will be a function of the bridge model, the random variables, and the component reliabilities.

5.6.1 Additional Failure Modes in the Superstructure

So far, only the failure reliability of the interior girders with respect to shear and moment has been considered in the analysis of Bridge E-17-AH. At this point, the girders will be divided into three types: interior, interior-exterior, and exterior as shown in Fig. 5.16. The limit state equations (Eqs. 5.34 and 5.35) and reliabilities for the interior girders due to shear and moment have already been calculated.

The exterior girders have a different size (WF33x125) from the other girders and therefore have a different plastic section modulus Z and different

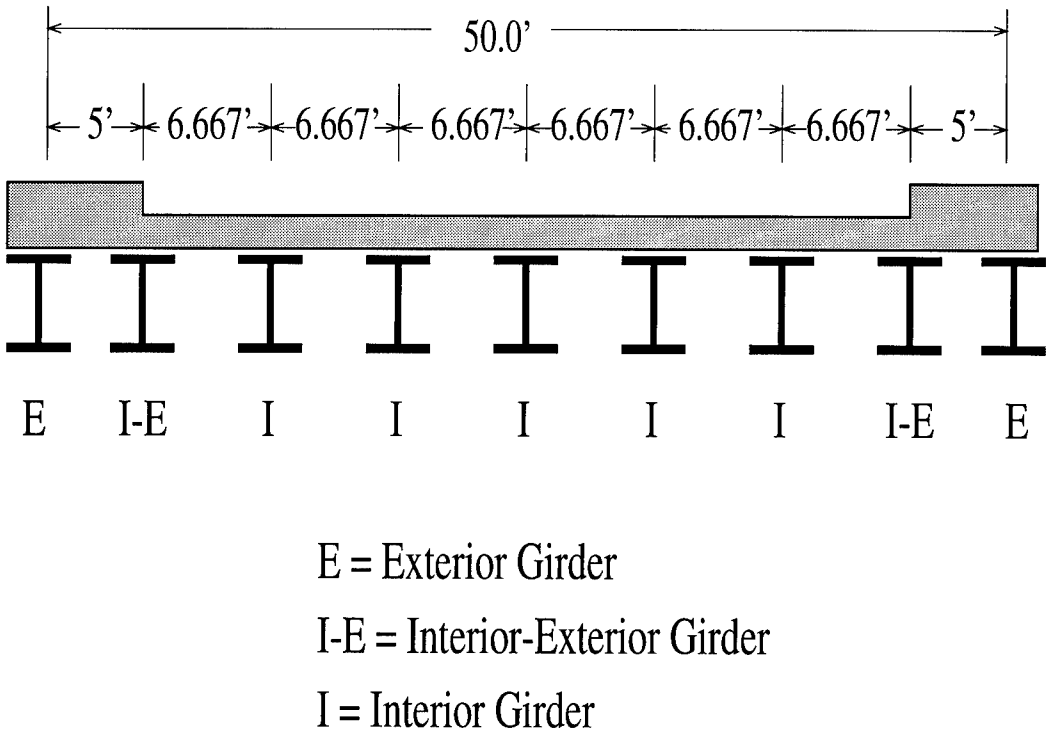

Figure 5.16: **Identification of Exterior, Interior-Exterior, and Interior Girders on Bridge E-17-AH**

web dimensions which will affect the moment and shear capacities of these girders. The exterior girders support the pedestrian walkway and should be capable of supporting a vehicle in an emergency situation. Because of the sidewalk and the reduced tributary area, the dead load will also be different on the exterior girders.

5.6.1.1 Moment and Shear on Exterior Girders

The dead load moment M_{dl} is a function of the concrete slab, the railings, and the self-weight of the steel

$$\begin{aligned} M_{dl} &= [\frac{\gamma_{conc} ts}{12} + w_{rail} + w_{stl}]\frac{l^2}{8} \\ &= [\frac{150lb/ft^3(9+10.375in)(2.5ft)\lambda_{conc}}{12} + (\frac{4160lb}{137.33ft}) \\ &\quad +125lb/ft)\lambda_{steel}]\frac{(43.833ft)^2}{8(1000lb/kip)} \\ &= 145.32\lambda_{conc} + 37.3\lambda_{steel} \end{aligned} \tag{5.48}$$

The live load moment M_{ll} is the product of the static moment caused by the live load truck M_{trk-e}, the impact factor I_{beam} and the girder distribution factor DF_e. The Nowak live load model is used for the exterior girder live load. The only difference is the number of occurrences. Rather than using the ADTT of 850 trucks/day, it is assumed that a truck will have to drive up on the 10 inch sidewalk once every six months. Using Eqs. 5.42 and 5.43 for a 50 year time period, the number of occurrences will be $n = 100$ and the values taken from the Nowak graphs for the single truck are the same as for the interior girders. For the 50 year load, this results in a mean maximum moment $M_{trk-e} = 416.38\ ft - kips$ $(564.53\ kN - m)$ and a standard

deviation of $\sigma_{M_{trk-e}} = 10.75\ ft - kips$ $(14.57\ kN - m)$. Recall that for the interior girder, these values were 435.6 $ft - kips$ (590.6 $kN - m$) and 14.76 $ft - kips$ (20.01 $kN - m$), respectively.

Because of the five foot spacing between the exterior girder and the interior-exterior girder, the deterministic girder distribution factor DF_e is

$$DF_e = s/5.5 = 5ft/5.5 = 0.909 \tag{5.49}$$

Using the bias factor and covariance from Zokaie *et al.* [1991] as shown in Table 5.2, the random variable DF_e has a mean of 0.982 and standard deviation of 0.122. The impact factor is the same as for the interior girder. The live load moment M_{ll} for the exterior girder is

$$M_{ll} = M_{trk_e} I_{beam} DF_e \tag{5.50}$$

The only change in the ultimate moment capacity for the exterior girder is the plastic section modulus $Z = 438.46\ in^3$ $(7185.1\ cm^3)$ for the WF33x125 steel girder.

$$M_u = ZF_y\lambda_{mfg} = \frac{438.46in^3}{12in/ft}F_y\lambda_{mfg} = 36.54F_y\lambda_{mfg} \tag{5.51}$$

The limit state equation $g(4)$ for failure due to moment on an exterior girder becomes

$$\begin{aligned} g(4) &= M_u - M_{dl} - M_{ll} = 0 \\ &= 36.54F_y\gamma_{mfg} - 145.32\lambda_{conc} - 37.3\lambda_{steel} - M_{trk-e}DF_eI_{beam} \end{aligned} \tag{5.52}$$

Using the exact same reasoning and assumptions as for moment, the limit state equation for the failure of the exterior girder due to shear $g(5)$ is

$$\begin{aligned} g(5) &= V_u - V_{dl} - V_{ll} = 0 \\ &= 10.38F_y\gamma_{msg} - 13.27\lambda_{conc} - 3.4\lambda_{steel} \\ &\quad -28.33V_{trk-e}DF_eI_{beam} \end{aligned} \tag{5.53}$$

5.6.1.2 Moment and Shear on Interior-Exterior Girders

The only major differences between the interior girders and the interior-exterior girders are the girder distribution factor, the dead load due to a portion of the concrete sidewalk, and the difference in girder spacing. The spacing for the girder distribution factor is the average between 5 ft (1.52 m) and 6.667 ft (2.03 m). The deterministic distribution factor DF_{i-e} is

$$DF_{i-e} = \frac{S}{5.5} = \frac{(5ft + 6.667ft)}{2(5.5)} = 1.06 \tag{5.54}$$

Using the random bias and covariance found in Table 5.2 [Zokaie *et al.* 1991], the mean and standard deviation for DF_{i-e} are 1.14 and 0.142 respectively. The limit state equation for failure of an interior-exterior girder due to moment $g(6)$ becomes

$$g(6) = 39.8F_y\gamma_{mfg} - 244.08\lambda_{conc} - 28.8\lambda_{asph} - 31.7\lambda_{steel} - M_{trk-i}DF_{i-e}I_{beam} \tag{5.55}$$

and the equation for failure due to shear $g(7)$ is

$$g(7) = 10.55F_y\gamma_{msg} - 22.29\lambda_{conc} - 2.63\lambda_{asph} - 2.89\lambda_{steel} - 28.33V_{trk-i}DF_{i-e}I_{beam} \tag{5.56}$$

5.6.2 Failure Modes in the Substructure

Although the substructure is ignored in the load rating analysis because it rarely governs, there are a number of strength modes in which the substructure could fail. This section examines potential failure modes such as shear and moment in the pier cap, crushing of the pier columns, and failure in the footing. The list is not all-inclusive. Failure modes such as bearing failure of the soil and failure of the abutment piles, for example, were not considered. In each case, the design equation is used to assess capacity and the load model determines the demand. Both are used to form a limit state equation from which a reliability analysis can be performed. Accurately defining the uncertainty in the random variables is the most difficult aspect of the process.

5.6.2.1 Failure Due to Shear, Positive Moment, and Negative Moment in the Pier Cap

The pier cap is modeled as an indeterminate beam as shown in Fig. 5.17 where the load is transferred from the girders. The beam reaction supports represent the four columns in the pier. The source of the load is the dead load weight of the asphalt surface, concrete slab and steel girders; the live load of the trucks passing over the bridge; and the self-weight of the pier cap. These loads will result in different shear and moment demands throughout the pier cap. An analysis is required to find the points of maximum shear, positive moment, and negative moment. The bending steel and cross-sectional dimensions are constant throughout the pier cap so the moment capacity is

constant throughout. The spacing of the shear stirrups is different in different sections of the pier cap which results in differing shear capacities. This section will develop limit state equations for failure of the pier cap with respect to shear $g(8)$, positive moment $g(9)$, and negative moment $g(10)$.

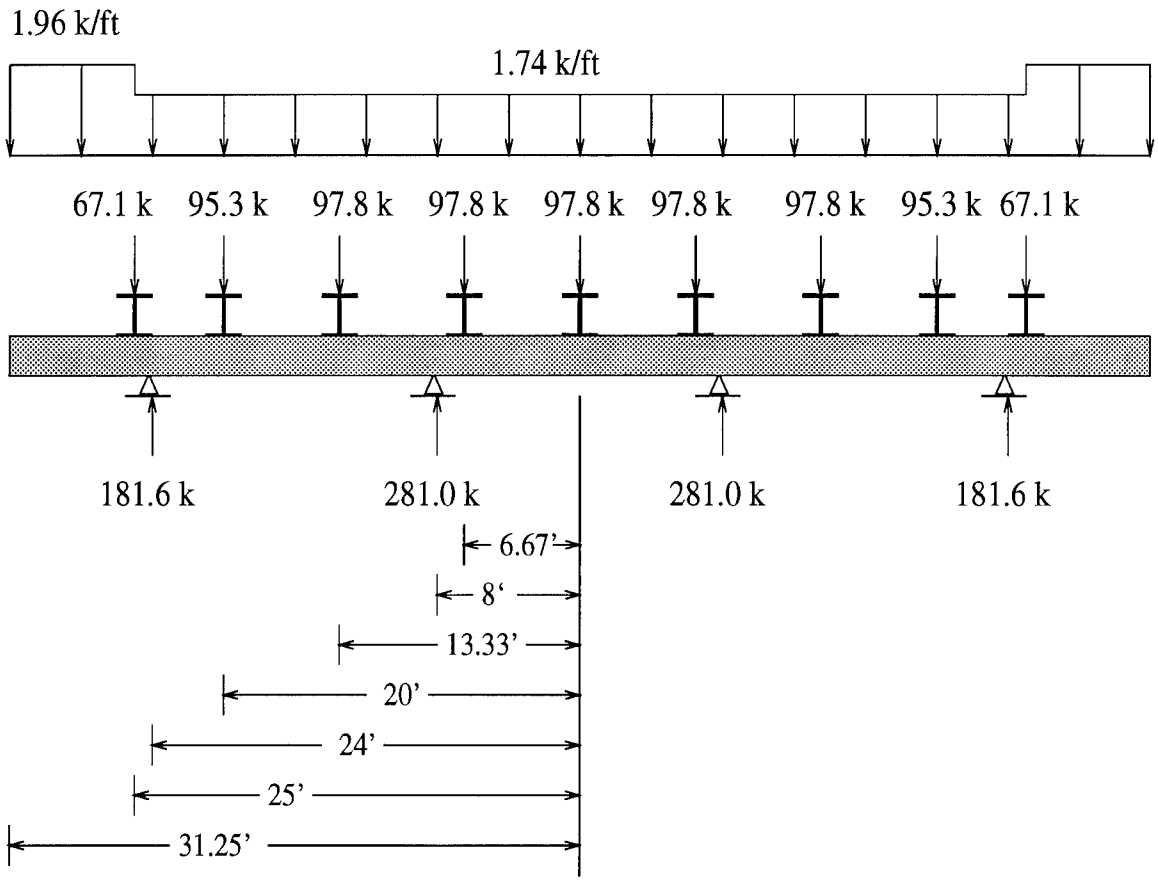

Figure 5.17: **Critical Loading Condition on Pier Cap Modeled as an Indeterminate Beam**

To determine the demand on the pier cap, shear and moment diagrams are needed. Because the different live and dead loads all have different

uncertainties associated with them, each load is considered separately and composite shear and moment diagrams are developed from superposition of the individual effects. The dead load of the asphalt, slab, and girders is transferred to the pier cap as a point load through the bearings at the ends of the girders. These point loads were computed earlier as dead load shear reactions based on unit weight of material and tributary area. Table 5.10 shows the contributions of each of the materials. The steel weight is greater in the lighter exterior girder because the metal railing is included in the quantity.

The live load is also transferred as a point load. The assumption was made that the worst case represented by four trucks side-by-side passed over the bridge simultaneously. The number of occurrences where this case exists is far less than that of a single truck going over the bridge. Some studies [Nowak 1993] have included this decreased likelihood of multiple presence and the correlation between the vehicles. For example, Nowak [1994] concluded that on a two lane bridge, two trucks were side-by-side as they passed over the bridge in only one out of every 50-100 cases. This study used the Nowak [1994] assumptions and treated the east and westbound portions as two separate two-lane roads where the trucks were side-by side one out of every 50 times and the two separate lanes coincided one out of every 100 times that the maximum two-lane condition was met. This resulted in the four lane side-by-side conditions occurring one out of every 5,000 occurrences of a single truck passing over the bridge which is still conservative.

The self-weight of the pier cap is treated as a distributed load. Based

on the cross-sectional dimensions of the pier cap shown in Fig 5.19, the area is 11.58 ft^2 (1.076 m^2). Using a unit weight of reinforced concrete γ_{conc} = 150 lb/ft^3 (2403 kg/m^3), the distributed load is 1.74 $kips/ft$ (25.39 kN/m). The pier cap has more concrete at the end (Fig. 5.4) which results in a distributed load of 1.96 $kips/ft$ (28.60 kN/m).

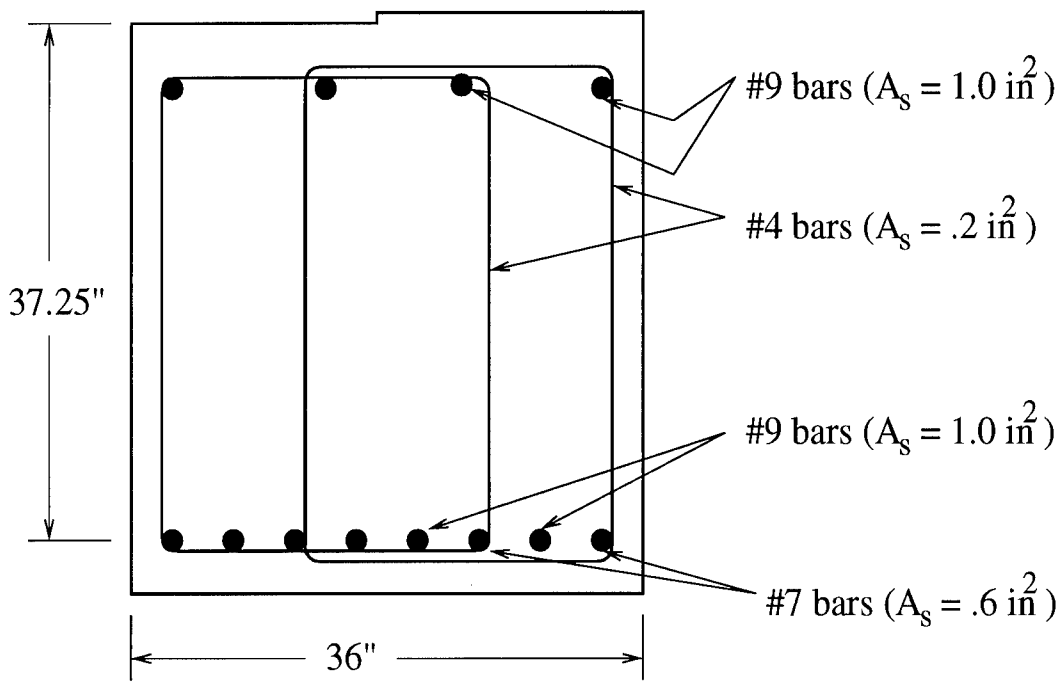

Figure 5.18: **Cross-section of Pier Cap 3 in the Positive Moment Area (Note there are 8-#9 bars on the top row in the negative moment region)**

The composite shear diagram shown in Fig. 5.20 for the most critical four truck case is the sum of the separate components. The maximum shear occurs at the interior column supports. Fig. 5.21 shows the composite moment

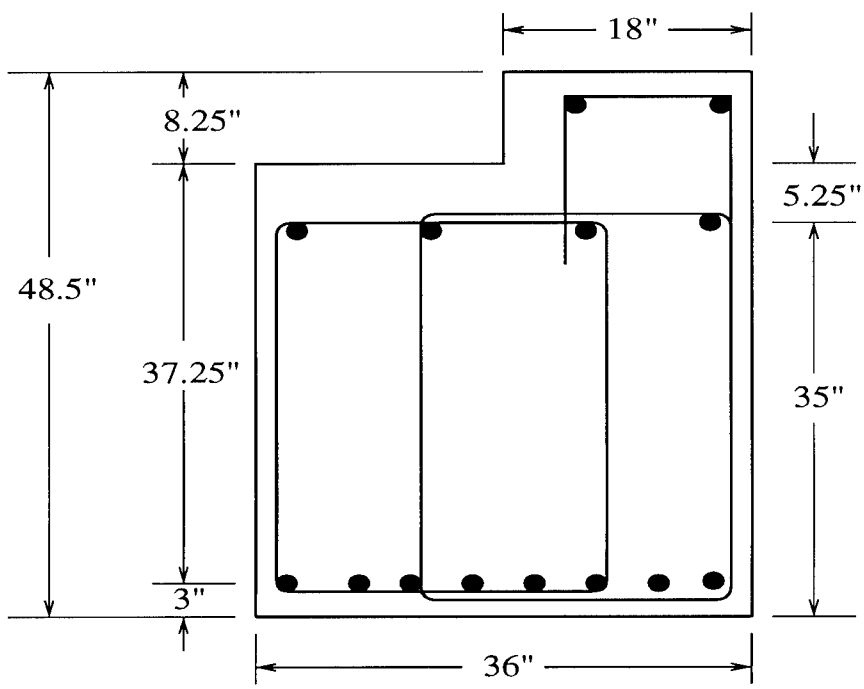

Figure 5.19: **Cross-section of Pier Cap 2 in the Positive Moment Area (Note there are 8-#9 bars on the top row in the negative moment region)**

Table 5.10: **Critical Loading on the Pier Cap**

Load Source	Int. Girder Point Load ($kips$)	Int.-Ext. Gird. Point Load ($kips$)	Ext. Girder Point Load ($kips$)	Dist. Load ($kips/ft$)	Uncert. Factor
asphalt	10.52	5.26	-	-	λ_{asph}
concrete slab	36.08	44.58	26.54	-	λ_{conc}
steel girder	6.68	6.57	7.14	-	λ_{steel}
live load	44.5	38.9	33.4	-	λ_{trk}
pier (int)	-	-	-	1.74	λ_{conc}
pier (ext)	-	-	-	1.96	λ_{conc}

diagram. The largest positive moment occurs where the interior-exterior girder meets the pier cap and the largest negative moment occurs at the interior column.

The dead load and live load shear and moment demands for the pier cap limit state equations can be found from the values on the shear and moment diagrams at their critical locations multiplied by their respective uncertainty factors. The critical location on the shear diagram is not obvious because the shear capacity of the beam is not constant due to the variable spacing of the shear steel. Fig. 5.22 shows the spacing of the shear steel in the pier cap relative to the total shear diagram. The spacing of the shear steel is 12 inches (30.5 cm) in the area where the shear is either low or where the pier cap is directly supported by the column. The spacing is reduced to 6 inches

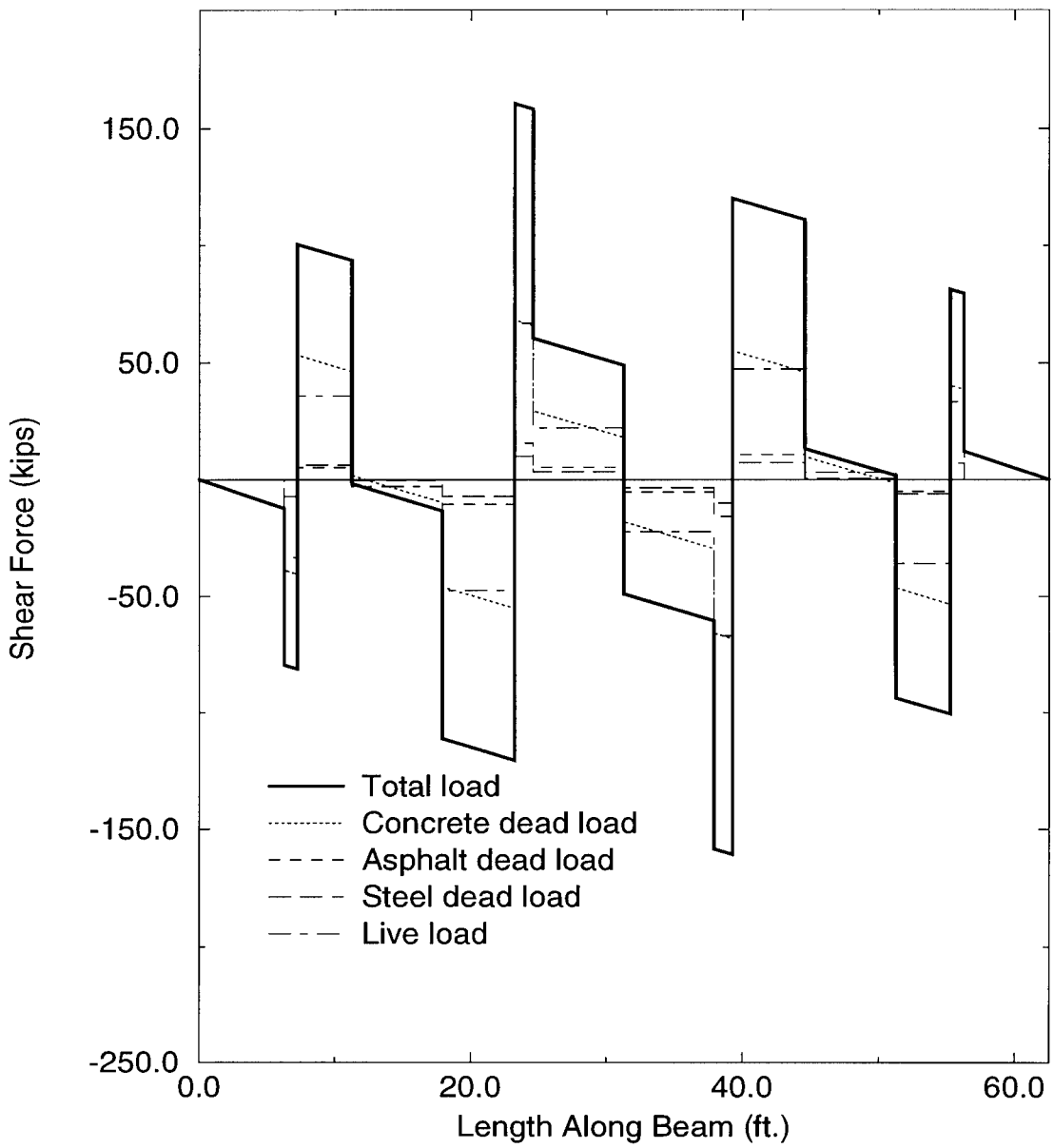

Figure 5.20: **Composite Shear Diagram for the Pier Cap on Bridge E-17-AH for the Most Critical Four Truck Case**

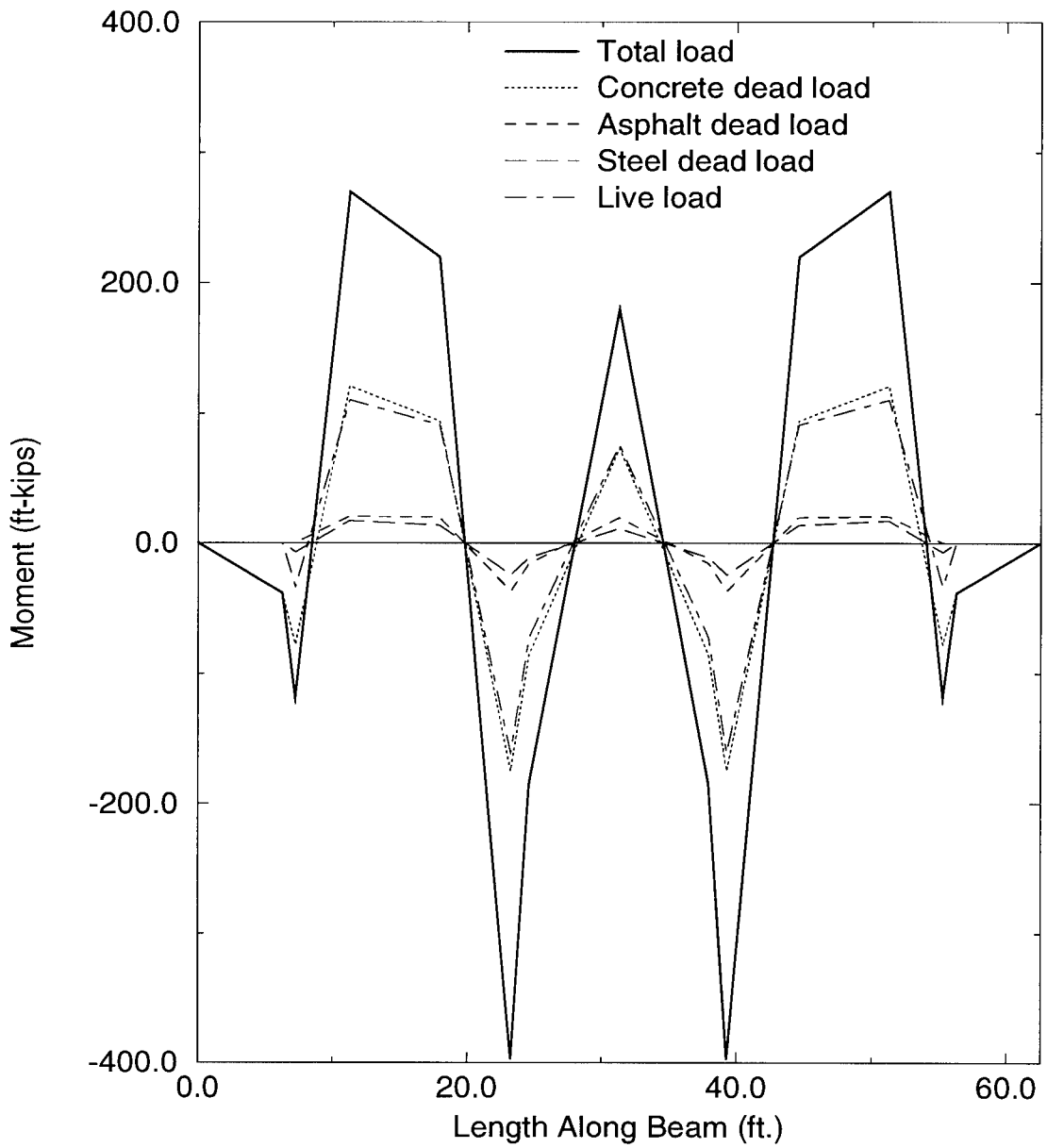

Figure 5.21: **Composite Moment Diagram for the Pier Cap on Bridge E-17-AH for the Most Critical Four Truck Case**

(15.2 cm) as the shear gets higher near the column supports and is reduced further to 4.5 inches (11.4 cm) where the shear is largest. A deterministic analysis helped identify the critical portion of the pier cap.

The largest shear values V_{max} read from the shear diagram are 160.6 *kips* (714.3 kN), 120.4 *kips* (535.5 kN), and 60.5 *kips* (269.1 kN) in the areas where the spacing was 4.5 *in* (11.4 *cm*), 6 *in* (15.2 *cm*), and 12 *in* (30.5 *cm*), respectively. The shear capacity of the pier cap is the sum of the shear strength of the concrete V_c and the shear strength of the steel V_s. The cross section of pier cap 3 is shown in Fig. 5.18.

The shear capacity provided by the steel V_s is given by

$$V_s = \frac{A_v f_y d}{s} = \frac{(.8in^2)(50ksi)(37.25in)}{s} = \frac{1490}{s} \tag{5.57}$$

where A_v = the area of shear steel which in this case is four #4 bars ($A_s = .2in^2$ (129 mm^2) per bar), f_y = the yield strength of the reinforcing steel, d = the effective depth of the beam as shown in Fig. 5.18, and s is the spacing of the shear reinforcement.

The shear capacity of the concrete V_c is a function of the 28-day compressive strength of the concrete f'_c, the width of the beam b_w, the effective depth d, and a factor λ which is equal to 1.0 for normal concrete.

$$V_c = 2.0\lambda\sqrt{f'_c}b_w d = 2.0(1.0)\sqrt{3000psi}\frac{36in(37.25in)}{1000lb/kip} = 146.9\ kips\ (653.4\ kN) \tag{5.58}$$

Table 5.11 shows the results of the deterministic factor of safety analysis for the three spacings of shear steel. The section of the pier cap where the spacing

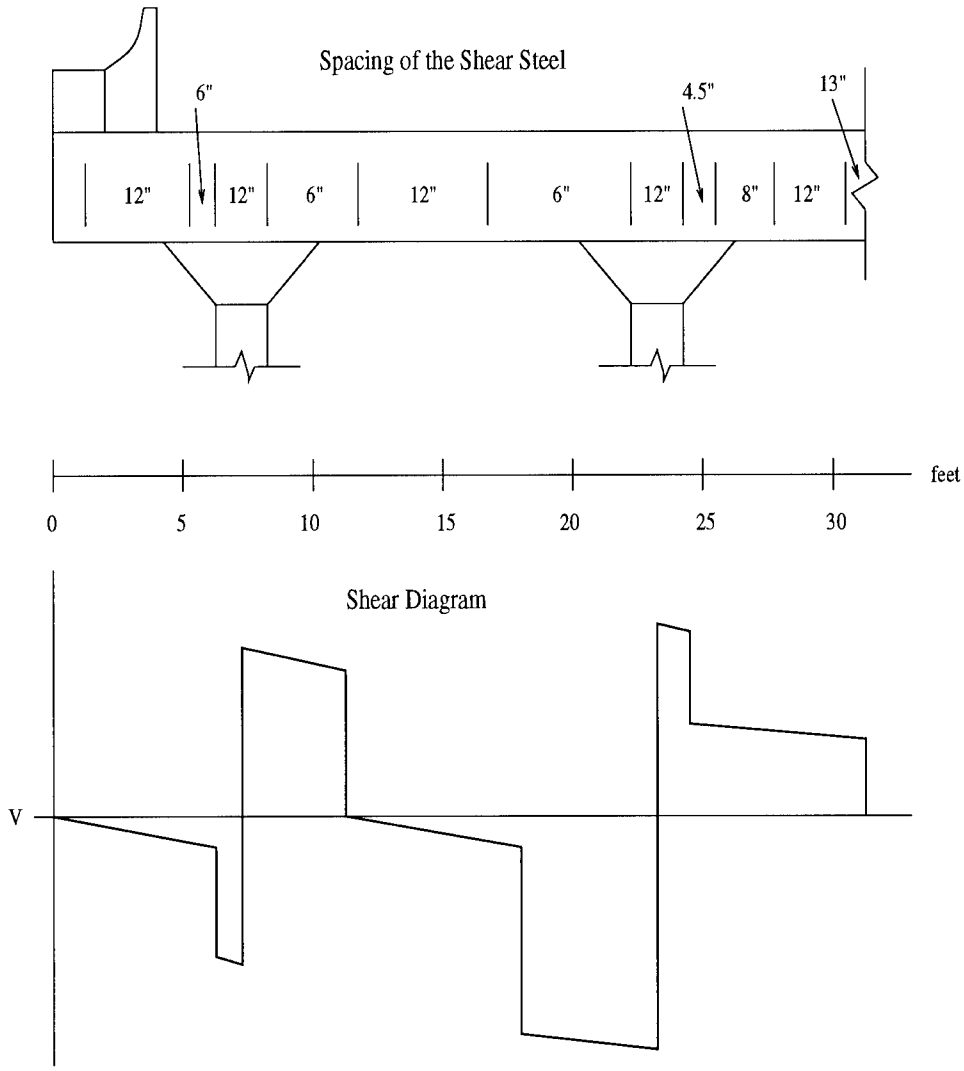

Figure 5.22: **Location and Spacing of Shear Steel in the Pier Cap Compared with the Locations of Maximum Shear**

is 4.5 *in* (11.4 *cm*) has the lowest factor of safety $FS = 2.98$ so this will be the portion of the beam considered in the reliability analysis.

Table 5.11: **Deterministic Analysis of the Pier Cap to Determine the Most Critical Section With Respect to Shear**

V_{max}	s	V_s	V_c	$V_{tot} = V_s + V_c$	Factor of
kips	*inches*	*kips*	*kips*	*kips*	Safety
160.62	4.5	331.1	146.9	478	2.98
120.38	6	248.3	146.9	395.2	3.28
60.51	12	124.2	146.9	271.1	4.48

The limit state equation with respect to failure of the pier cap due to shear can now be written. Eqs. 5.57 and 5.58 are used to describe the shear capacity where A_v/s, f_y, and f'_c are random variables and $\lambda_{d_{eff}}$ and γ_{msc} are uncertainty factors as described in Tables 5.2 and 5.3.

$$V_{capacity} = V_s + V_c = (37.25\lambda_{d_{eff}}\frac{A_v}{s}f_y + 2.682\sqrt{f'_c})\gamma_{msc} \qquad (5.59)$$

The shear demand is determined by the values on the composite shear diagram at the point where the total shear is maximum and the stirrup spacing is 4.5 *in* (11.4 *cm*). The respective shear contributions are multiplied by their uncertainty factors.

$$V_{demand} = 15.78\gamma_{asph} + 68.04\gamma_{conc} + 10.02\gamma_{steel} + 42.50V_{trk-i}DF_iI_{beam} \qquad (5.60)$$

The limit state equation $g(8)$ becomes

$$\begin{aligned} g(8) &= V_{capacity} - V_{demand} \\ g(8) &= 37.25\lambda_{d_{eff}} A_v / s f_y \gamma_{msc} + 2.682\sqrt{f_c'}\gamma_{msc} - 15.78\lambda_{asph} - 68.04\lambda_{conc} \\ &\quad -10.02\lambda_{steel} - 42.50 V_{trk-i} DF_i I_{beam} \end{aligned} \tag{5.61}$$

The limit state equations for positive and negative moment are easier to obtain because the most critical points on the beam are the points where the moment is maximum. For the positive moment capacity, Figs. 5.18 and 5.19 show the dimensions and the placement of steel in the pier caps. After verifying that the reinforcement is above the minimum allowed by the ACI code, the compression steel does not yield, and that the area of steel is less than 75% of the balanced reinforcement [Nawy 1990], the pier cap is treated as a singly reinforced beam. The moment capacity is determined in a manner similar to the moment capacity of the slab.

$$M_{capacity} = A_s f_y [d - \frac{a}{2}] = A_s f_y [d - \frac{A_s f_y}{2(.85) f_c' b}] \tag{5.62}$$

Considering that A_s, f_y, and f_c' are random variables and there are uncertainty factors associated with the effective depth, $\lambda_{d_{eff}}$, and with the flexural concrete model, γ_{mfc}, as described in Tables 5.2 and 5.3, the moment capacity becomes

$$\begin{aligned} M_{capacity} &= \gamma_{mfc} A_s f_y [37.25\lambda_{d_{eff}} - \frac{a_s f_y}{2(.85) f_c'(36in)}] \\ &= 37.25\gamma_{mfc} A_s f_y \lambda_{d_{eff}} - .0163\gamma_{mfc} \frac{A_s^2 f_y^2}{f_c'} \end{aligned} \tag{5.63}$$

The moment demand is taken from the composite moment diagram at the point of maximum positive moment which is at the interior-exterior girder

(see Fig. 5.21). Considering the uncertainty factors associated with the loads contributing to the moment, the moment demand becomes

$$\begin{aligned} M_{demand} &= 20.61\gamma_{asph} + 121.41\gamma_{conc} + 17.18\gamma_{steel} + 15.67V_{trk-i}DF_iI_{beam} \\ &\quad +109.41V_{trk-i}DF_{i-e}I_{beam} \end{aligned} \tag{5.64}$$

By subtracting the moment demand from the moment capacity, the limit state equation $g(9)$ for positive moment failure on the pier cap is

$$\begin{aligned} g(9) &= 238.4\gamma_{mfc}\lambda_{rebar}\lambda_{d_{eff}}f_y - .6689\frac{\gamma_{mfc}\lambda_{rebar}^2 f_y^2}{f_c'} - 20.61\lambda_{asph} \\ &\quad -121.41\lambda_{conc} - 17.18\lambda_{steel} - 15.56V_{trk-i}DF_iI_{beam} \\ &\quad -109.41V_{trk-i}DF_{i-e}I_{beam} \end{aligned} \tag{5.65}$$

The maximum negative moment occurs at the interior column on the pier cap. The top row of reinforcing steel in the negative moment region of the pier cap increases to 8-#9 bars. Accounting for the capacity and demand due to negative moment in the exact same manner, the limit state equation $g(10)$ for failure of the pier cap due to negative moment becomes

$$\begin{aligned} g(10) &= 280.8\gamma_{mfc}\lambda_{rebar}f_y\lambda_{d_{eff}} - 1.043\frac{\gamma_{mfc}\lambda_{rebar}^2 f_y^2}{f_c'} - 36.73\lambda_{asph} \\ &\quad -174.84\lambda_{conc} - 24.32\lambda_{steel} - 138.69V_{trk-i}DF_iI_{beam} \\ &\quad -29.18V_{trk-i}DF_{i-e}I_{beam} - 6.68V_{trk-e}DF_eI_{beam} \end{aligned} \tag{5.66}$$

5.6.2.2 Failure Due to Crushing of the Columns

The pier cap is supported by four columns as shown in Fig. 5.4. The distribution of the critical load to the columns is shown in Fig. 5.17 with

the interior columns taking a larger share of the load. Since the columns are identical, the interior column is the critical column. It would be reasonable to perform a reliability analysis on all columns and treat the columns together as a parallel system. If the system reliability analysis reveals that crushing of the columns is a critical failure mode, then the parallel system analysis would be beneficial.

The columns are braced and tied together by a six foot shear wall fixed to the middle of the columns. It is assumed that this large shear wall would prevent the column from buckling as a 23 ft (7.01 m) column in either direction. For this to occur, the wall would have to buckle with it. Instead, the pier column will be divided into an upper column and a lower column, with each being analyzed separately. The upper column is not as large but it carries less weight.

Fig. 5.23 shows the cross-section dimensions and placement of steel in these tapered square columns. The column width is two feet (0.61 m) at the top and increases to 2.91 ft (0.887 m) at the bottom as shown in Fig. 5.23. Even modeling the columns as pinned-pinned columns results in a slenderness ratio kl/r that is small enough to treat the columns as short columns where crushing is the critical failure mode. The capacity of the column $P_{capacity}$ is a function of the the compressive strength of the concrete f'_c and the reinforcing steel f_y [Nawy 1990].

$$P_{capacity} = 0.85[0.85 f'_c(A_{conc} - A_{steel}) + A_{steel} f_y] \tag{5.67}$$

where the outermost factor of 0.85 is included in the ACI code to account

for eccentricity in tied columns. It will be treated as the model uncertainty associated with this effect [Nawy 1990].

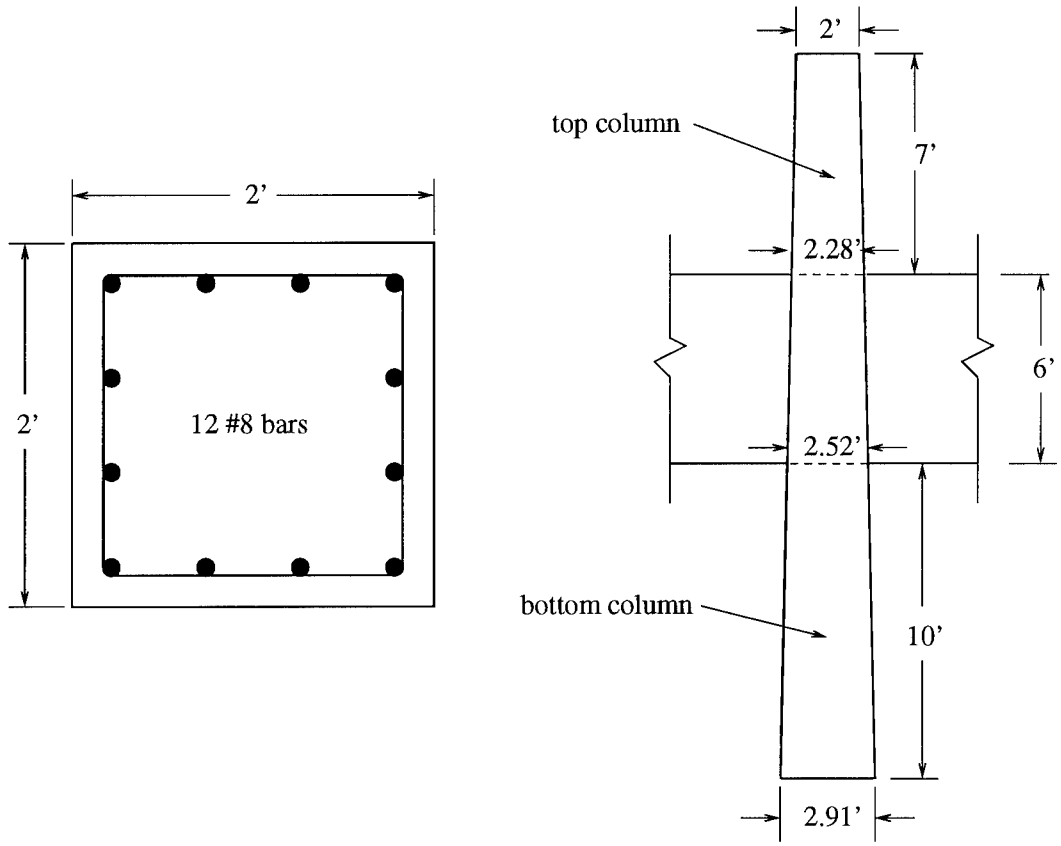

Figure 5.23: **Dimensions and Placement of Steel in the Top and Bottom Columns**

The conservative approach for the top column is to treat it as a prismatic square column with a constant depth of two feet. The area of the concrete cross-section is $A_{conc} = 576\ in^2$ ($3716\ cm^2$) and the area of the longitudinal reinforcing steel is $A_{steel} = 9.48\ in^2$ ($61.16\ cm^2$). The random variables contributing to the capacity are f'_c, f_y, and the uncertainty factors associated

with the area of the steel, λ_{rebar}, and model uncertainty, γ_{mcc}, (See Tables 5.2 and 5.3).

$$P_{capacity} = \gamma_{mcc}[489.6f'_c - 8.06f'_c\lambda_{rebar} + 9.48f_y\lambda_{rebar}] \tag{5.68}$$

The demand on the column P_{demand} is determined from the composite shear diagram (Fig. 5.20) for the pier cap at the point where it connects with an interior column. The limit state equation for failure with respect to crushing of a top column $g(11)$ is

$$\begin{aligned} g(11) &= 489.6\gamma_{mcc}f'_c - 8.06\gamma_{mcc}f'_c\lambda_{rebar} + 9.48\gamma_{mcc}\lambda_{rebar}f_y - 26.41\lambda_{asph} \\ &\quad -123.22\lambda_{conc} - 17.19\lambda_{steel} - 66.90V_{trk-i}DF_iI_{beam} \\ &\quad -8.41V_{trk-i}DF_{i-e}I_{beam} \end{aligned} \tag{5.69}$$

The bottom column is handled in the same manner. The capacity is increased because of the additional concrete in the lower portion of the tapered column. The demand is also increased by the self weight of the concrete column and shear wall above the bottom column. Considering these effects, the limit state equation for failure due to crushing of the bottom column $g(12)$ is

$$\begin{aligned} g(12) &= 777.3\gamma_{mcc}f'_c - 8.06\gamma_{mcc}f'_c\lambda_{rebar} + 9.48\gamma_{mcc}\lambda_{rebar}f_y - 26.41\lambda_{asph} \\ &\quad -145.8\lambda_{conc} - 17.19\lambda_{steel} - 66.90V_{trk-i}DF_iI_{beam} \\ &\quad -8.41V_{trk-i}DF_{i-e}I_{beam} \end{aligned} \tag{5.70}$$

5.6.2.3 Failure Due to Failure of the Column Footings

The column footings were modeled as isolated, two-way, concentrically loaded footings. Because all of the footings are identical, the most critical footings are those supporting interior columns which are carrying greater loads. The footings are analyzed with respect to failure by one-way shear, two-way or punching shear, and moment. The footings are assumed to be rigid and the underlying soil layers are elastic. The dimensions and placement of steel in the footings are shown in Fig. 5.24. The cumulative dead and live load to be transferred to the footing is assumed to be a concentrated load P which constitutes the demand on the footing. This will be the load transferred to the interior column from the pier cap plus the total weight of the column and proportional weight of the shear wall.

The critical plane on a footing with respect to one-way shear extends across the width of the footing at a distance d from the face of the concentrated load P. The distance d is the effective depth of the footing where $d = 20\ in\ (50.8\ cm)$ as shown in Fig. 5.24. The failure mechanism is assumed to be beam action at a distance d from the support face as shown in Fig. 5.25. The one way shear demand V_{demand} is calculated as the load intensity (the concentrated load P divided by the area of the footing A_{ftg}) multiplied by the footing width b_w and the distance x as shown in Fig. 5.25 [Nawy 1990]. This assumes that the soil exerts a uniformly distributed load on the bottom of the footing for a concentrically loaded column [Bowles 1982].

$$\begin{aligned} V_{demand} &= \frac{P}{A_{ftg}} x b_w \\ &= [26.41\gamma_{asph} + 159.7\gamma_{conc} + 17.19\gamma_{steel} + 66.90V_{trk-i}DF_iI_{beam} \end{aligned}$$

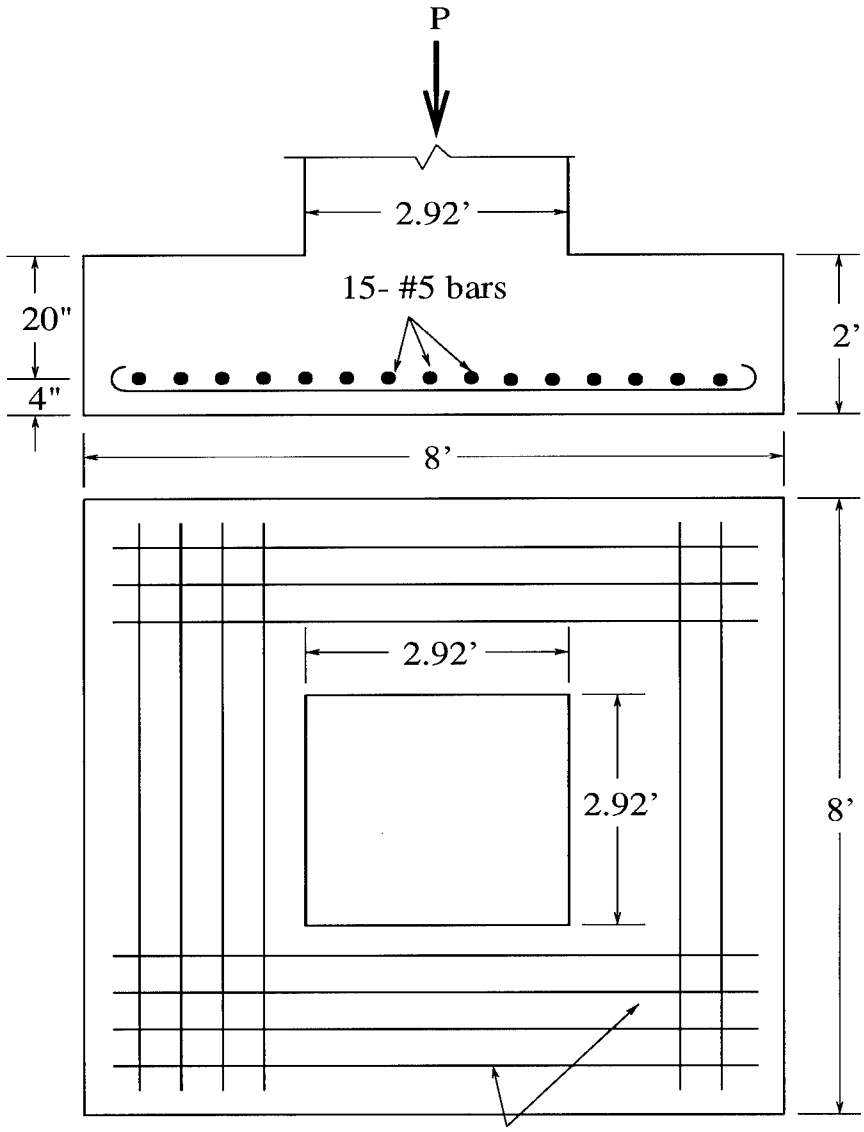

Figure 5.24: **Dimensions and Location of Steel Reinforcement in the Column Footings**

$$+8.41Vtrk - iDF_{i-e}I_{beam}]\frac{1}{64ft^2}(4ft - \frac{2.92ft}{2}$$
$$-\frac{20in}{12in/ft}\lambda_{d_{eff}})(8ft) \tag{5.71}$$

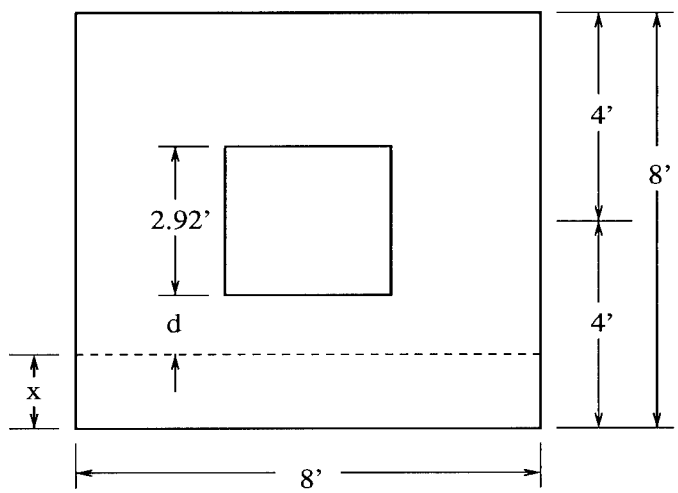

Figure 5.25: **One-Way Shear on Column Footing: Beam Action at a Distance d Away From the Support Face**

The shear capacity $V_{capacity}$ is a function of the 28-day concrete compressive strength f'_c, the width of the footing b_w, and the effective depth d [Nawy 1990].

$$V_{capacity} = 2\sqrt{f'_c}b_w d \tag{5.72}$$

The random variables are f'_c and the uncertainty factors relating to effective depth $\lambda_{d_{eff}}$ and model uncertainty γ_{msc}. By substitution, the shear capacity becomes

$$\begin{aligned} V_{capacity} &= 2\sqrt{1000lb/ft(f'_c)}\frac{8ft(12in/ft)(20in)}{1000lb/kip}\lambda_{d_{eff}}\gamma_{msc} \\ &= 121.43\sqrt{f'_c}\lambda_{d_{eff}}\gamma_{msc} \end{aligned} \tag{5.73}$$

The limit state equation for failure of the column footing with respect to one-way shear $g(13)$ is therefore,

$$\begin{aligned} g(13) &= 121.43\sqrt{f_c'}\lambda_{d_{eff}}\gamma_{msc} - (26.41\lambda_{asph} + 159.7\lambda_{conc} \\ &\quad +17.19\lambda_{steel} + 66.90V_{trk-i}DF_iI_{beam} + 8.41V_{trk-i}DF_{i-e}I_{beam}) \\ &\quad (.3175 - .2083\lambda_{d_{eff}}) \end{aligned} \tag{5.74}$$

The two-way shear failure mode is a failure in two directions where the column punches through the footing. The critical failure plane as shown in Fig. 5.26 is located at a distance $d/2$ from the support face where again d is the effective depth of the footing (i.e., $d = 20\ in\ (50.8\ cm)$). The shear demand is the load intensity P/A_{ftg} multiplied by the perimeter area surrounding the failure plane as shown in Fig. 5.26.

$$\begin{aligned} V_{demand} &= \frac{P}{A_{ftg}}[A_{ftg} - (b_{col} + d)^2] \\ &= [26.41\gamma_{asph} + 159.7\gamma_{conc} + 17.19\gamma_{steel} + 66.90V_{trk-i}DF_iI_{beam} \\ &\quad +8.41Vtrk - iDF_{i-e}I_{beam}]\frac{1}{8ft(8ft)}(4ft - \frac{2.92ft}{2} \\ &\quad -\frac{20in}{12in/ft}\lambda_{d_{eff}}(8ft) \end{aligned} \tag{5.75}$$

The two way shear capacity is determined from the smallest of the three following equations [Nawy 1990]:

$$V_{capacity} = (2 + \frac{4}{\beta_c})\sqrt{f_c'}b_od \tag{5.76}$$

$$V_{capacity} = (\frac{\alpha_s d}{b_o} + 2)\sqrt{f_c'}b_od \tag{5.77}$$

$$V_{capacity} = 4\sqrt{f_c'}b_od \tag{5.78}$$

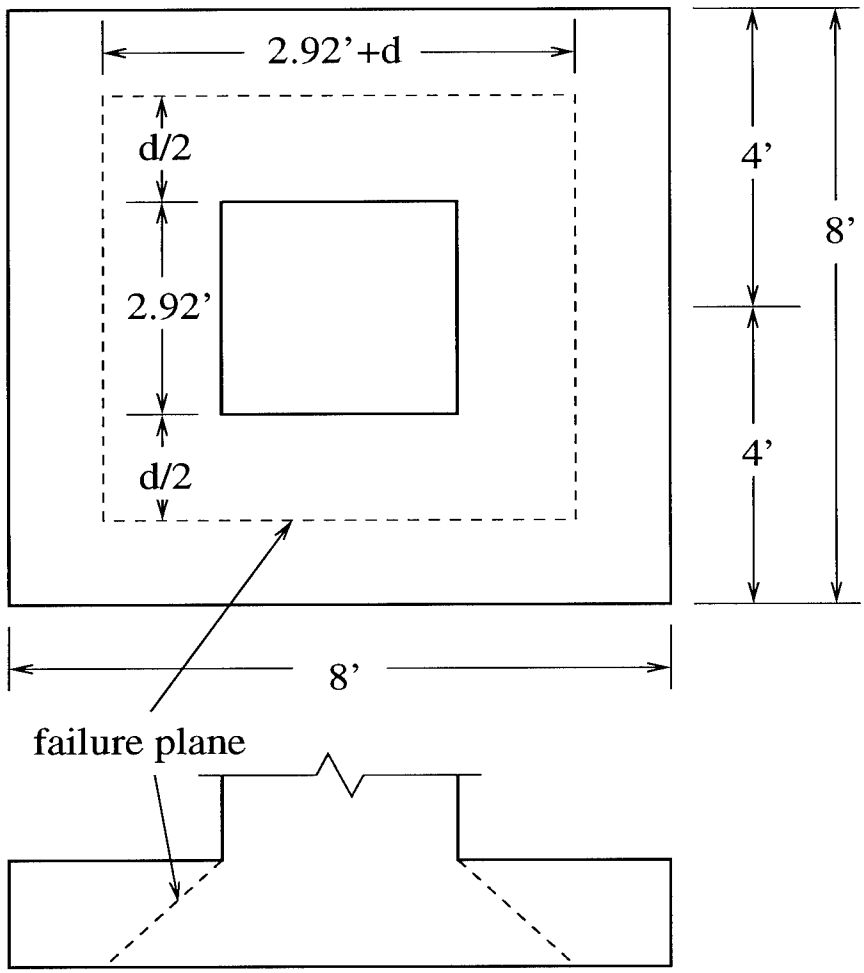

Figure 5.26: **Two-Way Shear on Column Footing: Failure Plane of Column Punching Through Footing**

where β_c is the ratio of the dimensions of the long side of the footing to the short side of the footing ($\beta_c = 1.0$ for the square footing), b_o is the perimeter of the critical failure plane, and α_s is a factor whose value is 40 for interior columns, 30 for edge columns, and 20 for corner columns. A deterministic analysis revealed that Eq. 5.78 provided the lowest value. From Eq. 5.78, the shear capacity for the reliability analysis will be

$$\begin{aligned} V_{capacity} &= 4\sqrt{f'_c} b_o d \gamma_{msc} \\ &= 4\sqrt{(1000lb/kips) f'_c}\; 4[2.92ft(12in/ft) + 20in\lambda_{d_{eff}}]20in\lambda_{d_{eff}}\gamma_{msc} \\ &= 278.1\sqrt{f'_c}\lambda_{d_{eff}}\gamma_{msc} + 202.4\lambda^2_{d_{eff}}\gamma_{msc} \end{aligned} \tag{5.79}$$

The limit state equation for failure of the footing due to two-way shear $g(14)$ is

$$\begin{aligned} g(14) &= 278.1\sqrt{f'_c}\lambda_{d_{eff}}\gamma_{msc} + 202.4\lambda^2_{d_{eff}}\gamma_{msc} - (26.41\lambda_{asph} + 159.7\lambda_{conc} \\ &\quad +17.19\lambda_{steel} + 66.90V_{trk-i}DF_iI_{beam} + 8.41V_{trk-i}DF_{i-e}I_{beam}) \\ &\quad (.918 - .0761\lambda_{d_{eff}} - .0434\lambda^2_{d_{eff}}) \end{aligned} \tag{5.80}$$

The critical plane when considering moment failure of the footing is at the face of the column as shown in Fig. 5.27 where the footing is treated like a cantilever beam with a distributed load. The moment arm is seen to be 2.54 ft (0.774 m). The demand moment (in $ft - kips$) at the failure plane is determined as

$$\begin{aligned} M_{demand} &= \frac{P}{A_{ftg}} b_w \frac{(moment\ arm)^2}{2} \\ &= \frac{P}{(8ft)(8ft)}(8ft)\frac{(2.54ft)^2}{2} = .403P \end{aligned}$$

$$= 10.65\gamma_{asph} + 64.4\gamma_{conc} + 6.93\gamma_{steel} + 27.0V_{trk-i}DF_iI_{beam}$$
$$+3.4V_{trk-i}DF_{i-e}I_{beam} \tag{5.81}$$

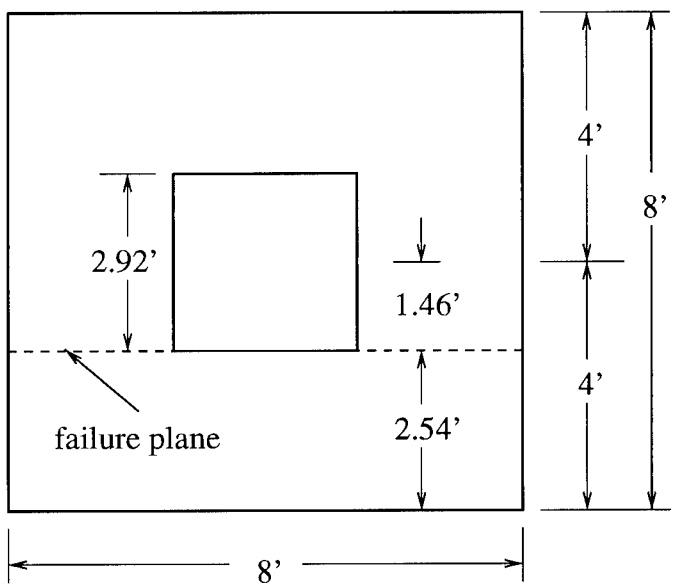

Figure 5.27: **Moment Failure on Column Footing: Critical Plane at the Support Face**

The moment capacity is again determined by the tensile force in the steel multiplied by the distance between the tension force and the compression force on the equivalent stress block (See Fig. 5.10). Using the same equation as was used for the pier cap (Eq. 5.62), the moment capacity of the concrete footing is

$$M_{capacity} = A_s f_y[d - \frac{a}{2}] = A_s f_y[d - \frac{A_s f_y}{2(.85)f'_c b}]$$
$$= 4.65in^2\lambda_{d_{eff}} f_y \frac{ft}{12in}[20in\lambda_{d_{eff}} - \frac{4.65in^2\lambda_{rebar} f_y}{2(.85)f'_c(8ft)(12in/ft)}]\gamma_{mfc}$$

$$= \quad 7.75\lambda_{rebar} f_y \lambda_{d_{eff}} \gamma_{mfc} - 0.132 \frac{\lambda_{rebar}^2 f_y^2}{f_c'} \gamma_{mfc} \tag{5.82}$$

The resulting limit state equation for failure of the footing due to moment $g(15)$ is expressed as

$$\begin{aligned} g(15) \quad = \quad & 7.75\lambda_{rebar} f_y \lambda_{d_{eff}} \gamma_{mfc} - .132 \frac{\lambda_{rebar}^2 f_y^2 \gamma_{mfc}}{f_c'} - 10.65\lambda_{asph} - 64.4\lambda_{conc} \\ & -6.93\lambda_{steel} - 27.0 V_{trk-i} DF_i I_{beam} - 3.4 V_{trk-i} DF_{i-e} I_{beam} \end{aligned} \tag{5.83}$$

5.6.2.4 Failure of the Expansion Bearings

The final failure mode to be considered is the analysis of Bridge E-17-AH is the expansion bearing whose dimensions are shown in Fig. 5.28. According to AASHTO [1994], cylindrical roller bearings are designed based on the contact stresses between two elastic bodies. The critical demand on the expansion bearing P_{demand} comes from the load transferred from an interior girder. The capacity of the bearing is

$$P_{capacity} = 8 \frac{w D_1}{1 - \frac{D_1}{D_2}} \frac{f_y^2}{E_s} \tag{5.84}$$

where: D_1 is the diameter of the bearing roller surface which is 23.5 in (59.7 cm) from Fig. 5.28; D_2 is the diameter of the mating surface which in this case is infinite since the surface is flat; w is the width of the bearing which is 11.5 in (29.2 cm); f_y is the yield strength of the steel; and E_s is the modulus of elasticity of the steel. The only random variables are F_y and E_s so

$$P_{capacity} = \frac{8(11.5in)(23.5in)}{1} \frac{f_y^2}{E_s} = 2162.0 \frac{f_y^2}{E_s} \tag{5.85}$$

The resulting limit state equation $g(16)$ is

$$g(16) = 2162.0\frac{f_y^2}{E_s} - 3.34\lambda_{steel} - 5.26\lambda_{asph} - 18.04\lambda_{conc} - 28.33V_{trk-i}DF_iI_{beam} \tag{5.86}$$

The reliability index of this component is only $\beta = 0.54$ which equates to a probability of failure of $P_f = 0.29$. AASHTO [1994] defines the design equation as a serviceability limit state. All other limit states in the system model are strength-based limit states.

The strength-based limit state that will be considered in this study will be failure due to crushing of the expansion joint. In this regard, the capacity of the bearing is the cross-sectional area A_s (From Fig. 5.28, $A_s = 25.25\ in^2$ ($162.9\ cm^2$)) multiplied by the compressive yield stress of the steel F_y. The limit state equation for failure due to crushing of the expansion bearing $g(16)$ is

$$g(16) = 25.25F_y - 3.34\lambda_{steel} - 5.26\lambda_{asph} - 18.04\lambda_{conc} - 28.33V_{trk-i}DF_iI_{beam} \tag{5.87}$$

Limit state equations have been derived for 16 possible failure modes. There are certainly others that could have been considered as well, such as failure of the soil in bearing, the abutment piles, the railings, or the diaphragms between girders but 16 failure modes is a reasonable start. This study also does not include the relationship of partial failure of one component to the failure of other components. For example, a common partial failure mode for expansion bearings is caused by the build-up of debris. This makes bearing rotation

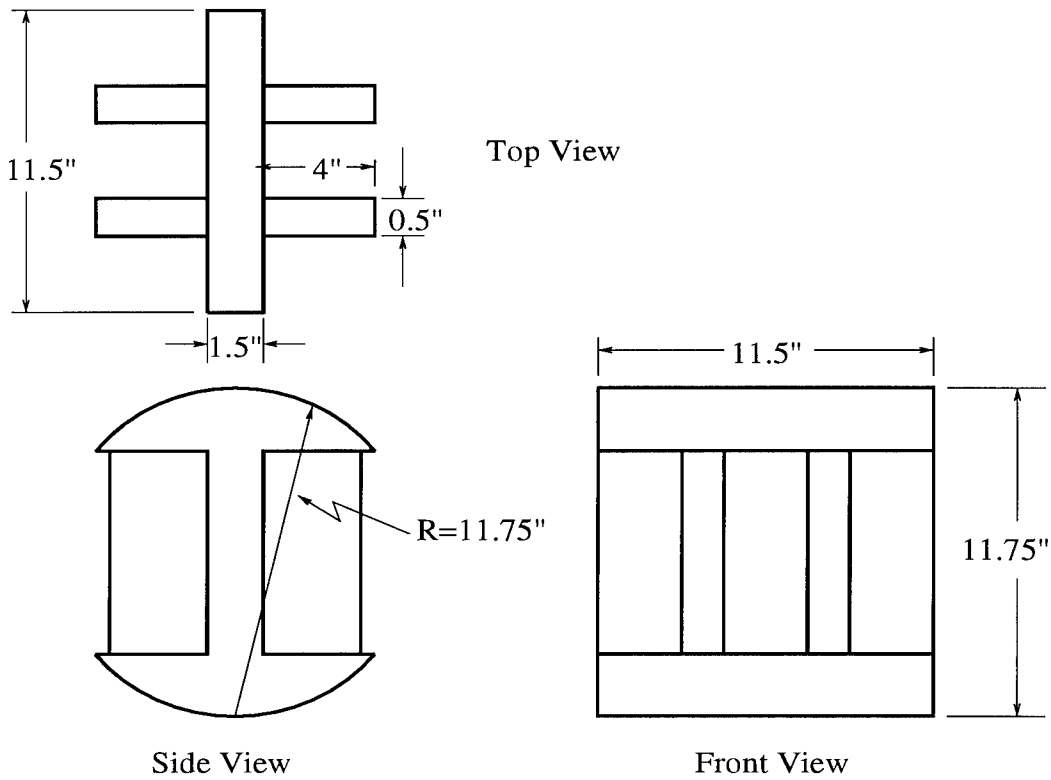

Figure 5.28: **Detail of the Expansion Bearing**

more difficult and may cause additional stresses on the girders which are not able to freely expand. Such considerations have not been explored. With all limit state equation and random variables defined, a reliability analysis on all components can now be completed.

5.7 Component Reliability Results

The reliabilities of the 16 possible failure modes as computed by RELSYS are listed in Table 5.12. The live load on the bridge was the 50 year Nowak [1994] live load. As expected, the component with the lowest reliability ($\beta = 2.44$) was the failure of the interior girder due to flexure. Surprisingly, the next lowest component was failure of the interior column footing due to flexure ($\beta = 2.60$). Given the low reliability of the column footing due to moment, the initial assumptions of a rigid footing on an elastic soil foundation could be reexamined. The rest of the substructure components had much higher reliabilities. The reliabilities of some failure modes such as moment failure of the pier cap, crushing of the expansion bearing, and one-way shear failure of the footing were so high that they can safely be excluded from the system analysis.

5.7.1 Sensitivity With Respect To Random Variables

Reliability results are only as good as the knowledge of the random variables that are in the limit state equations. Varying the mean value, standard deviation, or type of distribution for any random variable will affect the

Table 5.12: **Reliability and Sensitivity Analysis of Failure Modes for Colorado Highway Bridge Number E-17-AH**

No.	Failure Mode	Reliab. Index	Failure Probability	Most Sensitive Variables
1	Concrete deck, flexure	5.51	$1.77 * 10^{-8}$	f_y
2	Interior girder, shear	6.22	$2.41 * 10^{-10}$	F_y, γ_{msg}
3	Interior girder, flexure	2.44	$7.29 * 10^{-3}$	F_y, γ_{mfg}
4	Exterior girder, flexure	4.02	$2.95 * 10^{-5}$	F_y, γ_{mfg}
5	Exterior girder, shear	7.13	$5.12 * 10^{-13}$	γ_{msg}
6	Ext.-int. girder, flexure	2.79	$2.72 * 10^{-3}$	F_y, γ_{mfg}
7	Ext.-int. girder, shear	6.43	$6.23 * 10^{-11}$	F_y, γ_{msg}
8	Pier cap, shear	3.83	$6.42 * 10^{-5}$	f_y, γ_{msc}
9	Pier cap, pos. moment	8.82	0.0	f_y
10	Pier cap, neg. moment	8.75	0.0	f_y
11	Top column, crushing	5.80	$3.27 * 10^{-9}$	f'_c, γ_{mcc}, f_y
12	Bottom column, crushing	5.72	$5.27 * 10^{-9}$	f'_c, γ_{mcc}, f_y
13	Footing, one-way shear	7.69	$7.21 * 10^{-15}$	f'_c, γ_{mcc}
14	Footing, two-way shear	5.28	$6.42 * 10^{-8}$	f'_c, γ_{mcc}
15	Footing, flexure	2.60	$4.60 * 10^{-3}$	f'_c, f_y
16	Exp. bearing, crushing	7.84	$2.33 * 10^{-15}$	F_y

results. Because obtaining accurate information on random variables can involve considerable research and expense, it is important to know which random variables are worth the investment. A sensitivity analysis identifies those random variables where slight changes in their values result in large changes in the reliability of the component. The sensitivity of the system reliability with respect to the random variables is not considered.

As mentioned in Chapter 3, the program RELSYS provides sensitivity values with respect to the mean and standard deviation of each random variable in a limit state equation. The sensitivity value for the mean is α_i which is the direction cosine of random variable i with respect to the reliability vector in standard normal space at the closest failure point. The sensitivity for the standard deviation is $-\beta\alpha_i^2$ where β is the reliability index [Hohenbichler *et al.* 1987]. These approximations of stochastic importance help determine which random variables are most important and most worthy of further investigation.

To test the validity and understand the limitations of the sensitivity data provided by RELSYS, a detailed analysis was completed on failure mode $g(3)$, failure of interior girder due to moment, where the live load was a deterministic HS-20 truck. The sensitivity with respect to the random variables using the RELSYS approximations is shown in Fig. 5.29. Limit state equation $g(3)$, failure of the interior girder with respect to moment contained random variables 6, 7, 9, 11, 13, 14, and 15 (λ_{asph}, λ_{conc}, F_y, λ_{steel}, DF_i, I_{beam}, γ_{mfg}) as listed in Tables 5.2 and 5.3. Fig. 5.29 shows that the mean value and standard deviation of the yield strength of the steel (μ_9 and σ_9) and the model

uncertainty of flexure in girders (μ_{15} and σ_{15}) are the most sensitive variables. The unit weight of the steel (μ_{11} and σ_{11}) appears to be the most insensitive variable.

To test these results, the mean and standard deviation for each random variable was separately varied by -20%, -10%, $+10\%$, and $+20\%$ while holding all other random variables constant. The effect on the reliability index for variation of the mean values is shown in Fig. 5.30. Comparing Fig. 5.29 to Fig. 5.30, the order of importance of the random variables is the same. Variables 9 and 15 are the most sensitive and variable 11 is the least sensitive. The best measures of sensitivity are the slopes of the lines in Fig. 5.30 which indicate that variables 9 and 15 are equally sensitive and that variable 6 is much less sensitive than variable 7. Looking at Fig. 5.29, one would conclude that variables 9 and 15 are equally sensitive and also that variables 6 and 7 are equally sensitive.

The same exact analysis of the standard deviations of the random variables is shown in Fig. 5.31. Comparing Fig. 5.31 and Fig. 5.29, the order of importance and the relative importance of the random variables seems to match well. Fig. 5.32 is the same graph as Fig. 5.31 but plotted on the same vertical scale as the mean values in Fig. 5.30. A comparison of Fig. 5.31 and Fig. 5.30 reveals that reliability of the component is less sensitive with respect to the standard deviation than to the mean value of the same random variable. Fig. 5.29 is therefore misleading. It conveys that the reliability is more sensitive with respect to the standard deviation of variables 9 and 15

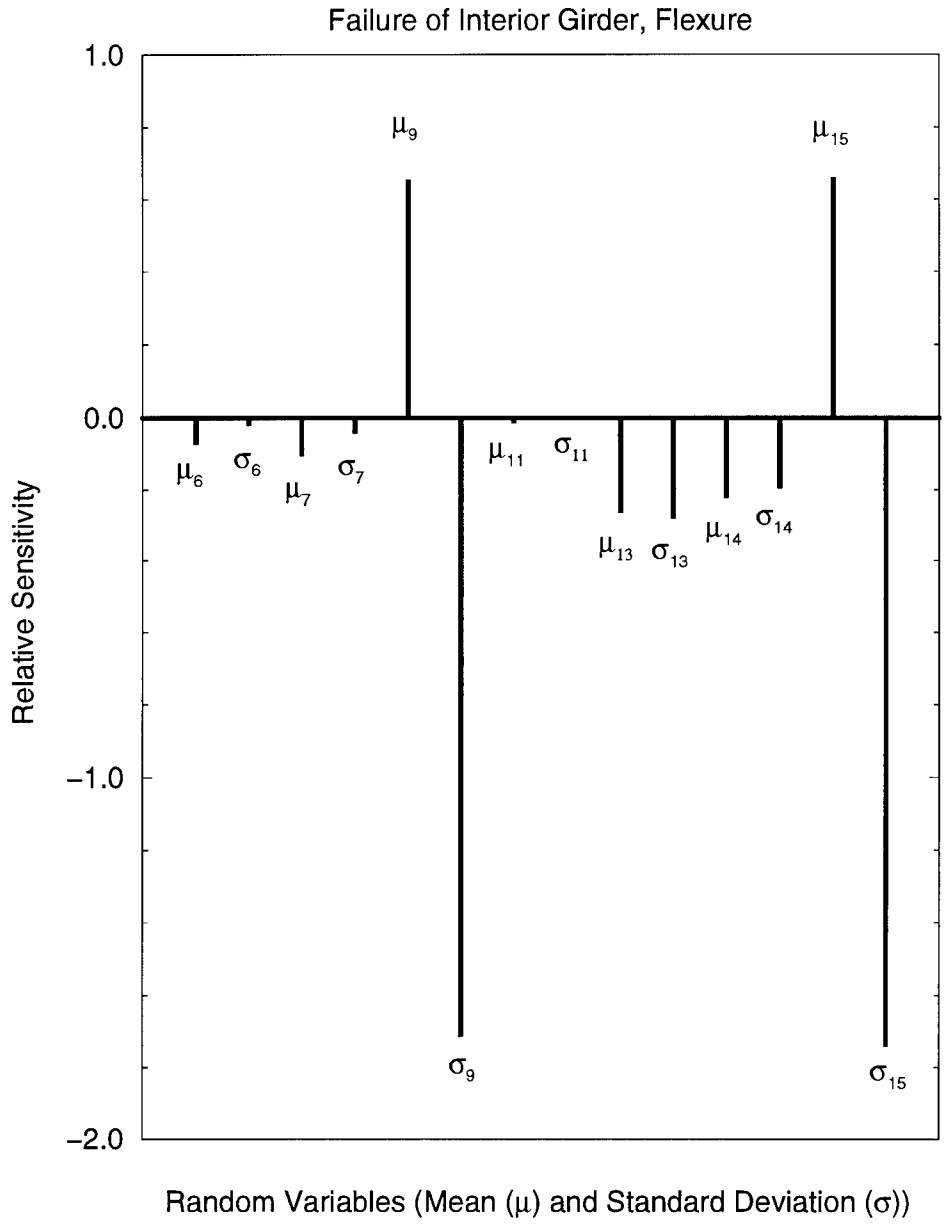

Figure 5.29: **RELSYS Sensitivity Values for Each Random Variable for Failure Due to Moment on an Interior Girder on Bridge E-17-AH With a Deterministic HS-20 Truck Live Load**

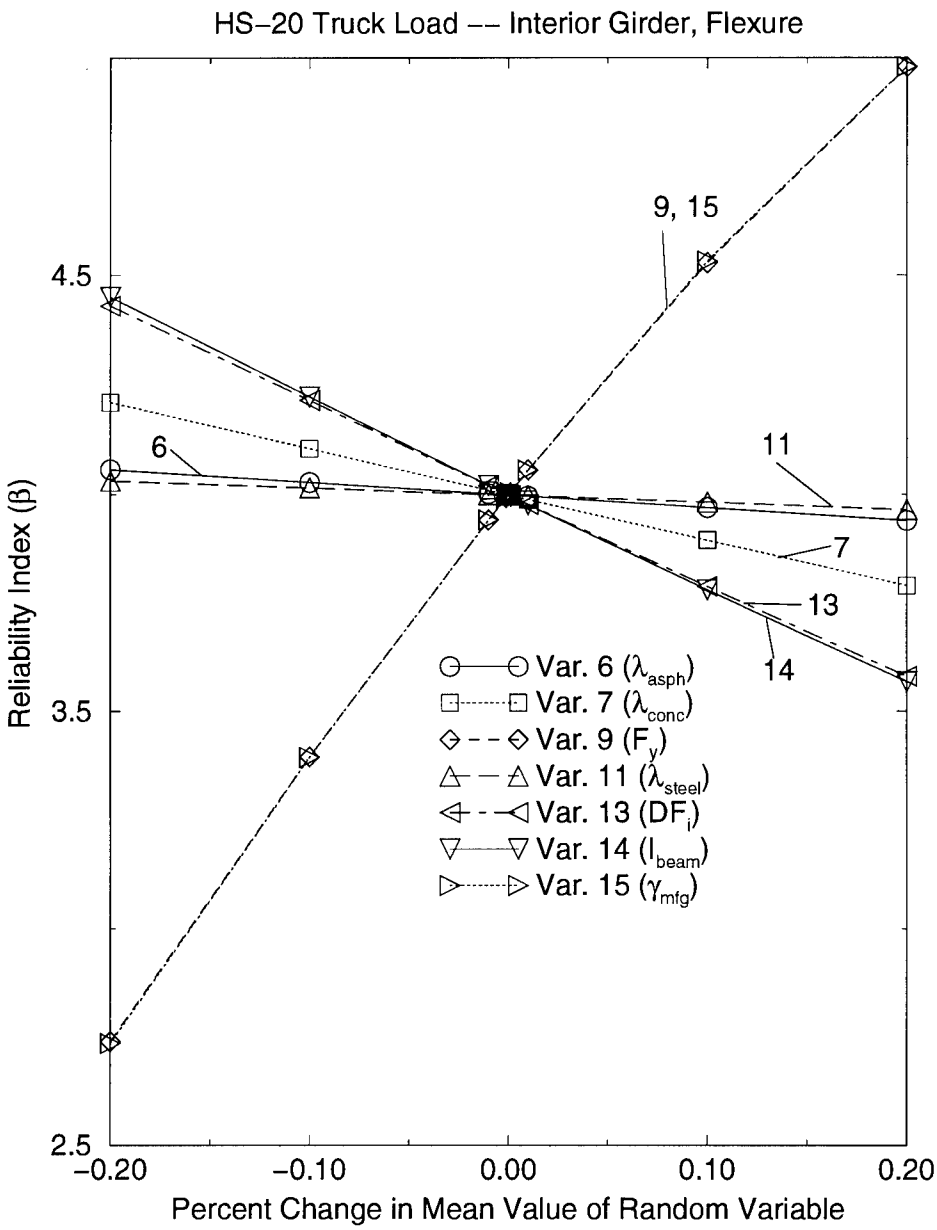

Figure 5.30: **Exact Sensitivity Values for Mean Values of Each Random Variable for Failure Due to Moment on an Interior Girder on Bridge E-17-AH With a Deterministic HS-20 Truck Live Load**

than with respect to the means of variables 9 and 15, which clearly is not true. From the exact analysis, one can conclude that the RELSYS sensitivity values are good approximations for the relative sensitivity of random variables but the means and standard deviations must be considered separately.

In order to understand the strengths and limitations of the RELSYS sensitivity values, a sensitivity analysis was performed for all failure modes and using the 50 year Nowak live load which produced the results in Table 5.12. The relative sensitivities with respect to the random variables associated with failure of the concrete deck $g(1)$ and with failure of the interior girder due to shear $g(2)$ are shown in Fig. 5.33 and those associated with $g(3)$ and $g(4)$ are shown in Fig. 5.34.

The analysis was completed for limit state equations $g(5) - g(16)$ as well. The most sensitive variables for each failure mode are listed in Table 5.12. In each case, the strength of the material (f'_c, f_y, F_y) and the model uncertainty ($\gamma_{mfc}, \gamma_{mcc}, \gamma_{msg}$) were the most sensitive variables, both of which appear on the capacity side of the limit state equations. Given limited time and resources, the investigation of the uncertainty associated with these random variables would provide the greatest benefit toward obtaining accurate reliability results.

5.8 Reliability of the Bridge as a System at a Fixed Point of Time

In order to compute the reliability of a system, there needs to be a model which describes the behavior of the system and the relationship of the individual components to the overall system. In order to use RELSYS,

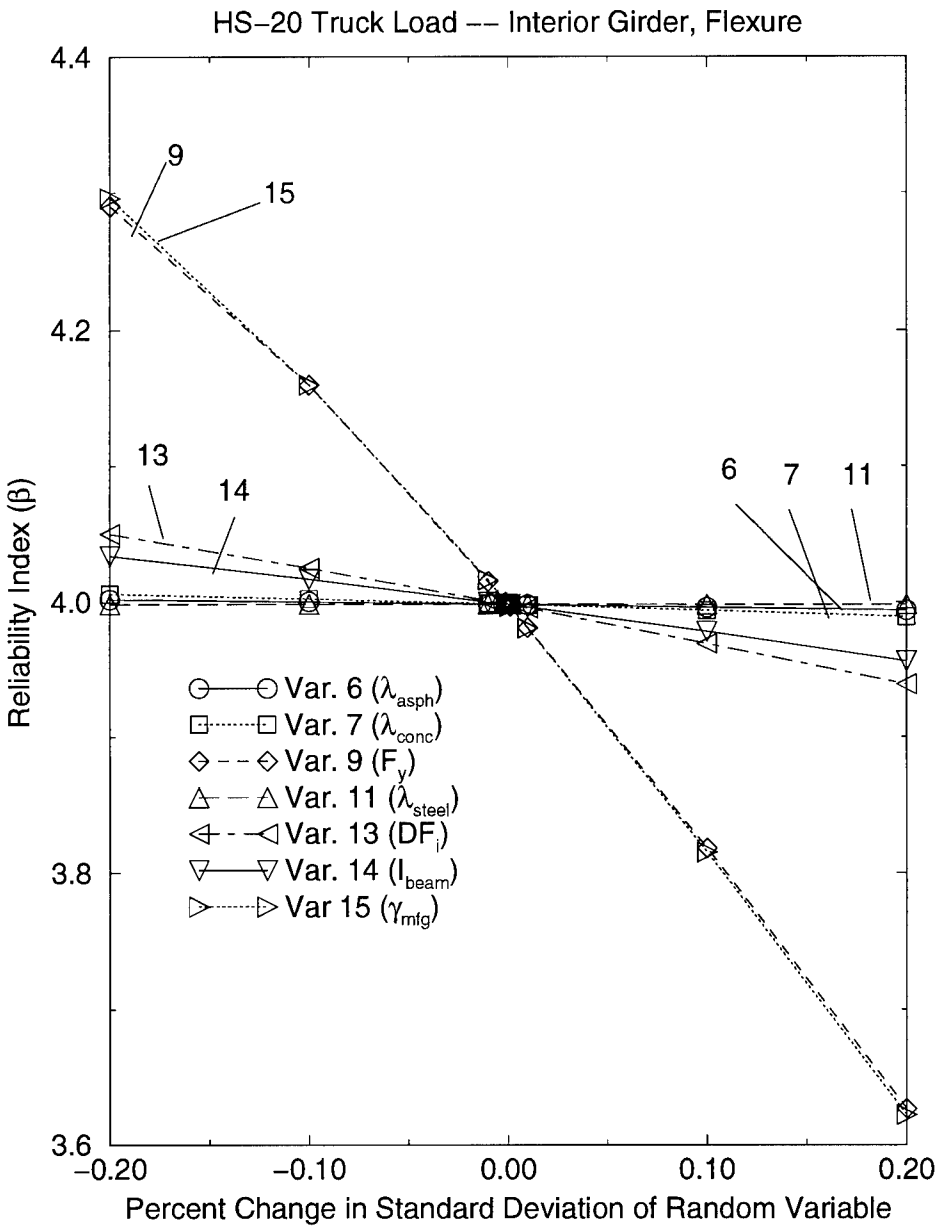

Figure 5.31: **Exact Sensitivity Values for Standard Deviation of Each Random Variable for Failure Due to Moment on an Interior Girder on Bridge E-17-AH With a Deterministic HS-20 Truck Live Load**

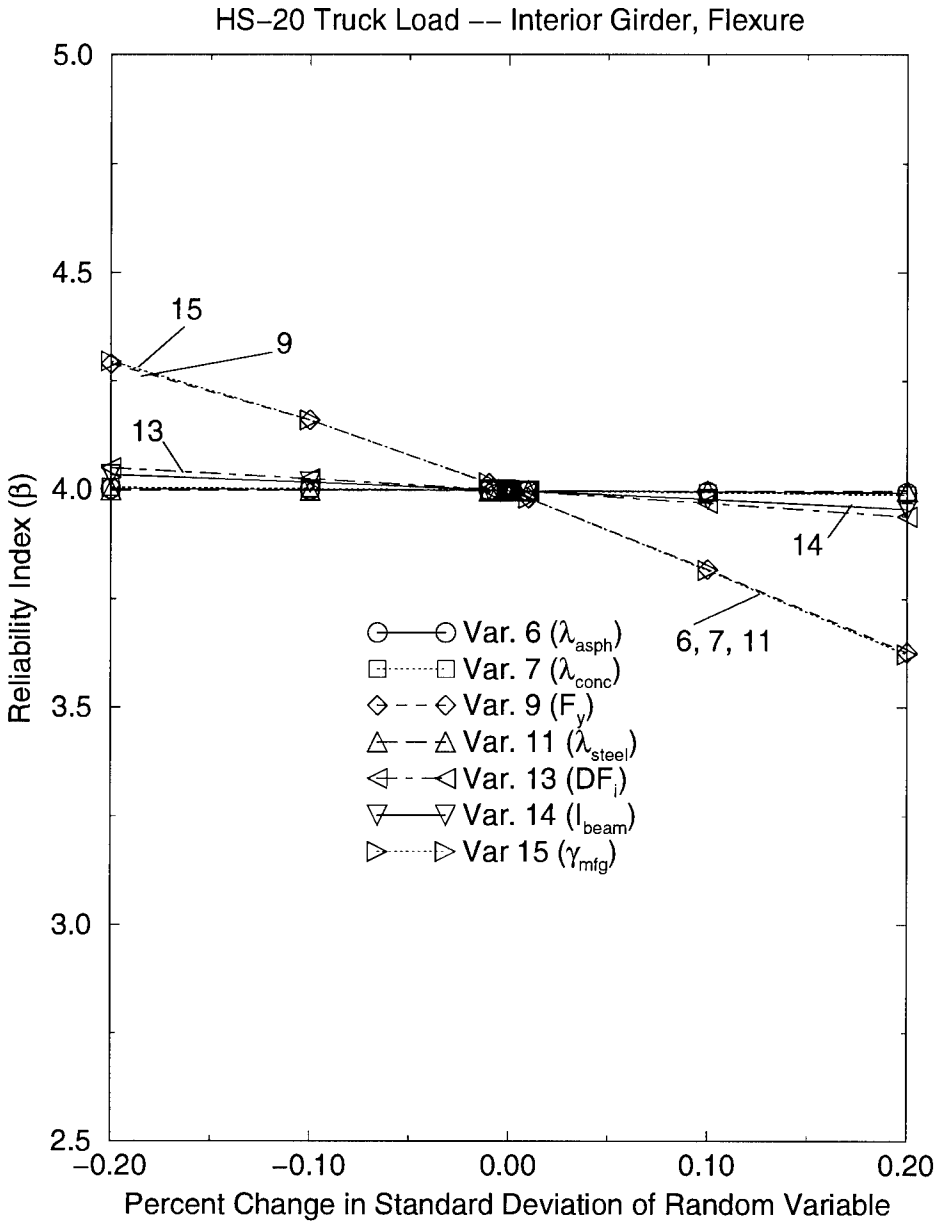

Figure 5.32: **Exact Sensitivity Values for Standard Deviation Plotted on the Same Scale as the Mean Values of Each Random Variable for Failure Due to Moment on an Interior Girder on Bridge E-17-AH With a Deterministic HS-20 Truck Live Load**

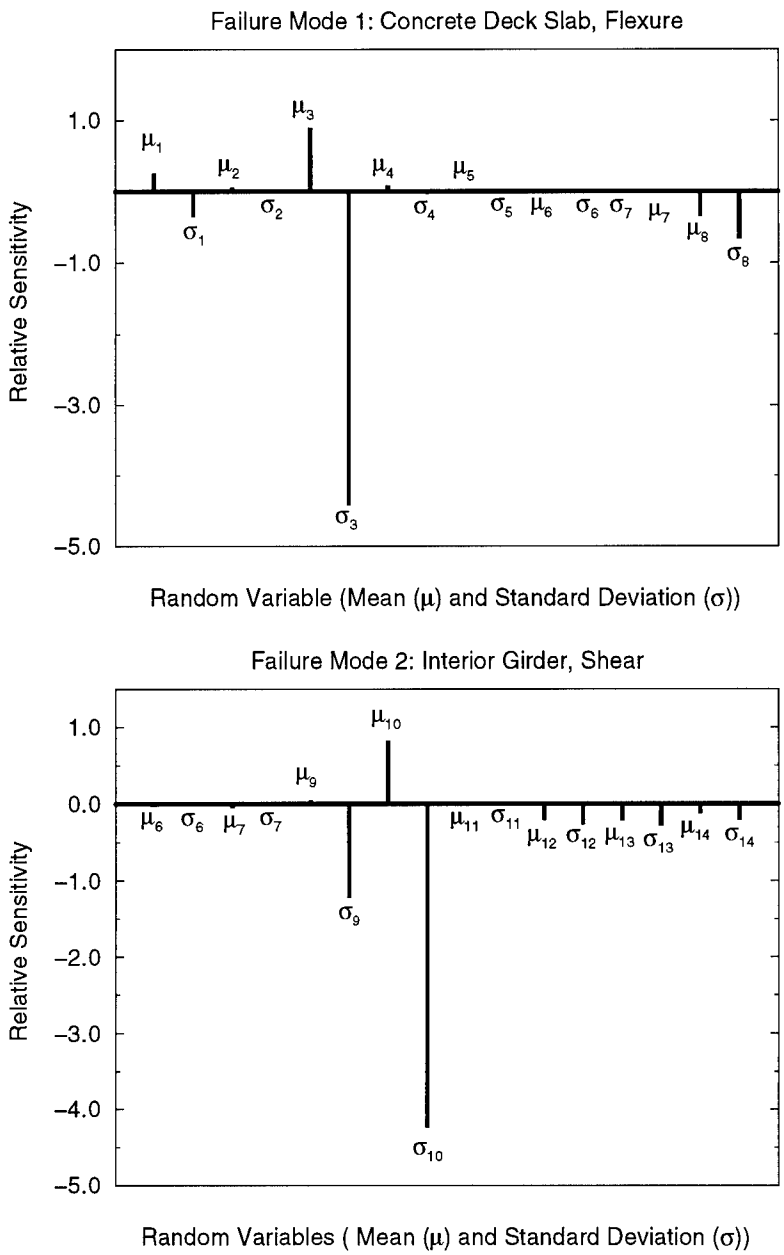

Figure 5.33: **Sensitivity Analysis on Random Variables: Failure Modes 1 (Concrete Slab) and 2 (Interior Girder due to Shear)**

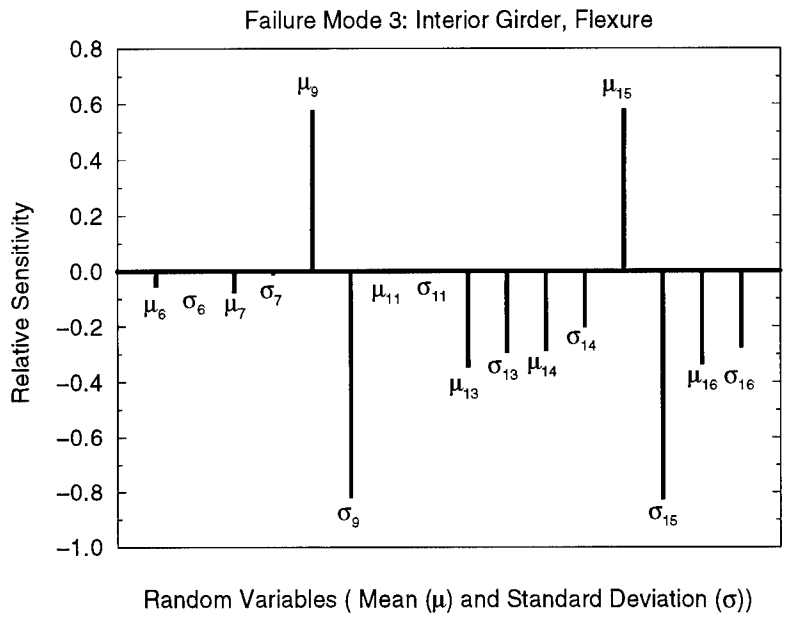

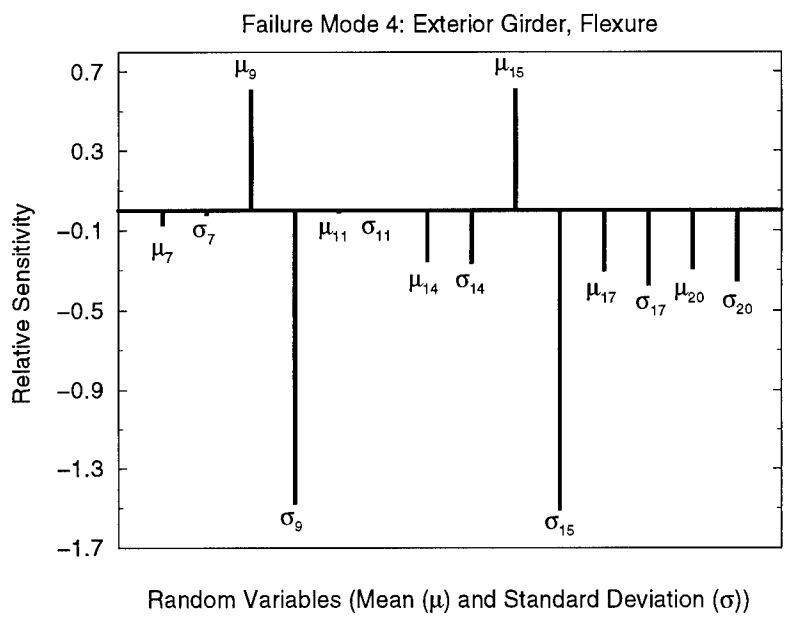

Figure 5.34: **Sensitivity Analysis on Random Variables: Failure Modes 3 (interior Girder due to Moment) and 4 (Exterior Girder due to Moment)**

a series-parallel model that eventually is comprised of the individual failure modes as described by limit state equations ($g(1) - g(16)$) needs to be developed. At the highest level, the bridge is a series system comprised of the deck, superstructure, and substructure. Fig. 5.35 considers the superstructure. It is composed of three spans in series, where the failure of any span constitutes failure of the bridge. Each span consists of nine girders where several model alternatives exist. Three possibilities for the girders are a series system, a parallel system where two adjacent girders must fail for the span to fail, or a parallel system where three adjacent girders must fail. Given the distribution of the live load and the interconnection between girders caused by the slab and the diaphragms, an argument could be made for any of the these three cases. Each girder can fail due to shear, moment, or crushing of the expansion bearing which finally reduces the model to the component limit state equations derived earlier.

Fig. 5.36 provides the same breakdown for the substructure and the slab. The substructure consists of two abutments and two column piers. The column piers are a series system of a pier cap, columns, and column footings. The pier cap is a series system which can fail due to positive moment, negative moment or shear. The columns are actually a parallel system where the failure of four columns are required to fail the system. The interior columns were the most critical and the failure of an interior column would greatly affect the performance of the pier cap above it. It is conservative and reasonable, given the high reliability of the columns, to model only the interior column which

is a series system of the top and bottom interior column. Likewise, only the interior column footing is modeled. It is a series system of one-way shear, two-way shear and moment.

The slab can be broken down as far as practicable. One equation could apply to the slab for the entire bridge, for an entire span, for a section of span between any two girders, or the slab could be divided into a grid pattern with each square of the grid having its own reliability. Several of these options are shown in Fig. 5.36.

Fig. 5.37 is the resulting system model in terms of limit state equations ($g(1) - g(16)$) for Bridge E-17-AH assuming that the concrete deck is identical throughout a span, three adjacent girders must fail for the superstructure to fail, and the abutment reliability is not considered. Using the 50-year Nowak live load and assuming no deterioration of the structure over time, the system reliability for the bridge was $\beta_{sys} = 2.51$. It is possible to simplify this model further by making some reasonable assumptions.

If some of the failure modes with very high reliabilities are not considered because they have negligible effect on the reliability of the system, the most relevant failure modes in the substructure are failure of the pier cap due to shear ($g(8)$) and failure of the footing due to moment ($g(13)$). Failure of the expansion bearing ($g(16)$) can be eliminated from the girder. If the two column piers are assumed to be perfectly correlated which is reasonable since they are subjected to almost identical loads and have identical strengths, the model only needs to consider one column pier. The same assumption can be

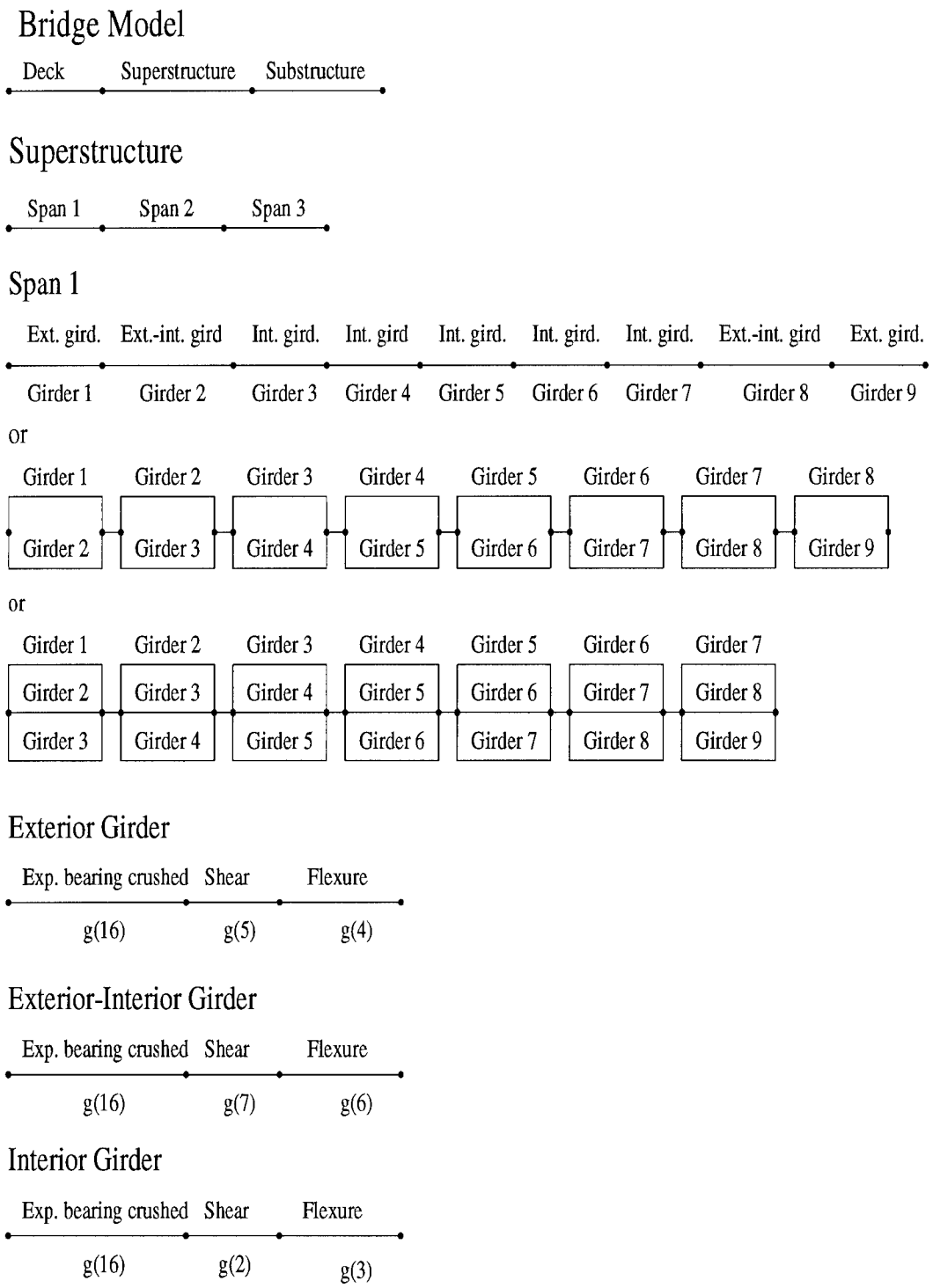

Figure 5.35: **Series-Parallel Model for Bridge E-17-AH: Superstructure**

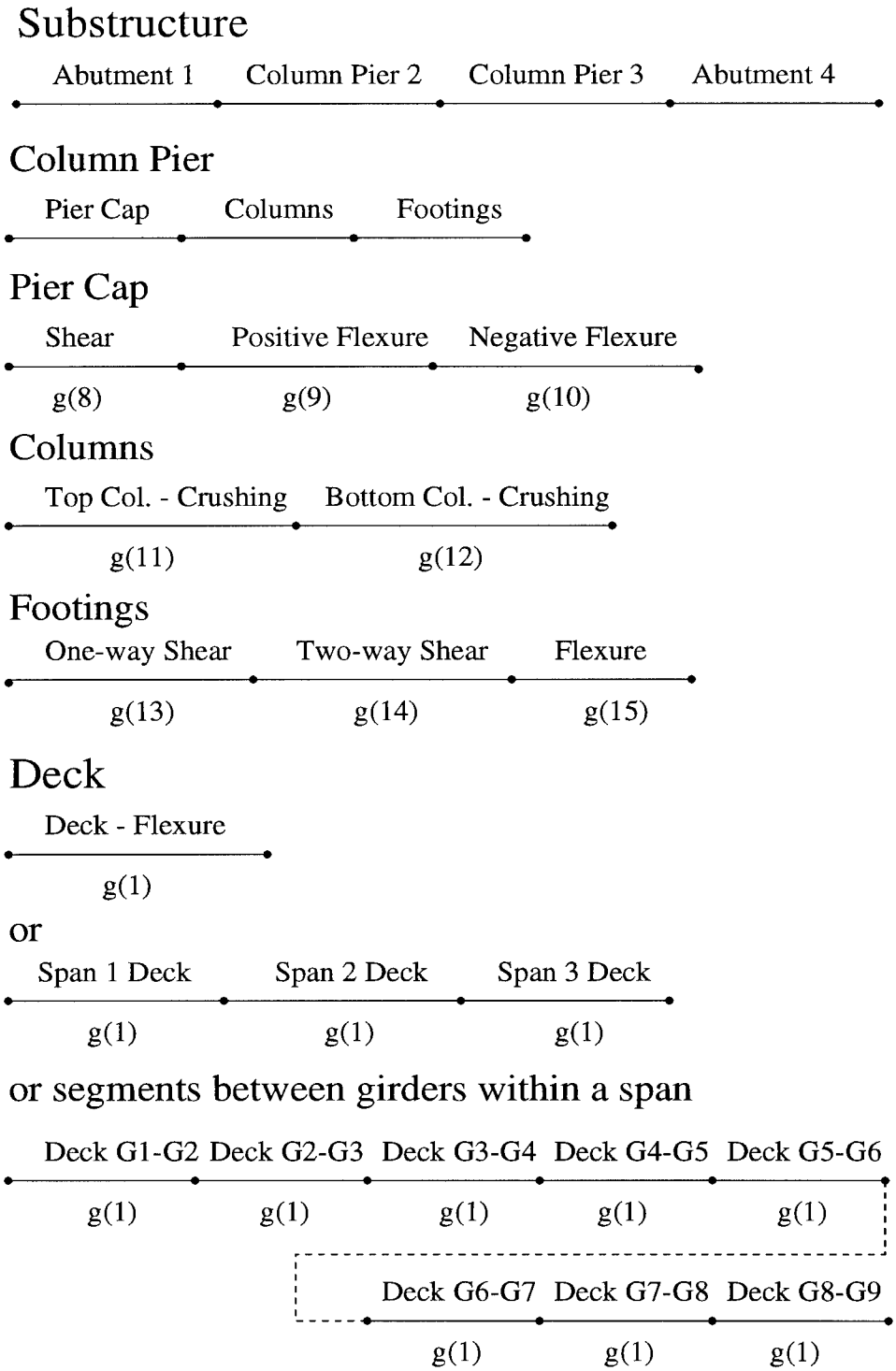

Figure 5.36: **Series-Parallel Model for Bridge E-17-AH: Substructure and Slab**

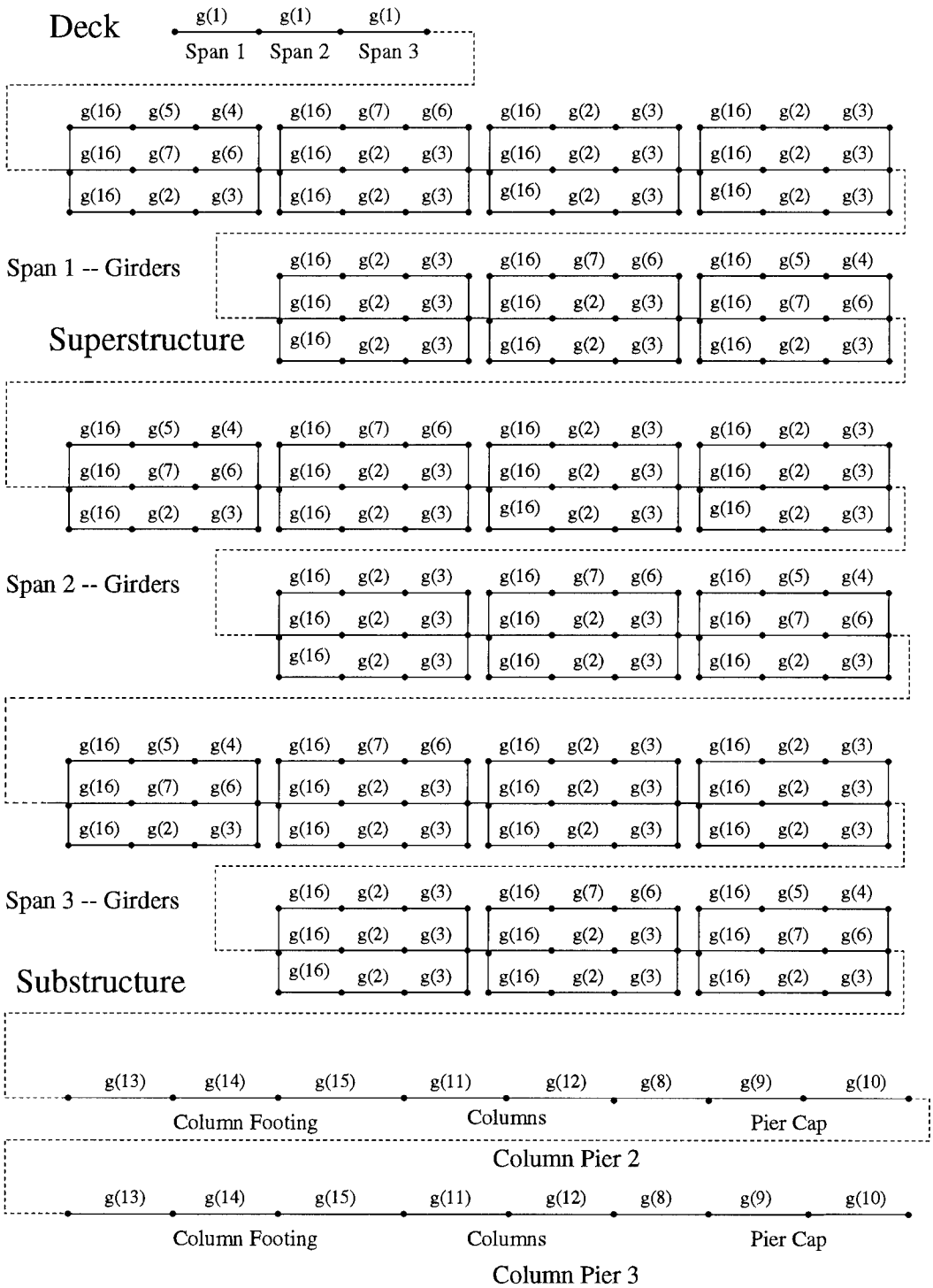

Figure 5.37: **Series-Parallel Model for Bridge E-17-AH: Deck, Superstructure, and Substructure**

made with regard to perfect correlation between the three equal-length spans for the slab and girders. Further if the spans are assumed to be perfectly correlated, and considering the symmetry within a span, the system model can be reduced to the model shown in Fig. 5.38 where three adjacent girders must still fail for the system to fail. The girders are numbered one through five as shown in Fig. 5.39. Using the simplified model and the 50 year Nowak live load model without deterioration, the system reliability was equal to $\beta_{sys} = 2.54$ which is very close to the more complex model in Fig. 5.37.

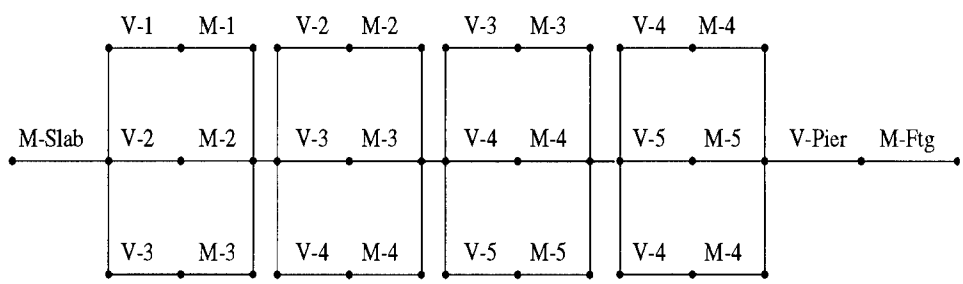

V-1: Failure Due to Shear in Girder 1

M-3: Failure Due to Moment in Girder 3

Figure 5.38: **Simplified Series-Parallel Model for Bridge E-17-AH: Failure of Three Adjacent Girders Required for System Failure**

The system model and the correlation between random variables will affect the system reliability of a structure. In the previous calculation, it was assumed that the girder resistances were uncorrelated ($\rho_{R_i,R_j} = 0.0$). Using the same simplified model, the system reliability was $\beta_{sys} = 2.49$ when the

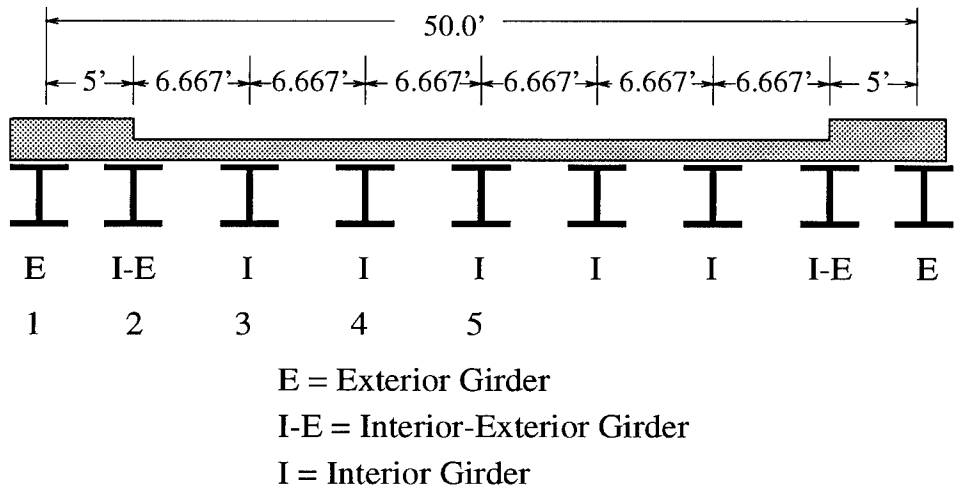

Figure 5.39: **Layout of Girders in Bridge E-17-AH**

resistance correlation was $\rho_{R_i,R_j} = 0.5$ and $\beta_{sys} = 2.31$ when $\rho_{R_i,R_j} = 1.0$. Similarly, the simplified model was revised as shown in Fig. 5.40 where only two adjacent girders have to fail for the system to fail and Fig. 5.41 where only a single girder must fail. The system reliability results for these revised models are shown in Table 5.13.

For the model in Fig. 5.41 which is entirely a series system, the increased correlation between the resistances improves the system reliability. For the parallel system models in Figs. 5.40 and 5.38, the increased correlation between the resistances decreases the system reliability. When there is perfect correlation between the resistances, the three models produce very similar results as expected. The correlation between other random variables could also be investigated along with other variations in the system model. Such analyses emphasize the importance of accurate input for reliability calculations. The

results obtained are only as good as the random variables, the correlation, and the system model that produces them.

Table 5.13: **System Reliability Results for Bridge E-17-AH Using Different System Models and Different Correlation Between Girder Resistances**

Failure Defined By	Correlation Between Girder Resistances		
	$\rho_{R_i,R_j} = 0.0$	$\rho_{R_i,R_j} = 0.5$	$\rho_{R_i,R_j} = 1.0$
Single Girder	1.97	2.06	2.23
Two Adjacent Girders	2.50	2.41	2.26
Three Adjacent Girders	2.54	2.49	2.31

5.9 Time Dependent Deterioration of the Bridge

Any structure will deteriorate over time which will affect the reliability of the system. A great deal of research has been undertaken to model the deterioration of structures and much more is clearly needed. Enright *et al.* [1996] have compiled a survey of deterioration models for concrete structures alone. For many cases of deterioration, we cannot not yet fully quantify how a structure loses capacity using a mathematical relationship. In such cases, deterioration models are developed by observing large numbers of structures over time and using regression analysis to fit the data into a linear or exponential relationship. Hearn *et al.* [1995] provides a comprehensive listing of these types of deterioration models as they relate to specific condition states

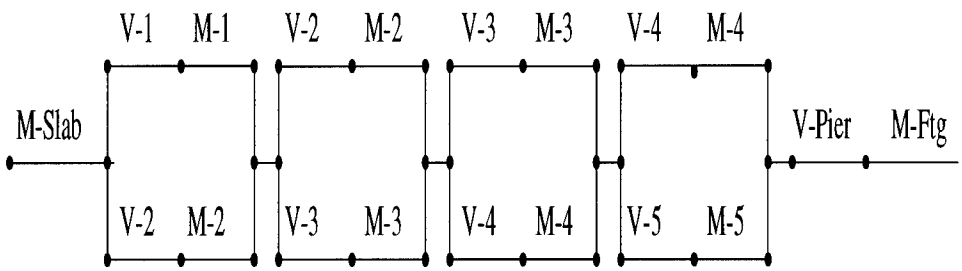

Figure 5.40: **Simplified Series-Parallel Model for Bridge E-17-AH: Failure of Two Adjacent Girders Required for System Failure**

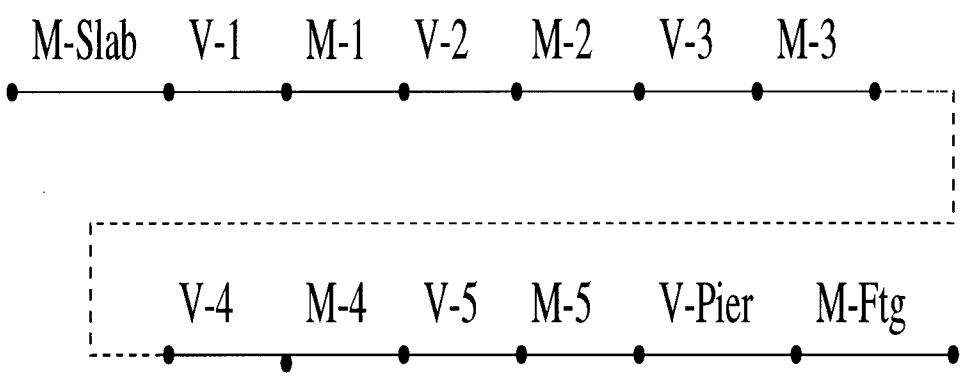

Figure 5.41: **Simplified Series-Parallel Model for Bridge E-17-AH: Failure of A Single Girder Required for System Failure**

developed by various researchers and state transportation departments.

This study will use available deterioration models to describe how the capacity of various elements of Bridge E-17-AH change over time. The system model to be used will be the simplified model in Fig. 5.38 where three adjacent girders must fail for the system to fail. The correlation between resistances is assumed to be $\rho_{R_i,R_j} = 0.5$. The live load is increasing over time in accordance with the Nowak live load model [Nowak 1993] and extreme value statistics. The capacity is evaluated at two year inspection intervals based on deterioration. This approach yields conservative results. For each evaluation, it is assumed that the maximum load is occurring at the time that the resistance is a minimum. In reality, the maximum live load could occur any time between the time of evaluation and when the bridge was placed in service. To account for this effect would require a much more complex analysis.

The bridge deterioration is assumed to be a result of corrosion of the steel girders and deterioration of the slab and pier cap due to chloride penetration of the concrete and subsequent corrosion of the steel reinforcement. The corrosion model for the girders was first proposed in Albrecht and Naeemi [1984] and has been used in many other studies [Sommer *et al.* 1993, Hendawi 1994, Jiang 1995]. The chloride penetration model was introduced in Cady and Weyers [1984], West and Hime [1985], and Takewaka and Mastumoto [1988]. The model was further developed and refined to include values for random variables by Thoft-Christensen *et al.* [1997].

5.9.1 Deterioration of the Concrete Slab and Pier Cap

Under normal circumstances, the reinforcing steel in concrete would not corrode. When concrete is placed around steel reinforcing, a protective passivation layer of gamma iron oxide is formed because of a chemical reaction between oxygen and the highly alkaline environment of the concrete. This high pH environment, if left alone, will keep this protective film stable [Takewaka and Mastumoto 1988]. Corrosion can result however if this environment is made more acidic which will cause the protective layer to decompose and then be exposed to oxygen and moisture.

The most common means of increasing the acidity of the environment is the process of carbonation or the penetration of chloride ions through the concrete. Carbonation occurs as carbon dioxide diffuses into the concrete and reacts with the calcium hydroxide of the cement [Enright *et al.* 1996]. The more common cause of increased acidity is through chloride ion penetration, most commonly the result of continued use of road salts to prevent freezing on the roadway during the winter months. The increased acidity breaks down the passivation layer and corrosion is initiated as the reinforcement is exposed to oxygen and moisture which have penetrated the microscopic cracks present in all concrete [Lin 1995]. Since practical experience [Thoft-Christensen *et al.* 1997] has shown chloride penetration to be a larger problem than carbonation, this study will focus on chloride penetration.

The chloride concentration at the reinforcement level must reach a minimum concentration before the corrosion process will start. This creates a two-step process. The first step is the penetration of chlorides from the

concrete surface over time until a sufficient chloride concentration C_{cr} has built up at the reinforcing steel. The rate of chloride penetration into concrete as a function of time t and space x has been shown to follow Fick's second law of diffusion [Takewaka and Mastumoto 1988]:

$$\frac{\partial C_{x,t}}{\partial t} = \frac{D_c \partial^2 C_{x,t}}{\partial x^2} \tag{5.88}$$

where $C_{x,t}$=chloride concentration at distance x from the surface at time t and D_c is the chloride diffusion coefficient. Assuming that the concentration of the chlorides at the surface is constant, the solution to Eq. 5.88 is

$$C_{x,t} = C_o[1 - erf(\frac{x}{2\sqrt{D_c t}})] \tag{5.89}$$

where C_o is the equilibrium chloride concentration on the concrete surface as a percent weight of the cement and erf is the error function. The error function erf is a special case of the incomplete gamma function and is defined by [Tuma 1987]

$$erf(x) = \frac{2}{\sqrt{\pi}} \int_0^x e^{-x^2} dx = \frac{2}{\sqrt{\pi}} (\frac{1}{0!}\frac{x}{1} - \frac{1}{1!}\frac{x^3}{3} + \frac{1}{2!}\frac{x^5}{5} - \frac{1}{3!}\frac{x^7}{7} + \cdots) \tag{5.90}$$

Press *et al.* [1986] provides the FORTRAN computer code needed to compute $erf(x)$.

In a time dependent study, the variable of interest is the corrosion initiation time T_I which is the amount of time between the application of the surface chloride and the onset of corrosion (which occurs when the critical chloride concentration C_{cr} is reached) at some distance x from the surface. The corrosion initiation time T_I can be expressed as [Thoft-Christensen *et al.*

1997]

$$T_I = \frac{(d_I - D_I/2)^2}{4D_c}(erf^{-1}(\frac{C_{cr} - C_o}{C_i - C_o}))^{-2} \tag{5.91}$$

where d_I = the concrete cover and D_I is the initial diameter of the reinforcement bar. C_i is the initial chloride concentration at the distance x which for this study will be assumed to be zero.

In reality, the initiation time T_I was found using Eq. 5.89 rather than trying to directly solve for an inverse error function. For a specific distance from the surface x, the time t was iteratively varied until the chloride concentration at the point in question $C_{x,t}$ was equal to the threshold or critical chloride concentration C_{cr} that will initiate corrosion. The time t when this occurs is the corrosion initiation time T_I.

The second step in the process is the actual corrosion of the steel reinforcement. Once corrosion has started, then the diameter of the reinforcement bars as a function of time $D_I(t)$ is modeled by

$$D_I(t) = D_I - C_{corr} i_{corr}(t - T_I) = D_I - 0.0203 i_{corr}(t - T_I) \tag{5.92}$$

where D_I = the initial diameter of the reinforcing bar (in inches), C_{corr} is a corrosion coefficient which for this study is estimated to be $C_{corr} = 0.0203$, and i_{corr} is a parameter related to the rate of corrosion. Since the area of available steel reinforcement $A(t)$ at any time t is the quantity needed to determine capacity in the limit state equations, that quantity is expressed as:

$$A(t) = \begin{cases} nD_i^2\frac{\pi}{4} & \text{for} \quad t \leq T_I \\ n(D(t))^2\frac{\pi}{4} & \text{for} \quad T_I < t < T_I + D_i/(0.0203 i_{corr}) \\ 0 & \text{for} \quad t \geq T_I + D_i/(0.0203 i_{corr}) \end{cases} \tag{5.93}$$

where $T_I + D_i/(0.0203 i_{corr})$ becomes an upper limit time beyond which the reinforcing bar is assumed to provide no strength to the structure.

This corrosion process is highly uncertain and a reliability analysis requires the introduction of many new random variables. One option is to include all of these random variables into the existing limit state equations. This would be very difficult since the corrosion of the steel is a function of the corrosion initiation time T_I which is itself computed from the inverse error function which is also a function of random variables. The limit state equation can be solved and the uncertainty in the corrosion process can be included if an approximate distribution for the area of steel $A(t)$ at any time can be found. The Point Estimate Method described in USACE [1992] is used to obtain the mean and standard deviation of $A(t)$.

The random variables used for this time-based reliability analysis and their associated values and distributions are taken from Thoft-Christensen *et al.* [1997] and are shown in Table 5.14. Note that the actual rate of corrosion r_{corr} can be computed using Eq. 5.92 and the value for the corrosion parameter i_{corr}, as follows:

$$\begin{aligned} r_{corr} &= 0.0203 i_{corr} = 0.0203(0.098) = 0.001989 \; in/yr \\ &= 1.989 \; mils/yr \; (0.051 \; mm/yr) \end{aligned} \tag{5.94}$$

This analysis is performed for both the concrete slab and the pier cap. It is assumed that the chloride concentration on the pier cap surface is two-thirds the concentration of the chlorides on the surface of the slab. Road salts are applied directly to the slab surface.

Table 5.14: **Random Variables (RV) Used To Compute the Deterioration of Reinforcing Steel in the Slab and Pier Cap Due To Chloride Penetration of the Concrete**

RV	Units	Description	Values*
C_o	%	Chloride concentration on the surface	N[1.08, 0.072] slab
			N[0.72, 0.048] pier
D_c	in^2/sec	Diffusion coefficient	N[5.42, 0.387](10^{-7})
x	in	Distance to reinforcement ($d_I - D_I/2$)	N[2.25, 0.337] slab
			N[2.0, 0.3] pier
C_{cr}	%	Critical chloride concentration	N[.40, 0.05]
D_I	in	Initial diameter of bar	N[0.625, 0.0187] slab
			N[0.5, 0.015] pier
i_{corr}	in/yr	Corrosion parameter	N[0.098, 0.0114]
*Unless specifically stated, values are for both slab and pier			

It is assumed that chlorides will leak through the pavement joints to reach the pier cap but will be diluted in the process. Similarly, it is assumed that the concentration of the chlorides is the same on the sides of the pier cap as it is on the top. The assumed deterioration in the pier cap is that the chlorides

penetrate from the side of the cap and corrode the outside stirrups as shown in Figs. 5.18 and 5.19. It will take the chlorides much longer to penetrate to the interior stirrup sections which will remain intact much longer. The corrosion model for the steel reinforcement is based on general corrosion and its statistical values. The model does not consider localized pitting corrosion which can result in a much higher weakening of the structure in specific areas [Thoft-Christensen *et al.* 1997].

The Point Estimate Method [USACE 1992] is used to first estimate the mean and standard deviation of the corrosion initiation time T_I and then compute the same parameters for the area of steel $A(t)$ at any time t. The Point Estimate Method approximates the probability integral by repeated deterministic analyses. It considers all possible combinations of the mean plus one standard deviation and the mean minus one standard deviation for all random variables. The results which conclude that the mean corrosion initiation time for the slab is $T_I = 19.60$ *years* with a standard deviation of 7.51 *years* are shown in Table 5.15. For each case, the iterative solution of Eq. 5.91 was obtained using the mean $\pm$ standard deviation values listed in Table 5.14. The same method was applied to the corrosion initiation time in the pier cap where the surface concentration of chlorides was less. On the pier cap, the mean corrosion initiation time was $T_I = 39.28$ *years* with a standard deviation of 21.21 *years*.

Once the parameters are obtained for the corrosion initiation time T_I, the area of steel $A(t)$ can be computed for any time t using the same

Table 5.15: **Point Estimate Method Results for Finding the Mean and Standard Deviation for the Corrosion Initiation Time T_I for the Concrete Slab**

Iteration Number	C_o %	D_c $in^2/sec * 10^{-7}$	x in	C_{cr} %	T_I $years$
1	1.15	5.81	2.59	0.45	24.76
2	1.15	5.81	2.59	0.35	17.26
3	1.15	5.81	1.91	0.45	13.53
4	1.15	5.81	1.91	0.35	9.43
5	1.15	5.03	2.59	0.45	28.57
6	1.15	5.03	2.59	0.35	19.91
7	1.15	5.03	1.91	0.45	15.61
8	1.15	5.03	1.91	0.35	10.88
9	1.01	5.81	2.59	0.45	31.48
10	1.01	5.81	2.59	0.35	20.65
11	1.01	5.81	1.91	0.45	17.20
12	1.01	5.81	1.91	0.35	11.28
13	1.01	5.03	2.59	0.45	36.32
14	1.01	5.03	2.59	0.35	23.83
15	1.01	5.03	1.91	0.45	19.84
16	1.01	5.03	1.91	0.35	13.02
$T_{I\ mean} = 19.60\ years$					
$T_{I\ std\ deviation} = 7.51\ years$					

technique. The results for the area of steel in the top of the slab after thirty years $A(30)$ for a one-foot (0.305 m) section of slab (i.e., two #4 bars, see Fig. 5.9) using Eq. 5.93 are shown in Table 5.16.

Table 5.16: **Point Estimate Method Results for Finding the Mean and Standard Deviation for the Area of Steel After 30 Years $A(30)$ for the Concrete Slab**

Iteration Number	D_i in	T_I $years$	i_{corr} $in/year$	$A(30)$ in^2
1	0.606	12.09	0.087	1.037
2	0.606	12.09	0.109	1.008
3	0.606	27.11	0.087	1.135
4	0.606	27.11	0.109	1.130
5	0.644	12.09	0.087	1.177
6	0.644	12.09	0.109	1.145
7	0.644	27.11	0.087	1.281
8	0.644	27.11	0.109	1.276
$A(30)_{mean} = 1.149\ in^2$				
$A(30)_{std\ deviation} = .0919\ in^2$				

The same procedure was used to compute the area of steel $A(t)$ in the top of a one foot (0.305 m) section of the slab for any time t. Fig. 5.42 shows the mean and standard deviation for $A(t)$ over a 70 year time period. The graph

can clearly be divided into three sections: the initial flat section where there is a high certainty that corrosion has not begun, a second portion where there is uncertainty about whether or not corrosion has been initiated, and a third steeper section where it is very likely that corrosion has begun. As time passes, the mean value of the area of steel is decreasing as the bar deteriorates while the standard deviation remains about the same. The coefficient of variation is therefore increasing over time.

Fig. 5.43 shows the coefficient of variation of $A(t)$ over time. The coefficient of variation (δ) rises most rapidly during the period where it is most uncertain whether or not corrosion has started. The cov continues to rise but at a lower rate once it is more certain that corrosion has started. Fig. 5.43 also demonstrates that the Point Estimate Method provides an approximation of $A(t)$ over time. The exact solution would not provide a flat curve in the initial section but would rather show a slight slope reflecting the tail of the distribution for the corrosion initiation time T_I. Similarly, the solution in the later life of the structure would reflect the other tail of the distribution and the possibility that corrosion has not been initiated. In this example, the Point Estimate Method provides a less conservative solution in the early life of the structure and a more conservative solution in the later life of the structure. The results however appear reasonable and an exact solution would have been much more difficult to obtain. The exact same method was used to calculate the deteriorating area of shear steel in the pier cap over time. The time dependent area of steel mean and standard deviation are used in the limit

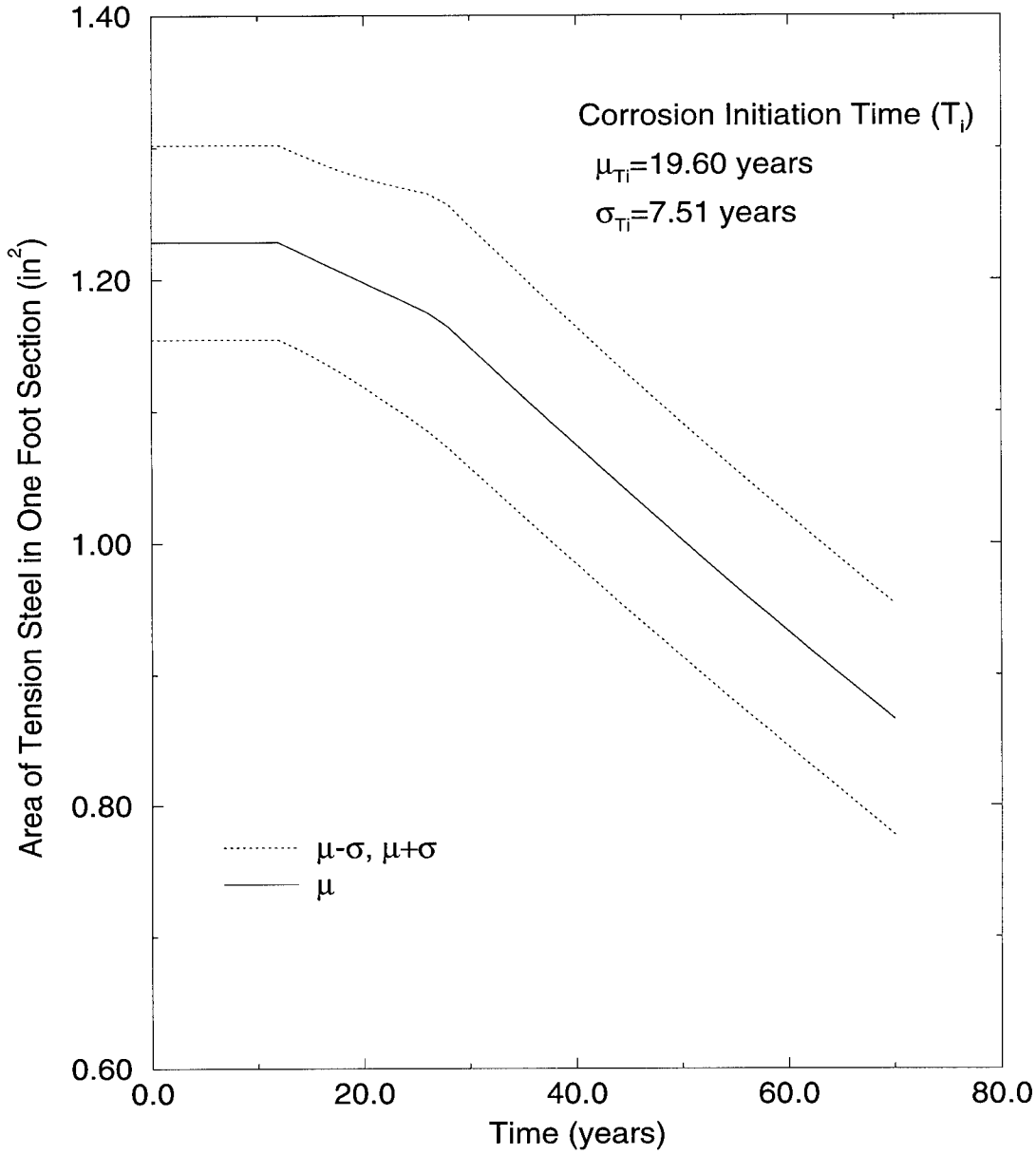

Figure 5.42: **Area of Reinforcing Steel in the Top of a One-Foot (0.305 m) Section of the Slab Over Time With Deterioration Caused by Chloride Penetration of the Concrete**

state equations for the failure of the slab $g(1)$ and the failure of the pier cap due to shear $g(8)$ to compute the reliability of these failure modes over time.

5.9.2 Deterioration of the Girders

While the chlorides are penetrating the concrete deck and cause the steel reinforcement to corrode, the exposed steel girders are also subject to corrosion. Corrosion deterioration is common among steel structures, particularly those which accumulate water. Corrosion is an electrochemical process involving oxidation and reduction. The corroding metal is the anode; the existing rust is the cathode; and the water film provides the electrolyte through which the current flows [Scully 1990]. Over time, the corrosion will pit and destroy the steel surface causing a reduction in the cross-section area. The reduction of the web area will lower the shear capacity of the structure and the plastic section modulus reduction will lower the moment capacity. This study focuses on the material loss which accompanies corrosion. Other effects of corrosion such as the pressure exerted on other elements which may cause stresses and eccentricities or the locking of bearings are not included.

Corrosion is difficult to predict and can take many forms such as pitting, crevice, galvanic, or stress corrosion. Pitting corrosion is localized and difficult to predict. It often begins with a defect on the surface and may cause local stress concentrations. Crevice corrosion often occurs at joints and tight spaces where different members are very close together. Similarly galvanic corrosion is a problem at joints where uncommon materials are connected electrically such as welds. The presence of a tensile force tends to increase

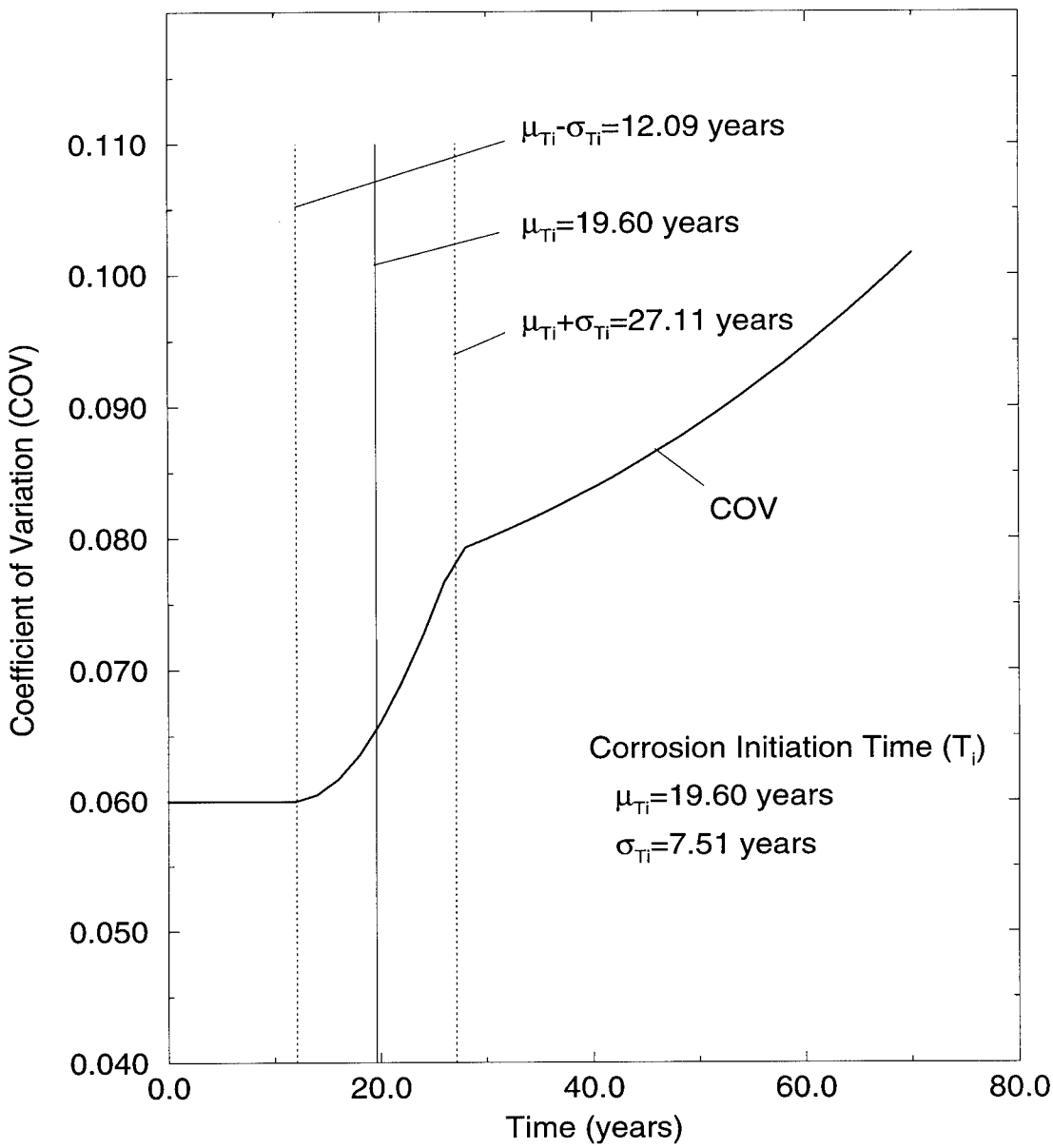

Figure 5.43: **Coefficient of Variation of the Area of Steel Over Time Subject to Corrosion of the Reinforcing Steel**

the rate of corrosion which is known as stress corrosion [Sommer *et al.* 1993]. This study, however, includes only general corrosion which is assumed to be uniformly distributed on the surface and is the most common type of corrosion.

Even general corrosion is difficult to predict since it is dependent on the type of steel, the local environment, the presence of moisture, and even the location of the steel member on the structure. The presence of chlorides from road salts increases corrosion. Steel girders on the same bridge will deteriorate differently as more road spray and salts tend to get deposited on the exterior girders. Even within a girder, the corrosion pattern can differ as more water and debris will accumulate near the joints rather than the middle.

Albrecht and Naeemi [1984] made a comprehensive study to attempt to predict corrosion in different environments for both carbon and weathering steel based on field studies in 46 locations worldwide. Using regression analysis of the field results, they developed a corrosion propagation model which predicts the average corrosion penetration $C(t)$ in micrometers ($10^{-6}m$) at any time t where t is in *years*. The corrosion penetration $C(t)$ is

$$C(t) = At^B \tag{5.95}$$

where A and B are the regression parameters based on the environment and type of steel. The environments were classified as urban/industrial, rural, or marine. Bridge E-17-AH is located in the metro Denver area and is best classified as an urban environment (environment 1) which contains the sulfur oxides and nitrogen oxides from fossil fuels and automobile exhaust which

enhance corrosion. It is readily apparent from an inspection of this bridge that the exterior and interior-exterior girders are corroding much faster than the interior girders. Perhaps the interior girders are better shielded from the urban contaminants (environment 2).

For this study, it will be assumed that the exterior and interior-exterior girders are exposed to the urban environment (environment 1), while the exposure to the interior girders is more clearly represented by the rural environment (environment 2). The bridge girders are carbon steel. The parameters that will be used to predict corrosion deterioration of the girders are shown in Table 5.17. The parameters A and B are random variables that must be included in the reliability analysis. This study does not consider the protective benefit provided by the paint on the girders.

The assumed corrosion pattern for the girders is shown in Fig. 5.44 where the corrosion extends all the way up the web at the supports and only a quarter of the way up the web at the center. Similar assumptions were made in Sommer *et al.* [1993] and Hendawi [1994].

To compute the reliability of the girders over time, the Point Estimate Method will again be used to compute the mean and standard deviation of the plastic section modulus Z and the area of the shear web $d_w t_w$. The reduced plastic section modulus will reduce the moment capacities in the girders as described in limit state equations $g(3)$, $g(4)$, and $g(6)$. Similarly, the reduced web area will reduce the shear capacity in limit state equations $g(2)$, $g(5)$, and $g(7)$.

Table 5.17: **Statistical Parameters A and B for Predicting the Corrosion Propagation in the Bridge E-17-AH Girders [Albrecht and Naeemi 1984]**

Parameter	A	B
Interior Girders (Environment 2)		
Mean value, μ	34.0	0.65
Coefficient of Variation, σ/μ	0.09	0.10
Correlation coefficient, $\rho_{A,B}$	0.0*	-
Exterior and Interior-Exterior Girders (Environment 1)		
Mean value, μ	80.2	0.593
Coefficient of Variation, σ/μ	0.42	0.40
Correlation coefficient, $\rho_{A,B}$	0.68	-
* Correlation data not available, variables assumed to be uncorrelated		

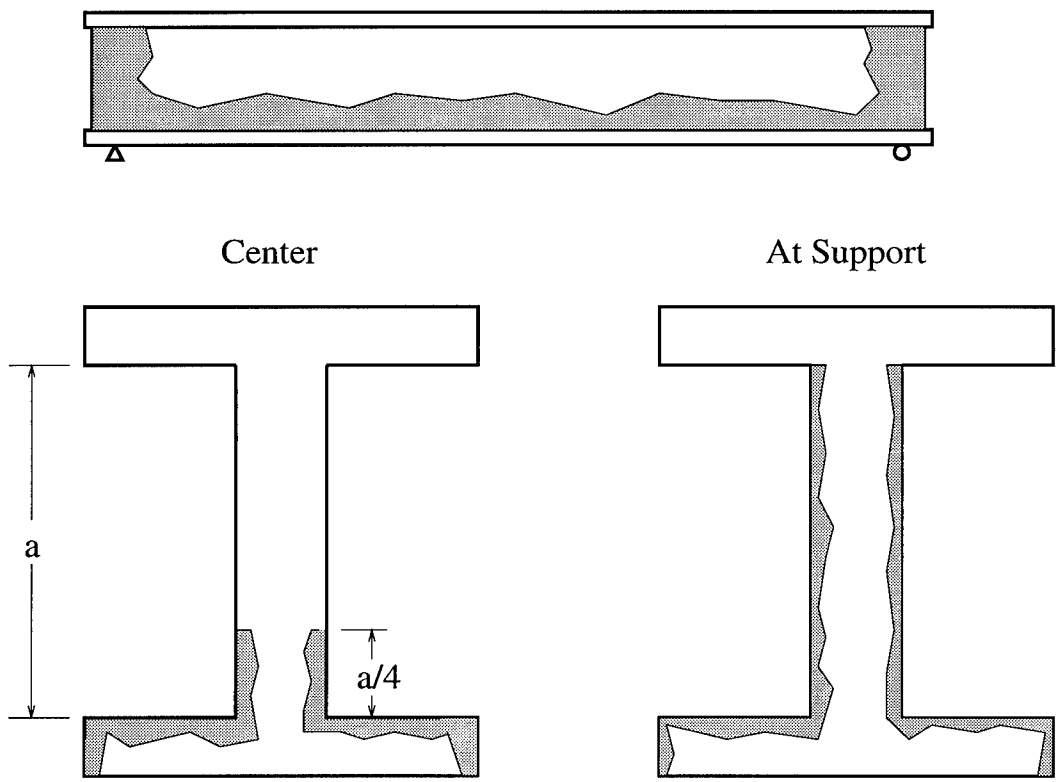

Figure 5.44: **Corrosion Pattern on Steel Girders on Bridge E-17-AH**

The plastic section modulus Z must be computed over time. The initial section properties of the steel girders are known and are considered to be deterministic. They are the depth of the beam d, the thickness t_w and depth d_w of the web, and the thickness t_f and width b_f of the flange. The depth of corrosion d_{corr}, a lognormally distributed random variable, is computed for any period of time. Other dimensions are defined as shown in Fig. 5.45.

$$\begin{aligned} p &= 0.75(d - 2t_f) \\ c &= b_f - 2d_{corr} \\ r &= t_f - d_{corr} \\ g &= t_w - 2d_{corr} \\ s &= p/3 + d_{corr} \end{aligned} \tag{5.96}$$

The first step is to determine the location of the plastic neutral axis (N.A) as shown in Fig. 5.45 which indicates the point where the areas above and below the plastic neutral axis are equal. The distance cg from the bottom of the beam to the neutral axis is computed as

$$\begin{aligned} Area &= b_f(t_f) + t_w(p) + s(g) + r(c) \\ cg &= d - t_f - \frac{(Area/2 - t_f(b_f)}{t_w} \end{aligned} \tag{5.97}$$

The plastic section modulus Z is the first moment of area about the plastic neutral axis for the sections shown in dotted lines in Fig. 5.45.

$$\begin{aligned} Z &= (cg - r/2)r(c) + (cg - r - s/2)s(g) + (d - t_f - cg)t_w(d - t_f - cg)/2 \\ &\quad + \frac{(d - t_f/2 - cg)}{2} + (d - t_f/2 - cg)t_f(b_f) \end{aligned}$$

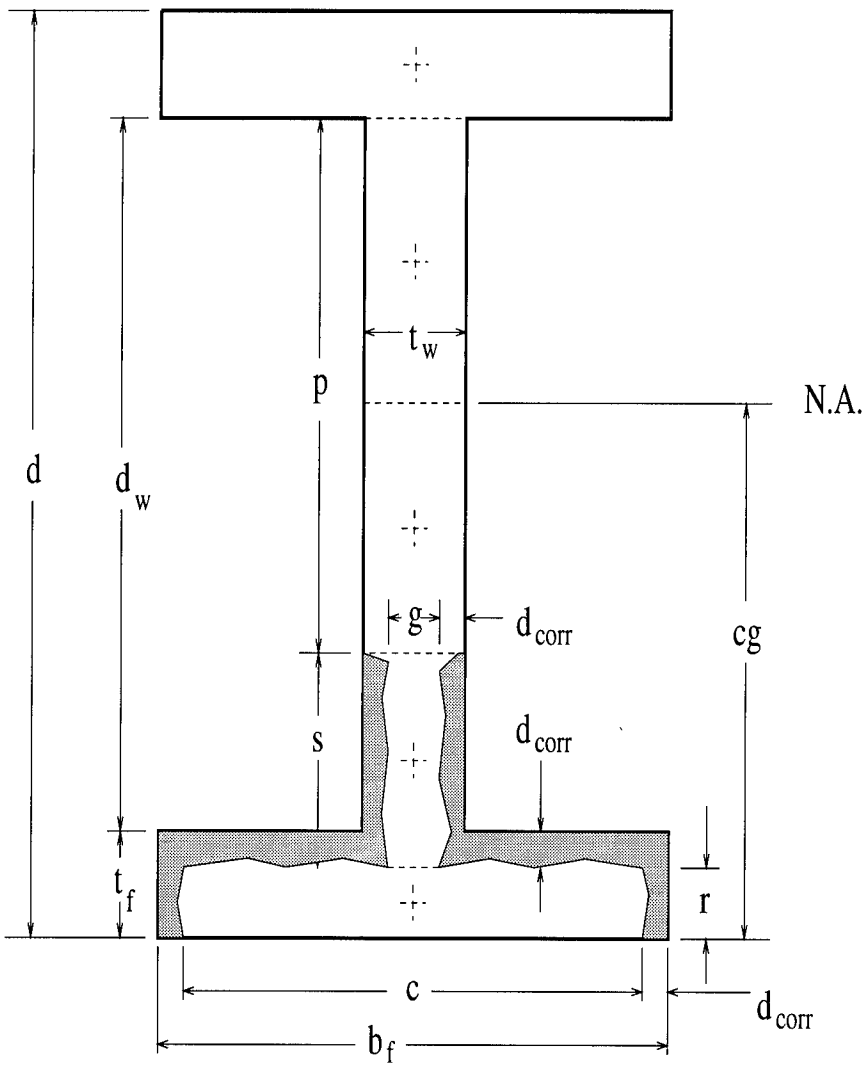

Figure 5.45: **Dimensions for Computing the Plastic Section Modulus of a Steel Beam Corroding Over Time**

$$+(p-(d-t_f-cg))t_w\frac{p-(d-t_f-cg)}{2} \tag{5.98}$$

The Point Estimate Method is used to compute the mean and standard deviation of Z at any time t. The only random variables in the analysis are the corrosion parameters A and B which are correlated for the exterior and interior-exterior girders. The Point Estimate Method accounts for correlation between random variables by using weighted probability concentrations. There are four possible probability combinations P_{AB} using the corrosion parameters A and B: P_{++}, P_{+-}, P_{-+}, and P_{--} where + indicates mean plus standard deviation for the individual variable and − indicates mean minus standard deviation. The weight assigned to each possibility is [USACE 1992]

$$\begin{aligned}(P_{A+})(P_{B+}) &= (P_{A-})(P_{B-}) = (0.5)(0.5)+(0.25)\rho_{AB}\\ (P_{A+})(P_{B-}) &= (P_{A-})(P_{B+}) = (0.5)(0.5)-(0.25)\rho_{AB}\end{aligned} \tag{5.99}$$

Table 5.18 shows the results for the plastic section modulus $Z(30)$ for the interior-exterior girder subject to corrosion for a time period of 30 years. Recall that the interior-exterior girder is a WF 33x132 standard shape beam whose initial dimensions are shown in Fig. 5.5. The corrosion parameters are: $\mu_A = 80.2$, $\sigma_A = 33.68$, $\mu_B = .593$, $\sigma_B = .237$, and $\rho_{A,B} = 0.68$ as shown in Table 5.17. For 30 years, the mean value for the plastic section modulus for the interior-exterior girder is $Z(30) = 458.21\ in^3$ ($7508.7\ cm^3$) with a standard deviation of $19.98\ in^3$ ($327.4\ cm^3$).

The mean and standard deviation for Z over a 70 year life for the interior-exterior girder is shown in Fig. 5.46. The uncertainty associated with

Table 5.18: **Point Estimate Method Results for Finding the Mean and Standard Deviation for the Plastic Section Modulus After 30 Years, $Z(30)$, for the Interior-Exterior Girder**

Iteration	A	B	Z (in^3)	P_{AB}
1	46.5	0.356	467.93	0.42
2	46.5	0.830	460.55	0.08
3	113.9	0.356	465.29	0.08
4	113.9	0.830	446.69	0.42
$Z(30)_{mean}$ $.42(446.69 + 467.93) + .08(465.29 + 460.55) = 458.21\ in^3$				
$Z(30)_{std\ deviation} = 19.98\ in^3$				

the plastic section modulus expands linearly as time passes and more corrosion occurs. The deterioration of the interior girder over time is much less as shown in Fig. 5.47 which makes sense since the corrosion parameters were smaller and had lower coefficients of variation (see Table 5.17).

The area of the web A_w over time is much easier to calculate.

$$A_w = d_w(t_w - 2d_{corr}) \tag{5.100}$$

where d_w is the depth of the web, t_w is the thickness of the web, and d_{corr} is the depth of corrosion at the time being considered. The Point Estimate Method is used to determine the mean and standard deviation of A_w. The deterioration of the shear web over a 70 year time period for an interior-exterior girder is shown in Fig. 5.48.

The uncertainty as shown by the coefficients of variation over time for all three types of girders for both the deterioration of the web area A_w and plastic section modulus Z are shown in Fig. 5.49. In all cases the coefficient of variation rises over time as the random corrosion process progresses. The interior girder uncertainty is much less than that associated with the exterior and interior-exterior girders. The uncertainty associated with A_w is much greater than that of Z which makes sense since the shear area is deteriorating at a much greater rate than the loss of plastic section modulus given the model described in Fig. 5.44.

Clearly more research is needed in the area of corrosion deterioration. While the Albrecht and Naeemi [1984] study included 46 samples in diverse

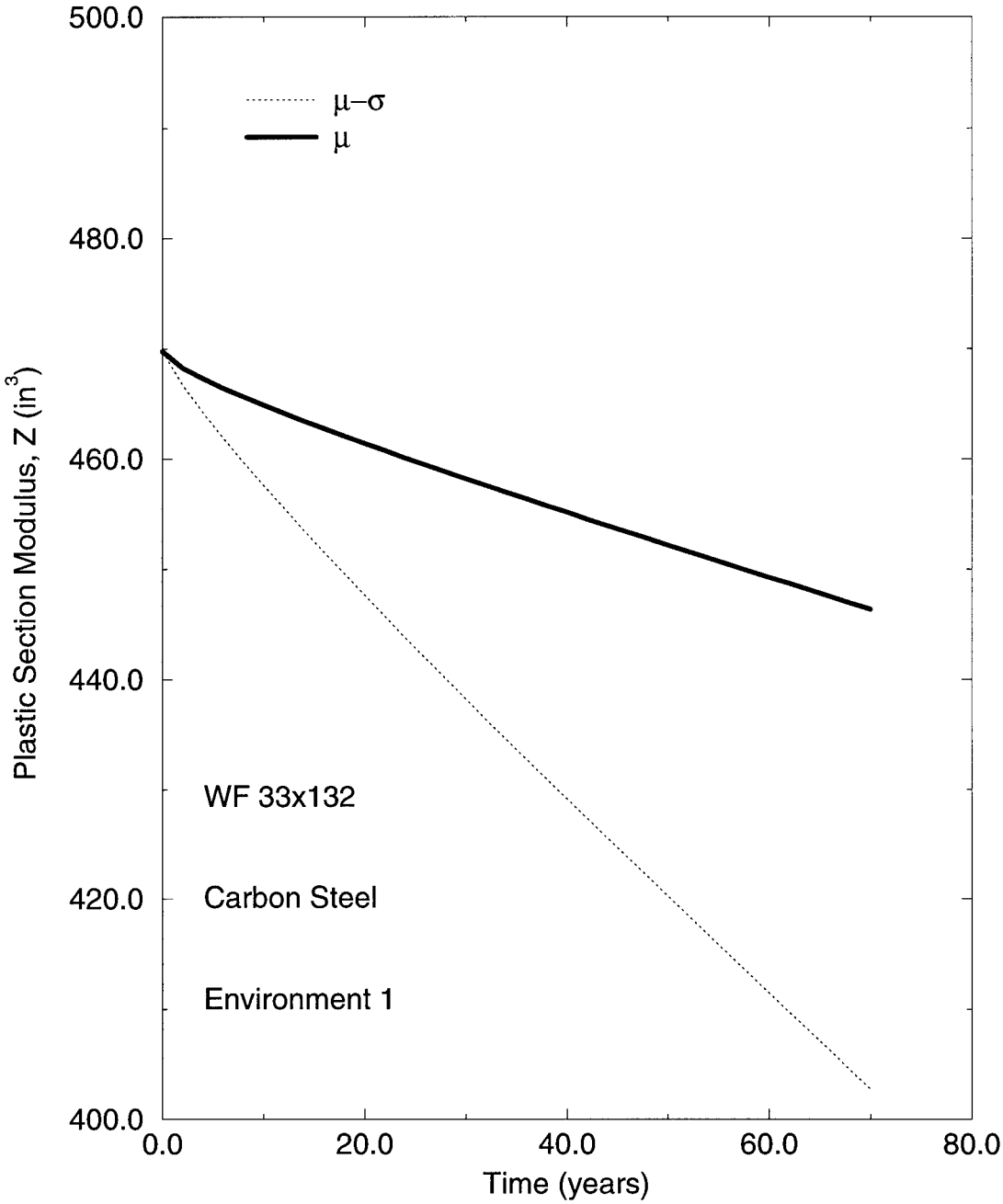

Figure 5.46: **Deterioration of the Plastic Section Modulus Z Due to Corrosion at the Midpoint of an Interior-Exterior Girder**

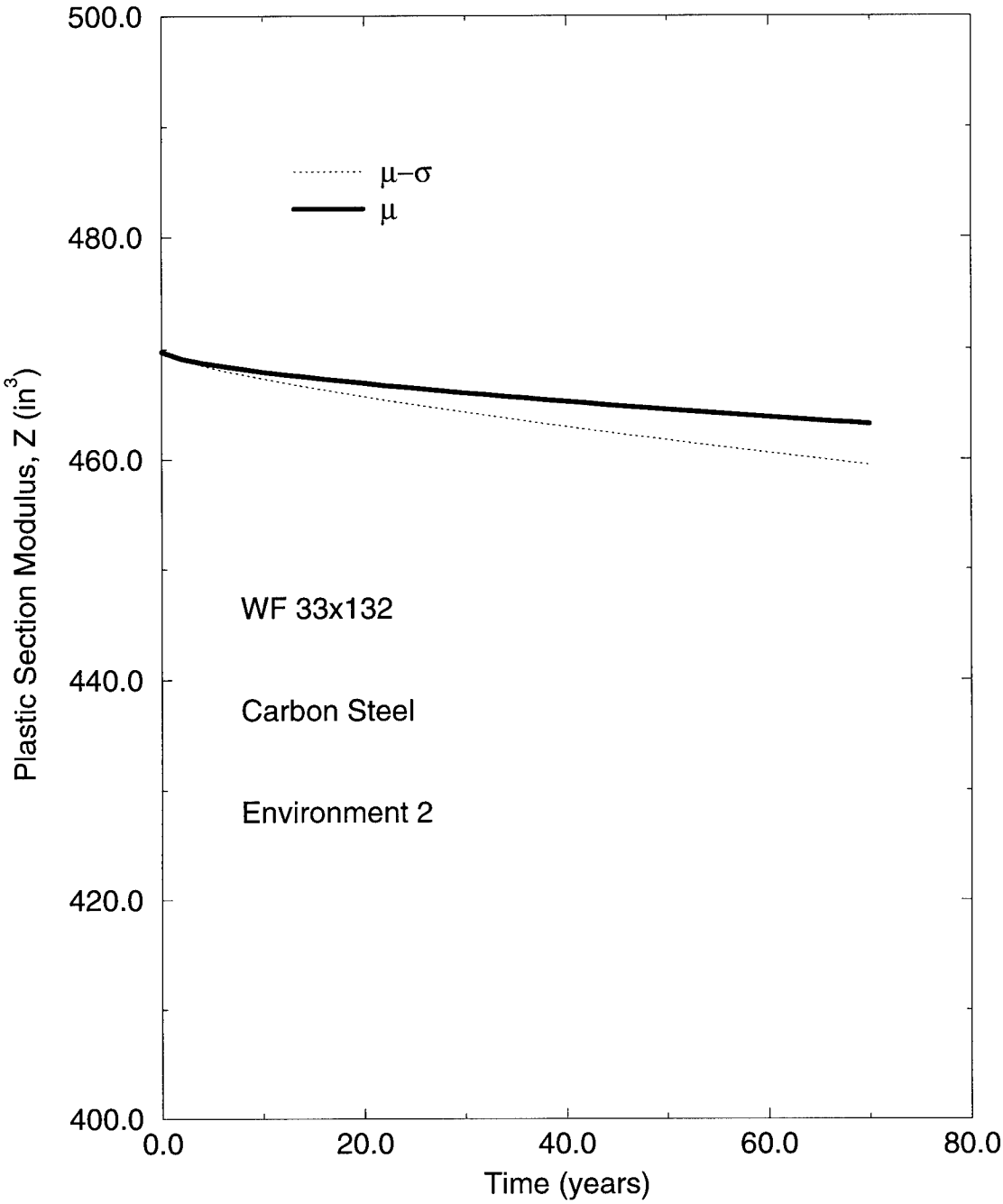

Figure 5.47: **Deterioration of the Plastic Section Modulus Z Due to Corrosion at the Midpoint of an Interior Girder**

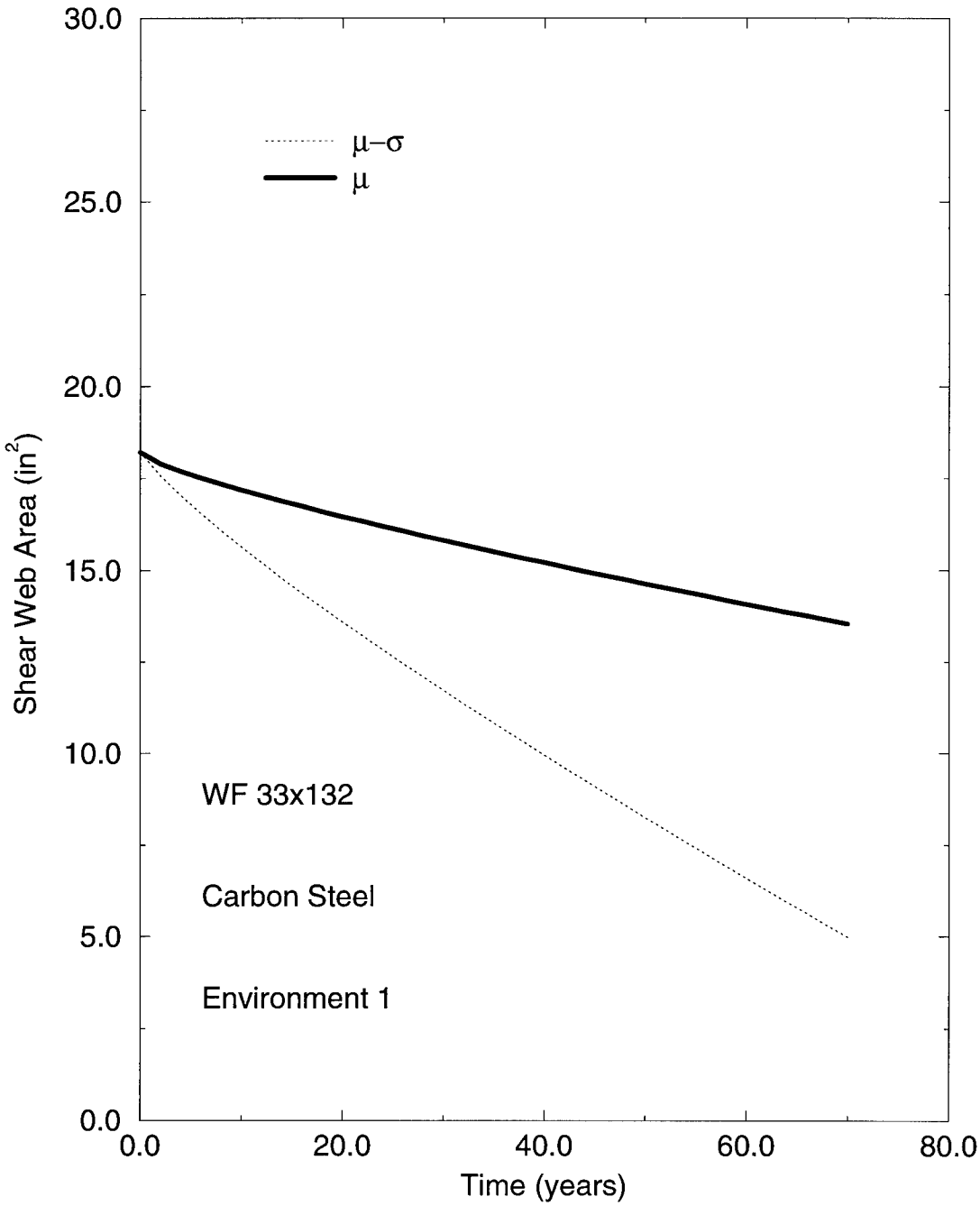

Figure 5.48: **Deterioration of the Web Area A_w Due to Corrosion at the Support of an Interior-Exterior Girder**

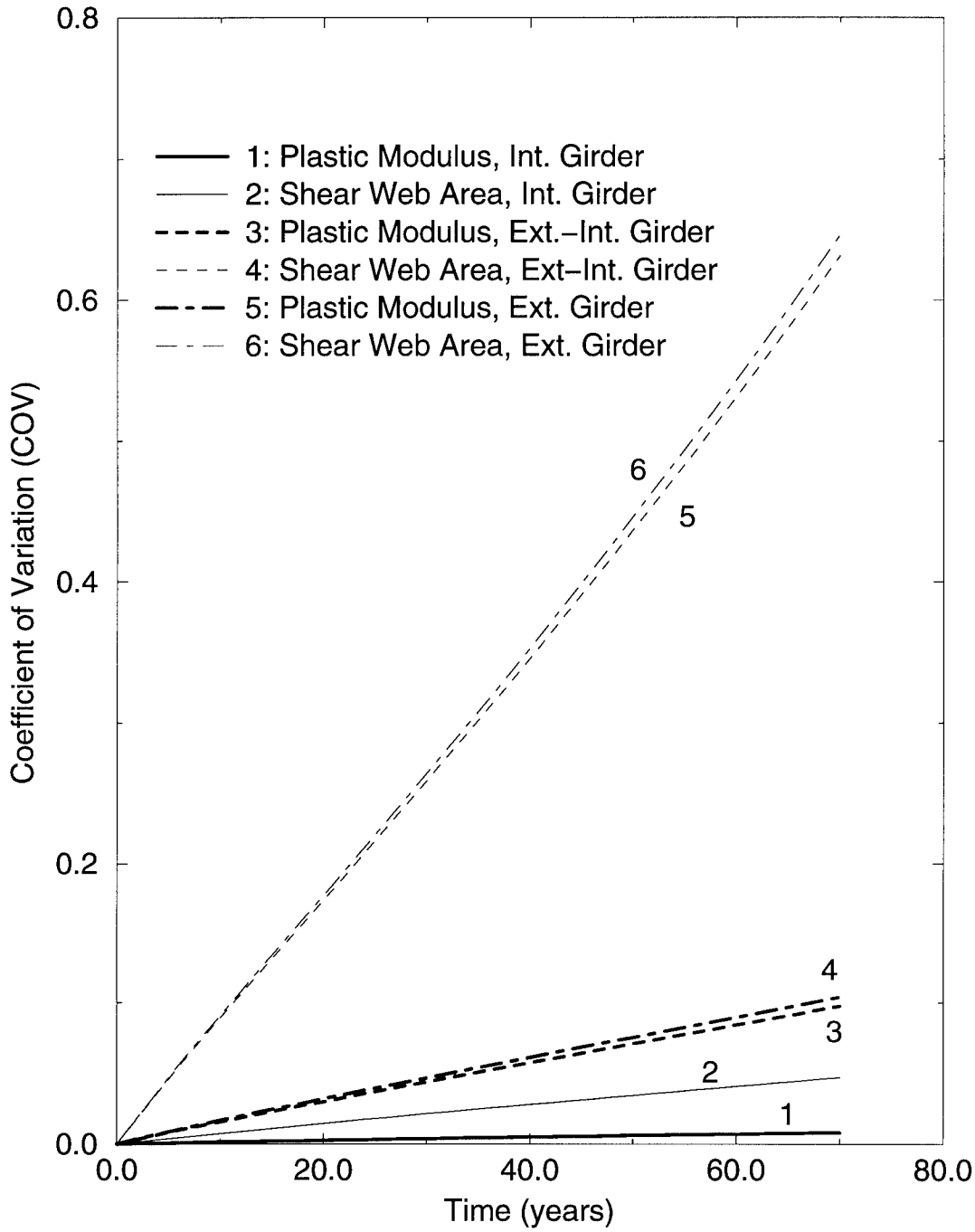

Figure 5.49: **Coefficient of Variation over Time for the Plastic Section Modulus Z and the Web Area A_w for Corroding Girders in Bridge E-17-AH**

locations, the results provide only a rough idea of corrosion propagation. Once the samples were classified by material and environment type, the number of test samples in any single category was very small. The corrosion parameters A and B that were used for the interior girders for example (i.e., carbon steel in a rural environment (environment 1)) were based on only two samples located in Saylorsburg, Pennsylvania and Olpe, Federal Republic of Germany. Hopefully further study will provide a larger number of cases from which to obtain data.

5.10 System Reliability Over Time

Having defined limit state equations for the components of the bridge in terms of the random variables and determined their respective reliabilities, Bridge E-17-AH was modeled as a simplified series parallel system as shown in Fig. 5.38. The model included the nine dominant failure modes and required the failure of three adjacent girders for the system to fail. The increase in live load (Section 5.5.2) and the deterioration of the structure over time (Section 5.9) have been modeled. It is now possible to examine the reliability of the system over time.

Using the assumptions listed in Section 5.8, the model in Fig. 5.38, and a correlation between the resistances of the girders of $\rho_{R_i,R_j} = 0.5$, the program RELSYS computed the system and component reliabilities for Bridge E-17-AH assuming a 70 year expected life. Inspections were conducted and the reliability was computed every two years. Figs. 5.50, 5.51, and 5.52 show the time-dependent component and system reliability results. Fig. 5.50 shows the system reliability along with the reliability of the three types of girders with

respect to moment. The interior girder has the lowest initial component reliability, but has the slowest deterioration rate. In fact, there is a crossover point around 60 years where the reliability of the interior-exterior girder becomes less than that of the interior girder. After an initial drop, caused mostly by the increased number of live load occurrences, the system reliability remains relatively flat for 30 years. The system reliability drops almost linearly from there. If a minimum system reliability of $\beta_{min} = 2.0$ was imposed, some type of remedial action would be needed after 50 years.

Fig. 5.51 shows the system reliability and the reliability of the girders with respect to shear. The shear component reliabilities are initially very high but the rapid deterioration of the web area causes the reliabilities of the exterior and interior-exterior girders to drop quickly. After 40 years, the reliability of these girders with respect to shear is below the reliability of the system. This occurs because of the parallel nature of the system model. Because three girders must fail for the system to fail, the interior girder which is not deteriorating as quickly is maintaining the reliability of the system.

Fig. 5.52 shows the system reliability and the component reliabilities of the slab, pier cap, and column footing. These components are all in the series portion of the system model and will therefore always reflect reliabilities that are higher than the reliability of the system. The reliability of the column footing dictates the reliability of the system in the early life of the bridge. While the interior girder moment component reliability was lower than the column footing component reliability, the interior girders are part of

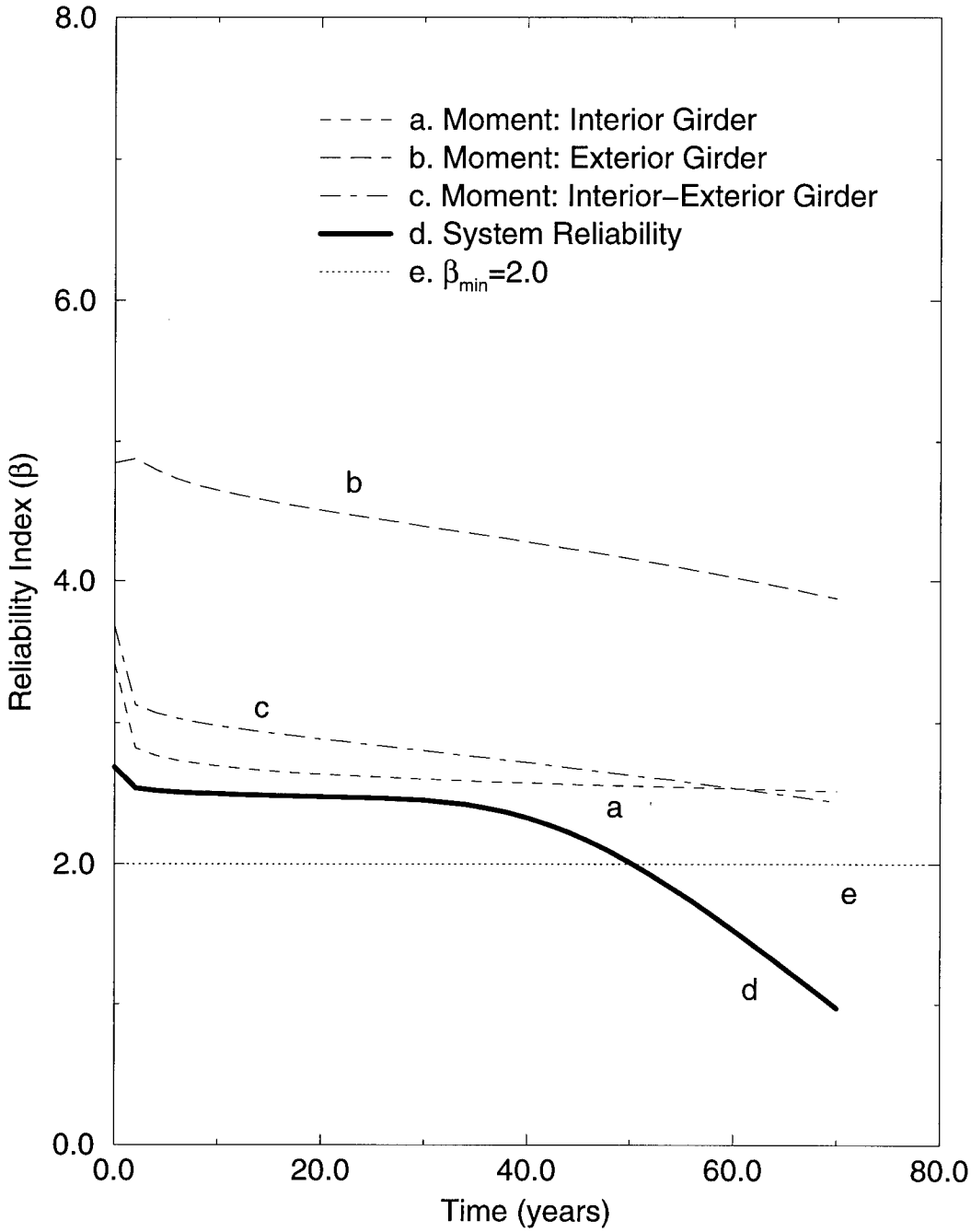

Figure 5.50: **System and Girder Moment Component Reliability Over Time for Bridge E-17-AH**

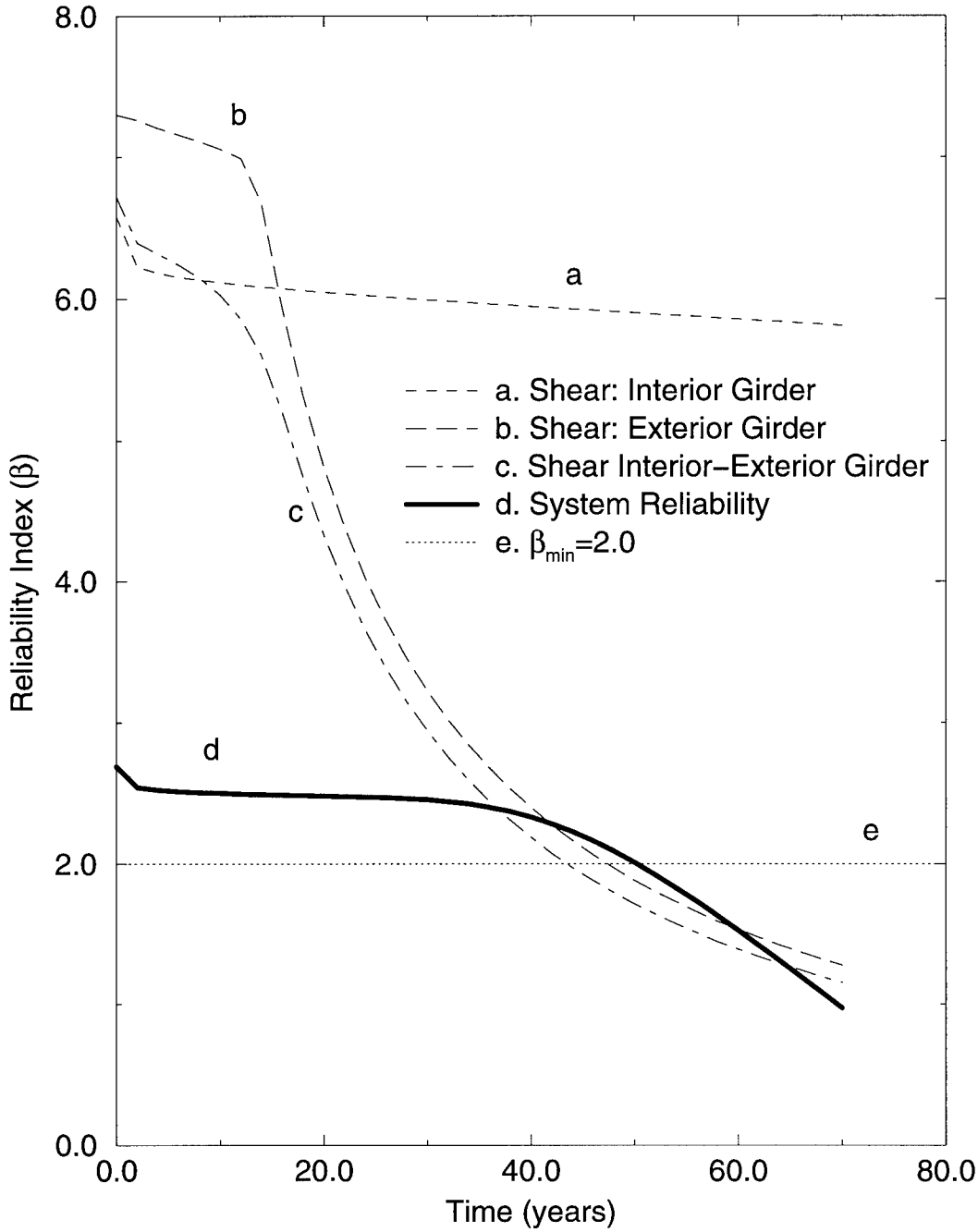

Figure 5.51: **System and Girder Shear Component Reliability Over Time for Bridge E-17-AH**

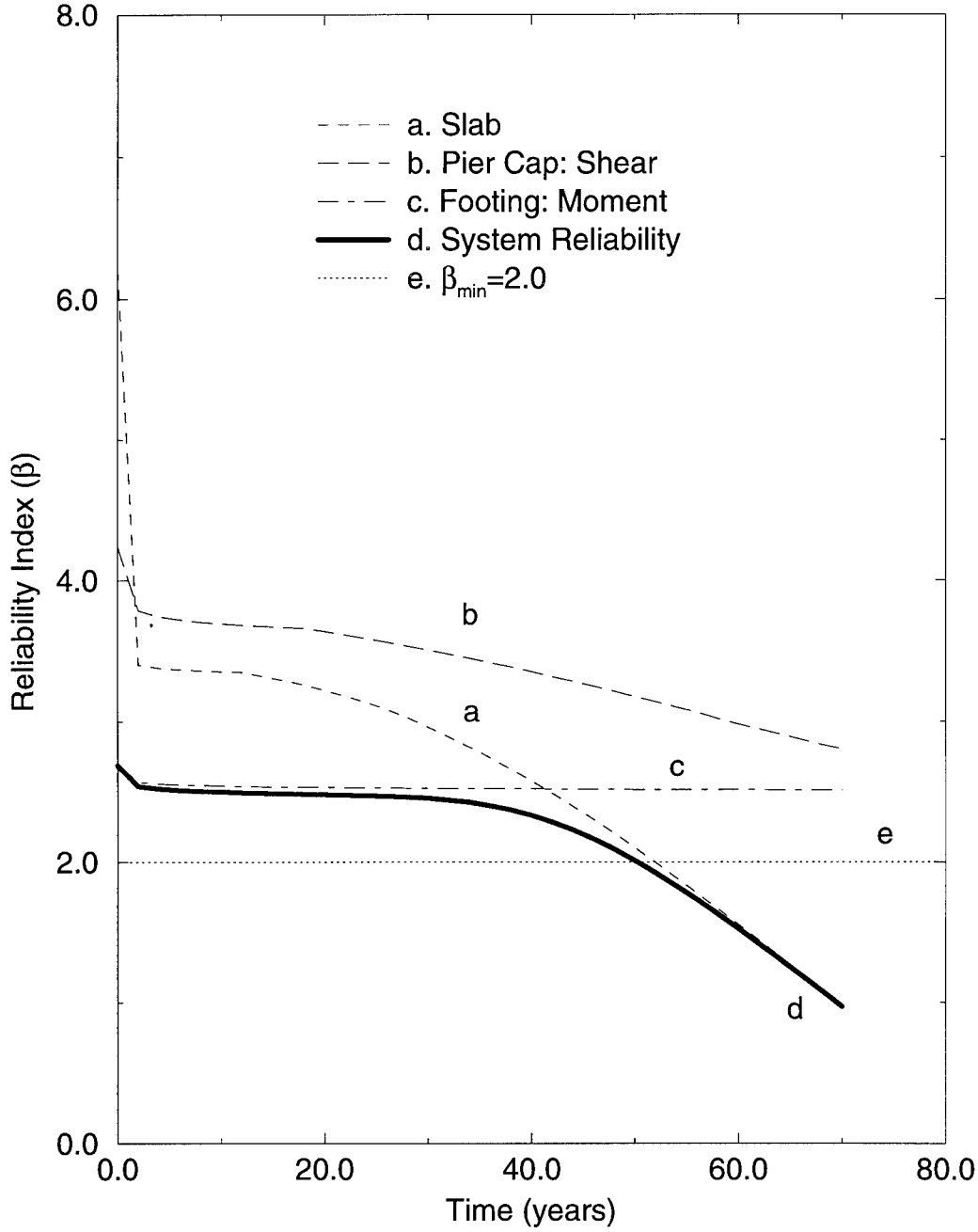

Figure 5.52: **Slab, Pier Cap, and Column Footing Component Reliability and System Reliability Over Time for Bridge E-17-AH**

the parallel portion of the system model. The column footing was assumed to have negligible deterioration relative to the rest of the bridge. Its reliability remains almost constant throughout the life of the structure and only drops due to increased live load. The drop in system reliability later in the life of the structure is due to the deterioration of the concrete slab. The pier cap is not deteriorating as quickly because the surface concentration of chlorides was not as high and only the exterior portions of the reinforcing stirrups are corroding.

Figs. 5.50, 5.51, and 5.52 demonstrate that the reliability of a system depends on the series-parallel model of the system and its deterioration. The component with the lowest reliability may not be the most important component and does not necessarily control the reliability of the system. The most important component early in the life of the structure may not be the most important during the later periods. It is difficult to predict the reliability of the system even if the reliability of all of the components are known, and therefore a repair strategy based solely on component reliabilities would probably be inefficient.

5.11 Repair Criteria and Repair Options

Since system reliability can be computed over the lifetime of a structure, a decision must be made regarding the time when remedial action must be taken. This decision should be based on the reliability of the system rather than the reliability of any of the individual components. The repair criteria should include a minimum system reliability below which the structure must

not be allowed to fall. There could be a dual criteria where one value lists when a structure should be repaired subject to availability of funds and a second value where a structure absolutely must be repaired to ensure public safety.

The repair criteria are statements of acceptable risk. Such an analysis includes assessing the importance of the structure, the cost of failure, and the costs of performing the repairs. The analysis must also incorporate the assumptions and model used to compute the reliability. Many studies have been completed which assess the reliability of current design codes. Lin [1995], for example, concluded that a reinforced concrete T-beam designed by AASHTO specifications would have a reliability between $\beta = 3.0$ and $\beta = 3.5$. The study used a deterministic HS-20 truck as the live load. As indicated in Fig. 5.50, the initial system reliability of this bridge is only $\beta_{sys} = 2.7$ but there were a number of assumptions which produced that value to include the use of the Nowak live load model as described in Section 5.5.2.

Establishing a minimum allowable system reliability $\beta_{min} = 3.0$ would clearly be unrealistic for Bridge E-17-AH since it would need to be repaired or replaced on the day it was built. This study does not undertake the failure cost analysis that would be needed to establish a minimum allowable system reliability β_{min}. Rather the arbitrary criterion that $\beta_{min} = 2.0$ is established. An alternative criterion could be used and its effect on the repair strategy can easily be seen from the figures that will follow. For this study, whenever the system reliability of the bridge β_{sys} falls below $\beta_{min} = 2.0$, a repair or replacement action must take place.

With the repair criterion established, the repair options and their associated costs must be developed. A technique was introduced and illustrated in Chapter 4 which established a $\beta_{threshold}$ value for components which was varied until an optimum solution was found. All components whose individual reliabilities were below $\beta_{threshold}$ were repaired and those whose reliabilities were above $\beta_{threshold}$ were not repaired at the point where β_{sys} fell below the minimum allowable value. While this technique worked well for the trusses in Chapter 4, it did not work well for this particular bridge.

The failure modes and the failure actions were not easily separated. For example, when the pier cap was repaired for shear, it was also repaired for positive and negative moment. Also, if one decided to replace all of the girders to improve their shear and moment strength, the slab would be replaced as well due to the natural sequence of construction. For Bridge E-17-AH, the better approach was to define distinct repair options and try all possible combinations of those options to determine an optimum strategy.

The development of realistic repair options involved some real-life constraints. For example, Bridge E-17-AH has a sufficiency rating of 60.8 out of a possible 100. It has been declared to be functionally obsolete because the roadway width is only 40 feet (12.2 m). For a repair project to qualify for federal funding, the sufficiency rating would have to be raised to at least 80 and the repair should last at least 10 years [White 1996]. Painting the steel girders to delay corrosion would ordinarily be a reasonable maintenance option. Given the environmental restrictions involving the lead-based paint

currently on the girders, that option is prohibitively expensive.

Merely replacing portions of the existing bridge in their current form would not meet the National Bridge Replacement and Rehabilitation Program funding requirements [FHWA 1988b], which could realistically determine whether or not a project will be approved. A significant redesign and widening of the bridge would be required. Similarly, the load rating on this bridge is only HS 17.8 due to serviceability of the girders as illustrated in Section 5.3.4. Modern bridges should have a minimum load rating of HS 20 and most are being designed for HS 25. A replacement of the superstructure would probably include a redesign to incorporate larger girders, continuous girders, or some type of composite action between the girders and slab to boost the load rating. The considerations of obtaining federal money, correcting vulnerability and safety deficiencies, and the need for redesign all affect the real world selection of repair options.

Since this study specifically chose not to undertake the broader and more complex issues of design and to deliberately neglect those repairs not associated with deterioration, the problem was simplified to exclude those considerations. For the purpose of this study, it was assumed that Bridge E-17-AH was adequate in all respects and that a replacement bridge would be of the same type. Given the existing bridge and deterioration models, five realistic repair options and their present day costs were developed in consult with the Colorado DOT. Using expert opinion [Wilson 1996, White 1996], historical cost data for actual bridge repairs [CDOT 1994, CDOT 1995a], and

the actual original cost of the bridge ($393,000 in 1942), the repair options and costs are shown in Table 5.19, along with the limit state equations affected by the repair. The sources conflicted on some cost estimates so a reasonable compromise was reached in each case.

Table 5.19: **Repair Options and Associated Repair Costs for Bridge E-17-AH (Using 1996 U.S. Dollars)**

#	Repair Option	Repair Cost ($)	Limit State Eqns.
0	Do nothing	0	none
1	Replace deck	225,600	$g(1)$
2	Replace exterior girders	229,200	$g(4,5,6,7)$
3	Replace exterior girders and deck	341,800	$g(1,4,5,6,7)$
4	Replace superstructure	487,100	$g(1,2,3,4,5,6,7)$
5	Replace bridge	659,900	all

Option 1 is to replace the entire deck which would include the concrete slab, sidewalk, guardrails and fresh layer of asphalt. The replacement of a portion of the slab was not considered because the slab sections were assumed to be perfectly correlated in the simplified series-parallel model of the bridge. Option 2 is to replace the exterior and interior-exterior girders which are deteriorating faster than the interior girders. The options include replacement of four girders, sidewalk, guard rails, and only that portion of the

slab above the replaced girders. Option 3 is the same as option 2 except the entire deck is replaced. Option 4 is to replace the entire superstructure which includes all nine girders and the entire deck as described in option 1. Finally, option 5 is to replace the entire bridge using the current design.

5.12 Optimum Lifetime Repair Strategy

An optimum repair strategy can be developed by using all feasible combinations of the repair options listed in Table 5.19. The various options are tried until replacement of the bridge is the only remaining option. For any expected life of the structure, an optimum repair strategy is determined. The repair criterion $\beta_{min} = 2.0$ is first applied to Bridge E-17-AH using the simplified series-parallel model shown in Fig. 5.38 and the live load and deterioration models used in Section 5.10. Figs. 5.50, 5.51, and 5.52 reflect option 0 which is to do nothing. Under this option, the bridge will last 50 years before some action is required.

Fig. 5.53 shows the effect of continuously repairing the slab (option 1). Fig. 5.53 is a combination of Figs. 5.50, 5.51, and 5.52 except that the bridge system is being repaired whenever β_{sys} falls below $\beta_{min} = 2.0$. The only component being repaired is the slab which gets replaced at year 50 and year 94. The slab is repaired again at year 106 but the repair does not cause the system reliability to rise above 2.0 at which point some repair other than replacing the deck must be made.

The same analysis is completed for replacing the entire superstruc-

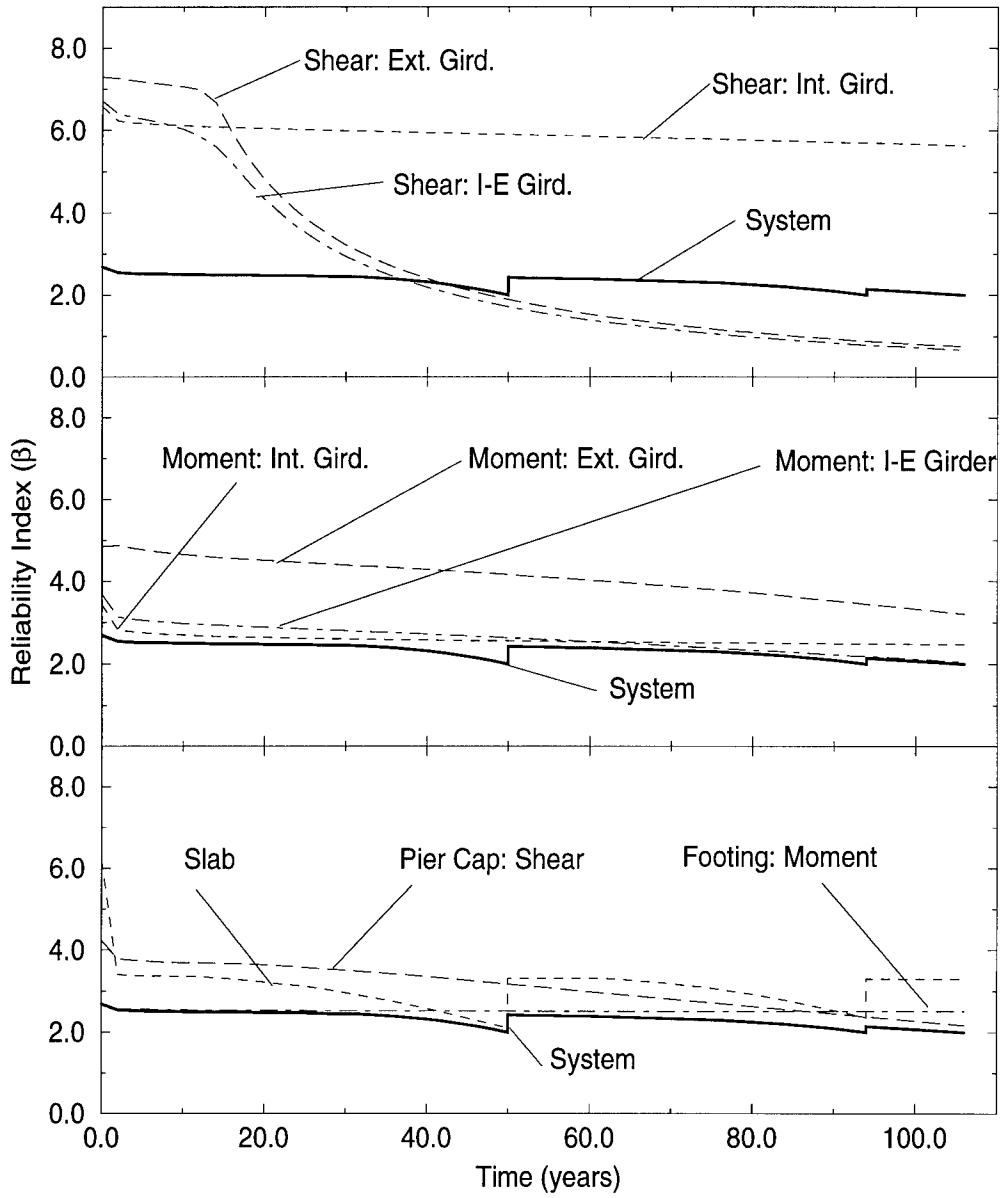

Figure 5.53: **Results of Repair Option 1 on Bridge E-17-AH Using Simplified Series-Parallel Model Requiring the Failure of Three Adjacent Girders**

ture (option 4) as shown in Fig. 5.54. In this example, seven of the nine components are being repaired whenever the system reliability index falls below 2.0. In fact, everything except the pier cap and column footings are being repaired. Surprisingly, this has little effect on the system reliability relative to repairing the slab. The superstructure is replaced at year 50 and year 94. The only difference is that the system reliability does not fall below 2.0 until year 108 instead of year 106. It appears that replacing the superstructure would be a waste of money and resources, relative to replacing the deck.

The optimum repair strategy for any expected life of the structure can be found from Fig. 5.55 where all feasible options and their associated costs are considered. The costs are computed using the present day (1996) costs listed in Table 5.19 discounted over time using an discount interest rate of 2%. The present value cost C_{PV}, for example, of replacing the deck at year 50 is computed as

$$C_{PV} = \frac{C_{rep}}{(1+r)^n} = \frac{\$225,600}{(1+0.02)^{50}} = \$83,813 \tag{5.101}$$

where C_{rep} is the cost of the repair option as shown in Table 5.19, r is the discount rate, and n is the number of years in the future that the repair will be made.

The discount rate used is the difference between the return obtainable from a risk-free investment such as short term government securities and the rate of inflation. Historically, this rate has been around 2-3% [Weston and Brigham 1981]. Other organizations use higher discount rates in their cost benefit analysis to reflect the lowest rate of return that knowledgeable investors

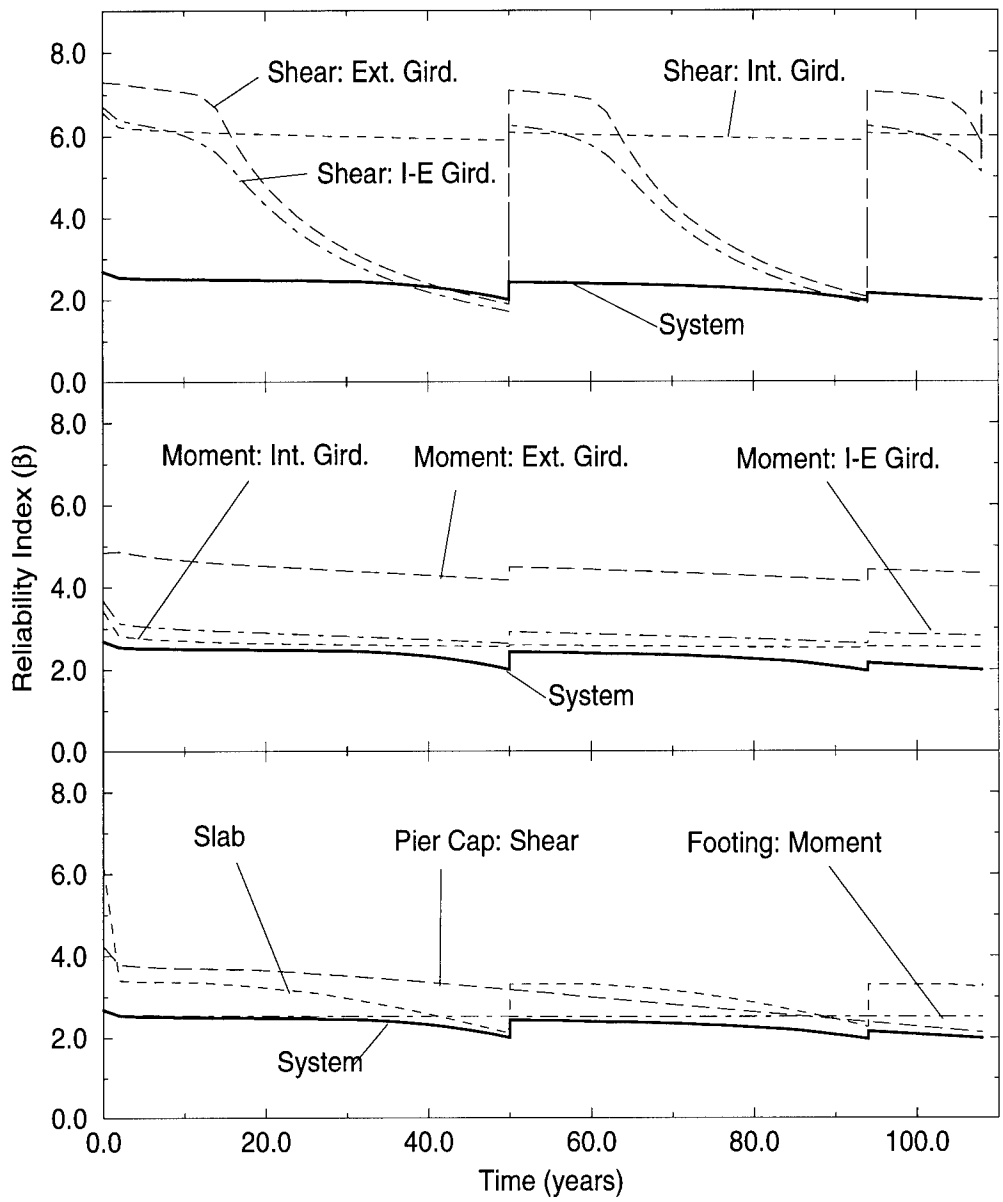

Figure 5.54: **Results of Repair Option 4 on Bridge E-17-AH Using Simplified Series-Parallel Model Requiring the Failure of Three Adjacent Girders**

will accept in the investment market. These rates include AASHTO (4-5%), U.S. Department of Agriculture (4%), Wisconsin and Pennsylvania Departments of Transportation (6%), and the Office of Management and Budget (10%) [FHWA 1989].

Fig. 5.55 shows that options 1, 3, and 4 yield the same benefit in extended life for different costs, where option 1 is the most economical. Therefore, for subsequent repairs, options 3 and 4 for the initial repair were eliminated from consideration. Option 2 was not considered because it did not improve the system reliability of the bridge above $\beta_{min} = 2.0$. The process was continued until there was no choice but to replace the bridge. The optimum lifetime repair strategy based on Fig. 5.55 is summarized in Table 5.20. It is unrealistic to believe that one would choose a more expensive repair strategy just to obtain two extra years of useful life (i.e., 106-108 years), but the analysis does reflect option 3 as the optimum second repair for that very small increase in the expected life span.

A change in the random variables, the structure model, or the deterioration model can change these results significantly. The expected life of the bridge given the repair options and the models used was at most 108 years before the bridge had to be replaced. This was dictated by the diminishing reliability of the pier cap whose steel was corroding due to chloride penetration of the concrete. If just one critical variable, such as the rate of corrosion, i_{corr}, from Eq. 5.92 is varied, the results would be much different. Fig. 5.56 shows the results for replacing the deck (option 1) when the corrosion rate parameter

Table 5.20: **Optimum Lifetime Repair Strategy for Bridge E-17-AH Using Simplified Series-Parallel Model Requiring Failure of Three Adjacent Girders**

Expected Life (years)	Optimum Repair Strategy	Cost ($)
0-50	Do nothing	0
50-94	1@50	83,813
94-106	1@50, 1@94	118,881
106-108	1@50, 3@94	136,945
>108	1@50, 5@94	186,393
1@50 indicates option 1 (replace deck) at year 50		

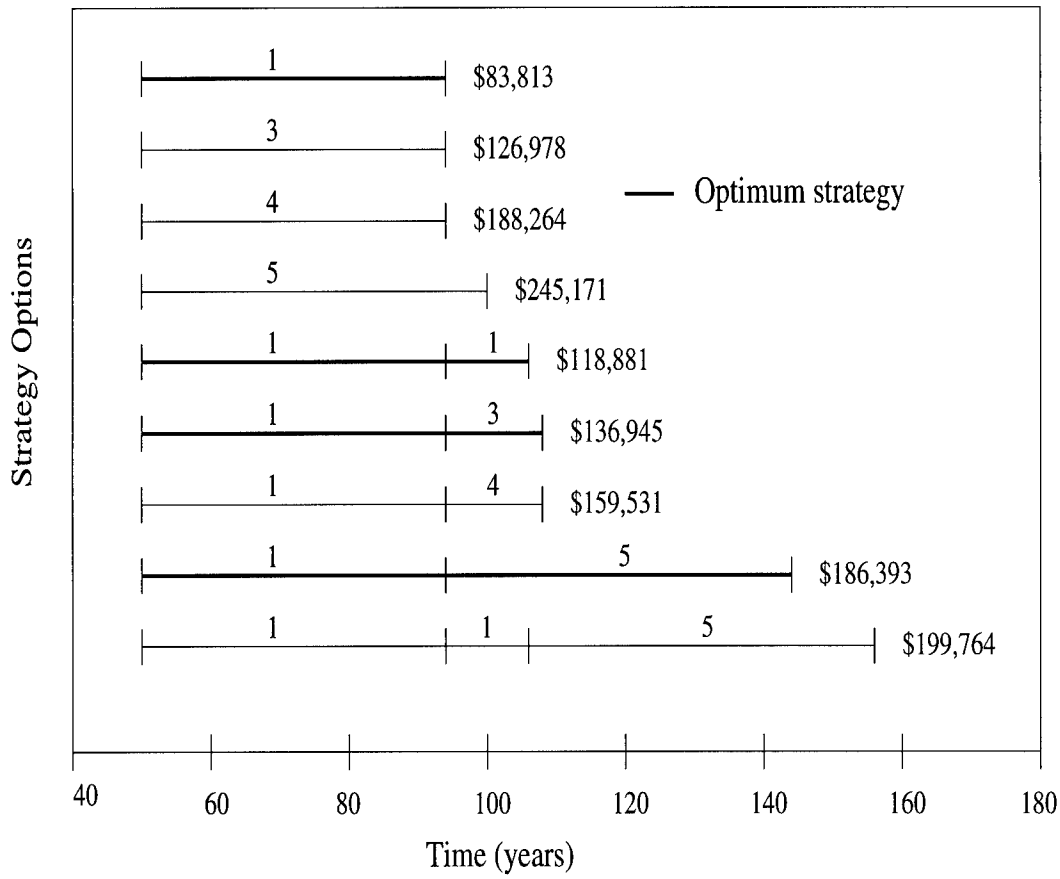

Figure 5.55: **All Feasible Repair Options For Bridge E-17-AH Using Simplified Series-Parallel Model Requiring the Failure of Three Adjacent Girders**

i_{corr} is halved from $i_{corr} = 0.098$ as shown in Table 5.14 to $i_{corr} = 0.049$ for the pier cap. The life of the bridge is extended from 104 years (Fig. 5.53) to 180 years where additional slab repairs sufficiently improve the bridge system reliability since the pier cap is not deteriorating as fast. The slab is repaired at year 52, year 100, and year 146. At year 180, the deck replacement is no longer sufficient due to the diminished reliability of the pier cap.

The results of all possible options are shown in Fig. 5.57. Again the parallel nature of the series-parallel model that requires three adjacent girders to fail renders the replacement of the girders or superstructure an ineffective option. The optimum lifetime repair strategy based on Fig. 5.57 is summarized in Table 5.21. Clearly, varying other variables would have produced a different strategy while there are some variables that could be modified with no change in the results.

If the series-parallel model of the system is revised to consider that the failure of only two adjacent girders constitutes failure of the system as shown in Fig. 5.40, the repair strategy will change. The effect of repairing the exterior girders will be more important to the system reliability. In the previous model (Fig. 5.38), the bridge would not fail until an interior girder failed. Using the two adjacent girder model and the original pier cap corrosion rate, Fig. 5.58 shows the results for option 1 if only the deck is replaced. The slab is replaced at year 50 and a second slab repair at year 70 is not sufficient to meet minimum system reliability requirements. Fig. 5.59 shows the effect of replacing the slab at year 50 (option 1) and replacing the slab and exterior

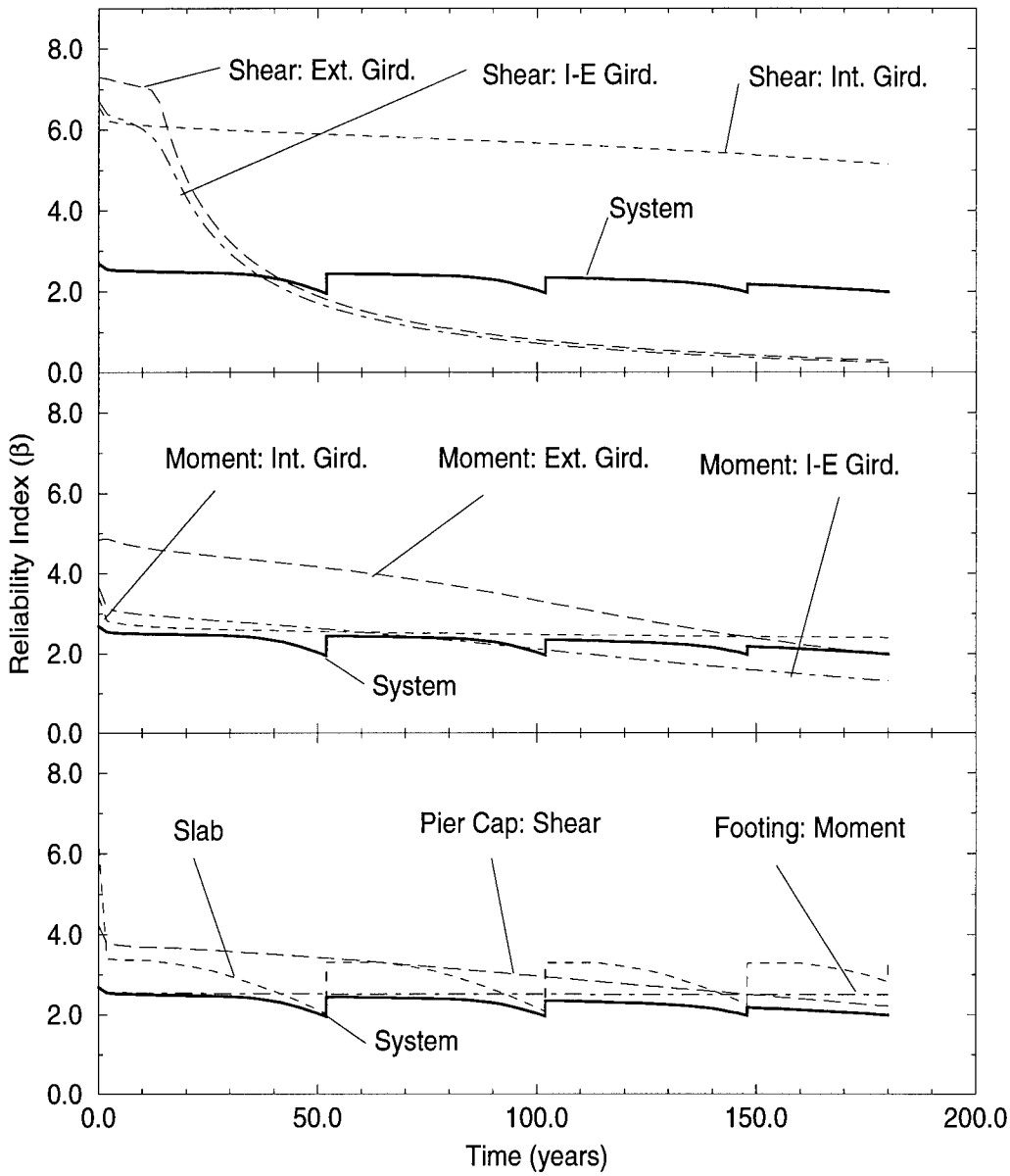

Figure 5.56: **Results of Repair Option 1 on Bridge E-17-AH Using Simplified Series-Parallel Model Requiring the Failure of Three Adjacent Girders and the Corrosion Rate of the Pier Cap is Halved** ($i_{corr} = 0.049$)

Table 5.21: **Optimum Lifetime Repair Strategy for Bridge E-17-AH Using Simplified Series-Parallel Model Requiring Failure of Three Adjacent Girders and the Corrosion Rate of the Pier Cap is Halved**

Expected Life (years)	Optimum Repair Strategy	Cost ($)
0-52	Do nothing	0
52-100	1@52	80,562
100-146	1@52, 1@100	111,695
146-180	1@52, 1@100, 1@146	124,216
180-186	1@52, 1@100, 1@146 4@180	138,001
>186	1@52, 1@100, 1@146 5@180	142,891
1@52 indicates option 1 (replace deck) at year 52		

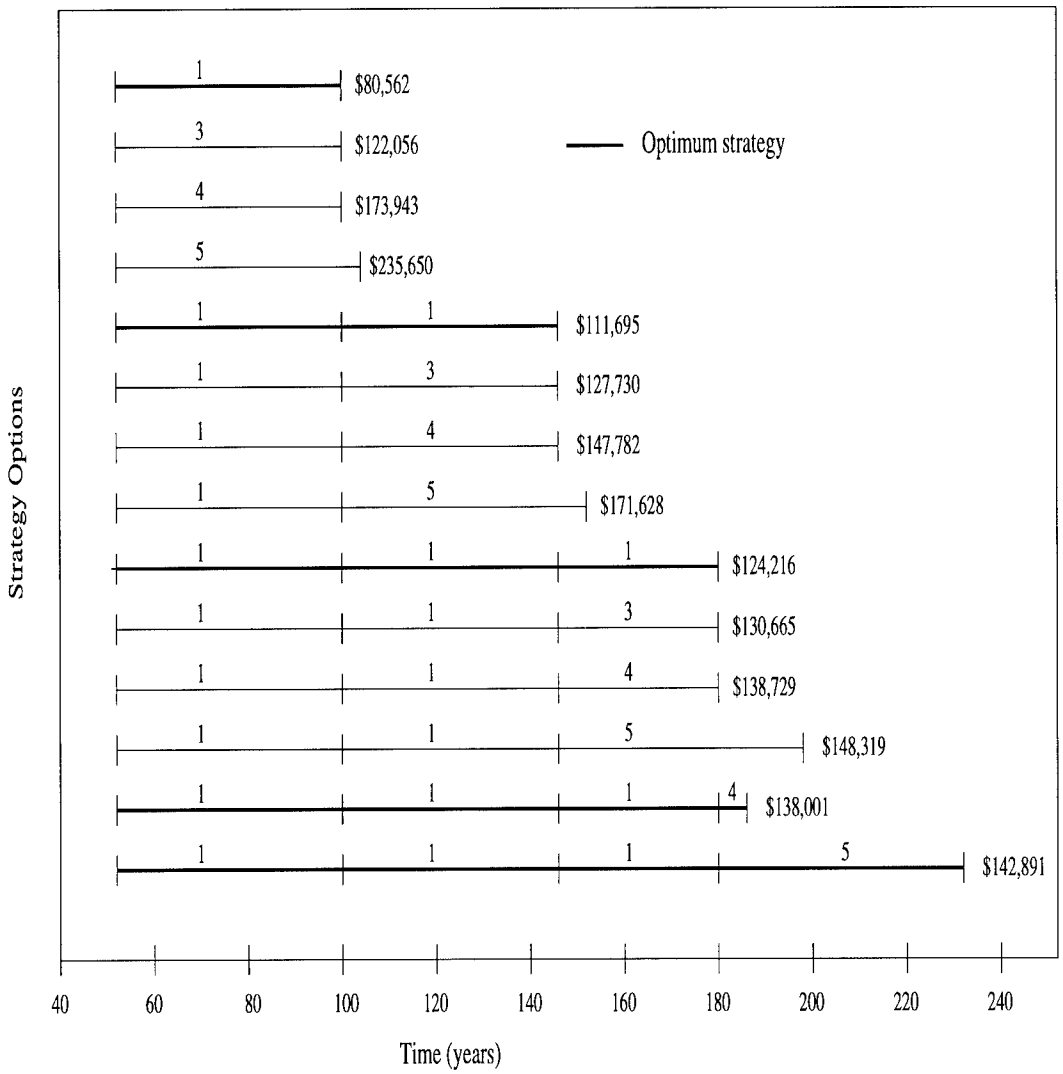

Figure 5.57: **All Feasible Repair Options For Bridge E-17-AH Using Simplified Series-Parallel Model Requiring the Failure of Three Adjacent Girders and the Pier Cap Corrosion Rate is Halved**

girders at year 70 (option 3). The repair effect lasts until year 102 when the pier cap deterioration becomes dominant.

The number of competitive repair options is greater using this model as shown in Fig. 5.60. The optimum repair strategy for any expected life for the two adjacent girder series-parallel model from Fig. 5.40 is summarized in Table 5.22.

Table 5.22: **Optimum Lifetime Repair Strategy for Bridge E-17-AH Using Simplified Series-Parallel Model Requiring Failure of Two Adjacent Girders**

Expected Life (years)	Optimum Repair Strategy	Cost ($)
0-50	Do nothing	0
50-70	1@50	83,813
70-92	3@50	126,979
92-100	3@50, 1@92	163,458
100-104	1@50, 3@70	169,269
104-106	1@50, 4@70	205,588
>106	3@50, 5@92	233,685
1@50 indicates option 1 (replace deck) at year 50		

When competitive repair options are present, the prevailing discount rate could affect the outcome. The results in Fig. 5.60 and Table 5.22 are based on a discount rate of 2%. Higher discount rates tend to make repairs made late

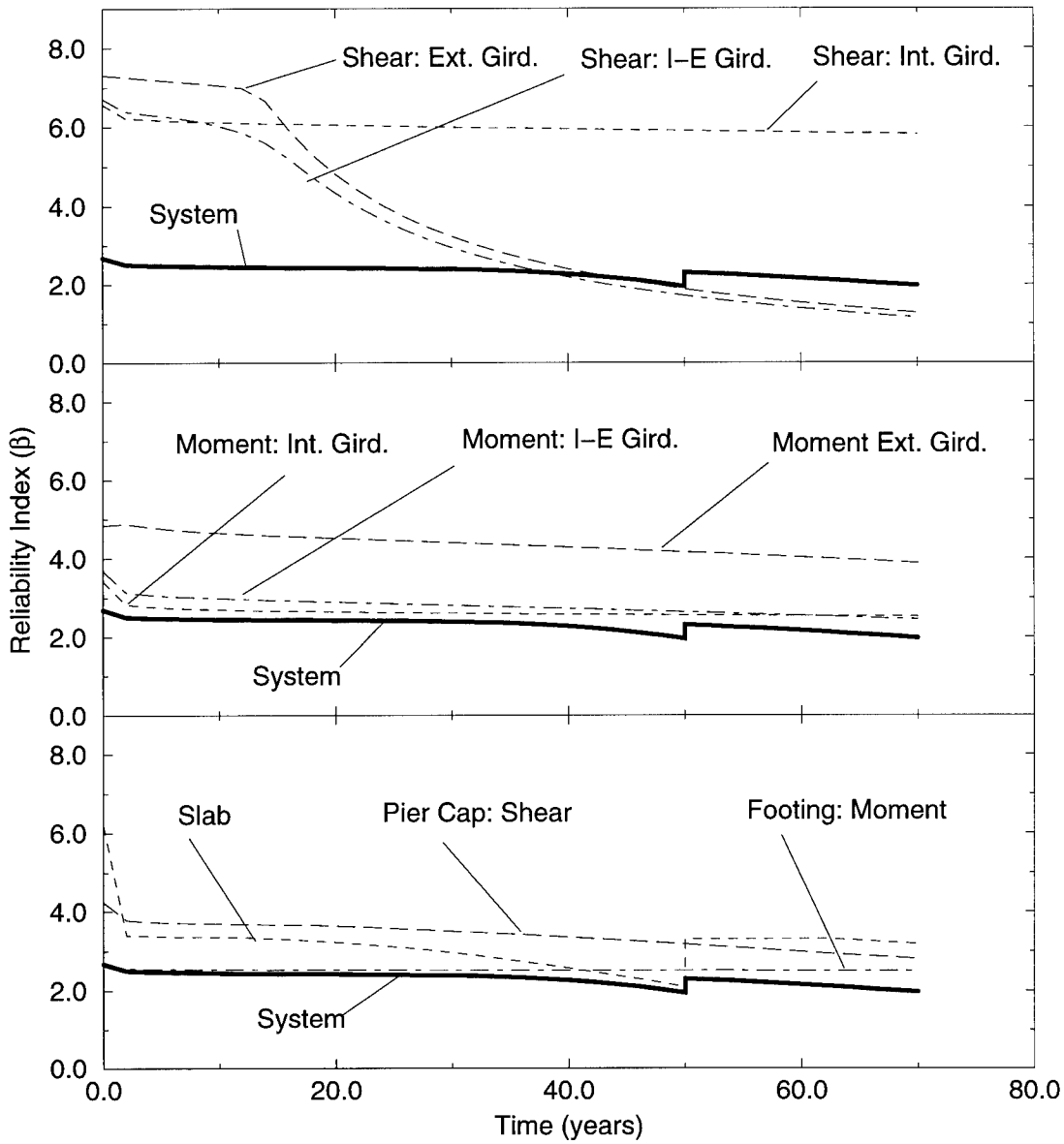

Figure 5.58: **Results of Repair Option 1 (Replace Slab) on Bridge E-17-AH Using Simplified Series-Parallel Model Requiring the Failure of Two Adjacent Girders**

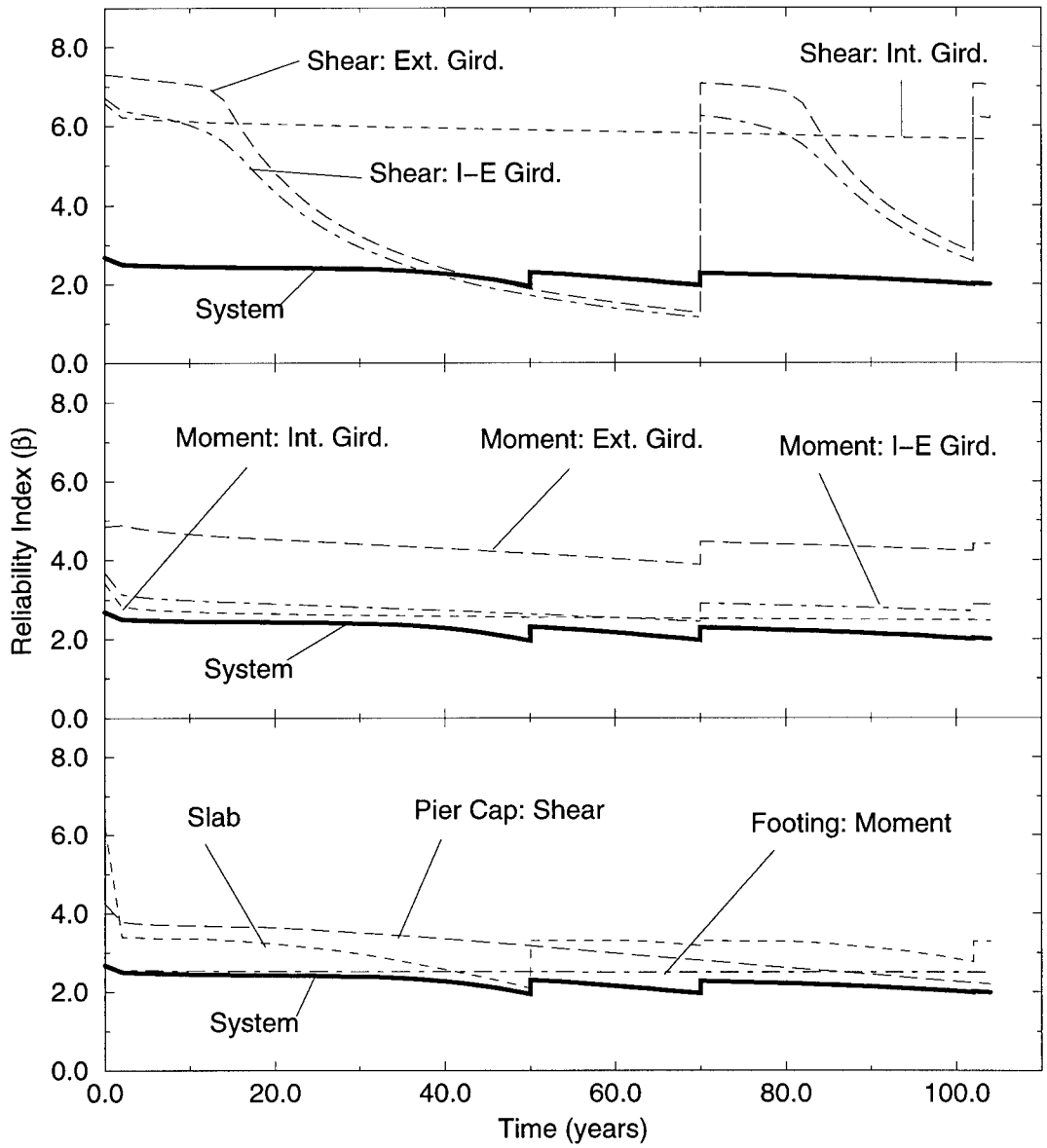

Figure 5.59: **Results of Repair Option 1 (Replace Slab) Followed By Repair Option 3 (Replace Slab and Exterior Girders) on Bridge E-17-AH Using Simplified Series-Parallel Model Requiring the Failure of Two Adjacent Girders**

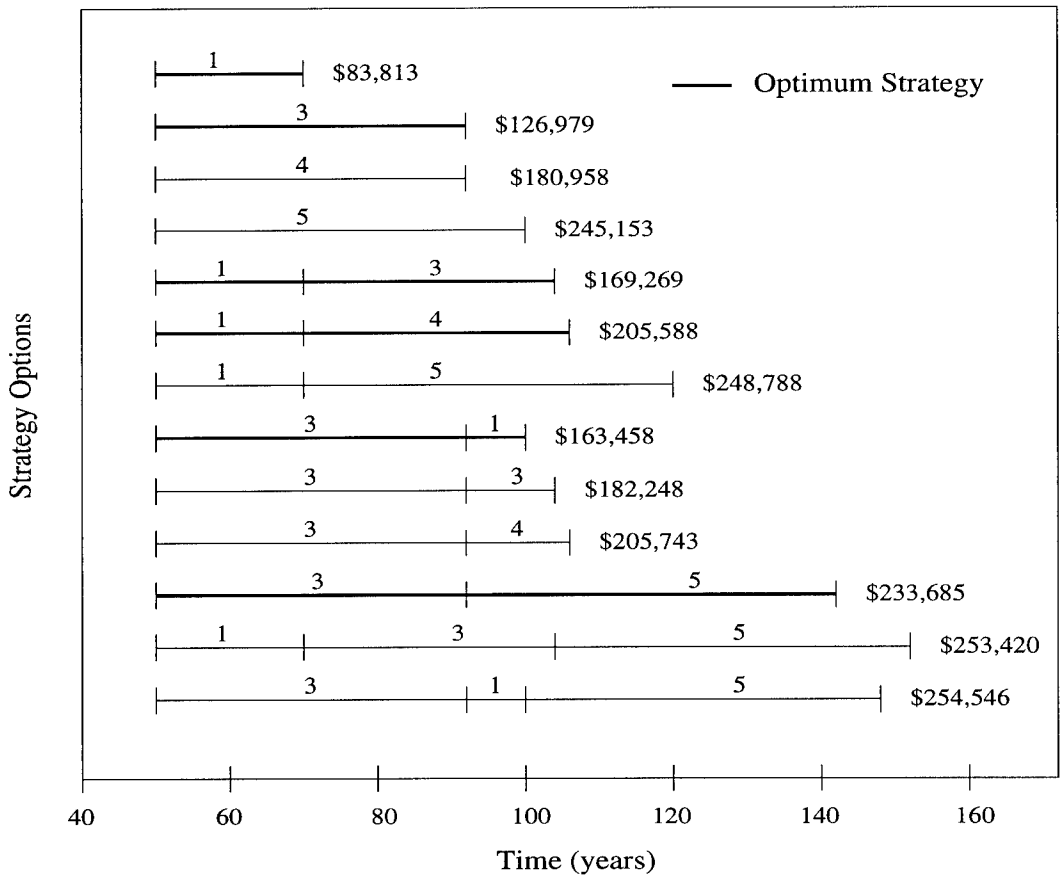

Figure 5.60: **All Feasible Repair Options For Bridge E-17-AH Using Simplified Series-Parallel Model Requiring the Failure of Two Adjacent Girders Using A Discount Rate of 2%**

in the life of the structure more attractive. The available repair options are the same regardless of interest rates. Table 5.23 compares the costs associated with all repair options from Fig. 5.60 for discounts rates ranging from one to six percent.

While the costs associated with each repair option are very different for the three interest rates, their relative attractiveness changes as well. For a discount rate of one percent, the optimum repair strategies are identical to those shown in Table 5.22 for two percent. For the discount rate of three percent, the optimum strategies are almost identical as those shown in Table 5.22. The only difference is for the expected structural life between 104-106 years, the strategy 3@50, 4@92 ($110,065) is more attractive than the 1@50, 4@70 ($112,980) strategy shown in Table 5.22. The jump to 4% offers no new strategy changes.

Once the discount rate jumps to 5% and beyond, it is more advantageous to replace the deck at year 50 and postpone the more expensive repairs as long as possible. At 6%, it is actually less expensive to replace the slab at year 50 (option 1) and then replace the exterior girders and slab at year 70 (option 3) than to just execute option 3 at year 50. The optimum strategy for a discount rate of 6% is shown in Table 5.24 which can be compared to the 2% strategy in Table 5.22. All possible strategies and associated costs using the 6% rate are shown in Fig. 5.61 which can be compared to Fig. 5.60 which reflects the 2% discount rate.

Finally, the repair of the girders becomes even more important, if

Table 5.23: **Cost of Available Repair Strategy for Bridge E-17-AH Using Simplified Series-Parallel Model Requiring Failure of Two Adjacent Girders for Discount Rates of 1% Through 6%**

Repair Strategy	Cost of Strategy ($)					
	$r = 1\%$	$r = 2\%$	$r = 3\%$	$r = 4\%$	$r = 5\%$	$r = 6\%$
Do nothing	0	0	0	0	0	0
1@50	137,165	83,813	51,459	31,745	19,673	12,247
3@50	207,814	126,979	77,965	48,096	29,806	18,556
4@50	296,157	180,958	111,108	68,541	42,477	26,444
5@50	401,219	245,153	150,523	92,856	57,546	35,825
1@50, 3@70	307,484	169,269	94,628	53,695	30,907	18,033
1@50, 4@70	379,887	205,588	112,980	63,026	35,682	20,492
1@50, 5@70	465,993	248,788	134,804	74,123	41,361	23,417
3@50, 1@92	298,122	163,458	92,832	52,209	32,341	19,616
3@50, 3@92	344,637	182,248	100,490	57,358	33,646	20,162
3@50, 4@92	402,800	205,743	110,065	61,295	35,279	20,844
3@50, 5@92	471,972	233,685	121,452	65,978	37,220	21,656
1@50, 3@70, 5@104	541,946	253,420	125,115	64,864	35,035	19,573
3@50, 1@92, 5@100	542,087	254,546	123,319	65,275	37,359	21,561

1@50 indicates option 1 (replace deck) at year 50

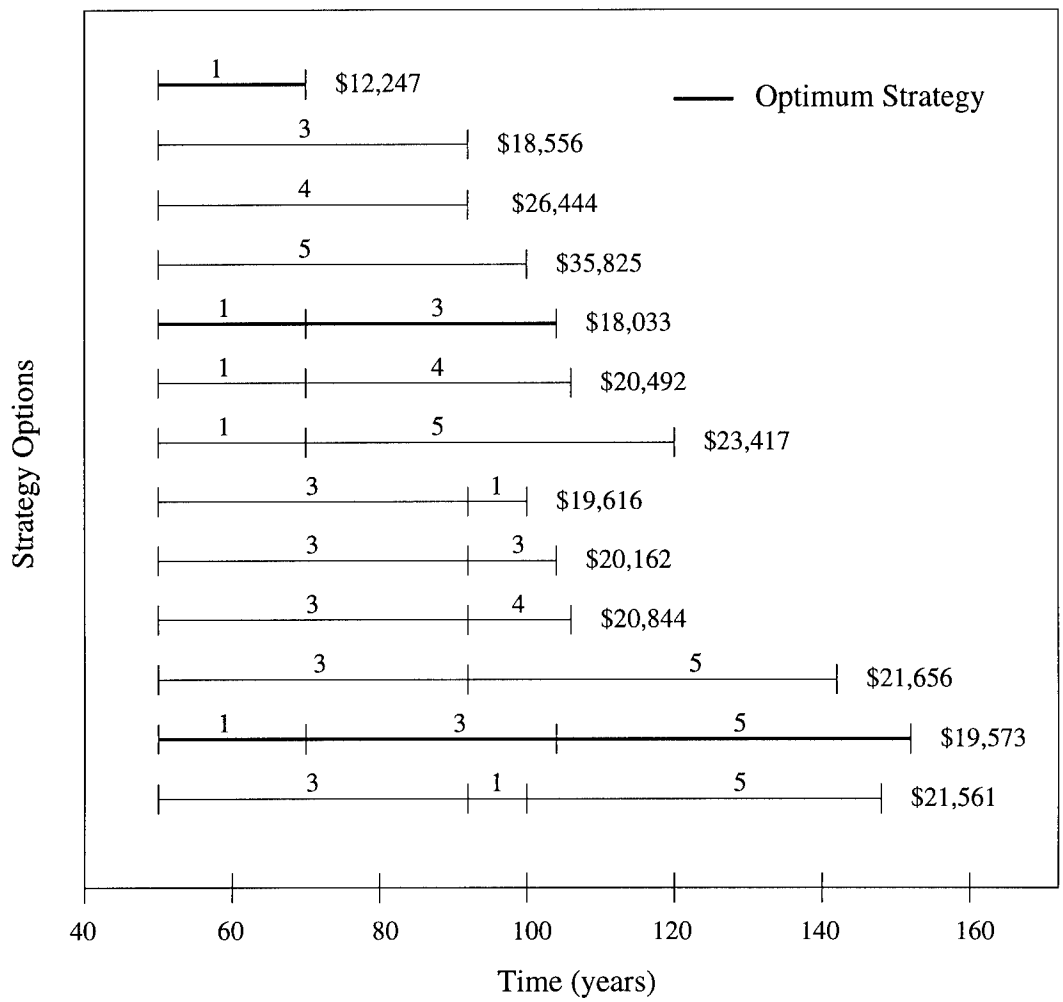

Figure 5.61: **All Feasible Repair Options For Bridge E-17-AH Using Simplified Series-Parallel Model Requiring the Failure of Two Adjacent Girders Using A Discount Rate of 6%**

Table 5.24: **Optimum Lifetime Repair Strategy for Bridge E-17-AH Using Simplified Series-Parallel Model Requiring Failure of Two Adjacent Girders With the Discount Rate Raised to 6%**

Expected Life (years)	Optimum Repair Strategy	Cost ($)
0-50	Do nothing	0
50-70	1@50	12,247
70-104	1@50, 3@70	18,033
>104	1@50, 3@70, 5@104	19,573
1@50 indicates option 1 (replace deck) at year 50		

the bridge is modeled as a series system where the failure of any girder would cause failure of the bridge as shown in Fig. 5.41. For the series system model, Fig. 5.62 shows the system and component reliability for repair option 3 where both the exterior girders and the slab are replaced. The repairs are made at year 32, year 60, and year 74. At year 76, another repair is made but is not sufficient to meet the minimum system reliability constraint. Using this model, the repairs are made sooner in the life of the structure and the effect of the repair on the system reliability is less. The effect of the repair at year 74 is almost undetectable from the graph. Using the series model, replacement of the exterior girders provides more benefit than replacing the deck which was certainly not the case in the two adjacent girder and three adjacent girder models.

The possible repair option combinations and their costs for the two percent discount rate are shown in Fig. 5.63. The replacement costs are greater that the previous cases because the actions are taken earlier in the life of the structure. Table 5.25 provides the optimum repair strategy for any expected life of structure. The optimum bridge replacement time is earlier (i.e., 80 years as opposed to 106 years for the two and three adjacent girder models) for the series model. As these various examples indicate, the reliability analysis results and optimum repair strategy are dependent on the input in the form of the random variables, limit state equations, series-parallel model, and live load and deterioration models.

5.13 Serviceability Flags

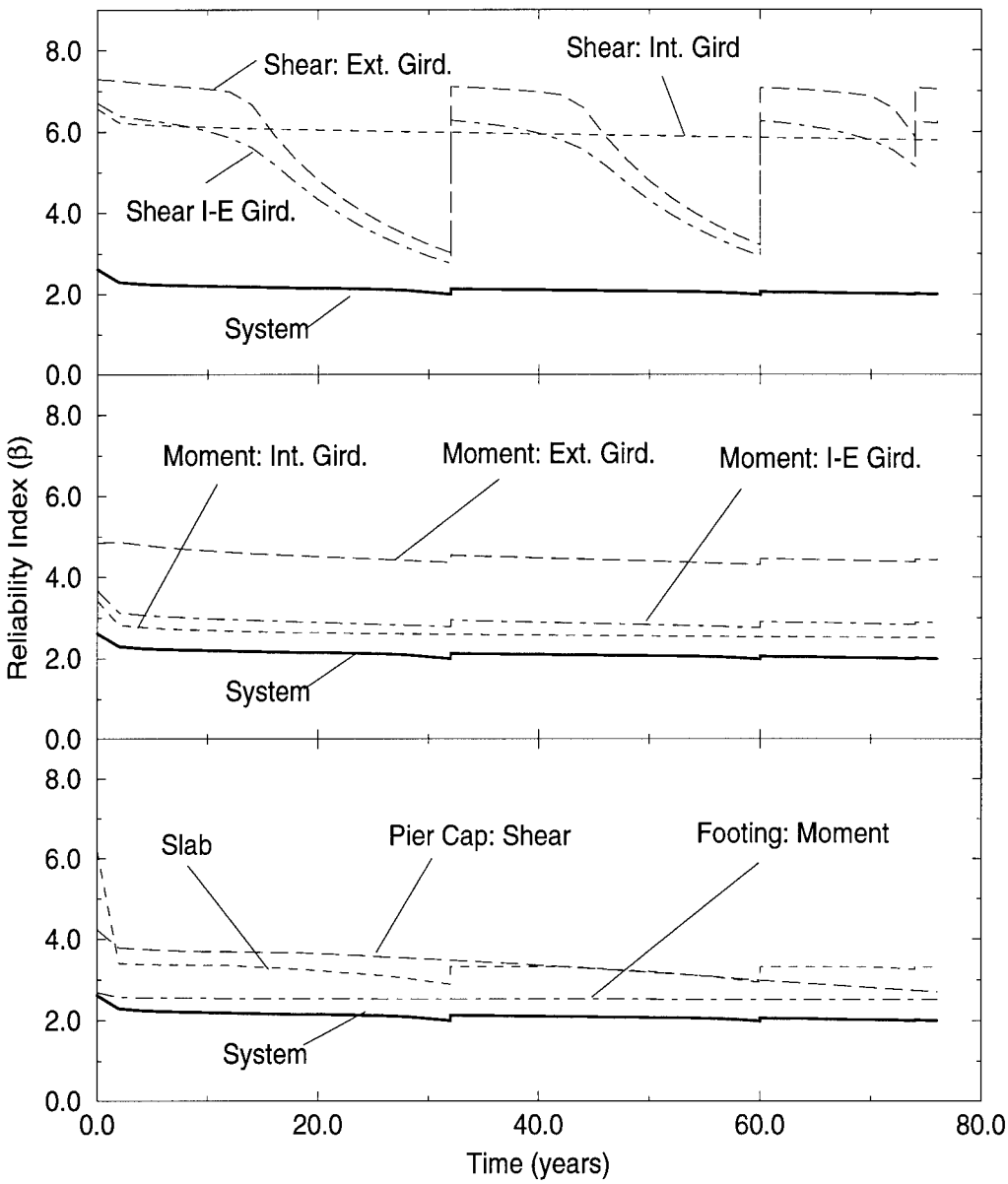

Figure 5.62: **Results of Repair Option 3 (Replace Slab and Exterior Girders) on Bridge E-17-AH Using Simplified Series Model Requiring the Failure of a Single Girder**

Table 5.25: **Optimum Lifetime Repair Strategy for Bridge E-17-AH Using Simplified Series Model Requiring Failure of a Single Girder**

Expected Life (years)	Optimum Repair Strategy	Cost ($)
0-32	Do nothing	0
32-44	2@32	121,613
44-60	3@32	181,359
60-68	3@32, 2@60,	251,219
68-74	3@32, 3@60	285,540
74-80	3@32, 4@60	329,827
>80	3@32, 5@60	382,497
1@50 indicates option 1 (replace deck) at year 50		

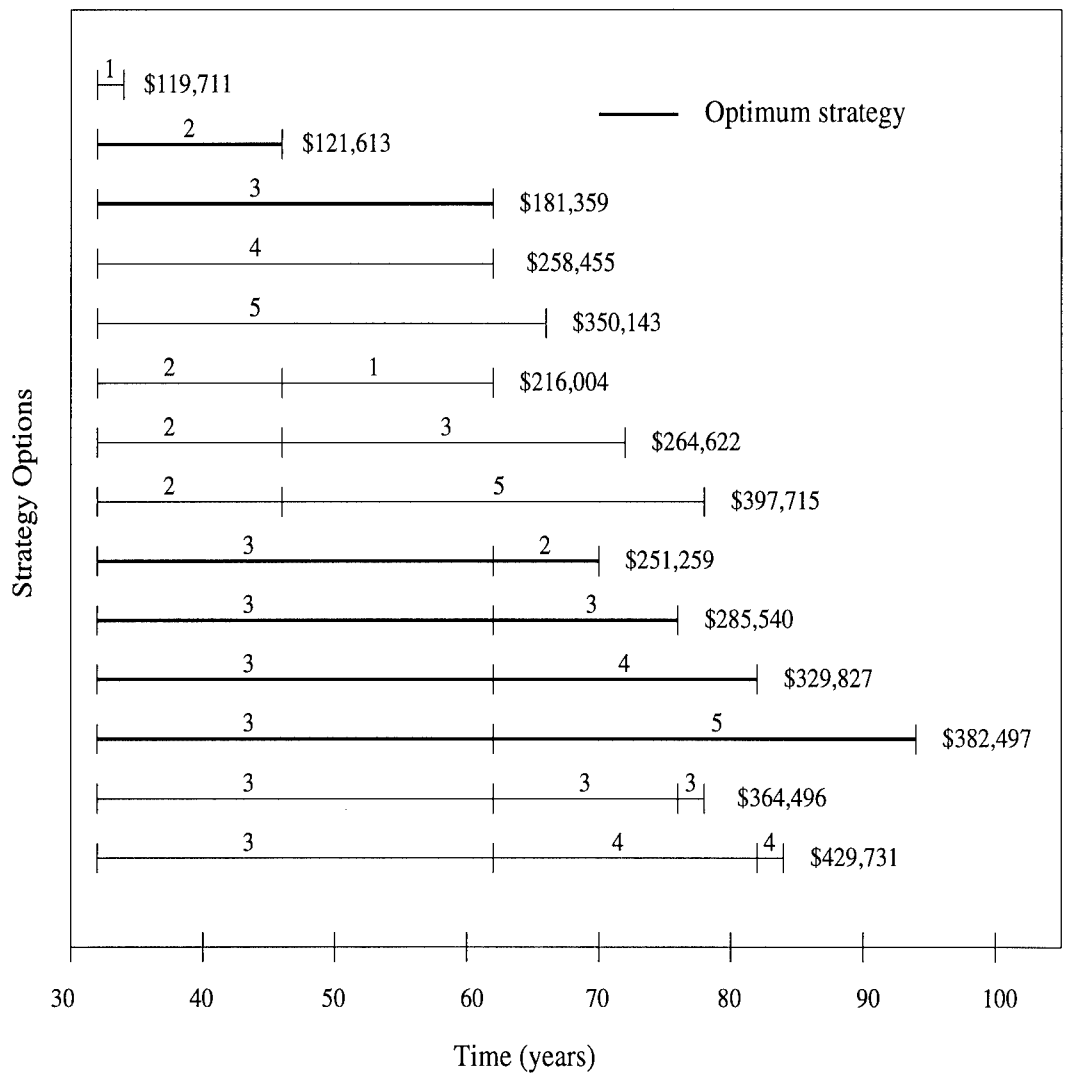

Figure 5.63: **All Feasible Repair Options For Bridge E-17-AH Using Simplified Series Model Requiring the Failure of a Single Girder**

The bridge reliability analysis has focused entirely on strength-based equations. It has not included serviceability concerns such as pot holes in the concrete deck, excessive deflections, or spalling on the concrete columns which may necessitate a bridge repair but which will not cause the bridge to collapse. It is extremely difficult to incorporate these items into a system reliability analysis because the level of concern over serviceability issues is not as high since the cost of failure involves driver discomfort, aesthetics, or public concern, rather than collapse of the bridge. The minimum system reliability index for this bridge is $\beta_{min} = 2.0$ which equates to a notional probability of failure of 0.022 or one chance in fifty. With potholes in a deck, we may be willing to accept a ten percent chance of them occurring or even a fifty percent chance before making the repair. Such disparity is reflected in current design procedures where load and resistance factors are applied to strength-based concerns but not to the serviceability equations. It is difficult to incorporate a serviceability limit state equation into a series-parallel system model when the level of concern regarding that serviceability component is different.

For example, consider a series system for a girder consisting of components relating to failure by shear, moment, and excessive deflection. If the minimum system reliability was established as $\beta_{min} = 2.0$, then the bridge would be overly constrained on its deflections. Conversely, if the system reliability was based on allowing the deflection mode to reach $\beta_{min} = 1.0$, the shear and moment failure modes could become unacceptably low. Using current serviceability criteria, the strength and serviceability modes can not be

incorporated together in a series-parallel model.

A separate system reliability model exclusively for serviceability does not make sense either. In this study, relevant serviceability issues will be included as serviceability flags. A serviceability flag can be inserted by the user to accommodate an additional concern on a structure that is not addressed in the strength-based limit state equations. For example, if the user believes that a deck will have to be replaced every 30 years due to excessive potholes which do not significantly affect the slab strength but which present unacceptable driving conditions, then a serviceability flag is created. The serviceability flag may override the strength-based solution. In this case, the slab would be repaired every 30 years or whenever the strength-based solution dictates, whichever is sooner.

It is up to the engineer to decide which serviceability flags to insert. For Bridge E-17-AH, three potential concerns are addressed. The deck may need to be replaced due to potholes and spalls prior to strength becoming critical. Only the pier cap deterioration is modeled in the analysis of the substructure. The remainder of the substructure is deteriorating but there was no reasonable model available to describe the deterioration. Finally, the steel railing is deteriorating but was not included in the analysis. Therefore, serviceability flags will be used for the concrete deck, the railings, and the substructure, as a whole. In this example, it is concluded that the strength-based analysis of the girders is sufficient and no serviceability flag will be added.

The information source for the serviceability flags will be historical data. A large number of studies have been conducted in many different States to obtain this historical data and use it to provide prediction models. Hearn *et al.* [1995] provides a summary of many of these studies and their accompanying results. Most of these studies and models describe how existing bridges have progressed through prescribed condition states which provide a general description of the bridge's deterioration. The reasons or the mechanisms that caused the deterioration are not addressed in these models. The models merely reflect how a large number of bridges have behaved over time. These models are used for serviceability flags because they are the best way to incorporate all of the non strength-based intangibles that have not or cannot be quantified.

The danger in using these models is that the unique structure being considered and its environment (i.e., Bridge E-17-AH) may be very different from the majority of the structures from which the data was taken. For example, the substructure of Bridge E-17-AH is different from most bridge substructures because a railroad runs underneath the bridge. Many bridges are over water where the substructure is subject to scour and many bridges are over highways where trucks and cars driving underneath expose the substructure to splashed water and pollutants. The substructure of Bridge E-17-AH could reasonably be expected to last longer than the data provided for the average bridge would indicate.

5.13.1 Condition States

Most recent deterioration studies are based on the National Bridge Inventory (NBI) Condition Ratings. As part of the National Bridge Inspection Program, States are required to inspect their bridges every two years and report the results to the Federal Highway Administration (FHWA) in a standardized format of condition ratings. The ratings as listed in Table 5.26 range from a high score of 9 indicating a bridge in excellent condition to a low of 0 indicating a bridge that has already failed [FHWA 1988a]. The FHWA requires separate ratings for the deck, superstructure, and substructure. This rating information, along with other required data on the nation's bridges, comprise the National Bridge Inventory data base from which many of these studies find their data. Some studies attempt to include all bridges into a single model while others break the data down by location, type of bridge, traffic volume, and environment.

As Bridge Management Systems have progressed, many States have developed programs to include much more information than the minimum required by the Federal Government. Attempts to study how different bridge components behave over time have been made for railings, joints, bearings, and all types of decks, girders, and substructures. In many cases, the States have developed their own condition states with more precise descriptions for every bridge element that gets inspected. These individual condition states are then converted to the NBI scale for federal reporting requirements.

In Colorado, for example, which uses the PONTIS Bridge Management System, an asphalt concrete deck is rated according to one of five condi-

Table 5.26: **National Bridge Inventory Condition Ratings, Their Meaning, and Associated Repair Actions**

NBI Rating	Description	Repair Action
9	Excellent condition	None
8	Very good condition	None
7	Good condition	Minor maintenance
6	Satisfactory condition	Major maintenance
5	Fair condition	Minor repair
4	Poor condition	Major repair
3	Serious condition	Rehabilitate
2	Critical condition	Replace
1	Imminent failure condition	Close bridge and evaluate
0	Failed condition	Beyond corrective action

tion states list in Table 5.27 [PONTIS, 1995]. Such reporting has allowed the data for specific bridge elements to be collected, studied and modeled.

Table 5.27: **PONTIS [1995] Condition State (CS) Ratings for An Unprotected Concrete Deck with Asphalt Concrete Overlay**

CS	Description
1	The surfacing of the deck has no repaired areas and there are no potholes in this surfacing
2	Repaired areas and/or potholes or impending potholes exist. Their combined area is less than 2% of the deck area.
3	Repaired areas and/or potholes or impending potholes exist. Their combined area is less than 10% of the deck area.
4	Repaired areas and/or potholes or impending potholes exist. Their combined area is more than 10% but less than 25% of the deck area.
5	Repaired areas and/or potholes or impending potholes exist. Their combined area is less than 25% of the deck area.

5.13.2 Condition State Deterioration Models

Some available models will be considered to develop serviceability flags for the deck, railings and substructure for Bridge E-17-AH. Many of the models are based on a linear deterioration of condition states where the deterioration rate can be expressed in terms of condition rating loss per year ($CR/year$) where the condition rating at any time t can be computed. Looking

specifically at reinforced concrete (RC) decks, railings and RC substructures, the results of several studies based on linear models as described in Hearn *et al.* [1995] are shown in Table 5.28. The source of the study and whether it was based on data or the opinion of experts is included. Given the condition state deterioration rate, the number of years required to reach NBI condition state 4 (poor condition) and condition state 3 (serious condition) are given.

Some of the studies became more specific regarding traffic volume and location. The Chen and Johnston [1987] study found the time to condition state 4 for the RC decks where the average daily traffic (ADT) was greater than 4000 was 39 years, rather than the 41 years for all RC decks. The ADT for Bridge E-17-AH is 8500. Similarly the James *et al.* [1993] study found that the condition state deterioration rate for RC decks on State highways in the western region of the U.S. was 0.176 rather than 0.210 for all RC decks, which equates to 28 years to condition state 4 and and 34 years to condition state 3.

Similar detail could be added to the substructure estimates as well. The Chen and Johnston study [1987] actually listed three condition state deterioration rates (0.102, 0.119, and 0.114) for the coastal , mountain and piedmont regions of North Carolina, respectively. A Pennsylvania study determined the expected service life of a deck with uncoated reinforcement to be 25 years and a substructure to be 100 years [Hearn *et al.* 1996]. Jiang and Sinha [1989] developed the following polynomial model for a concrete bridge

Table 5.28: **Linear Condition State Deterioration Models for RC Decks, Railings, and RC Substructures [Hearn *et al.* 1995]**

Element	Source	Basis	Time to NBI=4 *years*	Time to NBI=3 *years*	Deter. Rate *CR/year*
RC Deck	James *et al.* 1993	Data	24	29	0.210
RC Deck	Stukhart *et al.* 1991	Expert	33	39	0.152
RC Deck	Chen & Johnston 1987	Data	41	49	0.123
RC Deck	Morrow & Johnston 1994	Data	45	54	0.111
RC Deck	Al Rahim & Johnston 1991	Data	48	58	0.104
Steel Rail	Morrow & Johnston 1994	Data	37	44	0.135
RC Sub.	James *et al.* 1993	Data	23	27	0.219
RC Sub.	Stukhart *et al.* 1991	Expert	35	42	0.143
RC Sub.	Chen & Johnston 1987	Data	44	53	0.114
RC Sub.	Morrow & Johnston 1994	Data	42	50	0.119
RC Sub.	Al Rahim & Johnston 1991	Data	42	50	0.119

superstructure

$$CS(t) = 9.0 - 0.28877329t + 0.0093685t^2 - 0.00008877t^3 \qquad (5.102)$$

where $CS(t)$ is the condition rating of the bridge at time t where t is the age of the bridge in *years*, which translates to 71 years to condition state 4. Weyers *et al.* [1988] computed an average condition state deterioration rate for replacing a substructure is 0.077 $CR/year$ which indicates 65 years to condition state 4 and 78 years to condition state 3. There is no exact agreement between these studies and the result is an average deterioration rate. To create a serviceability flag which incorporates a probability (i.e., 10%, 20%, 30% chance) of being at a particular condition state, one could use Markov chains.

5.13.3 Markov Chain Models

Markov chains can be used to model NBI condition ratings based on the data from large numbers of bridges using transitional probabilities. Jiang and Sinha [1989] used Markov chains to model the condition of bridge substructures in Indiana. Table 5.29 shows the transitional probabilities for concrete bridge substructures. In this case the transitional probabilities change as the bridge ages.

The value p_9 indicates the probability that a bridge that is currently in condition state 9 will remain in condition state 9 for the next year. For a new bridge that is only 0 to 6 years old, this probability is $p_9 = 0.705$. Assuming that a bridge can only change one condition state in a given year,

Table 5.29: **Transition Probabilities for Concrete Bridge Substructures Using Markov Chains [Jiang and Sinha 1989]**

Bridge Age (years)	p_9	p_8	p_7	p_6	p_5	p_4
0-6	0.705	0.818	0.810	0.802	0.801	0.800
7-12	0.980	0.709	0.711	0.980	0.980	0.856
13-18	0.638	0.639	0.748	0.980	.0980	0.980
19-24	0.798	0.791	0.788	0.980	0.870	0.824
25-30	0.794	0.810	0.773	0.980	0.980	0.980
31-36	0.815	0.794	0.787	0.980	0.980	0.737
37-42	0.800	0.798	0.815	0.980	0.850	0.980
43-48	0.800	0.800	0.309	0.938	0.980	0.050
49-54	0.800	0.800	0.800	0.711	0.707	0.768
55-60	0.800	0.800	0.800	0.05	0.05	0.505

the probability that the bridge will fall to condition state 8 is $1 - p_9$ which for the new bridge is $1 - 0.705 = 0.295$. Once this new bridge $(0 - 6\ years)$ has transitioned to condition state 8, the probability that it will remain in condition state 8 is $p_8 = 0.818$, and so forth. Using Table 5.29 the bridge has only been modeled to condition state 3.

It is possible to conduct a simulation to determine the probability of the concrete substructure being in any condition state at any given time. For each year, a random number between 0.0 and 1.0 is generated and compared to the transition probability to determine whether the bridge will change condition states or remain in the same condition state. The results of a simulation for 10,000 bridges conducted for a 70 year time period using the transitional probabilities in Table 5.29 are shown in Tables 5.30 and 5.31 and Fig. 5.64. Table 5.30 shows that there is a 10% chance of the concrete substructure being in condition state 3 (i.e., 1000 bridges) between 34-35 years. Similarly, Table 5.31 indicates that there is a 13% chance (i.e., about 1300 bridges) between 41-42 years and a 50% chance (i.e., about 5000 bridges) between 53-54 years of being in condition state 3. These could be used to define probabilistic serviceability flags. The curves in Fig. 5.64 are very uneven due to the degree which the transition probabilities change over time.

The distribution curves are much smoother when the transition probabilities do not change over time and the process is stationary. Cesare *et al.* [1992] used Markov chains to model many bridge elements in New York State using a data base of 850 bridges and 2,000 individual spans. The New York

Table 5.30: **Simulation Results for 10,000 Concrete Bridge Substructures Using Markov Chains (Year 0-35)**

Bridge Age	Number of Bridges in Each Condition State (CS)						
(*years*)	CS_9	CS_8	CS_7	CS_6	CS_5	CS_4	CS_3
0	10000	0	0	0	0	0	0
1	7016	2984	0	0	0	0	0
2	4951	4549	500	0	0	0	0
3	3529	5150	1225	96	0	0	0
4	2512	5215	1943	306	24	0	0
5	1764	5006	2531	624	73	2	0
6	1260	4567	2987	970	199	16	1
7	1238	3280	3449	1800	214	16	3
8	1214	2334	3432	2750	248	14	8
9	1185	1699	3086	3714	289	15	12
10	1169	1202	2723	4511	367	14	14
11	1134	886	2307	5211	427	18	17
12	1107	625	1935	5767	526	21	19
13	700	811	1677	6139	627	27	19
14	432	784	1555	6423	747	40	19
15	274	666	1454	6679	850	55	22
16	177	537	1284	6932	977	69	24
17	109	401	1152	7142	1083	86	27
18	72	287	997	7296	1212	108	28
19	62	251	831	7348	1214	264	30
20	51	205	703	7392	1197	417	35
21	41	160	610	7395	1193	560	41
22	30	146	514	7368	1167	724	51
23	23	125	445	7340	1149	852	66
24	17	104	391	7284	1135	989	80
25	13	90	327	7197	1282	988	103
26	9	76	268	7109	1423	999	116
27	8	60	213	7027	1552	1012	128
28	7	51	159	6950	1665	1017	151
29	5	42	134	6837	1768	1039	175
30	5	34	113	6714	1884	1053	197
31	4	29	101	6600	1977	805	484
32	3	21	88	6498	2046	622	722
33	3	17	72	6389	2138	495	886
34	3	14	61	6282	2209	438	993
35	2	10	58	6174	2290	368	1098

Table 5.31: **Simulation Results for 10,000 Concrete Bridge Substructures Using Markov Chains (Year 36-70)**

Bridge Age	Number of Bridges in Each Condition State (CS)						
(*years*)	CS_9	CS_8	CS_7	CS_6	CS_5	CS_4	CS_3
36	2	7	46	6063	2382	314	1186
37	1	7	40	5963	2148	649	1192
38	1	5	37	5864	1914	969	1210
39	1	5	28	5755	1729	1252	1230
40	1	3	24	5651	1604	1451	1266
41	1	3	20	5548	1472	1662	1294
42	1	3	16	5447	1369	1835	1329
43	1	3	5	5095	1698	133	3065
44	1	3	1	4784	1986	30	3195
45	1	3	1	4472	2260	38	3225
46	1	3	0	4205	2485	44	3262
47	1	3	0	3946	2699	50	3301
48	0	4	0	3719	2865	63	3349
49	0	3	1	2631	3119	885	3361
50	0	2	2	1832	3015	1566	3583
51	0	1	3	1289	2648	2122	3937
52	0	1	2	925	2233	2406	4433
53	0	1	1	681	1831	2518	4968
54	0	0	2	504	1478	2462	5554
55	0	0	2	33	552	2685	6728
56	0	0	2	1	62	1823	8112
57	0	0	2	0	3	985	9010
58	0	0	2	0	0	489	9509
59	0	0	1	1	0	267	9731
60	0	0	0	1	1	129	9869
61	0	0	0	0	1	70	9929
62	0	0	0	0	0	30	9970
63	0	0	0	0	0	15	9985
64	0	0	0	0	0	13	9987
65	0	0	0	0	0	3	9997
66	0	0	0	0	0	2	9998
67	0	0	0	0	0	1	9999
68	0	0	0	0	0	1	9999
69	0	0	0	0	0	0	10000
70	0	0	0	0	0	0	10000

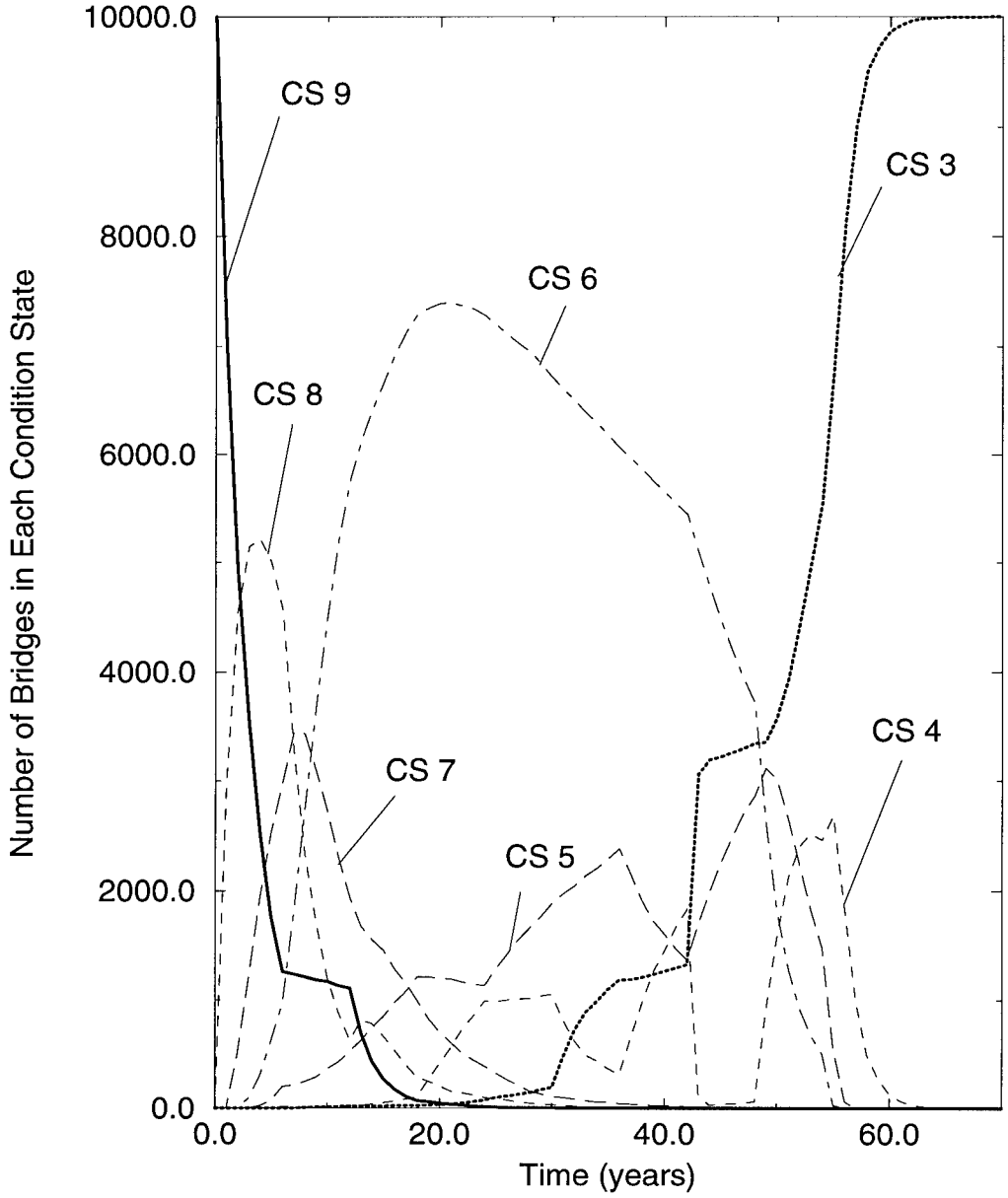

Figure 5.64: **Condition States (CS) for Concrete Bridge Substructures Over Time Using Markov Chains**

condition ratings range from 7 (high) to 1 (low) as shown in Table 5.32

Table 5.32: **New York State Condition Ratings and Their Definitions [Cesare *et al.* 1992]**

New York Rating	Description
7	New condition
6	Between new condition and minor deterioration
5	Minor deterioration
4	Between minor and serious deterioration
3	Serious deterioration
2	Between serious deterioration and potentially hazardous
1	Potentially hazardous

Based on these New York condition ratings, Cesare *et al.* [1992] developed stationary transition probabilities for numerous bridge elements. For a structural cast-in-place bridge deck with uncoated bars, the transitional probabilities are: $p_7 = 0.937$, $p_6 = 0.940$, $p_5 = 0.971$, $p_4 = 0.974$, $p_3 = 0.977$, and $p_2 = 0.961$ where $p_2 = 0.961$ means that if the bridge deck is in Condition State 2, there is a 96.1% likelihood that it will remain in Condition State for the next year. Using these probabilities and a simulation of 10,000 bridges, Fig. 5.65 shows the probabilities of being in any given condition state at any time. The curves are much smoother when the probabilities do not change. The probabilistic serviceability flags can be developed for any bridge element for which the Markov chain data is available.

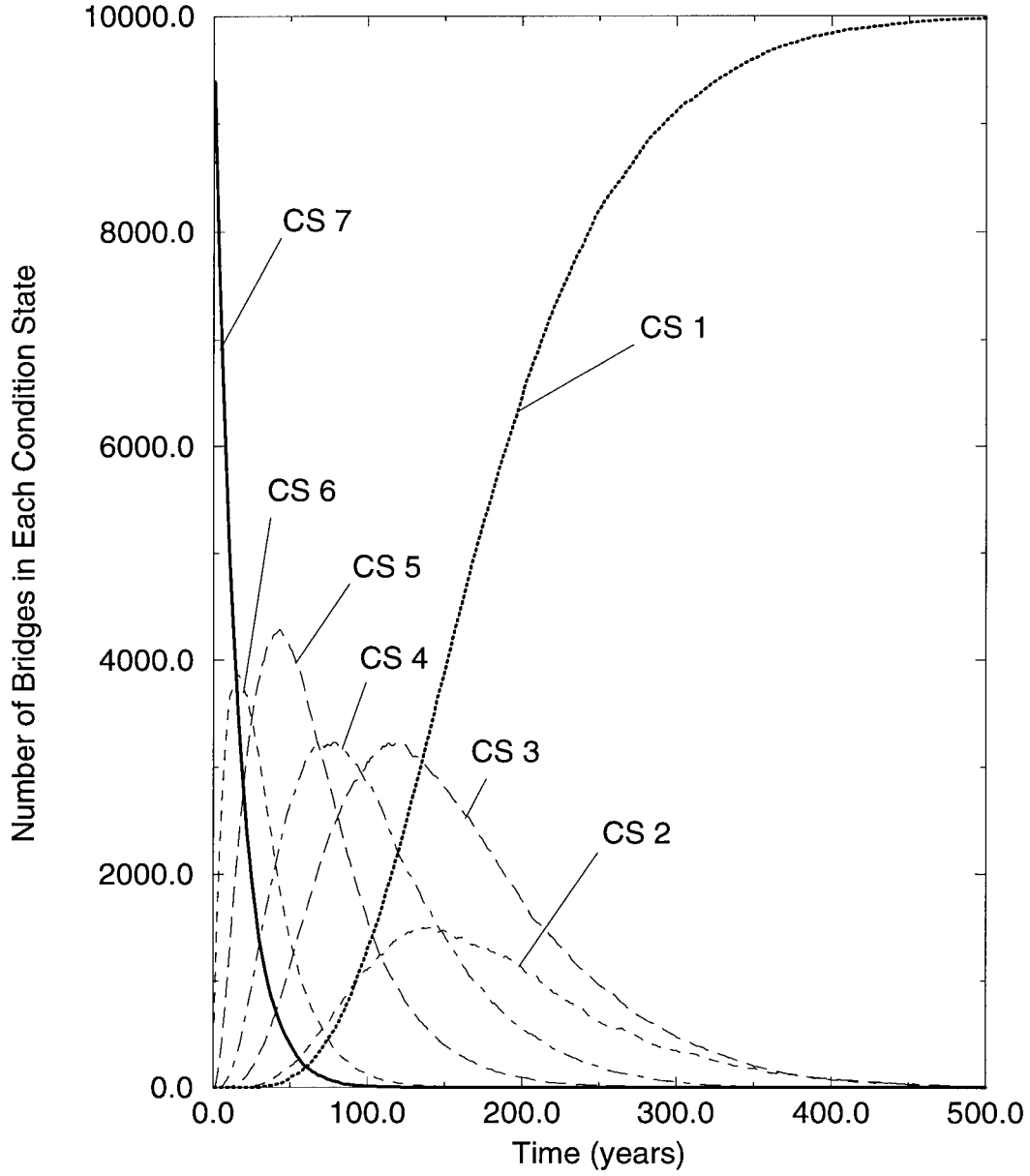

Figure 5.65: **Condition States (CS) for Cast-In-Place Bridge Deck Over Time Using Markov Chains and New York State Condition Ratings (1-7)**

5.13.4 Example Using Serviceability Flags

It is clear that the data can differ significantly from study to study. The engineer must use the study and assumptions that best fit the structure being considered when developing serviceability flags. For the case of Bridge E-17-AH, the following serviceability flags will be adopted to account for deterioration of the slab, the railing, and the substructure. The concrete slab will be replaced every 28 years using the James *et al.* [1993] study for RC slabs on state highways in the western region deteriorating to condition state 4. The railings will be replaced every 37 years using the Morrow and Johnston [1994] study as shown in Table 5.28. Considering that only a railroad runs underneath the bridge, the substructure will be replaced every 65 years using the Weyers et al. [1988] study.

The results for Repair Option 1 (Replace Slab) with these serviceability flags are shown in Fig. 5.66 and can be compared to Fig. 5.53 for the same situation where serviceability flags were not in effect. The railing serviceability flag is never executed because the railing is replaced every time the slab gets replaced (every 28 years). In Fig. 5.66, the slab is replaced twice (years 28 and 56) which is before the strength constraint requires it. As a result, there is little effect on the system reliability from the slab replacement. Slab repair is no longer effective at year 65 where the serviceability flag requires that the substructure, and thus the bridge, be replaced.

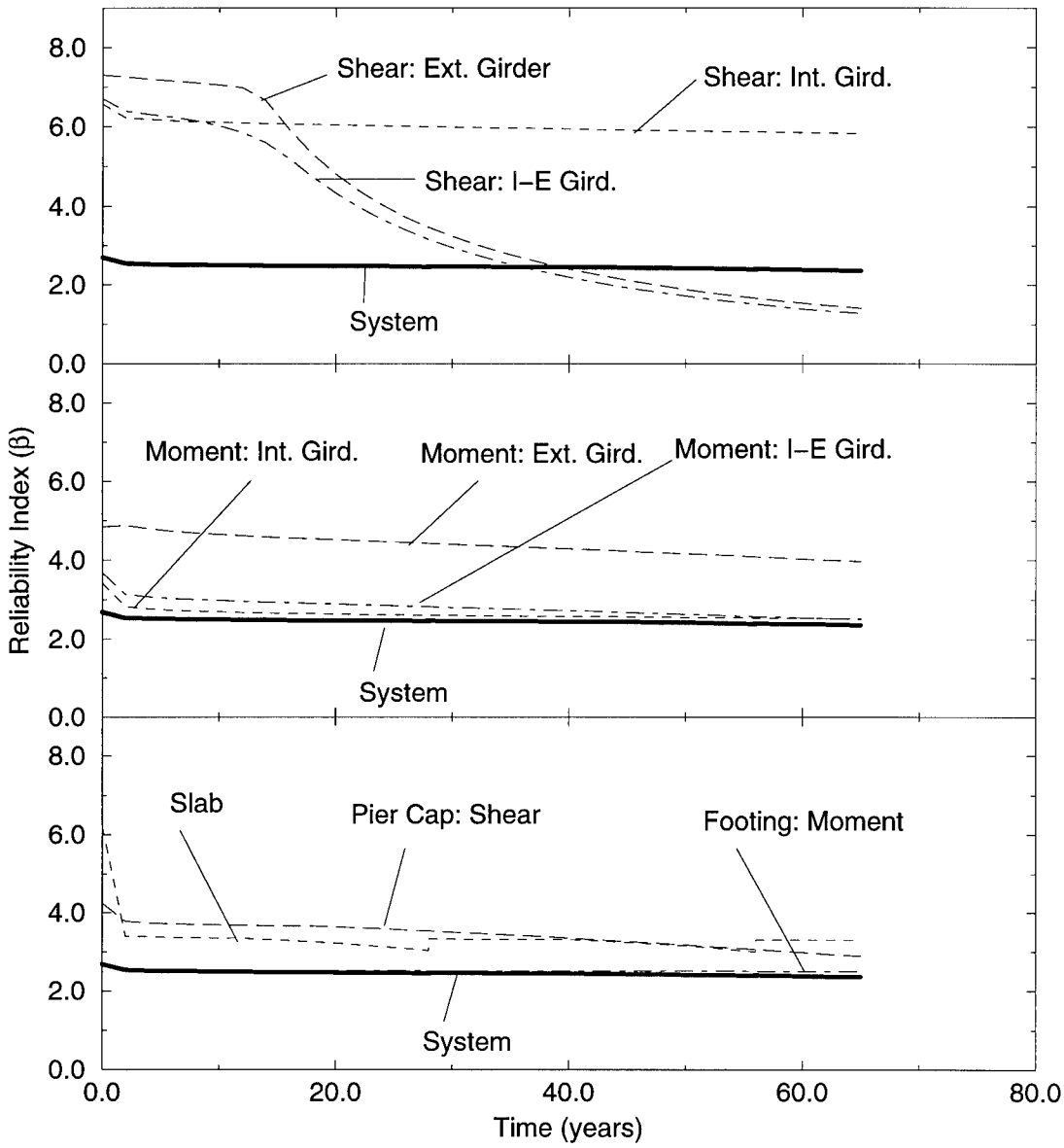

Figure 5.66: **Results of Repair Option 1 (Replace Slab) on Bridge E-17-AH Using Simplified Series-Parallel Model Requiring the Failure of Three Adjacent Girder Including Serviceability Flags**

All feasible repair options for the series-parallel bridge model where three adjacent girders are required to fail with serviceability flags implemented are shown in Fig. 5.67. These options can be compared to Fig. 5.55 where the serviceability flags are not used. The optimum repair strategy based on these options including serviceability flags is shown in Table 5.33. Compared to the optimum repair strategy without serviceability flags shown in Table 5.20, the serviceability flags result in earlier repairs, a shorter expected life of the bridge, and a more expensive optimum repair strategy. This will always be the case. At the most extreme case where all serviceability flags are overridden by strength concerns, the optimal solution would be the strength-based case. A serviceability flag will only shorten the life of the structure.

Table 5.33: **Optimum Lifetime Repair Strategy for Bridge E-17-AH Using Simplified Series-Parallel Model Requiring Failure of Three Adjacent Girders (Serviceability Flags Included)**

Expected Life (years)	Optimum Repair Strategy	Cost ($)
0-28	Do nothing	0
28-56	1@28	129,579
56-65	1@28, 1@56	204,006
>65	1@28, 5@56	347,284
1@28 indicates option 1 (replace deck) at year 28		

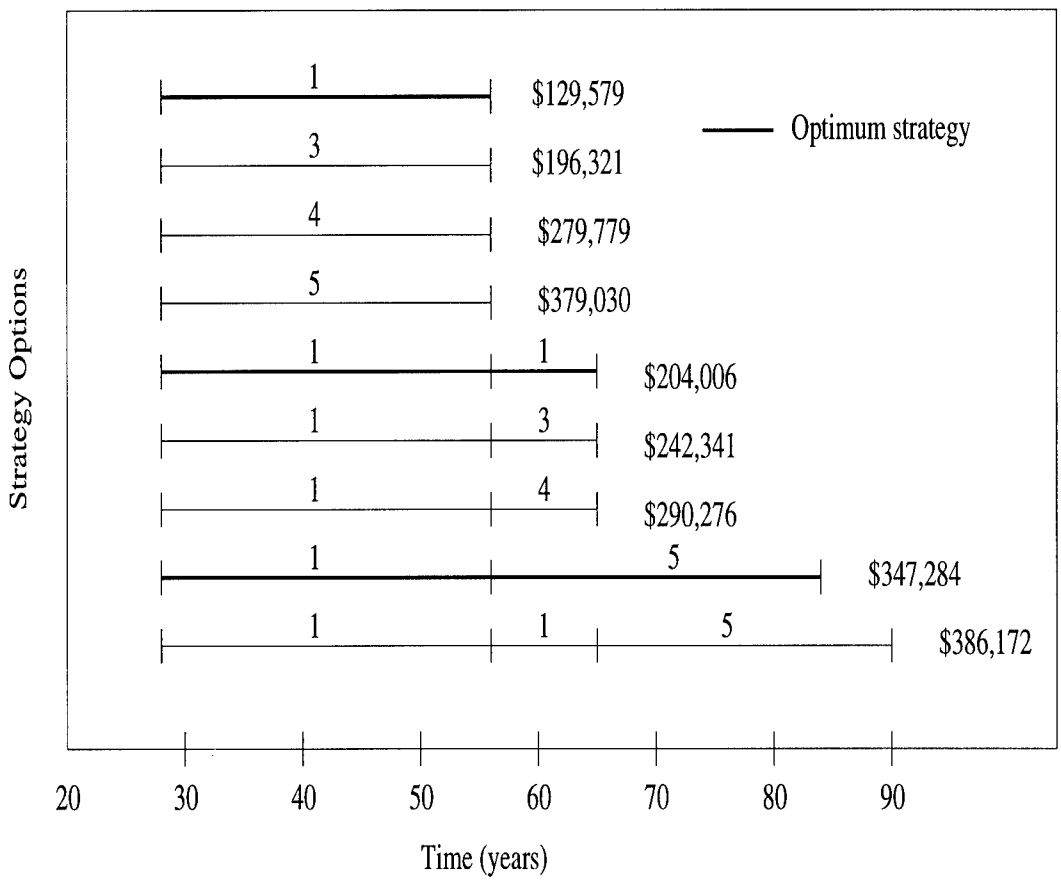

Figure 5.67: **All Feasible Repair Options For Bridge E-17-AH Using Simplified Series-Parallel Model Requiring the Failure of Three Adjacent Girders (Serviceability Flags Included)**

5.14 Summary

This chapter has applied a system reliability optimization technique to an existing highway bridge, E-17-AH, that currently exists in Denver, Colorado. The application of this technique was significantly more involved and complex for an actual bridge than for the hypothetical trusses using imaginary data in Chapter 4. There were numerous opportunities for assumption and engineering judgement along the way. The choice of failure modes, random variables, series-parallel models, live load and deterioration models, repair options, discount rates, costs, and serviceability flags are all subject to debate and a change in any of them can produce radically different results. The choice of input data is therefore critically important and time consuming, yet very imprecise. This is an area that will only be improved through further use of the method and more research.

With accurate input, the method demonstrates real potential for minimizing lifetime costs while maintaining a prescribed level of structural safety. While current deterministic design methods are certainly easier to implement, this proposed methodology accounts for uncertainty associated with the entire design process, structure redundancy, failure mode correlation, and the variability of conditions over time. The structure is considered as a total system rather than an a collection of unrelated individual components.

The proposed system reliability optimization process produces an

optimum repair strategy for initial lifetime planning purposes. When a plan attempts to forecast the condition of a structure 30, 50 or even 100 years in the future, inevitably some of the initial assumptions will be proven to be wrong. Still, a plan based on sound concepts that can be modified as assumptions are verified, is far more useful than no plan or a plan based on faulty logic. It is therefore important for the optimized plan to be updated based on inspection results.

Considering Bridge E-17-AH as an example, none of the plans put forth in this chapter accurately portray what has actually happened to this bridge over the last 54 years. Even the most optimistic forecasted lifetime strategy (see Table 5.20) predicted that the slab would have to be replaced after 50 years. The serviceability flag stated that the slab would be replaced after 28 years. In reality, Bridge E-17-AH has had no major replacements since it was originally constructed in 1942. The only major repair was to the bridge approach in 1992 for a cost of $68,000 which would not have been included in this model. In fact, after the most recent inspection [CDOT 1996b], the bridge was given NBI condition ratings for the slab, superstructure, and substructure of 6, 6, and 5, respectively. This would indicate that the bridge still has many years of expected life remaining.

These results do not demean any of the plans or methods used in this chapter. Rather, they emphasize the need to modify and update the plan over time to account for actual behavior based on the results of inspections. For Bridge E-17-AH, any of the plans offered in this chapter would have been

modified over time and the assumptions would have been verified or altered. The methods for revising both the strength-based plan and the serviceability flags based on inspection results will be the subject of the next chapter.